GROUND-BASED RADIO WAVE PROPAGATION STUDIES OF THE LOWER IONOSPHERE

CONFERENCE PROCEEDINGS

11-15 APRIL, 1966

OTTAWA, CANADA

VOLUME I

DECEMBER 1967

CONFERENCE ON GROUND-BASED RADIO WAVE PROPAGATION STUDIES OF THE LOWER IONOSPHERE

First Row: Mr. T.J. Elkins, AFCRL – Dr. W. Elling, Max-Planck Inst. Germany – Mr. L.W. Hewitt, DRTE – Dr. R.C. Whitten, SRI – Dr. William Swider, Jr., AFCRL – Dr. W. Pfister, AFCRL – Mr. Samuel Horowitz, AFCRL – Dr. J.S. Belrose, DRTE – Dr. Klaus Bibl, Lowell Tech., – Dr. H. Volland, U. of Bonn, Germany – Dr. R.A. Smith, U. of New England, Australia – Mr. Glenn Falcon, ITSA – Mr. L.R. Megill, ITSA.

Second Row: Mr. D.P. Hayes, Lowell Tech. – Dr. A.C. Aikin, NASA/GSFC – Dr. T.M. Georges, ITSA – Mr. Richard S. Allen, AFCRL – Dr. E.V. Thrane, NDRE, Norway – Dr. Ben Segal, DRTE – Frank T. Davies, CS/DRTE – Lt. Col. J.D. Brown, DASA – Mr. V.E. Hildebrand, U.S. Naval Ord. Lab. – Dr. Gary S. Sales, AFCRL – Dr. E.S. Owen Jones, Bedford College, England – Dr. H.A. von Biel, Cornell Aero Labs. – Mr. B.R. May, RSRS, Slough, England.

Third Row: Dr. J.S. Shirke, U. of Illinois – Mr. D.B. Ross, DRTE – Miss Doris H. Jelly, DRTE – Dr. J.A. Kane, NASA/GSFC – Dr. R.I. Fenwick, Stanford U. – Mr. K. Olson, Lowell Tech. – Mr. B.W. Reinisch, Lowell Tech. – Dr. A.K. Paul, Max-Planck Inst. Germany – Dr. J.W. Wright, ITSA – Dr. G. Lanza, Northeastern U. – Mr. D. Reitz, GE/TEMPO – Mr. Jerry T. Jones, IIT Research Inst.

Fourth Row: Mr. G.W. Adams, Douglas MSSD – Dr. A.H. Manson, Chicago U. – Dr. J.B. Gregory, U. of Saskatchewan – Dr. I. Bourne, DRTE – Mr. W.T. Roberts, NASA/MSFC – Mr. Arne Haug, NDRE, Norway – Dr. M.L.V. Pitteway, Nottingham U. England – Dr. L.M. La Londe, Cornell U. – Mr. Arne Pedersen, NASA/GSFC – Mr. Noboru Wakai, ITSA – Lt. J.E. Barety, USAF Weapons Lab. – Dr. E. Gossard, U.S. Navy Electronics Lab.

VOLUME 1

PROCEEDINGS OF A CONFERENCE HELD 11 TO 15 APRIL, 1966

AT

DEFENCE RESEARCH TELECOMMUNICATIONS ESTABLISHMENT
RADIO PHYSICS LABORATORY
Shirley Bay, Ottawa, Ontario, Canada

GROUND-BASED RADIO WAVE PROPAGATION STUDIES OF THE LOWER IONOSPHERE

Compiled by

J.S. Belrose, I.A. Bourne and L.W. Hewitt

SPONSORED BY

Defence Research Telecommunications Establishment
Ottawa, Ontario

and

Air Force Cambridge Research Laboratories
Hanscom Field, Massachusetts, U.S.A.

December 1967

Defence Research Board
Department of National Defence
Canada

66-571

96413—1½

CONFERENCE PLANNING AND DRTE MANAGEMENT STAFF

Conference General Chairman

Dr. J.S. Belrose

Secretary

Mrs. Edna Robertson

Program Planning

Dr. J.S. Belrose	–	Defence Research Telecommunications Establishment Ottawa 4
Dr. W. Pfister	–	Geophysics Research Directorate Air Force Cambridge Research Laboratories Bedford, Massachusetts

Local Arrangements

Dr. I.A. Bourne	–	Publications
Mr. L.W. Hewitt	–	Chief Reporter
Mr. H.E. Checkley	–	Facilities
Mrs. Judy Mulvihill	–	Conference Secretarial Assistance

DRTE Management

Mr. Frank T. Davies	–	Chief Superintendent
Dr. John H. Chapman	–	Deputy Chief Superintendent
Dr. Irvine Paghis	–	Superintendent, Radio Physics Laboratory
Dr. J.H. Meek	–	Superintendent, Communications Laboratory
Dr. R.C. Langille	–	Superintendent, Electronics Laboratory

PREFACE

The lower ionosphere, consisting of the D region and part of the E region below about 120 km. in height, is perhaps the most imperfectly understood part of the ionosphere at the present time. This is partly because of observational limitations and partly because of difficulties in interpreting the observational data that have been obtained. Under normal conditions the electron number densities are so low that low frequencies are needed for reflection in this height range. Despite an abundance of experimental data, few results have, until recently, emerged from these studies. Under abnormal conditions (SID, PCA, and auroral disturbances) the attenuation of radio waves propagating within the region can become so great that radio reflections, other than from the base of the ionosphere, are not obtained. The dynamic range of variation is large: under normal conditions the electron density and collision frequency values change by up to five orders of magnitude in the height range 30 to 120 km.; and under disturbance conditions electron density increases by several orders of magnitude can occur at low heights.

Thus, while ground-based studies of the lower ionosphere are both scarce and difficult to interpret, the situation is not much improved in the case of experiments conducted "in situ". The relative high gas densities make environmental measurements with sounding rockets difficult, and most experiments have been designed to provide information about the ionosphere at heights above about 90 km. A few results have been obtained for the normal D region, but in general these are less reliable than those obtained at times when radio wave absorption was great.

The magnitude of the electron density and its variation with height in the lower ionosphere is roughly known, at least at middle latitudes, but superimposed on a general increase with height are important structural features, the dynamic changes of which cannot be studied by means of rockets. For example it is becoming increasingly evident that meteorology plays an important part in the variability of the undisturbed D region. There is therefore a need for a reliable means of studying the lower ionosphere by ground-based experiments capable of synoptic application. In recent years, several new techniques have been developed for studying the lower ionosphere, e.g., partial reflections and pulse cross modulation, and new progress is being made in the numerical interpretation of low frequency propagation data. Since an increasing number of research laboratories and organizations are exploiting one or more of these techniques, it is important at this time to evaluate the reliability of the data, so that the best experiments can be undertaken in a synoptic application. It is important at this epoch of the solar cycle to increase the latitude coverage of D-region observations before solar activity increases.

With this aim in mind, a working conference was planned to bring together specialists concerned with the various ground-based experiments. The various experimental techniques were reviewed, emphasizing the state of the art and the problems to be resolved, and new and stimulating results not yet appearing in the literature were presented. When soliciting papers for the conference, it was made clear that a Conference Proceedings would be published, and that an edited discussion following each paper would be included. Even so, it was our intention to keep the atmosphere of the conference as informal as possible so as to promote discussion (or debate), even to the extent of intentionally forcing an argument. This procedure sometimes worked so well, it later proved difficult to obtain final manuscripts from some of the speakers, and the task of preparing an edited version of the discussions was a difficult one.

Unfortunately, the three main experiments (partial reflections, pulse cross modulation, and LF propagation) have little in common, apart from the fact that they are concerned with the reflection and propagation of radio waves in the ionosphere, and workers in the three fields do not necessarily have a good understanding of all the experiments or, for that matter, of the D region.

The purpose of Session 1 was therefore to give a general background of D-region properties, insofar as they are currently known, and to show the difficulties that are encountered because of limited knowledge concerning the existence of minor constituents and the uncertainties of dominant production and loss rates. The majority of the work in Session 1 is a summary of previously published work, of which a knowledge is necessary if the merits (and defects) of the partial reflection, wave interaction, and LF propagation experiments, which are discussed in the main sessions of the conference, are to be appreciated.

The partial reflection and the pulse cross modulation experiments and observational results obtained by these techniques, and the long wave propagation interpretive results, are the subjects of Sessions 2, 3, and 4 respectively. Other experiments, e.g., ionosondes and radio wave absorption, and observational results obtained from an analysis of these data, are the subjects of Sessions 5 and 6.

The concluding discussion is intended to compare the various data, to update the present knowledge summaries given in Session 1 in the light of the new observational results presented at this conference, and to define the areas where new observational data or new interpretations are needed.

In setting up this conference, we were guided by the concept that its prime purpose should be the dissemination of viewpoints, technical information, and scientific results among a relatively small number of active researchers, following a pre-arranged program of subject material. Accordingly, the meeting was not open to all who might have desired to attend. We hope that this record will be of some value to them, and that it will serve as a basic text to be used by future investigators of the lower ionosphere.

John S. Belrose
Conference Chairman

ACKNOWLEDGMENTS

Any success achieved by the Conference or its Proceedings is undoubtedly due to the authors of the various papers and to the speakers and session chairmen. All participants are to be congratulated for the quality of the material brought to the conference and for the willingness with which they responded to the critical spirit of the meetings.

We have wielded a heavy and sometimes arbitrary editorial hand in preparing the papers, especially the discussions, in a coherent form for printing. Accordingly, we take full responsibility for any misquotation or misrepresentation of a participant's remarks which may appear.

The help freely given by the many members of the Defence Research Board staff in the organization of the conference and the production of this volume is gratefully acknowledged. The whole hearted co-operation of Dr. L.W. Billingsley and the DRB/DSIS staff who organized the technical production of this Proceedings, and of Mr. E.A. Atkins of the DRTE Publications Section, deserves particular mention. Mr. A.F. Adams and Mr. J.E. Colbert of the DRTE Illustration and Photography Sections also gave able assistance.

Special mention should be made of the DRTE technical staff who operated projection and recording facilities during the conference, and of the secretarial staff, especially Mrs. Edna Robertson, who prepared typed copy of the many discussions.

J.S. Belrose
I.A. Bourne
L.W. Hewitt
Editorial Committee

LIST OF ATTENDEES AT CONFERENCE

Mr. Gene Adams
Douglas MSSD.,
Santa Monica, California, U.S.A.

Dr. A.C. Aikin
NASA/GSFC,
Greenbelt, Maryland, U.S.A.

Dr. Richard Allen
Air Force Cambridge Research Laboratories,
Bedford, Massachusetts, U.S.A.

Dr. Ian Axford
Cornell University,
Astronomy Department,
Ithaca, New York, U.S.A.

Lt. J.E. Barety
Kirtland Air Force Base,
Air Force Weapons Laboratory,
Albuquerque, New Mexico, U.S.A.

Dr. R.E. Barrington
Defence Research Telecommunications Establishment,
Ottawa, Canada.

Mr. C.D. Bell
Pennsylvania State University,
University Park,
Pennsylvania, U.S.A.

Dr. J.S. Belrose
Defence Research Telecommunications Establishment,
Ottawa, Canada.

Dr. K. Bibl
Lowell Technological Institute Research Foundation,
Lowell, Massachusetts, U.S.A.

Dr. I.A. Bourne
Defence Research Telecommunications Establishment,
Ottawa, Canada.

Lt.-Col. J.D. Brown
Department of Defence,
Defence Atomic Support Agency,
Washington, D.C., U.S.A.

Mr. J.W. Cox
Defence Research Telecommunications Establishment,
Ottawa, Canada.

Dr. C.M. Crain
The Rand Corporation,
1700 Main Street,
Santa Monica, California, U.S.A.

Dr. A. Dalgarno
Department of Applied Mathematics,
Queens University of Belfast
Belfast, Northern Ireland.

Mr. Frank T. Davies
Chief Superintendent
Defence Research Telecommunications Establishment,
Ottawa, Canada

Mr. Terence J. Elkins
Wentworth Institute,
550 Huntington Avenue,
Boston, Massachusetts, U.S.A.

Dr. W. Elling
Max-Planck Institut Fur Aeronomie,
Lindau UB. North /Han., Germany.

Mr. G. Falcan
Institute for Telecommunication Sciences and Aeronomy,
Environmental Science Services Administration,
Boulder, Colorado, U.S.A.

Dr. R.B. Fenwick
Radioscience Laboratory,
Stanford University,
Stanford, California, U.S.A.

Dr. A.J. Ferraro
Ionospheric Research Laboratory,
Pennsylvania State University,
University Park,
Pennsylvania, U.S.A.

Dr. P.A. Forsyth
Department of Physics,
University of Western Ontario,
London, Ontario, Canada.

Mr. T.M. Georges
Institute for Telecommunication Sciences and Aeronomy,
Environmental Science Services Administration,
Boulder, Colorado, U.S.A.

Dr. E.E. Gossard
US Navy Electronics Laboratory,
San Diego, California, U.S.A.

Dr. J.B. Gregory
University of Saskatchewan,
Saskatoon, Saskatchewan, Canada.

Dr. T.R. Hartz
Defence Research Telecommunications Establishment,
Ottawa, Canada.

Mr. A. Haug
Norwegian Defence Research Establishment,
P.O. Box 25,
Kjeller/Lillistrom, Norway.

Mr. Daniel P. Hayes
Lowell Technological Institute Research Foundation,
450 Aiken Street,
Lowell, Massachusetts, U.S.A.

96413—2

Dr. R.J.W. Henry
NASA/GSFC,
Greenbelt, Maryland, U.S.A.

Mr. L.W. Hewitt
Defence Research Telecommunications Establishment,
Ottawa, Canada.

Mr. Verne E. Hildebrand
Naval Ordnance Laboratory,
Corona, California, U.S.A.

Mr. S. Horowitz
Air Force Cambridge Research Laboratories,
Bedford, Massachusetts, U.S.A.

Miss Doris Jelly
Defence Research Telecommunications Establishment,
Ottawa, Ontario, Canada.

Dr. J.R. Johler
Institute for Telecommunication Sciences and Aeronomy,
Environmental Science Services Administration,
Boulder, Colorado, U.S.A.

Dr. E.S.O. Jones
Bedford College, Physics Department,
Regents Park, London N.W. 1, England.

Mr. Jerry Jones
IIT Research Institute,
10 West 35th Street,
Chicago, Illinois, U.S.A.

Dr. J.A. Kane
NASA/GSFC,
Greenbelt, Maryland, U.S.A.

Dr. Arthur J. Kantor
Air Force Cambridge Research Laboratories,
Bedford, Massachusetts, U.S.A.

Mr. J. Kert
Space Information Systems,
North American Aviation Incorporated,
Downey, California, U.S.A.

Dr. L.M. Lalonde
Clark Hall, Cornell University,
Ithaca, New York, U.S.A.

Dr. G. Lanza
Physics Department,
Northeastern University,
Boston, Massachusetts, U.S.A.

Dr. H.S. Lee,
Pennsylvania State University,
University Park,
Pennsylvania, U.S.A.

Dr. Alan Henry Manson
University of Chicago,
Chicago 37, Illinois, U.S.A.

Mr. B.R. May
Radio and Space Research Station,
Ditton Park,
Slough, Bucks, England.

Mr. L.R. Megill
Institute for Telecommunication Sciences and Aeronomy,
Environmental Science Services Administration,
Boulder, Colorado, U.S.A.

Mr. K.V. Narasinga Rao
Air Force Cambridge Research Laboratories,
Bedford, Massachusetts, U.S.A.

Dr. G.L. Nelms
Defence Research Telecommunications Establishment,
Ottawa, Canada.

Mr. Kirtland Olson
Lowell Technological Institute Research Foundation,
450 Aiken Street,
Lowell, Massachusetts, U.S.A.

Dr. I. Paghis
Defence Research Telecommunications Establishment,
Ottawa, Canada.

Dr. A.K. Paul
Max-Planck Institut Fur Aeronomie,
Lindau UB. North/Han., Germany.

Mr. Arne Pedersen
NASA/GSFC,
Greenbelt, Maryland, U.S.A.

Mr. L. Petrie
Defence Research Telecommunications Establishment,
Ottawa, Ontario, Canada.

Dr. W. Pfister
Geophysics Research Directorate,
Air Force Cambridge Research Laboratories,
Bedford, Massachusetts, U.S.A.

Mr. T.P. Pinkerton
Pennsylvania State University,
University Park,
Pennsylvania, U.S.A.

Dr. M.L.V. Pitteway
Cripps Computing Centre,
Nottingham University,
Nottingham, England.

Lt. R.M. Price
Institute for Exploratory Research, Division C,
Department of Army, US Army Electronics Command,
Fort Monmouth, New Jersey, U.S.A.

Mr. Bodo Reinisch
Lowell Technological Institute, Research Foundation,
450 Aiken Street,
Lowell, Massachusetts, U.S.A.

Mr. David Reitz
DASA Information + Analysis Center, GE. Tempo,
816 State Street,
Santa Barbara, California, U.S.A.

Dr. D. Rice
Defence Research Telecommunications Establishment,
Ottawa, Canada.

Mr. W.T. Roberts
NASA,
Marshall Space Flight Center,
Huntsville, Alabama, U.S.A.

Mr. D.B. Ross
Defence Research Telecommunications Establishment,
Ottawa, Canada.

Dr. Gary S. Sales
Upper Atmosphere Physics Laboratory,
Air Force Cambridge Research Laboratories,
Bedford, Massachusetts, U.S.A.

Dr. B. Segal
Defence Research Telecommunications Establishment,
Ottawa, Canada.

Dr. J.S. Shirke
Department of Electrical Engineering,
University of Illinois,
Urbana, Illinois,
U.S.A.

Dr. R.A. Smith
University of New England,
Armidale, N.S.W., Australia.

Dr. Wm. Swider, Jr.
Air Force Cambridge Research Laboratories,
Bedford, Massachusetts, U.S.A.

Dr. E. Thrane
Norwegian Defence Research Establishment,
P.O. Box 25,
Kjeller/Lillistrom, Norway.

Dr. H. Volland
Mitteilungen Der Astromischen Institute,
Der Universitat Bonn,
Bonn, Germany.

Dr. A. von Biel
Cornell Aeronautical Laboratory Incorporated,
Buffalo 21, New York, U.S.A.

Dr. E.S. Warren
Defence Research Telecommunications Establishment,
Ottawa, Canada.

Mr. Noboru Wakai
Institute for Telecommunication Sciences and Aeronomy,
Environmental Science Services Administration,
Boulder, Colorado, U.S.A.

Dr. A.H. Waynick
Ionosphere Research Laboratory,
Pennsylvania State University,
University Park,
Pennsylvania, U.S.A.

Dr. R.C. Whitten
Department of Atmospherics Sciences,
Stanford Research Institute,
Menlo Park, California, U.S.A.

Dr. J.W. Wright
Institute for Telecommunication Sciences and Aeronomy,
Environmental Science Services Administration,
Boulder, Colorado, U.S.A.

Dr. S.P. Zimmerman
Air Force Cambridge Research Laboratories,
Bedford, Massachusetts, U.S.A.

TABLE OF CONTENTS

SECTION 5 – Ionospheric Sounding
Chairman – Dr. G.L. Nelms,
DRTE, Ottawa

SECTION 6 – Ionospheric Absorption
Chairman – Dr. W. Pfister,
AFCRL, Bedford

SECTION 7 – Discussion
Chairman – Dr. J.S. Belrose,
DRTE, Ottawa 653

SECTION 8 – Epilogue

SECTION 1

REVIEW OF PRESENT KNOWLEDGE

1.1 ELECTRON IONIZATION AND LOSS PROCESSES AND RATES

by

C.M. Crain

The Rand Corporation
Santa Monica, California

1. Introduction

My talk today is essentially one of a review nature. I plan to summarize factors which relate to the ionization state in the region below roughly 100 km., and will include contributions from work of several people, including some in the audience. In trying to cover a large number of items in the short time available I may not give proper credit to some sources used in preparing some of the figures. I intend to summarize high points, emphasize areas of uncertainty in the different approaches, and include examples illustrating the implications of some of these uncertainties with which we are faced in the region below 100 km. Some figures are self-explanatory, some are not, and I will try to cover the more important aspects.

2. Ionization Sources

The list that follows shows some of the ionization sources of concern from time to time for those working in the region below 100 km.; most of the terms are fairly obvious.

Ionization Sources in the Lower Atmosphere

Xrays	Fission Betas
Lyman	Fission Gammas
Cosmic Rays	Neutron Betas
Protons	Meteors
Electrons	Chem – Ionization
Alpha Particles etc.	Miscellaneous

I have included such things as fission betas and gammas, and neutron betas. Papers involving these sources have appeared in the last few years dealing with the effects that followed nuclear tests, both by the United States and the Soviet Union. The understanding of these effects on the ionosphere worldwide has been getting more and more attention. I will spend most of my time discussing all but the last three items.

Fig. 1 shows fairly classical deposition values for protons and electrons impinging on the earth's atmosphere, and gives an indication of the altitude, if one neglects the earth's magnetic field, to which both high energy electrons and protons penetrate. In more recent years we have become much more concerned with the role of the magnetic field and its importance in deposition calculations.

Dr. Lutomirski at RAND provided results he calculated for protons at different combinations of pitch angle and dip angle impinging on the earth's atmosphere (Fig. 2). These results are applicable to protons which are born within the earth's magnetic field and not to protons coming in from, say, the sun, where the shielding effects of the earth's field must be included in the analysis. They indicate the effect of the longer travel distance of spiraling particles. The values of beta are 1 and .433; D is the dip angle and α_L is the pitch angle. A beta of .433 would apply for a dip angle of 60° and a pitch angle of 30°. The figure indicates

the variation in height of the depositing of the energy of the proton due to magnetic effects. If one considers fairly low dip angles and small pitch angles, these height differences can be large, i.e., there is quite a variability in the altitude at which a given energy particle will give up its energy to the atmosphere.

Fig. 3 is for 10 mev protons; particles in this energy range give up most of their energy in ionizing the height range of the normal lower D layer.

Fig. 4 shows the same calculations for 100 mev protons. The deposition heights where most of the energy is actually deposited are in the 30- to 40-km. height range. These curves can be run out for any sort of combination of dip angle, pitch angle, and energy of the particles, using standard theory.

Fig. 5 indicates the deposition of energy in the atmosphere below a typical source of fission debris that is, say, well above the atmosphere — like a layer of debris. The important point to be indicated here is the role of the magnetic field and particularly the sizable differences in production rates at the altitude ranges, say, below 70 km. at the different dip angles. This sort of difference would likewise occur for electrons of natural origin.

Fig. 6 shows still another production rate profile in which we have become interested in recent years while studying D layer ionization effects of neutron decay beta particles produced by high-altitude nuclear detonations. Again I want to emphasize the sizable variability in the height range below 75 km. of production rate with magnetic field dip angle. At 60 km., for example, there is a difference of over a factor of ten in the production rate from a given impinging source of beta particles, for dip angles of 35° and 75°. These are electrons that have a number spectrum of about 0 to 780 kv. with a peak value at roughly 300 kv.

The two tables following are from work which Arnold and Pierce of SRI published two or three years ago.

TABLE 1. Ion Production Rate due to Lyman-α (Solar Maximum)

Height (KM)	NO CM^{-3}	Zenith Angle (Deg)			Night
		0	40	80	
60	7.9×10^{6}	2.5×10^{-5}	—	—	—
70	3.2×10^{6}	1.1×10^{-1}	4.8×10^{-2}	1.4×10^{-7}	—
80	6.3×10^{5}	2.4×10^{-1}	2.1×10^{-1}	2.5×10^{-2}	2.0×10^{-4}
90	7.9×10^{4}	4.5×10^{-2}	4.4×10^{-2}	3.4×10^{-2}	7.2×10^{-5}
100	7.9×10^{4}	4.7×10^{-2}	4.6×10^{-2}	4.4×10^{-2}	7.2×10^{-5}

Day Values Based on Flux of 5 ERGS CM^{-2} SEC^{-1}

TABLE 2. Ion Production by Cosmic Radiation for 1964

Height (KM)	Geomagnetic Latitude (Deg)			
	0	20	40	60
40	1.2×10^{-1}	1.6×10^{-1}	3.6×10^{-1}	2.0
50	3.4×10^{-2}	4.3×10^{-2}	9.8×10^{-2}	5.4×10^{-1}
60	1.1×10^{-2}	1.4×10^{-2}	3.2×10^{-2}	1.8×10^{-1}
70	3.1×10^{-3}	4.0×10^{-3}	9.1×10^{-3}	5.0×10^{-2}
80	6.6×10^{-4}	8.5×10^{-4}	1.9×10^{-3}	1.1×10^{-2}
90	6.9×10^{-5}	1.1×10^{-4}	2.6×10^{-4}	1.4×10^{-3}
100	1.2×10^{-5}	1.5×10^{-5}	3.4×10^{-5}	1.9×10^{-4}

Table 1 shows production due to Lyman α radiation for various altitudes and solar zenith angles. The ionization production values tabulated are for an assumed solar maximum condition (5 ergs/sq.cm./sec.) and are based on the assumed NO concentrations indicated. All of the model Lyman α curves of these types have to be based on some assumption as to the NO concentration versus height. This concentration is not satisfactorily resolved and the numbers shown have to be directly associated with the vertical distribution assumed. Dr. C. Barth's measurements, for example, would indicate that these values are low; however, the validity of his measurements, I think, lacks confirmation. Also, the concentration may depend on season, location, atmospheric circulation, etc. The slide indicates the significant role of the zenith angle from 0° to 80°. At the 70-km. height, comparing the values for the sun overhead with those for the sun at 80°, one obtains about 6 orders of magnitude difference in the production rate of ionization.

Table 2 reviews the expected role of ionization from cosmic radiation in the region below 100 km. It is based on the work of several people, who have looked at various aspects of cosmic ray ionization, including its variability over the solar cycle. The important thing here, taking these numbers at face value, is the variability from the equator to high latitudes. At 70 km., for example, note that the cosmic ray production at zero magnetic latitude is about a factor of six below the value at 60° magnetic latitude. I have the impression that some think that at the magnetic equator all D-layer cosmic ray ionization effects vanish; however, the table shows this is not correct.

Fig. 7 shows the ionization below 90 km. from a homogeneous layer of typical debris from a nuclear detonation which has deposited debris above this altitude. This is a curve from a paper in the JGR a few years ago illustrating another point — the persisting ionization effects following high-altitude nuclear testing. Probably the most interesting thing is the peak production around 30 km. and 70 km. due to the gammas and betas respectively, and the fact that the total ionization production is within a factor of ten constant from 20 to 90 km. from this kind of source function. A factor of ten is small relative to some of the other sources we have looked at throughout this height range. The ionization due to betas depends on magnetic dip angle, as indicated in Fig. 5; the gamma ionization is independent of dip angle.

Fig. 8 is an attempt to consider debris ionization together with some of the natural sources of ionization production as a function of altitude and to show under what conditions debris ionization can be of interest. The relation between the value of maximum ionization production, P_M, and other factors is shown in Fig. 5. It turns out that if you have, say, a megaton of fission debris spread homogeneously over 8,000 km. radius, 24 hours after the detonation it would cause a P_M value of about unity. After about two weeks, debris from one megaton of fission yield, if spread homogeneously over all the earth, would cause a P_M value of about 10^{-2}. These numbers and Fig. 8 give some indication of what this source of ionization can be, relative to the sources of background ionization. The cosmic ray curve here is based on the type of analysis that was shown in Table 2, calculated for a latitude of 20° on the 1964 cosmic ray model given by Arnold and Pierce. Included in the curve was the Lyman α at night — which was added quite arbitrarily — using estimates summarized by Arnold and Pierce. The ionization production due to nighttime Lyman α is still a very interesting and uncertain subject.

Figs. 9 and 10 review the general features of xray ionization. Fig. 9 shows the penetration heights of various monoenergetic xrays from 1 Å. unit up to 25 Å. The most interesting aspect of these curves — the point that I want to emphasize — is the very sharp cutoffs at the low altitudes, for example, from 60 to 70 km. for 3 Å. If one is considering ionization at 65 km., the monoenergetic 5 Å. xray would not be very effective; according to these curves it is five orders of magnitude below the 3 Å. curve. Of course, one of the complications of practical D-region xray sources is that they are never monoenergetic; so one has to look at the energy spectrum of the xrays and integrate the production throughout the spectrum, which means that if one is to get accurate electron production values from xrays, at least in the lower altitude here, he needs to know the source spectrum accurately.

Fig. 10 indicates another variable factor that needs to be considered in assessing xray effects — the solar zenith angle. This figure was also taken from calculations published by Arnold and Pierce, and is based on standard xray deposition theory. This emphasizes the variability of the xray deposition as a function of solar zenith angle for zenith angles from 0 to 80°, and it is important to note the great variability in production with height at the various zenith angles for a monoenergetic source. Again, it should be emphasized that practical sources contain a range of energies; however, it is clear that the source spectrum must be accurately known if D-region ionization production is to be accurately determined.

3. Ionization Loss Mechanisms

I shall not spend as much time on ionization source functions in the D region as on the loss mechanisms, which I consider an area in which there is more confusion and need for better understanding. This may be because I have worked more with loss mechanisms, loss rates, and so forth. The remainder of the paper emphasizes factors relating to ionization loss, both electrons and ions, in the lower ionosphere.

Two types of general approach are being used in looking at ionization loss in the lower ionosphere. These are the lumped parameter and multiple species — chemical kinetic approaches. The lumped parameter approach is indicated by these equations:

$$\frac{dN}{dt} = P - AN - BNN^{+} + C(N^{+} - N),$$

$$\frac{dN^{+}}{dt} = P - BNN^{+} - EN^{+}(N^{+} - N),$$

where P is the electron production rate,
N^{+} is the positive ion density,
A is the electron attachment coefficient,
B is the electron-ion recombination coefficient,
C is the electron detachment coefficient,
E is the ion-ion recombination coefficient.

The terms are fairly obvious and well-known. The negative ions are not considered explicitly, but are simply the difference between the positive ions and electrons, and determined by the rate equations shown.

Clearly, the actual species of charged and neutral particles do not enter directly into the lumped parameter analysis. One uses height-dependent values for the various parameters which have evolved from consideration of laboratory measurements of some of the reactions considered most important, and from a large number of various types of ground-based radio propagation and rocket observations. The actual molecular and atomic species involved are not explicit in such models; the rates adopted, however, reflect conclusions by the investigator relative to the importance of various species. By such a process the lumped constant approach has led to rather simple models which appear to give fairly satisfactory agreement with many observations for which comparison can be made.

Even though such a happy state of affairs can be achieved, there are many scientifically unsatisfactory aspects to this approach. Simply stated, there are enough unknown and adjustable parameters in such models that one can choose various different combinations of the height-dependent lumped parameters which give satisfactory answers when compared to particular propagation or rocket probe observations. Even though such models may have sizable differences in the individual coefficients, they may give very similar answers for a particular situation. The more advanced — and hence more valuable — models are those in which empirical adjustments have been made to give best agreement with the widest range of situations for which some kind of valid data exists. Today the greatest deficiency in models available is in predicting time-dependent or transient phenomena, such as sunrise and sunset ionization changes. This factor alone tends to emphasize the fact that much better understanding of the species controlling the lumped parameters is essential.

When one currently explores the species route, he finds wide divergence of viewpoint as to which negative ions, for example, play significant roles (O_2^-, NO_2^-, O^-, O_3^-, OH^-, etc.) and to what degree their role is dependent on factors such as level of ionization, time after perturbation, magnitudes of minor constituents such as O_3 and O, etc., etc. These gross uncertainties in effect require continued use of the lumped parameter approach in most practical applications. It is fairly well agreed that the attachment time is that due to attachment of electrons to O_2 to form O_2^-. The actual species with which we are dealing and which determine the other coefficients listed, at various altitudes or times, etc., must be considered as unsatisfactorily resolved in general. Despite the question of the species, using the lumped parameter type of approach one can arrive at values — as a function of altitude — for each of these parameters which give calculated values that reasonably agree with values deduced by various measurements for a wide range of ionization situations.

Some of the radio data such as Belrose and his colleagues have obtained on nighttime electron density in the polar night, and the Stanford Research Institute data that LeLevier, Gambill, Knapp and others have analyzed on recovery from an xray impulse following the Starfish high-altitude burst, have had sizable influence on the determination of lumped parameter coefficients. Again, the model must reasonably agree with the available observations if it is to have any credibility. I will discuss later actual lumped parameter values in current use.

There has been considerable interest in the last few years in studying the effects of a large transient ionization impulse in the ionosphere and the effects of ambient ionization on the recovery characteristics. If one solves the two previous equations, using an impulsive ionization production source added to the ambient production, he obtains the following result, under the condition that electron-ion and ion-ion recombination values are equal.

Excess Electron Density after Ionization Impulse

$$n = \Delta N \left[e^{(BN_\infty^+ - A - C)t} \right] \left[\frac{2N_\infty^+}{(2N_\infty^+ + \Delta N) e^{2N_\infty^+ Bt} - \Delta N} \right] \left[1 - \frac{BN_\infty - C}{A + C - BN_\infty^+} \left(e^{(A+C-BN_\infty^+)t} - 1 \right) \right]$$

n = Excess electron density at time t
ΔN = Impulse of electron density
N_∞^+ = Ambient positive ion density
N_∞ = Ambient electron density
A = Attachment coefficient
B = Recombination coefficient (electron and ion)
C = Detachment coefficient

Although the assumption of equal coefficient is approximate, it does lead to an analytic solution of the above rate equations; even though these coefficients are unequal, this equal coefficient solution should give insight into the nature of the effect of ambient on the recovery process. We have done both the equal and unequal solutions, using a digital computer, and have concluded that the equal coefficient solution illustrates quite well the significant role of the ambient ionization.

The following equation illustrates an important aspect of the impulse recovery solution:

Daytime Electron Density at Late Times

$$n = \Delta N \frac{\frac{2N_\infty^+}{\Delta N}}{\frac{2N_\infty^+ + \Delta N}{\Delta N} e^{2BN_\infty^+ t} - 1} \frac{C}{A+C}$$

when $e^{(A+C-BN_\infty^+)t} >> 1$

This result is for daytime conditions and is applicable to ambient impulses below about 10^4 electrons/c.c. — which is still a sizable impulse as far as radio effects are concerned. It is seen that at late times the recovery is controlled mainly by the ambient value and not by the other rates. To illustrate this further I have used the following lumped parameters

Electron attachment rate (where Z is the density in atmospheres)	$= 10^8 Z^2 + 10^2 Z$/SEC
Electron-ion recombination rate	$= 10^{-7}$/SEC
Photo-detachment rate	= .4/SEC
Ion-ion recombination rate	$= 10^{-7}$/SEC

and the ambient charge density values of Fig. 11 to calculate the recovery from impulses of 10^2 to 10^4 electrons/c.c. at various D-region heights. Using these assumed parameters and ambient models, one obtains the results of Fig. 12 at altitudes of 55, 65, 75, and on up to 115 km. The validity of this approach I would say becomes quite questionable at the higher altitudes. The rather interesting thing is that the persistence of ionization maximizes around 75 km. after the daytime impulse. The 75-km. ionization will live longer than, say, at 85 or 95 km. and so on.

Fig. 13 shows the same sort of analysis at night. I won't defend with vigor the constants used or the precise numerical values in the reaction rates, but independent of the precise ones used, you get this general picture, i.e., of ionization persisting longer — at least for impulses in this range of 10^2 and 10^4 — around 95 km., a lower persistence at 115 km., and so on.

Fig. 14 illustrates another aspect of the effects of ionization impulse on the D region. For example, one may wish to determine recombination parameters from propagation data obtained following a large impulse such as may be produced by xrays from a high altitude nuclear explosion such as Starfish. Clearly the height region contributing the principal absorption changes appreciably with time; hence, the data analysis and interpretation must reflect this fact. Such factors can appreciably complicate the interpretation of, say, riometer data where only an integrated effect can be determined. Fig. 14 shows results for impulses of 10^5 and 10^7 or greater, using the parameters of Fig. 11. An impulse greater than 10^7 doesn't make any difference in the values shown for times of 10 sec. or more due to the saturation effect of the ionosphere.

Numerous lumped parameter models of the D region have appeared in the literature in recent years. The most recent and thorough study of which I am aware is that by Knapp and colleagues at General Electric-TEMPO. Fig. 15 shows their most recent model, in which the nomenclature is somewhat different from that used on page 4. D is detachment rate, α_i is ion-ion recombination rate and α_d is electron-ion recombination rate.

Considered as a family of parameters, the values of Fig. 15 appear to give reasonable agreement with a wide variety of D layer ionization situations, such as quasi-equilibrium day and night profiles, recovery from ionization impulses such as produced by the xrays from the Starfish high-altitude burst, etc.; however, change in one parameter can be accommodated by appropriate changes in the other in such a way that much of the various experimental data and the modified model are also in reasonable agreement. Thus, while such models are our most valuable tool available for predicting effects to be expected from various natural or artificial ionization situations, they must be considered with reservation as far as understanding of the actual chemical processes and species that dominate these processes is concerned. Time does not permit adequate discussion of how the parameters of Fig. 15 have been chosen — to what extent thoughts about what species were dominating a particular parameter at a particular height were included, radio and rocket data for which comparisons were made, etc.; however, all these factors have been considered as objectively, I believe, as current knowledge permits. Future improvements in our knowledge of the actual positive and negative ion species, in reaction rates involving negative ions and minor constituents such as 0 and 0_3, in understanding of how these quantities are dependent on time of day, season, vertical mixing in the atmosphere, etc., should make possible a much improved situation.

The other approach in studying time-dependent atmospheric deionization processes involves considering singly and collectively all the charged and neutral molecular and atomic species possibly involved. Investigators using this approach have identified some hundred-odd reactions which may occur and have actively pursued the problem of determining which ones may be the most significant in a particular situation. Studies by Keneshea at AFCRL and by Bortner and Galbraith at General Electric are noteworthy in this area. Fig. 16 was taken from a report by Bortner and Galbraith and shows a comparison of electron density versus time following a 10^{10} electron/c.c. ionization impulse at 70 km. as obtained by various approaches. The calculations were carried out using a computer program developed by Keneshea which could accommodate 143 reactions and 15 species. The various curves were calculated using different adopted versions of species and rates as indicated. The curve marked "T" used somewhat different values from those presented in Fig. 15. Added to Bortner's curves is the result one would calculate from the quite elementary model I presented in the JGR in 1961.

Fig. 17 shows similar comparisons at an altitude of 50 km. I won't detail here why the various models gave such divergent results, particularly at late times. The point I hope to make is that we can have a sizable variation in results obtained by different current workers and their preferred models. In brief, this is simply a result of not really knowing either all the species which can be important or their pertinent reaction rates.

Some of this group have been concerned with the role of ions, particularly under disturbed conditions, in LF and VLF propagation. I believe that ions can be quite important; however, their significance relative to electrons cannot be fully determined until we know better the mass of the ions, their collision frequency with neutral molecules, and, of course, their density. If one has molecular oxygen and nitrogen ions, the mass is some 60,000 times that of the electron and the collision frequency is perhaps 1/40 that for electrons. Thus, the total density of positive and negative ions must be something like 1500 times the electron density for ionic effects to equal electronic effects on VLF and LF propagation where the significant parameter is $n/m\nu$ in the lower D region. Ions of other masses and collision frequency will, of course, require proportionally calculated densities. To illustrate the range of uncertainty in this area, I have shown in Fig. 18 some impulse recovery calculations by Knapp, using two plausible models of reaction rates at an altitude of 80 km. Model A leads to exceedingly large ratios of ions to electrons after about 10 sec., while in model B the ion density never exceeds the electron density enough to be significant. At lower altitudes the various models give results which indicate ions are important following such impulses or during abnormal ionization periods such as polar cap events; however, the degree of importance one calculates is quite dependent on the parameters adopted. Again, sizable and important uncertainty exists.

Fig. 19 is from a 1964 article in the JGR by Booker and myself which pointed out the possibly significant role of ions. Our approach in obtaining the results on this slide was fairly approximate, both in the ionization loss rate models and the propagation analysis; however, we believe the general characteristics obtained are quite realistic. Fig. 19 applies to a transmission frequency of 50 Kc. and an 80° angle of incidence at the level of reflection. Electron production rates in the height range of 30 to 80 km. apparently are as large as 10^4 to 10^5 electrons in some polar cap events. For a production rate of 10^4, for example, Fig. 19 shows that ions would contribute the principal absorption of the wave during the reflection process. Although not apparent in the figure, the analysis showed that the height of the reflection region was largely determined by ions at this level of production. Johler and Berry at ITSA have extended the analysis of the effects of ions, using various production rate models and ionization parameters and a full wave propagation analysis, and have published a group of papers on this subject recently. Their work generally confirms that ions can play a significant role; however, this subject needs further attention.

Fig. 20 needs more explanation than time permits; however, it gives an indication of the approximate number of ions alone which are necessary at various altitudes to produce reflection for frequencies of 10, 20, and 50 Kc., using the analysis on which Fig. 19 was based.

Figs. 21 and 22 were taken from recent work by Knapp et al., and illustrate the calculated electron and ion density distributions one gets using the reaction rates of Fig. 15 and normal ionization production values appropriate for a given location and time. Again, full description of the ingredients used to derive the curves is not feasible here; however, they show one feature I want to point out. Note that in Fig. 21 the electron density below about 65 km. is less at noon than shortly after sunrise. This is a direct consequence of a model in which the ion-ion recombination rate is smaller than the electron-ion recombination rate. Hargreaves and others have pointed this out previously in the literature, but the question of "What is the electron density variation in the lower D region following sunrise ?" is still only partially understood at best. There is evidence it is seasonally dependent, latitude dependent, etc., which I cannot pursue here.

Fig. 23 is taken from the report by Bortner and Galbraith discussed earlier. It is included to indicate the type of analysis that can be done with digital computers and many species models. This particular result for 90-km. altitude indicates how some 15 of the most significant species in their 1965 model varied with time following a 10^{10} electron/c.c. impulse. They indicate in their report that such calculations consume some 2 min. of 7094 time. They also indicate the magnitude of the problem of examining the effects of using maximum, mean, and minimum expected rate constants, in all combinations, of 143 reactions they have considered. It turns out to be 10^{68} computer runs. Even for 20 reactions such a procedure leads to some 10^{9} runs.

Further analysis using the reaction rate values of Fig. 15 illustrates differences one may expect from this model of reaction rates for day and night conditions at various levels of production rate and at various altitudes. Fig. 24 indicates that, for production rates between 10^{1} and 10^{5} electrons/c.c./sec., sizable differences in day-night electron densities occur around 70 km. but at 90 and 50 km. the day-night differences are small. Fig. 25 shows the day-night ratios as a function of altitude for various production rates. The important feature here is that the model predicts great variation in the day-night ratio at intermediate D-layer heights with level of ionization production. Finally, Fig. 26 shows the calculated day and night 30 Mc. vertical one-way absorption distributions for a production level of 10^{3} at altitudes between 50 and 90 km. This level of production is apparently attained in many polar cap events.

REFERENCES

Arnold, H.R. and E.T. Pierce. The ionosphere below 100 km. (D region). Research Memo. 11, Stanford Research Inst., September 1963.

Bortner, M.H. and H.J. Galbraith. Study of the accuracy of rate constants for deionization calculations. DASA Report No. 1667, General Electric Co., May 1965.

Crain, C.M. Decay of ionization impulses in the D and E regions of the ionosphere. JGR, 68, April 15, 1963.

Crain, C.M. and H.G. Booker. The effects of ions on low frequency propagation in an abnormally ionized atmosphere. JGR, 69, November 1, 1965.

Crain, C.M. A note on persisting radio propagation effects after high altitude nuclear bursts. JGR, 69, November 1, 1964.

Knapp, Warren, et al. General Electric Co.-TEMPO, Private Communications.

Lutomirski, Richard. The RAND Corporation, Private Communication.

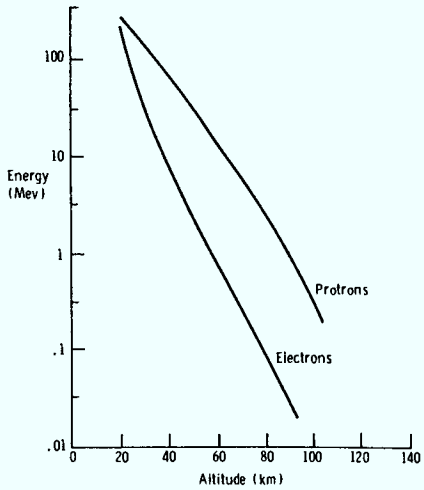

Fig. 1. Electron and proton energy versus altitude of penetration (Neglecting earth's magnetic field).

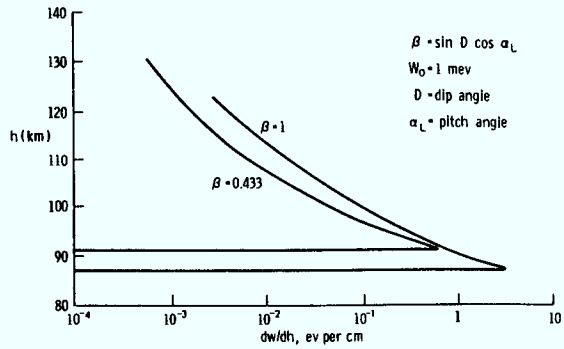

Fig. 2.

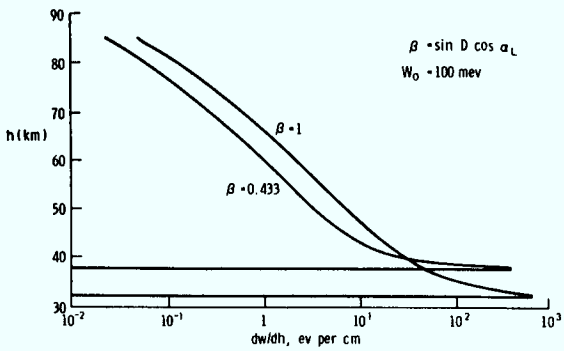

Fig. 3.

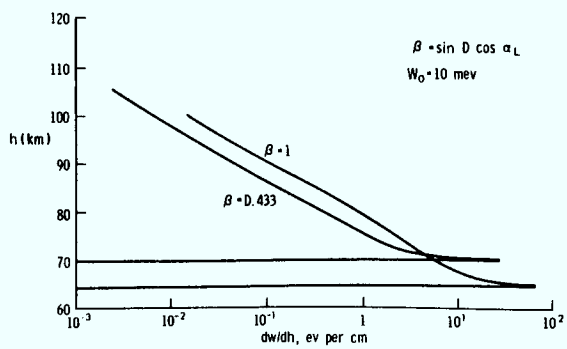

Fig. 4.

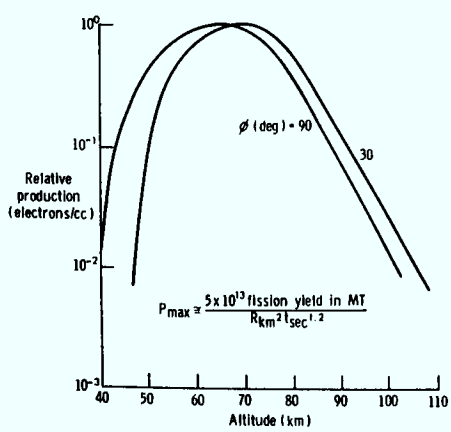

Fig. 5. Relative production rate from fission beta particles.

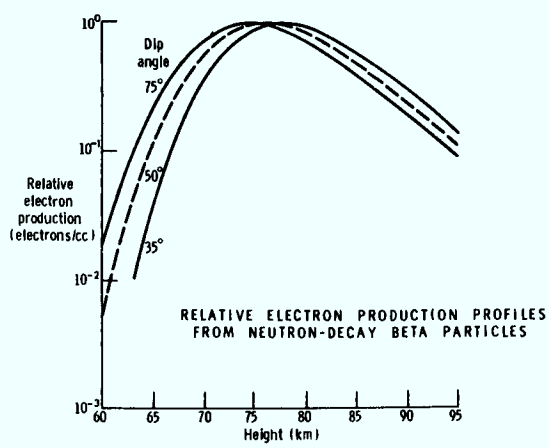

Fig. 6. Relative electron production profiles from neutron-decay beta particles.

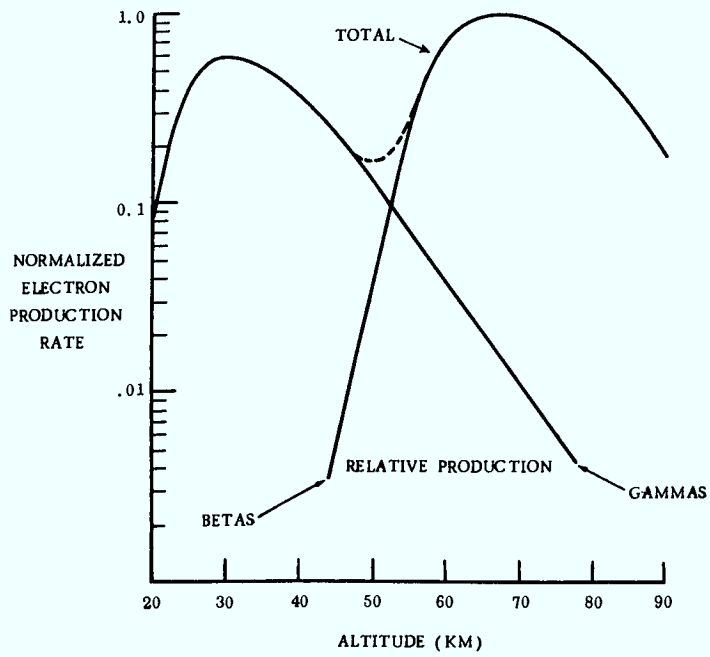

Fig. 7. Typical electron production distribution for homogeneous layer of fission debris at altitudes above 90 km.

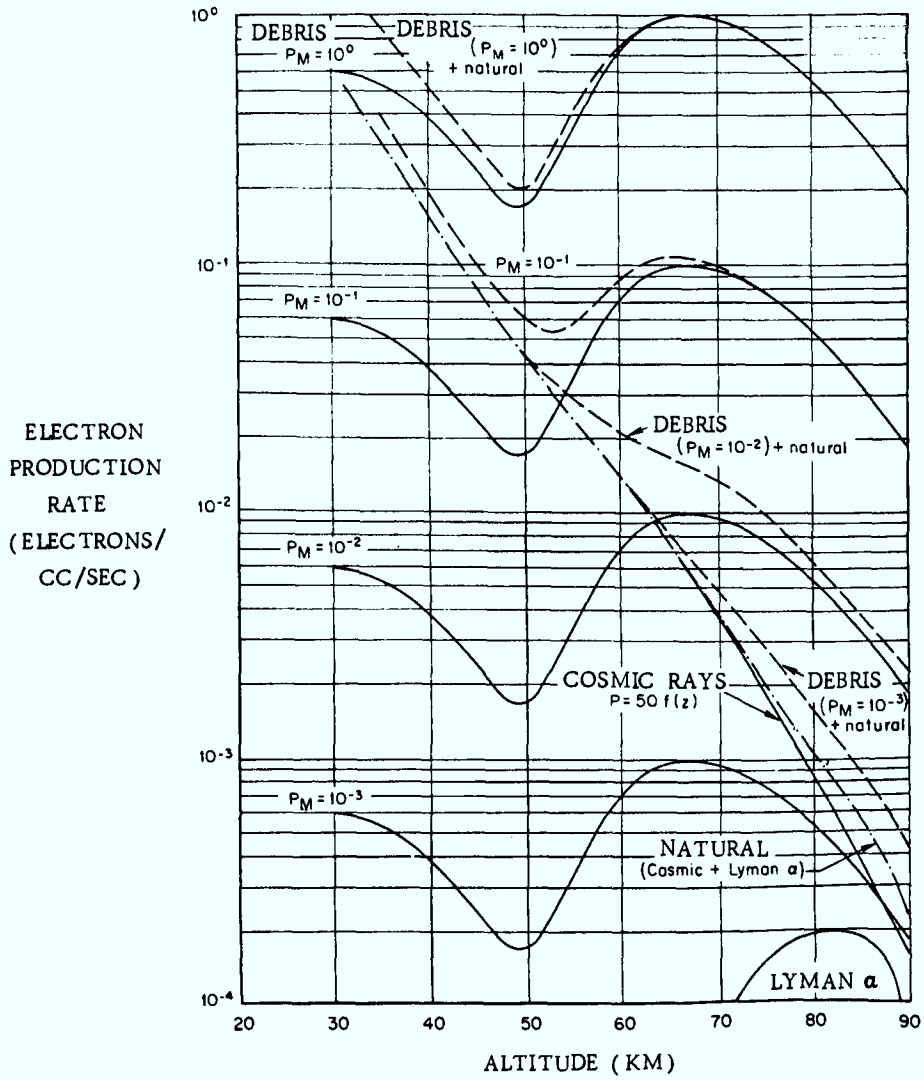

Fig. 8. Typical nighttime natural and debris production profiles, low latitude.

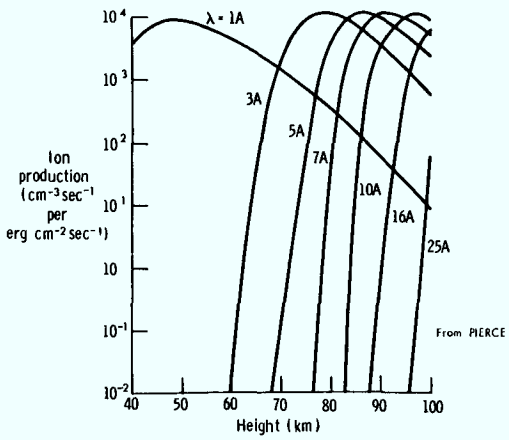

Fig. 9. Ion production due to xrays as a function of height and wavelength (Zenith angle = 0°).

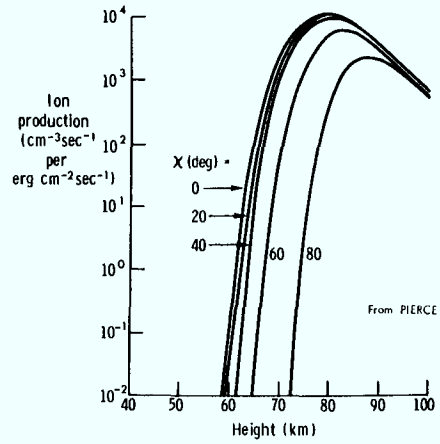

Fig. 10. Ion production due to 3 Å xrays as a function of height and zenith angle.

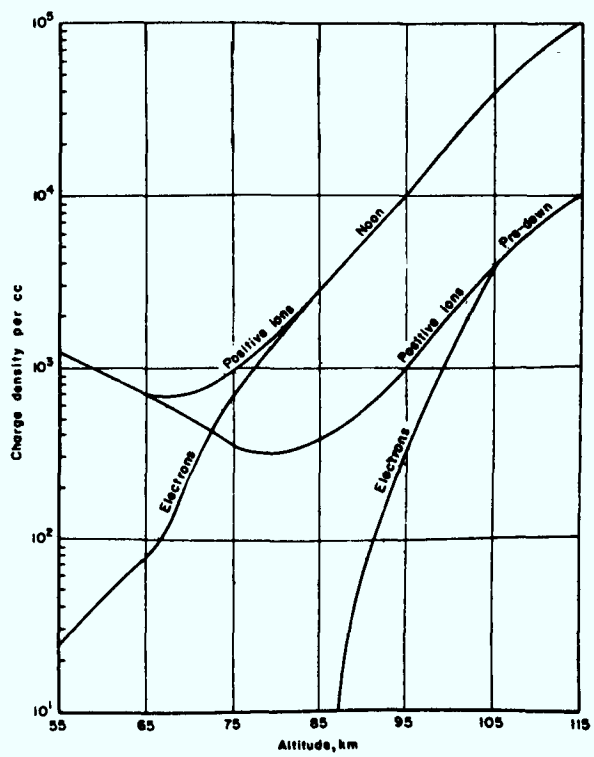

Fig. 11. Assumed ambient charge densities.

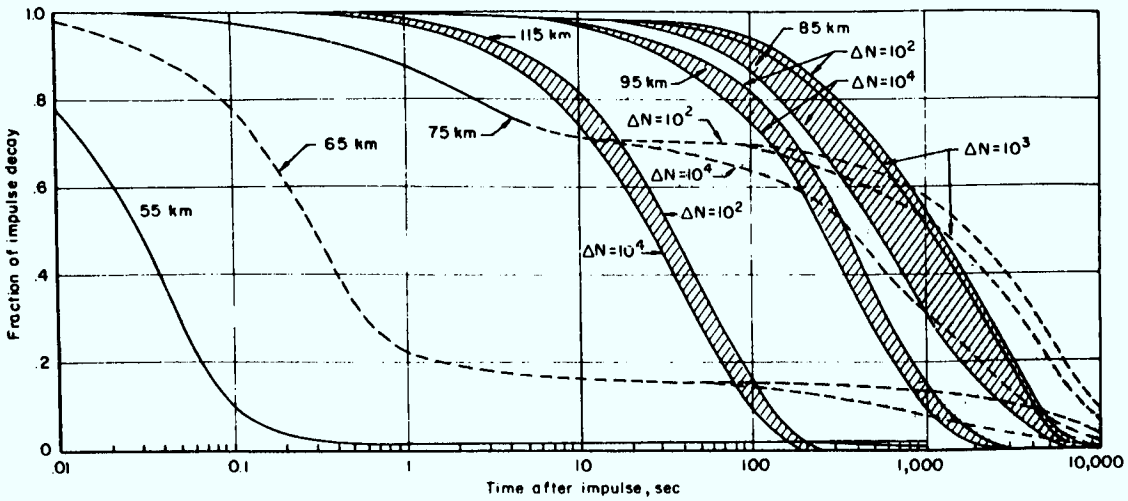

Fig. 12. Daytime impulse recovery characteristics impulse range, 10^2 to 10^4 electrons/c.c.: Altitude, 55 to 115 km.

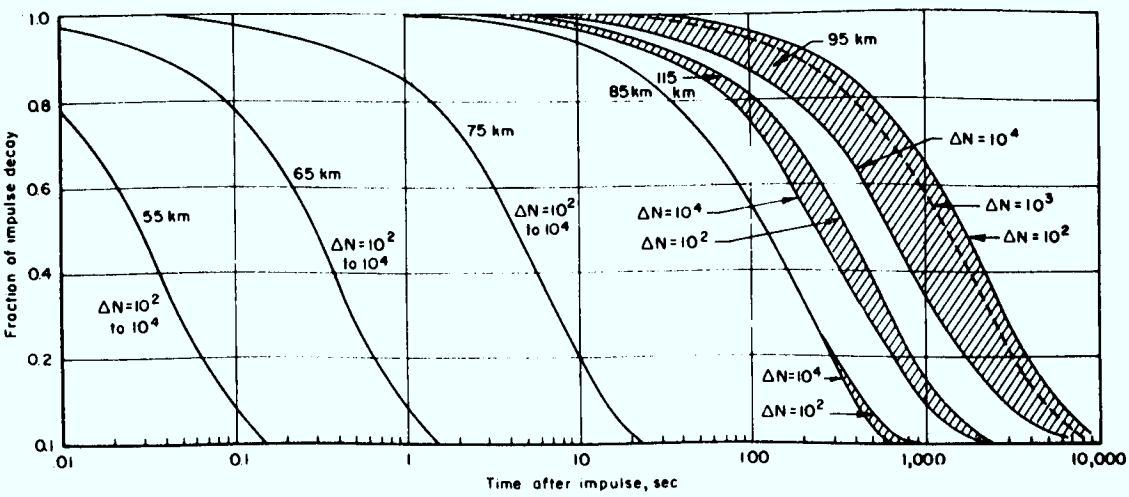

Fig. 13. Nighttime impulse recovery characteristics impulse range, 10^2 to 10^4 electrons/c.c.: Altitude, 55 to 115 km.

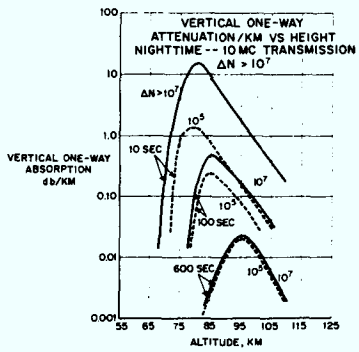

Fig. 14. Vertical one-way attenuation/km. vs height nighttime – 10 Mc. transmission N 10^7.

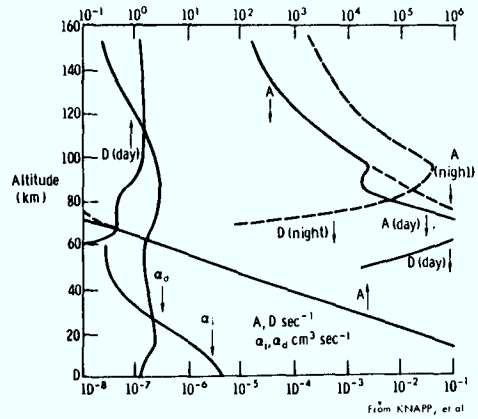

Fig. 15. Nominal values of reaction rates as a function of altitude.

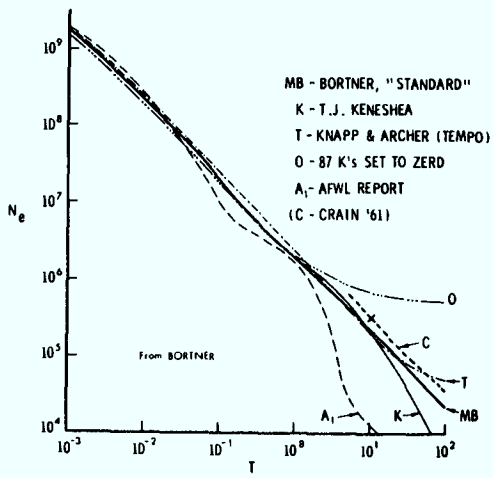

Fig. 16. Electron density predictions as given by various "sets" of rate constants, 70 km.

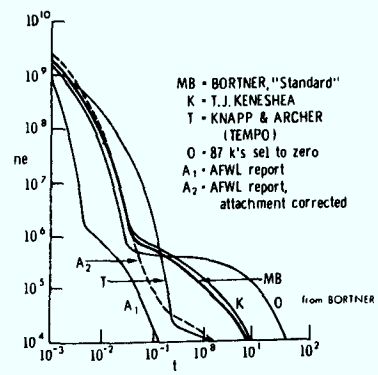

Fig. 17. Effect of various sets of rate constants, 50 km.

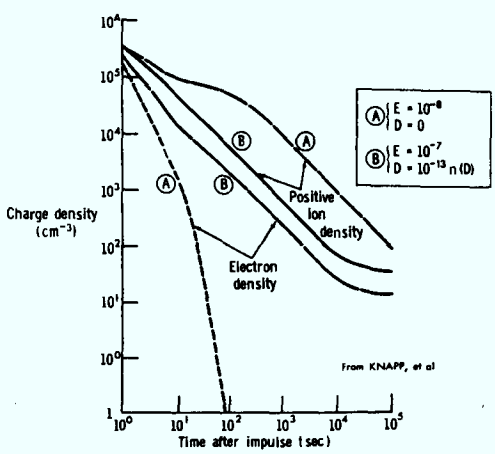

Fig. 18. Electron and ion densities at 80 km. following ionization impulse.

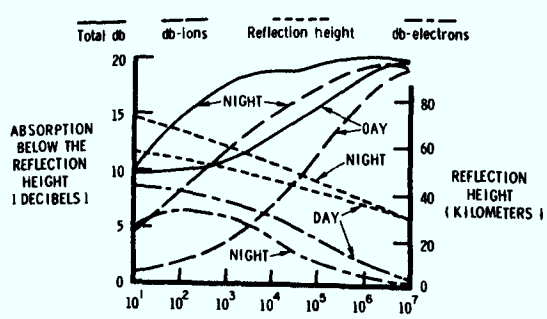

Fig. 19. Production rate, P, electrons/c.c./sec.

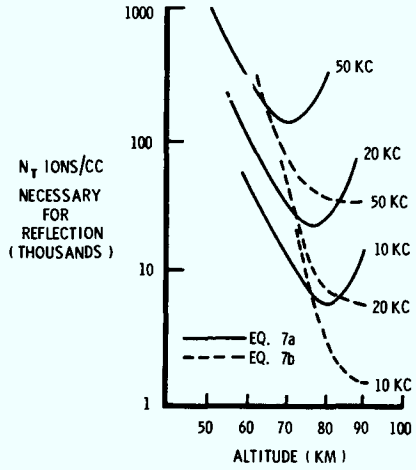

Fig. 20.

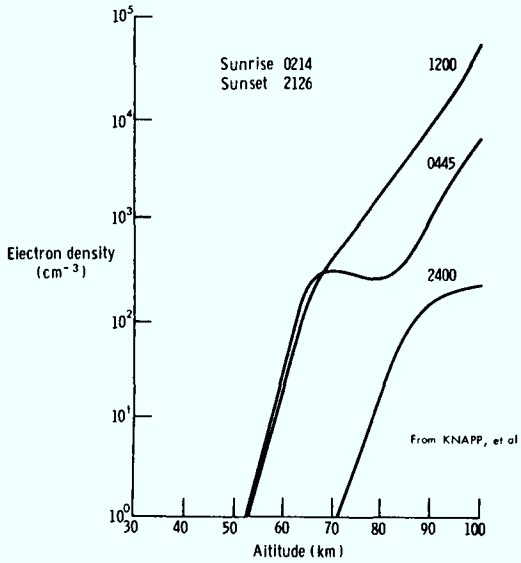

Fig. 21. Electron density versus time.

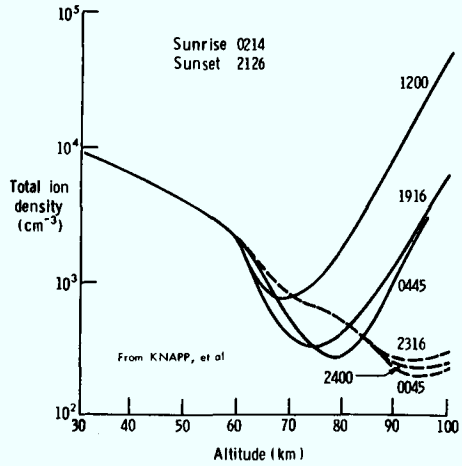

Fig. 22. Total ion density versus time.

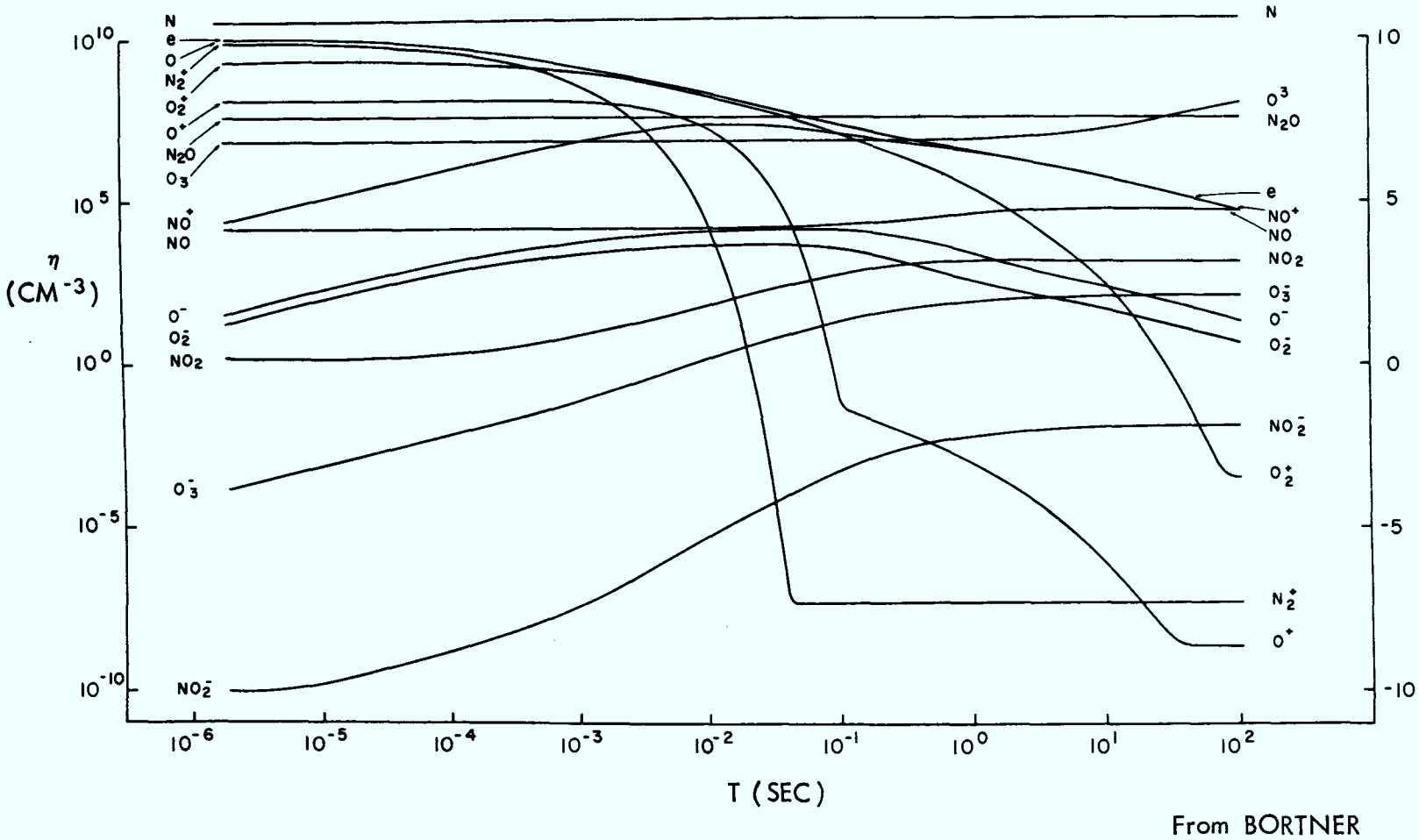

Fig. 23. Concentrations of all species, 90 km.

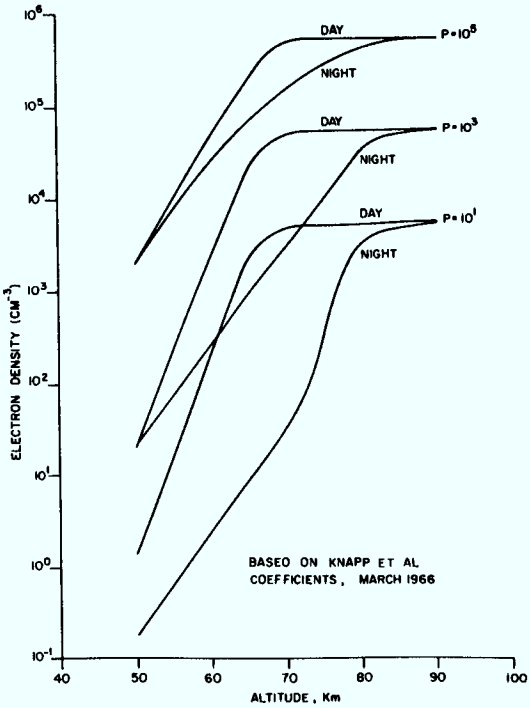

Fig. 24.

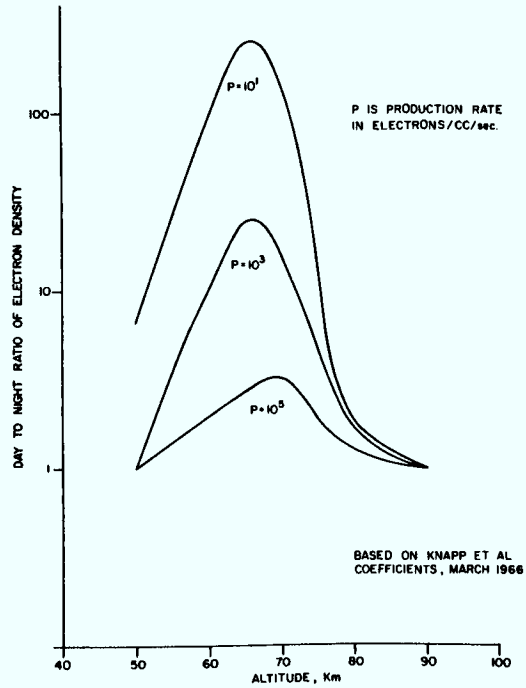

Fig. 25.

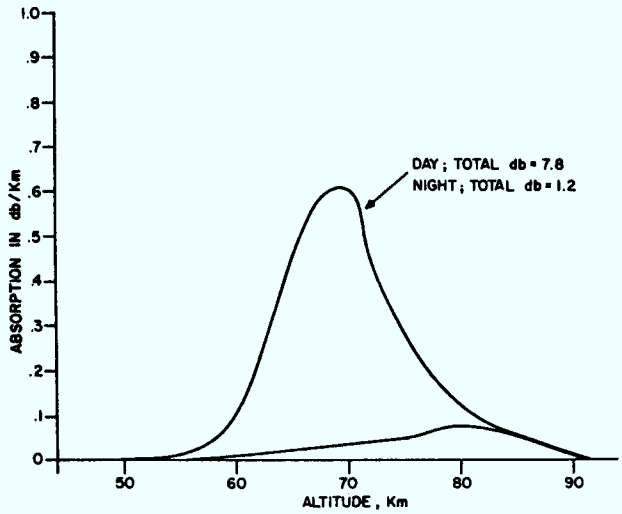

Fig. 26. 30 Mc. vertical; one way absorption distributions for $P = 10^3$.

Discussion on Paper 1.1 presented by C.M. Crain

Bibl: Was the 7.8 db absorption shown in Fig. 26 for a special riometer event?

Crain: This was just an arbitrary example, which was supposedly in the ball park for the production rates which were obtained in one of the polar cap events of November, 1961, I think.

Bibl: Cosmic ray radiation depends on geomagnetic latitude and you have shown a factor of five between 40° and 60°. Could you give a short reason for this?

Crain: Well, this is based on models, not my own work but theoretical work of Webber's, and I think Webber got it from someone else. The variability of the incoming cosmic flux is related by cos 4th θ. Were you questioning the numbers or just wondering where it came from?

Bibl: I wondered why it is so big.

Crain: The cosmic rays vary as cos 4th θ. I think this would be valid up to 60° or 65° magnetic latitude, and then maybe it levels off or doesn't follow this sort of cos 4th law. That is my interpretation at least of the modelling of the cosmic ray influx data.

1.2 THEORETICAL MODELS OF THE LOWER IONOSPHERE

by

A.C. Aikin

NASA – Goddard Space Flight Center, Greenbelt, Maryland

1. Introduction

Nicolet and Aikin considered three sources of ionization in their theory of D region formation:

1. Cosmic radiation
2. Solar Lyman alpha ionization of nitric oxide
3. Solar xrays, 2-8A, which vary in intensity with solar activity.

Positive ions, produced by these sources, recombine with electrons or negative ions, which result from attachment of electrons to neutral molecules.

Recently rocket measurements have been made of positive ion composition, electron and positive ion densities, as well as neutral nitric oxide. In this paper the D region problem is re-examined, taking into consideration the rocket measurements and the sources of ionization listed above. Calculations of the diurnal variation of the D region are also presented for several nitric oxide profiles to determine what can be learned about the allowable range of dissociative recombination coefficients.

2. Electron and Positive Ion Densities

Electron and positive ion profiles obtained during the period 1963 to 1964 at geographic latitudes 30° to 40°N, and representative of "quiet" solar conditions are shown in Fig. 1. The data presented are:

1. Electron density (Aikin et al.)
2. Ion density (Bourdeau et al.)
3. Ion density (Narcisi and Bailey).

Similar electron density profiles have been reported by Hall and Bullough, although the minimum at 83 km. is not as pronounced. The densities measured by rocket are very similar to the empirical profiles derived from long-wave ionosphere soundings by Nertney, and Pfister, more than a decade ago.

There is disagreement between the ion density data of Bourdeau et al., which agree with the electron density at 80 km., and the results of AFCRL. The AFCRL results are one order of magnitude greater than the electron density and the Bourdeau et al. ion density profile. Comparison of the AFCRL ion densities with the electron density profile shows that the negative ion density must exceed electron density throughout the daytime D region, provided that solar conditions were the same for both measurements.

3. Positive Ion Composition

Ion composition as measured by Narcisi and Bailey is displayed in Fig. 2. The number densities of the various species of ions were obtained by normalizing the total ion current to the ion density data of Sagalyn, whose instrument was carried on the same rocket as the mass spectrometer.

On the basis of the ionization mechanisms mentioned in the introduction, one would expect primarily NO^+, O_2^+ and N_2^+ ions. However, the presence of reactions such as

$$N_2^+ + O_2 \rightarrow NO^+ + NO$$

and

$$O_2^+ + N_2 \rightarrow NO^+ + NO$$

should lead to NO^+ as the predominant ion in the D region. As can be seen from Fig. 2, NO^+ comprises only 10 per cent of the total ions. The major ions have masses 19^+, 37^+ and higher. These ions are attributed by Narcisi and Bailey to reactions involving water vapor. Since the ionization potential of H_2O is 12.6 eV, only xrays and cosmic radiation can produce H_2O^+ ions directly in the D region. The majority of H_2O^+ ions must arise from the charge exchange process

$$N_2^+ + H_2O \rightarrow H_2O^+ + N_2 \qquad (1)$$

The complex 19^+ and 37^+ ions are products of the processes

$$H_2O^+ + H_2O \rightarrow H_3O^+ + OH \qquad (2)$$

$$H_3O^+ + H_2O + M \rightarrow H_5O_2^+ + M \qquad (3)$$

$$N_2^+ + H_2O \rightarrow N_2H^+ + OH \qquad (4)$$

$$N_2H^+ + H_2O \rightarrow H_3O^+ + N_2 \qquad (5)$$

While this sequence will lead to 19^+ and 37^+, it is important to keep in mind that the reaction

$$H_2O^+ + O_2 \rightarrow O_2^+ + H_2O$$

should be exothermic and that laboratory measurements by Fehsenfeld et al. and Warnecke lead to a rate of 1×10^{-10} c.c./sec. for

$$N_2^+ + O_2 \rightarrow O_2^+ + N_2$$

implying that large concentrations of water vapor are required if N_2^+ is to be lost by reactions with H_2O rather than O_2. According to process 1, the D region arises from the production of N_2^+ for which the production rate is the order of 10^{-3} ion pairs/c.c./sec. for a quiet sun. This is insufficient to account for the observed ionization. In view of these objections,

alternate explanations should be considered, such as the formation of complex hydrated ions from reactions involving NO^+. Lyman alpha could be retained as the ionizing agent, if it ionizes other minor constituents that subsequently form 19^+, 37^+, etc.

4. Diurnal Variation

Following the detection of nitric oxide in the mesosphere and lower thermosphere by Barth, there has been considerable discussion concerning the implications of densities of 4 to 6 × 10^7/c.c. for the formation of the D region. Aikin et al. considered the effective recombination coefficient deduced from the electron density profile of Fig. 1 for a production function employing this NO density. The origin of such large NO concentrations has been discussed by Nicolet. The ionospheric situation is further complicated by a wide range of values quoted for the dissociative recombination coefficient of nitric oxide ions.

Recently both theoretical and experimental determinations have been carried out on the dissociative recombination coefficient of NO^+. Stabler has derived an expression of the form

$$\alpha_{DNO} = 1.4 \times 10^{-7}(300/T_e)^{\frac{1}{2}}$$

for electron temperatures, T_e, below 1000°K. On the basis of laboratory measurements, Gunton and Shaw report an approximate temperature dependence of $T^{-1.2}$ for the recombination coefficient, where T is the neutral gas temperature. Measurements made at temperatures of 196 and 358°K yield values $10^{+2}_{-4} \times 10^{-7}$ and $3.5\ ^{+0.2}_{-0.5} \times 10^{-7}$c.c./sec. respectively. Stabler's expression leads to a value at T = 200°K of 1.7 × 10^{-7}c.c./sec.

In this section the form of the diurnal variation of the D region, assuming NO^+ to be the principle positive ion, will be discussed for the range of dissociative recombination coefficients and neutral nitric oxide densities given in Table 1.

TABLE 1

	α_{DNO}	n(NO)
Case 1	3 × 10^{-7}c.c./sec.	1.37 × 10^{-9}n(M)
Case 2	1.6 × 10^{-6}c.c./sec.	3.9 × 10^7
Case 3	3 × 10^{-8}c.c./sec.	1.1 × 10^{-10}n(M)

In cases 1 and 3, the theoretical electron density profile has been normalized so as to agree with the experimental electron density profile of Fig. 1 at 80 km. In these cases, the incident flux of Lyman alpha is taken to be 4.5 ergs/sq.cm./sec. An intensity 3 ergs/sq.cm./sec. is employed in case 2. The intensity and spectrum of xrays are those employed by Aikin et al. A summary of the processes affecting the charged particle distribution in the D region together with values assumed for the rate coefficients is given as Table 2. The photodetachment rate of electrons from O_2^- and O^- are 0.44/sec. and 1.4/sec. throughout the day except during twilight, where scattering and absorption processes were included. This procedure is analogous to calculations by Archer.

TABLE 2

Process	Rate
$N_2^+ + e \rightarrow N + N$	2.8×10^{-7} c.c./sec.
$O_2^+ + e \rightarrow O + O$	1.7×10^{-7} c.c./sec.
$NO^+ + e \rightarrow N + O$	α_{DNO}
$e + 2O_2 \rightarrow O_2^- + O$	1.5×10^{-30} cm^6/sec.
$O_2^- + h\nu \rightarrow O_2 + e$	d
$O + O_2 + e \rightarrow O^- + O_2$	3×10^{-29} cm^6/sec.
$XY^- + XZ^+ \rightarrow XY + XZ$	1×10^{-7} c.c./sec.
$O_2^- + O \rightarrow O_3 + e$	1×10^{-13} c.c./sec.
$O^- + O \rightarrow O_2 + e$	1×10^{-3} c.c./sec.
$O^- + h\nu \rightarrow O + e$	g

The set of simultaneous differential equations describing the D region is solved with the aid of a computer.

The theoretical electron density profiles of cases 1 and 2 are compared with experimental results in Fig. 3. Although case 1 is in reasonable agreement with the experimental profile, case 2 leads to densities a factor of two above the experimental data. The profile of case 2 is less than the AFCRL total ion density curve, but Lyman alpha intensities of less than 3 ergs/sq.cm/sec. or α_{DNO} values exceeding 2×10^{-6} c.c./sec. must be chosen if the theoretical profile is to agree with the experimental electron density profile.

The diurnal variation at altitudes of 80 and 70 km. is illustrated in Figs. 4 and 5 for a 48-hour interval. For case 3 where $\alpha_{DNO} = 3 \times 10^{-8}$ c.c./sec., the equilibrium solution assumed at the beginning of the computation is not reached after 24 hr. There is a marked asymmetry about local noon, which also appears for the case where $\alpha_{DNO} = 3 \times 10^{-7}$ c.c./sec., but not when $\alpha_{DNO} = 1.6 \times 10^{-6}$ c.c./sec. At 80 km. the maximum ionization occurs 45 min. after local noon for case 1. This time-lag is in agreement with observations of 2.5 Mc/sec. absorption (Rao et al.). At 70 km., as illustrated in Fig. 5, the asymmetry about noon is even more marked. The larger production function of case 2 leads to densities which are more directly under solar control.

The calculations discussed above indicate that it should be possible to determine the recombination coefficient by observing the diurnal variation at a specific altitude. Information on the magnitude of the solar-controlled production function can be obtained from the diurnal variation at altitudes where comparisons can be made with cosmic ray ionization.

5. Nocturnal and Sunrise Electron Density Variations

Cosmic radiation is one source of ionization at night. Another is scattered Lyman alpha, which has an intensity of the order of 10^{-2} ergs/sq. cm./sec. There sources are not sufficient to prevent decay of the electron density after sunset, but, as can be seen in Fig. 5, densities of the order of 10^2/c.c. can be maintained at 80 km. At altitudes below 80 km. the electron density is strongly dependent on the negative ion distribution.

In the present calculations it has been assumed that the agent responsible for destruction of negative ions in the absence of photodetachment is associative detachment. The efficiency of this process is dependent on the atomic oxygen density which has a diurnal variation below 80 km. If presunrise values of O are employed, the electron density at 70 km. before sunrise will be 6×10^{-2}/c.c. as compared with 20/c.c. for daytime atomic oxygen profiles.

The importance of negative ions at sunrise has been well documented. However, most of the information is derived from riometers, VLF, and long wave propagation data. It is only recently that other techniques, such as rockets, and ground-based cross-modulation studies have begun to obtain detailed electron density profiles as a function of time. Fig. 6 shows a series of probe current profiles taken with the aid of rockets by Bowhill et al. It is difficult to interpret these currents in terms of the true electron density, since a normalization factor must be employed. However, there was a radio propagation experiment on board the rocket and this accounts for the quoted density at 70 km. of 25/c.c. for a solar zenith angle of 85°. As will be seen shortly, densities of this order should be reached well before ground sunrise if O_2^- is the principle negative ion.

It has been assumed in our calculations that O^- and O_2^- are the only species of negative ions. Other processes leading to O_3^-, NO_2^-, or OH^- may be operative, but not enough is known about the rates of different ion-atom, charge exchange, and photodetachment processes to warrant their inclusion. The calculated variation of electron density over sunrise is illustrated in Fig. 7 for all cases. The effect begins when the solar zenith angle equals 98°, in contrast to the experimental curves of Fig. 6. For cases where the dissociative recombination coefficient is larger than the ion-ion recombination coefficient there is a decrease of the cosmic ray layer following its initial build-up.

6. Conclusions

At present there is no consistent theory of the D region which will explain the electron density, ion composition data, neutral nitric oxide density determinations, and the sunrise effect. A great many worthwhile suggestions have been made concerning the D region, but in many instances there is not enough laboratory information on rates of pertinent processes to allow for a check between theory and experiment.

There is also an appalling lack of information concerning what really occurs. Only a small amount of information is available in the literature concerning the variation of the electron density with time of day, season, and location. In general, there are no simultaneous solar xray flux data. The two ion-density profiles quoted are in conflict by one order of magnitude. There are no negative ion composition measurements. These problems must be solved if an understanding of this important region of the ionosphere is to be achieved.

REFERENCES

Aikin, A.C., Kane, J.A. and J. Troim. J. Geophys. Res., 69, 4621, 1964.

Archer, D.E. J. Geophys. Res., 69, 991, 1964.

Barth, C.A. Space Res., 5, 767, 1965.

Bourdeau, R.E., Aikin, A.C. and J. Donley. J. Geophys. Res., 71, 727, 1966.

Bowhill, S.A. and L.G. Smith. Space Res., 6, 1966.

Fehsenfeld, F.C., Schmeltekopf, A.Y. and E.E. Ferguson. Planetary Space Sci., 13, 919, 1965.

Gunton, R.C. and T.M. Shaw. Phys. Rev. 140, No. 3A, 1965.

Hall, J.R. and K. Bullough. Nature, 200, No. 4907, 642, 1963.

Narcisi, R.S. and A.D. Bailey. J. Geophys. Res., 70, 3687, 1965.

Nertney, R.J. J. Atmos. Terres. Phys., 3, 92, 1953.

Nicolet, M. J. Geophys. Res., 70, 691, 1965.

Nicolet, M. and A.C. Aikin. J. Geophys. Res., 65, 1469, 1960.

Pfister, W. URSI Comm. III, The Hague Assembly 1954.

Rao, M.K., Magumdar, S.C. and S.N. Mitra. J. Atmos. Terres. Phys., 24, 245, 1962.

Stabler, R.C. Final Report NAS5-3649, RCA Laboratories.

Warnecke, P. Gaseous Electronics Conf., Minneapolis, Minn., 1965.

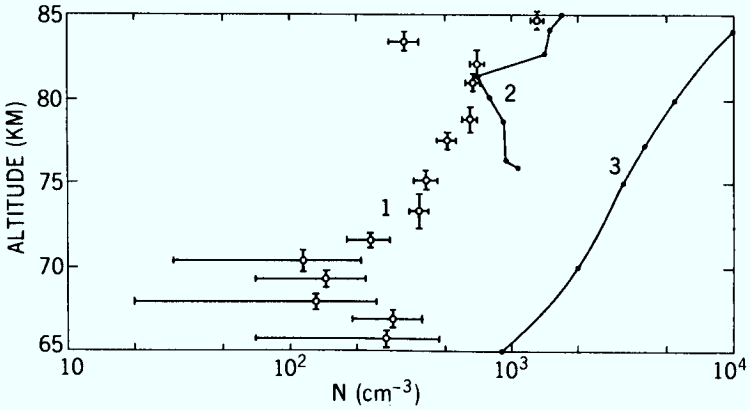

Fig. 1. Rocket measurements of:

1. *Electron density*
2. *Positive ion density (Bourdeau et al.)*
3. *Positive ion density (Narcisi and Bailey).*

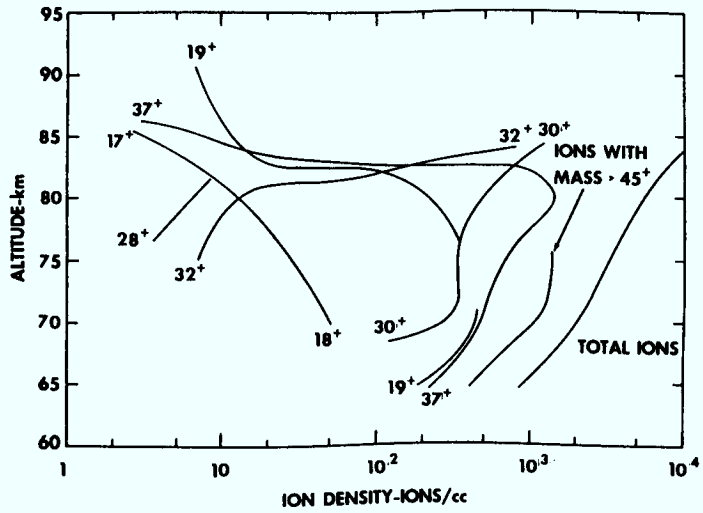

Fig. 2. D region ion composition.

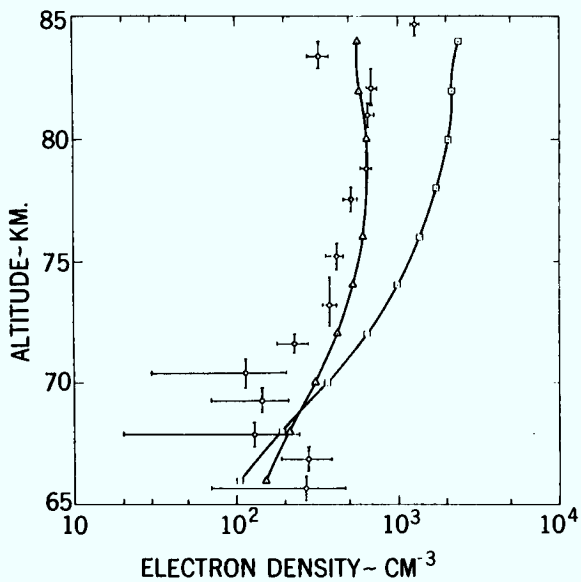

Fig. 3. Comparison of theoretical and experimental electron density profiles.

⊙ *Experimental*
△ *Case 1*
□ *Case 2*

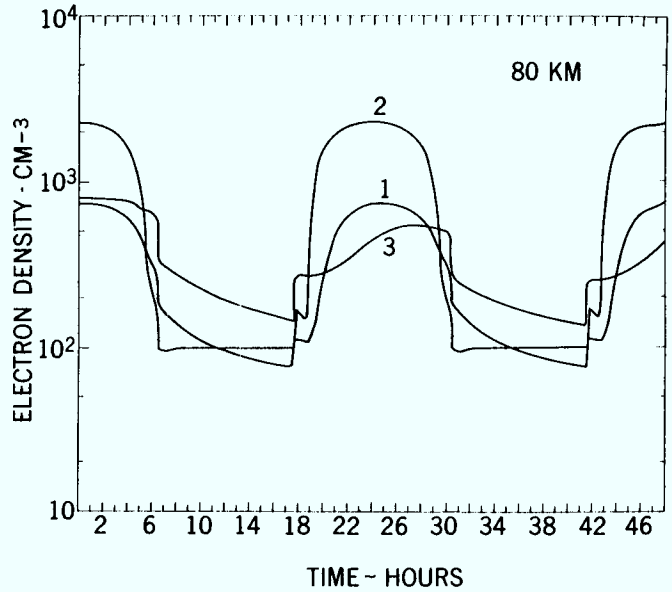

Fig. 4. Diurnal variation of electron density at 80 km. for:

(1) $a_{DNO} = 3 \times 10^{-7}$ *c.c./sec.*

(2) $a_{DNO} = 1.6 \times 10^{-6}$ *c.c./sec.*

(3) $a_{DNO} = 3 \times 10^{-8}$ *c.c./sec.*

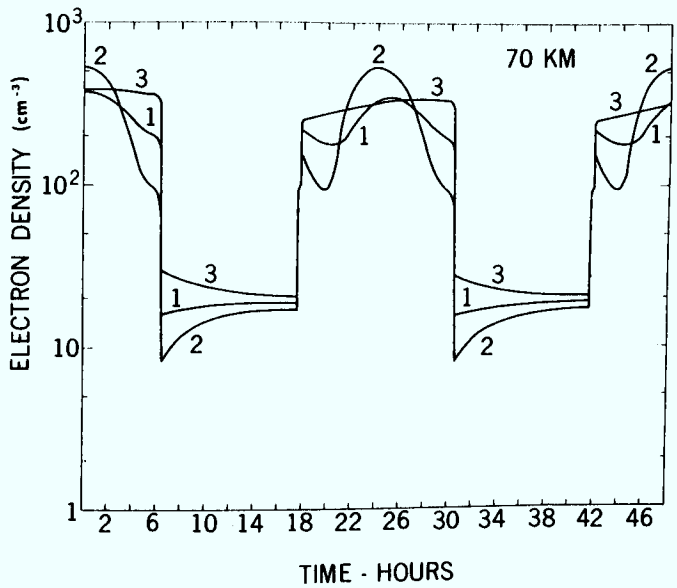

Fig. 5. Diurnal variation of electron density at 70 km. for:

(1) $a_{DNO} = 3 \times 10^{-7}$ *c.c./sec.*

(2) $a_{DNO} = 1.6 \times 10^{-6}$ *c.c./sec.*

(3) $a_{DNO} = 3 \times 10^{-8}$ *c.c./sec.*

A daytime atomic oxygen profile is employed.

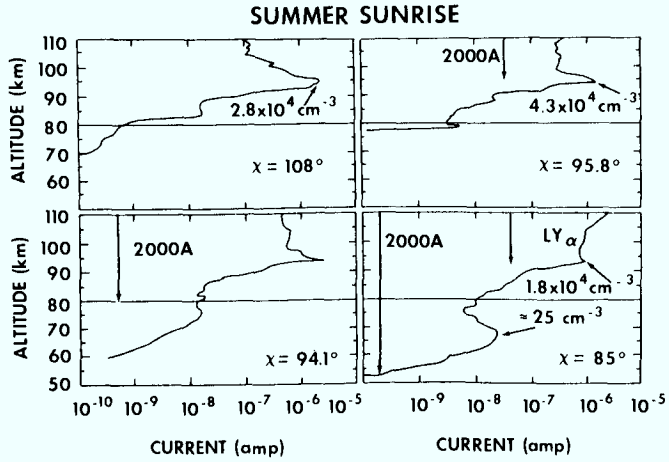

Fig. 6. Rocket measurements of the lower ionosphere during sunrise.

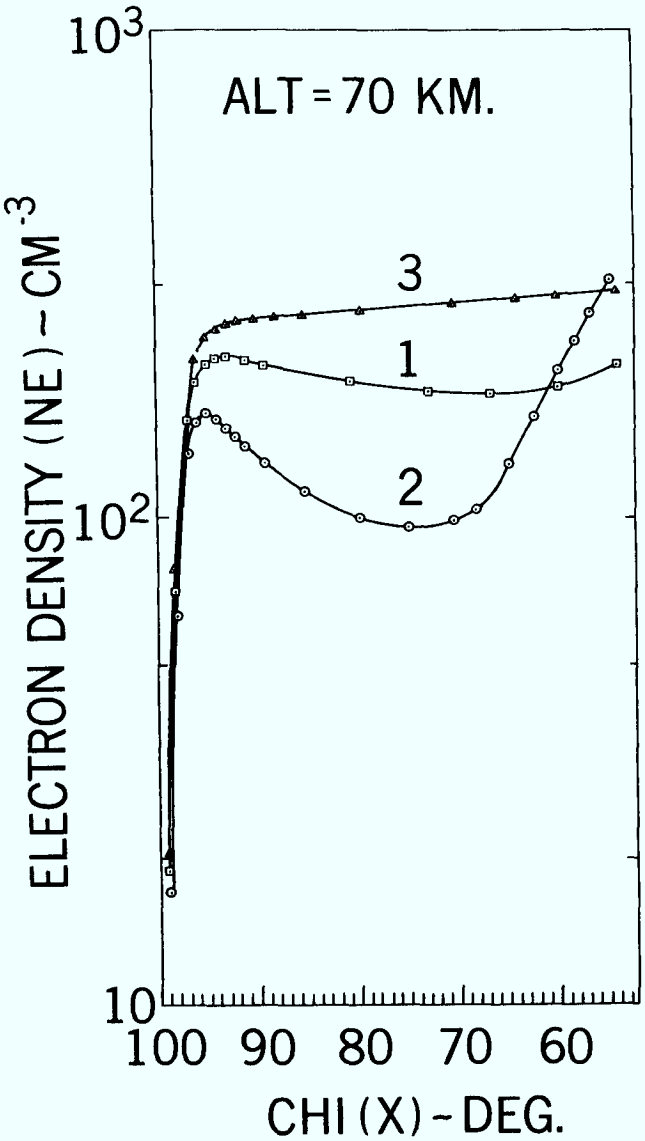

Fig. 7. Electron density variations as a function of solar zenith angle at 70 km. for:

(1) $\alpha_{DNO} = 3 \times 10^{-7}$ *c.c./sec.*

(2) $\alpha_{DNO} = 1.6 \times 10^{-6}$ *c.c./sec.*

(3) $\alpha_{DNO} = 3 \times 10^{-8}$ *c.c./sec.*

Discussion on Paper 1.2 presented by A.C. Aikin

Crain: I would like to comment on the problem people have with the associative recombination rate of NO, based on a model. The results are exceedingly sensitive to the other parameters chosen (i.e. attachment and detachment). If you change the attachment and detachment parameters, you can reach different conclusions about what αNO is. It is a sensitive circular game of consistent parameters, and if you chose a different value of attachment and detachment, you might end up with NO an order of magnitude smaller than you can justify on the basis of those values.

Aikin: That is right. You have to make some decision on what lambda is, and what the detaching agent is. At present, we do not have enough information to do anything, except something like the O_2^- hypothesis or modifications of it.

Crain: At 70 km., for example, the detachment is typically in the range of a few tenths to one, or something like that. The attachment term dominates the recombination terms, giving a recombination value which is dominated by a term 2 orders of magnitude larger than the previous value.

Belrose: For the purpose of knowing the present position of sunrise studies, could you comment on the success of the Goddard sunrise studies in New Zealand, and perhaps Dr. Shirke could tell us how Bowhill's analysis of the propagation data over sunrise has progressed. The data we saw were merely Langmuir probe data, with a spot electron density marked on it now and again.

Aikin: Dr. Kane is probably in a better position to comment on the Goddard data from New Zealand.

Kane: I should like to defer that until I talk with Dr. Gregory, who was making measurements at the same time as the rocket shots. We have not compared our results yet.

Shirke: I do not know of any addition to the work already reported by Bowhill.

Bourne: I believe Prof. Smith has new data(1), which he will present in a later paper, showing quantitative measurements of electron density changes during dawn. I think there is general agreement that the experimentalist can measure electron densities generally to better than a factor of 2, yet in the attachment rates, recombination rates, and uncertainties of the processes we talk about orders of magnitude uncertainties. What does a theoretician require from an experimentalist; a higher degree of accuracy, or data throughout the day measuring small changes as a function of time?

Aikin: It depends on what you look for. The present electron density profiles for one particular time are more than adequate. What we need is better measurements of the positive ion density, where we are now arguing about an order of magnitude, and of the effect of Lyman α at 70 km. Quantitative information for the sunrise electron density values is also very badly needed.

Dalgarno: In your discussion of the Narcisi data you appeared to imply the possibility that the concentration of water vapor might be comparable to that of molecular oxygen.

Aikin: I don't think that it is, but this is what would be implied.

Dalgarno: If the implication is accepted, then there would be no question about how the water vapor got there – it was taken there.

Aikin: I don't want to get involved in the controversy.

Smith: Dr. Bourne has mentioned some of the results I will be talking about on Wednesday. We have measured the dawn profile in successive changes of 1° in χ over the period from 100° to 85°, and following that during the day. These profiles are quantitative and suggest a layer forming. We will also be showing evidence that suggests or indicates to me that the cosmic ray profile decays. The only part of my profiles which I was not going to show, was the part which required recombination coefficients bigger than 10^{-6}. Had I known that such things were speculated and were real, I would have put those profiles in. I do remind vou that we are working on a delicate measurement, and I wasn't game at this

(1) Smith, R.A., Bourne, I.A., Loch, R.G. and T.N.R. Coyne. Small perturbation wave interaction in the lower ionosphere. Part III. Measurement of Electron Densities, These Proceedings, 1966.

stage to produce them even though the first interpretation of my data about 18 months ago required recombination coefficients bigger than 10^{-6}, which you are now talking about. The evidence seems to indicate strongly that there is definitely decay in the lower layer, going right up to 75 or 80 km. at very low electron densities. However, a lot of other factors are involved, and I think we would present quite a different picture about the ionization processes from what you talk about.

1.3 ON THE PRODUCTION OF IONIZATION BY H LYMAN ALPHA

by

W. Swider, Jr.

Air Force Cambridge Research Laboratories
Office of Aerospace Research, Bedford, Massachusetts

Abstract

It is argued that a daytime electron production rate near 0.1 c.c./sec. is required near 80 km. which can be supplied only by H Lyα. An estimate of the amount of NO which need be present is seen to agree with photochemical equilibrium studies by Nicolet. Nevertheless, it is pointed out that the observance of H_3O^+ and $H_5O_2^+$ ions by Narcisi and Bailey might be related to the ionization of CH_3 by H Lyα. Problems associated with their observance of ions greater than 48 atomic mass units are briefly discussed. The ionization of NO by H Lyα is noted to be possibly important in the daytime lower E region, near 85-90 km. A highly simplified model of a nighttime E region sustained only by scattered H Lyα ionizing NO is discussed.

1. Introduction

The importance of H Lyα as an ionizing agent in the upper atmosphere is due to the fact that an atmospheric "window" exists near 1216Å so that this radiation can penetrate relatively deeply into the atmosphere compared to neighboring wavelengths. (Unity optical depth is near 75 km. for an overhead sun.) The subsidiary requirements, flux intensity and sufficient photon energy, are also met. Even so, the role of H Lyα in creating ionization depends on the abundance of minor constituents at these altitudes. The major atmospheric constituents and many minor species cannot be ionized by H Lyα (10.14 eV) in their ground states. This can be seen from the following list.

Element	Ar	N_2	N	NO_2	O	H	OH
I.P.(eV)	15.8	15.6	14.5	13.9(9.73)	13.6	13.6	13.2

Element	CH_4	O_3	N_2O	H_2O	O_2	NH_3
I.P.(eV)	13.0	12.8	12.7	12.6	12.1	10.5

The ground states of certain minor atmospheric species, including metallic meteor atoms, are subject to ionization by H Lyα.

Element	CH_3	NO_2	NO	Si	Fe	Mg	Ni	Ca	Al	Na
I.P.(eV)	9.95	(9.73)	9.25	8.15	7.87	7.64	7.63	6.11	5.98	5.14

The ionization potentials in the above listings are taken from a tabulation by Hasted (1964), except for N_2O, which is taken from Curran and Fox (1961). Two ionization potentials are given for NO_2. We suspect the higher value (electron impact result) is probably correct.

While theoretically (Nicolet, 1965 a, b) there is sufficient NO in the D region for ionization purposes, mass-spectrometer results (Narcisi and Bailey, 1965, Narcisi, 1966) suggest a more complex ionic pattern. The role of H Lyα as an ionizing agent is discussed in terms of the results of the above authors.

At night, the presence of scattered H Lyα radiation is shown to provide a major portion of the nighttime E region if NO can attain densities as great as those suggested by Nicolet (1965 b). Negative ion formation is also considered in conjunction with the nighttime E region.

2. D-Region ionization by H Lyα

Fig. 1 illustrates what we will consider to be a minimum midday D region. Each profile was deduced via different methods and hence, by their compatibility, verify each other. Curve 1 is a midsummer noon electron density distribution as determined by Nertney (1953) from analysis of 150 Kc. measurements. A solar zenith angle, χ, of 20°–30° appears appropriate. The second curve is a mean of differential absorption and faraday rotation measurements by Aikin, et al. (1964) at $\chi \simeq 54°$. The final profile is a partial reflection result obtained by Belrose and Burke (1964); these authors emphasize the variability of the profile and the absence at times, of the minimum near 85 km. The minimum near 85 km. apparently exists only during low solar activity and is due, in part at least, to a minimum in production at this height (Aikin et al., 1964). The increase in the xray flux with solar activity eventually destroys this minimum (cf. Poppoff et al., 1964). The essential point here is that the xray ionization source rate is not more than 5×10^{-3} /c.c./sec. at 80 km. for solar minimum.

It appears that a noon electron production rate of about 10^{-1}/c.c./sec. is necessary in order that a sufficient number of electrons be created by noon. With 2×10^4 sec. between sunrise and noon, this rate would provide less than 2000 electrons/c.c. by noon, ignoring loss. Since the loss rate for NO^+ ions can exceed 10^{-7} c.c./sec. (Gunton and Shaw, 1965) a somewhat greater production rate may be necessary. Dawn detachment of electrons has been ignored. The work of Nertney (1953) implies that the number of electrons detached at dawn is a minor contribution to the noon electron density at 80 km. With a production rate of 0.1–0.2/c.c./sec. for NO^+ due to H Lyα, a nitric oxide density of $5\text{-}10 \times 10^5$/c.c. is required at 80 km. for unity optical depth with a 1215.7Å flux of 4 ergs/sq. cm./sec. This is 2.4×10^{11} photons/sq. cm./sec. at the "top" of the atmosphere and 1×10^{11} photons/sq. cm./sec. at 80 km. The ionization cross-section for NO is 2×10^{-18}/sq. cm. (Watanabe, 1954). Our estimated NO density is within the range suggested by Nicolet (1965 b), which is reproduced here in Fig. 2. His study can result in concentrations as low as 2×10^5/c.c. and as high as 4×10^6/c.c. at 80 km. using tentative estimates of the temperature variations at 85 km.* (see Table 1) at 45°N (Cole and Kantor, 1963) in the formula $n(NO)/n(O_2) = 10^{-1} \times \exp(-3000/T)$ of Nicolet (1965 a). This may relate to anomalous winter absorption since higher temperatures, and hence higher nitric oxide densities, occur in winter and day-to-day changes in the mesospheric temperature profile are possible (Nordberg, 1963). However, exact distributions for NO require a solution of transport conditions too.

TABLE 1. Estimated Temperature Variations at 85 km. versus Latitude (Cole and Kantor, 1963).

N. Lat.	15°	30°	45°	60°
Jan.	184	191	210	225°K
July	184	180	174	171

Narcisi and Bailey (1965) have found ions of atomic mass units 19 and 37 ± 1 to be more numerous than NO^+ ions below about 80 km. They suggest identifying these ions as H_3O^+ and $H_5O_2^+$. Perhaps $NO^+ + 2\,H_2O \rightarrow H_3O^+ + NO + OH$ followed by $H_3O^+ + 2\,H_2O \rightarrow H_5O_2^+ + H_2O$ occurred at the mass spectrometer entrance. A similar set of processes is possible beginning with O_2^+ ions. The three body reactions of water vapor with NO^+ and O_2^+ ions are exothermic by 0.75 eV and 3.5 eV, respectively, if (Hasted, 1964) $H_2O + H_2O \rightarrow H_3O^+ + OH^-$ is endothermic by 8.5 eV.

The creation of H_3O^+ and $H_5O_2^+$ ions from O_2^+ and NO^+ ions cannot be an ambient process. Again, a production rate near 0.1 c.c./sec. is needed and the water vapor fractional content of the stratosphere (Bates and Nicolet, 1965), which we adopt as a maximum for the mesosphere, is far too low, <10 ppm, to permit such a rate even with a very high three-body rate coefficient, 10^{-27} cm^6/sec. This argument is supported by the fact that the dissociative recombination rate of H_3O^+ ions, $\alpha(H_3O^+)$, is $2 - 3 \times 10^{-7}$ c.c./sec. at flame temperatures (Knewstubb, 1963), i.e., at 80 km., $\alpha(H_3O^+)\,[n(e)]^2 \simeq 10^{-1}$ c.c./sec. The value of $\alpha(H_3O^+)$ may be even larger at D-region temperatures. Temperature factors range from T^0 to $T^{-2.2}$ for dissociative recombination processes reported to date (Hasted, 1964). We surmise that the dissociative recombination rate for $H_5O_2^+$ ions is not less than that for H_3O^+ ions.

* It is assumed that mixing predominates below 85 km.

The molecule CH_3 is subject to ionization by H Lyα according to the ionization potentials listed earlier. This leads us to propose a possible mechanism for ambient H_3O^+ ion formation. The ion CH_3^+ cannot charge exchange with the major gases but the reaction $CH_3^+ + H_2O \rightarrow H_3O^+ + CH_2 + 0.4$ eV. is probably rapid. If the rate for this process is 10^{-9} c.c./sec., then a water vapor concentration of 10^8/c.c. is required to make this reaction important, i.e. H_3O^+ ions are then produced at a rate of 10^{-1} c.c./sec. A density of 10^8 c.c. for H_2O molecules appears possible (cf. Bates and Nicolet, 1965). Creation of $H_5O_2^+$ would require a very rapid three-body reaction rate since, again, a production of the order of 0.1 c.c./sec. must be attained. Yet, this is possible since preliminary measurements (Paulson, private communication, 1966) for $H_3O^+ + H_2O + N_2 \rightarrow H_5O_2^+ + N_2$ yield a rate coefficient near 10^{-27} cm^6/sec. and with $n(N_2) \approx 3 \times 10^{14}$/c.c. $N(H_2O) \approx 10^{-6}\ n(N_2)$/c.c. and $n(H_3O^+) \approx 10^3$/c.c. all near 80 km., we arrive at the desired figure. However, even if H_3O^+ ions are present in the D region, the observance of $H_5O_2^+$ ions may be a result of H_3O^+ ions interacting with the water vapor carried with the rocket rather than by ambient mechanisms.

The critical question involved is whether a sufficient amount of CH_3 can exist in the mesosphere. The quantity needed is obviously the same as the estimate made for NO, i.e. about 10^{-3} ppm., if the ionization cross-section of CH_3 is equal to that for NO. (The ionization cross-sections of CH_3 and NO at H Lyα probably lie within a factor of ten.) The molecule, CH_3, results from CH_4 + H Ly$\alpha \rightarrow CH_3$ + H. The density of methane, CH_4, is approximately 10 ppm. in the stratosphere (Bates and Nicolet, 1965) and hence it does not seem unreasonable that CH_3 could approach 10^{-3} ppm. near 75 to 80 km., even though $CH_4 + O \rightarrow CH_2 + H_2O$ also occurs (Bates and Nicolet, 1965).

The molecule CH_3 should exist only in a fairly narrow region near 75 to 80 km., i.e. in the vicinity of its production mechanism CH_4 + H Ly$\alpha \rightarrow CH_3$ + H since this molecule is subject to dissociation by ultraviolet radiation which penetrates to these altitudes and below. Anomalous winter absorption might be related to CH_3 ionization if sudden large transports of methane from the stratosphere into the mesosphere can occur or rather by strong depletions in the O concentration and hence suppression of the reaction $CH_4 + O \rightarrow CH_2 + H_2O$. Finally, it should be noted that the existence of important ionizable quantities of CH_3 or NO is not mutually exclusive.

3. Meteoric ions

The D-region problem is further complicated by the existence of heavy ions (amu >48) below about 75 km. (Narcisi and Bailey, 1965). These ions were found to be more numerous than even $H_5O_2^+$ and H_3O^+ ions. Recent results (Narcisi, 1966) suggests that these heavier ions are Fe^+, Ni^+ or possibly the corresponding oxidized ions. Evidence of Fe and Ni has been found in collections of noctilucent cloud particles (Witt et al. 1964).

The ionization of meteor atoms or oxides by H Lyα is probably unimportant. It is doubtful that both their ionization cross-sections and particle concentrations are comparable to those of nitric oxide. A competing mechanism for D-region ionization (versus that by H Lyα) could be the ionization of metallic oxides with ionization potentials less than about 7 eV, since a broad solar flux continuum (Nicolet, 1955) is then available. Meteor ions are not reported as important below 80 km. (Narcisi and Bailey, 1965; Narcisi, 1966) except possibly for Ni and Fe, since ions of mass >48 amu are seen. The ionization potentials of Fe and Ni exceed 7 eV however, so no broad solar flux continuum is available for ionization at D-region heights for these ions. Besides, since atomic ions have long lifetimes, the D region would not vary diurnally to any appreciable extent if the majority of the positive ions at 85 to 75 km. were atomic. A lack of variation is contrary to the observational evidence. If NiO and FeO have ionization potentials below 7 eV, their ionization coefficient may be sufficiently great so as to necessitate their consideration as important ionizable D-region constituents.

4. H Lyα in the lower E region

Bourdeau et al. (1966) suggested that $\alpha(NO^+) \approx 2 \times 10^{-8}$ c.c./sec. from 93 to 83 km. by balancing production and loss effects. Laboratory measurements (Gunton and Shaw, 1965) and most contemporary ionospheric studies indicate that $\alpha(NO^+) \gtrsim 10^{-7}$ c.c./sec. at these altitudes. The distribution (curve 5) shown in Fig. 2 permits the retention of the higher value by making the direct ionization of NO by H Lyα the dominant production source of electrons over this height interval. Furthermore, $\alpha(NO^+) \approx 2 \times 10^{-8}$ c.c./sec. would give a loss rate of only 0.007 c.c./sec. at 80 km., assuming $n(NO^+) = n(e) = 600$/c.c. (see Fig. 1). Yet, we have shown that the production rate should be about 0.1 c.c./sec. or more. The loss rate should be comparable if NO^+ is the dominant ion.

5. H Lyα at night

The nitric oxide distribution labeled curve 5 in Fig. 2 is constructed to stay roughly within the bounds suggested by Nicolet (1965b) to provide an example of how nitric oxide ionization can be important in the lower E region and to simplify calculations of the total content of the NO layer. The same distribution leads to a reasonable nighttime E-region profile of electron density. This nitric oxide distribution, which by inspection cannot be exact, yields a nighttime production rate of NO^+ ions and electrons when combined with the scattered H Lyα flux at night (Fastie et al., 1964) shown in Fig. 3 and the ionization cross-section for NO, 2×10^{-18} /sq. cm. at 1216Å (Watanabe, 1954). The resulting production rate of $q(NO^+) = q(e)$ yields an electron density $n(e) = n(NO^+) = \sqrt{q(NO^+/\alpha(NO^+)}$ given by the dotted line, curve 4, shown in Fig. 3 with a $(NO^+) = 10^{-7}$ c.c./sec. The agreement with the experimental data, curves labeled 1, 2 and 3, is reasonable. Curve 1 represents preliminary results of a standing wave impedance probe at 0315 local time (Ulwick and Pfister, private communication, 1966). Curve 2 is Langmuir probe data at 0435 local time by Smith (1962). The third curve is a result of calculations by Seliga (1965) of Mecktly's (1962) 512 kc. continuous wave measurements. The local time is about 0200.

6. Negative ions above 80 km. at night

Negative ions have been ignored in producing curve 4 in Fig. 3. Nicolet (1955) has stressed that the electron content of the nighttime E region is not indicative of any predominance of negative ions over electrons and that certain detachment processes discussed by Bates and Massey (1943) are probably operative. These processes are

$$O^- + O \rightarrow (\text{rate } d_1) \rightarrow O_2 + e \tag{1}$$

$$O_2^- + O \rightarrow (\text{rate } d_2) \rightarrow O_3 + e \tag{2}$$

However, in view of the fact that

$$O_2^- + O \rightarrow (\text{rate } c_1) \rightarrow O^- + O_2 \tag{3}$$

is exothermic by about 1 eV, we will ignore, for now, reaction (2) by assuming $c_1/d_2 \gtrsim 10$. The charge exchange reaction is likely to lie within the range $10^{-11} \pm 2$ c.c./sec. whereas d_1 (and probably d_2) may reach 10^{-15} c.c./sec. according to theoretical consideration of Bates and Massey (1943).

Attachment rates for both

$$e + 2O_2 \rightarrow (\text{rate } a_1) \rightarrow O_2^- + O_2 \tag{4}$$

and

$$e + O \rightarrow (\text{rate } a_2) \rightarrow O^- + h\nu \tag{5}$$

have been measured in the laboratory. The rates for these processes are about 2×10^{-30} cm^6 /sec. (Chanin, Phelps and Biondi, 1962) and 1×10^{-15} c.c./sec. (Branscomb, Burch, Smith and Geltman, 1958). We first show that adaption of these rates to the nighttime E region requires that production or detachment processes, or both, must be operative. Radiative attachment to O_2 is ignored since its rate appears to be very small (Branscomb, 1964).

The electron loss rate due to attachment alone is given by

$$\frac{1}{n(e)} \frac{dn(e)}{dt} = -a_1 \left[n(O_2)\right]^2 - a_2\, n(O) \tag{6}$$

The solution of this equation is simply

$$n(e) = n(e)_0 \left\{\exp -a_1 \left[n(O_2)\right]^2 - a_2\, n(O)\right\} t \tag{7}$$

The ratio of the electron density at $t = 3 \times 10^4$ seconds (about 8 hr.) versus the layer sunset electron density, $n(e)_0$, is given in the following table.

TABLE 2. Nighttime Attachment Rates and Parameters

Z(km)	$n(O_2)$	n(O)	$a_1 [n(O_2)]^2$	a_2 n(O)	$n(e)/n(e)_O$
120	7.1×10^{10}/c.c.	8.3×10^{10}/c.c.	1.0×10^{-8}/sec.	8.3×10^{-5}	8.2×10^{-2}
110	3.3×10^{11}	2.3×10^{11}	2.0×10^{-7}	2.3×10^{-4}	1.0×10^{-3}
100	1.6×10^{12}	5.5×10^{11}	5.1×10^{-6}	5.5×10^{-4}	7.0×10^{-8}
90	1.3×10^{13}	4.0×10^{11}	3.4×10^{-4}	4.0×10^{-4}	$\sim 10^{-10}$
80	8.0×10^{13}	(1.0×10^{11})	1.3×10^{-2}	1.0×10^{-4}	$\sim 10^{-8s}$

Notes: The n(O) densities are approximate. The density at 80 km. is a maximum value.

The production rate adapted in Fig. 3 for 100 km. (0.12 c.c./sec.) cannot balance the attachment loss rate at this altitude until n(e) declines to 2×10^2/c.c. Considering the fact that dissociative recombination has been ignored and that the nighttime production rate of electrons might well be less, a need for detachment processes is obvious.

In Table 2, the only attachment process important above 100 km. is process (5), radiative attachment to atomic oxygen. Therefore, only process (1) need be considered. The respective rates a_1 and d_1 for these reactions may both be 10^{-15} c.c./sec., as already noted. If so, the ratio $n(O^-)/n(e)$ has an upper limit of unity. (Nicolet, 1955, has pointed out this possibility). Since ion-ion recombination and dissociative recombination has been neglected, the ambient upper limit could be less. It would seem therefore, that both the experimentally determined rate $a_1 \simeq 10^{-15}$ c.c./sec. (Branscomb et al., 1958) and the theoretically estimated rate $d_1 \simeq 10^{-15}$ c.c./sec. Bates and Massey, 1943) are adaptable to the ionosphere. Since a_1 is the more reliably known parameter, low d_1 values, 10^{-17} c.c./sec. for example, would be unacceptable or electrons would be absent near 100 km.

Observational results of the electron density at night [Fig. 3, see also results by Smith (1962, 1964)] indicate no obvious effect of negative ions above 100 km. The decrease of electrons below 100 km. can be due to a decline in nighttime production rather than attachment processes. Nevertheless, the decrease of the electron density to a value of 10/c.c. near 80 km. cannot be due to dissociative recombination alone, which is limited according to $n(e) \rightarrow 1/\alpha t$. The ratio of negative ions to electrons undoubtedly lies within $10^1 \pm 1$ at this altitude past midnight. We are therefore led to the virtually trivial example (ion-ion and dissociative recombination can be neglected), by equating $a_1 [n(O_2)]^2$ n(e) with d_1 $n(O^-)$ n(O), that

$$d_1 = 10^{-13} \quad 10^{-14} \quad 10^{-15} \text{ c.c./sec.}$$

$$n(O^-)/n(e) = 1 \quad 10 \quad 10^2$$

If $c_1/d_2 < 1$ then $O_2^- + O \rightarrow O^- + O_2$ is unimportant and we balance $a_1 [n(O_2)]^2$ n(e) = $d_2 n(O_2^-) n(O)$ with the above rate estimates for d_1 applying to d_2.

This brief analysis leads to the conclusion that

$$d_1 > 10^{-16} \text{ c.c./sec.}$$

$$\text{if } c_1 > d_2, d_1 \simeq 10^{-14} \pm 1 \text{ c.c./sec.}$$

$$\text{if } c_1 < d_2, d_2 \simeq 10^{-14} \pm 1 \text{ c.c./sec.}$$

Since $c_1 > d_2$ is more likely, we feel it is d_1 which is near $10^{-14} \pm 1$ c.c./sec.

An exception to the conclusions above may exist. We have assumed the detachment process

$$O^- + N_2 \rightarrow (\text{rate } d_3) \rightarrow N_2O + e$$

is endothermic since the dissociation energy of N_2O appears to be less (Curran and Fox, 1961; Schulz, 1961) than the electron affinity of 0, about 1.47 eV. These authors point out that the thermochemical data gives $D_0(N_2O \rightarrow N_2 + O) > E.A.(O)$, however. If the thermochemical data is correct, the above process may

replace $O^- + O \rightarrow O_2 + e$. In that case, the rate d_3 need not be as great as the values for d_1 estimated above since $n(N_2) > n(O)$ at these altitudes.

7. Concluding Remarks

We have seen that H Lyα acting upon NO can sustain both the daytime D region and nighttime E region and may be important also in the lower daytime E region. Generally, this approach is in reasonable agreement with the observational evidence. The major exception is the ion composition results of Narcisi and Bailey (1965) in the daytime D region. We have indicated that it is difficult to decide at present whether these results properly represent ambient conditions below 80 km. Hopefully, the situation will become clarified in the near future. Till then, we hope that this brief paper may prove useful and stimulating to experimental workers in the field who must provide the evidence from which the physical constitution of the ionosphere can be deduced.

REFERENCES

Aikin, A.C., Kane, J.A. and J. Troim. J. Geophys. Res. 69, 4621, 1964.

Bates, D.R. and H.S.W. Massey. Phil. Trans. Roy. Soc., A-239, 269, 1943.

Bates, D.R. and M. Nicolet. Planet. Space Sci. 13, 905, 1965.

Belrose, J.S., and M.J. Burke. J. Geophys. Res., 69, 2799, 1964.

Bourdeau, R.E., Aikin, A.C. and J.L. Donley. NASA Report No. X-615-65-304, 1965, J. Geophys. Res. 71, 727, 1966.

Branscomb, L.M. Ann. Geophys. 20, 49, 1964.

Branscomb, L.M. Burch, D.S., Smith, S.J. and S. Geltman. Phys. Rev. 111, 504, 1958.

Chanin, L.M., Phelps, A.V. and M.A. Biondi. Phys. Rev. 128, 219, 1962.

Cole, A.E. and A.J. Kantor. Air Force Surveys in Geophysics No. 153, 1963.

Curran, R.K. and R.E. Fox. J. Chem. Phys. 34, 1590, 1961.

Fastie, W.G., Crosswhite, H.M. and D.F. Heath. J. Geophys. Res. 69, 4129, 1964.

Gunton, R.C. and T.M. Shaw. Phys. Rev. 140, A756, 1965.

Hasted, J.B. Physics of Atomic Collisions, Butterworth, London, 1964.

Knewstubb, P.K. Mass Spectrometry of Organic Ions, edited by F.W. McLafferty, Academic Press, New York, 1963.

Mecktly, E.A. Penn. State Univ. Ionosp. Res. Lab. Sci. Rep. No. 160, 1962.

Narcisi, R.S. to be presented at COSPAR, Vienna, 1966.

Narcisi, R.S. and A.D. Bailey. J. Geophys. Res. 70, 3687, 1965.

Nertney, R.J. J. Atmos. Terr. Phys. 3, 92, 1953.

Nicolet, M. J. Atmos. Terr. Phys. Suppl. 2, 99, 1955.

Nicolet, M. J. Geophys. Res. 70, 679, 1965a; ibid., 691, 1965b.

Nordberg, N. NASA Rep. No. X-651-63-244, 1963.

Poppoff, I.G. Whitten, R.C. and R.S. Edmonds. J. Geophys. Res. 69, 4081, 1965.

Schulz, G.J. J. Chem. Phys. 34, 1778, 1961.

Seliga, T.A. Penn. State Univ. Ionosp. Res. Lab. Rep. No. 254, 1965.

Smith, L.G. Geophys. Corp. Amer. Tech. Rep. No. 62-1-N, 1962.

Smith, L.G. COSPAR Inf. Bull. 17, 37, 1964.

Swider, Jr., W. J. Geophys. Res. 70, 4859, 1965.

Watanabe, K. J. Chem. Phys. 22, 1564, 1954.

Witt, G., Hemenway, C.L. and R.K. Soberman. Space Res. 4, 197, 1964.

Note added in proof

Fehsenfeld, Fergusson and Schmeltekopf's (J. Chem. Phys. 45, 1844, 1966) rate coefficients of 3×10^{-10} c.c./sec. for $O^- + O \rightarrow O_2 + e$, and 5×10^{-10} c.c./sec. for $O_2^- + O \rightarrow O_3 + e$ and $O_2^- + O \rightarrow O^- + O_2$, would ensure that negative ions are virtually non-existent in the nighttime E region. The low number of electrons at 80 km. and below (Fig. 3) would then imply that the atomic oxygen density is much lower at 80 km. than suggested by Table 2 and that perhaps O_2^- is not the dominant ion there.

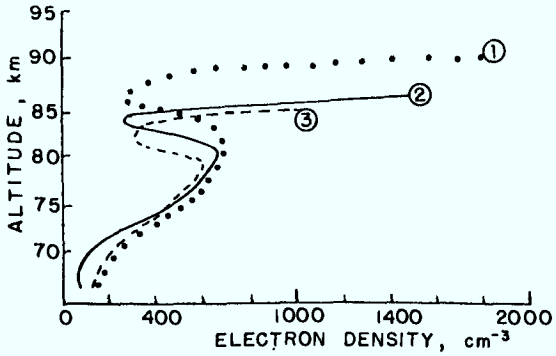

Fig. 1. Some minimum D-region electron density profiles (see text).

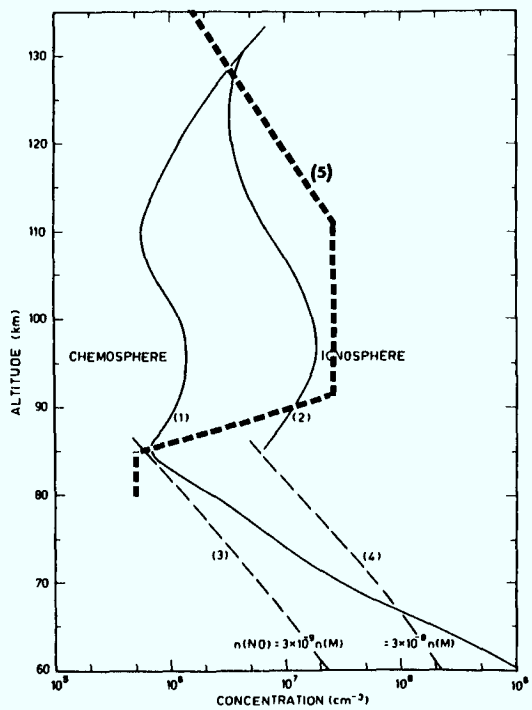

Fig. 2. Nitric oxide profiles due to Nicolet (1965) and, in addition, a simplified model in diffusive equilibrium above 111 km. with

$$\int n(NO)\, d_z = 9 \times 10^{13}/\text{sq. cm.}$$

above 85 km.

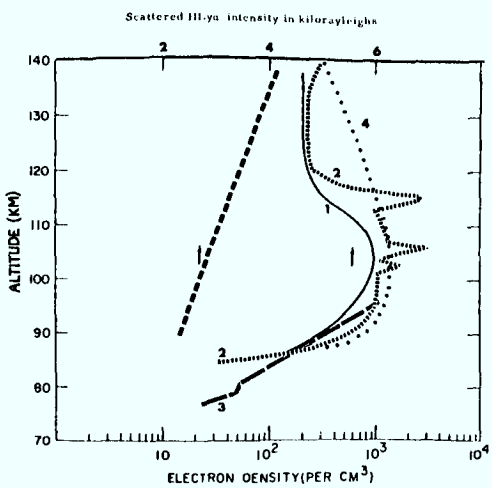

Fig. 3. Nighttime E-region measurements compared to a simple model (see text).

Discussion on Paper 1.3 presented by W. Swider, Jr.

Waynick: I think perhaps someone should both defend and attack Narcisi.

Swider: I know Narcisi well and am sure that he is taking a middle of the road attitude. This is what he honestly measured; there is no question about some of these meteor-ion profiles he has seen being very accurate. He has some interesting nighttime results, which will be presented at COSPAR(1), in which he sees a ledge of virtually pure meteor ions around 90 km. However, this is still not the total nighttime E region. With regard to the water vapor, you can say that we do not know; we cannot find either an ambient or non-ambient mechanism that definitely explains the problem.

Zimmerman: Hester, I believe, has shown or hypothesizes a vertical transport of water vapor where you have a constant ratio (since this is the mixing region) of something like 10^{-4} compared to the background. This would be ample to carry it up to 80 km. where dissociation of water vapor starts coming in by sunlight, and it seems to me that some of the measurements where he showed the cessation of the 19^+ and 37^+ at around 80 or 82 km. correspond nicely.

Swider: Well, the interesting thing is that the dissociation of water vapor corresponds to the regions where 19^+ and 37^+ fall off sharply so there is some definite reason to relate it to water vapor. I don't say that, but for production mechanism I cannot see how you can have the direct ionization of water vapor; this is impossible, as far as I can see, unless the loss rate would be very slow, and there is no evidence for this.

Zimmerman: I will agree that the production mechanism is in some argument, but the water vapor itself can get up there.

Swider: Yes, there is water vapor; however, there is also some evidence of contamination, because if you look at this data for higher altitudes (110 km.) you see an H_3O^+ ion. This cannot be an ambient ion; you just cannot get the neutral molecule H_3O. So certainly he wasn't measuring H_3O^+ from the atmosphere. It had to be made in his instrument, but at the D region this can be an entirely different mechanism.

Dalgarno: Could I clarify my position? The question I asked during discussion on the Aikin paper was whether the water vapor was comparable to the molecular oxygen. I am happy with this figure of 10^{-4}, but I don't think that is comparable.

Swider: There may be some misunderstanding on this point, but Narcisi never said or intimated that they were comparable.

Aikin: That is what I implied.

Pfister: Could you elaborate on the metallic ion Narcisi measured, especially in the nighttime D region?

Swider: These results will be presented at COSPAR(1). I did not mean to present them here, but since they are of intense interest I know Narcisi will forgive me. This 40^+ should be calcium ion or magnesium oxide ion; I am sure it must be the calcium ion because of the question of loss processes. The 24^+ will likely be magnesium and the 56^+ is iron. The nitric oxide is suppressed because there is a problem of charge transfer. Narcisi has suggested this, and I have been working on this problem independently in a different way by comparing ionization coefficients of metallic particles with reaction rates. He again saw the 37^+ but he could not see the 19^+ because he has a lower limit. The important thing to remember is that this flight was made about 36 hr. after a meteor shower. *Please* do not go away saying that this is the nighttime D region by any means, and also remember this is just ion current data; it is interesting and it does show that the meteor ions are really there.

Wright: Coincident with this flight, a sporadic E layer was observed on an ionsonde at the same altitude as the ion layer, and it can be traced back to about 4 p.m. of the previous day. It was about 105 or 106 km. altitude at that time.

Gregory: For many years one of the unexplained features of the lower ionosphere has been the persistence of weak ionization densities of a few ten per c.c. which persisted at about 85 km. right through the night hours. The recombination rates that have been assumed have always made this difficult to explain. However, the presence of this type of metallic ion is the sort of thing that one would like, to explain this data.

Swider: It is generally agreed that the D region does vary in a sort of Chapman-like way (as roughly as we know it) which means that the recombination coefficient must be fairly high. In other words, atomic positive ions are not the dominant ions of the D region, because the lifetimes of those ions would be too long. If atomic ions were the dominant ions of the D region, you wouldn't get any variation in the D region to speak of until nighttime, when suddenly you would have attachment and electrons that are going to disappear very rapidly. Narcisi has not identified a metallic ion in the D region. He only knows that he sees ions greater than 48^+ below about 75 km. by day, and these could be oxides of iron or nickel. At 80 km. it must be a molecular ion; below 70 or 75 km. it could be a metallic ion, but the processes there are governed in a different way perhaps.

Belrose: Can I raise again the question of the validity of Narcisi's results? Surely one can get a grasp of this, and presumably you who have seen his recent results already have this grasp, by looking at his day-night ratios. If we see vast differences between day and night then this can't be entirely a contamination problem. Does he give results on the descending leg or only on the ascending one?

Swider: In the results that were published, his descent data agreed well with his ascent data. This would then seem a strange contamination problem, because usually you would imagine there would be some difference in the out-gassing. In his nighttime results that I showed, the 37^+ values are not very different from his daytime, values except that they are a few km. higher; and as Narcisi has pointed out you do not have any dissociation of water vapor at night, so the water vapor layer is going to rise.

Wright: It is impossible to attribute this layer or any appreciable part of it to the rocket, because it was present 6 hr. earlier and continuously from then through the time the rocket was flown.

Swider: Which layer?

Wright: The layer of iron associated with the nighttime flight.

Swider: The iron problem is a different problem. We could talk all day about this water vapor below 85 km.

(1) Narcisi, R.S., Bailey, A.D. and L. Della Lucca. Composition measurements of Sporadic E in the Nighttime Lower Ionosphere, presented at COSPAR, Vienna, 1966. Abstract and figure published in these Proceedings, 1966.

1.3.1

COMPOSITION MEASUREMENTS OF SPORADIC E IN THE NIGHTTIME LOWER IONOSPHERE*

by

R.S. Narcisi, A.D. Bailey, and L. Della Lucca

Air Force Cambridge Research Laboratories, L.G. Hanscom Field
Bedford, Massachusetts

ABSTRACT

Measurements of positive ion composition of the lower ionosphere between 75 and 107 km. were made at Eglin Air Force Base, Florida, on 17 November, 1965 at 2320 CST. The experiment was similar to that described in an earlier paper of this meeting, except that the mass spectrum was scanned from 8 to 86 amu to determine the mass numbers of previously detected heavy ions. A sporadic E-like layer of less than 2 km. width at half height was detected at 89 km. Another layer, although not as intense as the lower layer, was found at 93 km. The layers were seen to be composed of Fe^+, Mg^+, Ca^+, and Ni^+, listed in order of decreasing abundance. The predominant ions from 85 to 95 km. were these metal ions. From 95 to 107 km. NO^+ was most abundant, with $NO^+/O_2{}^+ = 15 \pm 2$. The ion 37^+ was again detected to be the major ion below 86 km. and to disappear above this altitude. Conjunctive wind measurements were also performed during this night by another group for the comparison of sporadic E with wind shear.

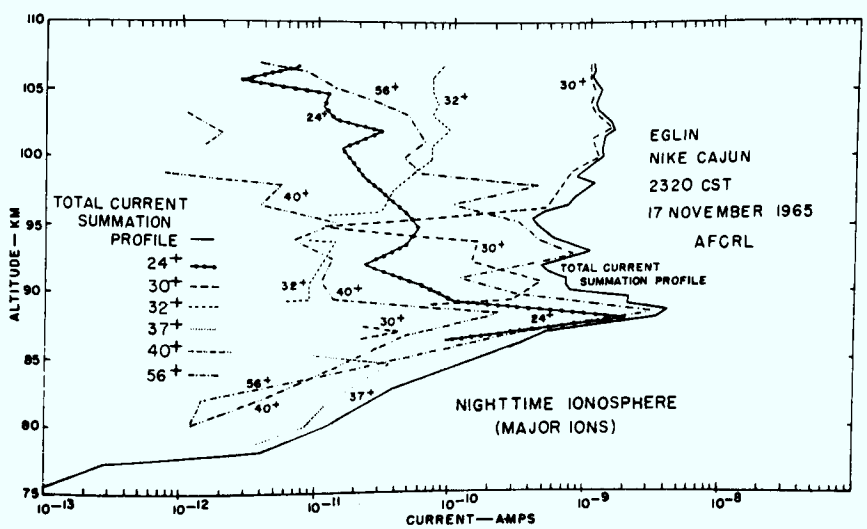

*To be submitted to the Journal of Geophysical Research.

Paper presented at COSPAR, Vienna, 1966. The results obtained by these workers were frequently referred to during the DRTE/AFCRL conference. We are pleased that the authors have kindly made this abstract and accompanying figure available for publication in this Proceedings. It should be noted that the figure shows ion current which is not simply related to the absolute total positive ion density.

1.4 HORIZONTAL AND VERTICAL DISTRIBUTIONS OF ATMOSPHERIC PRESSURE, 30 TO 90 KILOMETERS

by

A.J. Kantor

Design Climatology Branch
Air Force Cambridge Research Laboratories
Bedford, Massachusetts

Abstract

The variation of pressure with height and distance in the mesosphere and upper stratosphere can be an important factor in the study of radio wave propagation in the lower ionosphere. The distribution with latitude of atmospheric pressure is such that mean monthly pressures generally increase toward the equator in winter and toward the pole in summer, with the largest change near 60 km. At this height the mean maximum January gradient lies between 60 and 40°N, where the pressure changes by roughly one per cent of standard per degree of latitude. The height of smallest change is near 85 km. at which values remain between 106 and 111 per cent of standard. The largest January and July departures from standard occur near 65 km. in the Arctic, where the minimum January value is 65 per cent of standard and the maximum in July is 130 per cent of standard. A pressure increase near 60 km. of more than 7 per cent per degree of latitude can result from coexistence of typical cold and warm winter stratospheric thermal regimes within 600 miles over arctic regions. An extreme vertical pressure gradient of 23 per cent decrease per km. may exist near 85 km. for the coldest observed temperature, 130°K, at this level. Day-to-day variability of pressure increases with latitude and altitude to near 65 km. Estimated 2 standard deviations are largest at 60 to 65 km. at all latitudes, reaching ± 35 per cent during 60°N winter. Based on theoretically determined diurnal temperature changes of ± 5 or 6°K at 50 km., diurnal pressure variations have been calculated. They increase with height above 30 km. to at least 80 km., where deviations of ± 8 to 10 per cent approach seasonal and day-to-day values. These estimates compare favorably with values obtained from ARCAS-ROBIN soundings at Eglin AFB for May 1961 and October 1960 and 1962.

1. Introduction

Radio wave propagation is influenced considerably by the collision frequency of electron and neutral particles which in turn is dependent upon atmospheric pressure, and to a smaller extent, atmospheric temperature. As a result, the fluctuation of atmospheric pressure with height and distance in the mesosphere and upper stratosphere can be an important factor in the study of the propagation of radio waves, particularly in the lower portion of the ionosphere where absolute values of pressure are larger than at higher levels. Consequently, the horizontal and vertical distributions of atmospheric pressure are discussed for altitudes up to 90 km.

Estimates of January and July mean monthly pressure and temperature gradients at given altitudes as well as slopes of constant pressure surfaces can be determined from the vertical pressure and temperature profiles described in the Air Force Interim Supplemental Atmospheres to 90 km. These internally consistent atmospheres have been developed, assuming hydrostatic equilibrium, for 15, 30, 45, 60 and 75°N (Cole and Kantor, 1963). They will be published later this year through the Government Printing Office as the US Standard Atmosphere Supplements, 1966. In addition to these, mean monthly vertical pressure and temperature profiles to 80 km. have been calculated for every month for 30, 45 and 60°N, providing somewhat more detailed estimates between 30 and 60°N (Kantor and Cole, 1965).

For heights above 30 km., data are available neither in quantity nor in quality sufficient to provide frequency distributions of these gradients. However, if the atmosphere is assumed to be hydrostatically consistent, extreme values of pressure can be estimated by comparing available observations with the thermal structures that are associated with large pressure gradients.

2. Horizontal Gradients

The distribution with latitude of atmospheric pressure for January and July, expressed in per cent of the US Standard Atmosphere, 1962, is shown in Fig. 1 for 30 to 90 km. Values are based on the January and July Supplementary Atmospheres for 30, 45 and 60°N, and the mean annual Supplementary Atmosphere for 15°N. A mean annual atmosphere rather than monthly atmospheres was adopted for 15°N since the monthly variation of the temperature-height structure, the defining parameter, appears to be relatively small at these levels in the tropics. Since pressure profiles were not developed above 30 km. for 75°N, values between 30 and 90 km. for this latitude have been derived through extrapolation of data at lower altitudes and latitudes, and combination with fragmentary observations from polar stations at Thule AFB, Greenland (77°N), Point Barrow, Alaska (71°N), and McMurdo Sound, Antarctica (78°S).

Mean pressures shown in this figure generally increase toward the equator in January and toward the pole in July. The change in pressure with latitude is largest between 55 and 65 km. At these heights the maximum mean January gradient can be observed between 60 and 40°N, where the pressure changes from roughly 70 to 90 per cent of standard. This represents an increase of approximately 1 per cent of standard per degree of latitude, or almost 1.5 per cent increase in the 60°N pressure per degree of latitude. The height of smallest change with latitude between 30 and 90 km. lies near 85 km., where pressures apparently remain between approximately 106 and 111 per cent of standard. This level of quasi-constant pressure is illustrated in Fig. 2, in which pressure-height profiles for the Supplementary Atmospheres have been plotted as per cent departures from standard. The crossover near 85 km. is roughly 10 per cent greater than standard and results from the behavior of atmospheric temperature. That is, the vertical profiles of temperature for the various latitudes and seasons cross near 65 km., causing pressure and density gradient reversals to occur near 85 and 90 km. respectively.

The largest mean January and July departures of pressure from standard occur near 65 km. and poleward of 60°N, probably near 75 or 80°N. This was seen in Fig. 1. The mean minimum pressure in January is roughly 65 per cent of standard, whereas the mean maximum in July is twice that of January, or 130 per cent of standard. Minimum and maximum mean monthly pressures, however, do not necessarily occur in January and July at all levels between 30 and 90 km. This is apparent in Fig. 3, in which the estimated annual march of mean monthly pressure, again plotted as per cent departure from standard, is shown for 30, 45 and 60°N at 30 through 70 km. At 30°N, for example, mean monthly pressures are largest in May rather than July at 40, 50, and 60 km.; at 60°N pressures are smallest in December rather than January at 40, 50, 60, and 70 km.

Frequency distributions of horizontal pressure gradients are not yet available at heights above 30 km. since insufficient measurements have been taken, and data on the decay of correlation of pressure with distance have not been computed. However, estimates of extreme horizontal pressure gradients can be made by examining existing observations at these altitudes.

As suggested by the first two figures, the largest horizontal pressure changes tend to occur in winter at arctic and subarctic latitudes. The largest longitudinal as well as latitudinal differences in atmospheric conditions also generally occur in these regions during winter. This was indicated in Fig. 2 by the 60°N pressure profiles associated with typical cold and warm winter thermal regimes of the stratosphere and mesosphere. The frequency of occurrence of these thermal structures varies with longitude at both subarctic (60°N) and arctic (75°N) latitudes. Radiosonde observations between 20 and 30 km. demonstrate that the cold regime prevails over the warm by nearly four to one over north-central and northeastern Canada, whereas near the Aleutian Islands the warm regime prevails by approximately eight to one. At heights near 25 km. cold and warm winter regimes have been known to exist simultaneously within a 600-mile distance, as described by the Arctic Meteorology Group, McGill University (1963). This would result in a horizontal pressure change much larger than the maximum mean January gradient noted on the first figure. More specifically, the pressure increase in roughly one degree of latitude or 60 n.m., from the cold to the warm region would be more than 7.2 per cent near 62 km. This is almost five times larger than the maximum mean January gradient of 1.5 per cent increase per degree of latitude. For these conditions, estimates of per cent changes of pressure for heights 40 to 80 km. are shown in Table 1. These values, particularly across 600 n.m., are considered conservative estimates of extreme horizontal pressure gradients, since winds associated with such occurrences, assuming geostrophic balance, would be approximately 200 m./sec. at 60 km. These velocities have not, to my knowledge, been observed at this altitude.

TABLE 1. Pressure Increase (%) From Cold To Warm Winter Regime

Height (km.)	Pressure Increase 600 n.m.	60 n.m.
40	49%	4.9%
50	61	6.1
60	71	7.1
70	63	6.3
80	41	4.1

3. Vertical Gradients

From the barometric equation it is apparent that the greatest change in pressure with altitude occurs at the lowest mean temperature; that is, atmospheric pressure decreases in the vertical more rapidly in cold air than in warm air. Consequently, the largest mean monthly percentage change in pressure in the vertical between 30 and 90 km. would occur, according to the Supplementary Atmospheres, in the 80 to 90 km. layer during 60°N July, at a mean temperature of roughly 170°K. Under these conditions one would encounter on ascent a pressure decrease of 18 per cent per km. or 63 per cent in 5 km. For an incoming vehicle or descent through the atmosphere, these values correspond to pressure increases of 23 and 173 per cent at one and five km., respectively. Since these vertical pressure changes are based on mean monthly temperature-height profiles, they are exceeded at times as a result of day-to-day fluctuations in the thermal structure of the atmosphere. Unfortunately, frequency distributions of vertical pressure changes above 30 km. are not yet available. However, assuming a hydrostatically consistent atmosphere and utilizing the minimum observed temperatures in the mesosphere, estimates can be made of the largest gradients that are apt to occur at these altitudes.

The lowest temperatures known to have been observed in the mesosphere were obtained from a series of four rocket grenade soundings completed at Kronogard, Sweden, during the summer of 1963. The temperature approached 130°K near 85 km. at a time when noctilucent clouds were present (Bull. AMS, 1963). Consequently, for a one-km. layer with a mean temperature of 130°K, atmospheric pressure would decrease by 23 per cent or increase by 30 per cent. These values probably approach the maximum possible vertical pressure gradient. Provided this extreme temperature could persist for a five-km. interval, the pressure would decrease by 73 per cent or increase by 272 per cent through this layer.

A series of five curves is shown in Fig. 4, from which the per cent decrease in atmospheric pressure can be determined for layer thicknesses up to 12 km. and mean temperatures ranging from 130 to 290°K. A simplified form of the barometric equation, based on mean layer temperatures, also is shown to facilitate rapid calculation of approximate vertical pressure changes for the indicated mean temperatures and any given layer thickness, n. For the sample computation shown in the figure, a mean temperature of 210°K through a thickness of 4 km. yields a 48 per cent decrease of pressure in the vertical through use of $(0.84986)^4$ in the appropriate equation.

4. Day-to-day Variations

Estimated day-to-day variations of pressure which are exceeded less than 5 per cent of the time are shown in Table 2 as percentages around mean January and July values, surface to 80 km. Estimates to 30 km. are based on a large number of radiosonde observations taken at appropriate latitudes around the globe, whereas above 30 km. they are based on data from sensors released by rockets at approximately 18 launching sites between 8°S and 71°N.

As can be seen in the table, day-to-day variability generally increases with latitude and altitude in both January and July, although to a much smaller extent in July. Estimated two standard deviations are largest at 60 to 65 km. at all latitudes, reaching ± 35 per cent during 60°N winter. Variations seem to decrease above 65 km. to a probable minimum value, mentioned earlier, near 85 km. The estimated day-to-day variations shown in the table undoubtedly include some diurnal and semidiurnal fluctuations due to solar influences, particularly since the basic pressure data were not obtained at the same hours of the day nor were they sufficiently random to average out these solar effects. Envelopes of these estimated 95 per cent values should not be constructed since such pressures would not necessarily be found at all heights at any one given time and location. Decreases in atmospheric pressure in one layer, for example, often are associated with increases in another layer.

TABLE 2. Day-to-day Variations (%) Exceeded Less Than 5% of the Time Around Mean January and July Pressures

Height (km.)	January					July				
	75°N	60°N	45°N	30°N	15°N	15°N	30°N	45°N	60°N	75°N
0	±2.5	±3	±2.5	±1	±0.4	±0.4	±0.5	±1	±1	±1.5
10	7	4	3	2	0.8	0.7	0.8	2	3	4
20	10	10	10	7	4	2	2	3	3	3
30	20	16	14	12	7	4	4	4	5	5
40		±25	±20	±15	±8	±7	±8	±8	±10	
50		30	25	18	10	10	12	13	14	
60		35	30	20	12	12	14	16	18	
70		30	25	18	10	10	12	15	16	
80		20	16	12	8	8	9	10	10	

Extreme winter and summer pressure profiles observed at Fort Churchill (59°N) are compared in Fig. 5 with mean January and July pressure curves for 60°N. They are shown as percentage departures from the US Standard and effectively illustrate extreme deviations from monthly mean values that can be found at several levels simultaneously. The 27 January 1958 profile, determined by rocket grenade and falling sphere techniques, displays pressures 39 to 66 per cent smaller than standard between 30 and 80 km. Two days later, on 29 January 1958, another sounding reveals pressures which have increased to as much as 3 per cent greater than standard near 75 km. This represents a fluctuation, in only two days, from roughly -35 to +37 per cent of the January mean at 60 to 70 km., in general agreement with the estimated two standard deviation values which were noted in Table 2. Similar changes in pressure, although not as extreme, were observed several days later at radiosonde levels below 30 km., associated with a "sudden warming" of the stratosphere. Data indicate that when these warmings occur, they usually take place over north-central and northeastern Canada near the end of January or the beginning of February, although they have been known to appear any time from December through March.

The 15 July 1958 profile is a Churchill pressure measurement in which pressures were observed from roughly 30 to 50 per cent greater than standard between 40 and 80 km. This represents a profile approximately 10 to 20 per cent greater than the July mean at all levels from 40 to 80 km., also approximately as estimated in Table 2.

5. Diurnal Variations

Estimates of the diurnal variation of pressure can be made through theoretically determined diurnal temperature fluctuations that are associated with the absorption and radiation of solar energy by ozone and carbon dioxide. Murgatroyd and Goody's (1958) and Biriukova and Kastrov's (1961) temperature values were used for altitudes 30 to 80 km. Equal daytime heating and nocturnal cooling were assumed, even though one slightly exceeds the other near the winter and summer solstices. At 50 km. temperature changes of approximately ±5°K for 30°N and ±6°K for 60°N were applied to the mean July temperature-height profiles. Vertical pressure profiles were computed for these estimated daytime and nighttime conditions using the barometric equation. The temperature-height profiles for 30 and 60°N are shown in Fig. 6, and resulting vertical pressure distributions are described in the inserts as percentage departures from the appropriate mean July pressures. Values for January would be of similar magnitude. At lower altitudes, however, systematic pressure variations also are known to occur, attaining roughly ± 0.5 to 0.7 per cent near 20 km. (Harris, et al, 1962). Consequently, pressure deviations above 20 km. may be up to 0.7 per cent larger than the values shown in the figure.

Diurnal pressure fluctuations apparently increase with altitude above 30 km. to at least 80 km., where deviations of ± 8 to 10 per cent approach the seasonal and day-to-day deviations described earlier. This suggests that for heights up to roughly 90 or 100 km., pressure fluctuations are associated primarily with seasonal and latitudinal differences and synoptic events, whereas above these levels they gradually become diurnal in nature, varying with solar angle and solar activity.

These theoretically determined estimates of diurnal pressure fluctuations can be compared with available ARCAS-ROBIN soundings which have been launched primarily at Eglin AFB (30°N). Observations suitable for analysis were obtained at Eglin in May 1961 and October 1960 and 1962. By implementation of the hydrostatic equation, these ROBIN density measurements yield atmospheric pressure values; estimates of root mean square errors are 6 per cent at 60 to 70 km. and 3 per cent at 50 to 60 km. (Lenhard and Kantor, 1965).

May and October daytime and nighttime values for 50 and 60 km. are shown in Fig. 7 as per cent departures from the 30°N July mean pressures. For this analysis, day is considered 1000 through 2000 hr. local standard time and night is 2000 through 1000 hr. Unfortunately, the distribution of observations is uneven, and the number of nighttime values is very small. Nonetheless, it is apparent that mean daytime pressures are higher than mean nighttime pressures at both 50 and 60 km. At 50 km. the mean daytime pressure in May is 6 per cent larger than the mean nighttime value and 6.5 per cent larger at 60 km. Corresponding mean pressure differences for October are roughly 5 and 6 per cent at 50 and 60 km., respectively. The actual diurnal pressure range will be somewhat larger than the indicated 5 to 6.5 per cent since all values were averaged over as many as 8 hr. during the day and up to 13 hr. at night. The extreme observed range shown in the figure is 24 per cent at 60 km. for both May and October. However, these values include root mean square errors of 3 to 6 per cent, so that they appear to compare favorably with the theoretically determined ranges of 8 to 10 per cent at 50 km. and 11 to 13 per cent at 60 km.

6. Summary

1. The largest mean monthly horizontal pressure gradients generally occur in winter between 55 and 65 km. and poleward of 45°N. Pressures may increase by more than 7.2 per cent near 60 km. over distances of 60 n.m. The smallest horizontal pressure changes between 30 and 90 km. occur near 85 km., where the range of mean monthly values is roughly 5 per cent. The greatest mean monthly departures from the Standard Atmosphere occur near 65 km. over arctic and subarctic regions. Departures are approximately 65 per cent of standard in winter and 130 per cent of standard in summer at this altitude, an increase by a factor of two from winter to summer.

2. The largest vertical pressure gradient occurs at the coldest mean temperature through a given layer of the atmosphere. Consequently, the largest mean monthly decrease in pressure with altitude occurs in the 80 to 90 km. layer over arctic and subarctic regions during summer. For these conditions, a mean temperature near 170°K, pressure decreases in the vertical by 18 per cent per km. or 63 per cent in 5 km. For the coldest observed mesospheric temperature, 130°K, the pressure would decrease by 23 per cent, and 73 per cent through 1 and 5 km., respectively.

3. Seasonal, monthly and day-to-day variability of pressure generally increases with altitude to a maximum between 60 and 65 km. At these altitudes, values exceeded less than 5 per cent of the time are up to ± 35 per cent in winter. Variability with latitude increases towards the pole for all heights to roughly 80 km. Smallest percentage changes occur near 85 km. and near the surface. Changes at the surface are smallest in the tropics and subtropics where they decrease to roughly ± 0.5 per cent in summer.

4. Diurnal pressure variations increase with altitude to at least 80 km., probably approaching a range of 16 to 20 per cent at this level near 30 and 60°N, respectively. Available observations for May and October compare favorably with estimated diurnal variability, range roughly 8 to 13 per cent at 50 and 60 km. The time of maximum pressure appears to be between 1400 and 1500 hr. local standard time. All values no doubt include small semidiurnal pressure changes.

REFERENCES

AMS. Lowest measured temperature in earth's atmosphere recorded in US-Sweden experiments. Bull. Amer. Meteor. Soc., 44, 806, 1963.

Biriukova, L.A. and V.G. Kastrov. Diurnal temperature variations in the stratosphere. Meteorol. i. Gidrol., 8, 3-10, 1961.

Cole, A.E. and A.J. Kantor. Air Force interim supplemental atmospheres to 90 kilometers. Air Force Surveys in Geophysics No. 153, AFCRL-63-936, Air Force Cambridge Research Labs., Bedford, Mass., 29 pp. 1963.

Harris, M.F., Finger, F.G. and S. Teweles. Diurnal variation of wind, pressure and temperature in the troposphere and stratosphere over the Azores. J. Atmos. Sci., 19, 136-149, 1962.

Kantor, A.J. and A.E. Cole. Monthly atmospheric structure, surface to 80 km. J. Appl. Meteor., 4, 228-237, 1965.

Lenhard, R.W. and A.J. Kantor. A catalogue of ARCAS-ROBIN soundings. Environmental Research Papers No. 113, AFCRL-65-449, Air Force Cambridge Research Labs., Bedford, Mass., 17 pp. 1965.

McGill University, Arctic Meteorology Group. An atlas of stratospheric circulation. Publication in Meteorology No. 56, Montreal, 1963.

Murgatroyd, R.J. and R.M. Goody. Sources and sinks of radiative energy from 30 to 90 km. Quart. J.R. Meteor. Soc., 84, 225-234, 1958.

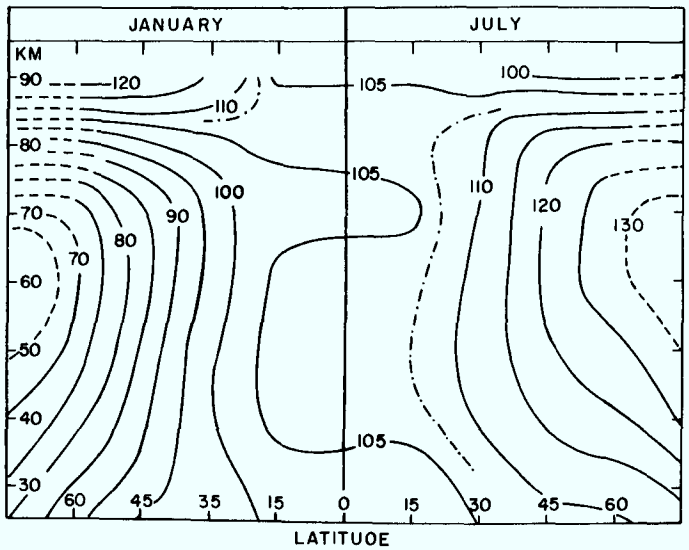

Fig. 1. Mean January and July pressure as per cent of US Standard Atmosphere, 1962.

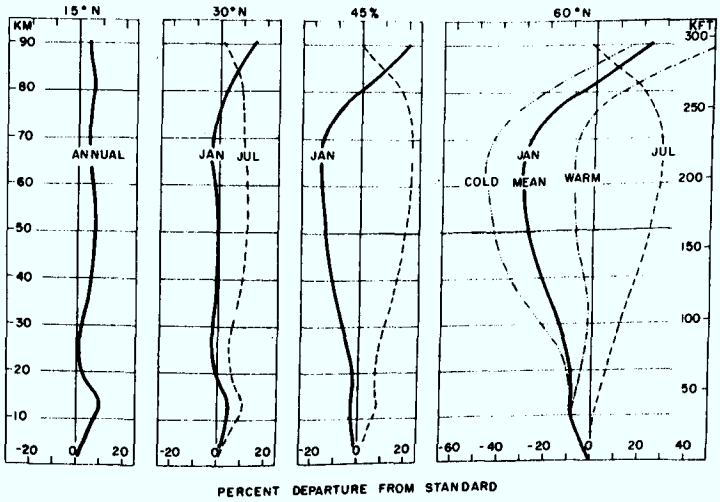

Fig. 2. Per cent departure of pressure of Supplementary Atmospheres from US Standard Atmosphere, 1962.

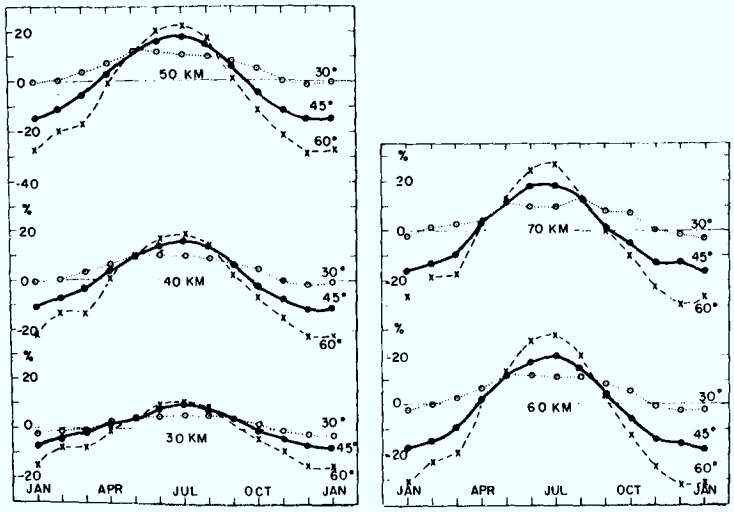

Fig. 3. Annual march of mean monthly pressure, 30, 45 and 60°N, as per cent departure from US Standard Atmosphere, 1962.

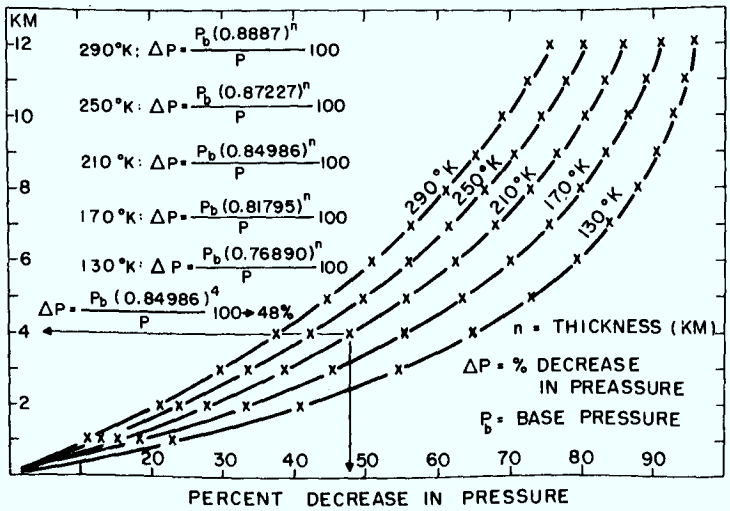

Fig. 4. Per cent decrease in pressure with altitude.

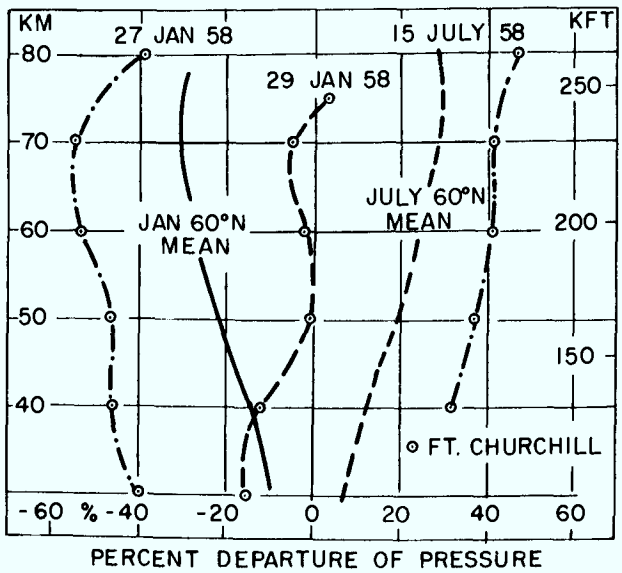

Fig. 5. Observed extreme January and July pressure profiles, Fort Churchill (59°N) as per cent departure from US Standard Atmosphere, 1962.

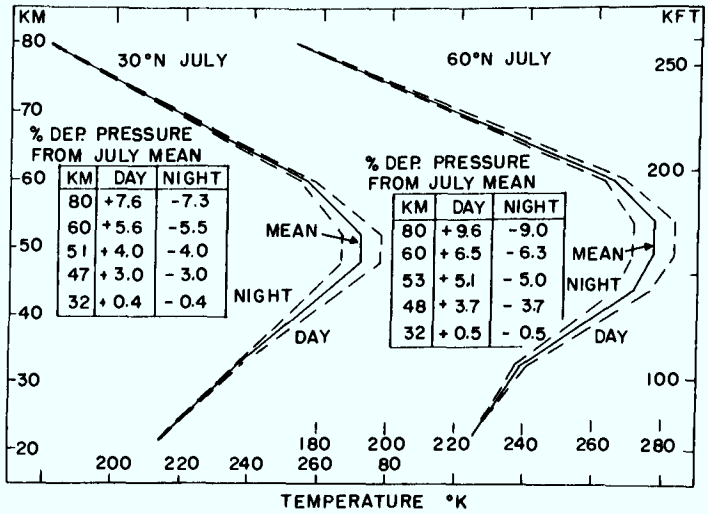

Fig. 6. Theoretical day-night temperature profiles and per cent departure of pressure from mean July values.

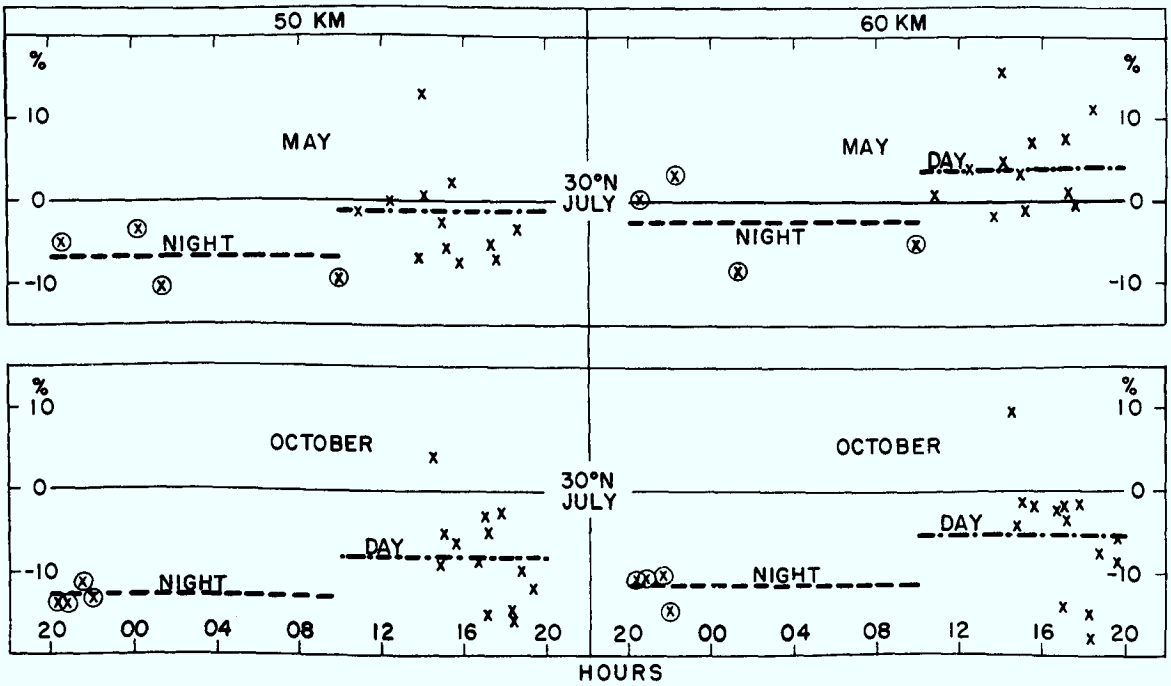

Fig. 7. May and October pressures, Eglin AFB, Florida (30°N), as per cent departure from 30°N mean July values.

Discussion on Paper 1.4 presented by A.J. Kantor

Bibl: Could large vertical and local gradients in pressure and temperature, found during winter, lead to small-scale turbulence in the lower E region in the daytime?

Kantor: They could lead to some small-scale turbulence. We prefer to see turbulence occurring due to changes in temperature rather than just pressure.

Belrose: Could you comment on regimes of correlation one might find during disturbances in winter? The reason for the question is the variability in radio wave absorption in winter months, and people have long been trying to correlate this with meteorological data. Due to absence of data at the higher heights, most of these studies have been correlating radio wave absorption with what is happening at the 10-millibar level which is down near 25 km. Have the meteorologists done any work on the possible correlation between what is happening down there and what is happening above? I gathered from your discussion that there might be no correlation whatsoever with what is happening at 60 km. and what is happening down below.

Kantor: We think of the atmosphere almost like a segmented balloon, and if you squeeze the lower portion it might pop out at some higher portion. We have several things going for us when we are talking about pressure, or temperature, or density. At about 8 km. we have the isopycnic level, where the density remains about the same regardless of time or place. We have another one, we think, at about 90 or 92 km., where the density remains relatively constant for time and space, which would mean that the surface density might increase; and the density then between 8 and 90 km., for example, would decrease, and then above it might increase again. So we have several crossovers, and we also have one quasi-constant in pressure at about 85 km. We think of all these things as being due to temperature, and since the temperatures generally seem to cross at about 60 to 70 km. regardless of season and latitude, this inevitably leads to the crossover in pressure at 85 km. and the crossover that you might have seen in the second figure at 90 or 92 km. There are correlations; the question now is for us to get away from theory and get enough observations between 30 and 100 km. as proof. We have some of these robin balloon observations that we are analyzing now, which will give us some correlations of temperature with temperature, pressure with pressure, density with pressure, and all the other combinations. Then we will have some answers for you.

Volland: I would like to address a question to Dr. Crain in connection with this. The equations of recombination effects are equations of conservation of mass, and yet you neglected the divergence term. What is the influence of this neglected term?

Crain: Any velocity effects on the basic recombination or the basic ionization balance equations are neglected. There is no consideration of dynamic effects at all in terms of air motion.

Volland: How great is the influence?

Crain: It depends on how much air motion there is. At low altitudes, things are very fast compared to any air motions, and at high altitudes they can be very slow compared to air motions. The convection and vertical motions of the atmosphere may be as important as the horizontal motions of the neutral constituents at low altitudes; they are probably unimportant in the ionization balance equations.

Gregory: Tomorrow I might throw a bit of light on the prospects of the motion which must be accompanying those large pressure changes that you mentioned.

Kantor: Are you talking about the seasonal changes or the day-to-day changes?

Gregory: I am talking about the day-to-day winter pressure changes that you mentioned. I would also like to suggest that we use the well-known meteorological unit of pressure, the bar and its sub-multiples, for quoting pressure effects in future. I believe that the only people who should be exempted from this are rocket experimenters who actually send up glass tubes full of mercury.

Kantor: Needless to say, I agree. We have used all the different units, but we prefer the millibar or the metric system.

Bourne: We have some partial reflection data from Ottawa which we believe is giving us collision frequency measurements near the 60-km. level. These measurements extended from 1961 up to the present time, although not continuously. If you look at our winter collision frequencies you find that in 1961 we have value S consistent with the standard profile, but in 1963 and 1964 all our data is significantly different by about a factor of 2.

Kantor: Are they larger or smaller?

Bourne: They are smaller. There would appear to have been a decrease in 1963 and 1964, while in the most recent data we seem to have come back to the 1961-62 level. To a meteorologist, is this factor of 2 a completely unacceptable value for a systematic pressure fluctuation through these winters?

Kantor: First let me clear up one other point. The standard atmosphere that I mentioned is merely a yardstick, and it is supposed to be typical of mean annual conditions at 45°N around the globe, which is pretty encompassing, so you have to be careful how you use that. We can't say that a factor of 2 is impossible but it seems very high. We are getting estimated 2 standard deviations of about ±35 or 40 per cent in that region. However, I might add that if such large fluctuations are going to occur, that would be the most probable altitude for them. I would like to see the data and study it.

Bourne: Some of these results will be presented in a later paper(1).

(1) Belrose J.S., Bourne, I.A. and L.W. Hewitt. A preliminary investigation of diurnal and seasonal changes in electron distribution over Ottawa, Churchill and Resolute Bay as observed by partial reflections. Fig. 15, these Proceedings, 1966.

1.5 ELECTRON TEMPERATURES IN THE D REGION

by

A. Dalgarno* and R.J.W. Henry+

*Department of Applied Mathematics, The Queen's University of Belfast
+Goddard Space Flight Center, Greenbelt, Maryland

Presented by A. Dalgarno

Detailed estimates are made of the rates of energy loss of electrons moving in the D region and it is argued that the electron gas has a negligible non-thermal component. The Maxwellian velocity distribution of the thermal component is brought about by collisions with molecular nitrogen involving rotational transitions and the distribution is determined by the neutral particle gas temperature.

1. Introduction

It is customary in analysing radio wave measurements in the D region to assume that the electrons have a Maxwellian velocity distribution characterized by an electron temperature T_e equal to the temperature T_g of the ambient neutral particle atmosphere. Evidence has accumulated in recent years that equality of electron and neutral particle temperatures does not prevail in the upper ionospheric regions (Boggess, Brace and Spencer 1959; Spencer, Brace and Carignan 1962; Brace, Spencer and Carignan 1963; Bowen, Boyd, Henderson and Willmore 1964; Evans and Loewenthal 1964; Brace, Spencer and Dalgarno 1965) and there have been suggestions that T_e exceeds T_g in the D region also. Thus from observations of cross-modulation, Rumi (1962) has derived an electron temperature of 1200°K at an altitude of 40 km. and Belrose and Hewitt (1964) have suggested that the collision frequency in the D region is correlated with solar activity, the correlation arising through variations of T_e and not of T_g. A tentative theory has been advanced by Sears (1963) which lends support to these observations, but we shall argue the contrary view.

2. Energy Loss Processes in the D Region

Fast electrons lose energy rapidly in the D region by exciting and ionizing the atmospheric constituents until their energy falls to about 7 eV. Below 7 eV energy is lost mainly in vibrational and rotational excitation of nitrogen and oxygen and in elastic collisions.

The cross sections $\sigma(0,\upsilon|E)$ for vibrational excitation of nitrogen by electrons of energy E

$$e+N_2(0)\rightarrow e+N_2(\upsilon) \qquad (1)$$

have been measured by Schulz (1964), and Chen (1964) has presented a theory which closely reproduces the measurements. The associated rate of energy loss for unit density of molecular nitrogen is

$$\frac{dE}{dt}=\left(\frac{2E}{m}\right)^{\frac{1}{2}}\sum_{\upsilon}\Delta(0,\upsilon)\sigma(0,\upsilon|E), \qquad (2)$$

where $\Delta(0,\upsilon)$ is the internal energy change occurring in the process. The rate of energy loss through vibrational excitation of N_2 is shown in Fig. 1 as a function of impact energy.

There is considerable uncertainty about the cross sections for vibrational excitation of molecular oxygen. Schulz and Dowell (1962) have measured a cross section at an energy of 0.3 eV of about 10^{-18} cm.^{2} which is an order of magnitude smaller than that derived by Phelps (1963) from an analysis of swarm data. The cross sections derived by Phelps are consistent with the energy loss rates in oxygen, shown in Fig. 1. There is also considerable uncertainty

about the cross sections for the excitation of the low lying electronic levels of molecular oxygen and we shall suppose that the oxygen curve of Fig. 1 includes also the contributions from electronic excitation processes.

To calculate the rate of energy loss associated with rotational transitions in molecular nitrogen

$$e+N_2(j)\rightarrow e+N_2(j'), \qquad (3)$$

we have employed the cross sections $\sigma(j,j'|E)$ computed by Dalgarno and Moffett (1963) who used the Born approximation and took into account the quadrupole interaction (Gerjuoy and Stein 1955) and the polarization interaction. By means of the distorted wave approximation (cf. Arthurs and Dalgarno 1960), attempts have been made to include the distorting effects of the long range polarization (Takayanagi and Geltman 1964; Mjolness and Samson 1964, 1965) but there remains considerable arbitrariness in the final results. The calculations of Dalgarno and Moffett are in reasonable harmony with the analysis of swarm data by Engelhardt, Phelps and Risk (1964).

The rate of energy loss for unit density of nitrogen at a temperature T_g is given by

$$\frac{dE}{dt}=\left(\frac{2E}{m}\right)^{\frac{1}{2}} \frac{\sum_{jj'}\sum \Delta(j,j')\sigma(j,j'|E)\ (2j+1)\exp[-Bj(j+1)/kT_g]}{\sum_j (2j+1)\exp[-Bj(j+1)/kT_g]}, \qquad (4)$$

where B is the rotational constant. Values of (4) are given in Fig. 2 for $T_g = 200^\circ K$.

We have carried out similar calculations for molecular oxygen, using the quadrupole moment and polarization anisotropy measured by Bridge and Buckingham (1964) and the values of dE/dt for electrons in molecular oxygen are also presented in Fig. 2.

The values of dE/dt in oxygen are much smaller than those measured by Mentzoni and Rao (1965) and Takayanagi and Geltman (1966) suggest that the short range forces (ignored in calculating Fig. 2) are very effective in causing rotational excitation of oxygen.

Energy can be lost in elastic collisions, the energy loss rate being

$$\frac{dE}{dt} = -\frac{2m}{m}\left(\frac{2E}{m}\right)^{\frac{1}{2}} Q_m(E - \frac{4}{3}E_g), \qquad (5)$$

where E_g is the thermal energy of the gas, M is the mass of the molecule and Q_m is the momentum transfer cross section. For nitrogen accurate values of Q_m have been derived by Engelhardt et al. (1964) and for oxygen less accurate values have been suggested by Phelps (1963). It follows from them that energy loss in elastic collisions with molecules is negligible compared to loss through rotational transitions.

In the upper ionospheric regions energy loss in elastic collisions with the ambient electrons is an important mechanism for preferentially heating the ambient electron gas and maintaining T_e above T_g (Hanson and Johnson 1961; Dalgarno, McElroy and Moffett 1963). If n_e cm^{-3} is the ambient electron density, the rate of energy loss by elastic electron-electron collisions is given approximately by

$$\frac{dE}{dt} = -\frac{7.7\times 10^{-6}}{E^{\frac{1}{2}}}\, n_e \ln\Lambda \, eVs^{-1}, \qquad (6)$$

where Λ depends upon n_e and T_e, and E is measured in eV (Butler and Buckingham 1962; Dalgarno et al. 1963). Values of $\ln\Lambda$ for various electron temperatures and densities are given in Table 1. The electron density in the D region rarely approaches 10^5 cm^{-3} even during periods of severe disturbance and an effective upper bound to (6) is accordingly

$$\left|\frac{dE}{dt}\right| < \frac{11}{E^{\frac{1}{2}}}\, eVs^{-1}. \qquad (7)$$

A comparison of (7) with the rate of energy loss from vibrational and rotational excitation of nitrogen and oxygen is given in Fig. 3 for electrons moving with energies of 1, 0.1 and 0.03 eV in the D region. It is clear that electron-electron interactions are rarely of any importance in the D region. The main mechanisms tending to establish equilibrium consist of rotational transitions in molecular nitrogen and oxygen so that if the electrons in the D region have a Maxwellian velocity distribution it will be characterized by the neutral particle gas temperature T_g.

TABLE 1

n_e (cm^{-3}) / T_e (^oK)	... 10	10^2	10^3	10^4	10^5	10^6	10^7
200	16.2	15.1	13.9	12.8	11.6	10.4	9.3
300	16.8	15.7	14.5	13.4	12.2	11.1	9.9
400	17.3	16.2	14.9	13.9	13.9	12.6	10.3
500	17.6	16.4	15.3	14.1	13.0	11.8	10.7
1000	18.6	17.5	16.3	15.2	14.0	12.9	11.7

Values of ln Λ (EQN.(6))

3. Production and Loss Mechanisms

The velocity distribution of the D region electrons depends on the electron production and removal mechanisms*. According to a recent review by Reid (1964a), the normal D region is produced by the absorption of Lyman α by nitric oxide and by the absorption of x-rays and cosmic rays. During disturbed conditions at middle and low latitudes, the flux of incident x-rays is enhanced, and at high latitudes an additional source of ionization is present, auroral absorption being due primarily to bombarding electrons and polar cap absorption to bombarding solar protons.

The fast electrons produced by the primary ionization processes lose energy rapidly. Some are removed by the two-body dissociative attachment process

$$O_2+e \rightarrow O^- + O, \qquad (8)$$

which has a peak cross section of about 1.4×10^{-18} cm^2 at an energy of about 6.5 eV (Buchelnikova 1959; Schulz 1962; Asundi, Craggs and Kurepa 1963), but most are removed by the three-body attachment process

$$O_2+O_2+e \rightarrow O_2^- + O_2, \qquad (9)$$

the rate of which has been measured by Chanin, Phelps and Biondi (1959).

A comparison of the mean times for energy loss associated with vibrational and rotational transitions and elastic scattering with the mean times for attachment is given in Fig. 4 as a function of energy for a neutral particle density of 10^{15} cm^{-3} (appropriate to an altitude of 70 km.) and in Figs. 5, 6 and 7 as a function of altitude for energies of respectively 1, 0.1 and 0.03 eV. The energy loss times are in all cases much shorter than the attachment times. Thus nearly all the electrons are converted into thermal electrons before their removal by attachment and the removal mechanism has little effect on the electron velocity distribution. The thermal electrons will have a Maxwellian velocity distribution characterized by the gas temperature T_g. Superimposed upon the thermal distribution there will be a small high energy component, the magnitude of which is enhanced by photodetachment.

4. Non-Thermal Electrons

After an electron attaches to form a negative ion, it is soon detached by the absorption of solar radiation. If the major negative ion is O_2^-, the free electron has an initial energy peaking at about 2 eV. This supply of 2 eV electrons in the

* We are ignoring the effects of electric fields and winds.

daytime D region is much larger than that provided by the primary ionization processes and it may give rise to a substantial non-thermal component in the velocity distribution (Sears 1963).

An estimate of the non-thermal component of the velocity distribution can be made by equating the number of electrons entering the energy interval dE in unit time to the number leaving it. Then if $f_a(E)\,dE$ is the number of electrons with energies lying between E and E + dE,

$$f_a(E) = -\sum_{E'} E\,q(E') \Big/ \frac{dE}{dt}, \qquad (10)$$

where q(E') is the rate of production of electrons of energy E'.

The shape of the distribution function corresponding to the O_2^- photodetachment source may be derived from the measured cross sections (cf. Branscomb 1964) and it is shown in Fig.8. The figure demonstrates the efficiency with which electrons with energies between 2 and 3 eV are degraded through exciting vibrational levels of nitrogen.

In equilibrium, the total number of non-thermal electrons with energies greater than 0.03 eV is approximately

$$n_a = \frac{3 \times 10^{11} n(O_2^-)}{N}\ \mathrm{cm}^{-3}, \qquad (11)$$

where $n(O_2^-)$ is the number density of O_2^- and N is the number density of neutral particles. The number varies inversely as N because the rate at which an electron loses energy is directly proportional to N. This has the simple consequence that the contribution of the non-thermal component to the collision frequency

$$\nu_a = \int f_a(E)\,\nu(E)\,dE/n_e \qquad (12)$$

depends upon altitude through the number density of negative ions only. The actual value of ν_a is given by

$$\nu_a = 7 \times 10^3\ \lambda s^{-1}, \qquad (13)$$

where λ is the ratio $n(O_2^-)/n_e$. It is negligible compared to the collision frequency ν_e of the thermal electrons. Thus at an altitude of 75 km., $\lambda \sim 1$, $\nu_a \sim 7 \times 10^3 s^{-1}$ and $\nu_e \sim 2 \times 10^6 s^{-1}$ and at 40 km., $\lambda \sim 100$, $\nu_a \sim 7 \times 10^5 s^{-1}$ and $\nu_e \sim 1 \times 10^8 s^{-1}$.

The contribution of the non-thermal component to radio wave absorption relative to that of the thermal component is still smaller since absorption of waves of frequency ω is controlled by the expression $n_e\nu/(\nu^2 + \omega^2)$, which at high energies and at low altitudes reduces to $n_e\nu^{-1}$.

Both the thermal and non-thermal components of the velocity distribution will be enhanced during distrubances in the D region. Because fast electrons slow down very rapidly, the shape of the distribution function of the additional non-thermal electrons will be closely similar to that shown in Fig. 8. If q $\mathrm{cm}^{-3}s^{-1}$ is the production rate of non-thermal electrons, we find that $n_e\nu_a \sim 10^4 q\ \mathrm{cm}^{-3}s^{-1}$.

During a strong auroral absorption event, q may be of the order of 10^4 so that $n_e\nu_a \sim 10^8\ \mathrm{cm}^{-3}s^{-1}$. With a radio frequency of 30 Mc/s, an absorption of about 0.001 db results from an altitude extent of 10 km., which is negligible compared to the measured absorption of greater than 1 db.

The contribution of non-thermal electrons to polar cap absorption similarly is less than 0.1% of the contribution of the thermal component and it appears unlikely that non-thermal electrons are significant in the quiet or disturbed D region.

The correlation between solar activity and collision frequency suggested by Belrose and Hewitt (1964) may perhaps be ascribed to variations of atmospheric pressure (Aikin, Kane and Troim 1964).

4.1 Auroral E Region

The velocity distribution of the low energy non-thermal electrons produced during an aurora is similar to that of Fig. 8 except that energy loss through excitation of the ^1D level of atomic oxygen causes some depletion of the electrons with energies above 2 eV and elastic collisions with the ambient electrons causes some depletion of the electrons with energies less than 1 eV. We may use our calculations to obtain an estimate of the contribution of non-thermal electrons to radio wave absorption during an aurora.

Visual auroras are classified according to an international brightness coefficient, I.B.C. θ and in a typical aurora located in the region of 105 km. the electron production rate is approximately $10^{3+\theta}\text{cm}^{-3}\text{s}^{-1}$ and the equilibrium electron concentration is $3 \times 10^{4+\frac{1}{2}\theta}$ cm^{-3} (cf. Dalgarno 1965; Ulwick, Pfister, Haycock and Baker 1965). The contribution of the non-thermal electrons to the parameter $n_e\nu$, which controls radio wave absorption in the E region, is about $3 \times 10^{7+\theta}\text{cm}^{-3}\text{s}^{-1}$ and the contribution of the thermal component is about $10^{9+\frac{1}{2}\theta}$. Thus the two contributions become comparable for an aurora of brightness I.B.C.III. The actual absorption is not large but Reid (1964b) has suggested that for brief periods during bright auroras the non-thermal absorption may be detectable.

5. Cooling in the D Region

If the electron gas in the D region is heated preferentially so that T_e exceeds T_g it will cool mainly by rotational excitation of molecular nitrogen if T is less than 1300°K and by vibrational excitation of molecular nitrogen if T_e exceeds 1300°K. The rate of cooling through rotational excitation may be derived from calculations by Dalgarno and Moffett (1962) and by Altshuler (1963). It is given approximately by

$$\frac{dT_e}{dt} = -\frac{2 \times 10^{-10}(T_e - T_g)}{T_e^{\frac{1}{2}}} N \text{ degKs}^{-1} \qquad (14)$$

where N is the N_2 density. Values of the cooling rate for a gas temperature of 200°K are given in Table 2. The rate of cooling through vibrational excitation may be derived from calculations by Chen (1964). Values of it are given in Table 2.

TABLE 2

T_e (°K)	200	300	500	1000	1500	2000
rotational (T_g = 200°K)	0	1×10^{-9}	3×10^{-9}	5×10^{-9}	7×10^{-9}	9×10^{-9}
vibrational	3×10^{-15}	8×10^{-13}	8×10^{-11}	2×10^{-9}	9×10^{-9}	2×10^{-8}

Cooling Rates – $(1/N)\,(dT_e/dt)$ for Rotational and Vibrational Excitation.

The electron temperature of 1200°K derived by Rumi (1962) at an altitude of 40 km. implies, according to Table 2, an energy deposition into the electron gas of the order of 10^7 eV $\text{cm}^{-3}\text{s}^{-1}$ for an electron density of 10^2cm^{-3}. Such an energy deposition rate seems unacceptably large and the interpretation of Rumi's observations through an enhanced electron temperature is implausible.

6. Electric Fields

Walker (1966) has demonstrated recently that electric fields in the D region cannot cause the electron temperature to rise significantly above the neutral particle temperature. A significant difference between T_e and T_g requires an electric field of at least 3.5×10^{-4} V cm^{-1}. The production of such a field by induction requires a neutral wind of at least 700 cm sec^{-1}.

The research reported in this paper has been sponsored in part by the Air Force Cambridge Research Laboratories OAR under Contract AF61(052)–780 with the European Office of Aerospace Research, United States Air Force and in part by the National Aeronautics and Space Administration.

REFERENCES

Aikin, A.C., Kane, J.A. and J. Troim. J. Geophys. Res., 69, 4621, 1964.

Altshuler, S. J. Geophys. Res., 68, 4707, 1963.

Arthurs, A.M. and A. Dalgarno. Proc. Roy. Soc. A, 256, 540, 1960.

Asundi, R.K., Craggs, J.D. and M.V. Kurepa. Proc. Phys. Soc., 82, 967, 1963.

Belrose, J.S. and L.N. Hewitt. Nature, Lond., 202, 267, 1964.

Bowen, P.J., Boyd, R.L.F., Henderson, C.L. and A.P. Willmore. Proc. Roy. Soc. A, 281, 514, 1964.

Brace, L.H., Spencer, N.W. and G.R. Carignan. J. Geophys. Res., 68, 5397, 1963.

Brace, L.H., Spencer, N.W. and A. Dalgarno. Planet. Space Sci., 13, 647, 1965.

Branscomb, L.M. Ann. Geophys., 20, 49, 1964.

Bridge, N.J. and A.D. Buckingham. J. Chem. Phys., 40, 2733, 1964.

Buchelnikova, I.S. Soviet Phys., (J.E.T.P.) 35, 783, 1959.

Boggess, R.L., Brace, L.H. and N.W. Spencer. J. Geophys. Res., 64, 1627, 1959.

Butler, S.T. and A.D. Buckingham. Phys. Rev. 126, 1, 1962.

Chanin, L.M., Phelps, A.V. and M.A. Biondi. Phys. Rev. Lett., 2, 344, 1959.

Chen, J.C.Y. J. Chem. Phys., 40, 3507; 3513; also private communication, 1964.

Dalgarno, A. Auroral phenomena (ed. M. Walt). Stanford University Press. 1965.

Dalgarno, A., McElroy, M.B. and R.J. Moffett. Planet. Space Sci., 11, 463, 1963.

Dalgarno, A. and R.J. Moffett. Planet. Space Sci., 9, 439, 1962.

Dalgarno, A. and R.J. Moffett. Proc. Nat. Acad. Sci. India, A, 33, 511, 1963.

Engelhardt, A.G., Phelps, A.V. and C.G. Risk. Phys. Rev., 135, A, 1566, 1964.

Evans, J.V. and M. Loewenthal. Planet. Space Sci., 10, 905, 1964.

Gerjuoy, E. and S. Stein. Phys. Rev. 98, 1848, 1955.

Hanson, W.B. and F.S. Johnson. Mem. Soc. Sci. Liège, Series 5, 4, 390, 1961.

Mentzoni, M.H. and N.K.V. Rao. Phys. Rev. Lett., 14, 779, 1965.

Mjolness, R.C. and D.H. Samson. Phys. Rev. Lett., 13, 812, 1964.

Mjolness, R.C. and D.H. Samson. Phys. Rev. Lett., 14, 89, 1965.

Phelps, A.V. Westinghouse Rep. 63-928-113-P6, 1963.

Reid, G.C. Rev. Geophys., 2, 311, 1964a.

Reid, G.C. J. Geophys. Res., 69, 3296, 1964b.

Rumi, G.C. I.R.E. Trans. Antennas Propag., 10, 594, 1962.

Schulz, G.J. Phys. Rev., 128, 178, 1962.

Schulz, G.J. Phys. Rev. 135, A, 988, 1964.

Schulz, G.J. and J.T. Dowell. Phys. Rev., 128, 174, 1962.

Sears, R.D. J. Geophys. Res., 68, 5135, 1963.

Spencer, N.W., Brace, L.H. and G.R. Carignan. J. Geophys. Res., 67, 157, 1962.

Takayanagi, K. and S. Geltman. Phys. Lett., 13, 135, 1964.

Takayanagi, K. and S. Geltman. Phys. Rev., (in press), 1966.

Ulwick, J.C., Pfister, W., Haycock, O.C. and K.D. Baker. Space Research V. (ed. P. Muller) North-Holland: Amsterdam, 1965.

Walker, J.C.G. Planet. Space Sci. (in press), 1966.

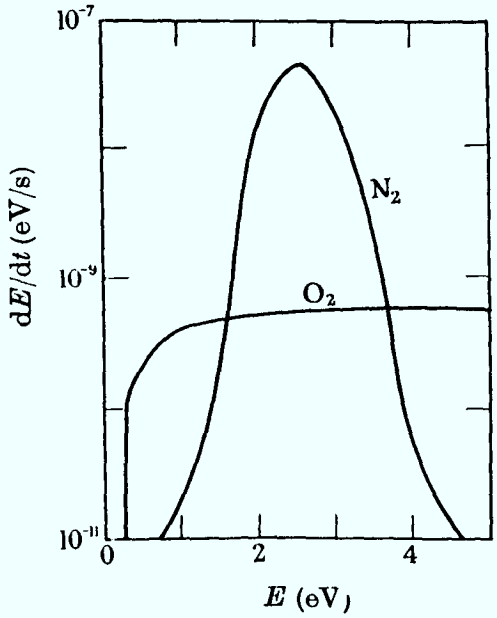

Fig. 1. Rates of energy loss through vibrational excitation of nitrogen and oxygen.

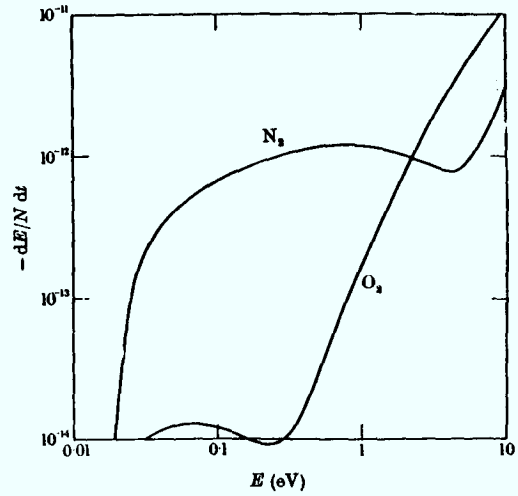

Fig. 2. Rates of energy loss through rotational excitation of nitrogen and oxygen.

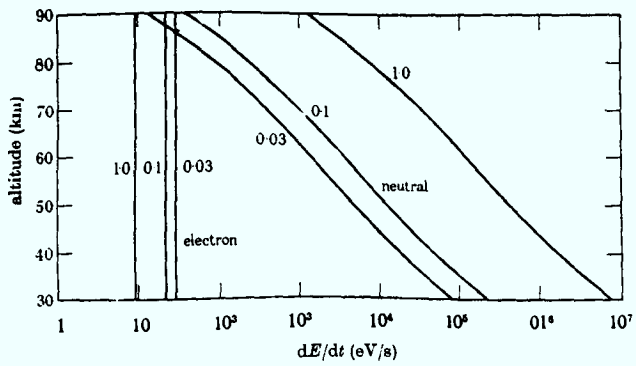

Fig. 3. Rates of energy loss in collisions with ambient electrons and with neutral particles for incident electrons with energies of 1, 0.1 and 0.03 eV.

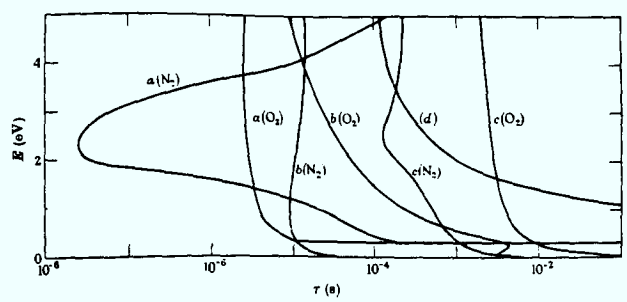

Fig. 4. Mean times for energy loss associated with (a) vibrational transitions, (b) rotational transitions, (c) elastic scattering and (d) the mean times for attachment as a function of incident energy at an altitude of 70 km.

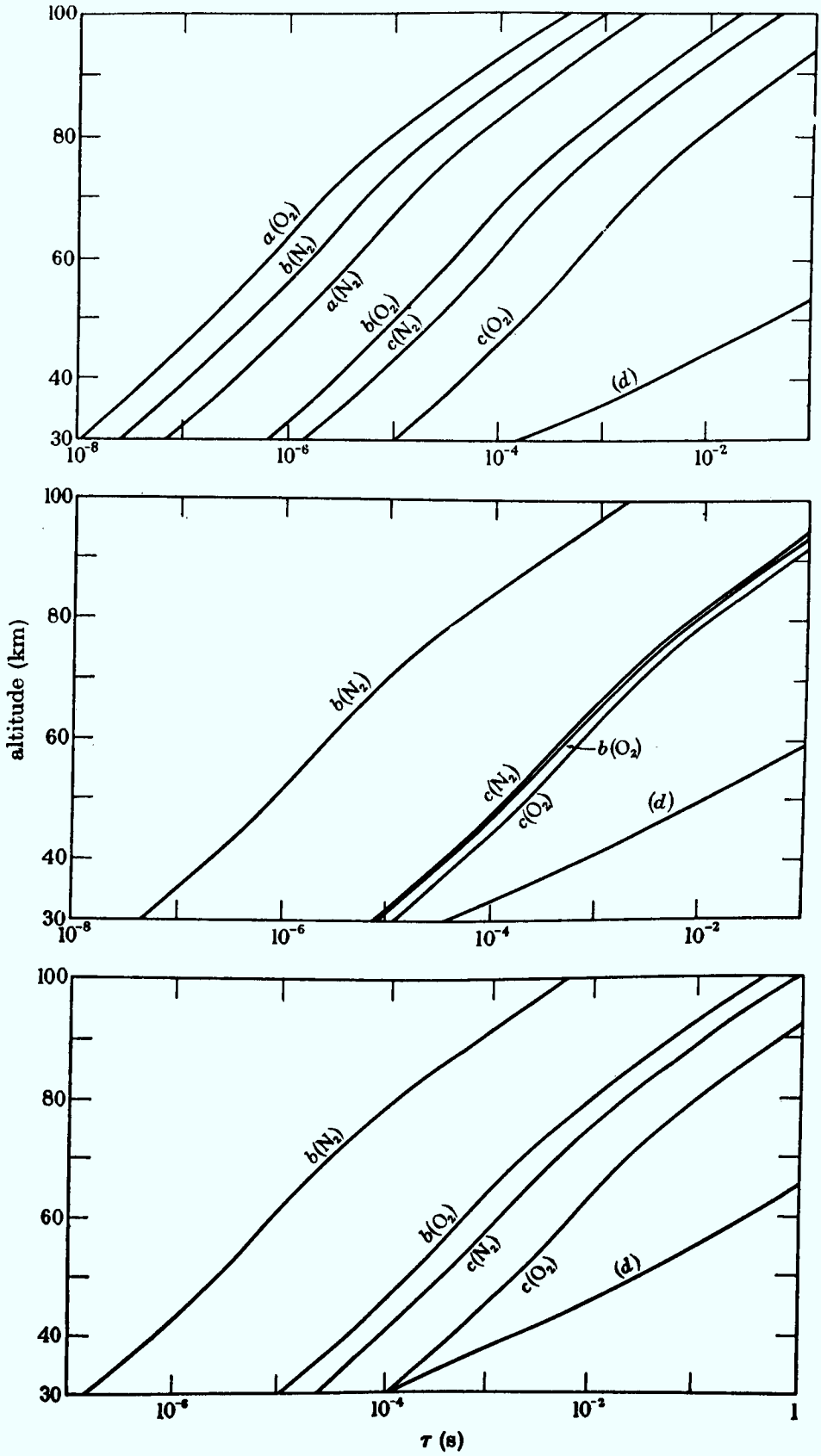

Figs. 5 to 7. Mean times as for Fig. 4 as a function of altitude for incident energies of 1 eV. (Fig. 5), 0.1 eV. (Fig. 6) and 0.03 eV. (Fig. 7).

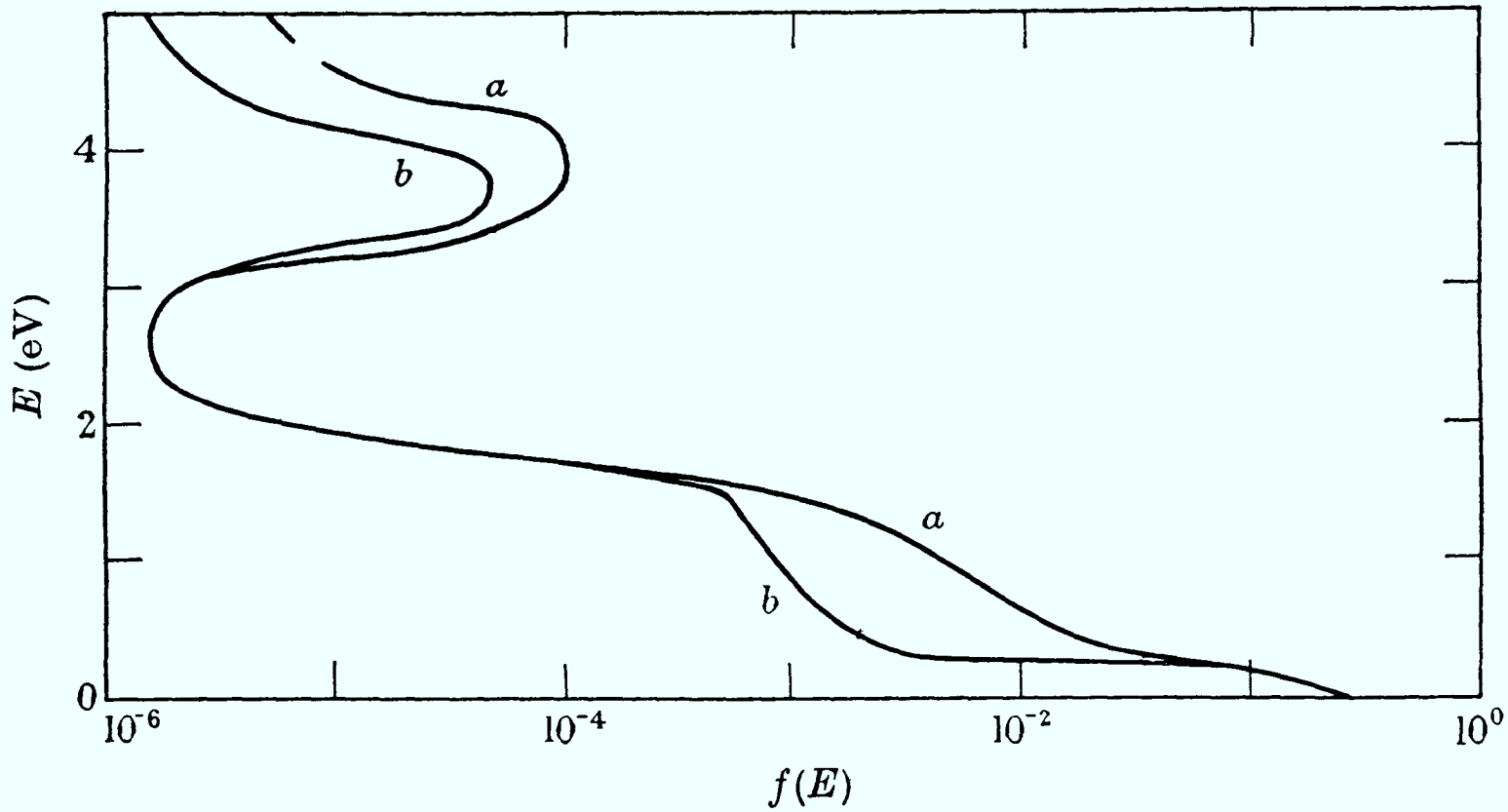

Fig. 8. The distribution function of the non-thermal electrons, ignoring vibrational excitation of oxygen (curve a), and including it (curve b).

Discussion on Paper 1.5 presented by A. Dalgarno

Gregory: Would you clarify that attachment time that you mention; does it refer to the mean lifetime of attachment?

Dalgarno: If the electron density is written as approximately $\frac{dNe}{dt} = -a$ etc., the time $1/a$ is that time. It is the half-life of the electron for attachment.

Zimmerman: Do you expect these high-energy electrons above 90 or 110 km.?

Dalgarno: Yes.

Zimmerman: I am not too familiar with all the data, but would they not have been observed by people who have done spectral analysis of these high-energy electrons with probes?

Dalgarno: When you are talking about measuring high-energy electrons you mean 10 kev. at least. When I am talking about high-energy electrons I mean 10 eV.

Aikin: I believe there are electron temperature measurements in the lower E region which do seem to exceed the gas temperature, but they are not generally talked about.

Dalgarno: Let me talk about them. I have an inborn suspicion of the theories of the experiments for those, especially on rockets. I do not say those measurements are wrong, I just do not understand them. If I accept those rocket data and calculate the heat input that they imply, and use that by any reasonable extrapolation in the D region, then the temperature difference again goes to zero; so they are at least consistent with what I have been discussing. I do not understand what the heat mechanism is. Maybe it is the electric field. The electric field discussion I am talking about is in the D region and there the argument is quite direct, but the E region gets a little more complicated. Perhaps Mr. Megill might have something to say.

Megill: If you stretch things pretty hard, you might possibly talk about a factor of 2 increase in electron temperature in the E region during auroral electrojets or something of this sort, but you are pushing pretty hard.

1.6 A SURVEY OF LABORATORY DATA FOR SLOW ELECTRONS IN AIR, NITROGEN, AND OXYGEN RELEVANT TO WAVE PROPAGATION AND WAVE INTERACTION IN THE LOWER IONOSPHERE

by

R.A. Smith

University of New England, Armidale, New South Wales, Australia

1. Introduction

In recent years considerable complication to the interpretation of radio propagation in the lower ionosphere, where collisions are important and may be dominant, has been added by the introduction of generalized magneto-ionic theories, which evaluate the conductivity matrix for a Maxwellian distribution of electron speeds and for a specified relation A(c) between the collision cross-section A and the electron speed c. The generalized theory of Sen and Wyller (1960) is based on a linear A(c) relation and its use in place of the simpler theory of Appleton and Hartree is now accepted. This major change in practice was initiated by claims (Phelps and Pack 1959, Huxley 1959) that the linear relation observed in the laboratory for thermal electrons in nitrogen would also apply in air and that radio measurements of collision frequency using rockets could then be made to agree with collision frequencies calculated from atmospheric and laboratory data (Phelps and Pack 1959).

One consequence in the study of the lower ionosphere of a change in magnetoionic theory is that it means the virtual abandonment of many previous results. This is particularly the case for electron densities derived from partial reflection and pulse wave interaction experiments, since the densities are not simply related to the raw data. On account of the role being played by these experiments in current research on the D region, it is highly desirable for the accuracy of the Sen and Wyller magnetoionic theory to be established unequivocally before the present major effort using these techniques is too advanced.

A further reason relates to gas temperature, which in the lower ionosphere varies considerably with height and at some heights is subject to large changes with season and with latitude. Should, as a result of collisions with oxvgen, the correct A(c) relation in air be non-linear, gas temperature would be an explicit parameter in a correct dispersion equation for wave propagation in the lower ionosphere and failure to allow for it would lead to errors in the electron density profile and, possibly, to incorrect interpretations of physical phenomena.

In this paper, laboratory data on the motions of electrons in air, oxygen, and nitrogen are examined from the viewpoint of one who recognizes the achievements in nitrogen and the difficulties of experimentation in the attaching gases, air and oxygen, but who feels that if the nature and importance of the problems were recognized, much could be done in the laboratory using existing techniques to provide a sound base for magnetoionic theory and to clarify aspects of energy losses at collisions needed in the study of radio wave interaction.

Results on the properties of electrons in air obtained at the University of New England from radio wave interaction measurements are described in Paper 3.2.1.

2. Drift velocity and diffusion data for air, nitrogen and oxygen

Except for the observations of Mentzoni (1965) and Veatch et al. (1965) to be described in Section 3, the experimental data for air, nitrogen and oxygen that we need to consider have been obtained using the diffusion methods introduced by Townsend. These methods are described in a well-known treatise by Healey and Reed (1941) and in a review article by Huxley and Crompton (1962), which summarizes recent theoretical developments.

The two quantities measured are the velocity of drift W of the electron swarm under a steady electric field E and the ratio W/D of W to the diffusion coefficient D. The measurement of W/D yields, provided the electron distribution function is assumed, the values of the Townsend energy factor k (= U/U_0, where U is the mean energy of the electron swarm and U_0 is the thermal energy of the gas) and the mean electron speed $\bar{c}$. By combining the measurement of W/D with the measurement of W, the mean collision frequency ν, the mean collision cross-section $\bar{A}$ and the mean energy η lost at a collision with a gas molecule can be derived. The properties of the electron swarm at a fixed gas temperature are functions of the parameter E/p, where p is the gas pressure, and the distribution function is usually assumed, as is done here, to be Maxwellian.

Historically, the problem of the behavior of near-thermal electrons in air first arose in the study of radio wave interaction. In their mathematical theory of this phenomenon Bailey and Martyn (1934), by extrapolation of the data ($k \geqslant 5.7$) of Townsend and Tizard (1913), adopted the hypothesis that the mean free path is approximately constant (i.e. $A \neq$ constant) and the hypothesis that

$$\eta = G(U-U_0) \tag{1}$$

where G is a constant of value $\sim 2.6 \times 10^{-3}$. In support of the form of (1) Bailey and Martyn invoked the theory of Pidduck (1915) of the motions of electrons in a gas, whose molecules behave as imperfectly elastic spheres. The Bailey and Martyn theory, with $G \sim 2 \times 10^{-3}$ and wave propagation discussed in terms of the Appleton-Hartree magneto-ionic theory, has had remarkable success in accounting for wave interaction observations made under a wide variety of experimental conditions.

In 1953 Crompton, Huxley and Sutton (C.H.S.) combined their measurements of W/D in air ($k \geqslant 4.0$) with the measurements of W ($k \geqslant 5.4$) made in 1937 by Nielsen and Bradbury (N.B.). They proposed the hypothesis that the collision cross-section of near-thermal electrons in air is proportional to the electron speed c and, as an alternative to (1), an energy loss formula which was subsequently withdrawn by Huxley (1955). The first of these hypotheses, being an unsubstantiated extrapolation over a large range of k, made little impact at the time, although it is now widely accepted on grounds to be discussed later.

On account of its importance to radio wave interaction and the study of the lower ionosphere generally, considerable effort has been made in the past decade to place knowledge of the behavior of near-thermal electrons in air on a sounder basis. This effort has been hampered by the apparent impossibility of making reliable measurements of W and W/D in the attaching gases, air and oxygen, when the value of the energy factor k is below about 5, but in nitrogen, the numerically major constituent of air, precise measurements have been made virtually to the thermal energy at room temperature. Near-thermal measurements in nitrogen have also been made at a temperature of 77°K.

Measurements of W and W/D for electrons in air, nitrogen, and oxygen we consider are as follows:

Air: W/D — Bailey (1925) ($k \geqslant 6.1$, 288°K); Crompton et al. (1953) ($k \geqslant 4.0$, 288°K); Rees and Jory* (1964) ($k \geqslant 10$, 293°K)
W — Nielsen and Bradbury (1937) ($k \geqslant 5.4$, 288°K)

Nitrogen: W/D — Warren and Parker (1963) ($k_{min} \sim 1.1$, 77.4°K); Crompton and Elford (1963, also see Appendix) ($K \geqslant 1.04$, 293°K)
W — Lowke *(1963a) (293°K, 77.6°K, $k_{min} < 1.05$)

Oxygen: W/D — Crompton and Sutton ($k \geqslant 4.7$, 288°K; see Appendix); Rees* (1965) ($k \geqslant 7.45$, 293°K)
W — Nielsen and Bradbury (1937) ($k \geqslant 8$, 288°K)

In brackets after each reference we give the temperature T_g of the gas and the lowest value of k. In the case of W, the lowest value of k has been estimated from the accompanying W/D data. The list of references is not comprehensive and has been selected as follows:

Only measurements of W by the use of electrical shutters are included, since this method can be more accurate than any other (Huxley and Crompton 1962). On this ground we have omitted for air the measurements of W by Townsend and Tizard (1913) and by Huxley and Zaazou (1949), which were obtained by the method of magnetic deflection. For air we have also omitted the measurements of W/D by these groups, since Townsend (1948) has attached greater weight to the W/D measurements of Bailey than to the measurements of Townsend and Tizard, and in the apparatus of Huxley and Zaazou the source and diffusion chambers were apparently insufficiently screened from each other (C.H.S.). Apart from these omissions, the list of references for air is comprehensive. For nitrogen and oxygen we have preferred, where available, measurements by Crompton and his colleagues (indicated in the list of references by an asterisk) at the Australian National University, Canberra, where the experimental techniques have been highly developed. For nitrogen, we have not listed, but give in the Appendix, the superseded measurements of W/D by Crompton and Sutton (1952) and the widely quoted, but unpublished, measurements of W and W/D by Crompton and Hall. The work of Phelps and his colleagues is referred to below. A comprehensive list of references to data for oxygen and nitrogen obtained before 1961 by a variety of methods has been given by Shkarofsky et al. (1961).

In air the agreement between the three sets of measurements of W/D (i.e. of k) is excellent for $E/p \geqslant 0.6$, the minimum value of this parameter in the experiments of Rees and Jory (see Fig. 5 and the Appendix). The measurements of Bailey and of C.H.S. were made to lower values of E/p and progressively diverge to produce, as will be shown later, marked differences in interpretation and in extrapolation to the thermal energy.

Huxley (1959), using the W and W/D data of Crompton and Hall (T_G = 288°K), found that in the range $1 < k < 4$ in nitrogen the collision cross-section is accurately proportional to the electron speed, with a constant of proportionality of 3.29×10^{-23} cm. sec. The slightly more accurate data of Lowke and of Crompton and Elford yield for this range in nitrogen the result

$$A_{N_2} = 3.16 \times 10^{-23} \text{ c sq. cm.}$$

Since the mean collision frequency ν is equal to $n\overline{Ac}$, where n is the gas particle density and the bar denotes an average, (2) implies that ν is proportional to the mean electron energy. This behavior in nitrogen was also found by Phelps (1960) using different experimental methods. The revised result (Pack and Phelps 1961)

$$\nu/n(N_2) = 1.12 \times 10^{-7} \text{ u c.c./sec.} \tag{3}$$

where u is the mean energy in eV, is in exact quantitative agreement with (2).

From the W and W/D data listed above, Lowke (1963b) has concluded that at a temperature of 77°K the relation between A and c in nitrogen is not strictly linear. Whether the departure from linearity is important at temperatures encountered in the lower ionosphere is unknown and it will be ignored in subsequent discussion.

3. The A(c) relation in air and oxygen

Phelps and Pack (1959) have estimated collision frequencies in the lower ionosphere by assuming that the approximate two-thirds ratio of collision cross-sections in oxygen and nitrogen, observed to hold down to an energy of 0.2eV (see Fig. 1), is maintained to thermal energies ($\sim$ 0.026 eV) so that "the error is less than 20% when the collision frequency for air is taken equal to that for the nitrogen alone". This hypothesis enabled them to neglect the "unknown" collisions with oxygen and is, in effect, an assumption that the A(c) relations in oxygen and nitrogen have essentially the same character over a decade of electron energy.

In a later paper Phelps (1960) gave for the energy range 0.03 to 0.2 eV in oxygen the relation

$$\nu/n(O_2) = 4 \times 10^{-9} u^{1/2} + 5 \times 10^{-8} u \text{ c.c./sec.} \tag{4}$$

which, for energies below 0.1 eV, can be replaced to an accuracy of ± 10% by

$$\nu/n(O_2) = 7 \times 10^{-8} u \text{ c.c./sec.} \tag{5}$$

Phelps based (4) on an assessment of available cross-sections for oxygen made by Shkarofsky et al. (1961) and both it and (5) can be criticized on the grounds discussed in the next two paragraphs.

In their assessment of data for oxygen Shkarofsky et al. preferred cross-sections obtained from data communicated privately by Crompton and Sutton, "in spite of their somewhat different energy dependence from the others, because their results are recent and some of the difficulties in experimentation in oxygen, such as attachment, are recognized. Also, they depend on the reliable values of Nielsen and Bradbury for the drift velocity". In Fig. 2b of their paper Shkarofsky et al. give three curves of cross-section as a function of energy. Of these, two are calculated from the experimental data for Maxwellian and Druyvesteyn distributions and are plotted for electron energies greater than 0.22 eV. The third, on which (4) is based, is subject to a more correct distribution and is extrapolated to an energy of 0.02 eV. This extrapolation compounded an extrapolation by Crompton and Sutton, who prior to private circulation of their data, had associated with their measurements of W/D for values of E/p of 0.2, 0.3 and 0.4 values of W which they had obtained by extrapolation of the drift velocity data ($E/p \geqslant 0.5$) of Nielsen and Bradbury (N.B.)*

For a gas temperature of 293°K the mean cross-section $\bar{A}$ and the mean speed $\bar{c}$ are given by

$$\left.\begin{aligned} \bar{c} &= 1.06 \times 10^{7} \; k^{1/2} \text{ cm./sec.} \\ \bar{A} &= 4.26 \times 10^{-9} (E/p)/(Wk^{1/2}) \text{ sq. cm.} \end{aligned}\right\} \tag{6}$$

when E/p and W are expressed in volts/cm.mmHg and cm./sec. respectively. These formulae, which

* The drift velocity associated by C.H.S. with their lowest value (4.0) of k in air is also an extrapolation.

apply for a Maxwellian distribution, can easily be derived from formulae given by Huxley and Crompton (1962). Curves 1 and 2 in Fig. 1 refer to oxygen and are calculated from (6) using the following data: 1 — W(N.B.), W/D(Crompton and Sutton); 2 — W(N.B.), W/D(Rees). The breaks indicate the part of curve 1 derived using the extrapolated values of W referred to above*. If the latter curve is accepted in its entirety, then the legitimate extrapolation to the thermal speed is a constant cross-section and not, as is implied by (4), a cross-section closely proportional to speed. If the broken part of curve 1 is ignored, its remaining part is in good agreement with curve 2 and in both curves the cross-section decreases slightly at low speeds. The reality of this decrease, however, depends on whether it has been introduced by the common factor of the two curves, the drift velocity data of N.B. For the range of speeds covered by curve 2 and the solid part of curve 1, the linear plot of W against E/p given by N.B. is contained in an area of the published diagram measuring 1.5 cm. by 0.8 cm. With no difficulty, and equal justification, the curve of best fit to the few, fairly rough, experimental points in this small area could be re-drawn to change the decrease in cross-section to an increase. Clearly, on the evidence presented, little weight can be attached to (4) representing the collision frequency in oxygen at thermal energies.

Recently, Phelps (1964) has derived the cross-sections for nitrogen shown in Fig. 2 to be consistent with DC measurements of electron drift velocity, of the ratio of electron diffusion coefficient to electron mobility, and of excitation and ionization coefficients. Although the cross-sections yielded by the technique used are not unique, they are claimed to be much more accurate than previously available data and to be consistent with most of known data. The cross-sections shown for oxygen in the figure have also been derived by Phelps using the same technique and are considered by him to be tentative, largely because of the lack of consistent experimental data. His assessment is that the cross-sections for oxygen are accurate to within ± 20 per cent for energies above 0.2 eV but are much less certain, although the best available at present, for energies below this value.

For energies below 0.07 eV the cross-sections for oxygen in Fig. 2 differ markedly both in magnitude and in energy dependence from previous estimates made by Phelps and, if correct, would imply that at thermal energies in air the A(c) relation is markedly different from that in nitrogen. This is shown by the broken curve in the figure, which is calculated for air from the cross-sections for nitrogen and oxygen using

$$A_{air} = 0.8A_{N_2} + 0.2A_{O_2} \tag{7}$$

Since the calculated cross-section is constant for energies below 0.04 eV, the possible implication with regard to current use of the Sen and Wyller magneto-ionic theory is obvious.

In his assessment of the contribution oxygen makes to the collision cross-section in air, Huxley (1959) did not use the W/D data for oxygen obtained by Crompton and Sutton but compared the cross-sections for nitrogen given by the W and W/D data of Crompton and Hall with the cross-sections for air given by the data of C.H.S. and N.B. He argued that the trend of the values for air ($k \geqslant 4$) with decreasing values of k required the contribution to be negligible when $1 < k < 4$ so that in this range

$$A_{air} \doteqdot 0.8A_{N_2}$$

In order to test this argument we have also shown in Fig. 1 curves of $\bar{A}$ against $\bar{c}$ labelled 3 to 7. Of these, curves 3 to 5 are calculated from formulae (6) using the following data:

3. Nitrogen (W, Lowke; W/D, Crompton and Elford)

4. Air (W, N.B.; W/D, C.H.S.)

5. Air (W, N.B.; W/D, Bailey)

The cross-sections for air in curve 6 are calculated using equation (7) and the cross-sections in curves 1 and 3. The cross-sections in curve 7 are 0.8 times the cross-sections in curve 3 for nitrogen. The parts of curves 4 and 6, which depend on extrapolated values of W, are shown as broken lines.

Curve 4 is seen to converge to curve 7 at low values of $\bar{c}$ suggesting, as Huxley pointed out, that collisions with oxygen make an unimportant contribution to the total cross-section in air at thermal velocities. However, $0.2A_{O_2}$ is the difference of two nearly equal large quantities and both of these must be known accurately if the trend of this difference is to be estimated with any certainty. The values of k for air measured by Bailey differ at most by 16 per cent from those measured by C.H.S., yet a comparison of curves 5 and 7 suggests a very different extrapolation of $0.2A_{O_2}$. Also, the predicted curve 6 for air does

* Since we are concerned here with unpublished data, it is noted that curve 1 is identical with a curve given by Huxley and Crompton (1962).

not agree perfectly with either of the experimental curves 4 and 5 in the range of $\bar{c}$ for which there are experimental data for oxygen. Since the success of Huxley's extrapolation depends on the accuracy of the W/D measurements of C.H.S. when combined with the W measurements of N.B., it is relevant that at E/p equal to 0.1, the lowest value of this parameter in the measurements of C.H.S., the value of W/D in the "easy gas" nitrogen measured by Crompton and Sutton (1952) at the same time as the measurements of C.H.S. were made differs by 18 per cent from the precise value measured by Crompton and Elford (see Table 2, Appendix).

Mentzoni (1965) and Veatch et al. (1965) have recently used microwave methods to measure the collision frequency of thermal electrons in afterglow plasmas in oxygen and have obtained the almost identical results

$$\nu/n(O_2) = C u \text{ c.c./sec.}$$

with C equal to 4.4×10^{-8} (Mentzoni) and 4.6×10^{-8} (Veatch et al.), when the electron energy u is expressed in eV. These results are in good agreement with (4) and (5).

Mentzoni measured as a function of pressure the insertion loss and the phase shift at an X-band frequency at several temperatures between room temperature and 900°K. A power law $\nu \propto c^r$ was assumed in the analysis and his value of 2 for r was obtained from comparisons of data for the different temperatures used.

In the experiments of Veatch et al., the plasma was immersed in a magnetic field and measurements were made at a number of pressures of the width of the cyclotron resonance absorption line and of the strength of the magnetic field which caused the modulation impressed by a pulsed disturbing wave (5.3 kMc/s) on a pulsed wanted wave (6.2 kMc/s) to be zero. The first of these measurements, when interpreted using formulae in which the energy dependence of the collision frequency is neglected, gave a value $\langle\nu''_b\rangle$* for the collision frequency which was lower than the value $\langle\nu'_b\rangle$ given by the second. Veatch et al. assumed also that $\nu \propto c^r$ and obtained the value of r from a plot of the ratio $\langle\nu''_b\rangle/\langle\nu'_b\rangle$ as a function of r calculated using factors given by Shkarofsky (1960). For r = 1 (A = const.) and r = 2 (A ∝ c) the calculated ratios are 0.93 and 0.74 respectively, so that the error in the value deduced for r is proportionately much larger than the error in the measured value of the ratio.+ To test their method Veatch et al. measured the collision cross-section and its energy dependence in helium and found good agreement with the results of other workers.

Despite the agreement between their results, the work of Mentzoni and of Veatch et al. has a number of unsatisfactory features which make us believe it is not the final answer to the problem of collisions of electrons with oxygen in the lower ionosphere.

In Fig. 1 of his paper, Mentzoni gave plots at three pressures of the variation of the total collision frequency (i.e., with ions and with neutral molecules) with time in the afterglow. This figure, which refers to a temperature of 894°K, is claimed to be typical of what is essentially the raw data, but in it the steady state is not attained at one pressure and is only roughly indicated at the other two. Since comparisons of steady state values for different temperatures are the basis of Mentzoni's method for determining the value of r, the poor quality of the data shown makes us treat his conclusion that r has the value 2 with considerable reserve. Mentzoni has also noted that the evidence for this value from data for temperatures below 569°K is not "as conclusive, pointing to possible noticeable contributions from collisions between ions and electrons". On this ground alone, the relevance of his result to the lower ionosphere (Tg ∿ 200°K) is questionable.

The method used by Veatch et al. is similar in many respects to the method used at the University of New England to determine collision frequencies in the nighttime lower ionosphere (see paper 3.2.1). It has the advantage over the method used by Mentzoni that the measurements are independent of the electron density when the plasma is weakly ionized. This advantage has been appreciated by Veatch et al., but the extremely small values of the density required in a cyclotron resonance experiment for this independence to be realized (see Smith et al., 1965) does not appear to have been recognized, since observations were made at a fixed delay in the afterglow and no attempt seems to have been made to determine whether results for widely different delays, and thus for widely different densities of electrons and ions, were consistent.

Fig. 3 is a reproduction of Fig. 14 in the report of Veatch et al. and shows the line from which they have deduced the value of $\langle\nu''_b\rangle/\omega p$. Clearly, the slope of this line has a large error and, more seriously, the line of best fit to the experimental points does not pass through the origin, as it should. This can mean that their observations at a fixed delay may have been biased by some pressure dependent property, e.g.

* The notation is that used by Veatch et al.

+ The method used by Mentzoni to determine the value of r also suffers from a similar difficulty.

ionization, of the afterglow. In explanation, Dr. Veatch* has stated that the errors in the points below 4 torr are large since at these pressures small variations in the magnetic field due to line voltage fluctuations made the half-width of the very narrow resonance difficult to measure. For this reason more weight was given to the measurements at the higher pressures. In support of their result for oxygen he has supplied Fig. 4, which is explained within the framework of the figure. Unfortunately, while the theoretical curve is stated to be normalized to the experimental points, an experimental point at the maximum of the theoretical curve is not shown. Also, the theoretical curve seems to have been calculated incorrectly, since it displays a cusp instead of a maximum at the gyro-frequency.

Although extreme care must be exercised if reliable collision frequencies are to be obtained from cyclotron resonance experiments in afterglows (Fehsenfeld et al. 1965), the method used by Veatch et al. is a powerful one and it is to be hoped that the investigation will be continued.

4. Energy losses in electron collisions

Electron energy loss in near-thermal collisions in air has been a long-standing problem in radio wave interaction theory, and many attempts have been made using laboratory data of one kind or another to improve our knowledge of this loss. With the use of high disturbing powers at the gyro-frequency by Smith et al. and the projected use of high disturbing powers by other groups, energy loss for mean electron energies up to about 1 eV has also assumed practical importance.

The mean energy η lost by an electron in a collision with a gas molecule can be shown to be proportional to W^2 (see Healey and Reed). Values of W^2 for air at 288°K are plotted against k in Fig. 5 using the drift velocity data of N.B. in association with each of the three sets of values of k yielded by the measurements of W/D listed in Section 2. In the range $10 < k < 25$ common to these measurements there is good agreement between the values of k, and the points in the figure lie on a straight line whose extension intercepts the k-axis at the point $k = 1$. For the corresponding range of mean electron energies we can thus use with some confidence for η the Bailey and Martyn formula (1), with $G = 1.7 \times 10^{-3}$, the value for the energy loss coefficient given by the slope of the line. This result for high electron energies will also apply to collisions in the lower ionosphere, since the properties of an electron swarm are independent of the gas temperature, when it is a small fraction of the electron temperature (Hall 1955).

Electron energies in the range we have just considered would require extreme radiated powers to be produced in the daytime D region, but almost certainly have already been produced at night near 85 km. by the transmitting installation for the gyro-frequency illustrated in paper 3.1.1. Unfortunately, in wave interaction experiments at night there appears to be no way of confining the effect observed on the wanted wave to that produced in the most strongly heated portion of the disturbed region, and in the analysis it is necessary to take into account all electron energies between the maximum and the thermal energy (Smith et al. 1965). In the range $6 < k < 10$ in Fig. 5, the values of k determined by Bailey give points lying on the straight line, whereas those determined by C.H.S. give points falling progressively further below it with decreasing k. This divergence makes the lowest energy in air to which (1) may be used with $G = 1.7 \times 10^{-3}$ uncertain and aggravates the problem in the interpretation of high power wave interaction observations raised by the lack of data for lower energies.

The hypothesis of Bailey and Martyn that η has the form (1) when the perturbation of the mean electron energy is small ($U - U_0 \ll U_0$) has been referred to in Section 2. In that section we also mentioned an alternate hypothesis due to C.H.S. The latter hypothesis has been revived recently (Benson 1964, Singh 1964), but can be disregarded on many grounds, one of which is that the formula, $\eta \propto (U - U_0)^2$, being an even function of $(U - U_0)$, is in conflict with the Second Law of Thermodynamics (Hibberd 1956, 1965). The points in Fig. 5 plotted using Bailey's value of k are obviously consistent with the Bailey and Martyn hypothesis and suggest that the energy loss coefficient has approximately the same value in a small perturbation as in the large one considered above. That such an extrapolation cannot be regarded as justification of the use of (1) in a small perturbation, or, if this can be done by other means, as a source of a reliable value for the energy loss coefficient, is shown by Fig. 6 in which W^2 in nitrogen at room temperature is plotted against k for the ranges $1 < k < 5$ and $1 < k < 20$. From this figure and from theories of energy loss in near-thermal collisions it is clear that when applied to such collisions the Bailey and Martyn formula must be regarded only as the first term in a power series expansion for η in the neighborhood of U_0.

When the electrons are drifting with a steady velocity W under a constant electric field E, the power supplied to the mean electron is EeW, where e is the electronic charge. This power is lost by collisions and we may write

$$EeW = (G\nu)(U - U_0) \tag{8}$$

regarding this equation as defining a quantity $(G\nu)$. In order to retain the formalism of Bailey and Martyn

* Private communication

we now put

$$(G\nu) = G\nu \tag{9}$$

where this relation between $(G\nu)$ and the mean collision frequency ν defines a dimensionless coefficient G, whose value is a function of U and U_0. When $(U - U_0)$ is a small perturbation (i.e., $U - U_0 \ll U_0$), the coefficient can be regarded as a function of U_0 only and will be distinguished from the more general G by the use of the subscript o.

In air, if energy loss in collisions with minor constituents is neglected, we have

$$G_{air}\nu_{air} = G_{N_2}\nu_{N_2} + G_{O_2}\nu_{O_2} \tag{10}$$

where on the right hand side each of the ν's is the mean number of collisions per second with the subscripted molecule. In terms of values at the same mean energy in pure nitrogen and oxygen

$$(G\nu/n)_{air} = 0.8\,(G\nu/n)_{N_2} + 0.2\,(G\nu/n)_{O_2} \tag{11}$$

where n is the gas particle density. Since $k = U/U_0$, it is easily shown from (8) and (9) that

$$G\nu/n = 8.0 \times 10^{-16}\,(E/p)W/(k - 1) \tag{12}$$

when E/p is in volts/cm.mm of Hg.

Using (12) we have plotted in Fig. 7, as a function of mean electron energy in eV, values of $G\nu/n$ in nitrogen (W, Lowke; k, Crompton and Elford) and air (W, N.B.; k, Bailey or C.H.S.) at room temperature, and values in nitrogen (W, Lowke; k, Warren and Parker) at a temperature of 77.4°K. The curve for air labelled 'predicted' has been calculated from (11) using, in the case of oxygen, the data of N.B. (W) and Crompton and Sutton (k). In plotting this curve and the curve labelled k(C.H.S.) we have included the extrapolated values of W discussed in Section 3,but, as in Fig. 1, have shown as a broken line the part of each curve derived using these values.

In nitrogen at 293°K the value of $G\nu/n$ is seen to increase from 0.77×10^{-11} at the lowest energy of measurement (k = 1.042) to a maximum of 0.97×10^{-11} at an energy of about 0.055 eV (k = 1.45). This increase at near-thermal energies may be significant, but it is more realistic to attribute it to errors in the experimental values of k*. Favoring the maximum value at 293°K, and adopting the asymptotic value at 77.4°K, we find the following values for a small perturbation in nitrogen;

$$(G\nu/n)_0 = 0.95 \times 10^{-11}\ (293°K) \text{ and } 1.5 \times 10^{-11}\ (77.4°K) \tag{13}$$

Here, the subscript o attached to $G\nu/n$ has the same significance as in the case of G_0. If, further, we assume that the relation (2) between A_{N_2} and c also applies at the temperature of 77.4°K, we obtain for nitrogen

$$G_0 = 2.2 \times 10^{-3}\ (293°K) \text{ and } 1.3 \times 10^{-2}\ (77.4°K) \tag{14}$$

Theoretical formulae for the variation of $(G\nu/n)_0$ in nitrogen with gas temperature have been given by Huxley (1959) and by Dalgarno and Moffett (1962). Huxley's formula is semi-empirical and is fitted to the W and W/D data of Crompton and Hall. In their calculation of electron collision loss by excitation of rotational levels of the nitrogen molecule Dalgarno and Moffett used for its quadrupole moment the value 1.01, which Frost and Phelps (1962) have found to be consistent with data from electron swarm experiments. The curve of $(G\nu/n)_0$ as a function of gas temperature given by Dalgarno and Moffett increases monotonically with decreasing temperature from a value of 1.2×10^{-11} at 300°K to a value of 1.85×10^{-11} at 100°K. The values given by Huxley's formula increase from 1.0×10^{-11} at 300°K to a maximum of 1.5×10^{-11} at about 150°K and then decrease to 1.3×10^{-11} at 100°K (see Dalgarno and Moffett). The experimental values (13) give no guide as to which of the predicted variations with temperature is the more reliable.

In the temperature range 150 — 300°K the two theoretical formulae for $(G\nu/n)_0$ give curves of similar shape. Taking $G_0 = 2.2 \times 10^{-3}$ at 293°K, the predicted values of G_0 in nitrogen at temperatures of 210°K, 190°K and 166°K are

$$3.8 \times 10^{-3}\ (210°K);\ 4.4 \times 10^{-3}(190°K);\ 5.2 \times 10^{-3}(166°K) \tag{15}$$

*When $k \neq 1$, the term $(k - 1)$ in the denominator of (12) makes exacting demands on the accuracy of the value for k.

Of these temperatures, the first is approximately the temperature near 70 km. in the lower D region, and 166°K is given in the ARDC (1959) atmospheric tables as the temperature at the mesopause near 85 km., where there is a minimum in the temperature. The values of G_0 in (15) are in the proportions 1:1.16:1.37.

In small perturbation wave interaction theory the modulation depth impressed on the wanted wave is inversely proportional to the product $G_0 T_g$. For the three temperatures just considered the predicted values of this product are in the proportions 1:1.05:1.08 and thus vary much less with temperature than the predicted values of the coefficient G_0.

These theoretical and experimental results for near-thermal energy loss in nitrogen are of direct value in the study of radio wave interaction in the ionosphere only if they can be supplemented by quantitative data for energy loss in oxygen. Huxley (1959) has proposed that when $k < 4$ ($T_g = 288°K$) the energy loss due to excitation of rotational changes in the molecule is roughly equal in oxygen and nitrogen, so that

$$(G\nu/n)_{air} \doteqdot (G\nu/n)_{N_2} \tag{16}$$

As part support of this proposal he pointed out that when $k = 4$ the value of $G\nu/n$ in nitrogen is almost equal to the value in air (see Fig. 7, in which the value 4 for k corresponds to the lowest energy in the broken part of the curve for air labelled k(C.H.S.)). Dalgarno and Moffett, using the result of Smith and Howard (1950) that the quadrupole moment of molecular oxygen is apparently very small, have suggested that rotational energy loss in oxygen is negligible and that

$$(G\nu/n)_{air} \doteqdot 0.8\,(G\nu/n)_{N_2} \tag{17}$$

In both (16) and (17) we have omitted from each side of the equation the subscript o.

If the collision cross-section in oxygen at thermal energies is small compared to the cross-section in nitrogen, then (16) would require the value of G_0 in air to be about 25 per cent larger than the value in nitrogen and (17) would require the values in the two gases to be about equal. According to the views of Huxley and of Dalgarno and Moffett, the value of G_0 in air would vary with gas temperature in the same manner as in nitrogen.

It is obvious from Fig. 7 that while the value of $G\nu/n$ in air is decreasing fairly rapidly with decreasing electron energy, any attempt to connect the experimental values for air to the near-thermal values for nitrogen requires guessing the behavior in air over almost a decade of energy. This guesswork is not made easier by the marked difference at the lower energies between the two experimental curves for air, and by the equally marked difference, except for those parts shown as broken lines, between either of these curves and the predicted curve. Huxley (1959) has commented that the behavior of electrons in nitrogen, oxygen and air serves to illustrate the failure of the method of mixtures in some circumstances and its validity in others, and that the use of (11) to calculate energy losses in a mixture such as air from separate data implies the assumption, which there is no reason to suppose is valid generally, that for the same mean energy the electrons are distributed in precisely the same manner in the mixture as in the gases separately. While this is a possible explanation of differences in Fig. 1 and 7 between observed and "methods of mixtures" data, it serves more as a reason, while these differences are unreconciled quantitatively, for placing little weight on quantitative inferences, particularly those involving extrapolation, from comparisons of this kind.

Finally, we note that if the values of k measured by C.H.S. are more accurate than those measured by Bailey, then there is the suggestion in Fig. 7 that the value of $G\nu/n$ in air could be approximately constant for mean electron energies less than about 0.15 eV. In a preliminary analysis of their high power wave interaction data, Smith et al. (1965) have found that this hypothesis, in conjunction with the hypothesis $A \propto c$ and values for G_0 etc. determined from small perturbation wave interaction experiments, gives agreement between the theoretical and observed variations of modulation depth with disturbing power and predicts the transient characteristics of the electron heating. Whether or not this agreement between theory and observation implies the correctness of each of these hypotheses up to electron energies of about this magnitude remains to be demonstrated, since it is possible that the same agreement could be achieved by modifying both in a complementary manner.

5. Concluding remarks

Two aspects of the behavior of slow electrons in air have been examined. One is the relation between collision cross-section and electron speed, which determines the form of generalized magnetoionic theory appropriate to wave propagation in the lower ionosphere, and the other is the energy loss in collisions, which is important in the study of radio wave interaction.

The generalized magneto-ionic theory of Sen and Wyller (1960) has embodied in it a linear relation between cross-section and speed, a behavior for thermal electrons in air that was first proposed as a postulate by Crompton et al. in 1953, and was later argued with much greater apparent force by Huxley and by Phelps and Pack in 1959, following experimental evidence of a similar behavior in nitrogen. In this paper we have made no attempt to assess whether or not a linear relation is the correct relation in air, since the laboratory data that we have considered do not, we believe, permit such an assessment. Instead, we have given reasons why we regard the assessments of Huxley and of Phelps and Pack with considerable scepticism, and have criticized the expression for the collision frequency of thermal electrons in oxygen, which Phelps gave in 1960. Recent developments, that have been discussed, are the cross-sections for nitrogen and oxygen which Phelps (1964) has derived to be compatible with a wide variety of experimental data and the results of Mentzoni (1965) and of Veatch et al. (1965) for the collision frequency of thermal electrons in afterglow plasmas in oxygen. Of these developments, the cross-sections for oxygen derived by Phelps contradict his earlier expression and imply, with the cross-sections for nitrogen, that the correct behavior for a thermal electron in air is a constant cross-section. On the other hand, the results from experiments in afterglows are in quantitative agreement with the expression and support the use of a linear relation for electrons in air. Reasons have been given why we do not regard the latter results from afterglows as the final answer to the problems of the collision frequency and its energy dependence in oxygen. By drawing attention to the present confusion and to the dangers confronting research on the lower ionosphere, it is hoped that this paper will stimulate further work aimed at providing a sound base for magneto-ionic theory.

The factor that perhaps has contributed most to the ready acceptance of the linear relation for thermal electrons in air is its plausibility. Since four-fifths of air is nitrogen and at high electron energies the collision cross-section in oxygen is known to be about two-thirds of the cross-section in nitrogen, it would seem a reasonable assumption to make that collisions with nitrogen in air are dominant at thermal energies. Such an assumption, however, takes no account of the marked decrease of the cross-section in nitrogen with decrease of the electron energy and the low temperatures that exist in the D and lower E regions. These circumstances combine to make it possible to postulate any number of "reasonable" cross-sections for thermal electrons in oxygen, that cause the relation between cross-section and speed to be different in air and nitrogen and, at the same time, do not lead to conflict between collision frequencies for the lower ionosphere from aeronomic and radio measurements. The cross-sections for oxygen derived by Phelps (1964) illustrate this point and the risk in making the assumption that oxygen is simply a dilutant in air.

The lack of experimental values of W and W/D in air and oxygen at low electron energies has led to widespread use of extrapolation. When the "result" is clearly recognizable as an hypothesis, no objection can be taken to the extrapolation, and in many instances, e.g. in the development of the theory of radio wave interaction by Bailey and Martyn, no alternative was possible. When, however, fictitious values of W and W/D (or D/μ, where $\mu = W/E$) are created by extrapolation and are used in deriving an experimental result, many dangers exist, since the implications may not be obvious in the paper and it is often the case that the end result only is remembered and quoted. An example of a paper in which extrapolated values of W and D/μ have been used is the important paper of Chanin et al. (1962) on attachment rates of electrons in oxygen. With regard to this paper the question may be asked why these values were used in it, if they are unnecessary for the final result for thermal electrons. In several places in this paper we have referred to an extrapolated value of W in air, noted as such by Crompton, Huxley and Sutton (1953), and three extrapolated values of W in oxygen, that were circulated privately by Dr. Crompton. These values should, of course, be ignored, but we have been forced to consider them, since they have appeared in the literature on an equal basis with measured values. Some idea of the confusion that has resulted from the extrapolated values of W in oxygen can be gained from the following extract, under the name of Dr. Elford, from Quarterly Report No. 21, July-September, 1965, Ion Diffusion Unit, Research School of Physical Sciences, Institute of Advanced Studies, The Australian National University, Canberra:

"In Q.R. 20 the difficulties involved in extending the range of E/p for which drift velocity data is available were discussed. Further investigation has shown that the present range of E/p, i.e. 0.15 to 20, cannot be significantly extended by using the Bradbury-Nielsen method. A search of the literature, however, has shown that the published data is inaccurate and in many cases has been incorrectly plotted in published curves, e.g. in the most recent compilation of drift velocity data in O_2 by Chanin, Phelps and Biondi (Phys. Rev. 128, 219, 1962), one curve listed as results by Crompton is fictitious as Crompton has never measured drift velocities in oxygen. A curve listed as that of Bradbury has as its reference the 1932 Bradbury measurements in O_2. Not only do the points of the Chanin, Phelps and Biondi paper not agree with the 1932 Bradbury data, the 1937 data of Bradbury and Nielsen for oxygen is omitted. This later data was taken by a much more accurate method than that used in 1932."

Apart from its relevance to the material in this paper, this extract is interesting in that the values of W in oxygen attributed by Chanin et al. to Crompton are the 1937 values of Nielsen and Bradbury, together with the extrapolated values which had been circulated privately by Crompton.

Despite the present confusion about properties of slow electrons in air and oxygen, there would appear to be no fundamental reason why this confusion cannot be resolved using present laboratory techniques. The

electron swarm experiment has the apparent limitation that reliable measurements of W and W/D in these attaching gases cannot be made for electron energies less than about five times the thermal energy. Also, there is the difficulty of including generally in the analysis of the data the correct formula, due to Davidson (1954), for the drift velocity. Nevertheless, much of the confusion has been caused by reliance on a few old and unsubstantiated values of W and W/D in these gases, and there is an urgent need for new data to the lowest values of E/p possible with modern techniques. In order that the measurements should serve both to clarify the confusion and to have direct application to the ionosphere, they should be made at room temperature and at a temperature $\sim$ 200°K, which can easily be produced by the use of solid carbon dioxide as a refrigerant. Measurements at the lower temperature should also be made in nitrogen.

For data at the thermal energy, the methods used by Veatch et al. to determine collision frequency and its energy dependence in afterglows are most promising, and their measurements could easily be supplemented by a measurement of the electron relaxation time to yield the value of the energy loss coefficient. The measurements should be made at room temperature and at 200°K and should be made in air, nitrogen, and oxygen separately, in order that their internal consistency can be checked and comparisons can be made, in the case of nitrogen, with results from electron swarm experiments and, in the case of air, with results from experiments on radio wave interaction in the ionosphere.

Once reliable and consistent results for air are available at the thermal energy and at the low energy limit of the swarm experiment, the energy gap should not be too difficult to bridge by means of large perturbation wave interaction experiments made either in the ionosphere or in the laboratory.

REFERENCES

Minzer, R.A., Champion, K.S.W. and H.L. Pond. ARDC Model Atmosphere. Air Force Surveys in Geophysics No. 115, (AFCRC-TR-59-267), Air Force Cambridge Research Center. 1959.

Bailey, V.A. Phil. Mag., 50, 825, 1925.

Bailey, V.A. and D.F. Martyn. Phil. Mag., 18, 369, 1934.

Benson, R.F. Radio Sci., 68D, 1123, 1964.

Chanin, L.M., Phelps, A.V. and M.A. Biondi. Phys. Rev., 128, 219, 1962.

Crompton, R.W., and M.T. Elford. Proc. Sixth Internat. Conf. on Gaseous Ionization Phenomena, Paris, 337, 1963.

Crompton, R.W. and D.J. Sutton. Proc. Roy. Soc. A, 215, 467, 1952.

Crompton, R.W., Huxley, L.G.H. and D.J. Sutton. Proc. Roy. Soc., A, 218, 507, 1953.

Dalgarno, A. and R.J. Moffett. Planet. Space Sci., 9, 439, 1962.

Davidson, P.M. Proc. Phys. Soc. B, 67, 159, 1954.

Fehsenfeld, F.C., Megill, L.R. and L.K. Droppleman. J. Chem. Phys., 43, 3518, 1965.

Frost, L.S., and A.V. Phelps. Phys. Rev., 127, 1621, 1962.

Hall, B.I.H. Aust. J. Phys., 8, 551, 1955.

Healey, R.H. and J.W. Reed. "The Behaviour of Slow Electrons in Gases", Amalgamated Wireless, Sydney, 1941.

Hibberd, F.H. Ph.D. Thesis, Univ. Sydney, 1956.

Hibberd, F.H. Radio Sci., 69D, 25, 1965.

Huxley, L.G.H. Proc. Roy. Soc. A, 229, 405, 1955.

Huxley, L.G.H. J. Atmos. Terr. Phys., 16, 46, 1959.

Huxley, L.G.H. and R.W. Crompton. "Atomic and Molecular Processes", ed. D.R. Bates, Academic Press (N.Y.), 1962.

Huxley, L.G.H. and A.A. Zaazou. Proc. Roy. Soc. A, 196, 402, 1949.

Lowke, J.J. Aust. J. Phys., 16, 115, 1963a.

Lowke, J.J. Ph.D. Thesis, Univ. Adelaide, 1963b.

Mentzoni, M.H. Radio Sci., 69D, 213, 1965.

Nielsen, R.A. and N. Bradbury. Phys. Rev., 51, 69, 1937.

Pack, J.L. and A.V. Phelps. Phys. Rev., 121, 798, 1961.

Phelps, A.V. J. Appl. Phys., 31, 1723, 1960.

Phelps, A.V. NBS Techn. Note No. 211, 5, 49, 1964.

Phelps, A.V. and J.L. Pack. Phys. Rev. Letters, 3, 340, 1959.

Pidduck, F.B. Proc. Lond. Math. Soc., 15, 89, 1915.

Rees, J.A. Aust. J. Phys., 18, 41, 1965.

Rees, J.A. and R.L. Jory. Aust. J. Phys., 17, 307, 1964.

Sen, H.K. and A.A. Wyller. J. Geophys. Res., 65, 3931, 1960.

Shkarofsky, I.P. Res. Rept. No. 7-801, Res. Labs. RCA Victor Ltd., Montreal, Canada, 1960.

Shkarofsky, I.P., Bachynski, M.P. and T.W. Johnston. Planet. Space Sci., 6, 24, 1961.

Singh, R.N. Planet. Space Sci., 12, 675, 1964.

Smith, R.A., Bourne, I.A., Loch, R.G., Setty, C.S.G.K., Coyne, T.N.R., Barratt, P.H. and B.S.N. Prasad. Scientific Report No. 3, and Final Report, Contract No. AF19(604)-6177, Univ. New England, 1965.

Smith, W.V. and R. Howard. Phys. Rev., 79, 132, 1950.

Townsend, J.S. "Electrons in Gases", Hutchinson Sci. and Tech. Publs., London, 1948.

Townsend, J.S. and H.T. Tizard. Proc. Roy. Soc., A, 88, 336, 1913.

Veatch, G.E., Verdeyen, J.T. and J.H. Cahn. Scientific Report No. 2, Contract No. AF19(628)-2391, Univ. Illinois, Urbana, Illinois, 1965.

Warren, R.W. and J.H. Parker. Phys. Rev., 128, 2661, 1962.

APPENDIX

Values of W and k for electrons in air, oxygen and nitrogen

In the main paper we have referred to and used privately communicated data. Also, in a number of the references, the values of W or k as a function of E/p are given in graphical form and are not easily recovered. This appendix covers data of both these kinds for electron energies below about 1 eV and includes some data tabulated in the original references. The unit of the parameter E/p is volt/cm. mm. of Hg, and a Maxwellian distribution is assumed.

Air (T_g = 288°K or 293°K)

W (Nielsen and Bradbury 1937): A convenient table is given in Crompton et al. (1953). In their table the value at E/p = 0.1 is an extrapolated value.

k (Bailey 1925): E/p = 0.312 (k = 6.1), 0.442 (7.6), 0.625 (9.9), 0.884 (13.7), 1.25 (18.5), 1.77 (25)

k (Crompton et al. 1953): See reference.

k (Rees and Jory 1964): E/p = 0.6 (k = 10.0), 0.7 (11.5), 8.0 (12.7), 1.0 (15.2), 1.20 (17.5), 1.4 (20.0), 1.6 (22.2), 1.8 (24.3), 2.0 (26.0)

(See Table III, Quarterly Report No. 12, April – June 1963, Ion Diffusion Unit, Research School of Physical Sciences, Institute of Advanced Studies, Australian National University, Canberra. The table in this report also contains values of k at E/p = 0.2, 0.3, 0.4 and 0.5, but these have been omitted by request.

Oxygen (T_g = 288°K or 293°K)

The values of W and k in the second and third columns of Table 1 were received from Dr. Crompton in 1959. At E/p ≥ 0.5, the values of W are those of Nielsen and Bradbury (1937). At E/p = 0.2, 0.3 and 0.4, the values are the extrapolated values of W discussed in Section 3. For comparison, the values of k determined by Rees (1965), although tabulated in his paper, are also given in Table 1.

TABLE 1. W and k in Oxygen at Room Temperature as a Function of E/p

E/p	$W \times 10^{-5}$ (cm./sec.)	k (Crompton & Sutton)	k (Rees, 1965)
0.2	8.1	4.7	
0.3	10.6	6.0	
0.4	12.8	7.1	7.45
0.5	14.6	8.2	8.2
0.6	16.2	9.0	8.9
0.7	17.7	10.0	
0.8	18.9	10.8	10.2
0.9	20.2	11.6	
1.0	21.3	12.5	11.6
1.2	23.4	14.5	
1.5	26.1	18.1	17.0
1.8	28.4	22.2	
2.0	29.8	25.5	23.8

Nitrogen

W (Lowke, 1963a): This reference gives values at temperatures of 293°K and 77.6°K in table form.

W & k (Crompton and Hall): Their unpublished values of W and k in nitrogen at room temperature were received from Dr. Crompton in 1959 and are shown in the second and fourth columns, respectively, of Table 2.

k (Crompton & Elford, T_g = 293°K): The values attributed in the fifth column of Table 2 to Crompton and Elford (1963) have not been read off their graph, but have been obtained from Table 2, Quarterly Report No. 19, January – March 1965, Ion Diffusion Unit, where they are referred to as the values plotted in the graph. The values in the sixth column under Crompton and Elford have been obtained from the same table and represent their latest determinations of k. Since Crompton and Elford have been continually refining their experimental techniques, we have used these values instead of the values in the fifth column. Table 2 also contains for comparison the values of k of Crompton and Sutton (1952).

k (Warren and Parker, 1962; T_g = 77.4°K): This reference gives in graphical form D/μ vs. E/p_{300}, where $\mu = W/E$ and p_{300} is the pressure exerted at a temperature of 300°K by the same number density of molecules. Tables of D/μ at odd values of E/p_{300} are given in Scientific Paper 62 - 908 - 113 - P6, June 4, 1962, Westinghouse Research Laboratories, Pittsburgh, and from these tables, by averaging "inner ratio" and "outer ratio" values of D/μ, we have derived the following values for k at (E/p) values standardized to a temperature of 293°K: $(E/p)_{293}$ = 0.004 (k = 1.110), 0.006 (1.23), 0.008 (1.37), 0.01 (1.52), 0.02 (2.46), 0.03 (3.6), 0.04 (4.8), 0.06 (7.8), 0.08 (11.0), 0.1 (14.0), 0.2 (27.0), 0.4 (49), 0.6 (68), 0.8 (80).

TABLE 2. W (Crompton and Hall) and k in Nitrogen at Room Temperature as a Function of E/p

	$W \times 10^{-5}$ (cm./sec.)	k			
	Crompton & Hall	Crompton & Sutton (1952)	Crompton & Hall	Crompton & Elford (1953)	Crompton & Elford (Quarterly Report No. 19 Ion Diffusion Unit)
0.006				1.027	1.042
0.008				1.050	1.069
0.01			1.09	1.079	1.098
0.015	1.60			1.169	1.188
0.02	1.90		1.29	1.284	1.298
0.025				1.413	1.424
0.03	2.32		1.56	1.554	1.564
0.04	2.62		1.87	1.872	1.877
0.05	2.73	3.1	2.20	2.23	2.224
0.06	2.84		2.56	2.60	2.592
0.07	2.94		2.90	2.98	2.972
0.08	3.02		3.26	3.36	3.347
0.09	3.08		3.65	3.74	3.720
0.10	3.14	4.8	4.00	4.10	4.076
0.15				5.75	5.713
0.20	3.75	8.0	7.13	7.25	7.196
0.3	4.2	10.9	9.90	10.12	10.09
0.4	4.8	13.6	12.7	12.96	12.91
0.5	5.3	16.2	15.2	15.56	15.54
0.6	5.8	18.3	17.5	17.80	17.80
0.7	6.3	20.2	19.5	19.70	19.75
0.8	6.9	22.1	21.0	21.4	21.42
0.9	7.4	23.4	22.3	22.9	22.82
1.0	7.9	24.7	23.8	24.1	24.10
1.5	10.5	29.3	28.5	28.7	28.60
2.0	12.9	32.9	31.6	31.7	31.64

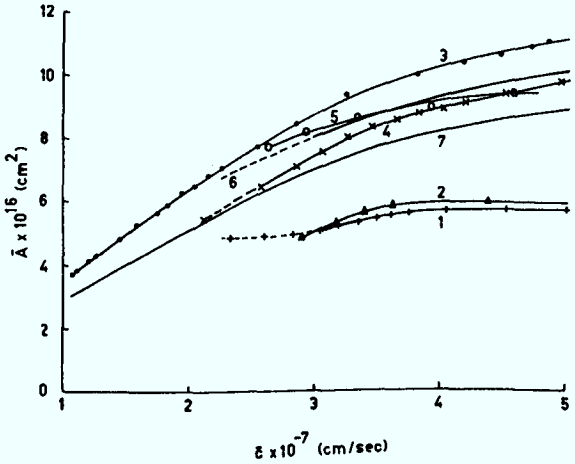

Fig. 1. Variation of $\bar{A}$ with $\bar{c}$ in air, nitrogen, and oxygen. See text for the code to the curves.

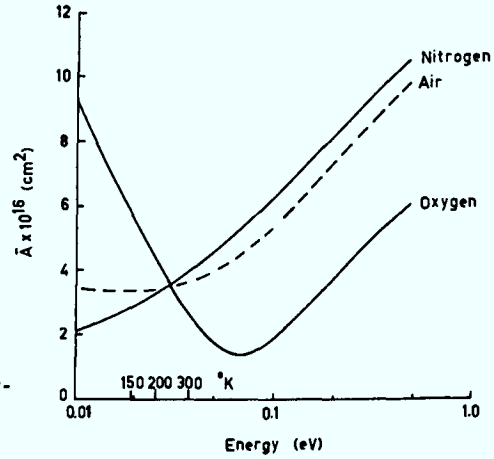

Fig. 2. Variation of A with electron energy in air, nitrogen, and oxygen. — Phelps (1964), ---- calculated for air from the cross-sections for nitrogen and oxygen.

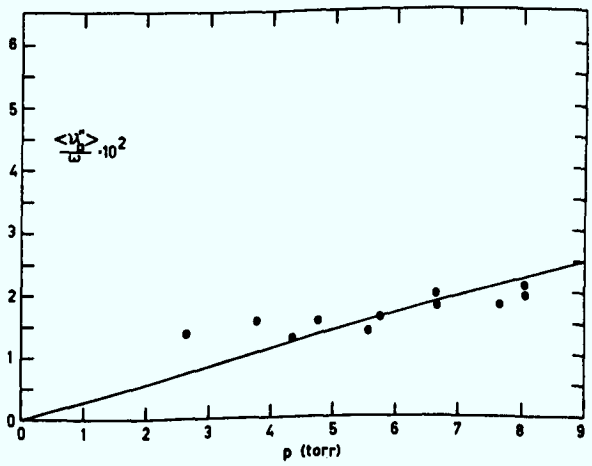

Fig. 3. $\langle \nu_b'' \rangle / \omega$ as a function of pressure in oxygen (Fig. 14 in Veatch et al. (1965)).

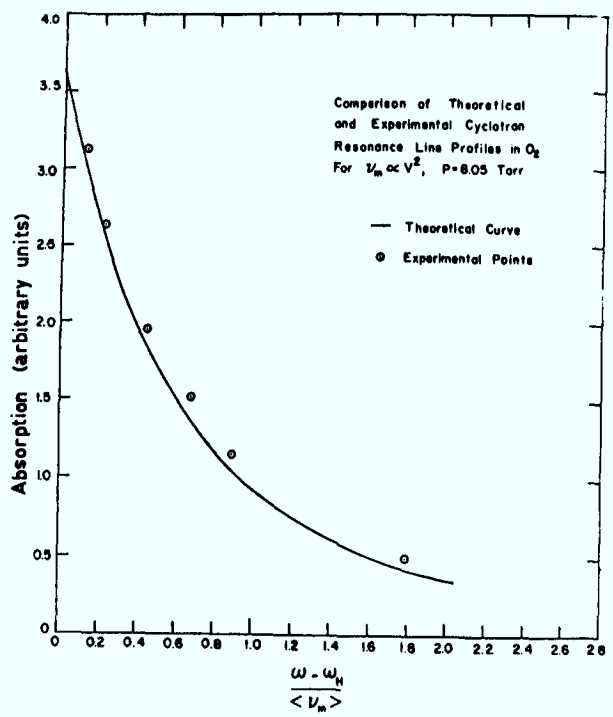

Fig. 4. Comparison of theoretical and experimental cyclotron resonance line profiles in oxygen (Veatch et al., private communication).

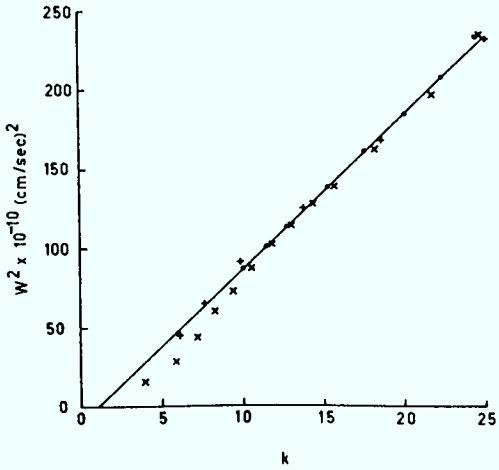

Fig. 5. W^2 as a function of k in air at room temperature. (W -- Nielsen and Bradbury; k -- + Bailey, x Crompton, Huxley and Sutton, • Rees and Jory)

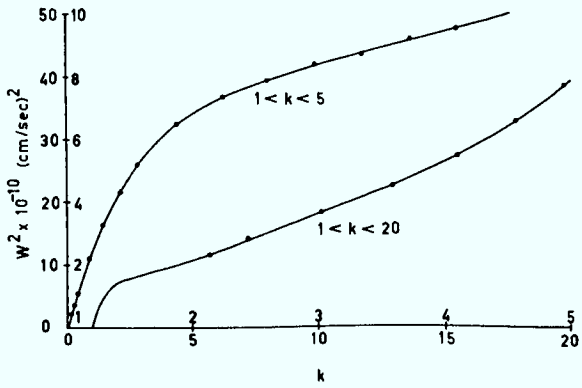

Fig. 6. W^2 as a function of k in nitrogen at a temperature of 293°K (W-- Lowke; k -- Crompton and Elford).
The experimental points for the range $1 < k < 5$ have been omitted from the curve shown for the range $1 < k < 20$. For the latter range of k, use the larger values of W^2.

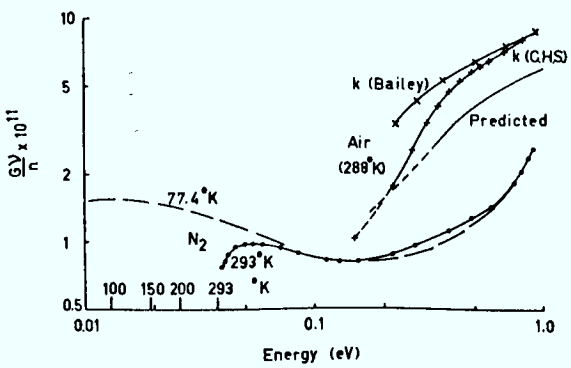

Fig. 7. $G\nu/n$ as a function of mean electron energy, in nitrogen at temperatures of 77.4° K and 293° K, and in air at a temperature of 288° K.

Discussion on Paper 1.6 presented by R.A. Smith

Waynick: I think Dr. Smith will permit me to mention that L.G.H. Huxley has been a close friend of mine for approximately 30 years, and he has continually pointed out the complexity and great difficulty in conducting these experiments in the laboratory at the very low energy levels involved.

Smith: I fully agree that they have carried the drift velocity measurements to the limit. But there are these newer methods of wave interaction which I think can solve the problem if somebody will do it.

Dalgarno: There is a general theoretical statement that one can make as to what the variation of the velocity really is. In the case of elastic scattering, the momentum cross-section of the electrons by an atom or molecule, q, is given by

$$q = A + \alpha C + \beta C \log C + \gamma C^2 + \ldots\ldots$$

and it is only valid in the limit of low velocities, but it probably covers the range of D region temperatures. I have no idea what values these parameters have, of course, but the general structural form of the cross-section is undoubtedly of this kind, and due to some chance cancellation in nitrogen it does happen, apparently, that all these terms become unimportant and A is nearly zero; you get a cross-section which is nearly proportional to C and the beta and gamma terms seem to cancel each other. It is remarkable, but it happens to work. It can be shown quite generally that A can be positive or negative. One might expect it to be close to zero. It would be surprising, on the grounds of probability, if this were nearly zero for both N_2 and O_2, so one would expect that as you go down to the low velocities the O_2 cross-section would approach a constant and it would, therefore, be larger than the N_2 cross-section which is approaching to zero. Strictly, A is not zero for N_2 because you can fit Phelps' data and Huxley's and Crompton's data by the general expression, and you find that A is not quite zero. The cross-section does not come down to the origin as their formulae imply.

Another point is that this expression is the first term in a Taylor series expansion, so it is necessarily true if you go near enough to zero.

Smith: Many of the results for oxygen which have been put in graphical form by Shkarofsky et al. show that some cross-sections increase and some attributed to the Ramsauer method decrease. If you take your pick, you can get any variation you like.

Narasinga Rao: Would you comment on some of the laboratory observations and the factors that distinguish these methods from your methods?

Smith: I don't feel competent to comment on the Mentzoni results because he does not give enough data to assess his work. The trouble, however, in their gyro interaction methods is that the theory is independent of electron density only if the electron density is very small. What they did was to measure the resonance width, and the conditions when $\frac{1}{N}\frac{d\kappa}{d\nu} = 0$. The theory they use is independent of N, but what they do not realize is how low N must be. The formula for the absorption of an extraordinary mode gyro wave shows that the conductivity is proportional to N at very low electron densities; however, the electron density must be remarkably low for this approximation to be applicable. For example, the electron density must be of the order of 50 electrons per c.c. or less for a 1.5 Mc/s gyro wave. The maximum absorption of the gyro wave does not occur at the gyro frequency except when the electron density is low, and that means you must have virtually $N \to 0$. I have nothing against their method if they demonstrate that the electron density is sufficiently low. If this is demonstrated and I criticize their method then I am criticizing my own work.

Narasinga Rao: Is it not true that in their method they go to extremely high frequencies, into the microwave region, and the value of $X = \frac{\omega p^2}{\omega^2}$ is very small.

Smith: Yes, but their degree of ionization is less than 10^{-4}. What they should have is less than 10^{-7} or 10^{-8}. On the figures presented in their report they could well have had too many electrons.

I think the method will provide the answers but what I am suggesting is that they should apply wave interaction techniques as used in the ionosphere to extend their measurements by another few milliseconds. If they plotted results as a function of time and got the same answers at 800 microsec. delay and 5 millisec. delay, then I would accept them implicitly.

Narasinga Rao: Unfortunately, at such delay times in the afterglow, the microwave method completely fails because of the fact that the densities are very low.

Smith: This is the case using their simple equipment. However, sophisticated equipment using Fejer techniques could extend the sensitivity by a factor of 1000 and greatly extend the useful delay times.

Narasinga Rao: I do not want to keep arguing this point in their defence, but I do not think there is any necessity to go to such delay times in the afterglow when the important parameter there is probably the ratio $\frac{\omega p^2}{\omega^2}$ and not necessarily the time in the afterglow.

Smith: Well, there is the fundamental flaw that this approximation only holds when the electron density is extremely low. I suggest to them that they take measurements at 2 or more delays and then if they get the same answer I'll believe them. If they do not do that then their work is under a cloud. The obvious thing to do is to take measurements at two delays and see if you in fact can verify the hypothesis in your theory that the measurements are independent of N.

1.7 THE ELECTRON DISTRIBUTION AND COLLISION FREQUENCY HEIGHT PROFILE FOR THE LOWER PART OF THE IONOSPHERE (THE D AND LOWER E REGIONS)

A REVIEW OF OBSERVATIONAL DATA

by

J.S. Belrose and I.A. Bourne

Radio Physics Laboratory
Defence Research Telecommunications Establishment
Ottawa, Ontario, Canada

1. Introduction

Several recent reviews (e.g., Belrose 1964, 1965; Aikin 1965, Whitten and Poppoff 1965, Ivanov-Kholodnyy 1964, Knecht 1963, and Holt and Landmark 1964) have summarized present knowledge of the distribution of electron number densities and collision frequencies in the lower ionosphere (the D and lower E regions) during disturbed and undisturbed times.

During the intervening years many additional profiles have been published and much unpublished data have been accumulated. The dissemination of this information was one of the main aims of this conference. Only profiles which have been determined with reasonable certainty are included in this review, but it must be admitted that the reliability of data is difficult to assess and different authors might have different views. Ratcliffe and Weeks (1960) have noted that conclusions derived from observational data on electron distribution and collision frequency are frequently based on a great number of assumptions. A knowledge of the reliability of the deduced ionospheric parameters is of prime importance, for although several theoretical models of the D region have been suggested none are fully consistent with experimentally derived parameters.

2. Collision Frequencies

Collisions between electrons and neutral molecules are of great importance to some aspects of radio wave propagation, particularly for the role they play in the attenuation of radio waves. The collision frequency height profile may be estimated from laboratory studies of the mobility of electrons in atmospheric gases, in combination with rocket-borne measurements of atmospheric temperature and number density (or pressure); or it may be determined quite independently from an analysis of radio wave propagation data. The appropriate analysis in the latter case is far more complex than had been first thought, but the theory now appears to be adequately developed (Sen and Wyller 1960, Shkarofsky 1961). As a result of the work of Crompton et al.(1953), Huxley (1959), and Phelps and Pack (1959), it became necessary to change the old concepts of collision frequency; these laboratory studies revealed that the collision frequency of low energy electrons in molecular nitrogen was proportioned to the energy of the electron. Earlier, when the Appleton-Hartree formulas were derived, it was believed that the collision cross-section was inversely proportional to velocity and the value of ν obtained was independent of electron energy. Thus our concepts of collision frequency have changed drastically during the past 5 years.

Also there is much recent evidence (both in radio and meteorological pressure data) to establish that the collision frequency height profile is not invariant, but changes with season, latitude, possibly time of day, and, at least in the E region, with solar activity;

there is also evidence of day-to-day changes, especially in winter months at high latitudes. The reported dependence of collision frequency on solar activity (Schlapp 1959, Beynon and Jones 1965) requires that the electron temperature, Te, and the neutral gas temperature, Tn, be different, since there is no evidence that neutral gas temperatures in the E region change by the required amount over the epoch of the solar cycle. The suggestion that electron and gas temperatures in the E region can be different is not accepted by all workers (cf. Dalgarno Paper 1.5) although there is some evidence derived from incoherent scatter radars that Te/Ti $\simeq 1.5$* in the E region (LaLonde Paper 2.5). These results are however inconsistent with results derived by other workers using the incoherent scatter radars (Perkins 1966), but doing a different experiment. Whether Te/Ti is different from unity in the E region seems to be yet unresolved.

Collision frequency height profiles calculated from average rocket pressure data, using the formula

$$\nu\, m = 1.04 \times 10^{8}\ p(\mathrm{mm.Hg})\ \mathrm{sec.}^{-1}$$

for 30°N, 45°N, and 60°N are compared with various radio data in Figs. 1 to 3. This formula was given by Phelps (1960), and while it differs from others derived from experimental measurements made only in nitrogen gas, it is probably reasonably accurate, particularly since van Lint et al. have revised their collision frequency value for O_2 upward by almost a factor of two (Phelps 1962).

The radio data employed in these investigations have taken into account recent revisions in the theoretical analysis of radio wave propagation, i.e., the generalized magnetoionic theory (Sen and Wyller 1960). In Fig. 1 the results obtained by Smith et al. (1965) have been measured at Armidale by a gyrofrequency radio wave pulse experiment; the extraordinary made gyro wave was used to disturb the ionosphere, thus localizing the height range where heating occurs, and the transferred modulation on two probing waves was observed. The result at 70 km. was determined from daytime observations, the result at 85 km. from nighttime observations. In Fig. 2 the results obtained by Schlapp (1959) have been measured at Cambridge by the E region group retardation method (Appleton 1935). The single value at 61 km. reported by Aikin et al. (1964) has been determined from a rocket experiment at Wallops Island, where a Faraday rotation experiment at 3 MHz. was used to examine the quiet D region. The value corresponds to a critical propagation condition at a height where there was reversal in the sense of rotation of the plane of polarization. The results attributed to Belrose have been reported by Belrose and Burke (1964), and were determined by the partial reflection experiment at Ottawa. The dashed curve labelled Curve 1 has been calculated by using the formula noted above and the COSPAR International Reference Atmosphere (CIRA 1961). It is included for reference, as this curve has been frequently used to determine electron density data from the DRTE partial reflection measurements. In Fig. 3 results obtained by Kane (1961) have been measured by a rocket propagation experiment at Fort Churchill during polar cap absorption events. The results of Jespersen et al. (1963) have been measured by a rocket-borne multifrequency experiment which measured differential absorption, differential phase, and ionospheric attenuation during auroral absorption events.

The collision frequency during disturbed and undisturbed times seems to be the same. It appears that there is substantial agreement between values deduced from the various methods. However, a period of consolidation still lies ahead as the laboratory measurements are extended to various species of neutral molecules and ionospheric observations are taken over a broader range of conditions. The data are limited in their geographic extent, and there is a need for measurement of rocket pressure data or collision frequencies at latitudes higher than 60°N.

3. The E Layer at Night

There is little information about the E layer at night because its penetration frequency lies below the working range of most ionosondes. The most extensive data which show the fine scale irregularity of the nocturnal E layer are the rocket-borne Langmuir probe measurements by Smith (1965a, b), some of which are illustrated in Fig. 4. It is noted that the electron densities increase from about 10^2/c.c. at 80 km. to 10^4/c.c. at 100 km., and decrease above this height reaching a minimum between 120 - 140 km.

*The positive ion temperature, Ti, has not been studied, but there seems to be little doubt that Tn and Ti are equal in the E region.

The data are too few to establish seasonal, latitudinal or sunspot cycle changes, but a long series of long wave propagation observations have been carried out through one or more solar cycles, and these data reveal certain characteristics which can be interpreted on a consistent basis. For example, steeply incident radio waves at 16 kHz. appear to be more strongly reflected at sunspot maximum than at sunspot minimum, whereas at 245 kHz. the reverse is true. We would expect increased attenuation of medium frequencies in sunspot maximum years, since increases in absorption, lasting a night or two, have been shown to follow large geomagnetic storms (Lauter and Springer 1952, Belrose 1958), but the mean amplitudes are still less in sunspot maximum years even if one attempts to remove obviously disturbed days.

A second effect referred to in the literature as the "breaking of the nocturnal E region" is observed to be associated with magnetic storms during which frequencies of about 150 kHz., normally reflected from heights of 90-120 km. are occasionally returned from much higher heights, near 120-150 km. (Watts and Brown 1951, Linquist 1953).

The data in Fig. 5 reveal some interesting facts about seasonal and diurnal changes. The monthly mean "phase height" of reflection of 15 kHz. waves steeply reflected from the ionosphere (Rugby-Cambridge) for July and December 1954 and 1955 are plotted against cos χ, the cosine of the solar zenith angle. This "phase height" variation probably indicates the variation of the level where the electron density is about 300/c.c. In July the phase heights for the same range of zenith angles are greater than in December. The regular variation throughout the night is the feature to note in the present discussion. The maximum phase height is reached about one hour after local apparent midnight, and the phase height then slowly decreases until a rapid decrease begins a few minutes before sunrise. This is evidence for a nocturnal production of ionization which is solar controlled, being minimum at local apparent midnight. The fact that the maximum phase heights are not reached until one hour afterwards is taken to be due to the "sluggishness" of the ionosphere, since a recombination coefficient in the expression $\tau = \frac{1}{2} \alpha N$ of $\sim 5 \times 10^{-7}$/c.c./sec. can account for the delay.

The seasonal change of the midnight phase heights is shown in more detail in Fig. 6. Minimum phase heights (middle curve in the figure) are reached in midwinter; this fact, together with the discussion in the paragraph above, is taken as evidence for the nocturnal production being larger in winter (or the electron loss rates are smaller) than in summer. The midsummer phase heights are less than those in April and August, and might be explained by light scattered around the edge of the solid earth, since ionization changes, albeit small, can be detected as early as $\chi \simeq 110^{\circ}$.

4. The Electron Content of the Daytime Lower Ionosphere

4.1 The Background Electron Distribution

Electron density height profiles for the undisturbed lower ionosphere measured by various techniques (see Table 1) are given in Fig. 7. While the major differences between the various curves is undoubtedly due to changes of location time and solar conditions, the existence of observational errors should not be neglected. Curve 1 (in two parts) was obtained by the partial reflection experimental technique; curves 3 and 9 were obtained by rocket-borne Langmuir probes; curves 4, 5, 8, 10 and 11 by rocket-borne radio wave propagation experiments that employed HF transmissions between the rocket and the ground facilities; curves 12 and 13 by rocket-borne radio wave propagation experiments that employed LF transmissions between the ground and rocket. Curve 6 was determined by a cross-modulation experiment; curve 7 was derived from ionosonde data and does not extend below the E region, a limitation of this technique. Curve 2 is a theoretical distribution calculated for a quiet sun at a low zenith angle (by Aikin 1963), although in the light of what has been said at this conference, concerning the uncertainties in theoretically calculating electron density profiles, we are not sure what Dr. Aikin would have calculated today.

The figure also shows two electron density profiles representative of the nighttime E region at middle latitudes, which are included to show more clearly the diurnal change.

Some general features of the daytime D region can be seen in several of the curves in Fig. 7; these are probably best defined by the curves 1 and 2 which show three "ledges" of ionization: (1) the base of the E layer at about 80 - 85 km.; (2) the D layer which reaches

a quasi-peak in the height range 75 - 80 km.; (3) a distinct region below about 70 km. which has been designated the C layer. Since the ledges exhibit quite different diurnal patterns and are ascribed to different ionization mechanisms, as we shall see later in this paper and in this conference (see e.g., Smith Paper 3.2.4), they are quite properly called "layers".

4.2 Seasonal Changes in D-region Ionization

Only a few attempts have been made to measure the seasonal changes in electron concentration in the D region. One set of measurements obtained by the partial reflection experiment at Ottawa is shown in Fig. 8. The data are winter (Dec. 1961), spring equinox (Mar. 1962), and summer (June 1962). It is clearly evident that there is much greater variability during winter than during summer; the winter variability is thought to be due to circulation changes in the mesosphere. Only in winter months is the C layer clearly observable, in summer it merges with the overlying D layer. The dashed and solid portions of the curves correspond to different analysis of the data (see Belrose and Burke 1964).

Data taken on five magnetically quiet days in each month from November 1961 to October 1962 were averaged and plotted in Fig. 9. The winter curve is the average for Nov., Dec. and Jan.; the summer curve is the average for June, July and August; March and September are plotted separately. While a different method of averaging of winter data has subsequently been used (see Belrose et al. Paper 2.3.2), Fig. 9 is included in this paper because it shows the very marked seasonal asymmetry in the D region: note that the September curve nearly resembles a summer month, whereas the March curve lies between winter and summer. This seasonal asymmetry is clearly seen in the midday reflection height of VLF radio curves steeply reflected from the ionosphere (top curve in Fig. 6), and has been previously referred to in the literature as "the November effect". The averaged data for three summer months (June, July, August 1962) and four winter months (November 1961 and 1962, December 1961, and January 1962) are shown in Fig. 10. The summer data show little variation from month to month, whereas the winter data show a considerable change. The minimum ionization densities are found in December.

The electron density height profiles in Fig. 11 have been deduced from an analysis of long wave propagation data. Curves 1, 2, 3 and 4 are from Krasnushkin and Kolesnikov (1962) and are for night, midday winter and summer at middle latitudes, and midday at equatorial latitudes respectively during sunspot maximum years. The profiles illustrate a disappearance of the C layer at equatorial latitudes, and suggest that at middle latitudes the electron densities in the C layer do not change with season. Curves 5, 6 and 7 are from Deeks (1966) and are for midday in winter, equinox, and summer at middle latitudes during sunspot minimum years. While there is a general agreement between the two sets of profiles there are important differences, e.g., Deeks' profiles predict a minimum between the lower C layer and the upper D layer, whereas in the Krasnushkin and Kolesnikov profiles the C and D layers partially overlap, the degree of overlapping varying with season. In winter, owing to the high altitude of the position of the D layer, the C layer is almost exposed. This feature, at least, is common with the electron density profiles over Ottawa measured by the method of partial reflection.

The general features of the curves in Fig. 11 change with the epoch of the solar cycle and latitude as expected: that is, the C layer is greatest at sunspot minimum (galactic cosmic rays are more intense during sunspot minimum years), whereas the D layer is greatest at sunspot maximum (the contribution to D-layer ionization by solar xrays would be expected to be greatest in sunspot maximum years); and the C layer is weakest (not there at all) at equatorial latitudes.

4.3 Diurnal Changes in Electron Distribution

Only a few attempts have been made to measure diurnal changes in electron concentration in the D region, and these in general were concerned with changes which occur after sunrise (e.g., Fejer and Vice (1961), Barrington et al. 1963, Nesterov and Serafimov 1964). The changes which occur during the twilight periods are of considerable importance, since they could provide some clue about the ionization processes responsible for the various layers (C, D and E layers).

The results presented in Fig. 12 show a series of measurements made by rocket-borne Langmuir probes for solar angles of 108°, 96° and 85°, which reveal a rather startling feature of the D-region ionization change over dawn. The profiles were obtained from a nose-tip Langmuir probe and although electron density is indicated the experiment measures probe current. The probe current is directly proportional to electron density for heights greater than about 85 km., but interpretation of probe currents in terms of electron densities can be considerably in error at low heights. All ascent profiles are shown, except for curve 3, which is a descent profile included because it showed considerable departure from the ascent profile (curve 2). The D region was fully illuminated by the visible part of the solar spectrum at the times of the last two rocket launches. The profiles show however that there was no increase in electron density at the time of the ascent profile, for which the solar zenith angle at the rocket was 95.8°. The profile obtained on the descent of the rocket ($\chi = 94.1^{\circ}$), shows the initial development of the C layer, which is well developed on the final rocket flight (curve 4). The electron density peak at 65 km. for this latter profile was estimated to be about 25/c.c. from a propagation experiment aboard the rocket.

It was concluded from comparison of these profiles that the increase of electron density in the D region begins when it is illuminated by radiation not from the visible part of the solar spectrum but from that part of the spectrum absorbed by the ozone layer. The wave lengths responsible for photo-detachment in the D region were therefore estimated to fall within the range 1800 to 2900 Å, since shorter wave lengths are absorbed higher in atmosphere while the longer wave lengths penetrate the ozone layer.

The suggested onset of sudden changes in the D-region ionization near $\chi \simeq 95^{\circ}$ is rather startling, and not entirely in accord with low frequency propagation data, which show that while there are noticeable features near $\chi \simeq 95^{\circ}$, signigicant changes occur very much earlier, near $\chi \gtrsim 100^{\circ}$.

There seems to be little doubt, at least at middle latitudes, that the D-region ionization contains two layers, the D and C layers, which have quite different diurnal variations. The C layer develops at dawn ($\chi > 98^{\circ}$) whereas the D-layer ionization is not significant until quite near ground sunrise ($\chi = 90^{\circ}\ 50'$). The daytime structural changes in the D-region ionization are largely a filling in of the ionization between the base of the D layer and the C-layer peak; the regular change of this ionization can be seen from the diurnal change of the phase height of reflection of VLF radio waves steeply reflected from the ionosphere.

The phase height of reflection of VLF radio waves steeply reflected from the ionosphere closely follows changes of the zenith angle of the sun, and departures from symmetry about the time of local noon are unmeasurably small in summer. In winter there is a more marked asymmetry, as is illustrated in Fig. 5. The seasonal change of this asymmetry is illustrated in a different way in the bottom curve of Fig. 6, which shows the time delay after sunset required for the phase height to attain the value that it had at sunrise. The delay is negligibly small in summer months and about 1½ hours in winter months.

4.4 D-region Ionization and Solar Activity

Except for the results shown in Fig. 11, most of the data summarized in this paper have been taken during the minimum epoch of the solar cycle. Indirect observations have, however, been carried through one or more solar cycles. For example, steeply incident radio waves at 16 kHz. appear to be more strongly reflected at sunspot maximum (by about 3 db) and the "phase height" of reflection is lower (by about 2 km.) than at sunspot minimum, whereas at 245 kHz. the reverse is true (the change being as large as 6 db). The stronger reflection of 16 kHz. waves can be attributed to an increased electron density gradient, while the decreased strength of the 245 kHz. return could result from increased absorption and increased electron content below the E layer. Several unexplained features have also been revealed, such as a maximizing of the absorption when the solar zenith angle is 70°, and a disappearance of the solar cycle variation at 245 kHz. during summer months. Monthly median values of the logarithm of the reflection coefficient are closely correlated to sunspot number R at 245 kHz., but the linear relation holds only up to R = 150 when a "saturation effect" sets in. A similar behavior is found in the case of HF absorption.

4.5 D-region Meteorology

We have already noted that measurements of electron densities in the D region indicate great regularity from day-to-day in summer and great irregularity from day-to-day in winter. In addition, seasonal changes are not symmetrical in their variation with the zenith angle of the sun. The winter irregularity and the seasonal asymmetry are likely to be related to meteorological effects in the D region rather than to variations in the ionizing radiations from the sun.

On some days in winter, marked increases in ionization are observed throughout the D region. This results in a marked increase in absorption of high frequency radio waves reflected at higher levels, to the point where a statistically significant winter anomaly is recognized. This little-understood phenomena (Belrose et al. 1966) has long been thought due to some sort of atmospheric meteorology (Dieminger 1952, 1955); on one occasion at least (Wexler 1956) the anomaly coincided with a drastic increase in the temperature of the stratosphere. Although no satisfactory explanation of it exists, the effect might be due to changes in the minor ionizable constituents of the lower D region, although the height where the ionization changes occur is not well established. The observational data of Gnanalingan and Weekes (1955) suggested sporadic increases of D-region ionization at heights near 85 km., whereas the "winter variability" discussed by Belrose et al. (1966) was concerned with heights below 80 km. It would thus appear that electron density increases can take place in both height regions and, on the basis of HF (2 MHz.) radio wave absorption alone, the height where the electron density increased cannot be located with certainty. There also seems to be some difficulty in recognizing a winter day of anomalous absorption. For example, a large absorption increase in February 1961 (see Belrose 1963, 1965 and Fig. 13) which did not appear to be connected with electron precipitation, and was therefore labelled a winter day of anomalous absorption, was associated with great absorption of 2.66 MHz. waves (up to and greater than 80 db over normal) and was primarily due to ionization changes below 80 km. It has since been realized that this period of excess absorption was also detected in Europe (Schwentek 1965), a fact which makes positive identification of the phenomenon difficult because one of the reasons for associating the winter anomaly with meteorological changes in the D region was the fact that HF absorption changes correlated over distance up to about 1000 km., but the correlation was poor or non-existent for greater distances.

The winter variability is briefly discussed elsewhere in these proceedings (cf. Paper 2.3.2 and Paper 6.5).

5. Electron Density Distributions at times of Ionospheric Disturbances (SID, PCA and AA)

Electron density changes by one or more orders of magnitude occur at times of ionospheric disturbances. The change which occurred during an SID associated with a class 2+ solar flare on 1 March, 1962, is given in Fig. 14. This profile was measured by the partial reflection experiment. The absorption recorded by a 30 MHz. riometer was about 1.2 db, which is a typical magnitude for a moderately large SID, but riometer absorption can amount to 3 db for large events, and 10 db occasionally.

Electron density profiles during PCA are given in Fig. 15. The numbers on the curves give the absorption measured by a 30 MHz. riometer, a 3 db event being the largest absorption for which a profile has been determined. Since PCA absorptions on occasion can reach 20 - 30 db, the electron density enhancements at low heights must be considerable at these times. The dashed extension of the curve labelled normal midday summer profile is an average profile (Knecht 1963) where some dozen or so results were averaged (some of which were given in Fig. 7). It is intended to illustrate that the main electron density enhancement occurs at low heights.

Fig. 16 gives electron density height profiles during auroral absorption events. The profiles show a marked difference between day and night results, although there is also a difference in the magnitude of the absorption. Although nighttime absorptions can be as large as daytime events, there is indirect evidence (Belrose 1965) based on LF propagation which suggests that even for large nighttime events the electron density profiles do not extend below about 70 km. The difference is thought due, at least in part, to the importance of photodetachment from negative ions during daytime. Since the largest absorption event for which data have been obtained is 4.2 db, and since 10 db absorption events can occur during

the night as well as during the day, there is a need to measure profiles during large disturbances - especially during the night - because at the heights where the nighttime ionization increase is thought to occur, the electron enhancements for a large absorption event must be very great because of the small collision frequencies.

One of the profiles in Fig. 16 was measured at a time when there was no auroral absorption detected by a 30 MHz. riometer (labelled A (0 db)). If these electron densities are compared with those measured at middle latitudes (see Fig. 4), it will be found that they are much greater. This difference is later redressed (in Paper 2.3.2) where it is suggested that nighttime ionization at auroral latitudes is strongly dominated by ionizing energetic electrons, and that weak electron fluxes probably result in enhancement of the nighttime electron densities even during so-called quiet times. This point is also made by Haug in Paper 2.3.1.

6. Conclusions

This paper has reviewed the observational data concerning the distribution of electron number densities and collision frequencies in the lower ionosphere. The following conclusions can be drawn:

(1) The collision frequencies (or pressures) in the lower ionosphere change with season and latitude; the greatest seasonal change occurs at high latitudes, where day-to-day changes as large as a factor of two can take place in winter. There is some evidence that diurnal pressure changes occur, being most pronounced at some heights (Whitehead et al. 1965), but a diurnal change in collision frequency has not been detected. There is also evidence that collision frequencies in the E layer change with solar activity. There is no evidence for collision frequency changes during particle bombardment of the lower ionosphere (auroral disturbances) or during sudden ionospheric disturbances, although short-lived effects could have occurred and been missed.

(2) The magnitude of the electron density and its variation with height is roughly known, during disturbed and undisturbed times, but superimposed on a general increase with height are important structural features which are currently receiving greater attention. New and previously unavailable results, presented at this conference, have detailed the general variation of the electron density distribution at dawn. If future experiments are to make significant contributions to our knowledge of electron production and loss, they should be capable of measuring the electron number density distribution with accuracy and be designed to study diurnal and seasonal changes at various latitudes. There are no measurements of the electron density below the 60 km. level under quiet conditions, since various experimental techniques rapidly lose sensitivity at lower heights. The variation of the electron density with height below the 60 km. level is consequently open to speculation.

(3) There is evidence in some profiles for a deep minimum in electron density at a height of about 82 km.

(4) The majority of the observational data summarized in this paper were made during quiet sun years. Experimental studies of the lower ionosphere should continue to be made during the next several years to more clearly delineate changes with solar activity. The association between magnetic activity and D-region electron densities observed at Ottawa (and discussed in Paper 2.3.2) suggest that significant changes can be expected at high magnetic latitudes.

(5) The nighttime electron density profile is very irregular, especially above a height of about 100 km. Some of the nocturnal sporadic E (or thin layer) structure has a fairly long lifetime, of the order of hours (see the thin layer in the 110 - 120 km. height range in Fig. 12 which can be recognized even after sunrise). There is some evidence that on some days there is structure below 85 km. (i.e., not merely an exponential increase of electron density with height).

(6) Nighttime electron density values in the height range 85 - 100 km. in auroral latitudes can be as large as during the daytime, even on so-called undisturbed nights (i.e., no auroral absorption measured by 30 MHz. riometers).

(7) Radio data (16 kHz. "phase height" of reflection) provide evidence for a nighttime production of electrons which is under solar control (a minimum at local midnight). The source of ionization is probably scattered Lyman Alpha. The calculated recombination coefficient at 90 km. is 5×10^{-7}/c.c./sec.

REFERENCES

Adey, A.W. and W.J. Heikkila. Rocket electron density measurements at Fort Churchill, Canada. Can. J. Phys., 39, 219 - 221, 1961.

Aikin, A.C. Formation of the equatorial ionospheric D region. Proc. of the Second International Symposium on Equatorial Aeronomy, (ed. F. de Mendonca), 1 - 13, 1965.

Aikin, A.C., Kane, J.A. and J. Troim. An interpretation of a rocket measurement of electron density in the lower ionosphere. Goddard Space Flight Center, Sci. Report X - 615 - 63 - 159, 1963.

Aikin, A.C., Kane, J.A. and J. Troim. Some results of rocket measurements in the quiet D region. J. Geophys. Res., 69, 4621 - 4628, 1964.

Appleton, E.V. A method of measuring the collision frequency of electrons in the ionosphere. Nature, 135, 618, 1935.

Barrington, R.E., Thrane, E.V. and B. Bjelland. Diurnal and seasonal variations in D-region electron densities derived from observations of cross-modulation. Can. J. Phys., 41, 271, 1963.

Belrose, J.S. Some investigations of the lowest ionosphere. Ph.D. Thesis Cambridge, England, 1958, (unpublished).

Belrose, J.S. Present knowledge of the lowest ionosphere. AGARDOgraph 74: Prop. of radio waves at frequencies below 300 kc., (ed. Blackband), Pergamon Press, 1963.

Belrose, J.S. The lower ionospheric regions. Physics of the Earth's Upper Atmosphere, (ed. Hines et al.) 46 - 72, Prentice-Hall Inc., 1965.

Belrose, J.A. and M.J. Burke. Study of the lower ionosphere using partial reflections. 1. Experimental technique and method of analysis. J. Geophys. Res., 69, 2799 - 2818, 1964.

Belrose, J.S. and E. Cetiner. Measurement of electron densities in the ionospheric D region at the time of a 2+ solar flare. Nature, 195, 688 - 690, 1962.

Belrose, J.S., Bourne, I.A. and L.W. Hewitt. The winter variability of electron density in the lower ionosphere over Ottawa. A discussion of results and possible cause. Electron Density Profiles in the Ionosphere and Exosphere, (ed. Frihagen), 48 - 60, North Holland Pub. Co., 1966.

Beynon, W.J.G. and E.S.O. Jones. Some medium latitude absorption studies. J. Atmosph. Terr. Phys., 27, 761 -773, 1965.

Bourdeau, R.E., Aikin, A.C. and J.L. Donley. Lower ionosphere at sunspot minimum. J. Geophys. Res., 71, 727 - 740, 1966.

Bowhill, S.A. and G.G. Kleiman, in NASA. University Program Review Conference, NASA, Special Pub. SP -85, U.S. Gov. Printing Office, Washington, D.C., March 1965.

Cole, A.E. and J. Kantor. Air Force interim supplemental atmospheres to 90 km. AF Surveys in Geophysics No. 153, AFCRL - 63 - 936, December 1963; Monthly atmospheric structure surface to 80 km., AFCRL 65 - 634, August 1965.

Crompton, R.W., Huxley, L.G.H. and D.J. Sutton. Experimental studies of the motions of slow electrons in air with application to the ionosphere. Proc. Roy. Soc., A., 218, 507, 1953.

Deeks, D.G. D-region electron density distributions in middle latitudes deduced from the reflection of long radio waves. Proc. Roy. Soc. A., 291, 413 -437, 1966.

Dieminger, W. Uber die Uracke de exzesiven absorption in der ionosphere an winter tagen. J. Atmosph. Terr. Phys., 2, 340 - 349, 1952.

Dieminger, W. Short wave echoes from the lower ionosphere. The Physics of the Ionosphere. (The Phy. Soc. Lond.), 53 -57, 1955.

Fejer, J.A. and R.W. Vice. An investigation of the ionospheric D region. J. Atmosph. Terr. Phys., 16, 291 - 306, 1959.

Friedman, H. Rocket observations of the ionosphere (summary paper). P.I.R.E., 47, 272 - 280, 1959.

Gnanalingham, S. and K. Weeks. D-region echoes observed with a radio wave of frequency 1.4 Mc/s. Report of the Conf. The Physics of the Ionosphere, 63 - 70. The Phys. Soc. London, 1955.

Hall, J.E. and J. Fooks. The electron distribution in the quiet D region derived from rocket measurements of low-frequency propagation. Planet. Space Sci., 13, 1013 - 1030, 1965.

Holt, O. and B. Landmark. Some experimental studies of the Arctic D-region AGARDOgraph 78, Arctic Communications, (ed. Landmark), 3 - 25, Pergamon Press, 1964.

Huxley, L.G. A discussion of the motion in nitrogen of free electrons with small energies with reference to the ionosphere. J. Atmosph. Terr. Phys., 16, 46, 1959.

Ivanov-Kholodnyy. Investigation of electron concentration in the lower part of the ionosphere. Review, Geomagnetism and Aeronomy, SSSR IV, 337 -496, 1964.

Jespersen, M., Petersen, O., Rybner, J., Bjelland, B., Holt, O. and B. Landmark. Electron density and collision frequency in the lower D region during auroral absorption. Ionospheric Lab. Royal Tech. Univ. Denmark, Report 16, 1963; and in Electron Density Distributions in the Ionosphere and Exosphere, (ed. Thrane), 22 - 35, North Holland Pub. Co., 1964.

Jespersen, M., Haug, A. and B. Landmark. Electron density and collision frequency observations in the Arctic D region. Electron density profiles in Ionosphere and Exosphere, (ed. Frihagen), 27 - 30, North Holland Pub. Co., 1966.

Kane, J.A. Re-evaluation of ionospheric electron densities and collisional frequencies derived from rocket measurements of refractive index and attenuation, J. Atmosph. Terr. Phys., 23, 338-347, 1961.

Knecht, R.W. The distribution of electrons in the lower and middle ionosphere. Proc. of XIV URSI General Assembly, 1963.

Kransnushkin, P.E. and N.L. Kolesnikov. Investigation of the lower ionosphere by means of long radio waves and low frequency probes installed in a rocket. Detection of a new ionospheric layer. Doklady Akademii nauk SSR, 146, 596 - 599, 1962 (transl. Aerospace Information Div. Library of Congress, AD Report 62-207, 1962).

Lacey, W.K. Private communication, 1965.

Lauter, E.A. and K. Springer. Nocturnal ionospheric disturbances in the lower ionosphere. Zeit. f. Met., 6, 161 - 173, 1952 (translation DSIS/DRB, Canada, Translation T826).

Linquist, R. An interpretation of vertical incidence equivalent height versus time recordings on 150 kc/s, J. Atmosph. Terr. Phys., 4, 10 - 27, 1953.

Nesterov, G. and K. Serafimov. Winter distribution of electron density in the ionospheric D region. Geomagnetism and Aeronomy SSSR, IV, 678 - 683, 1964.

Perkins, F. Private communication, 1966.

Phelps, A.V. Private communication, 1962.

Phelps, A.V. and J.L. Pack. Electron collision frequencies in nitrogen and in the lower ionosphere. Phy. Rev. Letters, 3, 340 -342, 1959.

Phelps, A.V. Propagation constants for electromagnetic waves in weakly ionized, dry air. J. App. Phys., 31, 1723 - 1729, 1960.

Ratcliffe, J.A. and K. Weekes. The ionosphere, physics of the upper atmosphere, (ed. Ratcliffe), 378 -470, Academic Press, 1960.

Robinson, B.J. Diurnal variation of the electron distribution in the ionospheric E layer. J. Atmosph. Terr. Phys., 18, 215 - 233, 1960.

Schlapp, D.M. Some measurements of collisional frequency in the E region of the ionosphere. J. Atmosph. Terr. Phys., 16, 340 - 343, 1959.

Schwentek, H. Private communication, 1965.

Sen, H.K. and A.A. Wyller. On the generalization of the Appleton-Hartree magnetoionic formula. J. Geophys. Res., 65, 3931 -3950, 1960.

Shkarofsky, I.P. Generalized Appleton-Hartree equations for any degree of ionization and application to the ionosphere. Proc. I.R.E., 49, 1857, 1961.

Smith, L.G. Rocket observations of sporadic E and related features of the E region. G.C.A. Tech. Report, 65 - 22 - N, August 1965.

Smith, L.G., Weeks, L.H. and P.J. McKinnon. Investigation of the D and E regions of the ionosphere during the international quiet sun year. NASA Report No. CR - 391, March 1966.

Smith, R.A., Bourne, I.A., Loch, R.G., Setty, C.S.G.K., Coyne, T.N.R., Barratt, P.H. and B.S.N. Prasad. Radio wave interaction using gyro-waves. Sci. Report. No. 3, and Final Report AFCRL 65-460, University of New England, Armidale, N.S.W., 1965.

van Lint, V.A.J., Wicker, E.G. and D.L. Trueblood. Rept. No. T.R. 59 - 43, General Atomic Div. of General Motors Corp., San Diego, Calif. (Unpublished and recent work as referenced by Phelps (1962)), 1959.

Watts, J.M. and J.N. Brown. Effects of ionospheric disturbances on low frequency propagation. J. Geophys. Res., 56, 403, 1951.

Wexler, H. A look at some suggested solar-weather relationships. The sun's effects in the earth's atmosphere. Inst. for Solar-Terrestrial Research, Tech. Report No. 2, High Altitude Observatory, Univ. Colorado, 21 -30, October, 1956.

Whitehead, V.S., Lancer, A.M., Harper, D.R. and W.J. Saucier. Atmospheric structure and circulation to 200 km. in terms of density. University of Oklahoma Research Institute. AFCRL Report No. 65-242, March, 1965.

Whitten, R.C. and I.G. Poppoff. Physics of the lower ionosphere. Prentice-Hall Inc., 1965.

Yonezawa, T. Probe measurements of the electron and positive ion densities in the E and F region by rockets. Proc. NATO Advanced Study Inst. on Electron Density Profiles in the Ionosphere and Exosphere, Skeikampen, Norway, 1961, (to be published).

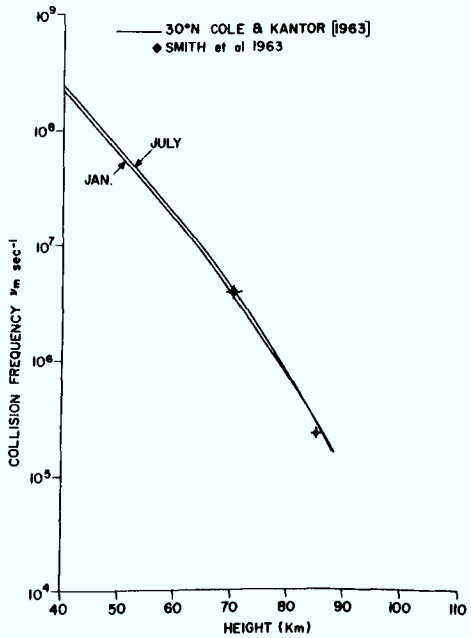

Fig. 1. Collision frequency of electrons νm plotted against height for 30°N. latitude.

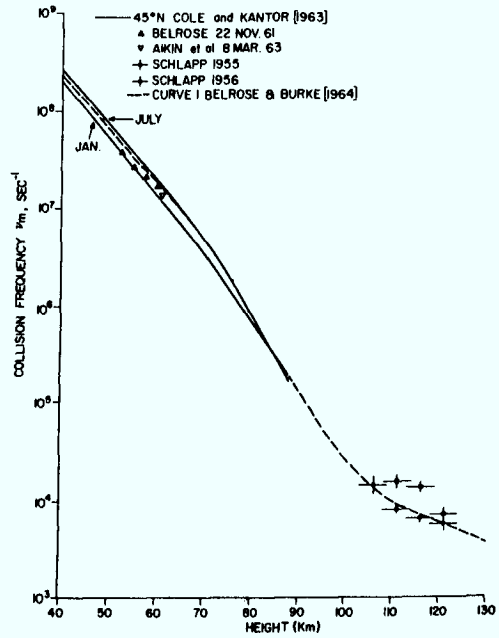

Fig. 2. Collision frequency of electrons νm plotted against height for 45°N. latitude.

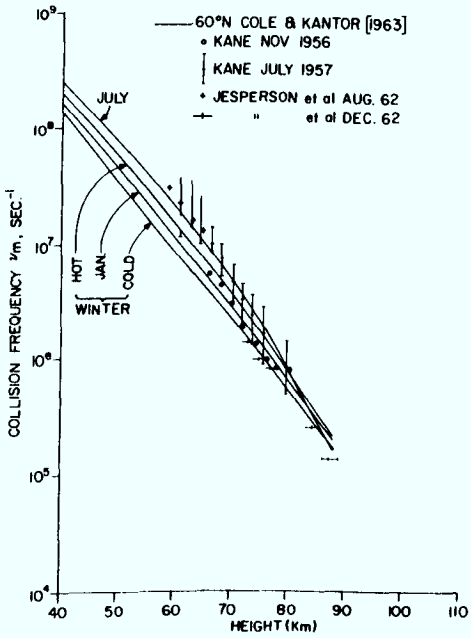

Fig. 3. Collision frequency of electrons νm plotted against height for 60°N. latitude.

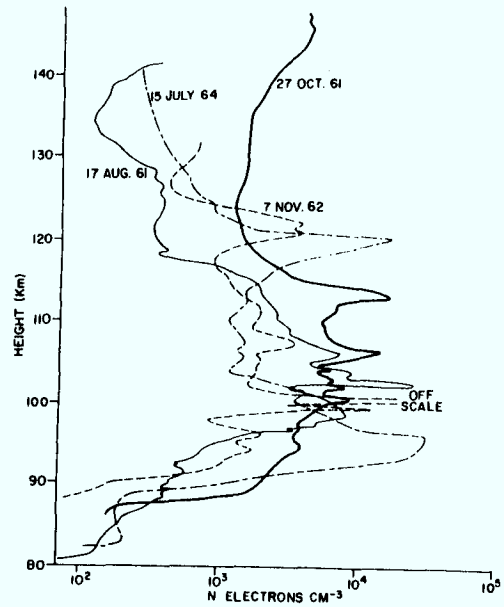

Fig. 4. Electron density-height profiles for the E region at night over Wallops Island measured by rocket-borne Langmuir probes (after Smith 1965).

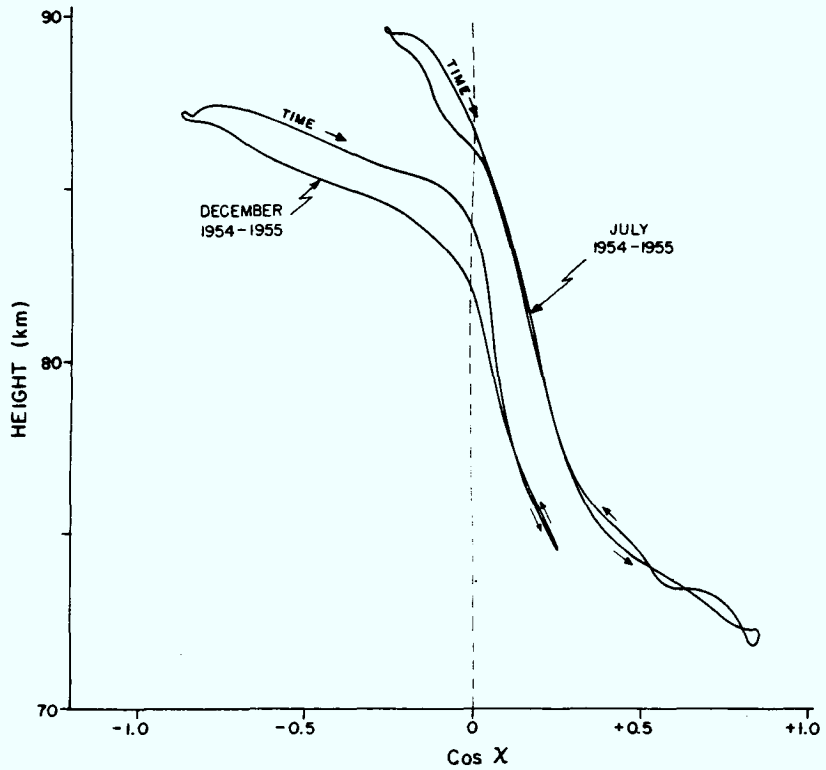

Fig. 5. Diurnal change of the "phase height" of reflection for 16 kHz. waves steeply reflected from the ionosphere (Rugby – Cambridge) during sunspot minimum years for July and December in 1954 and 1955.

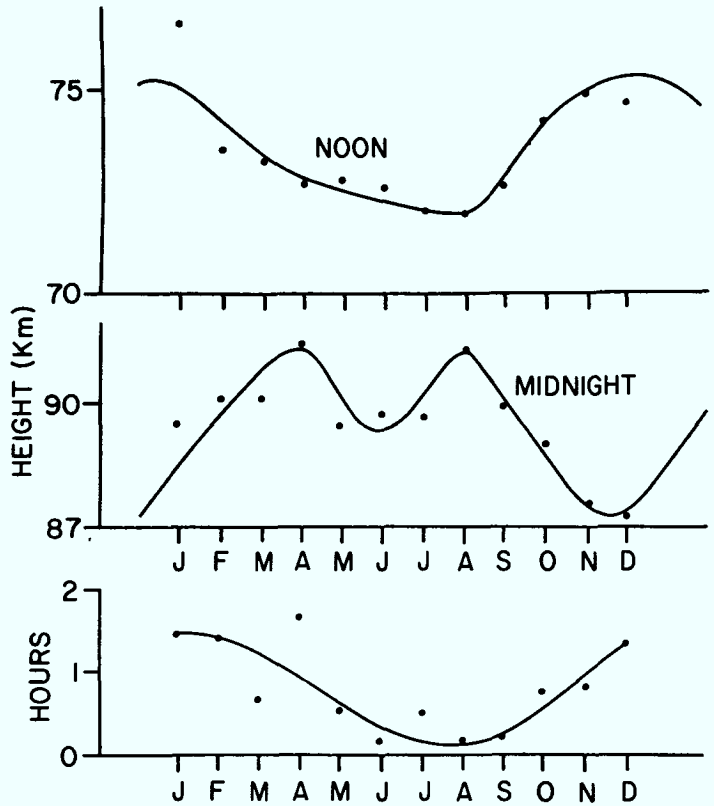

Fig. 6. Seasonal changes in the midday and midnight "phase height" of waves of frequency 16 kHz. observed at Cambridge from a transmitter at Rugby during 1954-55, i.e., sunspot minimum years, and the asymmetry (defined in the text) of the Monthly Mean Daily Variation (after Belrose 1958).

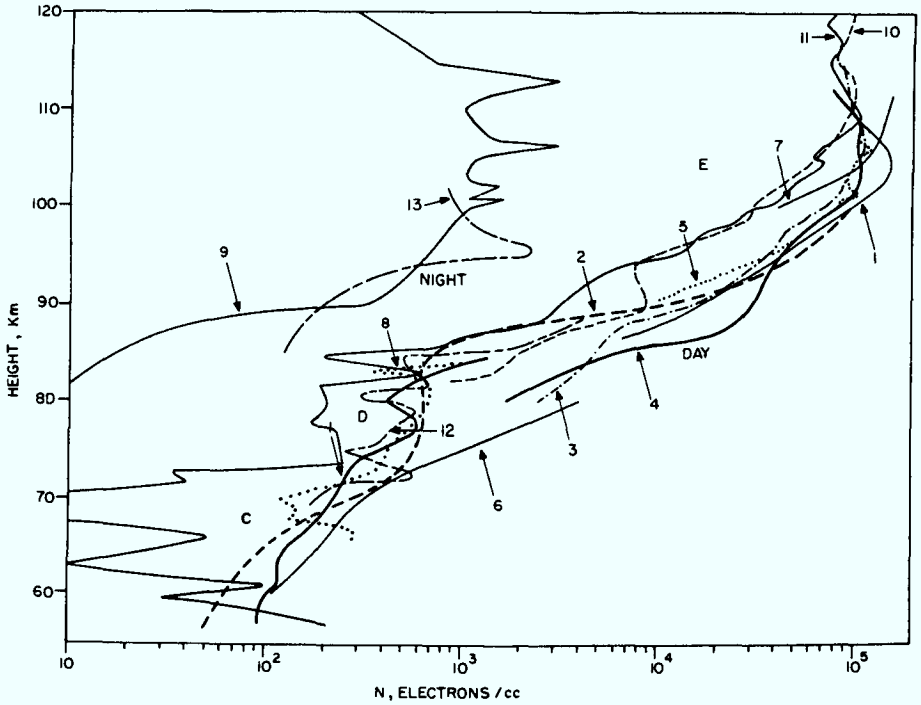

Fig. 7. Electron density height profiles for the undisturbed D and lower E regions. The details for the various curves are given in Table 1.

TABLE 1

ELECTRON DENSITY HEIGHT PROFILES FOR THE UNDISTURBED LOWER IONOSPHERE

Curve No.	Date	Time LST	Place	Experiment	Author
1	1 May 61	1030	Ottawa	Partial Reflection	Belrose & Burke,(1964)
2				Theoretical	Aikin et al. (1963)
3	22 Sept 60	1532	Michikawa	Rocket Langmuir Probe	Yonezawa (1961)
4	17 Sept 59	1237	Churchill	Rocket Propagation	Adey & Heikkila (1960)
5	26 June 54	1730	USSR Middle Lat.	Rocket Propagation	Reported by Friedman (1959)
6	March - April 60	10-14	Kjeller	Pulse cross modulation	Barrington & Thrane (1963)
7	27 Mar 57	Noon	Cambridge	Ionosonde	Robinson (1960)
8	8 Mar 63	1430	Wallops Is.	Rocket Faraday Rotation	Aikin et al. (1964)
9	27 Oct 61	0435	Wallops Is.	Rocket Langmuir Probe	Smith (1965)
10	22 Nov 64	1707	Wallops Is.	Rocket Propagation	Bourdeau et al.(1965)
11	15 Apr 64	1605	Wallops Is.	Rocket Propagation	Bowhill & Kleiman (1965)
12	20 Sept 62	1351	Woomera	Rocket LF Propagation	Hall & Fooks (1965)
13	15 Aug 62	0050	Woomera	Rocket LF Propagation	Hall & Fooks (1965)

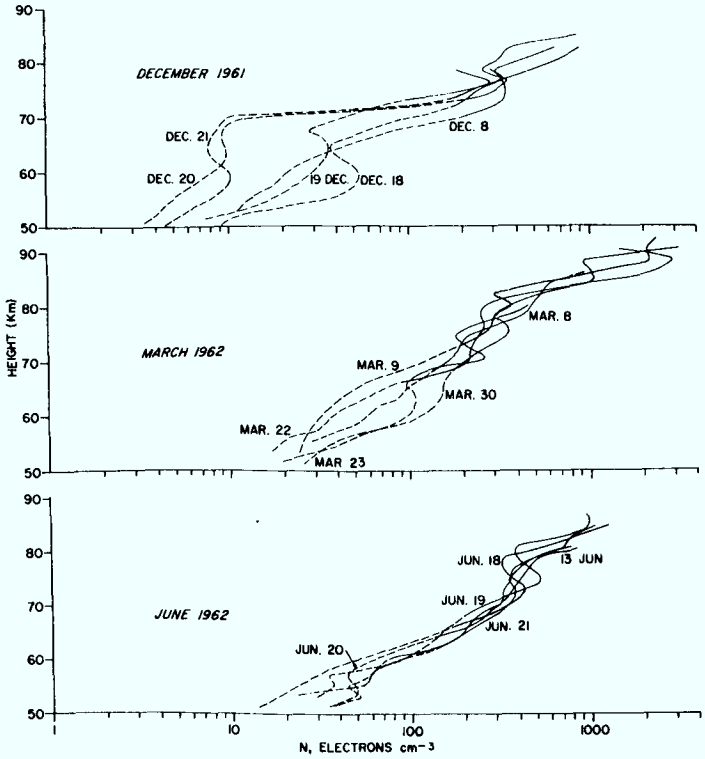

Fig. 8. Electron density height profiles by the method of partial reflection for midday Ottawa data on five magnetically quiet days during three seasons, winter (December 1961), Equinox (March 1962), and summer (June 1962), (after Belrose et al., 1965).

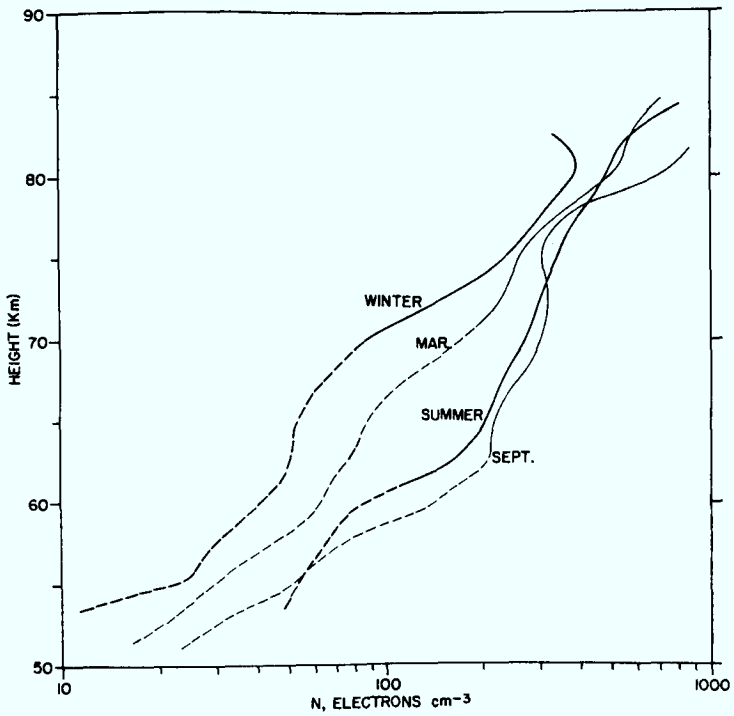

Fig. 9. Seasonal change of electron densities in the D region over Ottawa (after Belrose 1965).

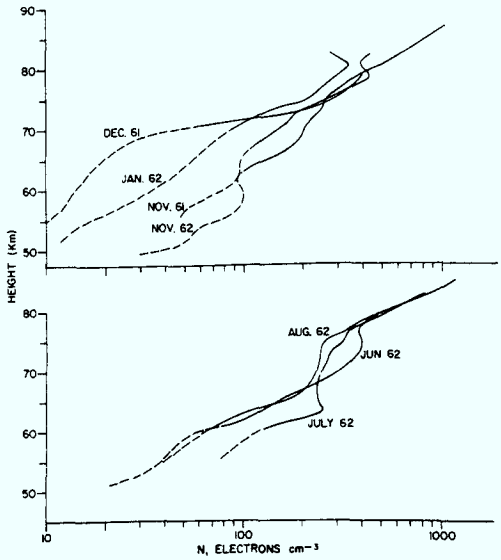

Fig. 10. Electron density height profiles by the method of partial reflection for midday Ottawa data on five magnetically quiet days during three summer months and four winter months.

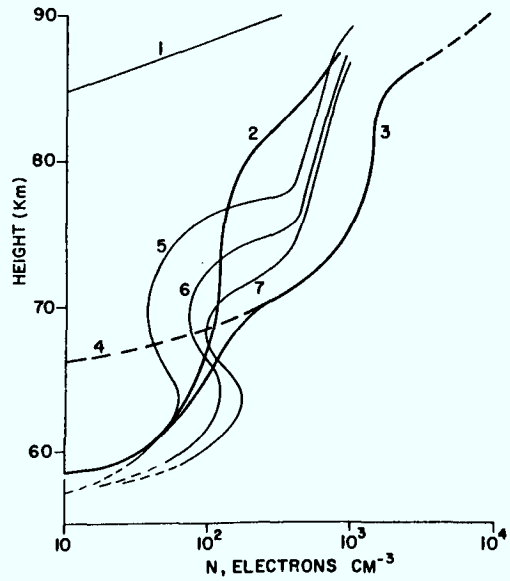

Fig. 11. Electron density height profiles deduced from an analysis of long wave propagation data. Curves 1, 2, 3 and 4 are from Krasnushkin and Kolesnikov (1962) and are for night, midday, winter and summer at middle latitudes, and midday at equatorial latitudes respectively. Curves 5, 6 and 7 are from Deeks (1966) and are for midday winter, equinox, and summer at middle latitudes during sunspot minimum years.

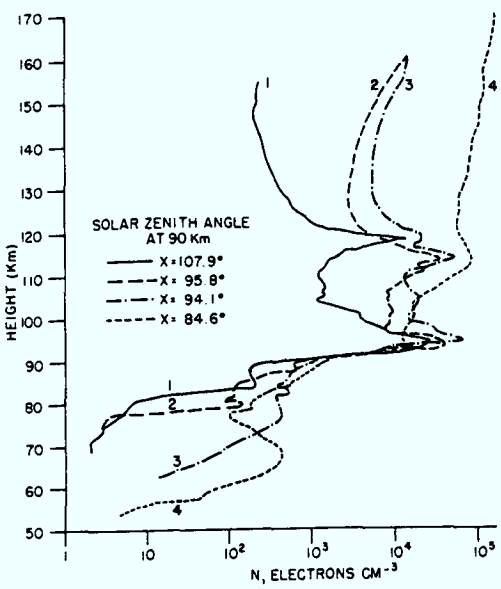

Fig. 12. Sequence of electron density profiles over Wallops Island on the morning of 15 July, 1964, measured by rocket-borne Langmuir probes, (after Smith (1965), Smith, et al. (1966)).

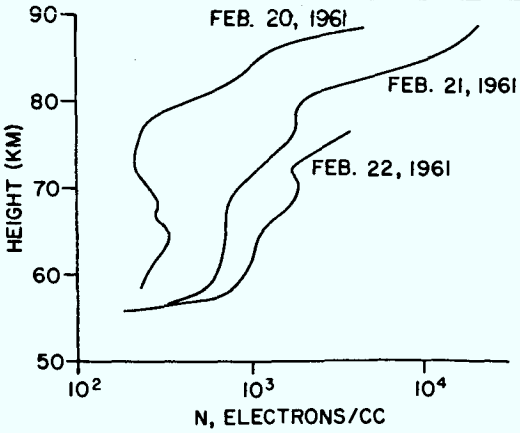

Fig. 13. Electron density profiles over Ottawa during several magnetically quiet days in February 1961 (after Belrose 1963, 1965).

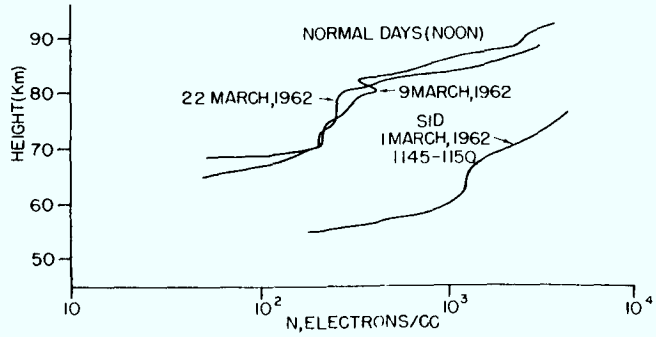

Fig. 14. Electron density height profiles for a Class 2+ Solar Flare and for quiet days in March measured by partial reflection experiment at Ottawa, (after Belrose and Cetiner 1962).

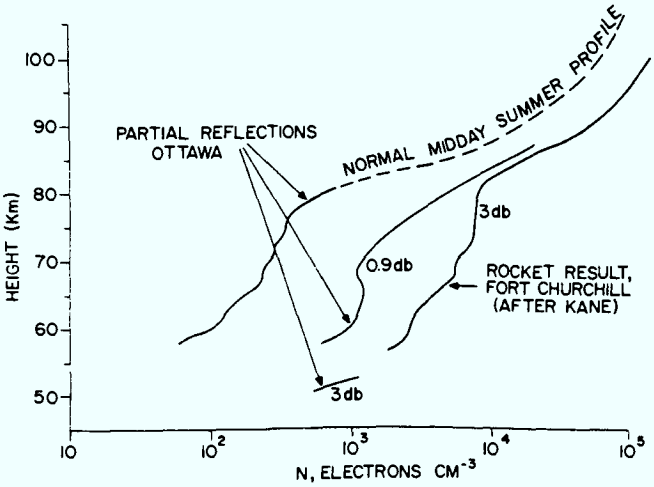

Fig. 15. Electron density height profiles during PCA and during quiet days in summer (June, July and August 1962 at Ottawa). The numbers marked on the curves give the absorption measured by a 30 MHz. Riometer, (after Belrose 1963).

Fig. 16. Electron density profiles during auroral absorption events. The numbers marked on the curves identify them and give the absorption measured by a 30 MHz. Riometer. The curves marked "F" are from Jespersen et al., (1965) and were measured by rocket-borne propagation experiments over Andoya, Norway. The curves marked "A" and "B" are from Lacey (1965), and were measured by a rocket-borne RF capacitance probe over Churchill, Canada.

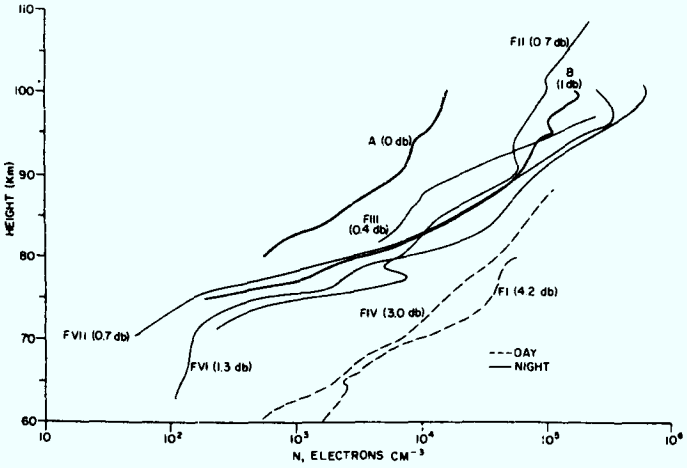

Discussion on Paper 1.7 presented by J.S. Belrose

Sales: You made the comment that the differences between the rocket flights (Fig. 12), which were separated by less than 2° of χ, could not be caused by visible light. There is a paper by Archer in J.G.R. in which he calculates the flux of visible light on the C-layer altitudes and shows that it is reasonable to expect not full development by say $\chi = 96°$, and full development shortly after when $\chi = 94°$, so there is a delay even for visible light due to Rayleigh scattering. I don't think you can rule out the possibility of visible light still being the detaching mechanism. The second point concerns diurnal variations below 60 km. It is important to decide whether there is a diurnal variation below 60 – 65 km.

Belrose: Some results which Dr. Smith[1] will be showing may shed more light on this. We certainly can't come to any outstanding conclusions on the basis of our observations here. The Norwegian cross modulation curves for Kjeller suggest a diurnal change of the electron density at 65 km. by about a factor of 2.

Thrane: That is correct.

Belrose: It is clearly important to establish the diurnal variation of electron densities at low heights better than it has been established at the moment. There is absolutely no doubt about that, but the point I wanted to bring out here was that the main diurnal change we see appears to be in the 65 – 75 km. region. (See Fig. 19, Paper 2.3.2.)

Shirke: On 10 January, 1966, which was a day of winter anomaly, we fired a rocket at $\chi = 60°$. The essential increase in the electron density was seen to occur close to 82 km. There is a factor of 10 increase in electron density near 82 km. over what was observed on 15 December, 1965 at the same zenith angle. There is not much change in the lower ionosphere.

Aikin: Would you please clarify what you mean by winter anomaly? Is this stratospheric warming or is this ground-based absorption?

Shirke: We judge this from ground-based measurements using vertical transmission. When the absorption was about 10 db higher we called it a winter anomaly and fired a rocket.

Belrose: I think the problem is; what is the winter anomaly? There is no doubt that the electron densities are widely variable in winter months, but are there several classes of winter anomalies or are they all meteorological phenomena?

Lalonde: Can you generate profiles every 5min.? If so, how similar are successive 5-minute profiles?

Belrose: Sometimes we can produce profiles every 5 min. It depends on the data. My impression is that when there is a disturbance like an SID we could average over a much shorter period of time and get good data. By good, I mean that if we measure the amplitude ratio between the two magnetoionic components as a function of height, and if we can draw a smooth curve that goes through nearly all data points – this is good data. Sometimes we can average over 5 min., as we did during this SID, and get good data; sometimes we don't get such good data. If you compare the amplitude of the O-ray as a function of height there are differences from one 5-minute period to another. We have shown with reasonable theoretical justification that the O-ray amplitude is approximately proportional to electron density.

Lalonde: Can you make 5-minute profiles during a normal day or do you require a disturbance?

Belrose: We can make a profile in 5 min. any time we want but it is not always as smooth a curve as if we average over 15 min. It depends on how accurately you want to measure your profile. The electron density depends critically on the slope of the amplitude ratio of the two magnetoionic components, and we want to determine the curve as accurately as we can. We will be seeing tomorrow that there is a tremendous range of variability in the scatter of the data which we get back[2]. Sometimes we get data back which has a very large scatter as a function of height; we have no explanation as to why it should be so large on some days compared with other days. Obviously, a day which shows a lot of scatter as a function of height is not going to be a day in which we can get constant answers from one 5-minute period to another.

Gregory: I would like to comment on your Fig. 13. I don't believe that it is an example of the so-called meteorological winter anomaly, and you can check this very easily by noting that this is a northern winter and a southern summer, therefore, photodetachment is much more operative in the Antarctic. If you look at the Antarctic records, you find that those days are in fact days definitely disturbed by some form of particle influx; 22 February was the concluding date of the particle influx event. I make this point because those curves have been put into the literature as a record of the winter anomaly by Reid, and in my opinion they are highly suspect as an example of the meteorological type variation which I shall be talking about[3].

(1) Smith, R.A., Bourne, I.A., Loch, R.G., and T.N.R. Coyne. *Small perturbation wave interaction in the lower ionosphere. Part III: Measurement of electron densities.* These Proceedings, 1966.

(2) Belrose, J.S., Bourne, I.A., and L.W. Hewitt. *A critical review of the Partial Reflection Experiment.* These Proceedings, 1966.

(3) Gregory, J.B. *Mesospheric Electron Densities at 43°S.* These Proceedings, 1966.

1.8 TRANSPORT MECHANISMS IN THE LOWER IONOSPHERE AS MEASURED BY NEUTRAL TRACERS

by

S.P. Zimmerman

Air Force Cambridge Research Laboratories
L.G. Hanscom Field, Bedford, Massachusetts

Abstract

The study by chemical tracers of upper atmospheric winds revealed a transition phenomenon at 105 ± 5 km. This transition was the sudden cessation of turbulence in the optically viewed tracers at this altitude, labelled the turbopause. The continued use of these tracers by various authors, to study the turbulent parameters below the turbopause will be reviewed here.

Although not in keeping within the original guidelines of my previous summary, a significant set of turbulent data as studied in radio meteors, is discussed and reanalyzed in an appendix to this paper.

1. Introduction

The study of upper atmospheric turbulence by neutral motion was by necessity initially limited to the observations of visible meteor trails (Millman 1959). With the advent of the small rocket, a means for the deposition and study of trace materials in the upper atmosphere was created (Manring et al. 1961, Zimmerman et al. 1961, Blamont and deJager 1961, Zimmerman and Champion 1961).

Initially these trace materials were high-temperature jets or explosions, respectively seeded with sodium and cesium, and to allow prolonged observations of the tracers, twilight conditions at the altitude of release were required. The scattered resonance radiation in the sodium trails was due to solar excitation of the 5893Å doublet, and the major lines of the cesium releases were the 8521Å doublet in the IR and the 4555Å in the visible (Fig. 1). Subsequent research (Pressman et al. 1956, Golomb 1962, and Rosenberg et al. 1963) showed the advisability of using chemical trails that react with the natural atomic oxygen of the atmosphere. The materials found to act best are NO and TMA (trimethylaluminum). These constituents react in some manner (not completely understood) with atomic oxygen in perhaps the following way (after Golomb et al. 1965 and Rosenberg et al. 1964).

$$NO + O \xrightarrow{k_1} NO_2 + h\nu \qquad (1)$$

where

$$k_1 = 2.5 \times 10^{-13} \text{c.c./sec.}$$

and

$$AlO + O \longrightarrow AlO_2^*$$

$$AlO_2^* \longrightarrow AlO_2 + \text{pseudo-continuum} \qquad (2)$$

The reaction above is for the non-sunlit radiation which is observed to be a continuum. The twilight sunlit spectrum of AlO shows definite radiation in the blue-green AlO bands of the $A^2\Sigma^+ - X^2\Sigma^+$ transition appears at 5337Å for the (0,2) transition, 5080Å (0,1), 4842 (0,0) and 4648Å for the (1,0) transition. Thus these reacting and passive chemical releases were shown to be effective tracers to determine transport phenomena in the upper atmosphere under twilight and nighttime conditions.

The problem then, simply stated, is to relate the measurements of the contaminant motion to turbulent atmospheric parameters.

2. Theory and Techniques

The approach to this problem has not been truly definitive in determining upper atmospheric turbulent parameters. The usual technique of analysis is to measure the rate of dispersion of the contaminants, and relate this dispersion rate to turbulent parameters by applying a theory of turbulent diffusion to the measured contaminant dispersion. This technique has been applied by Zimmerman et al. 1961, Blamont and deJager 1961, Zimmerman and Champion 1963, Noel 1963, and Cote 1965).

The usual technique in these measurements is to follow the time rate of change of a density or brightness contour of the chemical contaminant, assuming that it is of a gaussian distribution as per the solution of the diffusion equation where the diffusion coefficient K is independent of position. Thus, the density distribution $n(r,t)$ is

$$n(r,t) = \frac{4\pi\, n_{oo} r_o^3}{3\left(4\pi\, \overline{r^2}(t)\right)^{3/2}} \exp\left[-\frac{r^2}{2\,\overline{r^2}\,(t)}\right] \qquad (3)$$

where the total content $\left(Q = 2\pi \int_0^\infty n\,(r,t)\, r^2 dr\right)$ is a constant of time; which implies no chemical consumption of the contaminant.

n_{oo} is the center point density at t=0, and $\overline{r^2}(t)$ is the mean square deviation of the contaminant cloud.

Integrating over a specific density $\left[n(r,t)\right]$, then results in the number of particles per → cm^2 ← column, which for an optically thin source is directly proportional to the brightness of the source, and thus to the exposed atoms in the photographic film.

$$N(\rho,t) = \int_0^\infty n(r,t)\, dz, \qquad (4)$$

thus

$$N(\rho,t) = \frac{4\pi\, n_{oo} r_o^3}{6\sqrt{2}\left(4\pi\, \overline{r^2}(t)\right)} \exp\left[-\frac{\rho^2}{2\,\overline{r^2}(t)}\right] \qquad (5)$$

where $\rho^2 = x^2 + y^2$.

Thus the observed time dependence of some subtended density contour $N(\rho,t)$ will allow the description of $\overline{r^2}(t)$. The observations of $\overline{r^2}(t)$ are then related to turbulent parameters via the theory of turbulent diffusion.

Initially, in the study of diffusion using smoke puffs in the lower atmosphere (Kellogg 1956; Frenkiel and Katz 1956) the mean square deviation was related to turbulent parameters by Taylor's (1920, 1935) theory, which on a statistical basis described the mean square deviation of a particle migrating from a source as

$$\overline{r^2}(t) = 2\,\overline{v^2} \int_0^t \int_0^\tau R_\xi\, d\xi d\tau \qquad (6)$$

Since

$$R_\xi = \begin{cases} 1, & t \to o \\ 0, & t \to \infty \end{cases}$$

then

$$\overline{r^2}(t) = \begin{cases} \overline{v^2}t^2, & t \to o \\ 2\overline{v^2}It, & t \to \infty \end{cases}$$

where

$$I = \lim_{\tau\to\infty} \int_o^\tau R_\xi \, d_\xi,$$

$\overline{v^2}$ is the eddy intensity,

R_ξ is the Lagrangian auto-correlation function, and

τ is a dummy index.

Batchelor (1950), and subsequently Lin (1960), showed that while Taylor's statistical approach described the turbulent diffusion of a tracer element from a continuously emitting source, the diffusion of a point release must be described by the theory of the relative separation of two identical contaminant particles. Batchelor in his "similarity" theory has made the assumptions of isotropy, and limits the eddy scale controlling diffusion to much smaller than the sizes of the energy containing eddies, and much greater than the length $(\nu^3/\varepsilon)^{1/4}$ (i.e. within the inertial subrange). Then for the case of a finite contaminant release size (r_o) with zero initial velocity, he calculates the statistical relative behavior of two fluid particles.

$$\overline{r^2}(t) = \overline{r_o^2} + \frac{10}{3} C_1(r_o\varepsilon)^{2/3}t^2 + C_2 \varepsilon t^3 \qquad (7)$$

where

$\overline{r_o^2}$ is the initial (t=o) variance,

ε is the rate of viscous dissipation of turbulent kinetic energy, and

C_1 and C_2 are universal constants of the order unity.

Lin, studying the relative separation of two particles and considering the statistical average over an ensemble of such pairs, shows that for both isotropic and non-isotropic turbulence, and where the measuring time (t) is greater than τ_2, a specific time constant,

$$\overline{r^2} \approx \frac{2}{3} B \, t^3 \qquad (8)$$

where B, a constant, has the dimensions of ε. Thus the study of relative dispersion, where the effect of the initial variance upon $\overline{r^2}(t)$ has been allowed for, should show a t^2 relation followed by a t^3 relation.

Gifford (1957), and subsequently Zimmerman (1965), showed where some of the low altitude experiments of Kellogg's and Frenkiel and Katz's were adequately described by Batchelor's theory. However, most of the low altitude experiments and all of the upper atmospheric (~ 100 km.)experiments conducted in Project Firefly (1959 and 1960)*, and where a density

* These experiments are discussed as a series of papers in J. Geophys. Res. 68, 10, 2985-3063, 1963.

contour near the edge was examined, show no t^3 time dependence in the measured $\overline{r^2}(t)$. To explain these results Zimmerman and Champion (1963) and Zimmerman (1965a) apply Tchen's (1954) theory of shear-dominated turbulence to the measurements.

Tchen states that when the square of the vorticity is large compared to the square of the shear fields

$$\left[2\int_0^k F(k')\ k'^2\ dk' > \left(\frac{\partial U}{\partial z}\right)^2\right]$$

the spectral function will be $F(k')\ k'^{-5/3}$ and "similarity" predictions will hold. However, when

$$\left[2\int_0^k F(k')\ k'^2\ dk' < \left(\frac{\partial U}{\partial z}\right)^2\right],$$

$F(k') \sim k'^{-1}$ and the mean square deviation $(r^2(t))$ will be proportional to t^2 (Tchen, 1959) throughout the time of observation.

where

k' is the wave number,
$F(k')$ is the turbulent energy spectral function,
U is the velocity of the mean wind in the horizontal plane,
$(\partial U/\partial z)$ is the magnitude of the vertical shear, and the vorticity is defined by Tchen as

$\left[2\int_0^k F(k')k'^2dk'\right]^{1/2}$, which is derivable from the curl of the eddy velocity. In Tchen's derivation it is the product of a vorticity by an energy of shear origin which constitutes the transfer function (i.e., the mechanism whereby turbulent energy is transported down the spectrum of eddy sizes towards that eddy limited by viscosity).

3. Experimental Measurements

Blamont and deJager (1961), measuring the $\frac{1}{e}$th contour relative to the center point density, state that they observe turbulence up to $\sim$ 104± 8 km., and that molecular diffusion controls the dispersion above this region. Also that measurements of "blob" growths taken with a telescope indicate a t^3 type of growth representative of the intermediate time regime of Batchelor's "similarity" theory. The value of ε (the rate of turbulent viscous dissipation) determined from the slope of the $\overline{r^2}$ vs. t^3 curve is 70 cm.^{2}/sec.^{3}. The average size of the blobs was 90 m. 60 sec. after the material was deposited, and they grew to an average size of 500 m. in 120 sec. The value of ε measured this way is approximately the same as that reported by Greenhow (1959) from some observations of visible meteor trails. They also report that within the turbulent trail the smallest structure size observable is of the order of 50 to 100 m., very close to the value of 50 m. that Booker (1959) refers to as the isotropic scattering element of radio waves from the ionosphere. Kellogg (1964) comments that Blamont in a personal communication referred to a value of 700 e.g.s. for ε in sodium trails. This variation of ε has not been discussed by Blamont in the open literature. The exact altitude of the measurements was not stated by the authors; however, if we assume that the altitude in question was 95 km., then the viscous limited scale length

(given by the Kolmogoroff relation, $l_\nu = \left[\frac{\nu^3}{\varepsilon}\right]^{1/4}$ and using $\varepsilon = 70$ e.g.s., is of the order of 19 m. This is smaller than the structures reported by Blamont and deJager by a factor ≤ 5. Zimmerman and Champion (1961, 1963) measuring the radial growth of point cesium releases at 100 km. and 75 km., show that the relative dispersion does not follow Batchelor's "similarity" relation, but has only a t^2 time dependence. Following a contour near the visible edge of the release, they measured the transverse diffusion coefficient in a horizontal plane using their relations 10 and 12. These are respectively

$$r_o^2 = 2\,\overline{v^2}t^2 \left[1 + \ln\left(\frac{r_o^2 max}{2a^2}\right) - \ln\left(\frac{\overline{v^2}t^2}{a^2}\right)\right], \tag{9}$$

for turbulent diffusion, and

$$r_o^2 = 4Kt \left[1 + \ln\left(\frac{r_o^2 max}{2a^2}\right) - \ln\left(\frac{2Kt}{a^2}\right)\right] \tag{10}$$

for both molecular diffusion and a transport effect that has the appearance of molecular diffusion with a diffusion coefficient orders of magnitude larger than molecular. This is most likely a late time turbulent diffusion related to the energy of the explosive release (Zimmerman 1965b). Generally the contaminant clouds show initially this molecular-like diffusion, followed by a turbulent form of diffusion Fig. 2 which is attributed to atmospheric turbulence ($\overline{r^2} \sim t^2$). The results of Zimmerman and Champion's measurements are shown in Fig. 3, where they included some sodium and lithium data from trail releases supplied by Manring. The data representing the molecular-like diffusion coefficients are shown as the single points, and those representing turbulent diffusion coefficients ($K = \overline{v^2}t$) by the triangles with the connecting dashed lines. The theoretical curves are based on Chapman and Cowling's (1952) relation

$$D = \frac{3}{8n\,\sigma_{12}^2} \left[\frac{kT}{2\pi\mu}\right]^{1/2} \tag{11}$$

where

D is the molecular diffusion coefficient

n is ambient density

$\sigma_{12}^2 = \left(\frac{\sigma_1 + \sigma_2}{2}\right)^2$ is the mean collision cross-section of gas 1 in gas 2

k is Boltzmann's constant

T is the ambient temperature, and

μ is the reduced mass $\equiv \frac{m_1 \quad m_2}{m_1 + m_2}$

The authors also measured the "blob" diameters (Fig. 4). They noticed no special growth relation as reported by Blamont and deJager; and as noted in the illustration they compared these measured values to the scale sizes predicted by Booker (1956). The measured scale diameters range from 300 m. to 1.5 km. in the release at 100 km., and from $\sim$ 1.2 km. to 2.5 km. in the release at 103 km. These scale size values are roughly those reported by Blamont and deJager, and seem to substantiate their results. However, the lack of a regular growth pattern to these individual "blobs" conflicts with Blamont and deJager's measurements which allude to an average growth rate described by Batchelor's theory. Edwards et al. also have measured the growth rate of a number of their globules within the cesium clouds. They report that initially there is an extremely fast rate of growth of these globules, very close to the t^5 dependence predicted by Bolgiano (1959) for turbulent dispersion when buoyancy effects dominate. Very

shortly thereafter, there is a leveling-off phase where the globule does not grow, and finally another growth phase with a reported power dependence of 2.62. (i.e. $r^2 \sim t^{2.62}$). These conflicts in data continue to lend serious doubt to the usage of "similarity" theory or any turbulent diffusion theory to explain the variations observed in the individual "blobs". Continuing further the "blob" analysis, Noel (1963) reported on data supplied him by H. Edwards from Firefly releases. These were globules where the time history of the outer edge was measured. These data (Fig. 5) indicate a t^3 growth with diameters going from 800 m. to ~ 2 km. However, Cote (1965) analyzing the sodium trails from Wallops Island and reviewing some of the other reports data, which included Noel's, shows that since the globules studied lie within the contaminant cloud the effect of the varying background, which Noel did not take into account, upon the measurements could cause serious variance of $\overline{r^2}$ from the t^3 relation. Cote further states that his measurements of turbulent cloud growths, as observed from sodium trails, supports the $\overline{r^2} \sim t^2$ measurements of Zimmerman and Champion, where his measured coefficient (v^2) is of the order of 1 to 6 m.^{2}/sec.^{2}. This is somewhat in contrast to the reported value for v^2 of 15 m.^{2}/sec.^{2} as discussed by Zimmerman and Champion, which Cote points out could be reduced to 8 m.^{2}/sec.^{2} if a different value of the initial variance and the maximum observed radius were made, and the effect of molecular diffusion is also taken into account. Zimmerman (1965a) had considered the problem of the ambiguity involved in the measurements, when the uncertainties of initial and maximum radii, and molecular diffusion could not be properly measured. To minimize these effects he utilized a technique of measurement initially used by Frenkiel and Katz in the study of lower atmospheric smoke puffs. In essence this means taking the ln of equation 4 which would result in Zimmerman's equation 8

$$\rho^2 = -2\,\overline{r^2}\left[\ln\ 2\overline{r^2} + \ln\ \frac{\pi N}{Q}\right] \qquad (12)$$

where

$$\overline{r^2} = r_o^2 + 2Kt + \overline{v^2}\,t^2 \qquad (13)$$

Substituting (13) into (12) and dividing by t, would result in

$$\frac{\rho^2}{t} = -\left(\frac{2r_o^2}{t} + 4K + 2\,\overline{v^2_t}\right)\left[\ln\ 2\,\overline{r^2} + \ln\ \frac{\pi N}{Q}\right] \qquad (14)$$

It is evident that plotting $\frac{\rho^2}{t}$ vs. ln t would result in a straight line with a slope of $-4K$ when the effect of the initial radius and $\overline{v^2}$ is negligible. This can be observed from Fig. 6 which is $\frac{\rho^2}{t}$ vs. ln t. It is quite evident that for the assumed initial variance of 10^4 m.^{2}, $\overline{r_o^2}$ has little effect after 20 sec. and K may be fairly accurately determined. Similar reasoning holds in determining $\overline{v^2}$ by dividing by t^2 rather than t. This is shown in Fig. 7. For the experiment Echo, compare the value shown $\left(\overline{v^2}\right)^{1/2}$ = 490 cm./sec., (Table 1) or v^2 = 24 m.^{2}/sec.^{2} with Cote's estimate of ~ 8 m.^{2}/sec.^{2}. This discrepancy has still not been completely accounted for. Further results of such measurements on 3 chemical point cesium releases are shown in Table 1. Here ε (turbulent power dissipated by viscosity) is calculated two ways: (1) from the identity in Zimmerman (1966) for shear-dominated turbulence

$$\overline{v^2} \equiv \frac{K_3\,\varepsilon}{K_2\,\overline{U'}} \qquad (15)$$

where

$\overline{U'} \equiv \left(\frac{\partial U}{\partial z}\right)$ is the vertical shear of the mean horizontal wind, and K_3 and K_2 are unknown coefficients assumed unity in these measurements; and (2) from the relation $\varepsilon = \left(\overline{v^2}\right)^{3/2}/l$ where l is the measured blob diameter. Also shown are the values of the eddy

TABLE 1

Exp	Echo	Alpha	Susan
Altitude (m)	101×10^3	103×10^3	113×10^3
$\left\lvert\frac{\partial U}{\partial z}\right\rvert$ (sec.$^{-1}$)	$1.2 - 3 \times 10^{-2}$	$8\text{-}12 \times 10^{-2}$	$4\text{-}8 \times 10^{-3}$
$(\overline{v^2})^{\frac{1}{2}}$ (cm./sec.)	490	959	424
ε max (cm.^{2}/sec.^{3})	$3.2 - 7.5 \times 10^3$	$7.3 - 11 \times 10^4$	$7.2 - 14.4 \times 10^2$
ε (cm.^{2}/sec.)^3	2.35×10^3	5.8×10^3	7.62×10^2
l_k (cm.)	5×10^4	1.5×10^5	1×10^5
l_d (cm.)	$1.5 - 1.9 \times 10^3$	$1.8 - 1.9 \times 10^3$	$2.9 - 3.4 \times 10^4$
R_{e_k}	6.4×10^1	1.44×10^2	6.4

Reynolds number and the small-scale viscous limited scale size for the assumed large-scale length l_k. The eddy Reynolds number is calculated from the relation $R_{e_k} = \frac{v l_k}{\nu}$ where Zimmerman has shown that v^2 approximates the magnitude of $\overline{u_k^2}$ (the large-scale eddy kinetic energy). The small value of these numbers indicate that the inertial subrange, if it exists, or even the universal equilibrium subrange becomes quite small at approximately 100 km., and according to the release at 113 km. has disappeared. This would suggest that turbulence disappears at ~ 105 ± 5 km. as initially stated by Blamont and deJager.

Further, the measurement at 113 km. may not be truly turbulent, and some caution should be used before accepting it as such.

The values of the small viscous limited scale for the measurements at 100 and 103 km. is of the same order as Blamont and deJager's estimate at 95 km.

4. Conclusion

In this study, the experiments involving the use of chemical contaminants have been summarily reviewed. Some of their pertinent features have been the measurements of scale sizes, diffusion time dependence, and relation of the measurements to the theories of turbulent diffusion. What is quite apparent is that in the study of upper atmospheric turbulence there is no truly definitive experiment that unambiguously relates theory to the experiment. The present lack of subsidiary measurements, such as direct measurement of spectral density and atmospheric stability, deter markedly the more concise determination of the turbulent parameters, and thus the requirements upon turbulence theory.

Within these uncertainties, the measured and inferred structures indicate turbulent scale lengths from 12 m. to $\sim$ 2.5 km. and the rate of viscous dissipation varying from 70 cm.^{2}/sec.^{3} to the order of 10^5. This high value (reported in Zimmerman 1966) must be considered conservatively since the coefficients of equation 12 are unknown. Further discussion of other measurements will be considered in the Appendix, which I am including as almost a second chapter due to the different nature of the experiments.

5. Appendix

I have included the appendix in this paper primarily because the topics of research discussed are similar to the main topics of the meeting. Basically, this is the reflection of radio waves from an ionized medium in the upper atmosphere. The difference lies in the reflecting medium. This conference is mainly interested in the reflection from structure within the normal ionosphere, while the data I shall discuss is the reflection from ionized meteor trails within this same altitude range. Theoretically these meteor trails should pick up the structure of the medium, and these structures should be identifiable for analysis from the radar data.

The data in question is that of Roper (1962), and I shall limit myself for the most part to discussion of his reduced data. I recommend Roper's thesis for those who are interested in the experimental details. In this study, Roper determined the mean winds and the most probable turbulent velocity as respectively the mean of all measured winds within a certain time span, and the peak velocity deviations from this mean. To study the altitude separation of the observed winds, he used a system of doppler radar and triangulation. Thus, for a given period of integration time, turbulent velocities as a function of altitude are determined. Thus Roper has compiled various transverse eddy velocities as a function of vertical separation over the course of the year 1961. Then, following Batchelor (1963), he showed that the one-dimensional spatial relation between turbulent velocities in isotropic homogeneous turbulence, where the wave numbers lie in the inertial subrange part of the universal equilibrium range, may be expressed as

$$D_\xi = \overline{\left[u(z+\xi) - u(z)\right]^2} = 4\int_0^\infty \alpha\varepsilon^{2/3} k^{-5/3} \left\{1 - \frac{\sin(k\xi)}{(k\xi)}\right\} dk \qquad \text{(A-1)}$$

where

$D(\xi)$	is the structure function,
$u(z+\xi)$	is the turbulent velocity at a transverse separation ξ from z,
$u(z)$	is the turbulent velocity at altitude z,
k	is wave number,
α	is a constant of proportionality, initially assumed 2/3 for the thesis, and unity for the paper by Roper and Elford (1963). The experimentally determined value for α will be discussed later. The bar signifies a time averaging.

Solving A-1 gives

$$D = 3.2\ (\varepsilon\xi)^{2/3} \qquad \text{(A-2)}$$

where it has been assumed that $\alpha = 2/3$

In terms of the R.M.S. velocity differences Δv, where

$$D^{\frac{1}{2}} \equiv \overline{\Delta v} \equiv \left\{\left[u(z+\xi) - u(z)\right]^2\right\}^{\frac{1}{2}}, \qquad \text{(A-3)}$$

we arrive at Roper's equation 2.10.3

$$\overline{\Delta v} = 1.83\ (\varepsilon\ \Delta\ z)^{1/3} \qquad \text{(A-4)}$$

A typical example is shown in Fig. A-1 (Roper's Fig. 41) where the solid curve is an empirical fit of relation A-4 for ε = 420 cm.^{2}/sec.^{3}. However, a more proper empirical analysis could be considered by taking the ln of Δv vs. Δz as shown in Fig. A-2. As observed the 1/3 power relation of isotropic turbulence holds to a separation length of $\sim$ 450 m. for this example. Beyond this length the structure analysis results in $D(\Delta z) \sim (\Delta z)^{4/3}$. This 4/3 power relation is identical to that of the Blamont and deJager analysis, which they attributed to some mean wind phenomena, and which Zimmerman (1962) felt was descriptive of turbulent shear stress. However, this point has not been clearly proven or related, and will require further work. Further experimental evidence indicates that the structure analysis is descriptive of isotropic turbulence for some of the data and not at all for others. Two examples (Figs. A-3, A-4) show that for Fig. A-3 the 1/3 relation appears to hold for the separation distance of 2.5 km., the total lengths of the measurement; while for Fig. A-4 the observed relation does not bear any resemblance to the theory of isotropic turbulence. These data are more accurately described by $\Delta v \sim (\Delta z)^{2/3}$, or $D(\Delta z) \sim (\Delta z)^{4/3}$ as discussed above.

Using the above assumptions, and assigning the value of .44 for α, measured by Grant et al. (1962), we calculate the values for ε shown in Fig. A-5. The solid lines are from this analysis, and the dashed lines bracket the months which indicate no "inertial" or universal equilibrium range. The broken curve is from Roper and Elford as a comparison. Generally the results of this analysis are larger than those of Roper and Elford but show similar monthly variations. Roper noted a correspondence between the values of ε and the energy of the diurnal component of the mean wind (Fig. A-6, his Figs. 61 and 61b); repeating this comparison (Fig. A-7) we also observe a definite correlation. This substantiates Roper's statement that the magnitude of ε is proportional to the energy in the diurnal component of the mean wind. Why this seems to be so is not clearly explained. However, to apply some conjecture we shall assume that the diurnal mode is the dominant mode at 95 km. The vertical wavelength (given by Wilkes 1949) is approximated as

$$\lambda^2 = \frac{4\pi^2}{k^2} \cong 4\pi^2\ Hh \left\{\left[\frac{\gamma - 1}{\gamma} + \frac{\partial H}{\partial z}\right]\right\}$$

where

k	is the wave number
$\gamma(\approx 14)$	is the ratio of specific heats
z	is altitude
H	is the pressure scale height, and
h	is the "equivalent depth" of the atmosphere $\approx$ .63 km. (Siebert, 1963)

Using H = 5.9 km., and $\frac{\partial H}{\partial z}$ = .093 (U.S. Standard Atmosphere, 1962) we arrive at $\gamma \approx 7.5$ km. This value is indeed representative of the wavelengths measured at this altitude. Thus for a given wavelength of this size, and where the mean horizontal velocity or the wave amplitude is increasing, the local shears will also increase. This causes the atmosphere to become more unstable, and thus tend towards a more intense turbulent field. This example should be considered as merely illustrative in examining this problem; however, it does indicate a tentative relation between the mean wind and turbulent dissipation.

If we now consider that the separation length which marks the transition from the 1/3 to the 2/3 power relation is representative of the extent of the "inertial" or the "universal equilibrium" subrange, we can estimate the turbulent kinetic energy by the one-dimensional spectrum relation

$$\overline{v^2} = 2 \int_k^\infty E(k')\ dk' \qquad \text{(A-5)}$$

where $E(k') = .44\ \varepsilon^{2/3}\ k^{-5/3}$, and thus

$$\overline{v^2} = 1.32\ \varepsilon^{2/3}\ k^{-2/3}. \qquad \text{(A-6)}$$

Since $l \equiv k^{-1}$, and if we further assume that the height separation (Δz) is equal to l, then

$$\overline{v^2} = 1.32\ \varepsilon^{2/3} l^{2/3}. \qquad \text{(A-7)}$$

Fig. A-8 shows the measured values of l. Again the dotted line indicates no data. Included in this figure are the calculations of the Kolmogoroff microscale given by the relation $l_d = \left[\frac{\nu^3}{\ }\right]^{\frac{1}{2}}$. Applying the measurements of ε and l to equation A-7 results in the estimates shown in Fig. A-9; also shown is the turbulent kinetic energy per unit mass of the small microscales, calculated using the relation $v_\nu^2 = \left[\varepsilon\nu^{\frac{1}{2}}\right]$.

Finally I shall discuss the eddy Reynolds number (R_e) of this large eddy. This is simply expressed as

$$R_e = \frac{\left(\overline{v^2}\right)^{\frac{1}{2}} l}{\nu} \qquad \text{(A-8)}$$

substituting A-7 into A-8,

$$R_e = 1.15\ \frac{\varepsilon^{1/3} l^{4/3}}{\nu} \qquad \text{(A-9)}$$

This relation is similar to that derived by Zimmerman (1966) for the 3-dimensional case

$$R_{e_k} = .9\ \frac{\varepsilon^{1/3} k^{-4/3}}{\ }, \text{ where again } k^{-1} \equiv l.$$

The values determined using equation A-8 or A-9 are shown in Fig. A-10.

6. Summary

The values of the scale sizes and turbulent velocities discussed here agree quite well with values of scale lengths measured by Zimmerman and Champion, Blamont and deJager, Edwards et al., and Zimmerman using chemical tracers to measure turbulent parameters, as discussed in the main body of the report. The values of the viscous dissipation of turbulent kinetic energy (ε) are for the most part larger than that measured by Blamont and deJager, and fairly close (as in the data of August 1-6) to the estimate of Zimmerman and Champion, and Zimmerman (1965a) based on the measured velocity of expansion and the measured scale sizes. These values on the other hand, are much smaller than those calculated by Zimmerman (Table 1) for the case of shear-dominated turbulence where the coefficients of proportionality are assumed unity. The values for the eddy Reynolds number are also quite close to those of Zimmerman (Table 1), and substantiate the result stated in the main body of this text, that in the upper atmosphere the "inertial" subrange, if it exists, will be quite small. Indeed considering the size of the eddy Reynolds number ($<10^4$) there may well be no "inertial" range at all (cf. Batchelor 1950).

CORRECTION BY AUTHOR TO PAPER 1.8

THE TURBULENT STRUCTURE FUNCTION WHICH IS PRESENTED HERE AS AN ANALYSIS OF THE VERTICAL TURBULENT SPECTRUM IS INCORRECT. THE ANALYSIS IS THAT OF THE HORIZONTAL SPECTRUM.

REFERENCES

Batchelor, G.K. Quart. J. Roy. Meteorol. Soc., 76, 113-146, 1950.

Batchelor, G.K. Homogeneous Turbulence, Camb. Univ. Press, 1953.

Blamont, J.E., and C. deJager. Ann. Geophys., 17, 134-144, 1961.

Booker, H.G. J. Geophys. Res., 61, 673-705, 1956.

Booker, H.G. J. Geophys. Res., 64, 2146, 1959.

Chapman, S. and T.G. Cowling. The Mathematical Theory of Non-Uniform Gases, Camb. Univ. Press, 1939, 1952.

Cote, O. G.C.A. Tech. Report No. 65-5-N, NASA Contract No. NASA-1083, 1965.

Edwards, H.D. et al. AFCRL Report 64-700, Contract No. AF19(628)-3305, 1964.

Frenkiel, F.N. and I. Katz. J. Meteorol., 13, 384-394, 1956.

Gifford, F. Jr. J. Meteor., 14, 410-414, 1957.

Golomb, D. Project Firefly, IV, AFCRL No. 62-826, 103-111, 1956.

Golomb, D. et al. J. Geophys. Res., 70, 1155-1173, 1965.

Grant, H.L., Stewart, R.W., and A. Moilliet. J. Fluid Mech., 12, 241-268, 1962.

Kellogg, W.W. J. Meteorol., 13, 241-250, 1956.

Kellogg, W.W. Space Sci. Rev., 3, 2750316, 1964.

Lin, C.C. Proc. Nat. Acad. Sci., 46, 566-570, 1960.

Manring, E., Bedinger, J. and H. Knoflich. Space Res. II, 1107-1124, 1961.

Millman, P.M. J. Geophys. Res., 64, 2063-2084, 1959.

Noel, T.M. J. Geophys. Res., 68, 2862-2863, 1963.

Pressman, J., Aschenbrand, L.M., Marmo, F.F., Jursa, A., and M. Zelikoff. J. Chem. Phys., 25, 187, 1956.

Roper, R.G. Ph.D. Thesis, Univ. of Adelaide, 1962.

Roper, R.G. and W.G. Elford. Nature, 197, 963-964, 1963.

Rosenberg, N.W., Golomb, D., and E.F. Allen, Jr. J. Geophys. Res., 68, 5895-5898, 1963.

Rosenberg, N.W., Golomb, D., and E.F. Allen, Jr. Project Firefly Report AFCRL No. 64-364, 323-327, 1964.

Siebert, M. Advances in Geophys., 7, 105, 1961.

Taylor G.I. Proc. London Math. Soc., 2, 212, 1920.

Taylor, G.I. Proc. Roy. Soc. London, A, 151, 421, 1935.

Tchen, C.M. Phys. Rev., 93, 4-14, 1954.

Tchen, C.M. Advan. Geophys., 6, 165-174, 1959.

Wilkes, M.V. Oscillations of the Earth's Atmosphere, Camb. Univ. Press, 1949.

Zimmerman, S.P. Ann. Geophys., 18, 116-117, 1962.

Zimmerman, S.P. J. Applied Meteorol., 4, 279-288, 1965a.

Zimmerman, S.P. Space Res. VI, 1965b.

Zimmerman, S.P. To be published in J. Geophys. Res., 71, May 15, 1966.

Zimmerman, S.P. and K.S.W. Champion. J. Geophys. Res., 68, 2025-2029, 1963.

Zimmerman, S.P. and K.S.W. Champion. ARPA Report, AFCRL No. 256(I), 3049-3056, 1961.

Zimmerman, S.P., Majumdar, S.K., and K.S.W. Champion. Bull. Am. Phys. Soc., 1961.

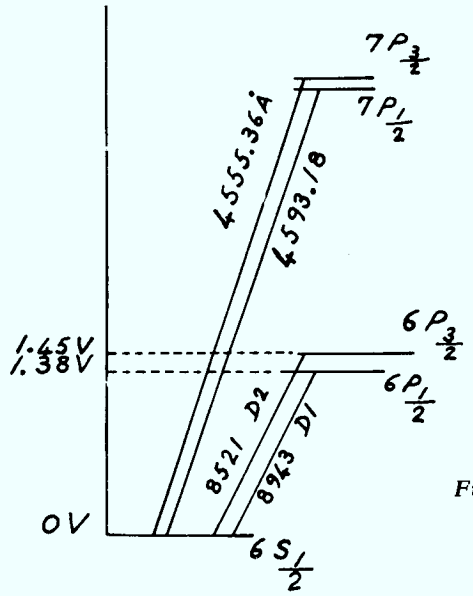

Fig. 1. Cesium energy level diagram.

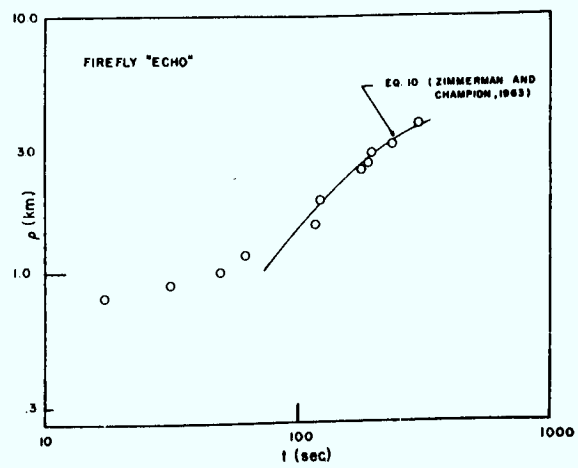

Fig. 2. Measurements of contaminant radius vs. time. Initially $r \sim t^{1/2}$ and after ~100 sec. $r \sim t$.

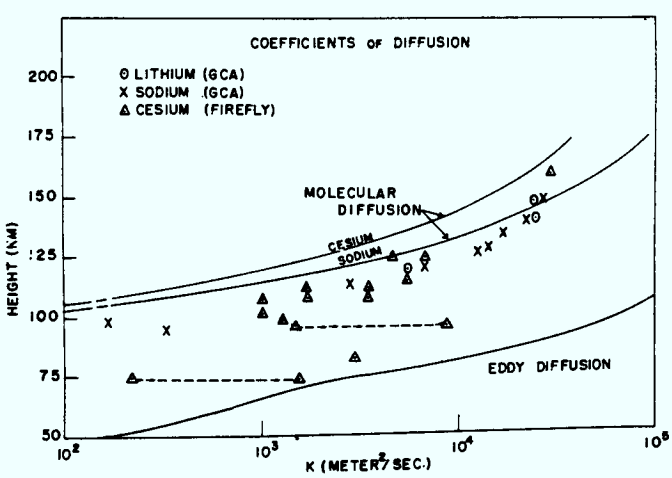

Fig. 3. Diffusion coefficients.

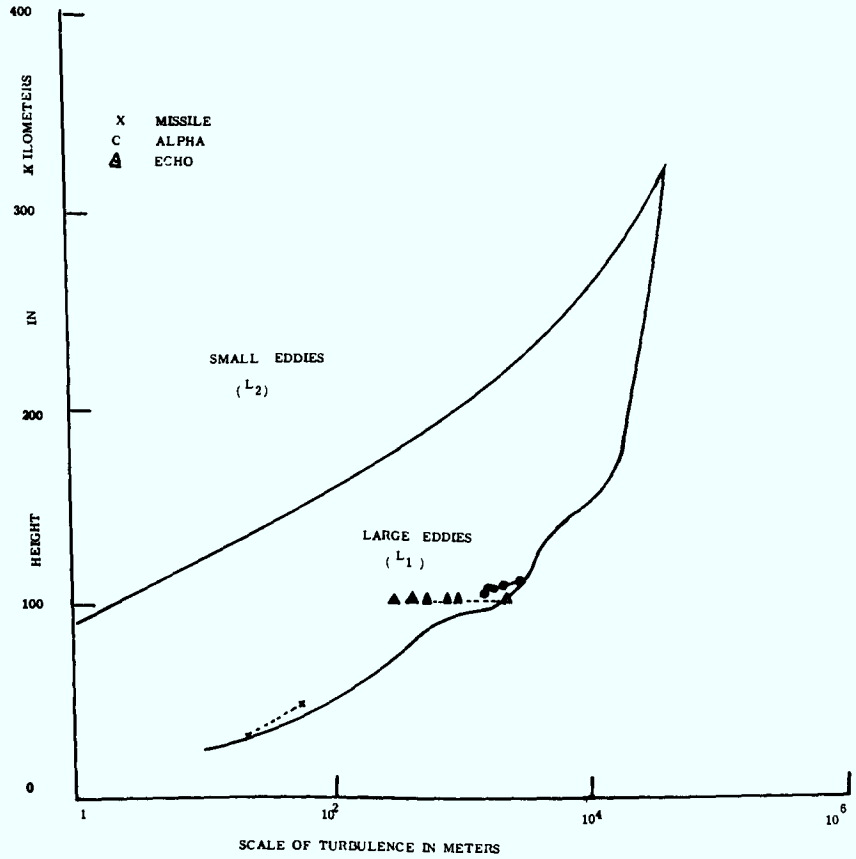

Fig. 4. Eddy scale sizes.

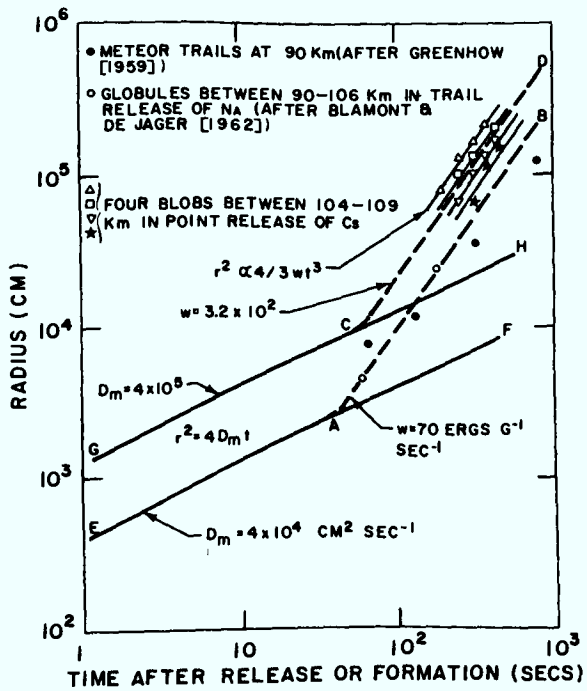

Fig. 5. Reproduction of Noel's Fig. 1.

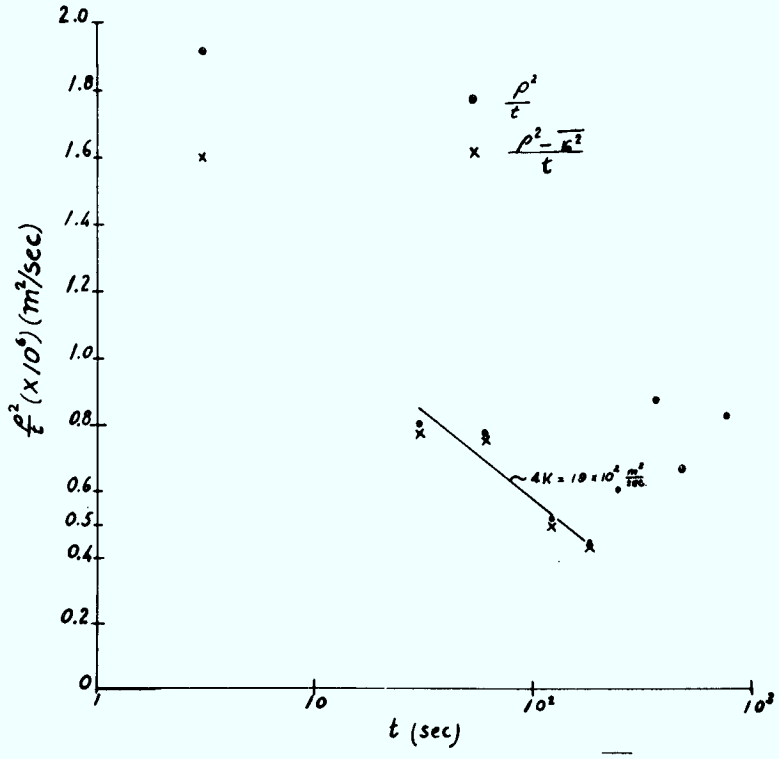

Fig. 6. The time dependence of $\frac{\rho^2}{t}$ *as compared to* $\frac{\rho^2 - \overline{r_o^2}}{t}$. *The measured values of 4K (the slope of the curve) for the experiment Margie (75 km.) are also given.*

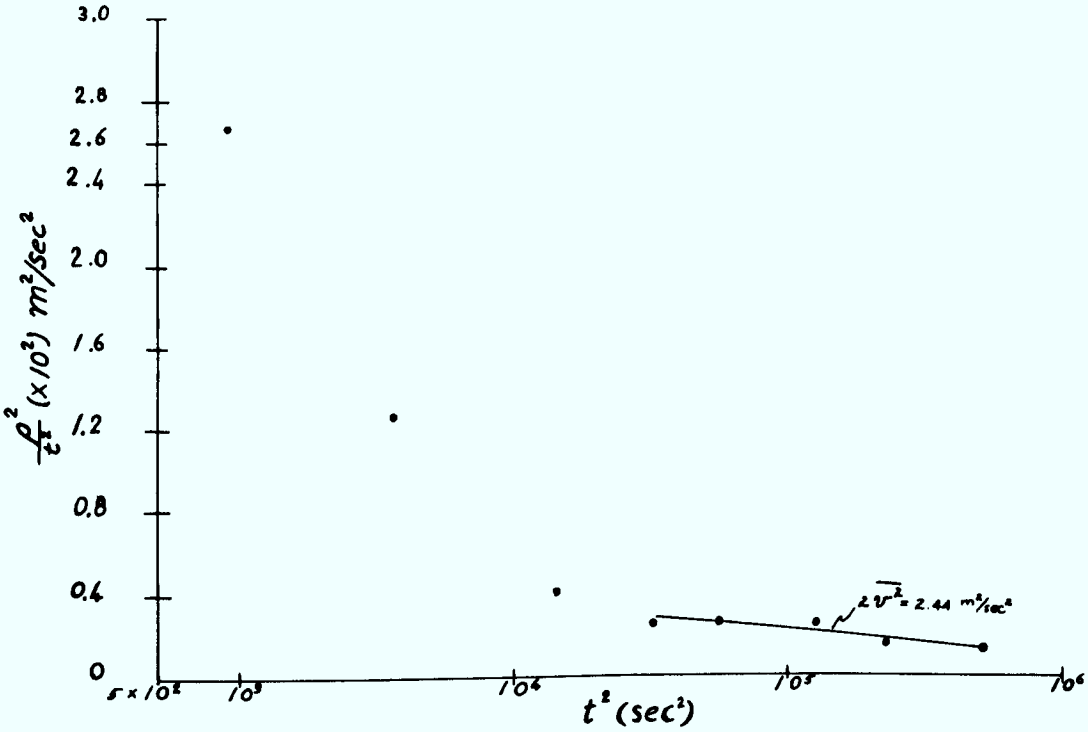

Fig. 7. The time dependence of $\frac{\rho^2}{t^2}$ *for Margie (75 km.) the value of* $2\,v^2$ *is also given.*

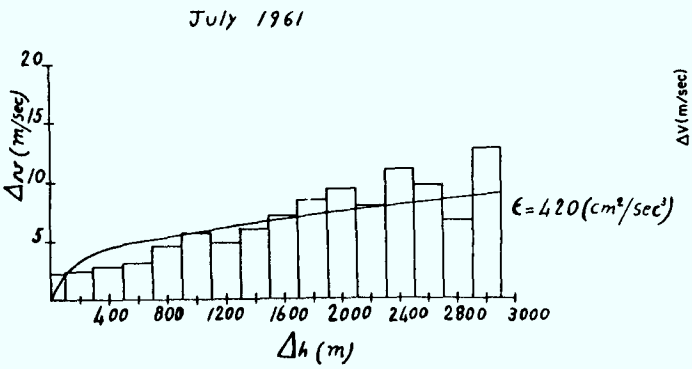

Fig. A-1. Reproduction of Roper's Fig. 41. $\overline{\Delta v}$ vs. Δz.

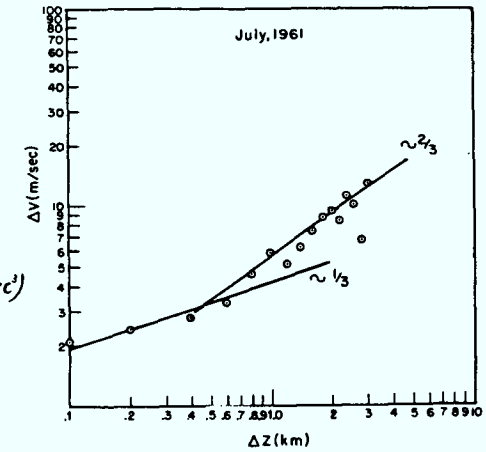

Fig. A-2. ln of Δv vs. ln Δz. The 1/3 power relation is equaled to an isotropic turbulent phenomenon, indicative of an equilibrium subrange.

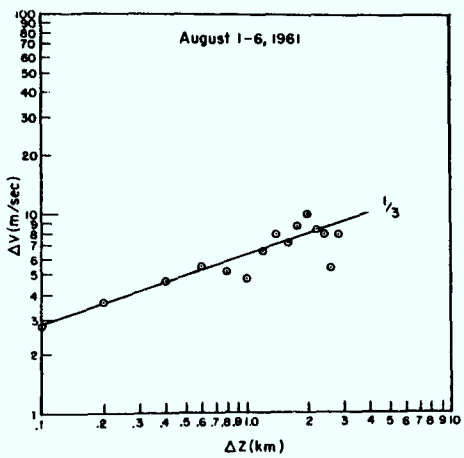

Fig. A-3. These data show isotropic turbulence for the complete measurement.

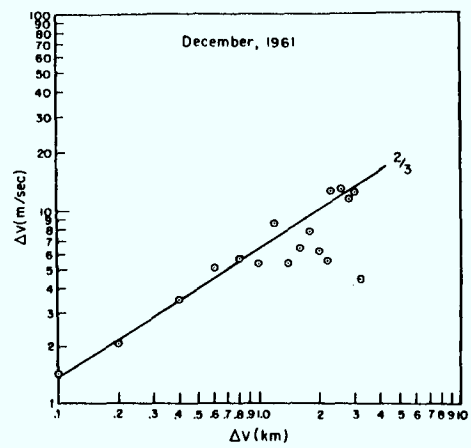

Fig. A-4. These data indicate no equilibrium subrange.

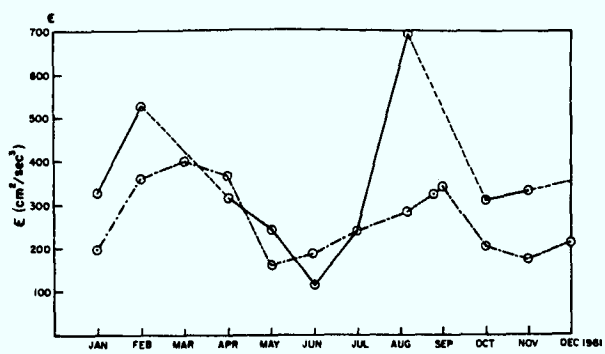

Fig. A-5. Comparison of ϵ for this analysis (solid line) with Roper's analysis (broken line).

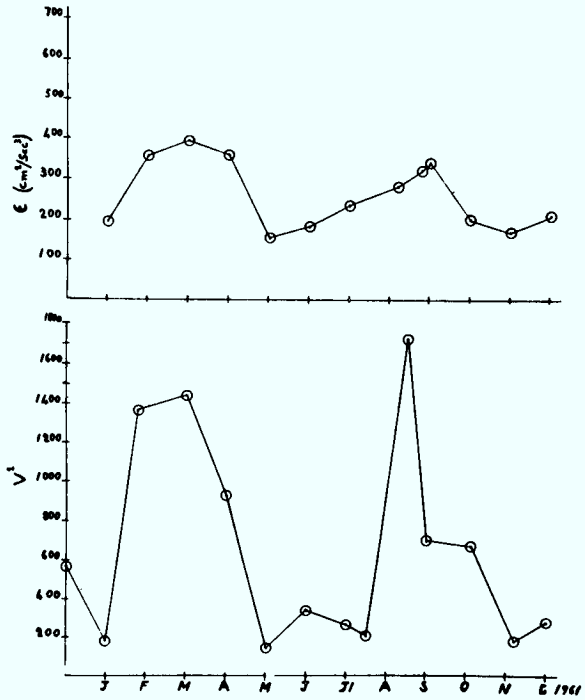

Fig. A-6. Roper's data showing the temperal variation of ϵ as compared to the temporal variation of the energy of the mean winds diurnal component.

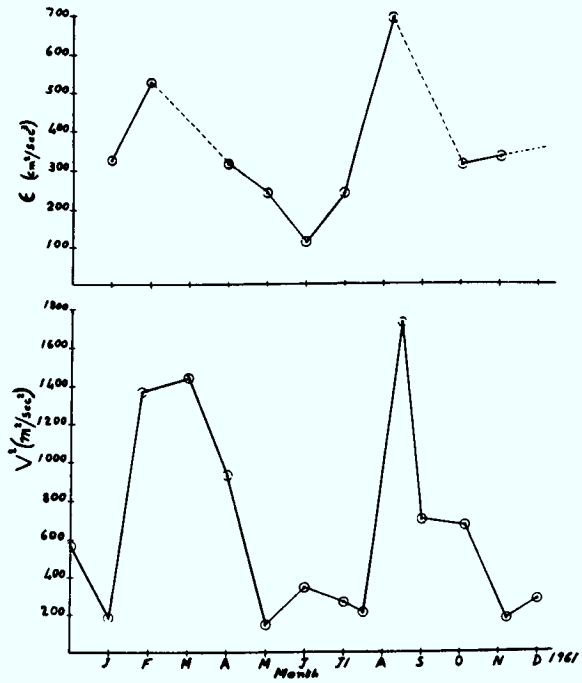

Fig. A-7. The temporal variation of ϵ due to this analysis compared to the mean winds diurnal component.

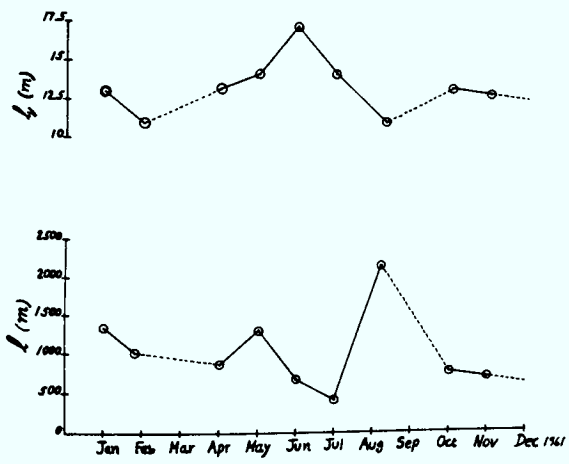

Fig. A-8. Large and small eddy scale sizes.

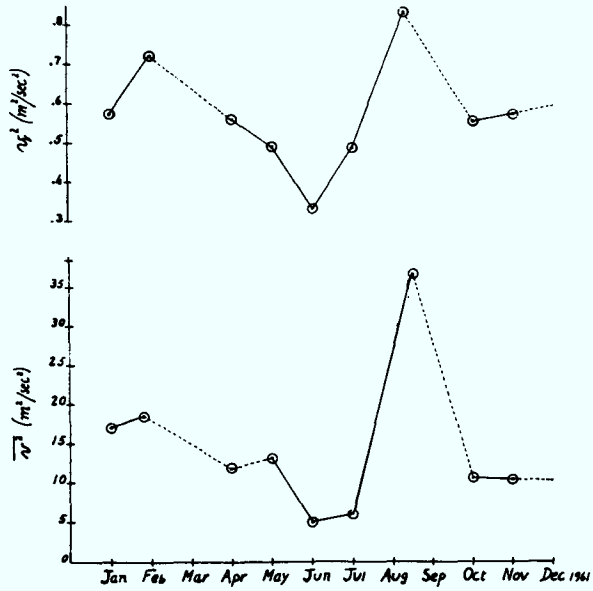

Fig. A-9. The kinetic energy of the large and small eddy scales.

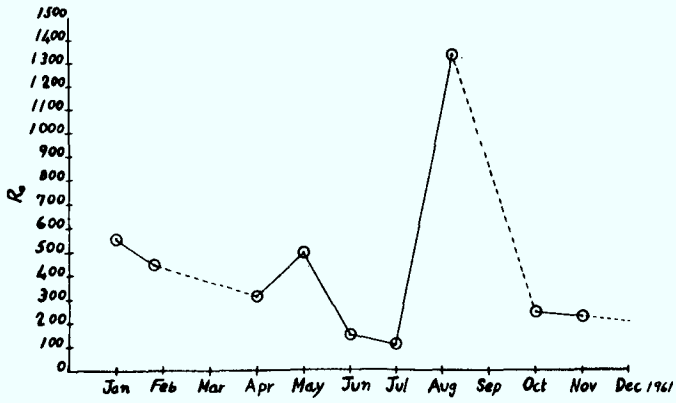

Fig. A-10. The eddy Reynolds number.

Discussion on Paper 1.8 presented by S.P. Zimmerman

Waynick: You quoted the altitude for the turbopause, but I didn't notice it on the slide.

Zimmerman: Yes, I should have mentioned that. The theory is that as the eddy Reynolds number goes to unity, the large-scale size and the small-scale size are in essence unity (1), and thus any energy which is imparted from a shear field would go to a single scale size, and by the same token be lost from that same scale size due to kinematic viscosity. Thus you would expect a cessation of turbulence, where that is apparent. However, this is based again on a simple idea.

Aikin: Lamont reported in a recent talk that he saw alternate regions of laminar flow and turbulent flow on the cloud which he attributes, I believe, to gravity waves. Do you see this sort of structure?

Zimmerman: We have observed a similar phenomenon on some trails, but not many; most of them do not show this. Since I am not familiar with his recent results, I think we ought to discuss this outside.

1.9 THE WIND SHEAR THEORY OF THE FORMATION OF TEMPERATE ZONE SPORADIC E LAYERS

by

W.I. Axford

Cornell-Sydney University Astronomy Center
Department of Astronomy, Cornell University, Ithaca, New York

The wind shear theory provides the most attractive mechanism so far proposed for the formation of temperate zone blanketing sporadic E layers. In this paper we outline briefly the basis of the theory and then go on to review some recent developments which were not discussed in our previous review (1) nor in the Proceedings of the Sporadic E Symposium, held in Estes Park, Colorado, during June 1965 (2).

As a first approximation, the equations of motion for ions in the ionospheric E region can be written

$$\underline{O} = e(\underline{E} + \frac{1}{c}\,\underline{u} \times \underline{H}_o) + \frac{1}{2}\, m_i \nu_i\, (\underline{U} - \underline{u}), \tag{1}$$

where e is the charge and m_i the mass of the ions, ν_i is the ion-neutral collision frequency, $\underline{H}_o$ the geomagnetic field, $\underline{E}$ the electric field, $\underline{U}$ the neutral wind velocity, and $\underline{u}$ the velocity of the ions. The effects of partial pressure gradients (i.e. diffusion) and gravity have been neglected in this equation, and it is assumed that $\underline{H}_o$ and $\underline{U}$ are unaffected by the presence of the charged particles. It is assumed that variations in the horizontal direction can be neglected compared with those in the vertical direction, since sporadic E layers are observed to be typically ~100 km. in horizontal extent and about 1 km. in thickness.

The mechanism underlying the wind-shear theory of temperate zone sporadic E can be understood easily by noting that in the frame in which the east-west component (V) of the neutral wind velocity vanishes, there is an induced electric field $E'_z = -\frac{1}{c} VH_oX$. (A set of Cartesian axes is chosen such that the xy plane is horizontal, the x axis points magnetically northward, y westward and z vertically upwards. We assume that $\partial/\partial x = \partial/\partial y = O$). The vertical velocity of the ions is therefore given approximately by

$$w \simeq W + \frac{2e}{m_i \nu_i}\,(E_z + E'_z) = W - \frac{X}{R_i}\,(V + cE_x/Z\,H_o), \tag{2}$$

where $R_i = cm_i\nu_i/2eH_o \gg 1$ and we have assumed that $\underline{E}\cdot\underline{H}_o \simeq O$. A sporadic E layer can be produced if there is a convergence of the vertical ion motion, and in a steady state the maximum ion density is obtained by equating the resultant rate of accumulation to the rate of loss by recombination; thus $n_i\, dw/dz \simeq -\alpha\, n_i n_e$ where α is the recombination coefficient, and hence (since dW/dz is probably small):

$$(n_e)_{max} \approx \frac{X}{\alpha R_i}\,\frac{dV}{dz}\,. \tag{3}$$

Clearly, the maximum must occur in a region where $dV/dz > O$, and it can also be shown that it will usually occur in the vicinity of the point where $w = O$.

It is implicit in this discussion that the electrons are able to follow the motion of the ions more or less freely so that charge neutrality can be maintained. In fact this is possible only if $Z \neq O$ for purely horizontal wind shears, since $R_e \ll 1$ at E region levels, and hence the electrons are largely constrained to move along the geomagnetic field lines. A more detailed analysis shows that for $Z \lesssim O(R_e)$ the wind shear mechanism becomes ineffective because large polarization fields are produced such that $w \simeq O$ (see Fig. 1). Indeed, a

zone of strongly reduced probability of occurrence of temperate zone sporadic E is observed to be associated with the geomagnetic dip equator. Elsewhere, if it can be assumed that the distribution of suitable wind shears is rather independent of position on the earth, then it is implied by (3) that the probability of occurrence should be correlated with the magnitude of the horizontal component of the geomagnetic field; this has been demonstrated by Heisler and Whitehead (3) to be the case, although Ovezgel'dyyer and Vasil'yeva (4) claim that the correlation is poor during the night hours.

On inserting favorable values for X/R_i and dV/dz in (3), it is found that $(n_e)_{max} \simeq 10^{-2}/\alpha$, and hence if the value of α is that appropriate to dissociative recombination of NO^+ and O_2^+ at 300-500°K (perhaps $1 - 3 \times 10^{-7}$ c.c./sec.), then clearly $(n_e)_{max} < 10^5$ c.c. It therefore seems difficult on this basis to explain the occurrence of intense layers which can at times have $(n_e)_{max} \simeq 10^6$ c.c. However it must be noted that the arguments which lead to (3) did not involve the assumption that all positive ions are involved, and in fact the result obtained is perfectly valid for individual species. Thus (3) implies that $(n_e)_{max}$ can indeed be very large, provided the ions concerned are those with relatively small recombination coefficients. Thus the wind shear mechanism effectively redistributes the ionic constituents of the ionosphere, and causes those ions with small recombination coefficients (especially ions of meteoritic origin which may have α as small as 10^{-12} c.c./sec.), to accumulate preferentially in sporadic E layers. If both O_2^+ and NO^+ have dissociative recombination coefficients of the order of 10^{-7} c.c./sec. or more, then it is predicted that sporadic E layers should be almost entirely comprised of ions of meteoritic origin, and indeed there is evidence that this might be the case. Various aspects of the wind shear theory with two or more positive ions present have been discussed by Cuchet (5), Whitehead (6), and Axford and Cunnold (1); a calculated sample of an equilibrium profile for the two-ion case neglecting diffusion is shown in Fig. 2, where it can be seen that not only do the slowly recombining ions comprise most of the layer, but the rapidly recombining ions are substantially depleted within the layer. Donahue (private communication) has pointed out that some support for the above ideas exists, in that the seasonal variation in the frequency of occurrence of temperate zone sporadic E resembles the variation in radar meteor rates, and also in that there have been isolated cases in which intense sporadic E accompanied a massive micrometeoritic shower (7).

Considerable effort has been put into attempts to verify the wind shear theory by comparing observations of the neutral wind structure from chemical releases with observations of sporadic E layers either by ionosondes or by measurement of the electron or ion density in situ with rocket-borne instruments. Perhaps the most impressive results obtained so far are those described by MacLeod (8), which show that in general sporadic E layers do occur in regions where $dV/dz > O$, but that rather weak layers which occur at 90 to 95 km. altitudes are often not associated with any pronounced east-west wind shear of either sign. It seems necessary to invoke some additional hypothesis to explain these anomalous layers, but it is quite possible that a relatively slight modification of the wind shear theory will suffice; suggestions have already been made that dust, or perhaps negatively charged particles other than electrons might be involved, or that the layers might be the remnants of otherwise normal sporadic E layers which have dissolved into a region where the winds have petered out.

The wind shear observations are useful; however, as a means of providing a test of the theory, they suffer from a number of disadvantages. Firstly, according to (2), the formation of sporadic E layers depends on E_x and W in addition to V, and unless one knows these quantities in a frame of reference in which the wind profile is more or less steady, the position of the layer cannot be predicted except to the extent that it should be in a region with $dV/dz > O$. Secondly, from the observational point of view, it is difficult to measure the wind and electron density coincidentally in space and time, and further uncertainty is introduced by the necessity for having to match altitudes determined separately for each profile. Finally, the wind measurements must be made during twilight or at night, when sporadic E might have a quite different character from that found during the day.

It has been suggested that a better test of the wind shear theory would be provided by measuring the magnetic field profile rather than the wind profile (9). If the contribution from W can be neglected, the variation of the total magnetic field intensity (H) is given by

$$\frac{dH}{dz} = en_eX\,(V + c\,E_x/ZH_O), \tag{4}$$

and hence H has a turning point where $V + c\,E_x/ZH_O = O$ which is approximately the position where the electron density has a turning value. For the case of a sporadic E layer where the turning value is a maximum, $dV/dz > O$ and hence $d^2H/dz^2 > O$, so that the magnetic field intensity has a minimum. Examples of calculated magnetic field intensity variations are shown in Fig. 3, where it can be seen that total variations of the order of a few gammas can be expected. Thus we see that a test of the wind shear theory is provided

by observing simultaneously the magnetic field intensity profile and the electron density profile and seeking correspondence between a minimum in H and the maximum of n_e. The advantages of this proposal are: (a) that electric fields are taken into account as well as the neutral wind; (b) the magnetometer and electron density probe can be placed on the same vehicle, thus avoiding difficulties associated with the usual measurements of electron density and wind profiles which are separated in space and time, and also eliminating the uncertainty introduced by the separate altitude determinations; (c) the experiment can take place at any time of day, and not just at night as is the case with wind measurements. The main disadvantage of the experiment is the accuracy and high time resolution required of the magnetometer, however this is offset to some extent by the fact that the layer can be transversed twice (on the up and down legs of the trajectory) thus improving the effective signal-to-noise ratio.

Some techniques for measuring the electron density in the ionosphere offer in addition the possibility of determining the electron temperature, although so far the results which have been obtained are confused and rather unconvincing (2). A general discussion of the electron temperature distribution to be expected in sporadic E layers has recently been given by Gleeson and Axford (10), who point out that according to the wind shear theory the electron temperature within a layer should normally be less than that found outside essentially because the electrons in the layer are a relatively older population. The treatment is somewhat more detailed than is usually given for problems of this nature (11), since effects such as work done by compression of the particles to form a sporadic E layer might not be negligible. However, if electric fields and heat conduction are neglected a relatively simple result can be obtained, namely

$$T_e - T_n = \frac{\frac{3}{2}kT_o + \left\{\left(\frac{n_e}{n_o}\right)^2 - 1\right\}\frac{5}{2}kT_e - \left(\frac{n_e}{n_o}\right)\frac{3}{2}kT_e}{L^*_{en}\left(\frac{1}{\alpha n_e}\right)\left(\frac{n_e}{n_o}\right)^2}, \tag{5}$$

where T_e and T_n are the electron and neutral temperatures respectively, k is Boltzmann's constant, n_o is the electron density to be expected in the absence of wind shear, L^*_{en} is the rate of loss of energy by individual electrons to neutrals, and $\frac{3}{2}kT_o$ is the effective "initial" energy with which the electrons first appear; near 110 km. altitude we have † $L^*_{en} \simeq 1.3\times10^{-4}\{1.2\times10^{-11}\, n(N_2) + (4\times10^{-14}\, T_e - 8\times10^{-12})n(O_2)\}$ ev/(°K sec) and $\frac{3}{2}kT_o \simeq 1$ ev. In Fig. 4, values of $(T_e - T_n)$ are plotted as a function of (n_e/n_o) for various assumed values of the parameters involved in equation (5). For the case in which a single type of positive ion is present, it is clear that T_e is larger than normal outside sporadic E layers (when $n_e/n_o < 1$) and less than normal within layers (where $1 < n_e/n_o < 10$); for a mixture of ions, the situation is similar. Aubry et al.(2) have found that $T_e < 365$°K inside and $T_e \simeq 780$°K outside a sporadic E layer which was observed at twilight; this result is consistent with the above discussions, although some parameters would have to be modified substantially to give agreement with the rather high temperatures observed outside the layer. The inclusion of heat conduction should not affect our conclusions, since this can only smear the electron temperature distribution slightly without altering its general shape; the inclusion of electric fields is also not expected to give significant effects. At night, when $(T_e - T_n)$ should be small everywhere in the E region at low latitudes, some care should be taken in interpreting observations of the electron temperature, since the neutral temperature itself can vary due to heating by viscous dissipation and the effects of adiabatic heating and cooling which must be associated with atmospheric gravity waves.

It is of some importance to understand the temporal behavior of sporadic E layers, especially their formation and their motion once they have been formed. Nguyen Minh Tri (12) and Gleeson (13) have considered the formation of a layer when only one type of positive ion is present, and have shown that during formation the layers are flat-topped. Cuchet (5) has discussed the case with two positive ions present, considering only the temporal behavior of $(n_e)_{max}$, and has shown that if the recombination coefficients for the two species differ markedly and the rapidly recombining ion is the more abundant, then at first the rapidly recombining ion forms a weak layer, but as the slowly recombining ions accumulate, the density of the former is gradually depressed so that eventually an equilibrium profile such as that shown in Fig. 1 is obtained. For the case of meteoritic ions in the ionosphere, where $w \simeq 1$ to 10 m./sec. the formation time must be of the order of 10^3 to 10^4 sec., since the ions must be drawn from a considerable altitude range (~±10 km. from the layer) in order to make a significant change in the electron density. In general, because wind shears are almost always present, one should expect meteoritic ions to be concentrated in

† $n(N_2)$, $n(O_2)$ in molecules/c.c.

this layer, although during the day these might not be noticeable as sporadic E layers (14); however, at sunset when the remainder of the E region decays these layers should remain, essentially undistorted, and appear as sporadic E layers after sunset. Observations obtained using the incoherent scatter technique at the Arecibo Ionospheric Observatory are effectively in agreement with this suggestion (15).

Finally, we note that consideration should be given to the internal structure of sporadic E layers. Ionosphere observations suggest that the layers are probably rather patchy since the highest frequency reflected is not necessarily equal to the blanketing frequency. It should not be too difficult to extend the wind shear theory to allow for some secondary structure in the wind which would lead to the formation of such patches. From the experimental point of view, however, it is not easy to investigate the patches in detail, except perhaps by the incoherent scatter technique using a very narrow beam radar. The possibility of making such observations at Arecibo is being considered at present, and it is hoped that some success will be obtained by adapting the equipment to permit two beams to be used simultaneously. This should allow us to prove the structure down to length scales of the order of 1 km., but for smaller scales other techniques will be necessary. Theoretical discussions of the stability of sporadic E layers suggest that structures with length scales of the order of tens of meters might occur (16), and indeed there is some experimental evidence that this is the case (17, 18).

Acknowledgments

This work was supported by the National Aeronautics and Space Administration under Grant NsG-382. I am indebted to Dr. L.J. Gleeson for his assistance in preparing this review and for useful discussions concerning the wind shear theory.

REFERENCES

1. Axford, W.I. and D.M. Cunnold. Radio Sci., 1, 191, 1966.

2. Proceedings of the Seminar on the Cause and Structure of Temperate Latitude Sporadic E, held at Estes Park, Colorado, June 1965; Radio Sci., 1, 129-252, 1966.

3. Heisler, L.H. and J.D. Whitehead. Nature, 187, 676, 1960.

4. Ovezgel'dyyev, O. and Ye. K. Vasil'yeva. Geomagnetism and Aeronomy, 4, 321, English translation, 1964.

5. Cuchet, L. Annals de Geophysique, 21, 477, 1965.

6. Whitehead, J.D. Radio Sci., 1, 198, 1966.

7. Dubin, M. Meteors (ed. T.R. Kaiser) p. 111, Pergamon Press, London, 1955.

8. MacLeod, M.A. Journal of the Atmospheric Sciences, 23, 96, 1966.

9. Axford, W.I., Cunnold, D.M. and L.J. Gleeson. Planet. Space Sci. in press, 1966.

10. Gleeson, L.J. and W.I. Axford. Planet. Space Sci. in press, 1966.

11. Geisler, J.E. and S.A. Bowhill. Ionospheric Temperature at Sunspot Minimum, J.A.T.P., 27, 457, 1965.

12. Tri, Nguyen Minh. Electron Density Profiles in the Ionosphere and Enosphere, North Holland, Amsterdam. 1966.

13. Gleeson, L.J. Paper in preparation.

14. Axford, W.I. Space Research VI, North Holland, Amsterdam, 1966.

15. LaLonde, M. Private communication.

16. Tsuda, T., Soto, T., and K. Maeda. Radio Sci., 1, 212, 1966.

17. Spizzichino, A., and A. Girard. Radio Sci., 1, 145, 1966.

18. Bowhill, S.A. Radio Sci., 1, 187, 1966.

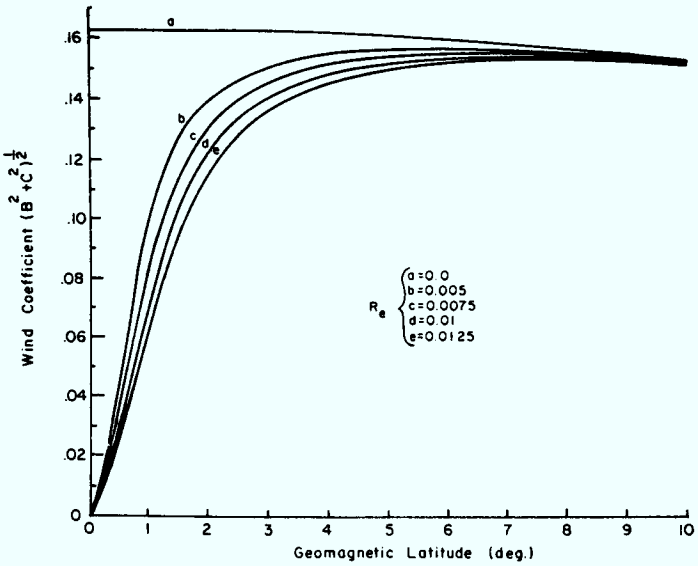

Fig. 1. **The Effective Wind-Shear Coefficient.** *The coefficient is a measure of the effectiveness of the wind-shear mechanism. In the E region R_e ~0.003. An ineffective zone at the magnetic equator is evident.*

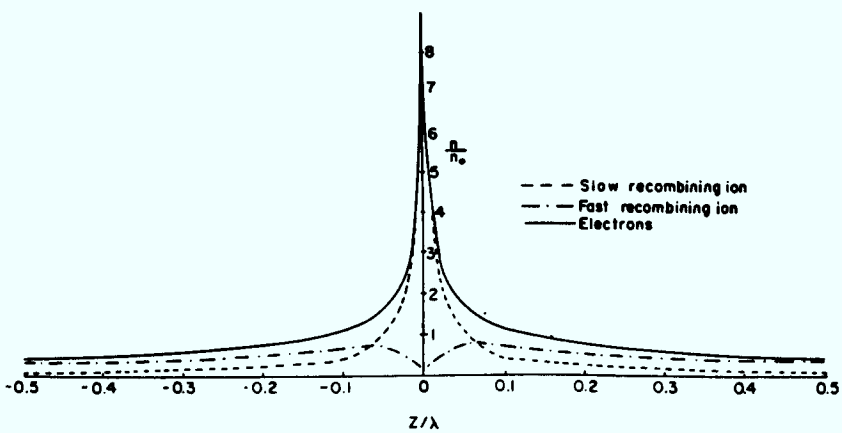

Fig. 2. **Calculated Ion and Electron Density Profiles – Mixed Ions.** *Conditions:* $E_x=E_y=0$, $B_x=0.27$ *gauss*, $B_z=-0.54$ *gauss*, $R_1=R_2=10$, $R_e=0.003$, $\underline{U}=(0,100\sin(2\pi z/\lambda),0)$ *m/s*, $\lambda=6$ *km*, $q_1=3.1\times10^7\ m^{-3}sec.^{-1}$, $\alpha_1=6\times10^{-15}\ m^3sec.^{-1}$, $q_2=2.8\times10^8\ m^{-3}sec.^{-1}$, $\alpha_2=6\times10^{-14}\ m^3sec.^{-1}$, *and* $n_o=10^{11}\ m^{-3}$.

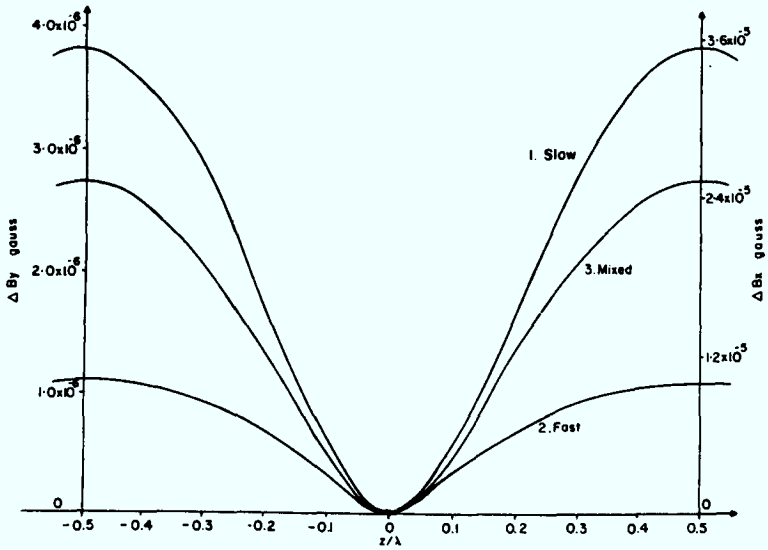

Fig. 3. **Calculated Magnetic Field Variations.** *The parameters assumed are given in the caption to Fig. 2. Profile (1) is for slowly recombining ions alone, (2) is for rapidly recombining ions alone, and (3) is for a mixture of these ions. In each case* $n_0 = 10^{11}\ m^{-3}$.

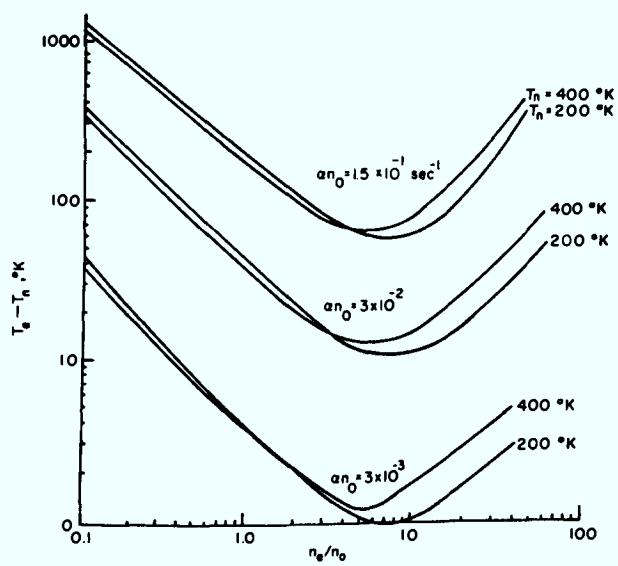

Fig. 4. **($T_e - T_n$) vs. n_e/n_0.** *The electric field and thermal conduction terms have been omitted. The calculations apply at 115 km. altitude with* $(3/2kT_0 = 1$ *ev and parameters* an_0 *and* T_n *as indicated.*

Discussion on Paper 1.9 presented by W.I. Axford

Dalgarno: You mentioned that a critical test of the wind shear theory would be this question of whether these layers are composed of meteoric ions. Supposing you simply have a region of enhanced electron density, and have two kinds of ions, one of which is slowly recombining, and one of which is rapidly recombining, the one that will be seen is the slowly recombining one, and that has nothing to do with wind shears?

Axford: No, but you have made a region of high electron density. You have to say how it got there.

Dalgarno: No, but if there were some other way of putting the electrons there the same thing would happen.

Axford: No, you have to actually pull the ions in, and there is no reason whatsoever that the meteoric ions would always come to the layer and just sit there for you. All the ions would come towards the layer as fast as they could, and in the meantime everything would recombine anyway.

Dalgarno: Leaving the slowly recombining ones!

Axford: No, because they wouldn't have got there in time. There are not many meteoric ions in the ionosphere. You have to collect them from 10 to 15 km. on either side of the layer and this takes quite a while. If you are just going to start with your pile of electrons sitting in a thin layer which is 1 km. thick, I would say that they would be gone in a few minutes, by which time you wouldn't have accumulated many meteoric ions unless you had some way of keeping them stoked up.

Zimmerman: You might be able to explain this (as suggested by Narcisi at AFCRL) by starting off with a neutral meteoric atom which can charge transfer from the diatomic species, and thus you don't have to introduce any other exotic mechanism of ionizing the meteoric ions separately.

Axford: That is much like bringing them in but I don't think that it is any good. You still must have a mechanism for enhancing the electron density. How are you going to do it? You must have an electron there to begin with or you have the same problem as Dalgarno. What you are saying ought to happen throughout the entire E region, and hence the entire E region would have a tendency to break up, but it doesn't.

Zimmerman: The meteoric ions for the most part have been observed as compiling in the lower part of the E region around 90 km.

Axford: Yes, but they occur in layers. Now if it was your mechanism, they would occur rather uniformly. The daytime E region is rather uniform, and has a rather uniform density. You see there is no reason why you should have restricted layers within that region.

Zimmerman: You have not taken into account vertical wind divergence.

Axford: No! Our theory is fact. There is no point, because we have explained everything without magic.

Swider: I want to show Narcisi's curve again (see paper 1.3.1). This is that nighttime flight that I mentioned earlier, and you see that around 90 km. there is this peak of ionization.

Axford: This is a little bit of a problem. Usually when one sees a sporadic E layer at this height, it doesn't have the right wind shear.

Swider: Well, of course not! This is at nighttime; the total electron density is lower.

Axford: Yes, okay, but it is still a problem to know just how this layer got there. If the same observation had been at a higher height and an ionosonde at the same time showed a sporadic E layer, I would have been happier.

Wright: That same sporadic E layer was at 105 km. and even higher earlier in the day, and was over a period of hours convected down to the altitude where you see it, and then over a period of about 3 hr. subsequent to this time, which was 23:21, it rose again, so there is a complete time continuity, and you have this period of several hours within which you wanted to sweep up these metallic ions.

With regard to the correlation with the magnetic field, Whitehead many years ago suggested that there should be a correlation in the probability of occurrence of sporadic E with the magnitude of the horizontal components of the magnetic field (static quantity), the probability being taken over the whole globe. He showed that there was such a correlation. There is a paper by two Russian authors which showed that this relation existed for sporadic E in the daytime and was washed out at night. Now this raises the possibility that these thin layers of very slowly recombining meteoric ions may be abandoned by the wind profile which produced them, and will diffuse back again, and more or less slowly float around, not being associated with any particular feature of the wind profile, while in the daytime, the relation between the wind profile and sporadic E might be expected to be more one to one. This emphasizes, I think, the necessity of getting some daytime wind measurements which are so far unavailable.

Axford: That by the way is another advantage of the magnetometer. It doesn't care about night or day.

Wright: My last question is about this argument that involves the magnetic field measurements, because the E_x which you have thrown in here was plucked out of the air. It is not the consequence of any mechanism?

Axford: It has nothing to do with the wind shear! It has to do with the main wind.

Wright: Through a dynamo process, yes, but the existence of that is somewhat speculative.

Axford: No, it is not. I know it is not because one now has emphatic ion experiments which show an E cross B motion which presumably isn't a wind motion. In other words, there are now measurements of an electric field.

Wright: In any case, I would like to ask just what light this throws on the wind shear process because if the region of enhanced electron density, therefore enhanced conductivity, exists and if the field exists, the current will flow, producing a magnetic field variation, and this says nothing about the cause of sporadic E.

Axford: What it does though, is just confuse the sporadic E theory. That is why I say it is not sufficient just to look at the winds.

Wright: I am saying it would contribute nothing other than a confidence that the current can cause a magnetic field, because one expects the current to be flowing in a region of enhanced conductivity if the electric field exists.

Axford: Sure, but it is a particular feature of the magnetic field record that matters. It has to be minimum, it is not just that there is a current there.

Wright: That feature is a consequence of J cross B and not a consequence of the wind shear theory. Isn't that right?

Axford: The J is a consequence of the V and the E, not just a consequence of the V, but the fact that it is a minimum is a consequence of the V. You can't make a shear in the electric field very easily, but you can make a shear in the wind, so the electric field alone doesn't give you a sort of electric field shear mechanism; but it nevertheless contributes to the mechanism, only in an unfortunate way.

Wright: About the equatorial problem. Blanketing sporadic E is observed at the equator with a probability of occurrence of 10 or 20 per cent in the daytime, compared with 80 or so per cent at temperate latitudes. The wind shear theorists can take some comfort from the fact that blanketing sporadic E is suppressed over the equator but it isn't absent, and I wonder what the explanation might be for it when it does occur?

Axford: Well, that is not too bad, because as I said, if you have absolutely horizontal sporadic E layers, then you get none within a couple of degrees of the equator, depending very much on the effect of the

collision frequency. Of course, the sporadic E layers are probably not absolutely horizontal, and you have only got to have them a little bit tilted for the effective dip equator to move several degrees north or south, so what the effect of a tilt on sporadic E layers would do is to iron that feature out. You won't even have a zero right at the equator, you may expect to see some blanketing sporadic E, but the fact that it is a factor of 8, as you say, down on what you see outside is very encouraging.

Wright: A critical test of the wind shear process might be to make measurements of the height of the sporadic E near the equator at separated points, and look for the tilt.

Axford: It might be; however, I have a feeling that most theories which involve the magnetic field will probably do the same at the equator.

SECTION 2

PARTIAL REFLECTIONS

2.1 A CRITICAL REVIEW OF THE PARTIAL REFLECTION EXPERIMENT

by

J.S. Belrose, I.A. Bourne and L.W. Hewitt

Defence Research Telecommunications Establishment

Presented by I.A. Bourne

1. Introduction

In this paper we discuss the partial reflection of medium frequency radio waves from the lower ionosphere. We are particularly concerned with a specific type of partial reflection experiment, originally devised by Gardner and Pawsey (1953) which provides useful information of ionospheric parameters below the 100 km. level. The technique is a promising approach to D region studies but has not been widely used and its advantages and limitations have not been clearly stated. It is our purpose, therefore, to summarize the main features of the experimental technique, to discuss the experimental difficulties and the characteristics of the experimental data, to critically examine the theoretical assumptions, and finally to attempt to assess the accuracy of the deduced electron number density estimates.

Although Gardner and Pawsey were the first to employ the partial reflection experiment in its present form, the existence of weak reflections from the D region had been detected by a number of observers. For example, Dieminger (1952, 1955) examined conventional ionosonde records and found:

a) in the frequency range 1.6 to 4.0 Mc/s, reflections were occasionally observed from heights of 75 - 90 km. in the daytime, exhibiting a diurnal variation,

b) the apparent reflection heights were independent of the probing frequency, and

c) the echoes were most frequent in winter.

Gnanalingam and Weekes (1954) used a sensitive swept frequency CW technique and detected echoes from heights of 75 to 80 km. More recently, Gregory (1956) used a sensitive system employing pulsed radio waves to detect preferred reflection heights. While these types of experiments give information concerning the amplitudes of the reflected waves, their fading rates and preferred reflection levels, they do not provide reliable quantitative measurements of the electron density or collision frequency profiles.

The revolutionary feature of Gardner and Pawsey's experiment was the measurement of the D region reflection coefficients for both the ordinary and extraordinary mode waves, and the demonstration that, if the reflections were caused by small irregularities in the electron density distribution, one could obtain an upper limit of the electron collision frequency near the base of the ionosphere; and, furthermore, if the collision frequency profile was known, it was possible to deduce the D region electron density profile.

The principal features of the experiment are illustrated in Fig. 1. A pulsed medium frequency radio wave is used to probe the ionosphere. The weak reflections from the D region are received by a polarized antenna system and amplified by a sensitive receiver. A number of different systems have been employed to record the receiver's output. Gardner and Pawsey used the signal to intensity-modulate a cathode ray oscillograph (CRO), and the intensity pattern was recorded on a continuously moving film. A narrow-slit optical system and photo cell were then employed to scale the film recordings. This is a relatively insensitive system and it was realized that a display system which would permit better amplitude and height resolution would be desirable in future experiments. The system shown in Fig. 1 is now in common use. The receiver's output is displayed on a CRO using a type A-scan. Between the reception of the ordinary and extraordinary mode waves the sense of deflection is reversed so that the upper and lower traces represent the ordinary mode and the extraordinary mode waves respectively.

TABLE 1

DATE	GROUP	LOCATION	TX ANTENNA POLARIZATION	DISPLAY	PUBLISHED RESULTS ν_m	PUBLISHED RESULTS N(h)	THEORY
MAY 1952	GARDNER & PAWSEY	BIMLOW AUSTRALIA 33°S, 151°E	LINEAR	INTENSITY RECORDING O,X,O SEQUENCE IN 1 MINUTE	1 VALUE	2 PROFILES	APPLETON-HARTREE
JAN-JUNE 1958	FEJER & VICE	FRANKENWALD SOUTH AFRICA 26°S, 28°E	CIRCULAR	DOUBLE TRACE A-SCAN O AND X SEPARATED BY 1/4 sec.	1 VALUE	1 PROFILE	APPLETON-HARTREE
1958 to 1964	HOLT, LANDMARK & LIED HOLT HAUG	LAVANGSDALEN NORWAY 69°N, 19°E	LINEAR	DOUBLE TRACE A-SCAN O AND X SEPARATED BY 1/50 sec.		22 PROFILES	SEN & WYLLER
1961 to 1965	BELROSE BELROSE & BURKE BELROSE & CETINER BELROSE & HEWITT BELROSE, BOURNE & HEWITT	OTTAWA CANADA 45°N, 76°W	CIRCULAR	DOUBLE TRACE A-SCAN O AND X SEPARATED BY 1/15 sec.	17 VALUES	33 PROFILES	SEN & WYLLER
1963 to 1965	BELROSE, BODE & HEWITT	RESOLUTE BAY CANADA 75°N, 95°W	CIRCULAR	DOUBLE TRACE A-SCAN O AND X SEPARATED BY 1/15 sec.	3 VALUES	1 PROFILE	SEN & WYLLER
1965	BELROSE, MATTHEWS & McNAMARA	CHURCHILL CANADA 58°N, 94°W	CIRCULAR	DOUBLE TRACE A-SCAN O AND X SEPARATED BY 1/15 sec.		1 PROFILE	SEN & WYLLER
1963 to 1965	GREGORY	CHRISTCHURCH NEW ZEALAND 43°S, 172°E	LINEAR	DOUBLE TRACE A-SCAN O AND X SEPARATED BY 1/50 sec.		14 PROFILES	APPLETON-HARTREE

Table 1 shows the quantity of data published prior to this conference by various groups using the partial reflection experiment. It is seen that most use of the technique has been made by groups in Canada and Norway and that only these groups have employed the generalized magnetoionic theory of Sen and Wyller (1960) in the analysis of their data. It should also be noted that, although the partial reflection experiment is apparently well suited for synoptic studies of the D region, relatively few measurements of the collision frequency or of the electron density distribution have been published. A final point to note is that some groups, including Gardner and Pawsey, have used a linearly polarized antenna for the

transmission of the probing wave and have relied on polarized receiving antennas to provide discrimination between the reflected ordinary and extraordinary mode waves. Experimental parameters used by the various groups are not shown. The probing frequencies employed have always been above the local gyrofrequency and frequently exceed the gyrofrequency by a factor ranging from 1.5 to 3. The exception is the work described by Belrose and Cetiner (1962) which used a probing frequency of 6.275 MHz. The choice of frequency depends, in part, on the height region and ionospheric condition to be studied. As the frequency is increased the experiment becomes less sensitive but can be used to greater heights and is better suited to investigations of periods of high absorption. It should be noted that the nature of the irregularities causing the partial reflections abruptly changes near the 100 km. level, and at present this level is an upper limit to the region where the partial reflection experiment can be usefully employed.

2. Characteristics of Partial Reflections

2.1 Echo Structure

The success or failure of the partial reflection experiment depends greatly on the characteristics of the reflections obtained from the D region. Some of these characteristics are partly dependent on the equipment parameters; a typical installation employed by DRTE has the following parameters:

Frequency: 2.66 MHz.
Peak Pulse Power: 100 kw.
Pulse width: 50 μsec.
O mode repetition rate: 1 p/s.
Delay between O and X mode pulses: 70 ms.
Antenna: 4 half-wave dipoles in the form of a square with parallel pairs fed in phase and adjacent sides fed in quadrature. A similar but separate antenna is used for reception.
Receiver: maximum gain 5×10^6.
Band width: 30 kHz.
Response: approximately linear.
Display: photographs are made of type A oscillograph display with the sense of deflection reversed between the reception of the O and X mode waves.

A number of echo structures that have been observed at high latitude stations using this type of equipment are shown in Fig. 2. The ground pulse starts near the left-hand side of each diagram and the upper and lower traces represent the X and O mode reflections respectively.

Fig. 2A is an example of turbulent echoes since echo peaks occur at a large number of levels, and the echoes are not well resolved. A sequence of frames shows that there are no preferred reflection levels. In this example it is evident that the peaks for the O and X mode reflections do not necessarily occur at the same heights and that more peaks can be seen on the O mode trace than on the X mode trace.

Fig. 2B shows a well-resolved stratified echo at the base of the D region. This example was selected from a sequence of photos which indicated that the echo was present at approximately the same height during the 20-min. recording period. Stratified echoes are frequently observed at low latitude stations (Gregory (1961)) and, while the height of the reflection levels may change from day to day, reflections are frequently detected from near the 64, 72, and 85 km. levels. Marked stratification is a mixed blessing, for while it enables accurate measurements to be made of the echo amplitudes at a few levels, it prevents the acquisition of data from intermediate levels; the result is a lack of detail in the computed electron density profiles and a restriction on the maximum electron densities that can be detected.

Fig. 2C is an example of a record obtained during a period of visual overhead aurora. The ratio of echo amplitudes falls from unity to a very small value in approximately 5 km. Under these conditions the computed electron density profile extends over a small height interval and it is probable that it underestimates the number of electrons present.

Fig. 2D shows an unresolved echo frequently seen at Resolute Bay and occasionally at other stations. While the peaks in the O and X mode records may occur at the same height, it is evident that the presence of strong echoes from slightly greater heights introduces significant errors into measurements of both the height of reflection and the amplitude of the echoes when these conditions prevail.

Fig. 3 shows an example of a completely different type of echo observed at Resolute Bay and Churchill. It is similar to echoes reported for other stations located near open water (Dowden 1957). The most striking feature is the presence of very low range echoes (~30 km) whose amplitudes generally decrease with increasing delay. This sequence of photographs, taken at 5-min. intervals, shows that marked changes occur in the echo structure although the changes occur slowly and are not readily detected within a period of a few seconds. It has been verified that they are true reflections and are not caused by large transients of 'ringing' in the receiver. It has been suggested that the echoes are ground and sea reflections, but in the case of the DRTE observations this has not yet been verified. In the examples shown the echo pattern is similar for the X and O mode waves; this is not always the case. These low range echoes may be absent for months but, once they occur, they may be regularly detected for similar periods. They have been detected in summer when there is open water near the experimental stations, and in winter when thick ice covers all water surfaces. There is some evidence that they are more pronounced during periods of abnormal D region absorption, but it should be noted that noise and interference levels are exceptionally low at these times.

While the low range echoes usually occur with apparent heights less than 40 km., they are sometimes detected up to the 70-km. heights and interfere with the more usual D region reflections that we wish to study. In this way low range echoes can effectively provide a limit to the useful sensitivity of future installations unless the cause of these reflections can be determined and the installation designed to eliminate them.

A less severe problem is presented by reflections from large aircraft which have been detected at distances in excess of 60 km. The systematic movement of the aircraft is a useful method for detecting this type of echo and rejecting it from any records which are used to calculate D region electron number density profiles.

2.2 Echo Fading Rates

Some installations use polarized transmitting and receiving antenna to obtain a high degree of discrimination between the ordinary and extraordinary mode waves; this necessitates a delay between the measurement of the echo amplitudes for the two modes and, if this delay is long, fading of the echoes can cause a large scatter in the measurements of the instantaneous ratio of the echo amplitudes.

Echo fading rates vary with time and echo type; in general the "turbulent" echoes appear to fade more rapidly than "stratified" echoes. No systematic measurements of fading characteristics have been made at DRTE although a number of tests have been conducted to ensure that negligible fading occurred in the 70 ms. delay between the reception of the O and X mode waves. Fig. 4 shows echo structures when two O mode waves are transmitted, instead of an O mode and an X mode wave. In records of this type the O mode amplitudes usually agree to within 1 or 2%. On the other hand, larger changes are frequently seen between echoes where the receiver output is the resultant of two or more waveforms and can depend critically on the relative phase relation between these waveforms.

Measurements have been made of the rate of change in the phase paths of well-stratified echoes at a low latitude station (Smith, et al. 1965). In general they show phase coherency for periods ranging from a few seconds to tens of minutes. On one occasion the phase path changed by less than 180° in a ½ hour period suggesting an extremely stable reflection level; it was also noted that for a given echo there was a constant phase relation between the ordinary and extraordinary mode reflected waves.

2.3 Echo Amplitudes

The ordinary mode echo amplitude changes rapidly with height and varies by approximately three orders of magnitude between the 50 and 80 km. levels. The mean ordinary mode amplitude in a given height interval varies from day to day and shows marked seasonal and latitudinal variations.

Experiments conducted at low latitude stations frequently show an almost complete absence of detectable reflections in some height ranges. Marked stratification has also been observed in Canada and Norway. Under quiet ionospheric conditions the number of detectable reflections from below the 70 km. level at Resolute Bay is very small and frequently results in an absence of information concerning this most interesting region.

Reflections from the D region are largest in winter months even though D region electron densities are then smaller than in the summer. The majority of echoes show marked fading, so that a large number of observations (50 or more) are needed before a reliable mean value can be obtained. Furthermore experimental constraints frequently prevent the deduction of reliable 'mean' values. For example, if there is a strong stratified echo near the 60 km. level, weak echoes at nearby levels are ignored since they would not be well resolved. On the other hand, an occasional large echo at nearby heights would be scaled. The result is that the true mean echo amplitude profile could be markedly stratified, while the mean of the scaled echo amplitudes may show little evidence of stratification.

3. Analysis of Partial Reflection Observational Data

3.1 Echo Selection Criteria

At DRTE two scaling criteria are used to help eliminate spurious pulses and off vertical echoes. The first is 'peak scaling'; that is, echoes are scaled only if the peaks on the O and X mode traces occur at the same height (within ± 1 km.). The second criterion is that the peak echo amplitude must exceed the noise level by at least a factor of two.

While there is generally good correlation between the occurrence of O and X mode echoes, the presence of an O mode echo does not necessarily mean that an X mode echo will also be detected. For the Canadian data — using the above criteria — approximately 1/10th of the O mode reflections show no corresponding X mode reflection. This may be due to a number of factors including:

(i) fading of the echoes in the 70 ms. period between the reception of the O and X mode waves
(ii) the presence of off vertical echoes
(iii) the reception of spurious RF pulses.

Furthermore, if echoes are not well resolved from above the 75 km. level, the part superposition and enhancement of two O mode echoes can occur when there is almost complete cancellation of the X mode wave (and vice versa) owing to differences in the phase paths of the two characteristic waves.

It is obvious that shorter pulses would assist in eliminating interference between echoes from neighbouring reflection levels. Tests conducted at DRTE show that a reduction of the pulse width to 25 μsec. does change the number of echoes that would be scaled in a given time interval, and that the vast majority of the peaks in the received echo signals represent true reflections and are not the result of the random summation of a number of weak echoes from numerous reflection levels.

3.2 Determination of the ratio Ax/Ao height curve

The basic experimental measurement concerns the ratio, $\frac{Ax}{Ao}$, of the relative amplitude of the extraordinary and ordinary mode waves, as a function of height. According to the theory of Gardner and Pawsey, the ratio should be independent of Ao and, at low heights, can provide a measure of the electron collision frequency. Unfortunately, the experimental data can show significant departures from the idealized case.

Fig. 5 shows a scatter plot of the amplitudes of the ordinary and extraordinary mode waves reflected from within a 2 km. height interval centered at 59.5 km. In this instance there is little scatter in the data points and the mean can be determined with fair precision. Fig. 6, on the other hand, shows a scatter plot of data obtained on a different date with a marked degree of scatter. For echoes reflected below 75 km. level, the scatter appears to be random. Echoes reflected above this level frequently show a systematic dependence of the ratio $\frac{Ax}{Ao}$ on the measured Ao value, as the data in Fig. 7 illustrates. This systematic dependence is thought to be caused by the presence of off vertical echoes reflected from low levels, which proportionally enhance the extraordinary mode components of the reflected waves. It is only when the O mode reflection (and hence the X mode reflection) is very much larger than the off vertical reflections that the desired ratio is obtained.

Fig. 8 is a plot of the ratios that were obtained in various 2 km. intervals on the same date, a day which was not noteworthy for producing either particularly good or bad records. Also shown are two curves obtained from the data points by different techniques. The data previously shown in Fig. 7 indicates that while both curves would underestimate the differential absorption taking place below the 80 km. level, the $\frac{\Sigma Ax}{\Sigma Ao}$ curve is probably the more reliable of the two, since it effectively weighs each $\frac{Ax}{Ao}$ ratio measurement by a term proportional to the O mode amplitude.

The presence of off vertical echoes has plagued the partial reflection experiment since the original observations by Gardner and Pawsey. Research groups in Canada and Norway can testify that they can be particularly troublesome when the ionosphere is disturbed (Belrose and Cetiner 1962, Holt 1963). The construction of large high-gain antenna arrays seems to be the only way to overcome this vexing problem. At DRTE a large antenna has been constructed for the 6.275 MHz. frequency, comprising a 128-dipole circularly polarized antenna covering 9 acres of ground. Tentative future plans include the possible construction of a 40-dipole array for 2.66 MHz.

If the scatter in the measurements of the ratio $\frac{Ax}{Ao}$ is random, the mean ratio can be determined with fair accuracy, if a large number of measurements are made. In practice, the number of echoes scaled in a 2 km. height interval can vary markedly with height. In Fig. 9 the mean Ao amplitude, the ratio $\frac{Ax}{Ao}$ and the number of echoes scaled in 2 km. height intervals are shown for 5 days in December 1961. The data for December 18 and 19 show a marked degree of stratification, in both the mean Ao value and the number of echoes scaled, which is almost completely absent on the 8th. The ratios measured at 57.5 and 59.5 km. on the 18th show markedly less scatter than the ratios measured at higher or lower heights and the larger number of echoes at these levels enables the mean ratio to be determined with a high degree of accuracy.

3.3 Comments on the Theory of Partial Reflections

A full development of the theory of partial reflections is beyond the scope of this survey. However, it is necessary to indicate some of the theoretical assumptions used and to estimate the effects of alternative theories on the computed D region parameters.

The first point to note is that the theory used by Gardner and Pawsey assumed that irregularities in the electron density distribution were the cause of the partial reflections. A number of groups using the partial reflection technique have known that irregularities in the electron collision frequency profile (if they exist) might also cause reflections (Piggott and Thrane 1966), but to date no conclusive evidence supporting either process has been published. The ratio of the relative amplitudes of the ordinary and extraordinary mode waves, $\frac{Rx}{Ro}$, in the absence of differential absorption depends markedly on whether an irregularity, ΔN, in the electron density, or an irregularity, $\Delta\nu$, in the collision frequency is causing the reflection or whether a combination of the two processes operates. Fig. 10 shows some curves, calculated by Burke (1963), which depict how the amplitude ratio $\frac{Rx}{Ro}$ depends on the

ratio $\frac{\Delta\nu m}{\nu m}/\frac{\Delta N}{N}$ at various heights (the collision frequency curve 1 of Belrose and Burke (1964) has been used in deducing these curves and it has been assumed that the irregularities ΔN and $\Delta\nu m$ occur at the same levels).

Note that at heights when $\frac{\Delta\nu m}{\nu m}/\frac{\Delta N}{N}$ is ~ 1 the ratio $\frac{Rx}{Ro}$ is very much less than either the pure ΔN or $\Delta\nu$ processes predict, but that there is a fairly rapid change to either ΔN or $\Delta\nu$ like ratios as $\frac{\Delta\nu m}{\nu m}/\frac{\Delta N}{N}$ departs from 1. In contrast, Fig. 11 shows that at higher levels when $\frac{\Delta\nu m}{\nu m}/\frac{\Delta N}{N}$ is 1, the ratio $\frac{Rx}{Ro}$ is approximately given by a ΔN type process and that $\frac{\Delta\nu m}{\nu m}/\frac{\Delta N}{N}$ must exceed 10 before $\Delta\nu m$ type ratios are obtained. We conclude that while $\frac{Rx}{Ro}$ ratios measured near the 85 km. level may support the ΔN hypothesis, they do not necessarily imply that the theory is adequate at lower levels.

The problem is further complicated if the irregularities ΔN and $\Delta\nu$ do not occur at the same level. Under those circumstances the ratio $\frac{Rx}{Ro}$ could be anywhere in the range 0 to ∞.

If ΔN and $\Delta\nu$ processes can operate independently, two degrees of freedom are introduced and additional information would be needed before ionospheric parameters could be determined. In principle, measurements of the difference between the phase paths of the ordinary and extraordinary waves could provide additional, but still insufficient, information. Fejer (1961) has suggested that, if a ΔN process operates, measurements of the difference in phase paths can be used to determine the electron density profile. To date this technique has not been employed. A consideration of the reflection process shows that allowance would have to be made for the difference, $\Delta\theta$, in the phase shifts suffered by the characteristic waves at the reflection level. Fig. 12 shows that $\Delta\theta$ should be readily detectable. If ΔN and $\Delta\nu m$ processes do not both occur, measurements of $\Delta\theta$ could be used in conjunction with the conventional partial reflection observations to determine which process operates.

Although irregularities in the collision frequency profile can theoretically cause reflections, it is stressed that the available experimental data, with one possible exception to be discussed later, is not inconsistent with the assumption that the reflections are caused by irregularities in the electron density profile. Nevertheless, in assessing the reliability of the experimental technique the possibility that some echoes are caused by collision frequency irregularities should not be overlooked. In the remainder of this paper, it is assumed that irregularities in the electron density profile cause the partial reflections unless explicitly stated otherwise.

The second point to note is that Gardner and Pawsey used the Appleton-Hartree theory, which is now considered inappropriate for ionospheric conditions that prevail in the D region. There is apparently no simple way to compare and contrast the electron densities deduced by the two theories, although Fig. 13 shows that profiles deduced by the two theories can be significantly different.

The third point is that in Gardner and Pawsey's original experiment a linearly polarized antenna was used for the transmission of the probing wave, and it was assumed that there was an equal division of the energy into the ordinary and extraordinary mode waves. A more detailed analysis by Smith et al. (1965) shows that this is strictly true only for longitudinal propagation. Furthermore, if the probing frequency is close to the gyro frequency and if a circularly polarized antenna is used to receive the weakly reflected waves, the reflection coefficients computed by Gardner and Pawsey can be in serious error as they then depend on the orientation of the transmitting antenna. Fig. 14 shows the expected dependence of the ratio $\frac{Rx}{Ro}$, of the amplitudes of the extraordinary and ordinary mode waves in the absence of absorption, on the antenna orientation for conditions at Armidale, N.S.W., Australia (ωH = 1.515 MHz., ω = 1.78 MHz.). Experimental measurements are in qualitative agreement with this analysis. If the receiving antenna are not accurately circularly polarized but are designed to receive only the characteristic waves, the dependence on the antenna orientations is less dramatic but still significant.

The final point to note is that the partial reflection experiment is not uniformly sensitive to electron densities within the D region. Fig. 15 shows a set of experimentally

determined ratios $\frac{Ax}{Ao}$ as a function of height. The solid curve represents the ratios $\frac{Rx}{Ro}$ that would have been detected in the absence of differential absorption assuming a certain collision frequency profile (collision frequency profile curve 1 (Belrose and Burke 1964 used). At low heights, where there is negligible differential absorption, the experimental data are consistent with this profile. At greater heights differential absorption causes the experimental data to fall below the $\frac{Rx}{Ro}$ curve, and theory shows that the electron density at a height h (assuming the collision frequency is known) is dependent only on the ratio $(A_x/A_o)_{h+1}/(A_x/A_o)_{h-1}$, or the slope of the log (Ax/Ao(h)) curve. Fig. 16 shows the dependence of the electron density on this ratio, which we shall call C, throughout the D region (again assuming the collision frequency curve 1). Since the ratio C is determined from experimental data, it is evident that a small error in the $\frac{Ax}{Ao}$ ratio measurements near the 60 or 85 km. levels can cause larger errors in the computed electron density than equivalent errors near the 75 km. level. Fig. 17 shows the departures from an assumed exponential profile that would be caused by various errors in the measurements of the ratio C. Since the electron density increases rapidly with height, the percentage error in the computed electron density profiles in roughly constant above the 75 km. level but increases very rapidly at lower levels.

3.4 The Reliability of the Deduced Collision Frequency and Electron Density Values

The basic experimental parameter we wish to determine is the dependence of the ratio $\frac{Ax}{Ao}$ on the height of the reflection level. Inaccuracies in the measurement of this relation are immediately reflected as errors in the computed values of the collision frequency and electron density. While a realistic evaluation of the magnitude of random and systematic errors associated with the ratio and height measurements result in unfortunately large uncertainties in the computed electron density profiles, they are probably no worse than the uncertainties associated with any other technique now available.

In discussing errors, attention should be given to the possible systematic and random errors associated with:

(1) The amplitude and height calibration of the receiving equipment,
(2) The scaling of the experimental data,
(3) The reduction of the experimental data,
(4) Polarization of the antenna systems.

These errors can be made small by the use of carefully controlled experimental procedures, and certainly should not account for more than a 2% uncertainty in the measurements of the ratios $\frac{Ax}{Ao}$ associated with a given 2 km. height level or an error exceeding ± 1 km. in measurement of the mean height of this interval. The scatter in the experimental data is very much greater than this figure and the influence of off vertical echoes can cause larger systematic errors near the 80 km. level. At low heights, poor signal-to-noise ratios can systematically cause the ratio $\frac{Ax}{Ao}$ to be underestimated.

Fig. 18 shows the scatter obtained in measuring the height of simulated echoes using the equipment operated by DRTE. The delay of a simulated 'echo' was systematically increased in 2 km. intervals and the normal scaling procedures used to determine its apparent reflection height. It is seen that only rarely was an error exceeding ± 1 km. obtained. In practice, echoes are not necessarily well resolved and a much larger degree of scatter is to be expected. Systematic errors of the order of ± 1 km. are not excluded.

Errors in ratio measurements can make very large errors in the estimated collision values if only data from very low heights are used. On the other hand, the ratio at higher heights is influenced by differential absorption. The majority of the data analysed by DRTE enables estimates to be made of the collision frequency near the 57 km. level; the possibility of systematic errors of ± 20% in the computed collision frequencies cannot be excluded.

Random height and ratio errors can exceed these values on any chosen day but can, to a large extent, be eliminated by averaging data, if only slow term variations are considered.

In a companion paper (Belrose et al. 1966) the yearly variations of the measured collision frequency values are discussed. The mean value for the 1963-64 winter corresponds to a height shift of the collision frequency profile by at least 6 km. (or to a decrease of more than 50% in the collision frequency) from the values observed during 1962. An alternative explanation is that the nature of the irregularities changed, being predominantly ΔN type reflections in 1961-62 and predominantly $\Delta\nu$ type reflections in 1963-64. When the characteristics of the experimental data are considered together with the computed mean electron density profiles for these winters, it seems highly probable that there was, in fact, a substantial change in both the gas pressure and the collision frequency and that the ΔN type reflection process was at all times the dominant reflection mechanism.

It is highly desirable that the estimates of the collision frequency near the 60 km. level be obtained when the experiment is used to deduce electron density distributions, since significant random and seasonal variations are known to occur in the pressure profiles. The upper diagram in Fig. 19 shows the effects of errors of ± 4 km. in choosing the location of a collision frequency profile on the computed electron densities. Below the 60 km. level and above the 75 km. level, the electron densities depart significantly from the assumed profile and errors of 50% occur near these levels. The lower diagram shows the effect of assuming the correct collision frequency profile but of making systematic errors (of ± 4 km.) in the measurement of the height of the reflection levels. Near the 70 km. level the computed electron density can be in error by approximately 100%.

Although the quality of the experimental data is variable, it is interesting to determine approximate limits on the range of electron densities that can be measured using the partial reflection technique. The lower limit is generally determined by the accuracy of the measurements of the ratio $C = (\frac{Ax}{Ao})_{h+1} / (\frac{Ax}{Ao})_{h-1}$. The upper limit is determined by the effective height resolution of the experiment, the height distribution of reflection levels, the smoothing of the experimental data and the presence of off vertical echoes. Fig. 20 shows estimated upper and lower limits for the 2.66 MHz. partial reflection experiment conducted at Ottawa. To the left of the left hand side curve a 5% error in the value of C causes a 100% error in the calculated electron density. As a general rule it is unlikely that this accuracy is exceeded in routine observations; the left hand side curve can also be used as a rough estimate of the uncertainty of a deduced electron density value under quiet D region conditions. If data for a number of days observations are available, the lower limit curve would not necessarily be appropriate as the mean ratio C may then be determined with a higher degree of accuracy. Electron densities to the right of the right hand curve cannot be measured, owing to the grouping of data into 2 km. height intervals and taking a 3-point running average of the measured $\frac{\Sigma Ax}{\Sigma Ao}$ ratio values. In practice, near the 80 km. level the measurable range of electron densities should be reduced owing to the weak X mode echoes at this level at midday and owing to the difficulties caused by off vertical echoes. Also shown are average electron density curves for summer and winter conditions. The dotted portion of these curves are extrapolated values assuming proportionality between electron densities and the mean Ao echo amplitudes. This suggestion was first made by Gardner and Pawsey and has been shown to be a good approximation, at least on some days, by Belrose and Burke (1964).

Mean values of ordinary mode echo amplitudes, electron density values, and total numbers of echoes scaled during the winter of 1961-62 and summer 1962 are shown in Fig. 21. The approximate proportionality between the electron densities and the echo amplitudes is clearly evident. However, it is noted that while the electron densities are larger in the summer than in the winter, the reverse is true of the mean amplitudes. Furthermore, there is a significant increase in the number of echoes scaled near the 55 km. level in the winter months. It is concluded that the lower ionosphere is less uniform in the winter than in the summer and that measurements of the Ao amplitude alone cannot provide reliable information on seasonal changes of the D region electron density.

As previously stated, one of the greatest problems in the partial reflection experiment concerns the possible existence of reflections from irregularities in the electron collision frequency profile. If irregularities exist in both the electron density profile and the

collision frequency profiles, there is no simple way of estimating the possible errors in the computed electron density profiles, although it can be confidently stated that the errors could be large. If reflections are observed only from collision frequency irregularities, while the analysis of the data assumed that the reflections were caused by irregularities in the electron density profile, the computed electron density profile would be in error. Figs. 22 and 23 show the relation between the computed electron density values $N_{\Delta N}$ (calculated on the assumption that ΔN irregularities were causing the reflections) and $N_{\Delta\nu}$ (the values calculated assuming that $\Delta\nu$ irregularities were the cause of the reflections). The data in Fig. 22 assumes that the collision frequency profile of Belrose and Burke (1964) has been used in both methods of analysis. The data shown in Fig. 23 assumes that different νm profiles are used in each type of analysis. The value of νm is chosen so that in the absence of differential absorption the reflection coefficient ratios are equal in both cases at 60 km. In this case there is no simple system of converting from $N_{\Delta N}$ values to approximate $N_{\Delta\nu}$ values; however, for electron densities found in the D region it is seen that $N_{\Delta\nu}$ probably does not differ from $N_{\Delta N}$ by more than approximately a factor of 3.

3.5 Comparison with other Experimental Results

Since D region electron densities at high latitudes show marked variations in both time and location, especially during the winter, data cannot be justifiably compared unless different experiments are conducted at the same place and time. One method is to obtain electron density profiles with two partial reflection experiments using different probing frequencies. The 2.66 MHz. and the 6.275 MHz. installations operated at Ottawa are poorly suited for this purpose, as they effectively probe different portions of the D region during undisturbed times; however, a comparison was made during a time when absorption was high (Belrose and Cetiner 1962).

Two experiments of this type have been conducted by DRTE. The first experiment enabled the electron density values and the collision value near the 60 km. level to be deduced from simultaneous partial reflection observations using probing frequencies of 2.66 MHz. and 6.275 MHz. during a S.I.D. on 1 March, 1962. The $\frac{\Sigma Ax}{\Sigma Ao}$ ratio data and the computed electron density profiles are shown in Figs. 24 and 26. It can be seen that similar collision frequencies would be deduced from both sets of data and that the electron density profiles are in good agreement at low heights; at greater heights there is a marked discrepancy between the computed electron density values. Belrose and Cetiner showed that the 6.275 MHz. data would be consistent with riometer recordings made during the S.I.D. The upper portions of the 2.66 MHz. electron density profile and the $\frac{\Sigma Ax}{\Sigma Ao}$ ratio curve are dotted, since it is believed that the ratios at these levels were strongly influenced by off vertical reflections. The variation with height of the mean 2.66 MHz. ordinary mode echo amplitude, shown in Fig. 25, differs markedly from the roughly exponential increase which is characteristic of quiet day records and the small amplitudes near the 75 km. level suggest that the wave was heavily absorbed at lower heights.

The second experiment employed a new installation with a 4.21 MHz. probing wave and compared the computed electron density and collision frequency values deduced from simultaneous data obtained with this frequency and the 2.66 Mc/s wave. The results obtained during a small disturbance on 30 March, 1966, are shown in Figs. 27, 28 and 29, from which it can be seen that the collision frequency values deduced from the two sets of data would not be inconsistent, that the mean Ao amplitudes vary with height in a similar manner and that there is good agreement between the computed electron density values near the 70 km. level. At greater heights the 2.66 MHz. data gives smaller electron density values than the 4.21 MHz. data. The 4.21 MHz. ordinary mode echo amplitudes are approximately a factor of 3 less than the 2.66 MHz. echo amplitudes, when allowance is made for the different sensitivity of the two installations.

The discrepancy at high heights between the electron density values deduced from the 2.66 MHz. data and the data obtained from the high probing frequencies is to be expected if off vertical reflections occur. It should be noted that disagreement between the various

profiles commences when the $\frac{\Sigma Ax}{\Sigma Ao}$ ratio, as measured on the 2.66 MHz. equipment, has fallen to a value near 0.7, which agrees well with the completely independent analysis presented in Section 3.2, which shows that there can be systematic dependence of measured $\frac{Ax}{Ao}$ ratios on Ao when $\frac{\Sigma Ax}{\Sigma Ao}$ has fallen to approximately this value. A simple theoretical analysis shows that the effect can be interpreted as being due to the presence of off vertical reflections, and there is experimental evidence which suggests that off verticals may be more troublesome during periods of high absorption. It is concluded that the various sets of data are consistent at low heights, but that care must be taken in interpreting the data at high heights as off vertical reflections can cause a systematic underestimation of the electron density.

Electron density and collision frequency profiles can also be deduced from wave interaction experiments and attempts have been made to compare the results with partial reflection experiments (Fejer and Vice 1959; Holt, Landmark and Lied 1961). Unfortunately, these analyses used the Appleton-Hartree theory and were not sufficiently accurate to really test the accuracy of the partial reflection experiment, although it was concluded that the two sets of experimental data were not inconsistent.

Using a generalized theory, Holt (1963) has compared partial reflection observations with the results of a rocket-borne experiment conducted by Jespersen et al. (1963) and concluded there was good agreement between the two sets of data over the 5 km. height range for which partial reflection data was available. The rocket and partial reflection experiments were conducted at locations separated by 140 km. and during a period of high, but fluctuating, D region absorption.

On 27 May, 1965 a rocket-borne propagation experiment was conducted by DRTE in conjunction with the 2.66 MHz. partial reflection experiments at Churchill. The rocket carried a receiver tuned to 2.66 MHz. which measured the differential absorption occurring between pulsed ordinary and extraordinary mode waves radiated from the ground-based station. Fig. 30 shows the computed electron density profiles (assuming the collision frequency profile, curve 1) and assuming that the partial reflections were caused by irregularities in the electron density distribution. While there is good agreement near the 70 and 85 km. levels, there is a factor of 2 discrepancy near the 80 km. level. As there was some uncertainty in the interpretation of the data from rocket experiments, the comparison was considered satisfactory. However, further analysis shows that if a second collision frequency profile is used and it is assumed that the reflections are caused by irregularities in the collision frequency profile better agreement between the two experiments is obtained.

Future comparisons of the two techniques are planned; it is hoped that modifications to the rocket-borne receiving equipment will eliminate much of the uncertainty in the interpretation of the data from the rocket-borne experiment.

4. Conclusions

There is certainly general agreement that the partial reflection experiment is one of the most valuable methods that has as yet been devised for the study of the lower ionosphere from a ground-based station.

This experiment has limitations, most of which have been discussed in this paper. In spite of possible errors introduced by some of these limitations, we feel that most errors can be minimized in a well-designed partial reflection experiment when the following features are incorporated into the experimental design:

1. High power transmitters (care being taken to restrict the power to a value which would not significantly change the collision frequency profile)
2. Polarized antennas for transmission and reception of the probing wave
3. The use of an appropriate magnetoionic theory and collision frequency profile: in the most desirable circumstances the latter should be determined from the experiment itself
4. The use of shorter RF pulses to improve height resolution
5. High gain antennas to reduce the influence of off vertical echoes

6. The simultaneous use of a number of probing frequencies
7. Analogue to Digital conversion systems that enable accurate reduction of echo heights and amplitudes.

The last point is particularly important if the partial reflection experiment is to be used for synoptic studies of the D region, since the scaling of photographic records is laborious and time-consuming. Although a suitable conversion system appears to be technically difficult, once developed, it could be of great assistance in numerous ionospheric investigations.

The major experimental difficulty is caused by the apparent variability of the ratio $\frac{Ax}{Ao}$ in a chosen height interval when the present experimental techniques are employed, and the variability in the number of echoes from various levels in the D region.

The one theoretical limitation which can affect the absolute accuracy of the determined N(h) profile and can not be minimized by the present experimental technique is the possibility that the partial reflections are also caused by discontinuities in the νm profile.

We feel that the assumption that electron density irregularities cause the reflections is a valid one, and we hope to carry out further experiments (such as the measurement of the difference in phase of the two magnetoionic components and further co-operative simultaneous ground-based and rocket experiments) in an attempt to provide justification for this assumption. Further experimental work on this problem should be encouraged to eliminate this possible inaccuracy in the profiles obtained by the partial reflection technique and further increase its value as one of the most simple and economic methods of obtaining reliable electron density profiles for the lower ionosphere.

REFERENCES

Belrose, J.S., Bourne, I.A. and L.W. Hewitt. A preliminary investigation of diurnal and seasonal changes in electron distribution over Ottawa, Churchill and Resolute Bay, These Proceedings, 1966.

Belrose, J.S. and M.J. Burke. Study of the lower ionosphere using partial reflections. 1. Experimental, technique and methods of analysis, J. Geophys. Res., 69, 2799-2818, 1964.

Belrose, J.S. and E. Cetiner. Measurement of electron densities in the ionospheric D region at the time of a 2+ solar flare, Nature, 195, 688-690, 1962.

Burke, M.J. Private communication, 1963.

Dieminger, W. Uber die Ursacke de exzesiven absorption in der ionosphere an wintertagen, J. Atmos. Terr. Phys., 2, 340-349, 1952.

Dieminger, W. Short-wave echoes from the lower ionosphere, 'Physics of the Ionosphere', 53, Phys. Soc., (London), 1955.

Dowden, R.L. Short range echoes observed on ionospheric recorders, J. Atmos. Terr. Phys., 11, 111-117, 1957.

Fejer, J.A. The absorption of short radio waves in the ionospheric D and E regions, J. Atmos. Terr. Phys., 23, 260-274, 1961.

Fejer, J.A.and R.W. Vice. An investigation of the ionospheric D region, J. Atmos. Terr. Phys., 16, 291-306, 1959.

Gardner, F.F. and J.L. Pawsey. Study of the ionospheric D region using partial reflections, J. Atmos. Terr. Phys., 3, 321, 1953.

Gnanalingam, S. and K. Weekes. D region echoes observed with a radio wave of frequency 1.4 Mc/s., 'Physics of the Ionosphere', 63-70, Phys. Soc., (London), 1955.

Gregory, J.B. Radio reflections from the mesosphere, 1, Heights of occurrence, J. Geophys. Res., 66, 429, 1961.

Gregory, J.B. Ionospheric reflections from heights below the E region, Austr. J. Phys., 9, 324, 1956.

Holt, O. Some experimental studies of the ionospheric D region at high latitudes, NDRE Report 46, Norwegian Defence Research Establishment, July 1963.

Holt, O., Landmark, B. and F. Lied. Observations of electron density and collision frequency during polar radio blackout conditions, J. Atmos. Terr. Phys., 23, 318, 1961.

Jespersen, M., Petersen, O., Rybner, J., Bjelland, B., Holt, O. and B. Landmark. Electron density and collision frequency observations in the lower D region during auroral absorption, Ionospheric Lab. Royal Tech. Univ. Denmark Rept. 16, March 1963.

Piggott, W.R. and W.V. Thrane. The effect of irregularities in collision frequency on the amplitude of weak partial reflections, J. Atmos. Terr. Phys., 28, 311, 1966.

Sen, H.K. and A.A. Wyller. On the generalization of the Appleton-Hartree magnetoionic formulas, J. Geophys. Res., 65, 3931-3950, 1960.

Smith, R.A., Bourne, I.A., Loch, R.G., Setty, C.S.G.K., Coyne, T.N.R. Barratt, P.H. and B.S.N. Prasod. Radio wave interaction using gyro-waves, Air Force Cambridge Research Lab. Report AFCRL 65, 460, 1965.

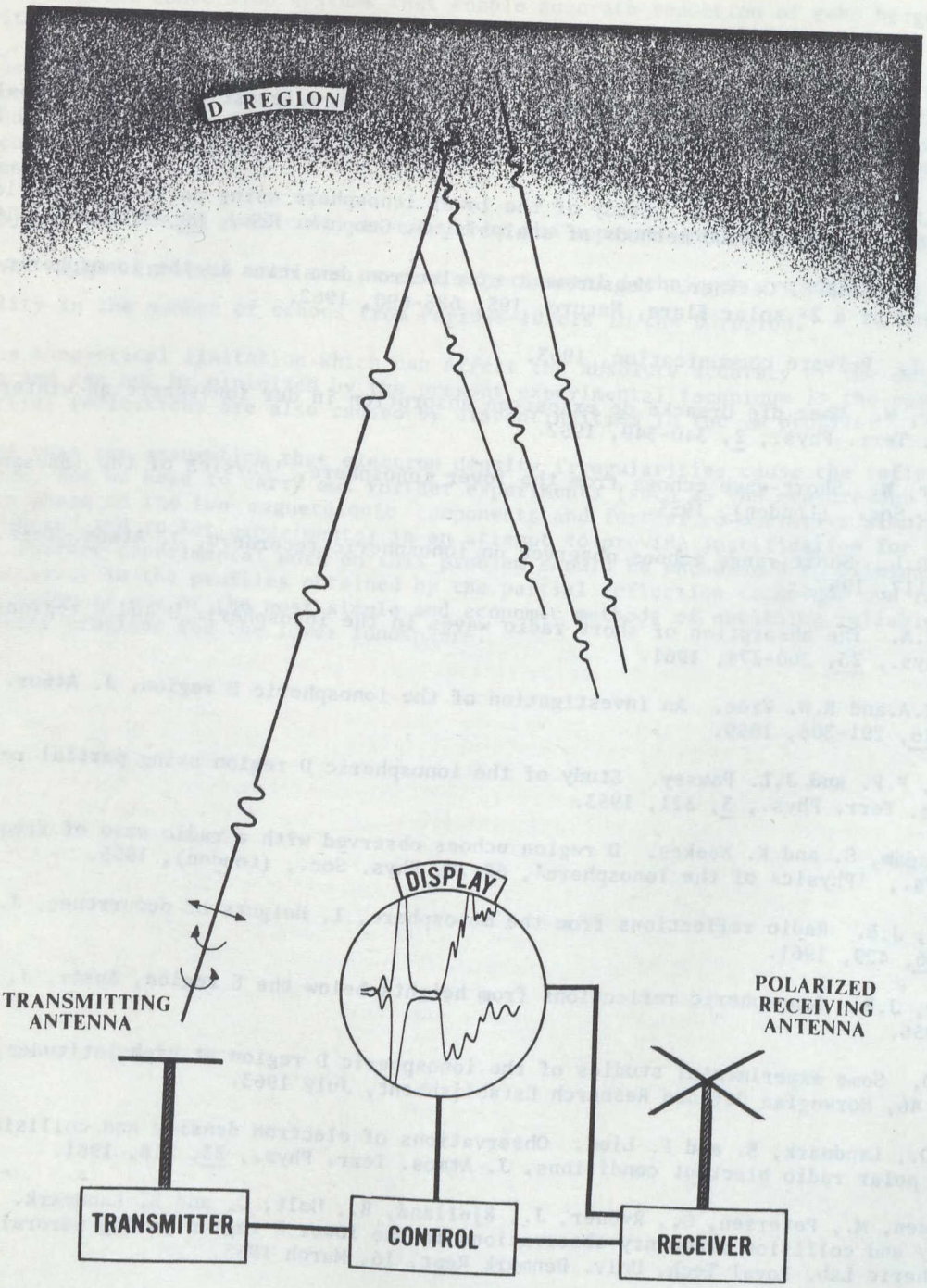

Fig. 1. Block diagram of a partial reflection experimental installation.

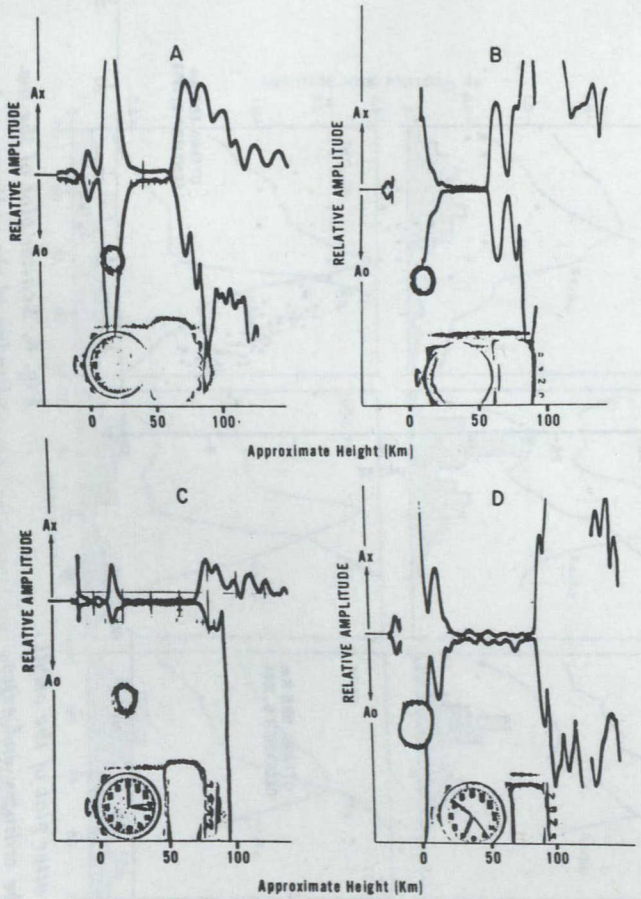

Fig. 2. Examples of recordings of partial reflections at high latitude stations.

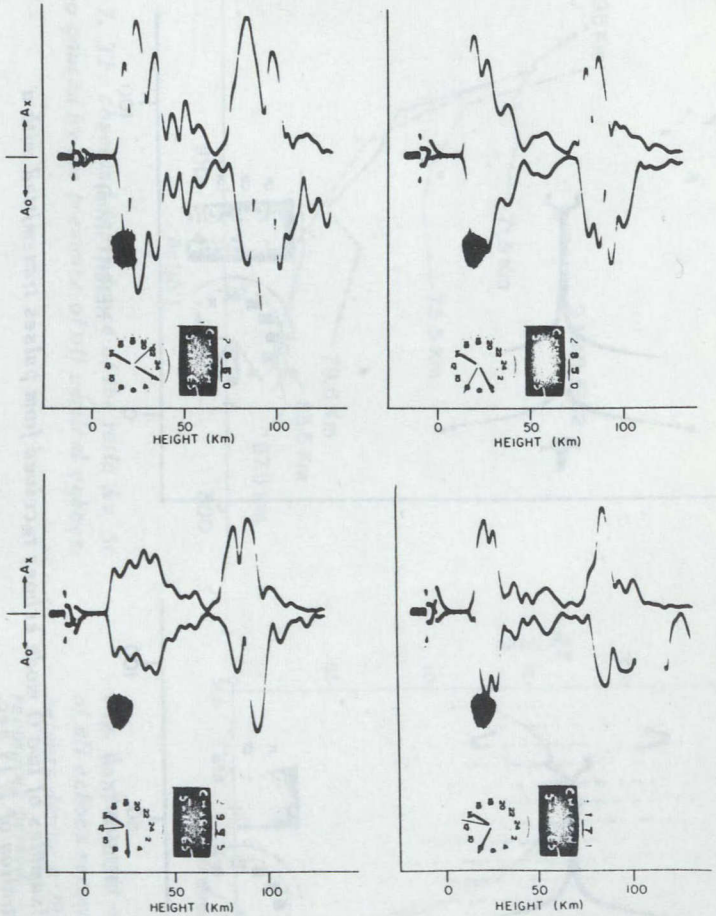

Fig. 3. Examples of unexplained low level echoes obtained at 5-min. intervals by the Churchill partial reflection installation.

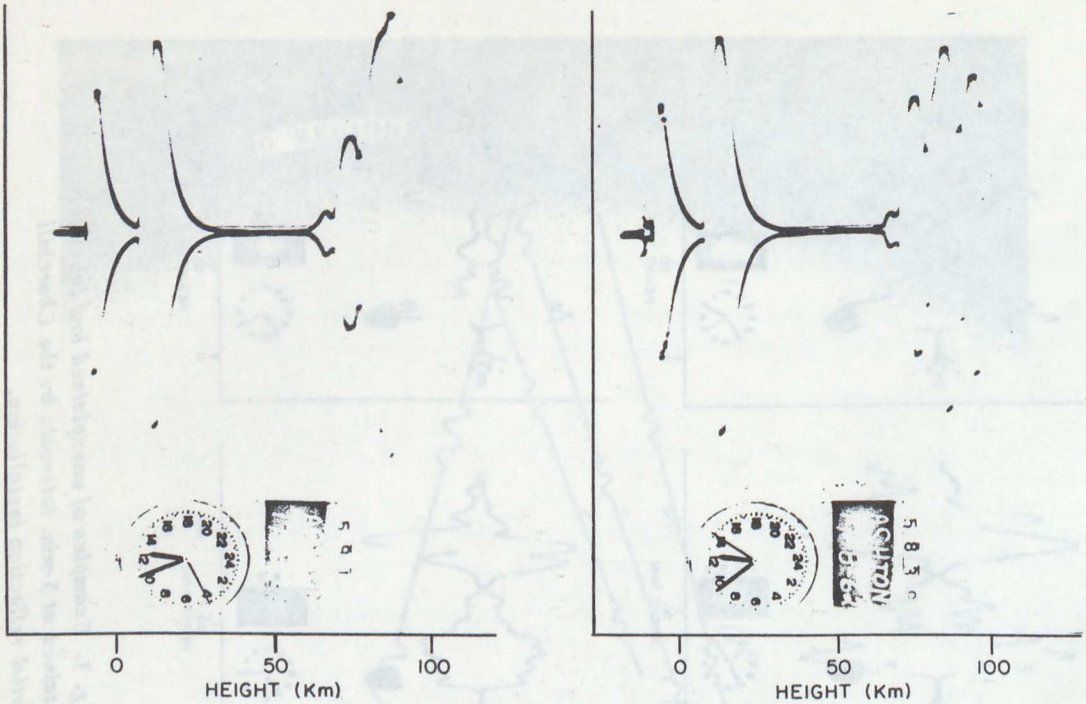

Fig. 4. Examples of two O mode echoes received from pulses transmitted with a time separation of 1/15 sec.

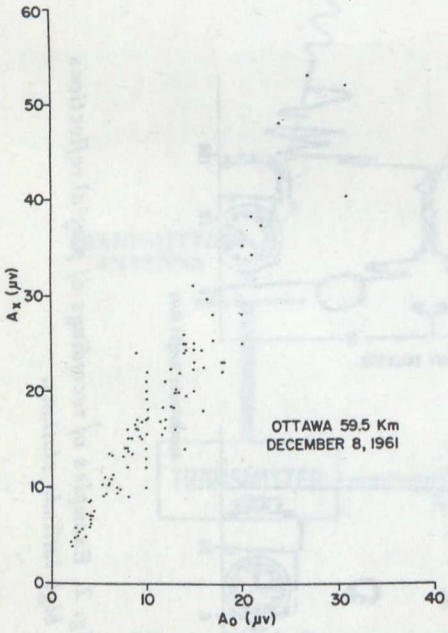

Fig. 5. Scatter plot of the amplitudes of the ordinary and extraordinary components of all echoes recorded in the height interval 58.5 to 60.5 km. during a 20-min. period, 8 Dec., 1961.

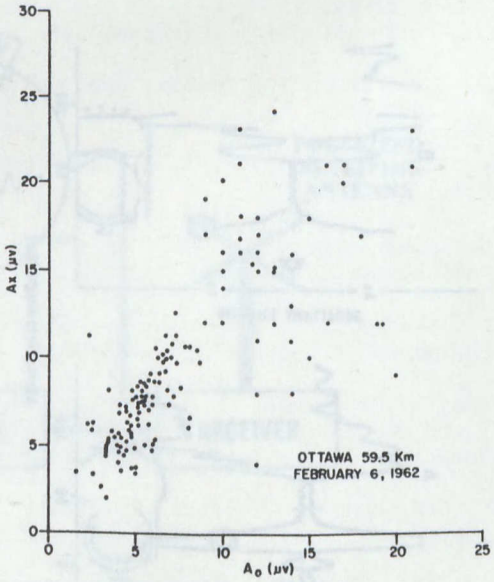

Fig. 6. Scatter plot of the amplitudes of the ordinary and extraordinary components of all echoes recorded in the height interval 58.5 to 60.5 km. during a 20-min. period, 6 Feb., 1962.

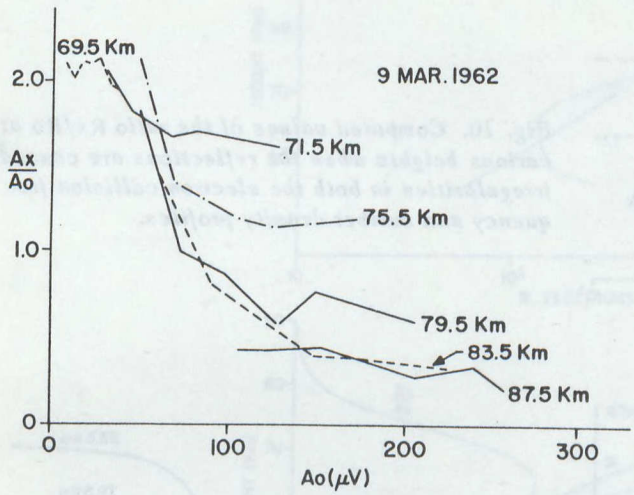

Fig. 7. The observed dependence of the ratio Ax/Ao on Ao caused by the presence of off vertical echoes.

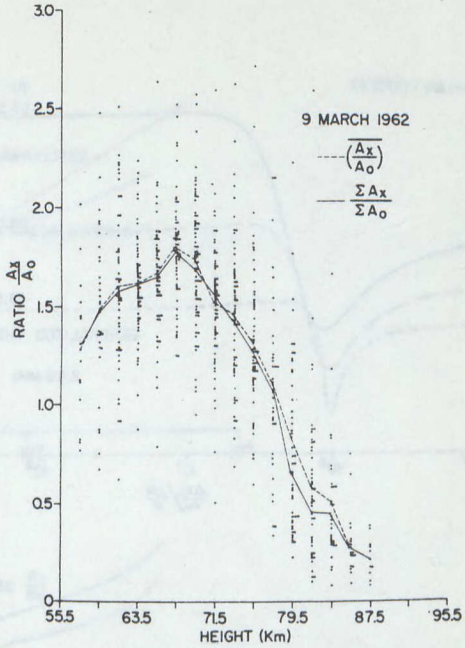

Fig. 8. Mass plot of ratio Ax/Ao of all echoes recorded at all heights during a 20-min. recording period.

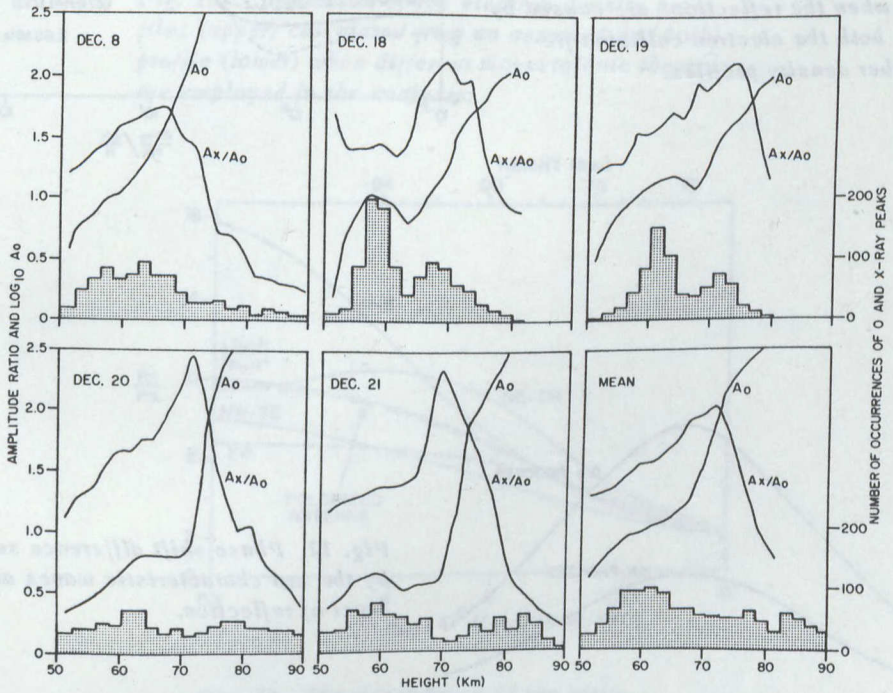

Fig. 9. Partial reflection observational data at Ottawa, showing the variation with height of the amplitude ratio Ax/Ao the O-ray amplitude Ao, and the histogram of occurrences of O- and X-ray peaks, for 5 magnetically quiet days in winter (December 1961).

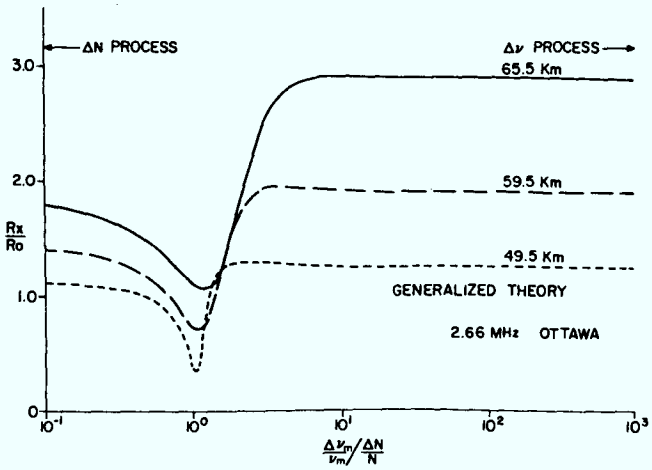

Fig. 10. Computed values of the ratio Rx/Ro at various heights when the reflections are caused by irregularities in both the electron collision frequency and number density profiles.

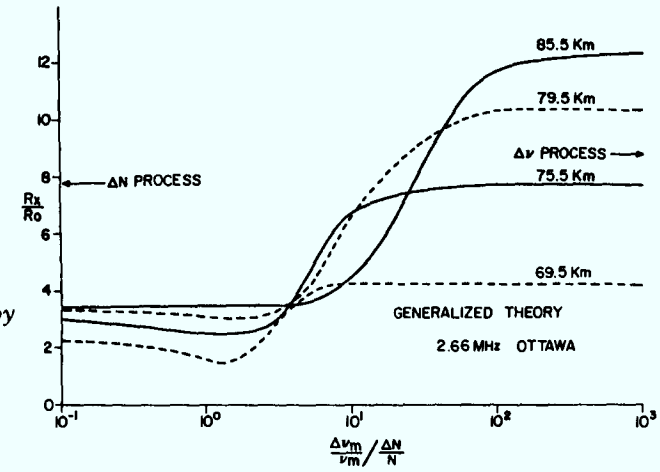

Fig. 11. Computed values of the ratio Rx/Ro at various heights when the reflections are caused by irregularities in both the electron collision frequency and number density profiles.

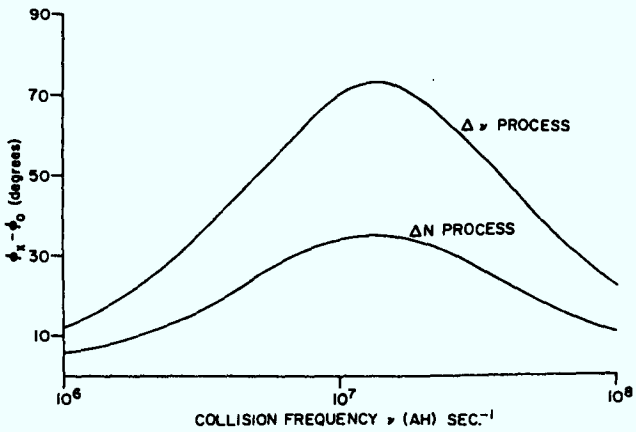

Fig. 12. Phase shift difference suffered by the two characteristic waves at the level of reflection.

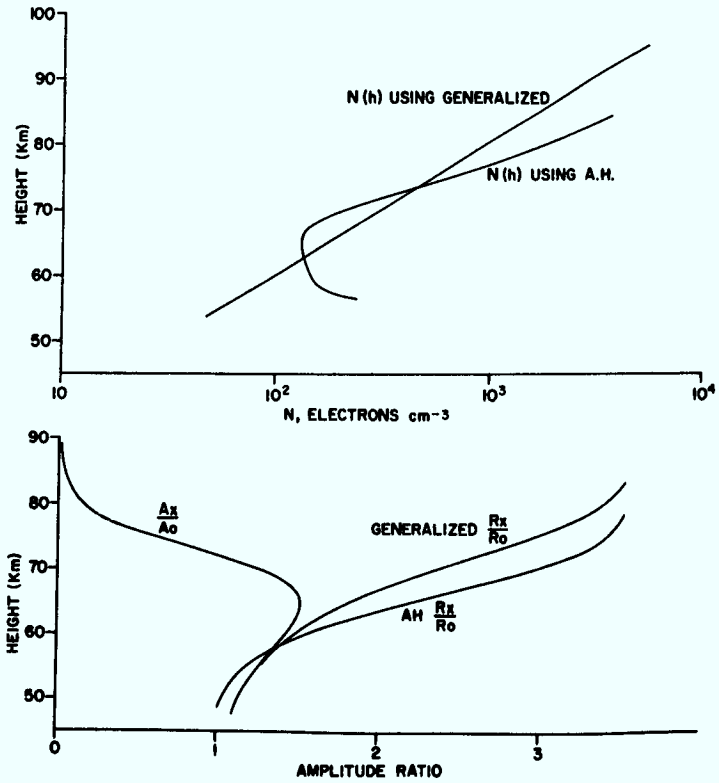

Fig. 13. Comparison of the electron density profiles (upper) calculated from an assumed Ax/Ao(h) profile (lower) when different magnetoionic theories are employed in the analysis.

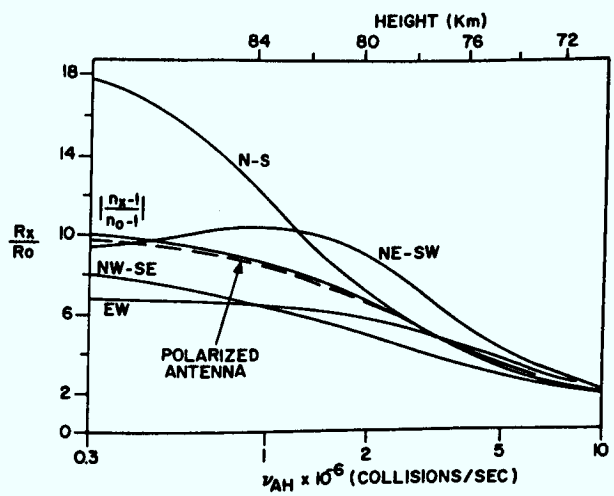

Fig. 14. The dependence of the ratio Rx/Ro on the orientation of a plane polarized transmitting antenna. Probing frequency 1.78 MHz., gyrofrequency 1.515 MHz., $\theta = 30°$ (Appleton-Hartree theory).

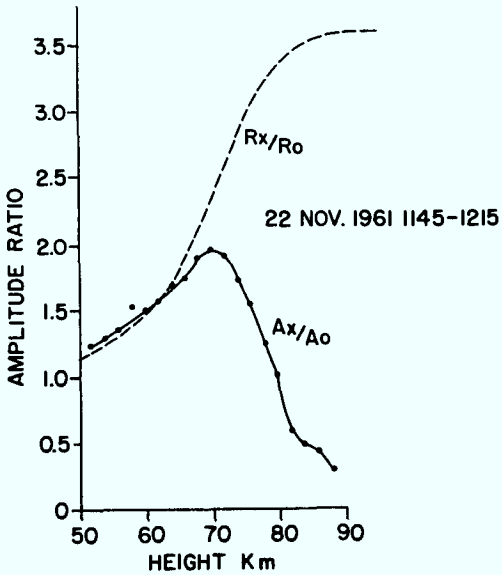

Fig. 15. Amplitude ratios Rx/Ro (calculated) and Ax/Ao (measured) as a function of height for 2.66 MHz. for a quiet day 22 November, 1961.

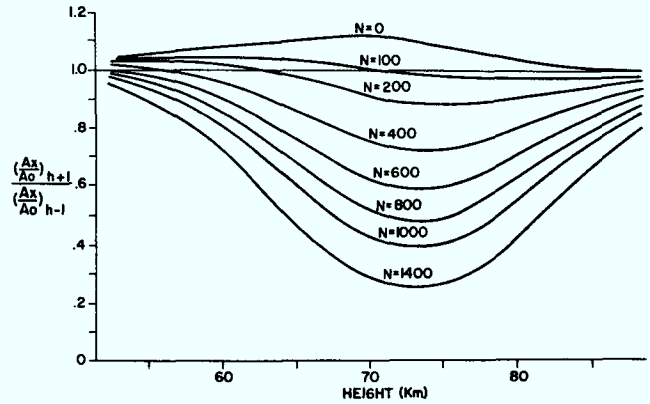

Fig. 16. The ratio $(Ax/Ao)_{(h+1)}/(Ax/Ao)_{(h-1)}$ as a function of height for various electron number density concentrations.

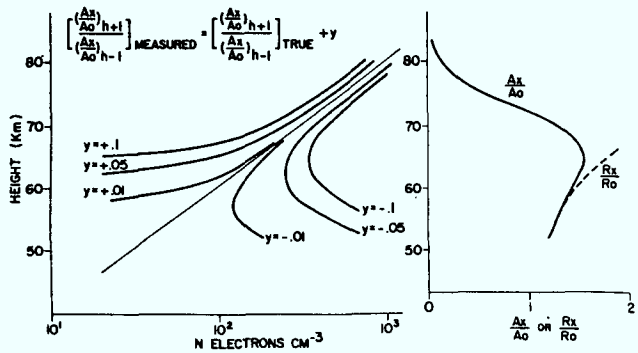

Fig. 17. Departure of the electron number density profile from an assumed exponential profile when various degrees of error are introduced into the measurement of the ratio $(Ax/Ao)_{(h+1)}/(Ax/Ao)_{(h-1)}$.

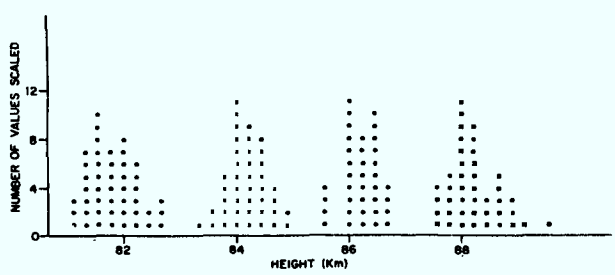

Fig. 18. Scatter obtained in the measured heights of simulated echoes.

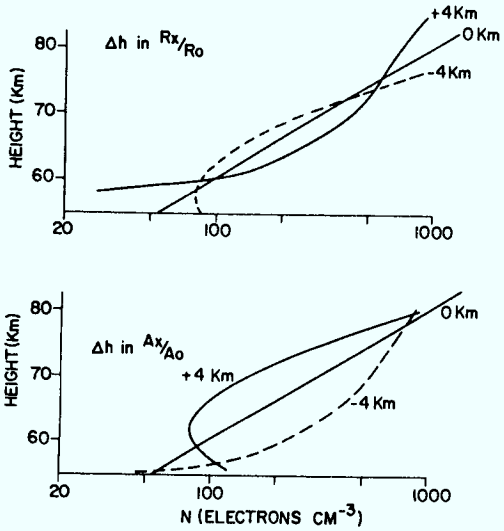

Fig. 19. Departure of the electron number density profile from an assumed exponential profile when ±4 km. errors are introduced in the height of the collision frequency profile (upper) and in the height of the Ax/Ao(h) curve (lower).

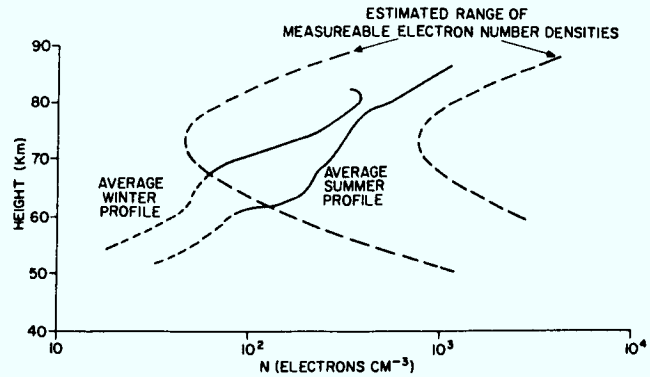

Fig. 20. Estimated upper and lower limits of the measurable electron number density as a function of height for the 2.66 MHz. experiment at Ottawa.

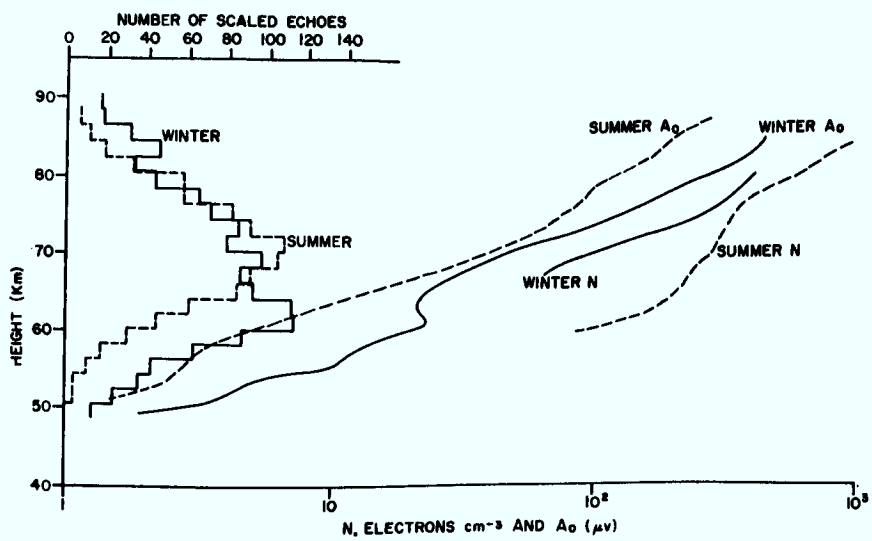

Fig. 21. Seasonal variation in the mean value of the Ao(h) profile, the N(h) profile and histogram of occurrences of O- and X-ray peaks.

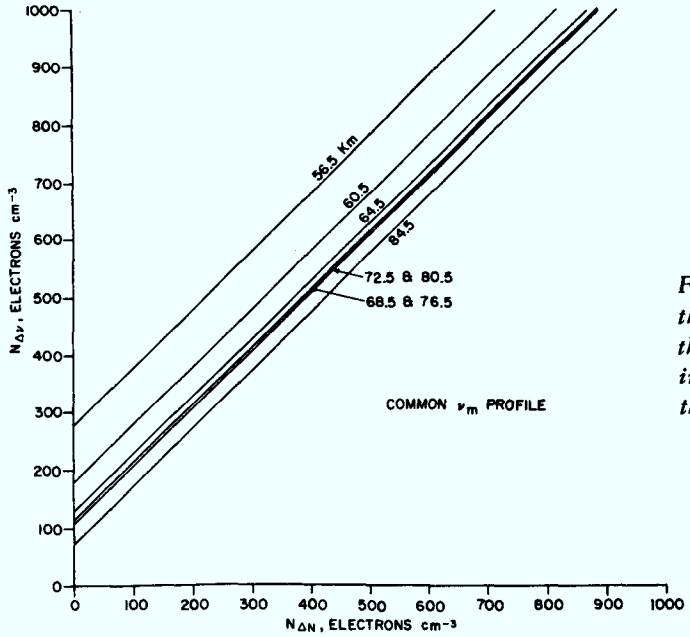

Fig. 22. Graph showing the increased values of the electron number density that would exist if the reflections were caused by a $\Delta\nu$ perturbation instead of a ΔN perturbation as was assumed in the original calculation.

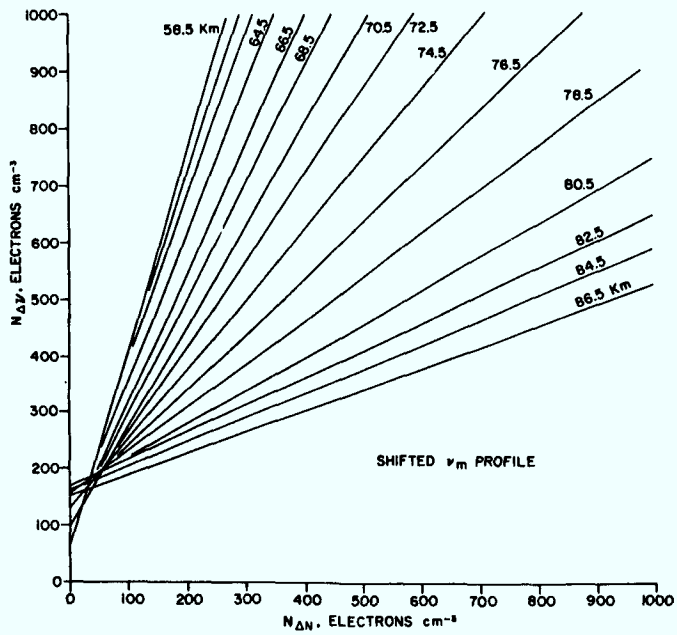

Fig. 23. Graph showing the values of the electron number density that would exist if the reflections were caused by a $\Delta\nu$ perturbation instead of a ΔN perturbation as was assumed in the original calculation.

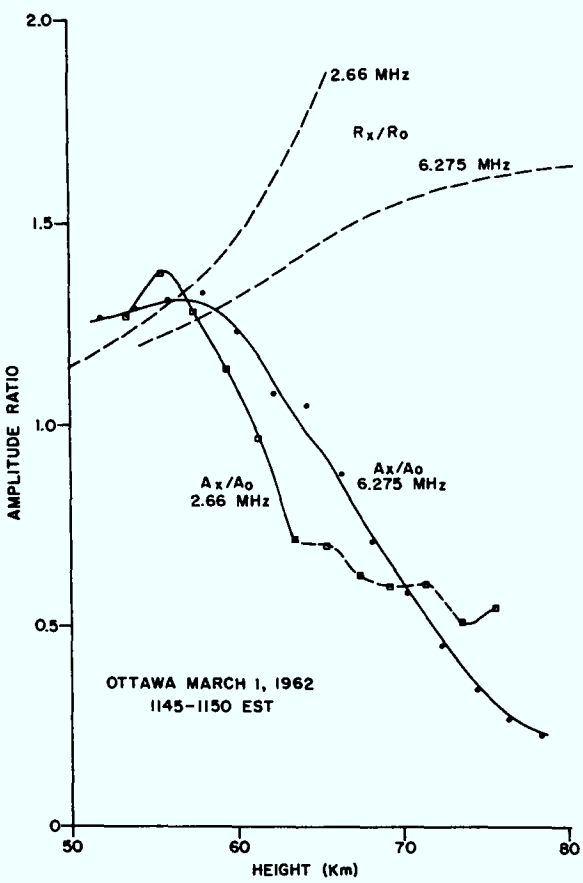

Fig. 24. Simultaneous amplitude ratio measurements, Ax/Ao, as a function of height for two probing frequencies.

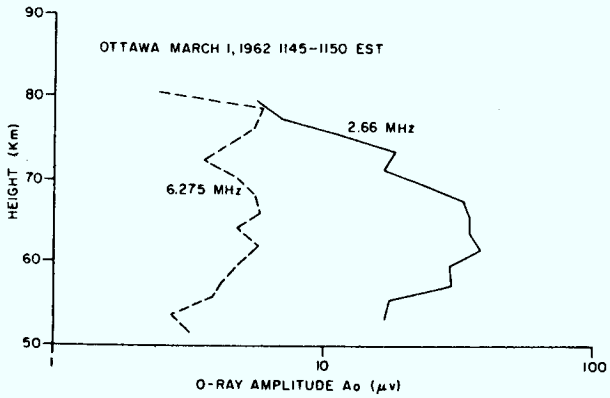

Fig. 25. Simultaneous values of the O-ray amplitude, Ao, as a function of height for two probing frequencies.

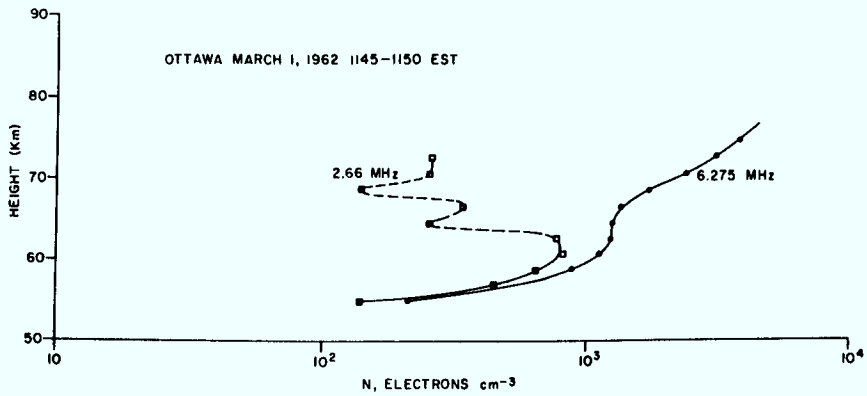

Fig. 26. A comparison of the electron number density profiles obtained from the simultaneous measurements of Ax/Ao(h) shown in Fig. 24.

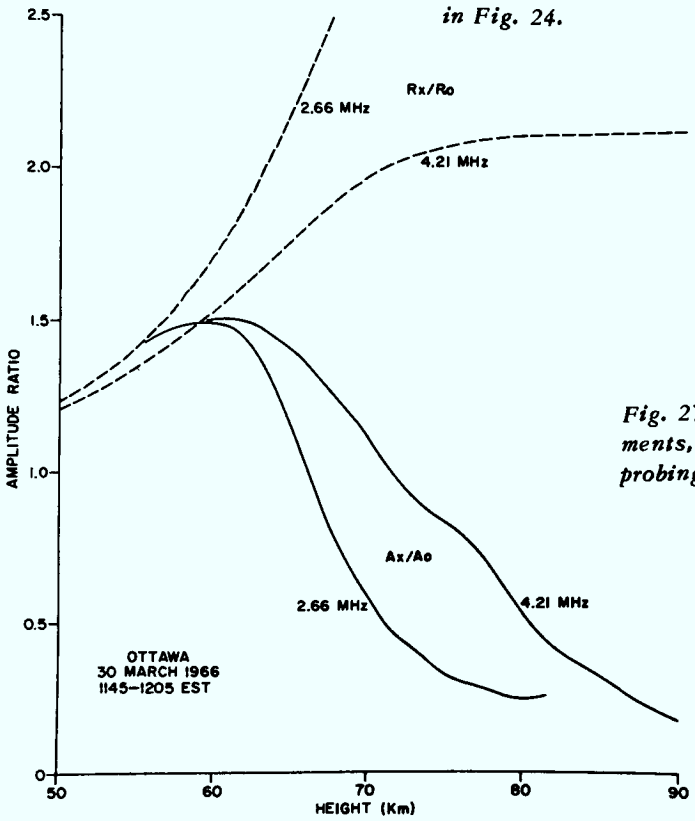

Fig. 27. Simultaneous amplitude ratio measurements, Ax/Ao, as a function of height for two probing frequencies.

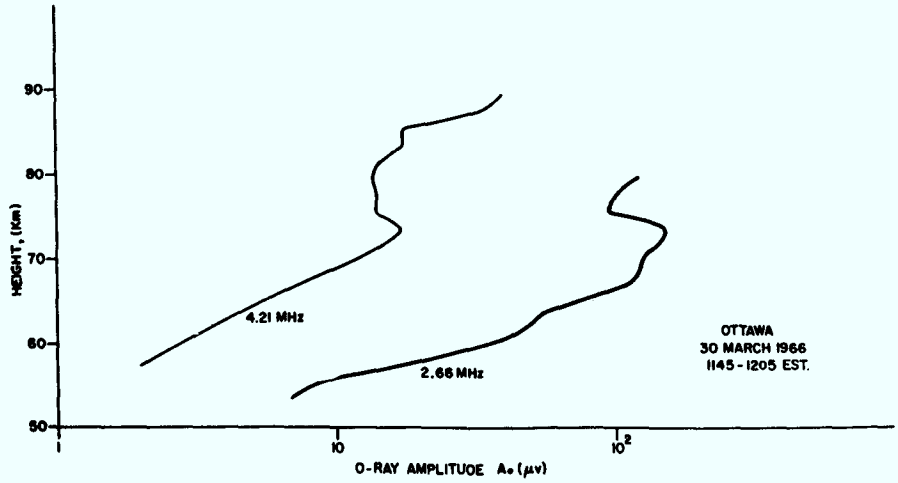

Fig. 28. Simultaneous values of the O-ray amplitude, Ao, as a function of height for two probing frequencies.

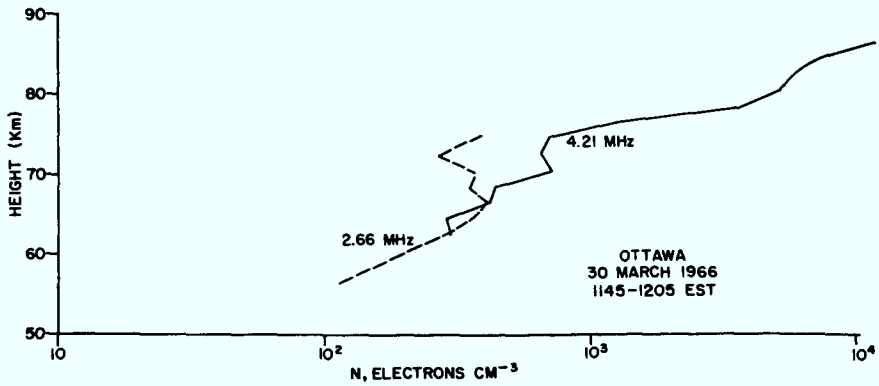

Fig. 29. A comparison of the electron number density profiles obtained from the simultaneous measurements of Ax/Ao(h) shown in Fig. 27.

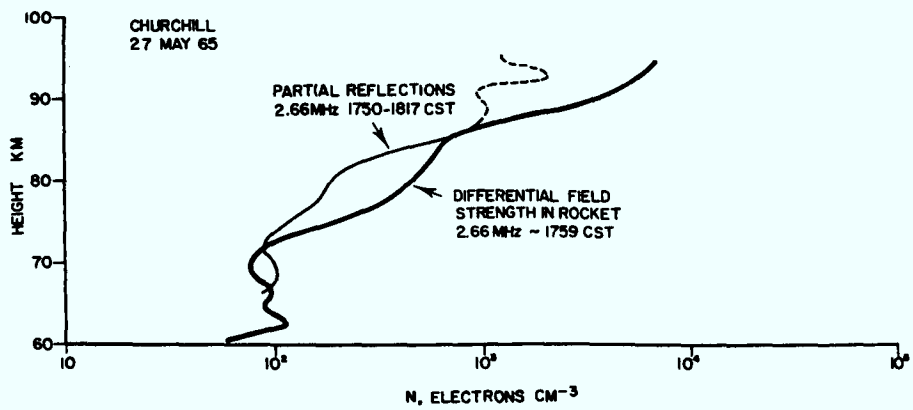

Fig. 30. A comparison of electron number density profiles obtained from simultaneous ground-based partial reflection observations and rocket-borne differential field strength measurements.

Discussion on Paper 2.1 presented by I.A. Bourne

Falcon: Why is it that your Ax/Ao curve is higher than the calculated Rx/Ro curve, in some cases at the low heights? What do you attribute this to?

Bourne: We have data which will be discussed later today, which strongly suggests that we get changes in the collision frequency, and these apparent changes are outside any experimental error that we can possibly attribute to our techniques. Assume we are looking at data from early winter, 1961-62. The ratio Ax/Ao at the 59.5 km. level is approximately 1.5. It consistently maintains this value until June 1962. In November 1962, the ratio has increased to 1.7, and in February 1963 to 1.9 or 2. In February 1964, the value is still high, but by February 1965 the ratio has returned to 1.5. These ratios were obtained from data which showed little or no differential absorption below the 60 km. level, and there is little day-to-day variation in the measured ratios. Under these conditions, the ratio should be a measure of the collision frequency if a $\Delta\nu$ process operates. As far as we are concerned, either there was a substantial change in the collision frequency, decreasing by approximately a factor of 2 in 1963-64, or during this period we observed reflections from a pure $\Delta\nu$ process. It seems to be either one or the other. We cannot find other evidence to suggest the $\Delta\nu$ process was operating, and we tend to believe the results indicate a substantial change in the collision frequency. There is some other indirect evidence supporting this conclusion. If you calculate the mean electron density profiles for the two winters, you find that they are similar, but there is a 6 km. height shift. The shift in the electron density profiles and the change in the collision frequency suggest that the whole atmosphere sank by 6 km. in this interval.

von Biel: You mention several sources of error, and I think it was pointed out, a factor of 2 is fairly good for this type of experiment. One cause of error which we have looked into at Cornell, which you did not mention, is that the entire theoretical derivation has conveniently neglected the pulse width, and unfortunately (for 50 μs. pulses which seem to be practical at the frequencies we are talking about), there can be a fair amount of absorption within the pulse itself. When that is thrown into the derivation (using Sen-Wyller) we can show (using the Belrose and Burke profiles published some time ago) that the electron density profile can change rather drastically, and I think this ought to be considered. Now the computational process gets messy if one considers the differential absorption within the pulse volume, but it is large enough to be considered for these practical pulses. You mentioned 50 μs. pulses. We are using 25 μs. pulses in our experiment, and if one could use 100 μs. at this frequency, probably the observational results would change drastically. Have you any comment?

Bourne: I am not too sure of your question, but I think you are assuming a random scatter from a large number of heights.

von Biel: No, I am willing to assume (and this is far-fetched) that we have a steady reflection. A 50 μs. pulse is being sent into a fairly slowly varying medium, and this pulse occupies a fair amount of distance in space. If we are going to make any sense out of the Ax/Ao curves, we cannot neglect the differential absorption in the pulse itself. We are generating a rather serious error.

Bourne: When analyzing the data, we assumed that the echoes we scale are resolved from other echoes; that means that there is not another echo occurring within roughly ± 3 km. This has been checked by using shorter pulse lengths. I will grant that echo structures can look complicated, and that the tails of some pulses can influence the measurement of ratios at nearby heights. This is a roughly random process which goes as the square of the signal amplitudes because the signals are randomly phased. The scaling criteria is designed to reject echoes which are not well resolved, i.e. separated by at least 6 km. If this assumption is correct, then it is not necessary to allow for the pulse length so long as the echo delay is measured from the center of the transmitter pulse to the center of the echo.

von Biel: Well, maybe I don't understand what you mean by echo. Are you proposing that there are discrete echoes, that there is not a continuum?

Bourne: I am definitely proposing that! Phase height records show that this just has to be the case, at least on some occasions. The stratified echo shown earlier was present during the 20-min. recording period, and didn't change its height; it faded, but it was a definite, clear, well-defined echo.

The structure that we are getting, at least on some occasions, is definitely inconsistent with the assumption that we obtain echoes from all heights at the same time, and that the 'echo' is the result of a large number of randomly phased reflections.

Belrose: In our experiments, we have made a great story about discrete echoes, and we think we are still scaling discrete echoes. This is why we scale only when there is a clearly defined peak, and we don't scale unless this peak occurs at the same height (within ± 1 km.) for the O and the X mode waves. We make an attempt to scale only discrete echoes and we conducted two experiments to determine that they were discrete echoes. We transmitted a 50 μs. pulse and a 25 μs. pulse separated by 1/15 sec., and displayed them in the normal manner. While we saw better resolution and the peaks were more clearly defined with 25 μs. pulses, the number of peaks and the reflection levels were unchanged. In another experiment, we transmitted two O mode pulses separated by a 15th of a second in time on frequencies of 2.66 Mc/s. and 2.66 + 40 kc/s. We saw the same echo structure at the two frequencies; the echo structure that we see is not a function of pulse width, and is not a rapidly varying function of frequency. There are probably other experiments that you can do, but these are the two that we conducted, and both suggest that we are observing discrete reflections.

Smith: You showed a number of different types of echo structure. What type of echo structure is in the data used to determine electron density profiles?

Bourne: We derive profiles from any data which looks as if it is giving a reasonable Ax/Ao profile. I can show a number of examples in which we have, for part of the time, the type of echoes we are calling turbulent echoes, which are replaced at a later time by a discrete, well-defined echo. The Ax/Ao ratio does not seem to depend on echo type. I don't think it matters much what type of echo we observe; whether it is a turbulent type echo or not, we get the same mean ratios. However, when we have a well-stratified echo, the scatter in the data is generally smaller.

Smith: A knowledge of the echo type is important when you are trying to determine the cause of the irregularities. I can understand a discrete layer being caused by a temperature inversion or some such thing. But if you get echoes jumping up and down, I would say that what you are observing is an interference pattern. You are not observing discrete echoes. I can't imagine that at one time you've got a stable layer at 62 km., and after another second you've got one at 64 km., and after one more second you have one at 60 km. What you have is a whole turbulent region, and you have an interference pattern, and you should, in fact, allow for this as an interference phenomenon.

Belrose: The experiments we have just described show that this is not an interference pattern, because we changed the pulse width and we changed the frequency, and the "interference pattern" did not change.

Bourne: I think this is a legitimate test.

Gregory: Is it not a fact that you are getting scattering out of a spherical cap whose width is the pulse? This is not what Dr. Smith calls interference. The type of interference to which Dr. Smith is referring would show when the frequency was changed. The description is turbulent scattering, as Booker and Gordon have used, and I think this is one class of possible reflection.

Bourne: We do not deny that we can get off vertical echoes, and our analysis of our data shows that their presence can frequently be detected. What we dispute is the assumption that 'echoes' that we scale are only an interference pattern caused by the superposition of a number of weak reflections simultaneously reflected from a large number of different levels.

Gregory: May I comment on this and go back to your Fig. 1. It seems to me that the results from your careful and admirable analysis of all the echoes does hinge on how you interpret your raw data. In Fig. 1, you notice that you have the possibility of interpreting the ratio in a number of ways at a given height. Now, we have used a different technique to yours. We haven't scaled photographs, which, of course, are a permanent record of the reflections at a certain time. We used a high-speed comparison technique

employing a rapidly switched attenuator, and this has given us perhaps a different view of the thing. In other words, we make a subjective judgment, as you must also, as to what we will accept as an experimental ratio. From Fig. 1, I conclude that what we have always done is accept only those reflections from the flat portion of the curve; that is, towards the higher signal strengths. We would not accept anything that comes up when the signal is changing. You see, we are able to watch this ratio changing under our eyes, and we match the two envelopes. Those of you who were navigators in the Air Force and used Loran will know this pulse-matching business. Now, unless these pulses fade together, we don't consider we have a reliable ratio, and I conclude from this that what we were doing was favouring the larger echo amplitudes. Now, when you do that, the number of heights at which you obtain acceptable data is greatly reduced, and in general, we never have had more than half a dozen heights in the interval between say, 60 and 90 km. That would be our maximum number of experimental points on a curve. Maybe this is pessimistic but it does give a different view of the discrimination of the profile which the method is able to provide. I believe you could do a little better than this, but I believe that probably the real truth of the discrimination lies between your very detailed profiles, which have no error bars by the way, and our rather crude profiles. Somewhere between the two there lies the optimum. But I wouldn't put more than six points on a curve.

2.2.1 MEASUREMENT OF SPATIAL VARIATIONS OF MESOSPHERIC REFRACTIVE INDEX

by

T.J. Elkins

Wentworth Institute, Boston

1. Introduction

Partial reflection experiments are capable of providing information about the following factors of significance in the study of small-scale mesospheric dynamics:

(i) Scale sizes and height distribution of scattering irregularities
(ii) Random and ordered components of velocity in the medium
(iii) Velocity of large-scale motions (winds).

Since the electrical conductivity of the mesosphere is negligibly small, the micro-meteorology of this region should be somewhat similar to that of the troposphere. Thus, since the adiabatic lapse rate considerably exceeds the ambient lapse rate, inherent gravitational stability must strongly inhibit vertical convection. Limited convection may, however, be possible under somewhat unusual conditions, such as in the vicinity of jets. In that event, a certain scale size, determined by the local properties of the medium, will predominate in the spatial refractive index spectrum. A similar form of this spectrum might be expected for any periodic structure, such as internal gravity waves, whose existence is thought very likely. The most widespread process generating the irregularities is most probably turbulence, which, for the special case of homogeneous, isotropic conditions, exhibits the well-known $-5/3$ power law spectrum. Such idealized conditions never exist in nature, the effects of anisotropy due to several factors modifying the situation quite markedly. Among the more important of these modifying factors are wind shear and horizontal stratification due to gravity.

Fig. 1 shows the types of refractive index spectrum which might exist under the various conditions described. Also shown are the idealized cases of a sharp discontinuity and a completely random spectrum. Measurement of these spectra is an obviously important practical objective. To this end, it may be shown that the intensity, $I(k, \theta)$ of broadband radiation scattered from a region of spatially varying refractive index, $n(z)$, is proportional to the Fourier transform of $n(z)$, denoted by $\Phi(k_1)$, where $k_1 = k \operatorname{Sin} \frac{\theta}{2}$.

$$\text{i.e.,} \quad I(k, \theta) \;\alpha\; \Phi(k \operatorname{Sin} \frac{\theta}{2}) \qquad \ldots\ldots(1)$$

where θ is the scattering angle (180° in the case of back scatter), defined in Fig. 2, which also shows the foreshortening of a horizontal dimension, a and k is the wavenumber of the scattered radiation (2π/wavelength).

Here the problem of measurement is greatly simplified by regarding the refractive index as varying with only one spatial co-ordinate instead of three. Although this situation applies naturally in several inherently one-dimensional cases, such as vertical discontinuities, it is an obvious limitation whose validity may often be questionable. The Fourier transforms of the refractive index spectra already considered are shown in Fig. 1 as a function of k_1. Although there are two "degrees of freedom", viz., the operating frequency and scattering angle, measurement of these spectra would, in practice, be scarcely feasible. Alternative methods, simpler to perform, but necessarily providing less information, are required. Out of practical considerations, it is desirable to see what can be done using only one frequency and one highly directive antenna.

2. Principle of the suggested measurements

In order to extract the maximum amount of information from a given measurement, it is helpful to determine the ultimate limits of available experimental precision. These can be found by suitable application of the Heisenberg Uncertainty Principle. The brief analysis which follows is quite general (for two-dimensional geometry) and makes no assumptions about the form of the irregularities. It reproduces all the essential features of the extensive literature relating to irregularities which are of general interest.

If the scattering medium is regarded as an array of sources of electromagnetic energy, the scattered field is composed of quanta of energy specified by two canonical quantities, e.g., position and momentum. Fig. 3 is a crude attempt to represent the Uncertainty Principle. If the shaded object represents a two-dimensional irregularity, with propagation in the Z-direction, the size may be defined by the intercepts Δx and Δy on the X- and Y-axes respectively. Then a quantum reflected or emitted by this irregularity is largely confined within a cone whose solid angle is specified by $\Delta\phi_x$ and $\Delta\phi_y$. These angles are defined in terms of observational spreads of the X- and Y-components of momentum, as shown in the lower half of Fig. 3. $|P|$ is the "true" momentum. By analogy with optical coherence theory, this solid angle may be called a "coherence angle". Similarly one might define a "coherence time", which is related to the precision with which an emitted quantum may be localized in the time domain.

There is a certain relation between these two parameters specifying the coherence of the wave field. The spectra in momentum (k_1) and configuration spaces are Fourier Transforms of each other, and the volume of an oscillation mode in phase space is h^3, where h is Planck's constant. In Cartesian co-ordinates, the Uncertainty Principle may be expressed as follows:

$$\Delta x \cdot \Delta P_x \sim h \qquad \text{.....(2)}$$

$$\Delta y \cdot \Delta P_y \sim h \qquad \text{.....(3)}$$

$$\Delta z \cdot \Delta P_z \sim h \qquad \text{.....(4)}$$

where $\Delta P_{x,y,z}$ are the observational spreads in the three momentum components.

For propagation in the Z-direction,

$$\text{Sin } \Delta\phi_{x,y} = \frac{\Delta P_{x,y}}{|P|} \qquad \text{...(5,6)}$$

where $$|P| = \frac{hk_1}{2\pi} \qquad \text{.....(7)}$$

Substituting (5), (6) and (7) into (2) and (3), one obtains

$$\left.\begin{aligned} \Delta x \cdot \text{Sin } \Delta\phi_x &\sim \lambda_1 \\ \Delta y \cdot \text{Sin } \Delta\phi_y &\sim \lambda_1 \end{aligned}\right\} \qquad \text{.....(8)}$$

Then since $$\Delta P_z = h/c \; \Delta\nu_1 \qquad \text{.....(9)}$$

and $$\Delta Z = C\,\Delta t \qquad \text{....(10)}$$

where $\Delta\nu_1$ is the spread in the quantity $(\frac{ck}{2\pi} \text{ Sin } \frac{\theta}{2})$

and Δt is the observation time (integration time in an experiment),

equation (4) gives

$$\Delta t \cdot \Delta(\nu \text{ Sin } \frac{\theta}{2}) \sim 1 \qquad \text{....(11)}$$

Equations (8) and (11) thus specify the coherence angles ($\Delta\phi_x$, $\Delta\phi_y$) and the coherence time (Δt) which set the ultimate limits upon the degree of precision which may be achieved in an experiment which simultaneously measures position and time for a given event, such as the reflection of a wave-packet.

From (11), it may be seen that, if $\Delta(\nu \text{ Sin } \frac{\theta}{2})$ is made very small, (implying a signal of high spectral purity and a small antenna aperture), then the coherence time becomes relatively large. In a physical measurement, the apparent coherence time would then be determined by other factors, notably the velocity of the scatterers. Measurement of the coherence angle and apparent coherence time of the scattered energy would then provide information about the velocity and size of the scattering irregularities.

3. Measurement of coherence angle and time

This may be done using either a Michelson interferometer or a spatial intensity correlation measurement, the former being the more sensitive since it uses additional information contained in the phase of the diffracted energy. If an observation is made in a time much longer than the coherence time, a spatially coherent beam shows no spatial fluctuations, although it will display time fluctuations. This corresponds to interference between separate oscillation modes in phase space. Thus a definite fringe pattern is observed with an interferometer, provided the angular resolution is smaller than the coherence angle, and that the measurement time considerably exceeds the coherence time. Alternatively, the correlation between field intensities at two arbitrary points remains constant, under the same conditions.

Similarly, if a measurement is made in a time much shorter than the coherence time, there will be no temporal fluctuations. However, a random interferometer fringe pattern will be observed if the antenna spacing exceeds the source scale size, and there will be no intensity correlation between two arbitrary points separated by a distance greater than the source scale size. The Uncertainty Principle states that a simultaneous measurement within both the coherence angle and coherence time is impossible.

An idealized experiment might consist of transmitting upwards a narrow highly monochromatic beam, and receiving the back-scattered energy coherently at two points, having a relatively small separation. An interference pattern is observed, but the intensity exhibits time fluctuations, the autocorrelation function of which diminishes to a small value in the coherence time (Δt). As the antennas are moved further apart, the fluctuations decrease and the fringes disappear as the angular resolution exceeds the coherence angle. If the height of the scatterers is known or assumed, the scale length (Δx) may thus be found from (8), whence the velocity ($\Delta x/\Delta t$) may be determined.

4. Suggested experiments

There are a number of ways in which these principles may be applied experimentally. Figs. 4 and 5 show block diagrams of two suggested experiments, which, operating in the frequency range now employed for D-region partial reflection work, should provide useful data on irregularities in this height range.

The first is a simple CW system, which might possibly be used in the interferometer mode as well, depending on the stability of the ground wave. The high-isolation hybrid separates the transmitted and received waves, and has provision for cancellation of both amplitude and phase of residual leakage, main-layer reflections, etc. The frequency synthesizer generates the local oscillator frequency (F-f), which together with the transmitted frequency (F+f), determines an IF frequency 2f. The phase detector operates at this frequency, and since it detects both in-phase and quadrature components of received energy, it allows a measurement of both instantaneous amplitude and phase. The output of the phase detector may be displayed as an Argand diagram on an oscilloscope, or recorded for digital processing. This equipment would allow a continuous measurement of apparent reflectivity, together with irregularity size and wind velocity.

Fig. 5 shows a FM/CW system, which would measure essentially the same parameters as the previous one, but with the addition of range resolution. The frequency synthesizer must provide a highly linear variation of frequency with time, determined by the sawtooth generator. The variable delay lines partially compensate for the propagation time, and provide a local oscillator frequency which determines a small resultant frequency for phase comparison. The function of the amplitude weighting device is to reduce the side-lobes in range space and provide better range resolution, should it be desirable for some purposes to sweep the frequency rapidly over a small interval. Height range information is obtained by varying the delay lines, and range resolution by varying the filter bandwidth. The local oscillator for the interferometer out-stations might be simply the ground-wave, suitably delayed and amplified, while the phase comparison might be made via radio links or telephone lines, or by separately recording the information for later comparison.

The main limitations to such techniques are:

(i) The operating frequency causes a selective bias in the observed sizes, since irregularities much larger than one wavelength are not observed, due to their small coherence angle.

(ii) The finite transmitted beam causes averaging over a volume. This can be partly overcome in the FM/CW experiment by using very narrow filters.

Acknowledgment

I am indebted to Dr. Sales, who cleared up some confusion regarding wind velocities and random velocities associated with irregularities.

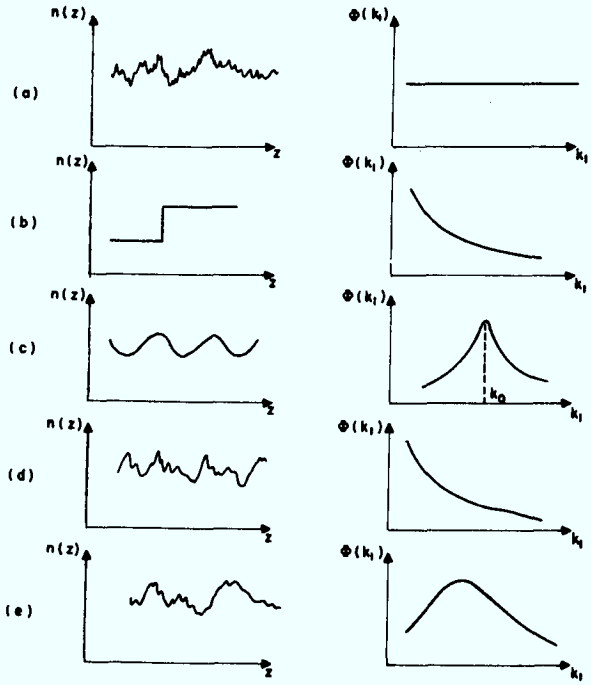

Fig. 1. Height profiles of refractive index n(z) with related power spectra $\Phi(k_1)$

(a) Random – $\Phi(k_1)$ = constant

(b) Step discontinuity – $\Phi(k_1) \propto k^{-2}$

(c) Periodic – $\Phi(k_1) \sim \delta(k - k_o)$

(d) Turbulence (isotropic) – $\Phi(k_1) \propto k^{-5/3}$

(e) Turbulence with shear.

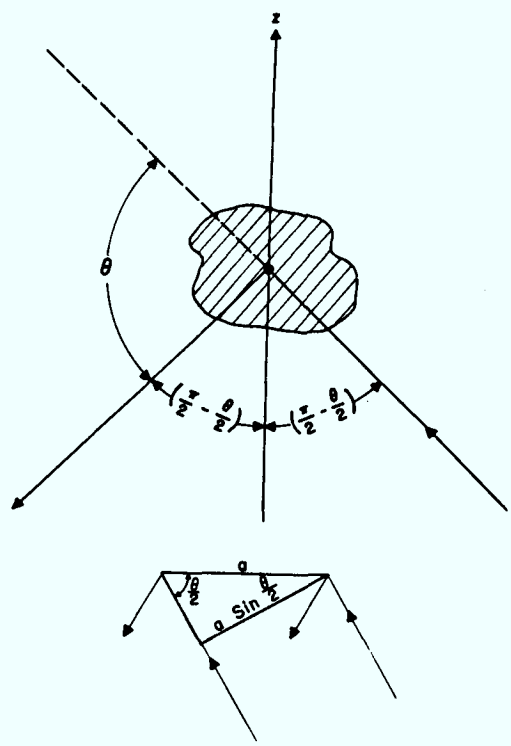

Fig. 2. Geometry of the problem.

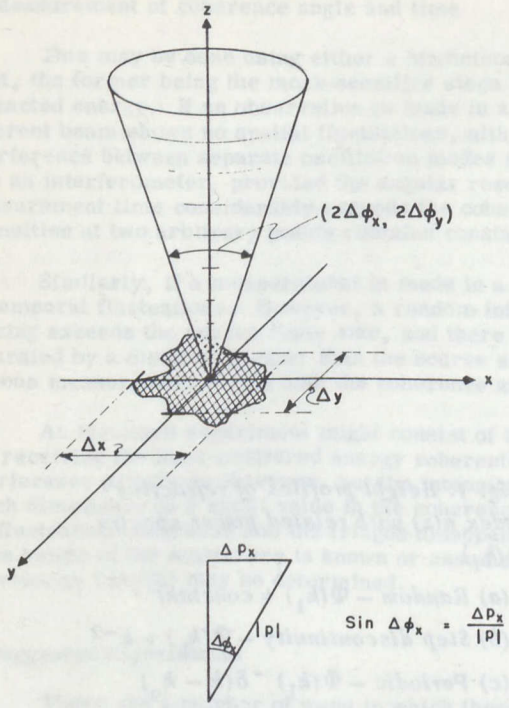

Fig. 3. Geometrical interpretation of uncertainty principle.

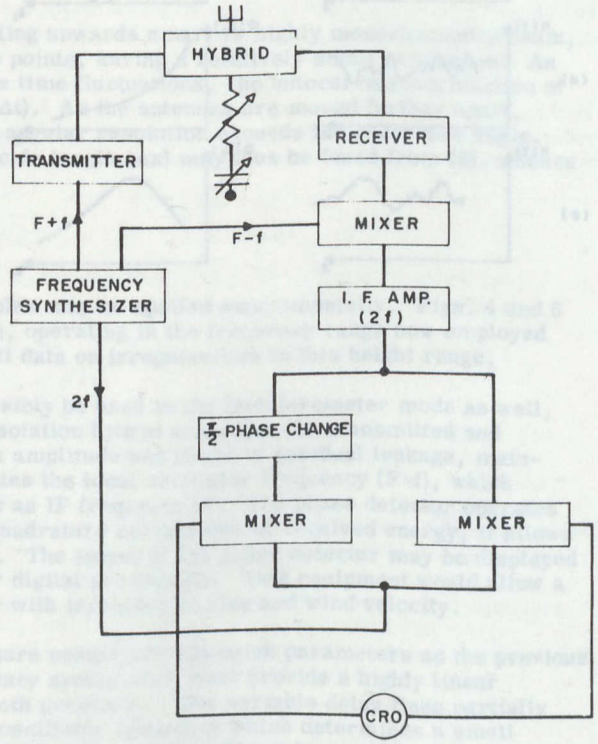

Fig. 4. FM/CW radar interferometer.

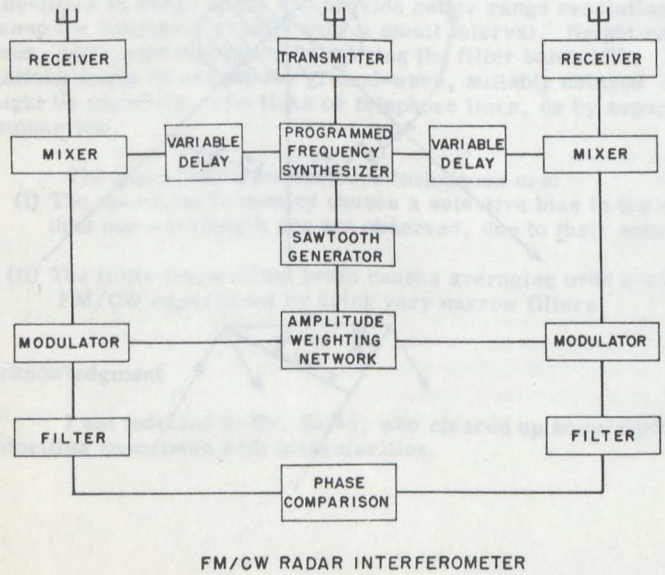

Fig. 5. CW radar.

Discussion on Paper 2.2.1 presented by T.J. Elkins

Belrose: What are your thoughts on this experiment, and are you contemplating putting some of them into practice?

Elkins: No, I am idly thinking about it, as I have no possibility of putting it into practice. What you need is a very large antenna and a high-powered transmitter such as those used by the people doing partial reflection experiments. The remainder of the equipment (the outlying field sites) could use relatively small antennas such as rhombics.

Belrose: You didn't mention polarization. If you don't use polarized aerials, you will have fading due to the interference between the two magnetoionic components.

Elkins: Yes, I assume that people doing partial reflection experiments are using polarized antennas. That is the case, isn't it?

Belrose: Yes.

Sales: You did not consider the possibility that these irregularities might change as they drift, that is, that a steady drift is not their only motion?

Elkins: The motions that are determined by this coherence time are the instantaneous motions, that is, the random motions connected with their turbulence velocity. In addition to that there is a large-scale steady motion such as a wind, which would also come out of this information, but it is not related to this coherence time at all. It is the instantaneous velocity, the random phase change, which is determined by this method.

Zimmerman: To get an eddy velocity out of this, would integration time be much less than the characteristic scale of an eddy?

Elkins: Yes, it would. Another way of getting the coherence time, rather than taking the auto-correlation function, might be to measure the half-widths of all the little fading peaks (and nulls), and take the average over a large time, which would give us once again the same answer as we get here.

Sales: But you don't; you integrate to get that fading time over a relatively long period.

Elkins: No, you integrate to get the spatial interference pattern.

Sales: You also integrate to get that correlogram.

Elkins: This could be done digitally.

Sales: But it is still integration over a relatively long time, over many fades. You need 100 fades maybe to get that correlogram reliably. One doesn't get that correlogram from a single fade.

Elkins: No, you don't. You take the same curve and you move it over a little bit, and you get the cross-correlation and so forth.

Sales: But I am talking about the length of the record.

Elkins: Oh, yes, that is not integration.

Wright: That is just averaging the variation.

Sales: But averaging is integration, over a long time. You are not getting the fade at any particular time, but are getting the average fade over a relatively long time, so you have integrated over a long time. Therefore, you end with only the drift velocity.

Wright: The correlogram expresses exactly the average width of those peaks. There is nothing wrong with that.

Sales: No, there is nothing wrong with it.

Elkins: When I speak of integration, I am talking about it in the experimental sense, where you have an RC time constant and actually lose this information. It is no longer available for use because you have no knowledge of what it is. You are averaging over a length of time, but this isn't integration, which involves loss of this short time period data. If the average half-width of fading peaks were just, for example, one second, we would still have information on the signal strength for times considerably less than one second.

Sales: What are you describing as the physical mechanism that causes the width of the peaks?

Elkins: This is the motion of the irregularities.

Sales: You have two things.

Elkins: Our bandwidth is very narrow so that it is the medium which determines the coherence time rather than the transmitter.

Sales: It is the sum of two motions, one turbulent and one a steady drift. It is not easy to separate these motions from the kind of measurements you have made.

Elkins: I really haven't been concerned too much with steady drifts, but they will appear as large features on the record. You are thinking of two separate orders of time here. Large drifts might be of the order of several seconds – ten seconds – perhaps.

Wright: A large drift will come out of any non-zero average of the instantaneous drift. The steady drift can be derived as an average of these instantaneous drifts.

Sales: But these are not instantaneous. They are over a period of 100 fades, so that they are not instantaneous. It is the average drift you will get.

von Biel: If I understand you correctly, the figure on the right hand side is nothing more than the auto-correlation function of the signal. If you take the Fourier transform of the auto-correlation function you have the power spectrum; consequently, you have the entire information, long-term drift as well as short-time drift right in the auto-correlation parameter function, and you can pick it out any time you want, depending on how long a record you take.

Elkins: Yes, that's true, depending on how long you sample the record, or the duration of the record.

von Biel: Yes, both the high and the low frequency components are there.

Belrose: Well, thank you very much, Mr. Elkins, for introducing some new thoughts into this subject. One can do many things with partial reflections which haven't been done in great detail. The study on the irregularities themselves hasn't been done in detail. Partial reflections to determine winds have been used in only one place, I think, by Dr. Fraser working with Dr. Gregory in New Zealand. Most of us are using them to determine only electron densities.

2.3.1 ELECTRON DENSITIES AT HIGH LATITUDES DURING QUIET IONOSPHERIC CONDITIONS

by

A. Haug

Norwegian Defence Research Establishment, Kjeller, Norway

1. Outline

In this paper the results from partial reflection measurements made at two high latitude stations in Norway are summarized. The measurements were made in March and July/August 1964 at Lavangsdalen (69.5°N), and in September 1964 and March/April 1965 at Kjeller (60°N). Lavangsdalen is close to the zone of maximum auroral activity (geomagnetic latitude 66°N) while Kjeller is located at 57.2° geomagnetic latitude. In section 2, the experimental method and the method of analysis is briefly discussed. The results are presented and discussed in section 3. A comparison of the solar zenith angle dependence of the electron density is made between the high latitude data and data from a middle latitude station at Crete (35.4°N). This comparison suggests the presence of a weak flux of auroral electrons at high latitudes, even during periods when no disturbances can be detected by riometer and magnetometer.

2. Experimental Method and Analysis

In the analysis the generalized magnetoionic theory (Sen and Wyller, 1960) has been applied to the Gardner and Pawsey method. A brief discussion of the experimental method is given in a companion paper (Haug and Thrane, these proceedings). However, some data concerning the high latitude stations are given in Table 1.

TABLE 1

	Lavangsdalen		Kjeller	
Geographic co-ordinates	69.5°N 19.3°E		60.0°N 11.1°E	
Geomagnetic latitude	66.0°N		57.2°N	
Gyrofrequency	1.44 MHz.		1.39 MHz.	
Rejection ratio between wanted and unwanted magnetoionic component	>20 db		>25 db	
Transmitter antenna	Single half-wave dipole		12 horizontal half-wave dipoles 11 db vertical gain relative to a single half-wave dipole	
Peak power of transmitter	20-50 kw.		50 kw.	
Period of measurements	March 64	July/August 64	September 64	March/April 65
Working frequency	2.25 MHz.	2.75 MHz.	2.75 MHz.	2.90 MHz.

All measurements were made at sunspot minimum (R_z less than 20) and in ionospherically quiet periods selected by the following criteria:

1) Riometer absorption at 27.6 MHz. less than 0.1 db.

2) The H-component of the magnetic field strength deviating less than 20γ from the normal. (Measured in Tromso, 30 km. north of Lavangsdalen).

3) No solar flares in excess of 1—.

It is assumed in the analysis that the reflections are caused by irregularities in the electron density. A discussion of the validity of this assumption is given by Piggott and Thrane (1966) and by Haug and Thrane (these proceedings).

Collision frequencies obtained by rocket measurements at Andoya (Jespersen et al. 1966) are given in Fig. 1. Andoya is situated 100 km. west of Lavangsdalen. In the figure a comparison is made with pressure measured by rockets at a latitude of 59°N (Nordberg et al. 1965; Nordberg and Stroud, 1961). It is seen that the pressure and the collision frequency have the same seasonal variation and the same gradients. The best agreement between the measurements is obtained when

$$\nu_M = 8.10^5 . p \tag{1}$$

(p measured in Nm^{-2}). Collision frequencies based on this relation and Nordberg's measurements have been used in the analysis. The September measurements were associated with the summer model and for the measurements in March the winter model was used.

3. Experimental Results and Discussion

From the measurements at Lavangsdalen during July/August 1964 it was possible to establish average profiles for three different times of day (Fig. 2). Few echoes were observed below 75 km. and the dashed part of the afternoon curve is drawn from a single profile, making this part less certain. It should be noted that the electron densities show no marked variation with solar zenith angle.

In Fig. 3 the results from Lavangsdalen are compared with results from measurements at a middle latitude station at Crete (Haug and Thrane, these proceedings). All profiles are averaged over the period of measurements. The figure shows a marked difference in zenith angle dependence of electron densities at the two stations. The profiles are similar for $X = 50°$, but for $X = 65°$ the electron densities at Lavangsdalen are larger by a factor of two than at Crete.

If this difference is caused by an additional source of ionization at high latitudes, this additional production, q_p, at a particular height is given by

$$q_p = q_h = q_m = \psi(N_h^2 - N_m^2) \tag{2}$$

where q_h and q_m represent total productions at this height, at high and middle latitudes respectively. N_h and N_m are the corresponding electron densities and ψ is the daytime effective recombination coefficient defined by

$$\psi = q/N \tag{3}$$

Fig. 4 presents some results from the measurements in March 1964 in Lavangsdalen, compared with a profile derived from a radio wave propagation experiment by a rocket (F VIII) launched from Andoya in the same period, also during a quiet condition (Jespersen et al. 1966). A nighttime profile measured by a Langmuir probe technique at a middle latitude (Smith, 1962) is also shown in the figure (marked NIGHT). The profiles measured by partial reflections at $X = 71.5°$ and at $X = 77°$ agree well with the profile marked F VIII. Due to interference, night measurements of partial reflections were very difficult and often impossible. In fact, the only quiet nighttime profile established in Lavangsdalen is the one marked $X = 109.5°$ in Fig. 4.

This single profile gives electron densities one order of magnitude greater than the night profile measured by Smith at the middle latitude station, supporting the assumption of an additional ionization source at high latitudes.

Let us now compare the ionization rates required by this nighttime profile measured in Lavangsdalen with the previously suggested additional daytime ionization source at high latitudes. If the two ionization sources are identical we have

$$q_p = \psi(N_h^2 - N_m^2) = q_h' = \psi'.N_h'^2 \qquad (4)$$

The marked symbols refer to night conditions. If N_h, N_m and N_h' are the observed densities, equation (4) gives a ratio between the recombination coefficient ψ' (night) and ψ (day) equal 9.0 in 82 km. and 5.2 in 88 km. This is consistent with present models of recombination processes in this height region. (e.g. Adams and Masley, 1965; Mitra, 1966; Webber, 1962; Whitten et al. 1965).

A comparison between the night profile measured in Lavangsdalen and rocket measurements at Andoya from periods with weak auroral absorption, 0.8 db at 27.6 MHz. (Fig. 5), indicates that the night profile could be caused by a background flux of ionizing electrons three orders of magnitude weaker than the flux causing the two rocket profiles, but with the same energy spectrum.

A disturbance of this magnitude would not cause detectable riometer absorption and the ionization could thus be due to a single disturbance not excluded by the quiet day criteria. The observed difference in zenith angle dependence of the averaged profiles at the high and middle latitude stations indicates, however, that a weak flux of auroral electrons may be present at high latitudes even during periods when no disturbances could be detected by riometer and magnetometer.

Fig. 6 gives results from Kjeller in September 1964 and March/April 1965. In these periods interference and radio disturbance made the results less certain, but the zenith angle dependence at this station shows better agreement with the results from Crete than with the results from Lavangsdalen. This suggests that the additional source of ionization is active only in the auroral zone.

No significant seasonal variation is detected from September 1964 to March 1965 at Kjeller.

The research described is partly sponsored by NATO Science Affairs Division under Research Grant No. 133.

REFERENCES

Adams, G.W. and A.J. Masley. J. Atm. Terr. Phys., 27, 289, 1965.

Haug, A. Electron density distribution in ionosphere and exosphere, Ed. J. Frihagen, North Holland Publishing Company, 61, 1966.

Haug, A. and E.V. Thrane. These proceedings.

Jespersen, M., Haug, A. and B. Landmark. Electron density distribution in ionosphere and exosphere, Ed. J. Frihagen, North Holland Publishing Company, 2F, 1966.

Nordberg, W. and W.G. Stroud. NASA Technical Note D-703, April 1961.

Nordberg, W., Katchen, L., Theon, J. and W.S. Smith. NASA TMX-55251 (X-651-65-154), April 1965.

Piggott, W.R. and E.V. Thrane. J. Atm. Terr. Phys., 28, 311, 1966.

Sen, H.K. and A.A. Wyller. J. Geophys. Res., 65, 3931, 1960.

Smith, L.G. Geophys. Corp. Am. Tech. Report, 62-1-N, 1962.

Webber, W. J. Geophys. Res., 6F, 5091, 1962.

Whitten, R.C., Poppoff, I.G. and R.S. Edmons. J. Geophys. Res., 70, 1737, 1965.

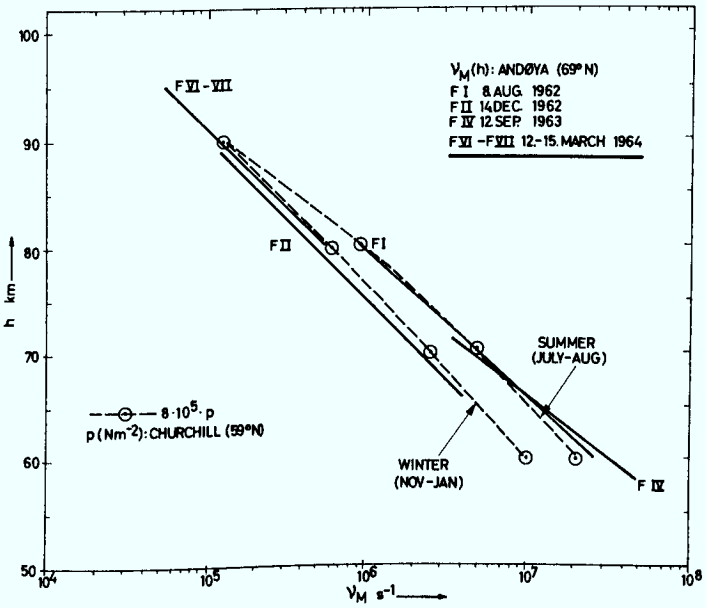

Fig. 1. Collision frequencies measured by Jespersen et al. (1966) compared with pressure measurements by Nordberg et al. (1965).

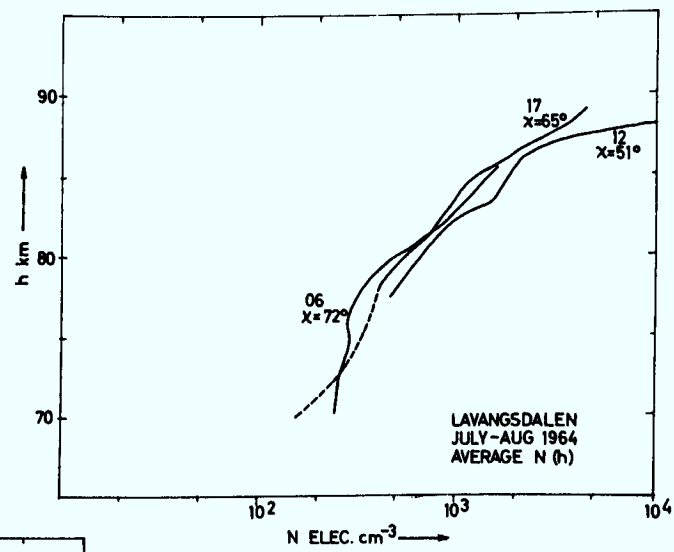

Fig. 2. Average electron density profiles for three solar zenith angles from July to August 1964.

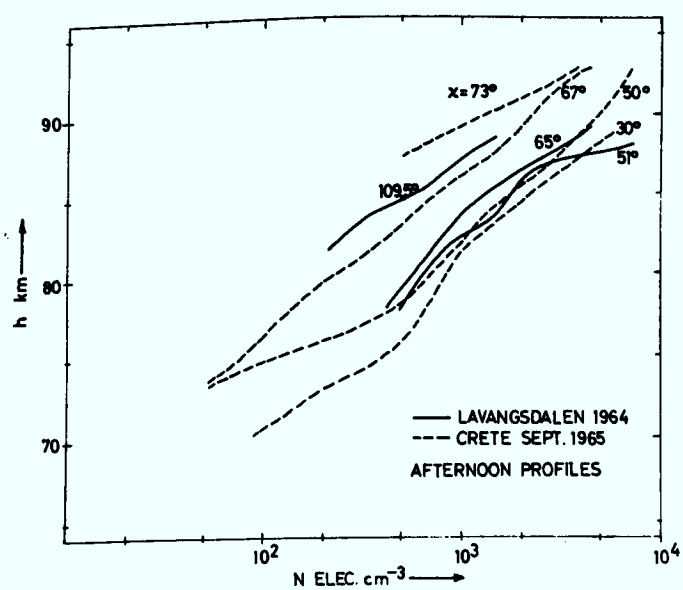

Fig. 3. Average electron density profiles at Lavangsdalen compared with results from measurements at Crete.

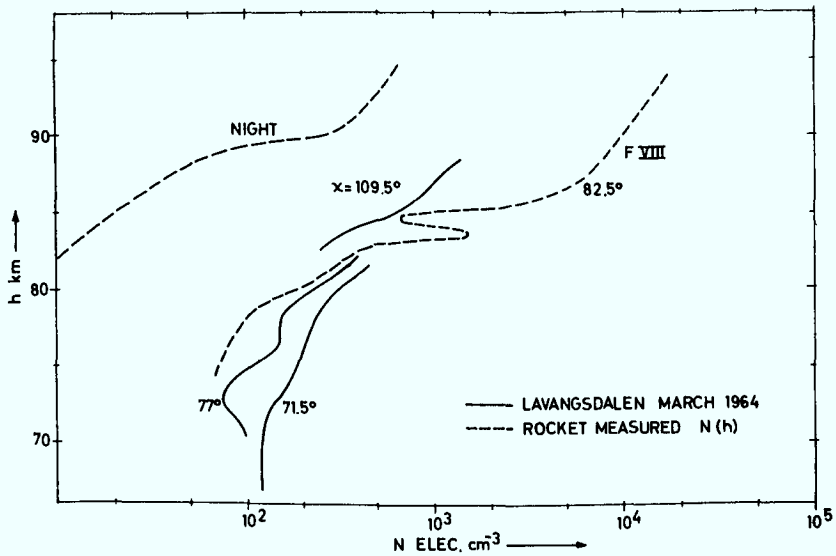

Fig. 4. Electron density profiles from March 1964 compared with a rocket measured profile (marked F VIII) in the same period and a nighttime profile measured by Smith (1962) at a middle latitude.

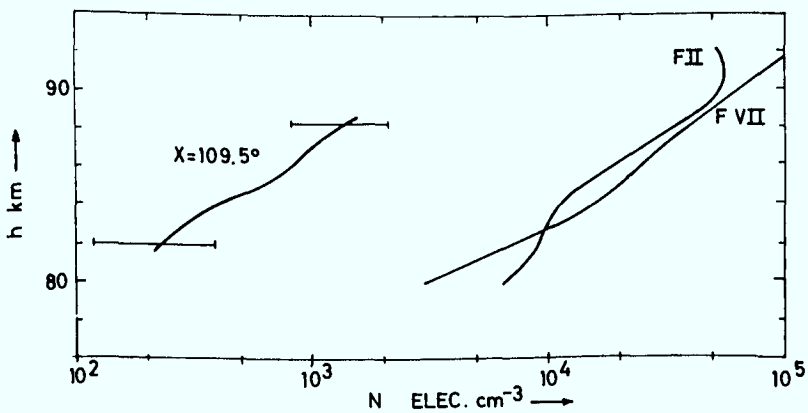

Fig. 5. Nighttime profile measured by partial reflections compared with rocket measured profiles from periods with weak auroral absorption.

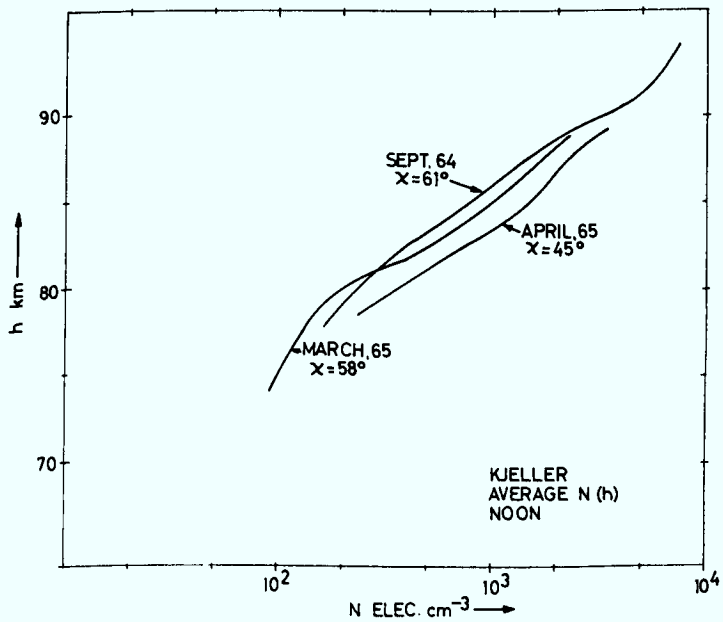

Fig. 6. Electron density profiles measured at Kjeller in September 1964 and March/April 1965.

Discussion on Paper 2.3.1 presented by A. Haug

Dalgarno: Do you know what the total energy flux is?

Haug: I did not calculate it.

Dalgarno: As these electrons come in, they will cause a luminosity. In particular, they will give rise to the emission of the first negative system of N_2^+ at 3940 angstroms, and if one could do a simultaneous measurement of this radiation, it would be a very decisive test of this hypothesis. There really is no other way to get this radiation.

Haug: You could compare the strength of the radiation with our profiles measured during an absorption of 0.8 db, just to get a feeling of the magnitude of the electron flux.

Dalgarno: Yes.

Pfister: Has this been measured in a rocket?

Haug: No, this is just the flux calculated to give such a profile.

Sales: Is it preferable to vary the recombination rate from day to night instead of assuming that the flux would have a diurnal variation? I think that it might be more reasonable to say that the flux would vary from day to night rather than conclude that the recombination rate changes by a factor of 9 from day to night.

Haug: Yes, it could do that, of course.

Sales: Then it might not be a real change of recombination rate?

Haug: Oh, no, of course.

Sales: Is there evidence for a change in recombination rate from day to night?

Unidentified speaker: Yes. With temperature.

Sales: With temperature; a factor of 9; is it that sensitive?

Haug: I think those numbers are sensitive.

Crain: Looking at the reaction rate and so forth, our conclusion is certainly that recombination rates not only vary greatly from day to night, but are not any fixed value. It depends on the production rate at night. So I don't think it is proper, even in a general sort of way, to talk about day-night ratios unless you define the level of the production rate for which you are calculating the day-night ratio.

Haug: Those factors will depend on the electron density too, of course.

2.3.2 A PRELIMINARY INVESTIGATION OF DIURNAL AND SEASONAL CHANGES IN ELECTRON DISTRIBUTION OVER OTTAWA, CHURCHILL AND RESOLUTE BAY

by

J.S. Belrose, I.A. Bourne and L.W. Hewitt

Radio Physics Laboratory
Defence Research Telecommunications Establishment

Presented by L.W. Hewitt

1. Introduction

The partial reflection experiment is being used to study the lower ionosphere at three sites in Canada: Ottawa at 45.4°N (magnetic shell latitude Λ = 58.2°), Churchill at 58.8°N (Λ = 70.5°) and Resolute Bay at 74.7°N (Λ = 84.2°). Ottawa is considered to be a middle latitude station (although its magnetic latitude is somewhat high), Churchill is located within the auroral zone, and Resolute Bay is located well within the polar cap. The experimental method devised by Gardner and Pawsey (1953), and developed by Holt (1963), Belrose and Burke (1964) and others, has proved to be a most valuable tool, capable of synoptic application, for investigating the lower ionosphere.

In previous communications (Belrose and Burke 1964 , Belrose et al., 1964b, 1966a, b) some observational results for Ottawa and Resolute Bay were discussed. The purpose of this paper is to summarize these and additional observational results (sects. 3.1 and 3.3), as well as to present some data obtained at Fort Churchill during the spring equinox of March 1965 (sect. 3.2), when efforts were made to compare average electron density distributions at all three places (sect. 3.4).

2. The experimental technique and equipment parameters

The study of the lower ionosphere by means of the partial reflection technique requires either high transmitter power or low receiving site noise, or both. At DRTE we are using a combination of high transmitter power and moderately low receiving site noise (site noise of $\sim$ 1μ volt across the 50Ω receiver input enables the measurement of effective voltage reflection coefficients at 75 km. of 10^{-6} for a transmitter power of 100 kw. or 3 x 10^{-7} for a transmitter power of 1000 kw.).

The experimental observations are amplitude height A-scan recordings at 2.66 MHz. made at one or two second intervals. O and X mode reflections are recorded sequentially by employing circular polarized transmissions separated in time by 1/15 sec. Separate four-dipole antenna systems are used for transmission and reception, and all three stations have identical antenna installations. Each four-dipole antenna system consists of four half-wave folded dipoles, one-quarter of a wave-length above the ground, arranged to form the sides of a square. Parallel dipoles are fed in phase with each other and in quadrature with the perpendicular pair to provide circular polarization. The rejection ratio between wanted and unwanted magnetoionic components is 40 to 60db.

The method of analysis is the same as that described by Belrose and Burke (1964). A complete description of the experimental equipment and a critical review of the experimental technique can be found in Belrose et al. (1964a) and Belrose et al., (1966c) respectively.

Table 1 gives a comparison of the equipment parameters at the three DRTE partial reflection installations.

TABLE 1 DRTE PARTIAL REFLECTION INSTALLATIONS

LOCATION	GEOGRAPHIC CO-ORDINATES	DIP ANGLE	ω_H	ANTENNA POLARIZATION Tx	Rx	TRANSMITTER POWER
RESOLUTE BAY	74.7°N 94.9°W	89°	9.736×10^6 RADIANS/SEC	CIRCULAR	CIRCULAR	80 - 100 KW.
CHURCHILL	58.8°N 94°W	83.9°	1.0247×10^7 RADIANS/SEC	CIRCULAR	CIRCULAR	80 - 100 KW.
OTTAWA	45.2°N 76°W	75.4°	9.753×10^6 RADIANS/SEC	CIRCULAR	CIRCULAR	800 - 1000 KW.

The lowest level from which partial reflections are detected varies with location. The level is as low as 50 km. at Ottawa, while at Fort Churchill echoes can be observed only down to the 60 km. level. At Resolute Bay echoes are not usually detected below the 65 km. level unless the ionosphere is in a disturbed state (radio wave absorption is high).

The high interference level at Ottawa prevents the observation of weak echoes at night. Although the high latitude stations have a voltage sensitivity a factor of 3 less than the Ottawa installation, the very low interference levels at these stations, both day and night, enable the equipment to be used at its maximum sensitivity at all times.

Typical records made at Ottawa for a quiet and disturbed day were given by Belrose and Burke (1964). Recordings obtained at high latitude stations are shown in Fig. 1; the records shown in 1(A) and 1(C) were made at Churchill while those in 1(B) and 1(D) were made at Resolute Bay.

Fig. 1(A) is the type of recording which is obtained from changing irregularities that are randomly distributed throughout the lower ionosphere. The amplitude of the X-mode echoes can be seen to decrease at higher heights, while the O-mode echo amplitudes increase with height. It can also be seen that the number of echoes and the height distribution of the echoes on the O and X polarizations are not the same. This is a feature which is seen more often at the high latitude stations than at Ottawa. Fig. 1(C), which was obtained during a period of visual overhead aurora at Churchill, shows a most spectacular onset of differential absorption and the ratio Ax/Ao drops to an unmeasurably small value. Fig. 1(B) shows a well-stratified echo which was obtained in July at local noon. This echo remained at a fixed height but varied in amplitude over a period of 20 min. Fig. 1(D) shows the type of record often seen at Resolute Bay during the winter months. The echo amplitude increases rapidly once echoes are detected and the amount of differential absorption is small. There is often a narrow echo peak located on the steeply rising O and X amplitude envelopes.

3. Observational Results

3.1 Resolute Bay

Observational data at Resolute Bay have been analyzed to investigate seasonal and diurnal changes. The average amplitude ratio Ax/Ao(h) curves (averaged over 4 to 7 days) for local noon and local midnight in December, March, and July 1964 are shown in Fig. 2. The various values of χ, the solar zenith angle, are marked. The dashed curve labelled Rx/Ro is the calculated reflection coefficient ratio, which depends on collision frequency, gyro-frequency, and wave frequency, and represents the amplitude ratios that would be measured in the absence of differential absorption assuming a collision frequency curve based on the CIRA 1961 Standard Atmosphere pressure profile (Belrose and Burke 1964).

Other points to be noted in Fig. 2 are: the electron density at noon in the D region clearly changes with season since the height where differential absorption begins (here taken as the height of $(Ax/Ao)_{max}$) changes with season from 88.5 km. in December, to 79.5 km. in March, and decreases to 71.5 km. in July. This change is largely because of the decreasing values of solar zenith angles from 98° in December to 53° in July, but the observational results given in the figure also show that there is a marked seasonal variation which is not proportionately connected with the change in solar zenith angle. The Ax/Ao(h) curves for March noon and July midnight are quite different even though the solar zenith angles are approximately the same at these times (about 80°). The electron density profile must also be different at these times, an observational result which suggests a seasonal change in ionizable constituents or electron loss rates.

Finally, it should be noticed in Fig. 2 that there is only a small diurnal change in mid-December, when the sun never rises ($\chi>98°$). In the absence of horizontal or vertical transport of ionization, this would be expected. In July, when the sun never sets ($\chi<83°$), there is a clear diurnal change. It should also be noted that the Ax/Ao(h) curves for December midnight and noon and for March midnight are not very different. This implies that the nocturnal electron production and loss rates are in equilibrium at these times, since similar results are obtained in December and March even though the length of the period of darkness varies from a month or more to a few hours.

Average diurnal changes are shown in greater detail in Figs. 3 and 4 for March 1964, which is a time of the year when the transition from night ($\chi>102°$) to day ($\chi<86°$) can be observed.

In Fig. 3 average data for Ax/Ao(h) for various solar zenith angles in the morning are shown. These solar zenith angles are 109° (local midnight), 102°, 98°, 94°, 90°, 86°, and 79° (local noon). There is a clear systematic diurnal change beginning as early as $\chi>98°$. The height of $(Ax/Ao)_{max}$ decreases from 87.5 km. before dawn (χ = 102°) to 79.5 km. at local noon (χ = 79°).

Fig. 4 shows averaged data for Ao(h) for the same solar conditions as in Fig. 3. The various curves in this figure again show regular changes over the dawn transition. There is a marked change in the slope of the Ao(h) curve between solar zenith angles 98° and 94° which is worthy of note since it probably indicates a steepening of the gradient of the electron density profile at this time.

It can be seen in Figs. 2 and 3 that the Rx/Ro(h) curve calculated from the $\nu m(h)$ curve 1 does not approach the Ax/Ao(h) at low heights as it should if differential absorption were small. This was previously interpreted (Belrose et al. 1966a) as suggesting high collision frequencies over Resolute Bay; but it is now thought that differential absorption at low heights may not be negligible due to the presence of a weakly ionized layer below the D layer. The irregularities in electron density in this low-lying layer must be too small to give detectable partial reflections.

The electron density height profiles shown in Fig. 5 are calculated from the data in Figs. 2 and 3. These profiles are considered to be provisional, since they have been calculated assuming reflection coefficient ratios calculated from collisional frequencies based on the CIRA 1961 standard atmosphere pressure profiles. These values of collisional frequency typically represent the values measured by the partial reflection experiment at Ottawa and Churchill.

The electron densities shown in Fig. 5 suggest that the electron densities near the 70 km. level are much smaller than would be expected from lower latitude results. These profiles also show a steep gradient in the 70 to 90 km. region. The height of this gradient appears to be under solar control. As indicated previously in Fig. 3, the Ax/Ao(h) data for July midnight and March noon suggest different electron density profiles at these times even though the solar zenith angles are similar. In Fig. 5 we can see that while the two profiles have similar gradients, the July midnight profile shows a layer of more or less constant electron density in the 75 to 85 km. region and also there are more electrons below 75 km. at midnight in July, which would account for the increased differential absorption.

3.2 Churchill

The observational data for Churchill have not yet been analyzed in the same quantity as at the other stations, and at present only data for quiet days in March 1965 are available. Fig. 6 shows the amplitude ratio Ax/Ao against height for a typical noon (5 March) compared with the average March noon on quiet days and two curves for midnight. The midnight Ax/Ao(h) curves were so variable from night to night that it was not deemed representative to obtain the average. The marked difference between the Churchill midnight Ax/Ao(h) curve and the Resolute Bay midnight Ax/Ao(h) curve is also illustrated.

Electron density as a function of height has been calculated from the data of Fig. 6 and is given in Fig. 7. The midnight electron densities, even on "undisturbed" nights (i.e. no absorption detected by a 30 MHz. riometer), can be as large at 75 km. heights as the daytime densities, but are undetectably small below about 70 km. The average noon electron density profile is similar to the profiles measured at lower latitudes at similar solar zenith angles. This point will be further discussed later in the paper.

3.3 Ottawa

Because of high nighttime noise and interference levels, as previously noted, it has not been possible to obtain observational data for Ottawa at night or over sunrise and sunset. While some results have established a clear diurnal variation during the day, the majority of our studies have been concerned with midday recordings. Results of these investigations are summarized in the following figures.

Figs. 8, 9, and 10 show the variation with height of the various observational parameters (the amplitude ratio Ax/Ao, the amplitude of the O-ray Ao, and the histogram of occurrences of O- and X-ray peaks) for the 5 magnetically quietest days for which data were available during the winter month of December, during the equinox month of March and during the summer month of June. The curves are not smoothed but are drawn through all data points. The sixth plot on these figures is the arithmetic mean of the three parameters for the five individual days shown. Electron density height profiles calculated from these data are shown in Fig. 11.

From examination of these data, one of the most evident features is the fact that while there are only small differences from day to day in summer, there are considerable variations in winter. This variability is exemplified in Fig. 11; however, several points in Figs. 8, 9, and 10 are worthy of note.

On individual days in December the ratio Ax/Ao reaches a maximum value greater than 2.0 and the mean Ax/Ao for December has a maximum of 2.0, while equinox and summer values rarely approach 2 and in fact have mean values of 1.75 and 1.68 respectively. The height at which the maximum value of Ax/Ao occurs is also seen to vary from around 70 km. in winter to 63 km. in summer. The lowering of the maximum value of Ax/Ao and the lowering of the height at which it occurred are both indications of increased differential absorption in summer months.

The histogram of occurrences of O- and X-ray peaks also exhibits great variability from day to day in winter, while remaining more like a normal distribution on equinox and summer days. In the height range 60 to 70 km., this parameter is dependent on both the frequency of occurrence and amplitude of the scatterers; at higher heights it is mainly dependent on the echo amplitude because of the recording technique and scaling criteria employed.

Because of the great variability from day-to-day in winter, it was not at first clear how to average the data so that the average would be representative of the profile which might be obtained on a particular day. It was finally decided to average the data according to a criterion established from the observational data itself. This criterion was established by grouping the days into categories which were indicative of the measured Ax/Ao at 75.5 km. The three subdivisions were: Ax/Ao>1.5, Ax/Ao between 0.5 and 1.5, and Ax/Ao<0.5; and were designated "quiet", "lightly disturbed" and "disturbed" respectively. Average electron density height profiles for these three groupings are shown in Fig. 12, where they are

compared with the average summer profile. It can be seen that, below the 75 km. level, the electron densities in winter can be greater than the average summer profile which is representative of magnetically quiet days in summer.

The variability of the partial reflection data is illustrated in Fig. 13, where various parameters of the partial reflection experiment (for data which have been scaled) are shown together with other geophysical data; the magnetic activity K-index at Agincourt, the solar index 2800 MHz. solar flux at Ottawa, and high stratospheric temperatures at Maniwaki. All available data have been plotted sequentially, although dates are not shown for individual readings. The curve labelled 'EXTRAPOLATED $\frac{Ax}{Ao}$ 59.5 km.' is an estimate of the ratio $\frac{Ax}{Ao}$ at 59.5 km., when allowance is made for differential absorption at lower levels.

As is evident, a major part of our data analysis was concentrated on winter months since, because of the greater variability, we were hopeful of establishing a stratospheric-ionospheric correlation; however, the major stratospheric warming which occurred during the past four years occurred in mid-January 1962, a period when high magnetic activity was also apparently affecting the ionosphere below 75 km.

The correlation between various parameters of the partial reflection data and the magnetic activity index is clearly evident in January, February, and November 1962 and November 1963. High magnetic activity results in lower values of Ax/Ao at 75.5 km., lower values of Ax/Ao maximum, and lower values of turnover height (i.e. the height where differential absorption becomes sufficient to cause the slope of the Ax/Ao(h) curve to become negative). The correlation of these three parameters as measured by the partial reflection experiment is good and this indicates self consistency within the experimental data. While there remains a possibility that the sudden change in the experimental parameters obtained from the partial reflection experiment in January 1962 could be associated with the stratospheric warming, it is worthy of note that changes of comparable magnitude were observed in February and November 1962 and November 1963 when there was little change in stratospheric temperatures.

Fig. 14 shows the correlation, on a day-to-day basis for the four winter months for which all data have been scaled, between the smoothed ratio Ax/Ao at 75.5 km. and total magnetic K-index at Agincourt. Because of the way in which data were selected for analysis during the remainder of the months (i.e. magnetically quiet periods), a more detailed correlation cannot be made.

The amplitude ratio Ax/Ao at low heights (say 57.5 or 59.5 km.) should provide a measure of collision frequency. Early results for November 1961 to February 1963 were interpreted as showing no seasonal variation in collision frequency, but apparently showed a clear dependence on solar activity (Belrose and Hewitt 1964). Additional data given in Fig. 13, which are, in the main, for periods of low solar activity, have not provided further evidence for such a dependence. In fact, if there is a dependence on solar activity during quiet sun years, it is masked by long-term variations which must be meteorological in origin. A clear seasonal variation has not yet been established.

Fig. 15 is a plot of the average weighted ratio Ax/Ao at 57.5 and 59.5 km. for all months for which we have data during the period November 1961 to February 1965. Although all the available data have not been scaled and days on which it was apparent that differential absorption was present at these heights have been omitted from the analysis, it is obvious that the ratios during the winters of 1962-63 and 1963-64 were much greater than during the winters of 1961-62 and 1965, suggesting that collision frequencies were lower by a factor of 2 or 3 during the winters of 1962-63 and 1963-64. The scales labelled Δh on this figure and on Fig. 13 represent the height variation of a fixed value of collision frequency.

As previously noted, only a few partial reflection observations have been made over the whole of the day for the purpose of determining the diurnal variation in electron density at Ottawa. Figs. 16, 17, 18, and 19 show the results of a set of observations obtained on 20 October, 1961.

Fig. 16 shows the variation with height of the amplitude ratio Ax/Ao for various times in the morning and for two times in the afternoon. The values of the solar zenith angle, χ,

associated with the middle of the various recording periods are: 77.5°, 67.5°, 60.5°, 56°, and 55° in the morning, and 57° and 83° in the afternoon. This figure shows a fairly uniform decrease throughout the morning of the value of the ratio Ax/Ao at high heights near 80 km. With the exception of the 1245 to 1300 data, there is reasonable agreement between the observed $\frac{Ax}{Ao}$ ratios and the calculated reflection coefficient ratios near the 60 km. height.

The marked disagreement between the 1245 to 1300 curve and other curves obtained near local noon is thought to be the result of a minor disturbance in the lower D region.

Fig. 17 is a plot of the ratio $\frac{Ax/Ao}{Rx/Ro}$ as a function of height throughout the day. While the "disturbance effect" is clearly evident in all curves near 1300 hours, it is not as marked at higher heights. The 81.5 km. values show a dependence on solar zenith angle which is almost symmetrical about local noon. The dashed curve shown near the 81.5 km. afternoon curve is a plot of the results which would be expected if the morning and afternoon curve were symmetrical about local noon (i.e. it is the mirror image of the morning curve about local noon).

Since the afternoon values were affected by a disturbance near 1300 hours, some degree of asymmetry could be expected from this cause alone. It is apparent that there is a definite diurnal variation of the absorption within the D region and that the partial reflection experiment can detect these variations. More diurnal studies must be undertaken.

Fig. 18 is a plot of the O-ray amplitude as a function of height for various solar zenith angles in the morning. The amplitudes below 65 km. show a slight decrease as χ decreases from 77.5°to 55°, while the amplitudes in the 75 km. region show an increase with decreasing values of χ until at local noon we have an exponential gradient in Ao which is typical of summer noon Ao(h) curves at Ottawa.

Fig. 19 shows the electron number density height profiles, which were deduced from the Ax/Ao curves shown in Fig. 16. The values of electron number densities shown in these profiles are calculated at all heights from the differential absorption data, (i.e. no attempt has been made to fit O-ray tails, as has been done for all other profiles shown in this paper). Although accuracy of the electron number densities calculated from differential absorption data below the turn-over height has always been poor, the figure definitely shows the existence of a minimum in electron number density in the 70 to 75 km. height region after sunrise (χ values of 77.5° and 67.5°). The depth of this valley in electron number density decreases throughout the morning as χ decreases, until at local noon we have an approximately exponential N(h) profile typical of a summer noon N(h) profile at Ottawa. This qualitatively agrees with the results given by Smith et al. (1966)*.

3.4 Latitudinal Variations

We have already noted that nighttime results for Ottawa cannot be obtained. Electron density distributions on quiet nights as deduced by partial reflections for Resolute Bay and Churchill are therefore compared in Fig. 20 with data obtained by rocket-borne experiments over Wallops Island. One rocket result for Churchill, on a night when there was no measurable riometer absorption, is also shown for comparison. These results indicate that the average electron densities at Resolute Bay are less than those at lower latitudes, while the electron densities at Churchill can be the same or larger than those measured at lower latitudes, especially at heights below 90 km. Fig. 7 shows that the electron density on some nights can be as large at 75 to 80 km. heights as during the day; the electron density at lower heights, however, decreases rapidly to small values. When the electron densities at Churchill become sufficiently enhanced, auroral absorption is measured by a 30 MHz. riometer.

A series of observations was made in March 1965 to compare average daytime electron densities at all three stations, Resolute Bay, Churchill, and Ottawa, at times in the morning when the solar zenith angles were the same. The high noise and interference levels at

* Fig. 19 was introduced in discussion as evidence supporting Dr. Smith's dawn profiles, but is included in the text of the paper prepared for the Proceedings for completeness.

Ottawa prevented us from obtaining partial reflection recordings at a solar zenith angle equal to the Resolute Bay noon value ($\chi = 80^{o}$).

In Fig. 21 we have shown the average Ax/Ao(h) curve for Resolute Bay noon ($\chi = 80^{o}$), which should be compared with the Churchill morning curve at the same solar zenith angle, and the curve for Churchill noon ($\chi = 63^{o}$), which should be compared with the Ottawa morning curve at the same solar zenith angle. Also shown are the three reflection coefficient ratios which are calculated for the three different stations, assuming the curve 1 collision frequency profile previously discussed. This figure indicates that the Resolute Bay profile must be considerably different than the others especially at low heights. This point will be discussed further in Figs. 22 and 23.

In Fig. 22 we have plotted the amplitude of the O-ray, Ao, as a function of height for the same solar conditions as for the Ax/Ao(h) data shown in the previous figure. The Ao(h) values for Ottawa have been reduced for this comparison to account for the increased transmitter power at Ottawa. The Ao(h) for Resolute Bay again appears quite different from the other three, and indicates lower electron densities since it has been shown with reasonable theoretical justification (Belrose and Burke 1964) that Ao is approximately proportional to electron density, although the proportionality varies from day-to-day and over the season.

In Fig. 23 we have plotted the electron density height profile for the results which were examined in Figs. 21 and 22. As was inferred from the data in Figs. 21 and 22, we can see that there is good agreement between the profiles for Churchill and Ottawa at the same solar zenith angle (63°), while the Resolute Bay and Churchill profiles, which were calculated from the results obtained at $\chi = 80^{o}$, are quite different especially at heights below 85 km.

4. Discussion

Assuming that the ionization in the undisturbed D region can be attributed to three sources: background cosmic radiation, solar X-rays 2 — 8A, and photoionization of nitric oxide by solar Lyman α radiation, the following main conclusions can be drawn from our observations which were made during quiet sun years when the ionization due to solar X-rays should be small.

1) The seasonal and latitude variations of electron densities are not in accord with a D region produced simply by background cosmic radiation and solar Lyman α, unless complex electron loss reactions are involved. The daytime electron densities at heights below 80 km. are much smaller at Resolute Bay than at Churchill and Ottawa (whereas the reverse would have been expected) and the greatest variability in the winter electron densities is found at low heights (below 75 km.) where the main source of ionization is thought to be background cosmic radiation. Since cosmic radiation will ionize all gas molecules in proportion to their mass abundance, it would have seemed more plausible, according to the ionospheric model, if the variability had been mainly in the D-layer ionization (since a trace ionizable constituent is involved at these heights).

2) The cause of the winter variability in electron densities is not clear. Bossolasco and Elena (1963), Shapley and Beynon (1965) and Gregory (1965) have established a connection with stratospheric temperatures. While the results for Ottawa have not established a clear stratosphere-ionosphere coupling, they do indicate that energetic particles (also) influence the ionization at low heights during the day (at Ottawa latitudes), since the electron densities in winter are correlated with magnetic activity.

3) The inferences concerning collision frequency suggest that, over Ottawa, the average collision frequencies on some winters can be considerably less than on other winters.There is undoubtedly considerable variability in collision frequency from day to day, especially in winter.

4) The nighttime ionization at auroral latitudes is strongly dominated by ionizing energetic electrons. This flux is very variable in time and space, but weak fluxes, which are very quasi-constant, can apparently enhance the nocturnal electron densities at auroral latitudes over those measured at other latitudes. This latter statement results from a study of all data available from our studies at DRTE, in particular the 80 kHz. transmissions between Ottawa and Churchill (the midpoint of this path lies within the auroral zone).

REFERENCES

Belrose, J.S., Bodé, L.R., Hewitt, L.W. and J.M. Griffin. An experimental system for studying partial reflections from the lower ionosphere, Defence Research Board, DRTE Report 1136, April 1964.

Belrose, J.S., Bodé, L.R. and L.W. Hewitt. Physical properties of the polar winter mesosphere obtained from low-frequency propagation and partial reflections, Radio Science J. of Res. NBS/USNC-URSI, 68D , 1319-1323, 1964.

Belrose, J.S. and M.J. Burke. Study of the lower ionosphere using partial reflection. 1. Experimental technique and methods of analysis, J. Geophys. Res., 69, 2799-2818, 1964.

Belrose, J.S. and L.W. Hewitt. Variation of collision frequency in the lowest ionosphere with solar activity, Nature, 202, 267-269, 1964.

Belrose, J.S., Bodé, L.R. and L.W. Hewitt. A preliminary investigation of diurnal and seasonal changes in electron number densities over Resolute Bay as observed by partial reflections, Electron Density Profiles in Ionosphere and Exosphere (ed. Frihagen), North Holland Publishing Co., Amsterdam, 1966.

Belrose, J.S., Bourne, I.A. and L.W. Hewitt. The winter variability of electron number densities in the lower ionosphere over Ottawa — A discussion of results and possible cause, ibid.

Belrose, J.S., Bourne, I.A. and L.W. Hewitt. A critical review of the partial reflection experiment. These Proceedings, 1966.

Bossolasco, M. and A. Elena. Absorption de la couche D et temperature de la mesosphere, Comptes Renclus, 256, 4491-4493, 1963.

COSPAR International Reference Atmosphere, North Holland Publishing Company, Amsterdam, 1961.

Gregory, J.B. The influence of atmospheric circulation on mesospheric electron densities in winter, J. Atmos. Sci., 22, 18-23, 1965.

Shapley, A.H. and W.J.G. Beynon. Winter anomaly in ionospheric absorption and stratospheric warmings, Nature, 206, 1242, 1965.

Smith, R.A., Bourne, I.A., Loch, R.G. and T.N.R. Coyne. Small perturbation wave interaction in the lower ionosphere, Part II. Experimental observations. These Proceedings, 1966.

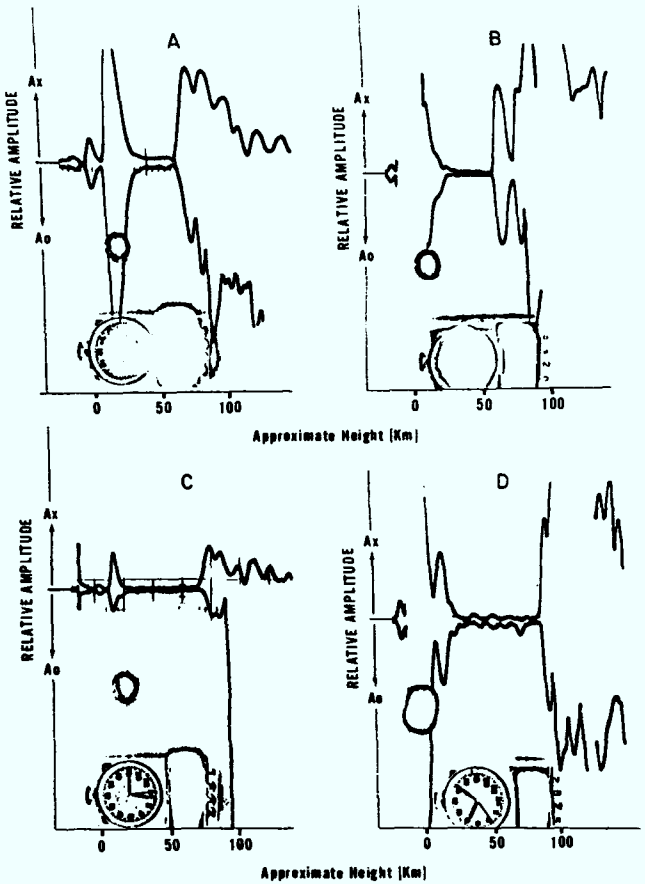

Fig. 1. Examples of recordings of partial reflections at high latitude stations.

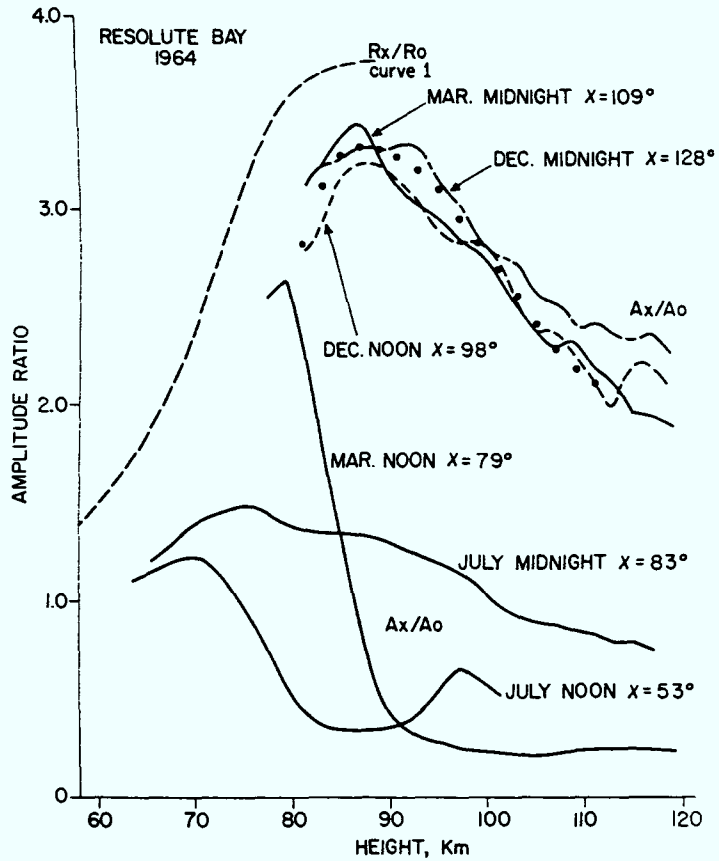

Fig. 2. Seasonal variation in average amplitude ratio, Ax/Ao, against height for midnight and noon at Resolute Bay.

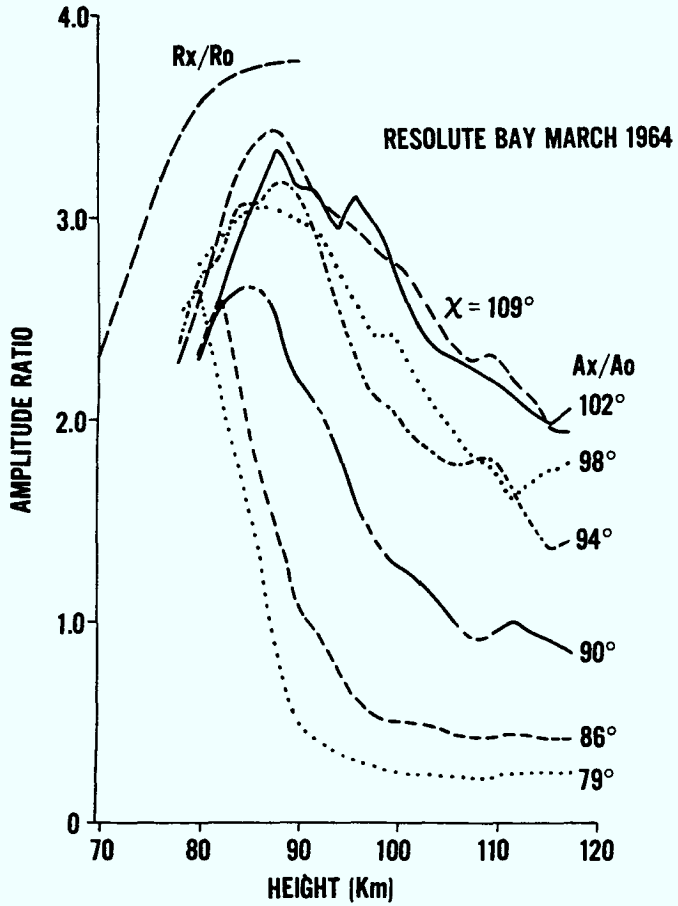

Fig. 3. Diurnal variation in average amplitude ratio, Ax/Ao, against height in March for midnight ($\chi = 109°$), noon ($\chi = 79°$) and over sunrise ($\chi = 102°$ to $86°$) at Resolute Bay.

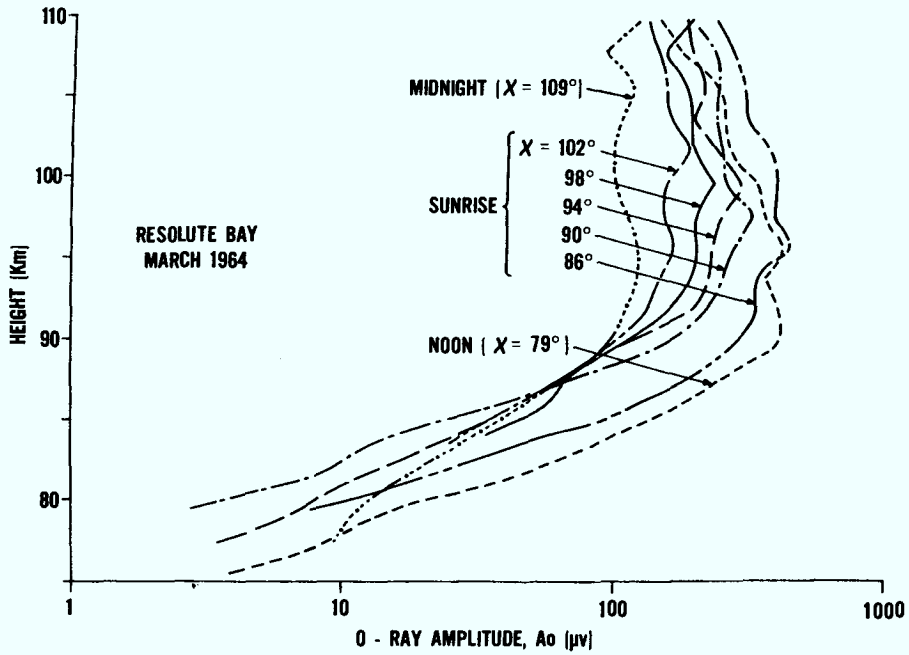

Fig. 4. Average diurnal variation of O-ray amplitude, Ao, against height in March for midnight ($\chi = 109°$), noon ($\chi = 79°$), and over sunrise ($\chi = 102°$ to $86°$) at Resolute Bay.

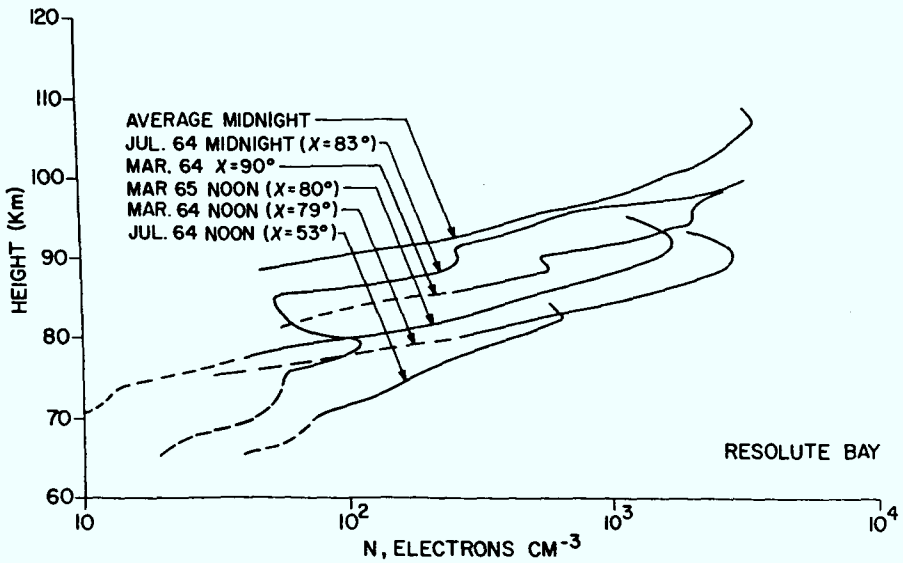

Fig. 5. Average electron number density against height at Resolute Bay for various solar conditions. Note these electron density values are calculated assuming collision frequencies based on the CIRA 1961 standard atmosphere pressure profile.

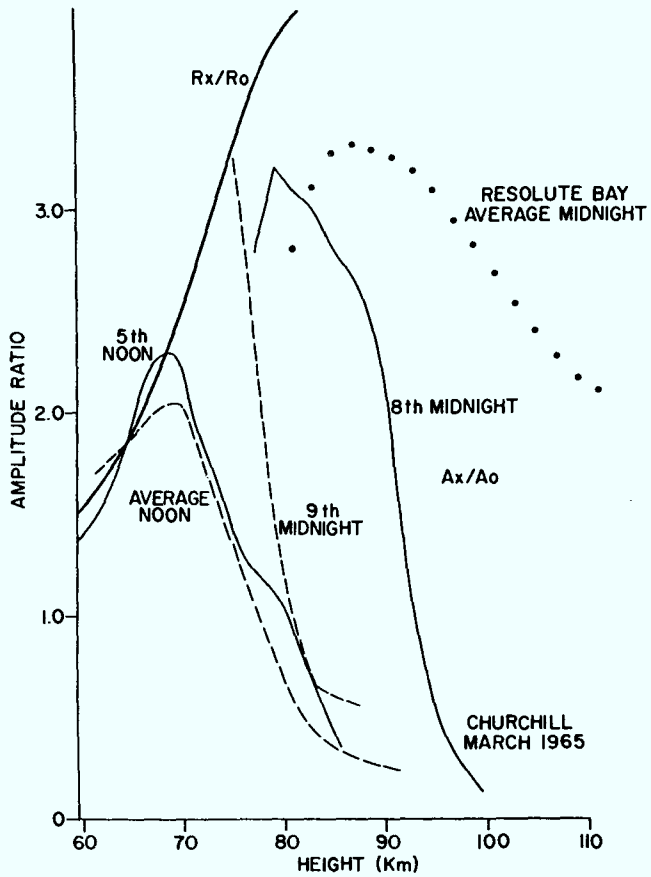

Fig. 6. Diurnal variation in amplitude ratio, Ax/Ao, against height in March for midnight and noon at Churchill. Average Resolute Bay midnight data are included for comparison.

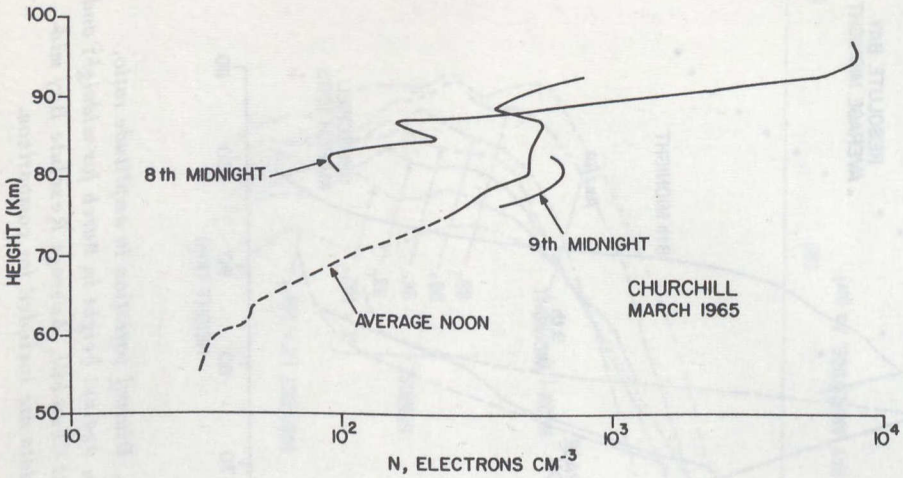

Fig. 7. Electron number density against height at Churchill in March 1965, for average noon and two quiet nights (i.e., no riometer absorption).

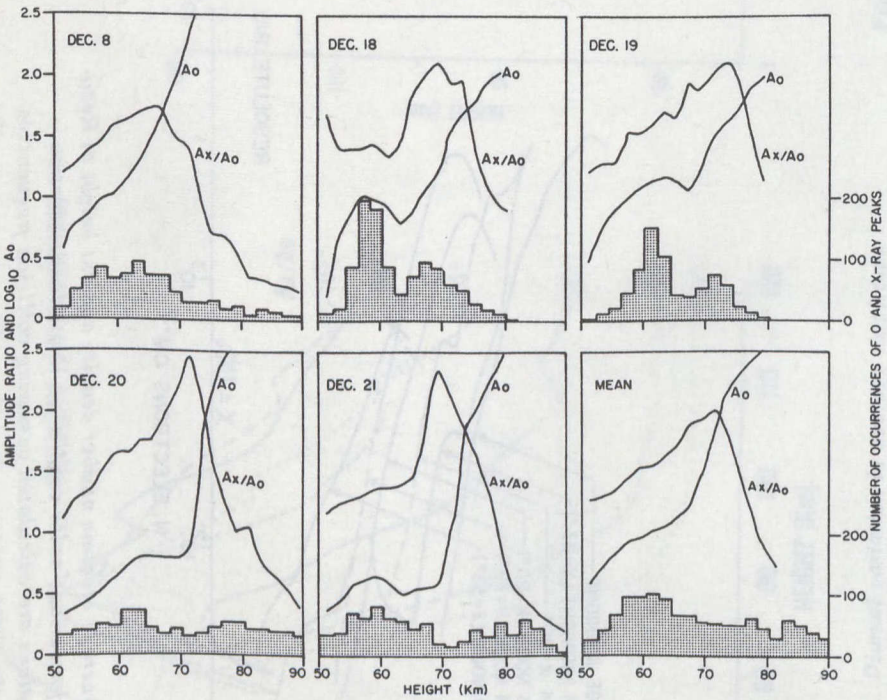

Fig. 8. Partial reflection observational data at Ottawa, showing the variation with height of the amplitude ratio Ax/Ao, the O-ray amplitude Ao, and the histogram of occurrences of O- and X-ray peaks, for 5 magnetically quiet days in winter (December 1961).

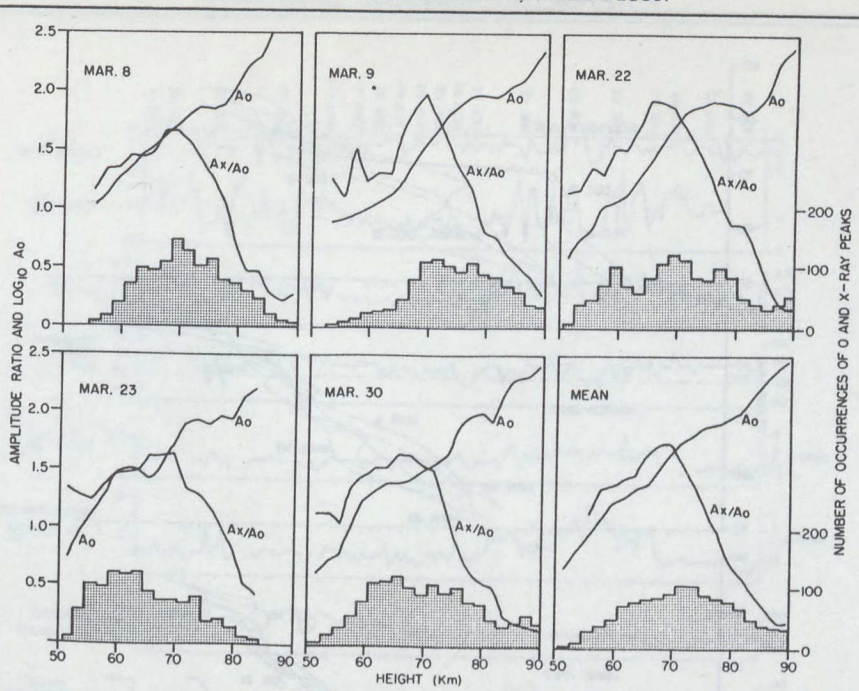

Fig. 9. Partial reflection observational data at Ottawa, showing the variation with height of the amplitude ratio Ax/Ao, the O-ray amplitude Ao, and the histogram of occurrence of O- and X-ray peaks, for 5 magnetically quiet days in spring equinox (March 1962).

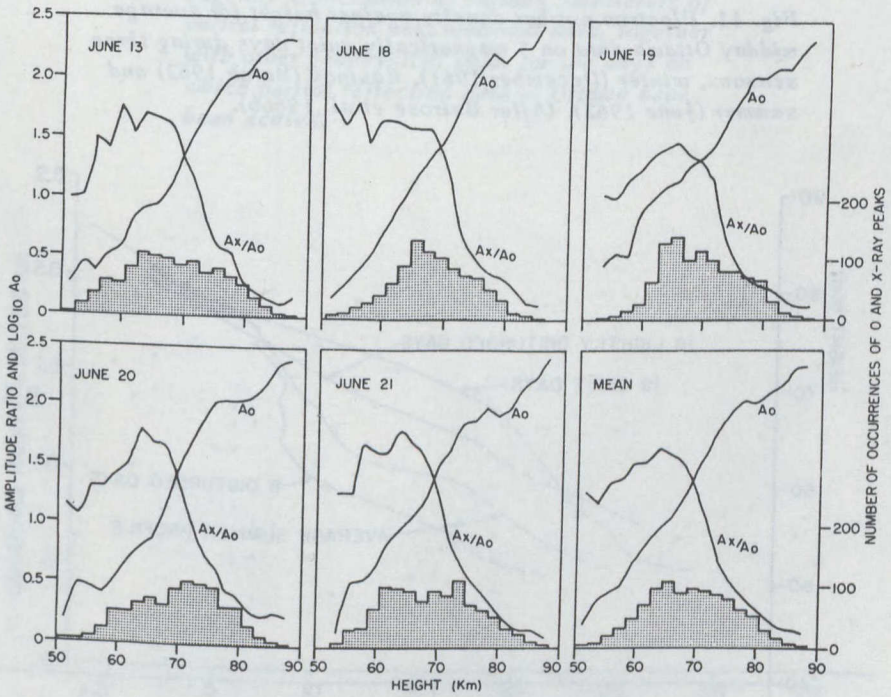

Fig. 10. Partial reflection observational data at Ottawa, showing the variation with height of the amplitude ratio Ax/Ao, the O-ray amplitude Ao, and the histogram of occurrences of O- and X-ray peaks, for 5 magnetically quiet days in summer (June 1962).

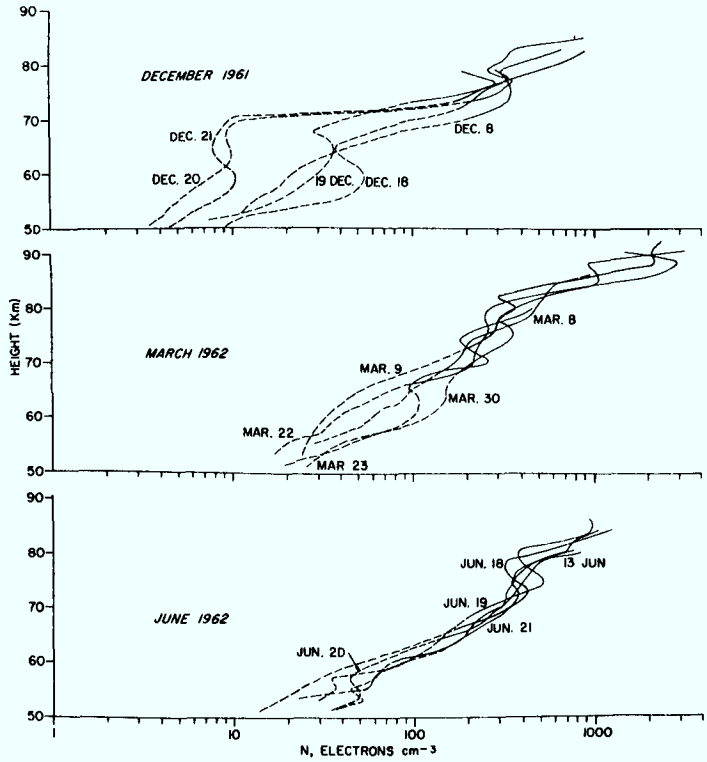

Fig. 11. Electron number density against height for average midday Ottawa data on 5 magnetically quiet days during three seasons, winter (December 1961), Equinox (March 1962) and summer (June 1962). (After Belrose et al. 1966b).

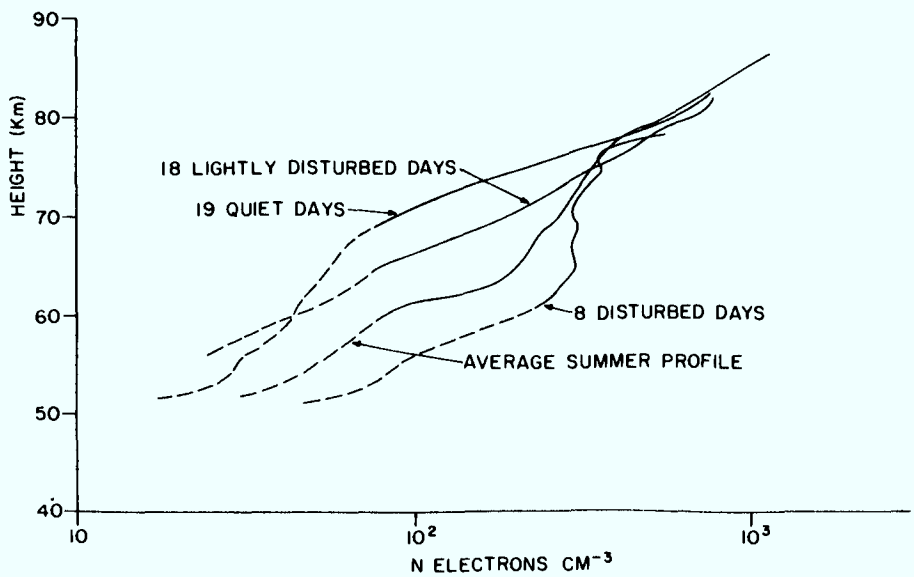

Fig. 12. Electron number density against height for average midday Ottawa data for various magnitudes of "disturbance". The degree of disturbance is judged from the partial reflection data.

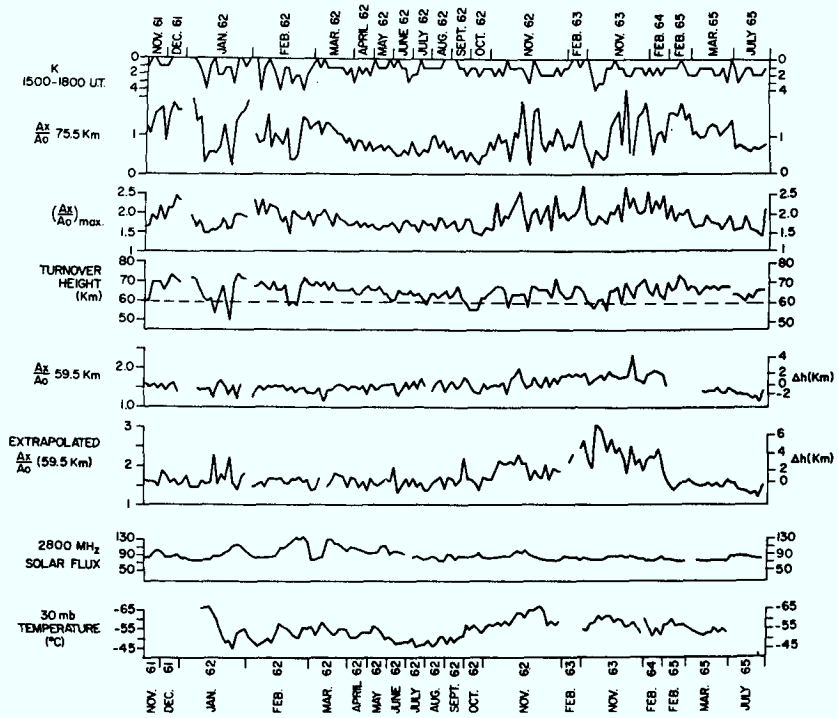

Fig. 13. Co-location of various parameters of partial reflection observational data, together with other geophysical data, for the days on which partial reflection data at Ottawa have been scaled.

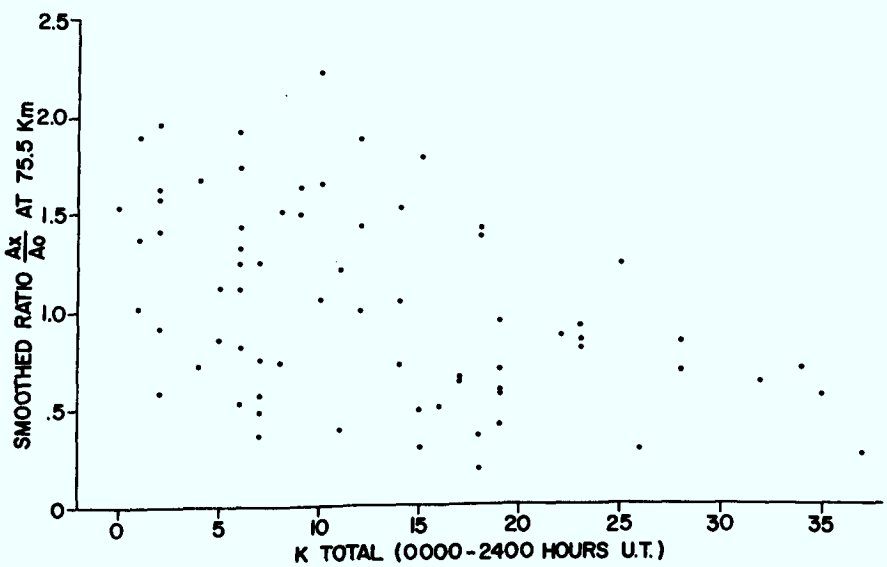

Fig. 14. Correlation between smoothed amplitude ratio, Ax/Ao, at 75.5 km. at Ottawa and total magnetic K-index at Agincourt.

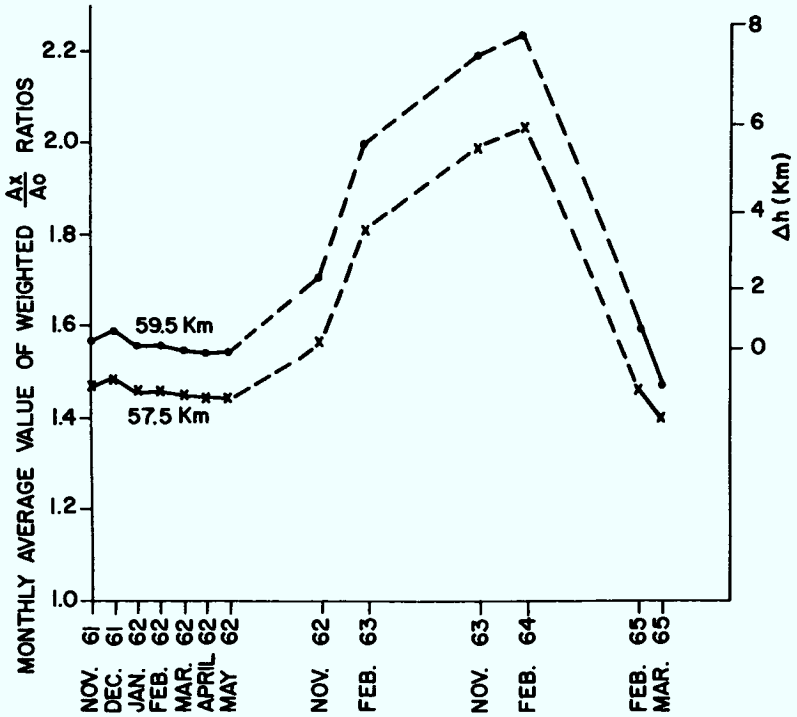

Fig. 15. The variation of the monthly averaged weighted value for the amplitude ratio, Ax/Ao, at 57.5 and 59.5 km. for the months on which data at Ottawa have been analyzed. The scale on the right of the figure represents the height variation of a fixed value of vm.

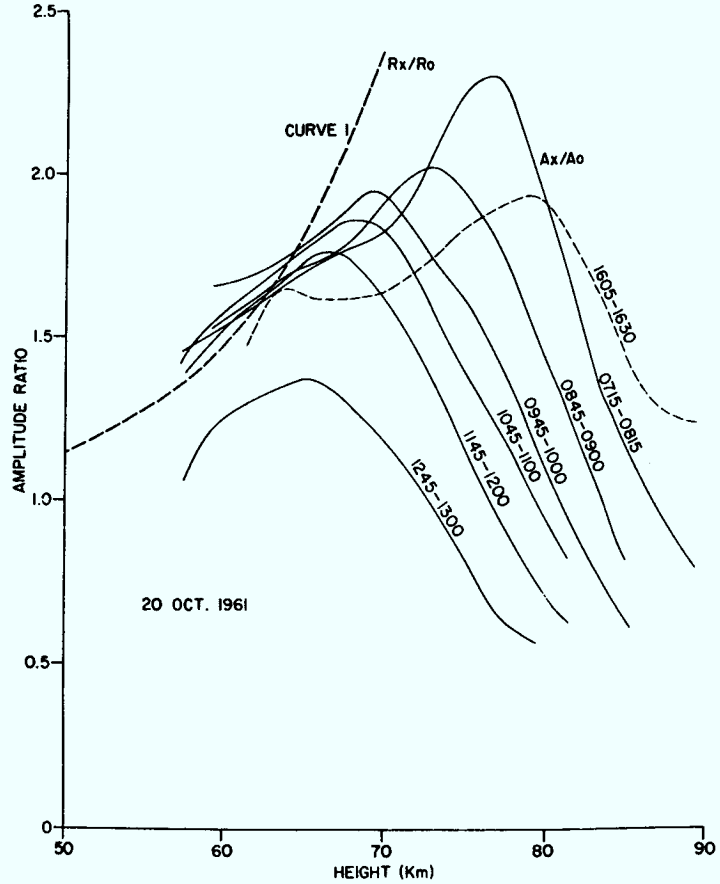

Fig. 16. Partial reflection observational data at Ottawa showing the diurnal variation in the amplitude ratio, Ax/Ao, against height for various times in the morning and for two times in the afternoon on 20 October, 1961. See text for corresponding values of solar zenith angle.

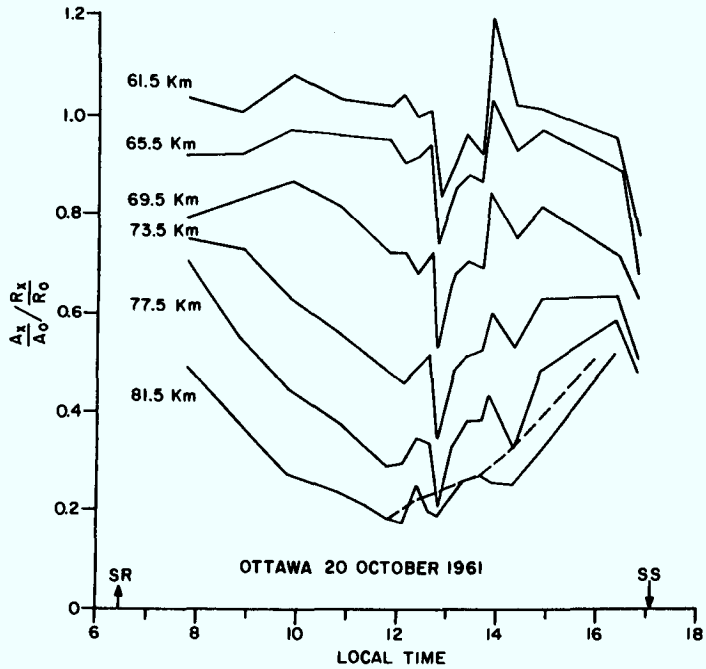

Fig. 17. Partial reflection observational data at Ottawa showing the diurnal variation of the ratio $\frac{Ax/Ao}{Rx/Ro}$ *at 4 km. height intervals on 20 October, 1961.*

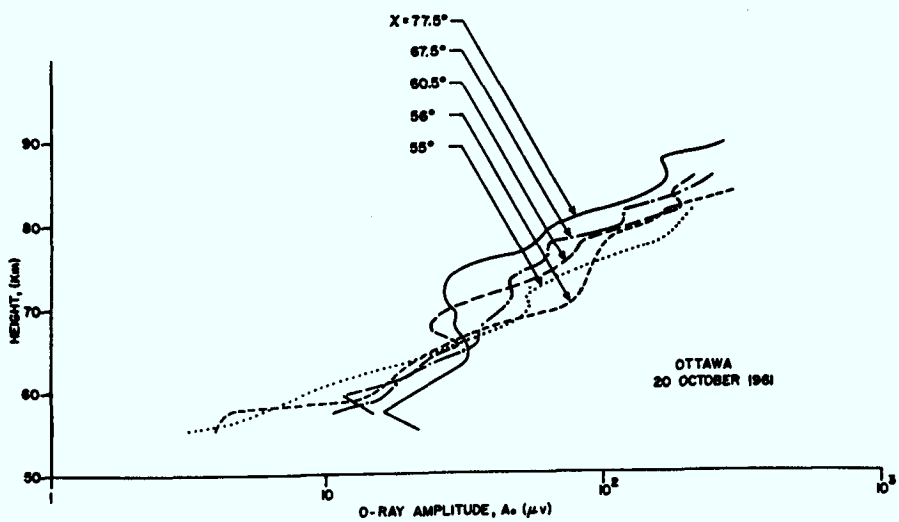

Fig. 18. Partial reflection observational data at Ottawa showing the diurnal variation of the O-ray amplitude, Ao, against height on 20 October, 1961, for various morning values of solar zenith angle.

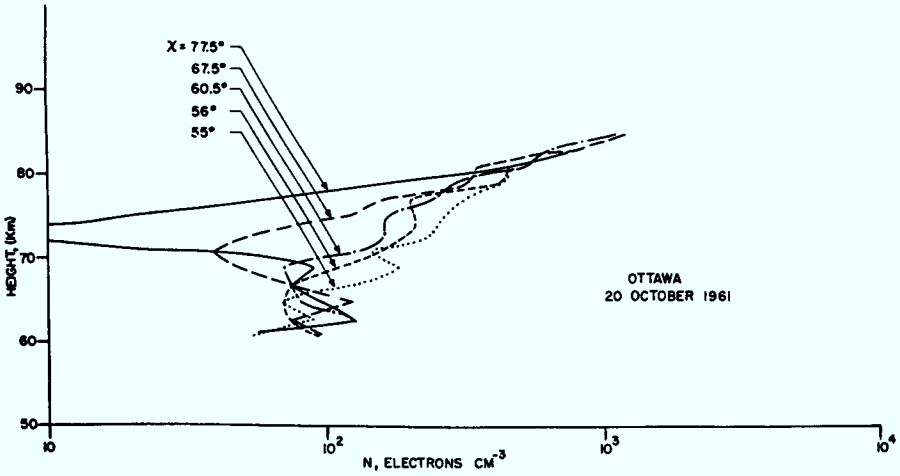

Fig. 19. Diurnal variation of electron number density against height for Ottawa data on 20 October, 1961, for various morning values of solar zenith angle.

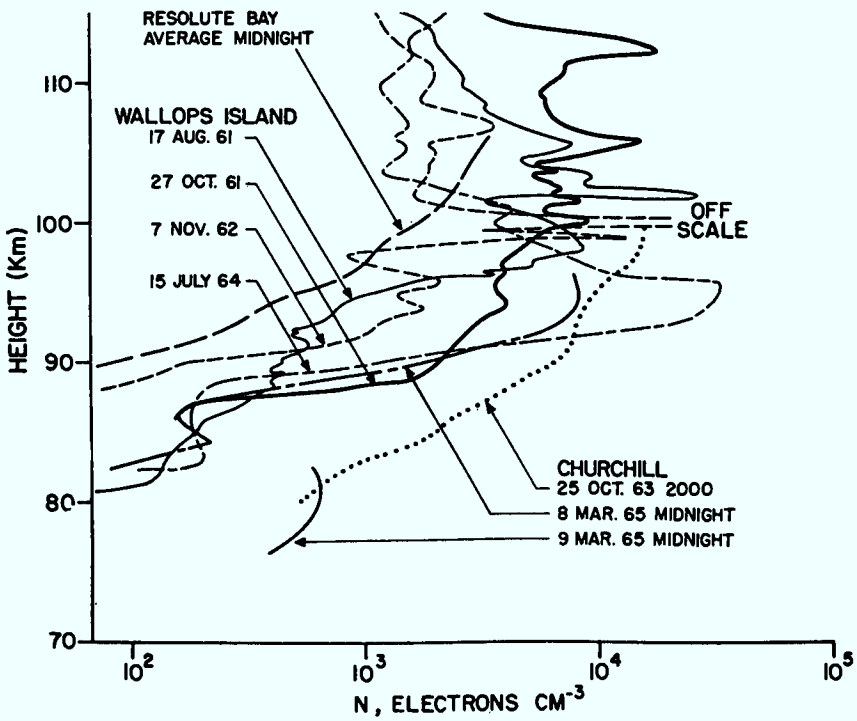

Fig. 20. Comparison of electron number density against height curves for quiet nights at high (Resolute Bay), auroral (Churchill), and middle (Wallops Island) latitudes.

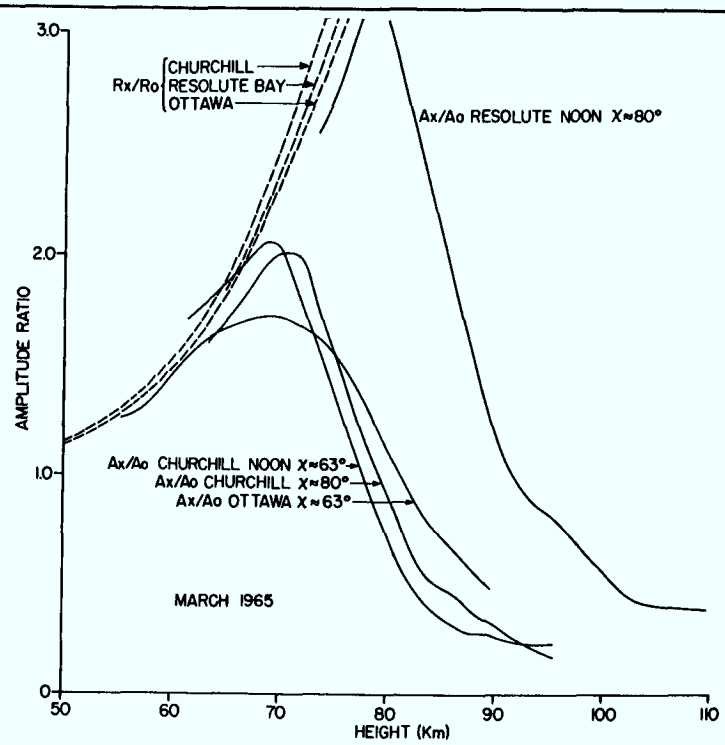

Fig. 21. Average amplitude ratio, Ax/Ao, against height in March 1965, for Resolute Bay noon ($\chi = 80°$) compared with Churchill in the morning at the same solar zenith angle, and Churchill noon ($\chi = 63°$) compared with Ottawa in the morning at the same solar zenith angle.

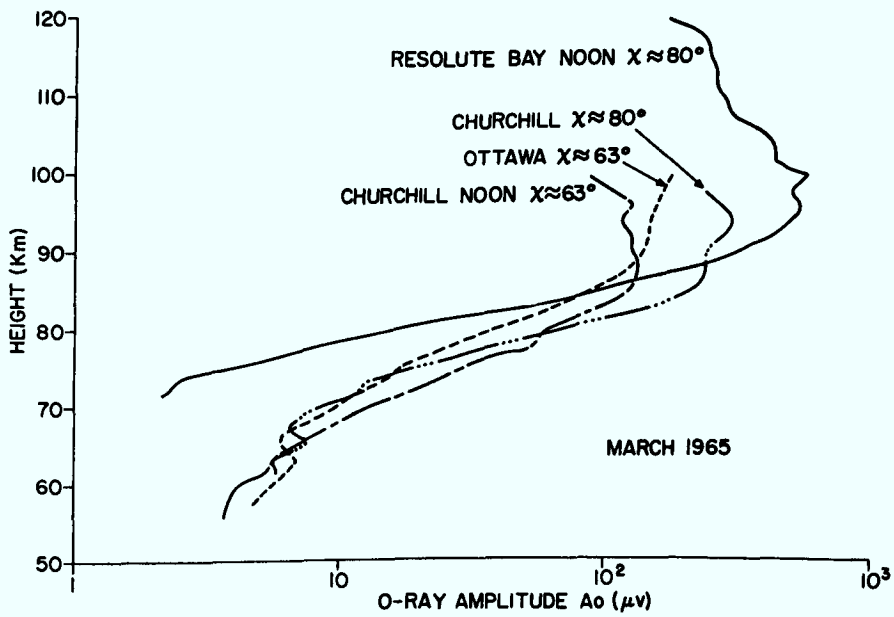

Fig. 22. Average O-ray amplitude, Ao, against height in March 1965, for Resolute Bay noon ($\chi = 80°$) compared with Churchill in the morning at the same solar zenith angle, and Churchill noon ($\chi = 63°$) compared with Ottawa in the morning at the same solar zenith angle.

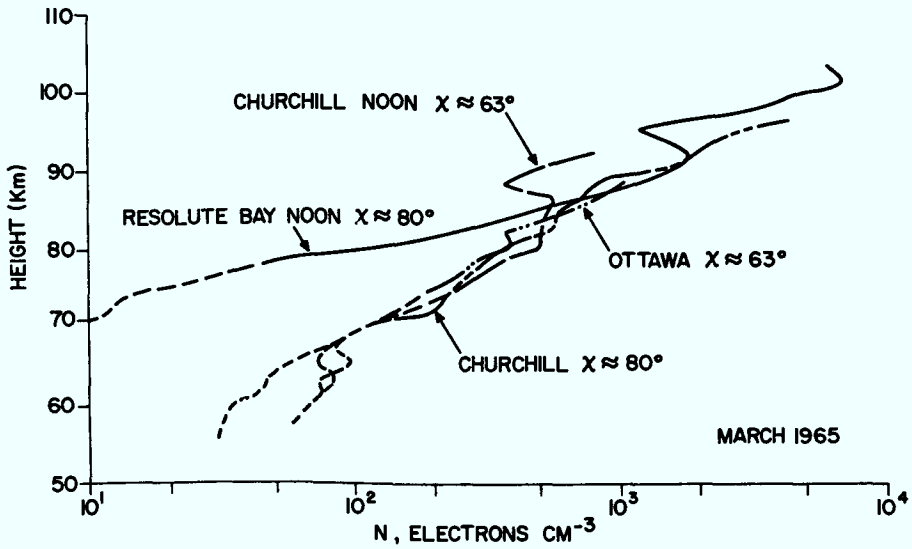

Fig. 23. Average electron number density against height in March 1965, for Resolute Bay noon ($\chi = 80°$) compared with Churchill in the morning at the same solar zenith angle, and Churchill noon ($\chi = 63°$) compared with Ottawa in the morning at the same solar zenith angle.

Discussion on Paper 2.3.2 presented by L.W. Hewitt

Bibl: Did you reduce your *Ao* values obtained at Ottawa to allow for the higher power of this station?

Hewitt: Yes. The *Ao* value has been reduced by a factor of 3 approximately.

Falcon: How do you calculate the electron densities where the *Ax/Ao* curve has a sharp peak near the 70 km. level, as for example, the Resolute Bay data?

Hewitt: Not one of the profiles here has shown calculated electron densities below the turnover height. The dotted portion of the curve, which in this case extends from 75 km. down, is proportional to the O-ray amplitude only, and it matches with the calculated curve at higher heights. The calculated curve is extended to lower heights using the proportionality with *Ao*.

Falcon: I am dividing our data into sub-intervals of about 3 km., and exact interpretation of the behaviour of this curve below this turnover height is frequently confusing, and you can get a wide range of calculated electron densities when you have only, say, two or three points below this peak.

Hewitt: Yes, below the heights where differential absorption sets in, the calculation is very sensitive, as was shown in some of Bourne's figures earlier this morning.

Falcon: Did you actually calculate electron densities from this portion of the curve and average the computed values obtained on a number of days?

Hewitt: No.

Bourne: We have done some analysis, mainly of winter data, and have subdivided the data into days having similar amounts of absorption. By lumping this data together, we effectively have a much higher degree of accuracy than we have on single days; we can then calculate electron densities 5 to 10 km. below the turnover height. These electron densities, as Hewitt mentioned, are very sensitive, but we are convinced that you can reliably extend the calculation to lower heights if you have the data.

Falcon: By averaging, do you calculate the electron density for each day on its own curve and then average the resulting electron densities, or do you take all of the ratios and average them, and then calculate your electron densities from that?

Bourne: We have taken the data on each individual day and weighed the data according to the number of echoes scaled on that day. Then we take a weighted mean of all these ratios – the resulting curves are extremely consistent. I don't trust them at very low heights, but certainly you can go below that turnover height with some degree of certainty.

Falcon: You average the ratio values, then use the average ratios to calculate the profile?

Hewitt: Yes.

Belrose: The point must be emphasized. It is pointless, on most days, to try to determine electron densities for heights below the turnover height. We have always determined electron densities only for heights above the turnover height where there is a significant degree of absorption in a 2 km. interval. The data is just too sensitive to small gradient changes in the *Ax/Ao* curve at low heights. The electron densities are meaningless unless you have a day in which there is very little scatter, or unless data are averaged in a careful manner and you use average data. This is a limitation of the partial reflection experiment. It seems to be a limitation of almost all experiments, whether you do rocket-borne experiments or radio-sounding experiments, you just cannot seem to get a decent base on the ionosphere. We put a base on our ionosphere by using O-ray amplitude, because it seems to be reasonably justified on some occasions, but one would like to have better sensitivities to see where the ionosphere actually begins.

von Biel: I have a question regarding the mechanics of recording the A-scan data; I believe you inferred that you have almost a simultaneous picture of X-ray and O-ray echo returns.

Hewitt: That is right.

von Biel: What is the dynamic range of the echoes as you normally observe them between, let us say, 60 and 90 km., and have you ascertained a linear relation in your receiver output over this dynamic range?

Hewitt: We use a stepped attenuator in the front of our receiver. Our receivers have a dynamic range which is in the order of 20 to 30 *db*, depending on where the gain is set. We also have stepped attenuators in the front end of the receiver, and we vary these in six *db* steps to give us another 30 *db*, so we have 60 *db* or more dynamic range. On the first pair of pulses, we have maximum gain; two seconds later we have a gain which is reduced by 6 *db*; two seconds later, we have a gain which is reduced by 12 *db*, and so on up to 30 *db*, and then we go back to maximum gain again. These attenuation factors are then used to multiply the scaled values.

von Biel: My second question – to what precision do you read your A-scans?

Hewitt: We scale them on with a Gerber scaling machine. We enlarge the record until the frame is approximately a foot square and the deflections and delays are read off in counts per inch. Bourne had a slide this morning showing height distribution of an echo which was moved in 2 km. steps. With this system, a change of 5 counts corresponds to a height shift of approximately 1 km. The machine reads off in two-hundredths of an inch, so we can scale the displayed amplitude and the height to parts in two-hundredths of an inch.

von Biel: I should rephrase the question. To what precision can you scale an *Ax* or *Ao* value? Is it closer to 1% or 0.1%?

Hewitt: If you are talking about one or two microvolt signal levels, the thickness of the trace is an appreciable percentage of the echo amplitude, whereas when you are talking about 100 microvolt echoes, the thickness of the trace is negligible. If there is a fairly decent echo of a few microvolts, we can certainly read it to the nearest microvolt.

Shirke: If I may repeat what I said yesterday; the rocket results on a winter anomaly day show excess ionization above 80 km., and little change below 80 km. This is slightly in conflict with your observations.

Belrose: I could comment on that again by repeating what I said yesterday, and that is that you have to be careful about what you call a winter day of anomalous absorption, and I think a good deal of study has to go into this subject yet. Most of the data presented in this paper illustrates winter variability. We are not talking about winter days of anomalous absorption – merely winter variability. Now there are winter days of anomalous absorption, and I showed one of them yesterday in which there were large electron densities at low heights, and this was not clearly connected with magnetic activity or with activity on the sun. I didn't stress this point; apparently it had very wide effects. Generally, a winter day of anomalous absorption, by the definition of people who have worked with it, is limited in extent to some thousand km., whereas on this particular day increased absorption at Ottawa was apparently correlated with absorption changes which were happening at Lindau in Germany.

Gregory: And in the Antarctic.

Belrose: So there is no doubt about it, there is a lot of variability in the winter months, sometimes it is anomalous absorption, but what do we mean by it? We are only talking about winter variability here.

Hewitt: On some of these particular days, when there was high magnetic activity and we saw enhancement of electron densities at 75 km., we probably weren't measuring electron densities much above 80 km. because detectable differential absorption was starting at 50 or 55 km. heights, and the *Ax/Ao* ratios above 75 km. were near the limiting values of .2 or .3 so that we couldn't determine the electron density distribution at the higher heights.

Shirke: I might mention that we do have some partial reflection records for the same day the rocket was flown, and the differential absorption also collaborates data shown by the rocket. The result is that the increased differential absorption occurred mainly above 80 km. on this particular day.

Gregory: Could we have the geomagnetic latitude of Wallops Island, where the firing was? I think Russian studies during the IGY showed that particle influx can be important unless the geomagnetic latitude is less than 45°.

NOTE: No one at the conference knew the geomagnetic latitude. Later investigations show that the invariant geomagnetic latitude would be approximately 52°.

2.3.3 D REGION ELECTRON DENSITIES DEDUCED FROM MEASUREMENTS OF PARTIAL REFLECTIONS AT A MIDDLE LATITUDE AND AT A LOW LATITUDE STATION

by

A. Haug and E.V. Thrane

Norwegian Defence Research Establishment

Presented by E.V. Thrane

1. Outline

The purpose of this paper is to present some preliminary results from measurements of partial reflections made during the International Quiet Sun Year, at a middle latitude station (Crete 35°N, 25°E) and at a low latitude station (Tsumeb 19°S, 18°E).

The first section describes the experimental technique, while the second section deals with the method of analysis. In the third section the deduced results are presented, and in a final section some of the possible limitations of the method, in particular as applied to the ionosphere at low and middle latitudes, are discussed.

2. Experimental Method

The partial reflection technique for finding the height variations of electron density in the lower ionosphere has been intensively and successfully applied in recent years (Gardner and Pawsey 1953; Fejer and Vice 1959; Belrose and Cetiner 1962; Holt 1964; Belrose and Burke 1964; Belrose and Hewitt 1964; Belrose 1964). The measurements discussed in this paper were made using a technique similar to the technique previously used in Norway by Holt et al. (1961).

A linearly polarized high frequency radio wave is transmitted vertically with a pulse length of 100 μsec. and a pulse repetition frequency of 50 Hz. The weakly scattered echoes from the D region are received by a polarimeter consisting of four horizontal half-wave dipoles forming a square. The phase of the signal from one pair of parallel dipoles is switched $\pm$ 90° relative to the signal from the other pair with a frequency of 25 Hz. This results in an alternate selection of one of the two circularly polarized components of the wave. The amplitude versus height of the received ordinary and extraordinary magnetoionic components are displayed on an oscilloscope, and recorded photographically with a rate of about 100 photographs per minute. The receiving equipment has been described by Bjelland (1966).

The present results were obtained at Crete, Greece and at Tsumeb, Southwest Africa. Some of the most important data concerning the two stations are given in Table 1.

TABLE 1

	Crete	Tsumeb
Geographic coordinates	35.4°N, 25.4°E	19.32°S, 17.71°E
Gyrofrequency	1.20 MHz.	0.90 MHz.
Angle of dip	50°	55°
Working frequency	2.54 MHz.	2.25 MHz.
Peak power of transmitter	50 kw.	30 kw.
Rejection ratio between wanted and unwanted magnetoionic components	20-25 db	25 db
Transmitter antenna	A system of 6 horizontal half-wave dipoles. Vertical gain relative to a single half-wave dipole about 8 db. The plane of polarization is at an angle of 45° to the magnetic meridian plane.	Vertical rombic (1.5-3 MHz.) with its plane of polarization in the magnetic meridian plane.

3. Method of Analysis

Our method of analysis is in principle the same as the method described by Gardner and Pawsey (1953) and Belrose and Burke (1964). It is based on the following assumptions:

(a) The weak partial echoes received from the D region are scattered from sharp local gradients in electron density.

(b) The incident wave is split into two independent magnetoionic modes below the height at which the lowest echo is observed (Smith et al. 1965).

(c) The formula for Fresnel reflection holds for each of the two weakly scattered magnetoionic modes, that is the reflection coefficient is given by

$$R_{o,x} = \frac{\Delta n_{o,x}}{2n_{o,x}} \qquad \ldots.(1)$$

where n is the complex refractive index of the medium, and Δn is the perturbation in n which causes the reflection.

(d) The rate of collisions of free electrons with neutral particles at a particular height does not vary with time of day or from day to day. The collision frequency is conveniently described in terms of ν_M, the collision frequency of electrons with energy kT. The adopted height variation of ν_M is shown in Fig. 1. It was derived from the average height distribution of atmospheric pressure at low and middle latitudes, published by Cole and Kantor (1965), using the relation $\nu_M = 8 \cdot 10^5$ p, where the pressure p is measured in N m^{-2}. (Haug, these proceedings; Thrane and Piggott 1966).

The validity of these assumptions will be discussed in a later section.

The well-known expression for the measured amplitude ratio of the extraordinary and ordinary echoes scattered from a height h can conveniently be written

$$\frac{A_x}{A_o} = \frac{A_x^{\,o}}{A_o^{\,o}} \left|\frac{R_x}{R_o}\right| e^{-2\int_{h_o}^{h} (\kappa_x - \kappa_o)\,dh} \qquad \ldots.(2)$$

when $A_x^{\,o}$ and $A_o^{\,o}$ are the amplitudes of the incident extraordinary and ordinary components at the height h_o when the lowest echo is observed. $\kappa_{o,x}$ is the absorption index.

The ratio $\frac{A_x^o}{A_o^o}$ will depend on the differential absorption below h_o and on how the energy in the incident wave is divided between the magnetoionic modes. In the height range of interest the ratio $\left|\frac{R_x}{R_o}\right|$ will depend only on ν_M and the absorption index $\kappa_{x,o}$ will be proportional to the electron density N. Thus, by taking the logarithm of both sides of equation (2) and differentiating with respect to height, the electron density N at a height $h > h_o$ can be expressed as

$$N = \frac{\Delta\left(\ln\left|\frac{R_x}{R_o}\right| - \ln\frac{A_x}{A_o}\right)}{\frac{1}{2N}(\kappa_x - \kappa_o)\,\Delta h} \qquad \ldots.(3)$$

Here $\Delta\left(\ln\left|\frac{R_x}{R_o}\right| - \ln\frac{A_x}{A_o}\right)$ is the change of the expression inside the parenthesis over the small height interval h to $h+\Delta h$. Note that the electron density does not depend on the differential absorption below the height of which the lowest echo is observed, nor does it depend on the separation of the energy of the incident wave between the two magnetoionic modes. It only depends on the specific absorption $\frac{1}{N}\kappa_{o,x}$ and on the relative slope of $\left|\frac{R_x}{R_o}\right|$ (h) and the measured ratio $\frac{A_x}{A_o}$ (h).

An electronic computer was programmed to give $\left|\frac{R_x}{R_o}\right|$ and $\frac{1}{N}(\kappa_x - \kappa_o)$ as a function of height using the height variation of ν_M given in Fig. 1 and the generalized magnetoionic theory described by Sen and Wyller (1960). As has been pointed out by Benson (1964), the use of the longitudinal approximation of Sen and Wyller's formulas for the refractive index can lead to considerable errors for low and middle latitudes, and the complete formula was therefore used in this work.

4. The Experimental Results

Measurements of partial reflections were carried out in the periods 13 to 31 March, 1965 at Tsumeb, and 30 August to 11 September, 1965 at Crete. Observations were made once or twice every hour throughout the day, each series of measurements consisting of about 300 amplitude-height A-scan records taken in the course of 3 to 4 min.

Weak partial echoes could normally be detected in the height range 70 to 95 km. during the daylight hours. At night, and often near sunrise and sunset, measurements were impossible because of interference. Only measurements from periods when no solar flares of importance greater than 1^- were observed, were used in the analysis. The electron density distributions obtained at Crete within zenith distance intervals of 10 degrees were averaged, and the average diurnal variation of the electron density thus obtained is illustrated in Fig. 2. Some profiles obtained during one single afternoon are shown in Fig. 3, and indicate that the smooth diurnal variation exhibited by the average profiles repeats from day to day. The analysis of the data from Tsumeb has not yet been completed, but some preliminary results are shown in Fig. 4. The profiles are average profiles for the morning and afternoon hours. The averages of the measured amplitude ratios are taken over zenith distance intervals of 10 degrees.

The profiles from Tsumeb are somewhat more uncertain than those obtained at Crete. The reason for this is that most of the partial echoes observed at Tsumeb were reflected from a small height interval. The prevalent height of reflection varied from about 75 km. during the middle of the day to about 80 km. near sunrise and sunset.

Discussion

In this section the validity of some of the assumptions on which our analysis is based will be discussed.

It has been pointed out by Piggott and Thrane (1966) that if the gradients of electron density which cause the weak reflections are accompanied by gradients in the collision frequency, then the usual theory for the partial reflection experiment needs revision. Suppose that the percentage perturbations in collision

frequency ν_M and electron density N are proportional so that $\alpha = (\Delta\nu_M/\nu_M)/(\Delta N/N)$. $\alpha = 0$ then corresponds to the case when only perturbations in N are important, and $\alpha = \infty$ corresponds to the other extreme when only perturbations in ν_M are present.

The height variation of the ratio $\left|\frac{R_X}{R_O}\right|$ has been computed for different values of α and the results for Tsumeb are given in Fig. 5. The curve for $\alpha = 0$ is the curve used to derive the electron densities discussed in the preceding section. As will be seen, $\left|\frac{R_X}{R_O}\right|$ varies considerably with α, and we conclude that the present analysis may be seriously in error if α deviates appreciably from zero. However, the fact that results from partial reflection measurements in general seem to agree well with data from other experiments suggests that α normally is small. (Thrane, these proceedings).

The curves for $\left|\frac{R_X}{R_O}\right|$ in Fig. 5 are calculated for a typical daytime electron density distribution, and the curves rise very steeply above 90 km. where the reflection region for the extraordinary wave is approached. At these heights, during the day, the ratio $\left|\frac{R_X}{R_O}\right|$ is no longer independent of N and the present method of analysis cannot be used.

Smith et al. (1965) have shown experimentally that, when a linearly polarized transmitter antenna is used at middle latitudes, the measured amplitude ratio $\frac{A_X}{A_O}$ depends on the orientation of the antenna relative to the plane through the vertical and the earth's magnetic field. This is also predicted by theory, since the separation of the energy in the incident wave between the two magnetoionic modes will depend on the orientation of the plane of polarization relative to the characteristic ellipses at the bottom of the ionosphere (Bailey 1937). However, Smith's measurements do not agree with the theoretical predictions.

It has already been shown that the unequal division of energy between the modes does not affect our analysis, provided the incident wave splits up into independent magnetoionic components below the region in which the echoes are observed. It is of interest to determine at what height this splitting is likely to occur.

According to Budden (1961, Chapter 19) the limiting polarization will be determined near the level at which

$$|\psi^2| \approx \left|\frac{1}{4}(n_O - n_X)^2 - \frac{1}{2}\, i\,(n_O' - n_X')^2\right| \qquad \ldots.(4)$$

where ψ is the coupling parameter given by $\psi = \frac{\rho_X'}{\rho_X^2 - 1}$.

The differentiation is with respect to height.

Above this level the magnetoionic components will propagate and be scattered independently, provided there is no critical coupling.

Below the level at which equation (3) holds, the incident and reflected waves will travel without changing their polarizations and they do not split up into magnetoionic components.

In order to find the height at which the limiting polarization is determined, the right and left hand sides of equation (4) have been computed as a function of height for various models of electron density. It was found that, for all reasonable daytime models, the limiting region occurs below 60 km. Suppose for example that the electron density below 70 km. varies with height as

$$N = 9.1 \cdot 10^{-13}\ e^{-\frac{h}{2.17}}\ (\mathrm{cm}^{-3})$$

h is the height in km.

The computations show that in this case the limiting region is at ≈ 52 km. at Crete and at ≈ 49 km. at Tsumeb. Thus it seems likely that at least during the day the limiting polarization will be determined well below 70 km., which is the lowest height at which a partial reflection has been observed during our measurements. Moreover, it is interesting to note that at these levels the collision frequency ν_M is very large and the characteristic polarizations as given by Sen and Wyller's formulas are very nearly circular, even at low and middle latitudes.

We conclude that the method introduced by Gardner and Pawsey can be used with some confidence to deduce D region electron densities at middle latitudes, provided the height variation of collision frequency is known, and provided irregularities in collision frequency do not play an important part in the scattering of high frequency radio waves from the lower ionosphere.

Acknowledgments

The research described in this paper is sponsored by NATO Scientific Affairs Division under Research Grant No.133, and the measurements were made by the Norwegian Defence Research Establishment in collaboration with the Ionospheric Institute of Athens, Greece, and with the Max-Planck Institut für Ionosphären-Physik, Lindau, West Germany.

REFERENCES

Bailey, V.A. Phil. Mag. S7 23, 929, 1937.

Belrose, J.S. Electron density distribution in the ionosphere and exosphere (Ed. E. Thrane), North Holland Publishing Co., Amsterdam. 41-49.

Belrose, J.S. and M.L. Burke. J. Geophys. Res. 69, 2799, 1964.

Belrose, J.S. and E. Cetiner. Nature, Lond. 195, 688, 1962.

Belrose, J.S. and L.W. Hewitt. Nature, Lond. 202, 267, 1964.

Benson, R.F. J. Res. NBS, 68D, 219, 1964.

Bjelland, B. Technical Note E-88 NDRE, 1966.

Budden, K.G. Radio waves in the ionosphere. Cambridge Univ. Press, 1961.

Cole, A.E. and A.J. Kantor. Air Force Surveys in Geophysics No. 153, 1963. L.G. Huscom Field, Bedford, Mass.

Fejer, J.A. and R.W. Vice. J. Atm. Terr. Phys. 16, 307, 1959.

Gardner, F.F. and J.L. Pawsey. J. Atm. Terr. Phys. 3, 321, 1953.

Haug, A. These proceedings.

Holt, O. Electron density distribution in ionosphere and exosphere, (Ed. E. Thrane), North Holland Publishing Co., Amsterdam. 36, 1964.

Holt, O., Landmark, B. and F. Lied. NDRE Report 35 parts I–III, Norwegian Defence Research Establishment, 1961.

Piggott, W.R. and E.V. Thrane. J. Atm. Terr. Phys. 28, 311, 1966.

Sen, H.K. and A.A. Wyller. J. Geophys. Res. 65, 3931, 1960.

Smith, R.A., Bourne, I.A., Loch, R.G., Setty, C.S.G.K., Coyne, T.N.R., Barratt, P.H., and B.S.N. Prasad. Radio wave interaction using gyro-waves. Air Force Cambridge Research Lab. Report AFCRL-65-460, 1965.

Thrane, E.V. These proceedings.

Thrane, E.V. In preparation.

Thrane, E.V. and W.R. Piggott. J. Atm. Terr. Phys. 1966. In press.

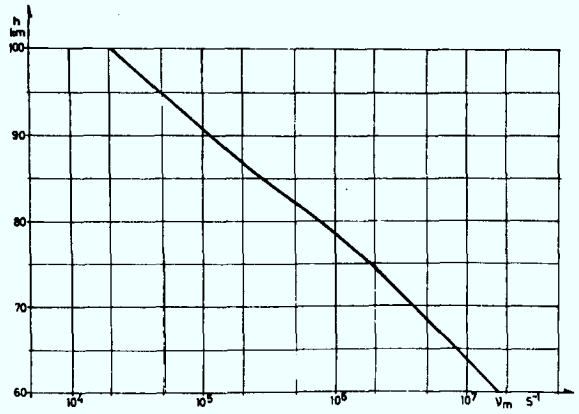

Fig. 1. The adopted height variation of the collision frequency ν_M.

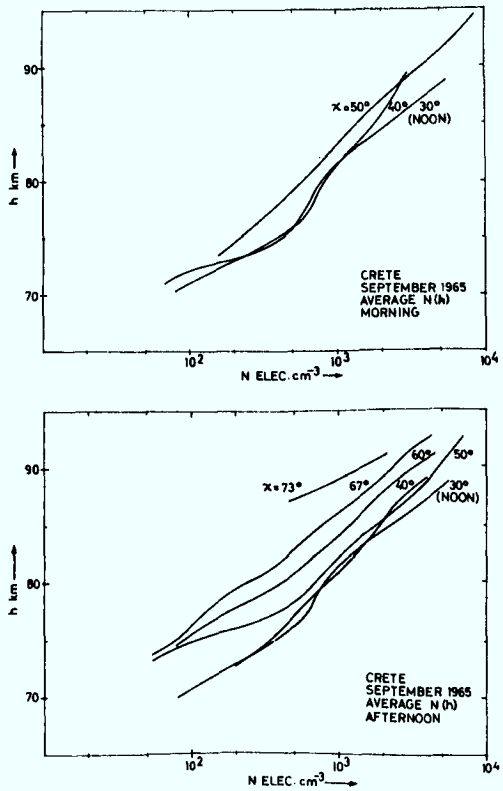

Fig. 2. Average electron density distributions for different solar zenith angles. Crete, September 1965.

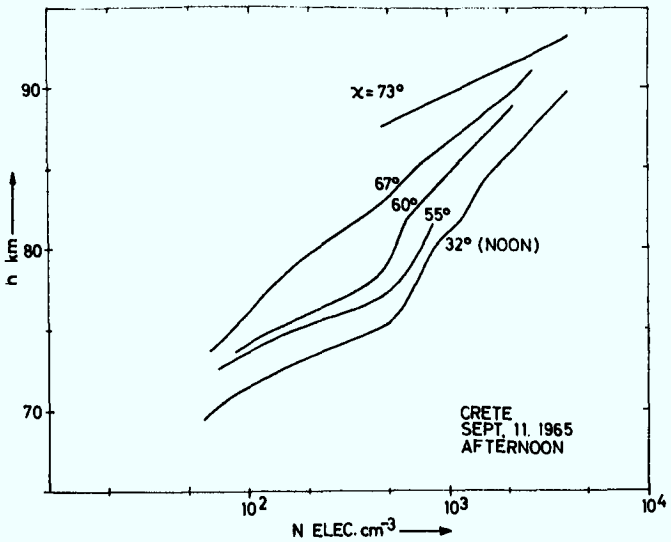

Fig. 3. Electron density distributions measured during one single afternoon.

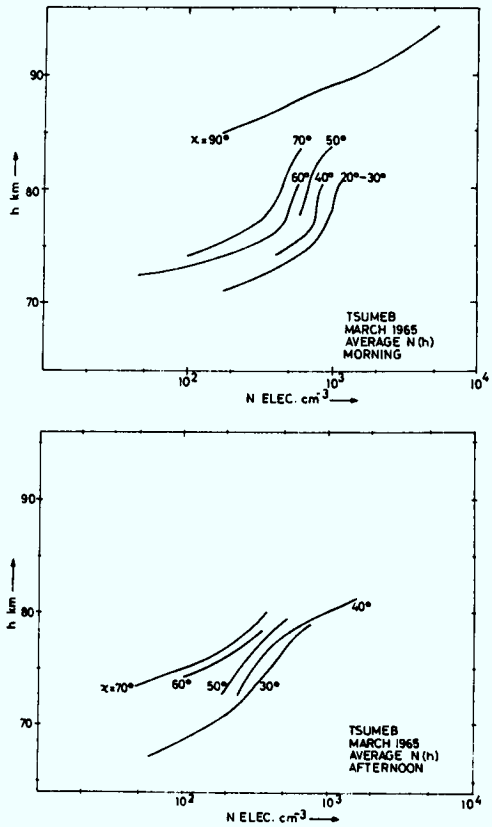

Fig. 4. Average electron density distributions for different solar zenith angles. Tsumeb, March 1965. These results are tentative.

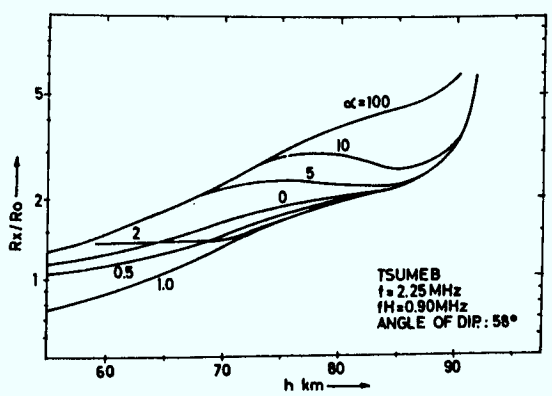

Fig. 5. Height variation of $\left|\frac{R_x}{R_o}\right|$ *for different values of* $a = (\Delta\nu/\nu)/(\Delta N/N)$.

Discussion on Paper 2.3.3 presented by E.V. Thrane

Smith: I find that last calculation hard to believe, especially as our polarization observations at Armidale were made on many echoes from the 70 km. region. We got this magnetic orientation effect as if the wave was incident in a vacuum on heights of 70 km. I just don't believe that calculation.

Thrane: I don't know. I knew I was probably sticking my neck out, but I don't really understand what is wrong here, if Budden is right. We have checked the calculations. At 70 km. the condition I had on the board here is far from being fulfilled, and you should expect the two waves to travel independently, and so any wave travelling downwards through the ionosphere should keep its characteristic polarization right down till it came to this region, shouldn't it?

Smith: Yes, but I wouldn't have thought that it was occurring so low down.

Thrane: Yes, this is what I expected too, but if my calculations are correct, this is what I get. I should be happy for any comments on this, if anyone can explain it.

Pfister: I want to say that this concept of a limiting polarization breaks down at any of the levels where you get a reflection. There really is coupling at the point of the partial reflection, so it must be coupling between the ordinary and extraordinary wave. You never talk about it, you say there is no coupling at this point.

Thrane: No, I tried to check this point also. As a matter of fact, I tried to calculate the reflection coefficients. Of course, there is coupling at the point where you have partial reflection, but this coupling is very small provided you don't have a great change in the collision frequency. If the gradient is in the electron density then you will have very little coupling.

Pfister: It depends on the gradient.

Thrane: It depends on the gradient, but I tried to put in reasonable sort of gradients that would give echoes of the order of magnitude you observe.

Bourne: We approached the problem in a slightly different way and noted that coupling was effective until the newly generated waves become out of phase with the waves from lower heights. For a typical D region profile this doesn't occur seriously until you get up to somewhere near 75 km. Below that the high collision frequency and the low electron density don't cause much differential phase shift between the two components. Without having gone into this in great detail, we would assume that coupling would be relatively effective up to this sort of level.

Thrane: Yes, I have no comments except that these calculations were made using Budden's theory.

2.3.4 STUDY OF THE LOWER IONOSPHERE BY MEANS OF PARTIAL REFLECTIONS

by

G.D. Falcon

ITSA/ESSA

National Bureau of Standards, Boulder, Colorado, U.S.A.

1. Introduction

This experiment was originally proposed by Gardner and Pawsey and improved by Belrose and Burke. The mechanism assumed for these reflections is that of Fresnel reflection due to sharp gradients or inhomogeneities of electron density in the lower ionosphere although the actual mechanism is most certainly more complicated than this. Piggott and Thrane recently called attention to the effect of irregularities of electron collision frequency, ν_m, on the reflection process. While specific values of the proportional change of ν_m relative to that of electronic density, N, would be difficult to determine, the resulting calculations of N can be determined for assumed values of $\frac{\Delta\nu}{\nu}/\frac{\Delta N}{N}$ in order to see where the effect is pronounced.

The received amplitude of the scattered echo can be expressed by $A_{e,o}=R_{e,o}\exp\left[-2\int K_{e,o}dh\right]$ where R = reflection coefficient, K = absorption coefficient, and the subscripts e and o refer to the extraordinary and ordinary components respectively. Thus the ratio of the received amplitudes is given by

$$\frac{A_e}{A_o} = \frac{R_e}{R_o} \exp\left[-2\int(K_e - K_o)dh\right]$$

The ratio of reflection coefficients, $\frac{R_e}{R_o}$, is almost completely independent of N when N is small, and is a function of the variable ν and of parameters wave frequency, electron gyrofrequency, and direction of propagation with respect to the earth's magnetic field. The collision frequency profile used in this analysis, from Belrose and Burke, is shown in Fig.1. The resulting calculated $\frac{R_e}{R_o}$ is given by the solid curve in Fig. 2. The dotted curve in Fig. 2 is computed for values of ν_m equal to one-half those of Fig. 1, at each respective height. The calculations of R_e/R_o are for a transmitted frequency of 2.666 Mc for conditions at Boulder, Colorado, where the experiments are being conducted.

2. Experimental Procedure

The present scheme uses a linearly polarized antenna to transmit a pulsed c.w. signal of 2.666 Mc vertically into the ionosphere. Peak transmitted power is 15 kw., the pulse width is 35 μs., and pulses are transmitted at the rate of 120 pulses per second. The receiving antenna consists of two perpendicular half-wave dipoles connected to two receivers in order to receive the ordinary and extraordinary components simultaneously. For the Boulder conditions, the received waves are both very nearly circularly polarized so that the variation of the ratio of reflection coefficients with the transmitting antenna orientation is quite small.

The received wave amplitudes are displayed on the different baselines on the same oscilloscope in A-scan presentation. The received pulse amplitude versus height presentation is recorded on 35 mm. film using a one-second exposure time. The photographs can be made at a rate down to 40 records per minute but a rate of 14 per minute is most commonly used. The high pulse repetition rate gives many oscilloscope traces during each film frame's exposure so that weak signal echoes are enhanced. Periodic checks are made to ensure the rejection of the ordinary mode signal in the X mode output channel and vice versa.

Measurements of A_e/A_o at a given height usually show considerable scatter, so that many samples of this quantity are necessary to give a statistically significant measure. Transmission periods of several minutes duration were used to obtain sufficient numbers of values of A_e/A_o over the desired height range.

Accuracy of determining the height of reflection is limited by the transmitted pulse length, receiver bandwidth, scaling error, and presence of echoes received from off-vertical directions. Thus the wave height resolution is limited to about 3 km.; hence the data is grouped into 3-km. subintervals.

3. Results

The A_e/A_o versus height data show considerable scatter for most transmission periods, so that the slope of this curve, which is required in the calculation, is difficult to determine in certain height regions. The slope is not so much in error at the higher altitudes where A_e/A_o falls off rapidly with height. At these heights, however, the calculated value of N is determined almost completely by the differential values of A_e/A_o because the value of R_e/R_o is changing very little in the region above, say 80 km. (see Fig. 2.). Hence as can be seen from the equation:

$$N(h) = \frac{1}{f(\nu)}\left[\left\{\ln\left(\frac{R_e}{R_o}\right)_{h+\Delta h} - \ln\left(\frac{R_e}{R_o}\right)_h\right\} - \left\{\ln\left(\frac{A_e}{A_o}\right)_{h+\Delta h} - \ln\left(\frac{A_e}{A_o}\right)_h\right\}\right]$$

the contribution to N from the $\left\{\ln\left(\frac{R_e}{R_o}\right)_{h+\Delta h} - \ln\left(\frac{R_e}{R_o}\right)_h\right\}$ term at higher altitudes becomes very small. In the height region from about 60 to 75 km., this same term has larger values due to the steeper slope of R_e/R_o. It is around the height of 70 km. that the A_e/A_o curve reaches a maximum before decreasing and it is here that its slope has the greatest uncertainty, so that the calculated electron density can be in serious error due to this term. The resulting error in N is not so great, however, because of the larger magnitude of the

$\left\{\ln\left(\frac{R_e}{R_o}\right)_{h+\Delta h} - \ln\left(\frac{R_e}{R_o}\right)_h\right\}$ term.

Fig. 3 shows electron density versus height for two days in July 1965. These and the following profiles are for near local noon periods unless otherwise specified. It could not be determined whether N continued to increase for heights down to 65 km., since echoes were not received at that height.

With regard to error bars for all of these profiles, a complete analysis of the contribution of all uncertainties to errors has not yet been made. The error in height has been mentioned before and is primarily due to off-vertical echoes, since scaling and A-scan presentation errors are not more than 1 km. At low heights the error in height should not be more than 2 or 3 km. due to oblique echoes. At higher altitudes, however, this effect becomes increasingly serious, so that at 90 km. the error could amount to several kilometers. Estimates of error in electron density, based on preliminary investigations, amounts to a factor of about three.

Figs. 4, 5, and 6 show profiles for days in September 1965, November 1965, and March 1966 respectively. These curves show that the average values of N at the higher altitudes are higher during the equinox periods than during the November period, but that the values at the lower heights show less seasonal variation. The relatively small change in N over the 70 to 80 km. height range cannot be explained at this time. It could be that the error factors mentioned before could mask small range variations over these altitudes.

It is emphasized that the error in height at 90 km. could be several kilometers due to oblique echoes, so that the values of N would be shifted downward by that error.

Attempts to establish a diurnal variation with the data analyzed so far have been inconclusive. The main problem during the winter months is that high noise conditions prevent good records except for two or three hours about local noon, when the variation appears to be within the experimental error. One good record in March 1966, is shown in Fig. 7. At this time the noise level was not excessive until about 1800 local time.

The effect on one profile shown earlier due to inclusion of the effects of perturbations of collision frequency is shown in Fig. 8. For this case, the fractional change of ν was assumed to be much larger than that of N. The modification is greatest at the lower heights and becomes quite small at higher altitudes.

The effect on calculated N for different assumed models of ν is shown in Fig. 9, where ν refers to values given in Fig. 1. Hence it is important to know ν as accurately as possible in evaluating numerical values of N. If ν could be determined independently, this would greatly improve the reliability of the derived electron density. One such method of determining ν has been proposed by Fejer. This involves measurement of the difference in phase, as well as amplitude of the two magnetoionic components. The differential phase versus path length is shown in Fig. 10 for two assumed electron density profiles. It appears feasible to measure differential phase at heights down to at least 70 km. Determinations of ν at only a few heights are likely to give a more accurate determination of ν over the region and time of interest than the use of a standard reference profile based on average conditions.

REFERENCES

Belrose, J.S. and M.J. Burke. J. Geophys. Res., 69, 2799-2818, 1964.

Fejer, J.A. J. Atmos. Terr. Phys., 23, 260-274, 1961.

Gardner, F.F. and J.L. Pawsey. J. Atmos. Terr. Phys., 3, 321-344, 1953.

Piggott, W.R. and E.V. Thrane. J. Atmos. Terr. Phys., 28, 311-314, 1966.

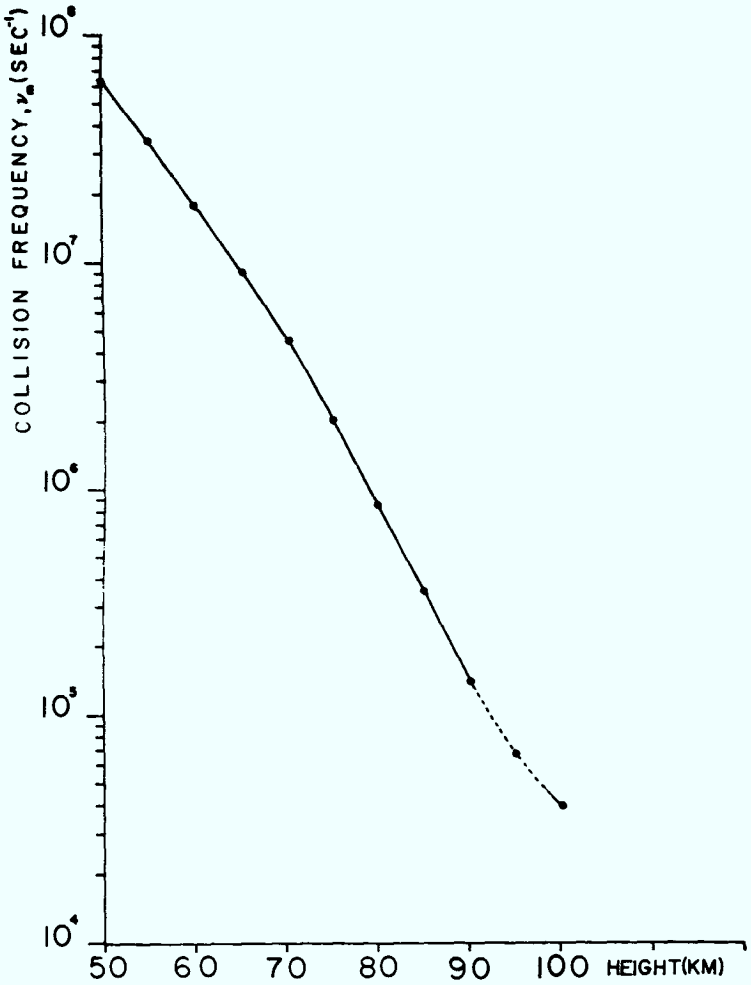

Fig. 1. Collision frequency of monoenergetic electrons vs height.

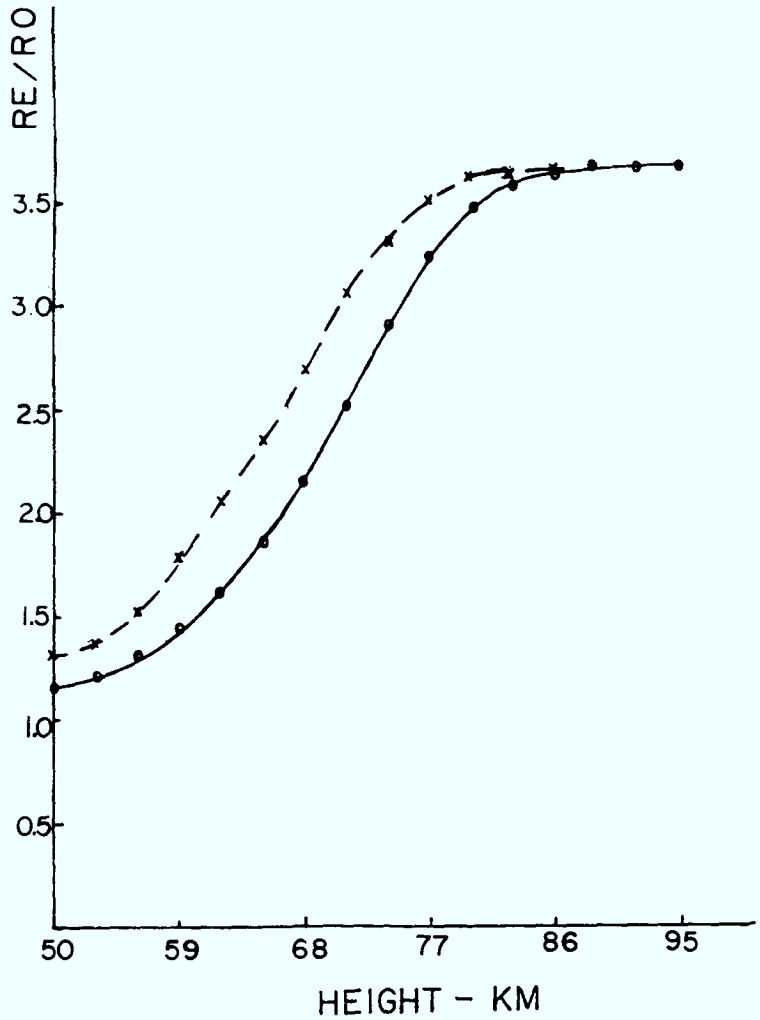

Fig. 2. Ratio of Reflection coefficients vs height.

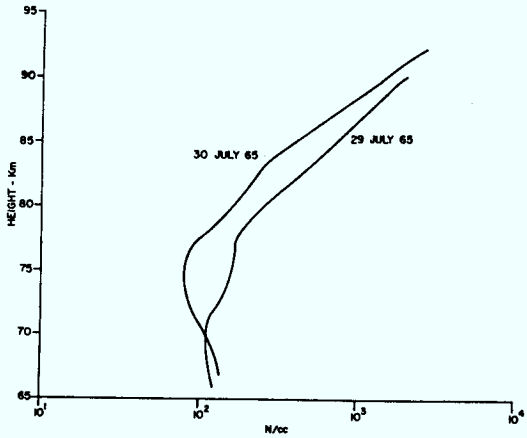

Fig. 3. Electron density – height profiles.

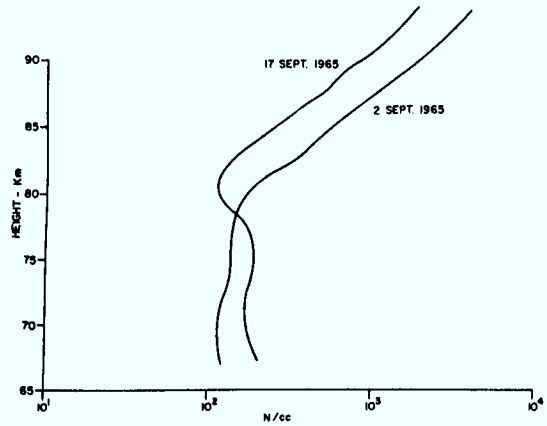

Fig. 4. Electron density – height profiles.

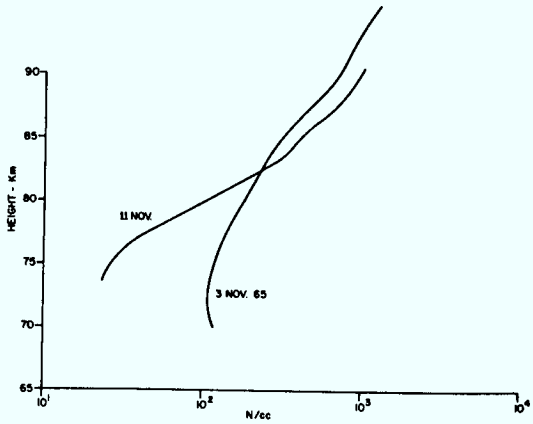

Fig. 5. Electron density – height profiles.

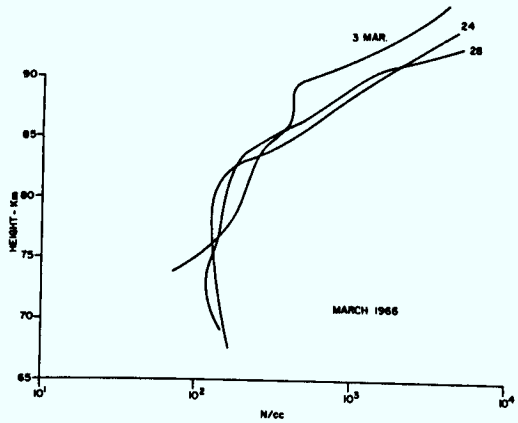

Fig. 6. Electron density – height profiles.

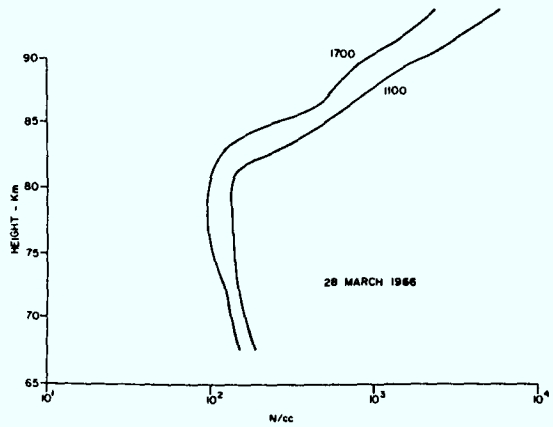

Fig. 7. Electron density – height profiles.

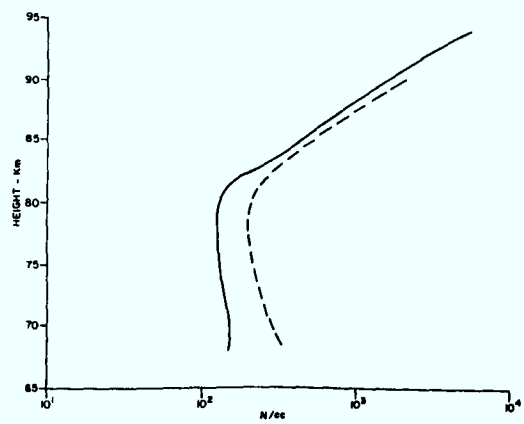

Fig. 8. Effect of considering $\frac{\Delta\nu}{\nu}$ in addition to $\frac{\Delta N}{N}$.

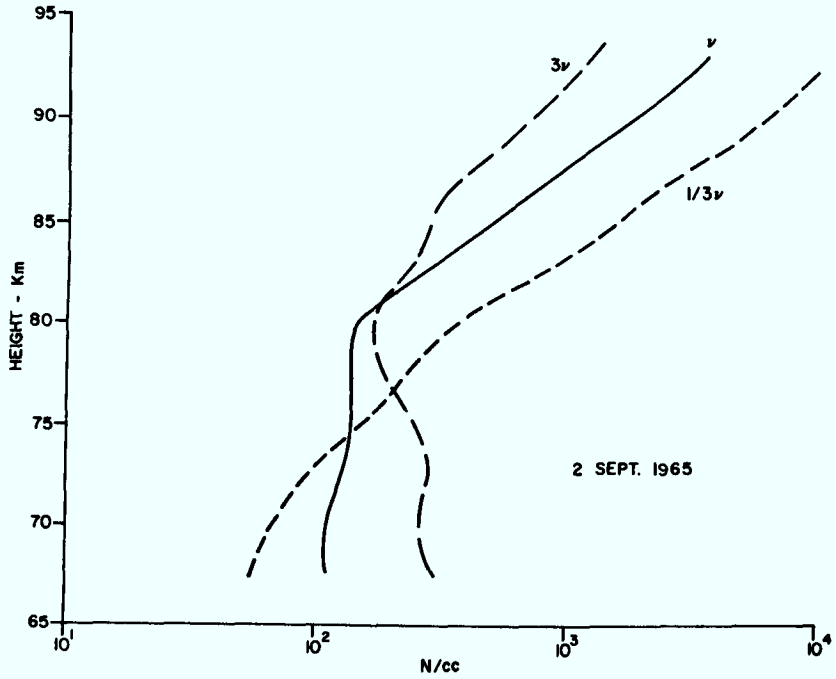

Fig. 9. Electron density – height profiles for various collision frequency profiles.

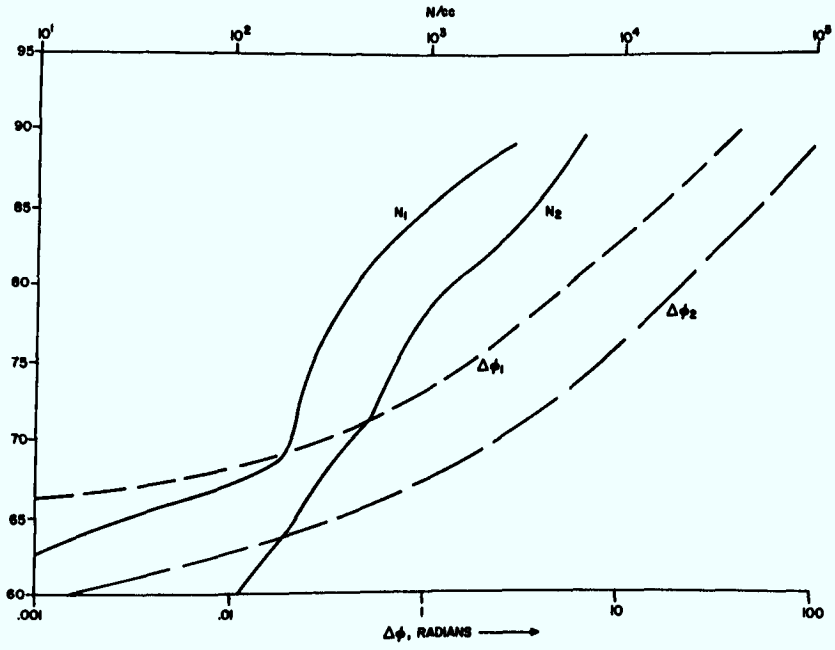

Fig. 10. Differential phase vs height for two different N(h) profiles.

Discussion on Paper 2.3.4 presented by G.D. Falcon

Belrose: My first comment is that if one compares the summer electron density profiles we have just seen with profiles measured at Ottawa and with those given by Dr. Thrane, we find that the profiles are in fact quite different. The lower latitude results for Crete have roughly exponential profiles in the range 70 to 85 km. or so. This is by and large true for Ottawa data; we go to slightly lower heights, but in summer the profiles are roughly exponential. They are also roughly exponential in March. The profiles shown by Mr. Falcon for summer months have almost constant electron densities over a height interval of 70 to 80 or 85 km. This seems curious, and is in discord with the other data seen this morning.

Falcon: This is true; in summer the values are approximately constant from about 70 to 75 or 77 km. I almost omitted the N values at low levels, because the calculation is extremely sensitive to the slope of the $\frac{Ax}{Ao}$ curve at these heights, since the electron densities are calculated from measurements near the turn-over point in the Ax/Ao curve. There probably is an increase in electron densities below 70 km., but I don't have reflections at low enough heights to tell whether they are going to increase or decrease at lower heights.

Belrose: At 80 km. you see far fewer electrons than shown by other data.

Falcon: The electron density value is about 2.6×10^2 at 80 km.

Belrose: That would differ from the results of the Ottawa data by approximately a factor of 5.

Haug: Do you have the zenith angle for your profile?

Falcon: No; these observations were probably obtained near 11 o'clock local time.

Elkins: I would like to ask about the spread in the data which could be answered, perhaps, by several of this morning's speakers. Could it not be due to a different type of reflection mechanism and might well be checked by determining the amplitude probability distribution? Have you done this yet?

Falcon: I am figuring out the distributions for the amplitudes to get some idea of what the reflection process actually is, but haven't completed this.

Elkins: It seems if you had true partial reflections, such as Bourne talked about this morning, you should have a displayed Gaussian type distribution in which the power of detected amplitude on the O and X wave should be proportional. However, if you have a scattering type of mechanism you would have a Rayleigh distributed amplitude distribution, and it is not so clear that the two would be proportional.

Falcon: Yes.

Hewitt: Do you know the gyro frequency and dip angle?

Falcon: The dip angle is $67\frac{1}{2}^\circ$ and the gyro frequency is about 1.42 Mc/s.

Bourne: In most of the simple theory, it is assumed that the perturbation in the electron density is a fairly sharp 'ledge'. However, it doesn't matter to the theory if there is a ledge or if the variation is smooth. In fact, an approximately exponential profile with a small sinusoidal 'noise-like' variation on it, extending over a few wave lengths, can be an extremely effective reflection mechanism, even though the perturbation in electron density is only of the order of 1 or so per cent. You don't need a very sharp gradient.

2.3.5 MESOSPHERIC ELECTRON DENSITIES AT 43°S

by

J.B. Gregory

Institute of Space and Atmospheric Studies
University of Saskatchewan, Saskatoon, Canada

1. Introduction

Observations of the lower ionosphere are often characterized by considerable variability. The nature of the variability is sometimes sufficiently obvious for the cause to be assigned with little ambiguity, for example in the solar proton influx at high geomagnetic latitudes. Other aspects of the variability have however resisted identification for a number of years, notably in respect to mid-latitude phenomena. This paper is concerned with the origin of a well-recognized but little-understood phenomenon of mid-latitudes, namely a variation which reaches its maximum in mid-winter, and which is in general a characteristic of the winter period. This variation has become known to workers in the northern hemisphere as "the winter anomaly of ionospheric absorption", but as will be shown its implications are not confined to the effect of ionospheric variations on radio waves. From a purely ionospheric point of view, however, the phenomenon involves both the electron density and collision frequencies. It may be identified in observations of the scattering of radio waves, both vertically and in the oblique forward mode, as well as in absorption. The basic origin of this winter effect will be shown to lie essentially outside the realm of ionospheric physics, and the observations in which electron densities play a prominent part are to be regarded as an advantageous method of investigating a dynamical phenomenon of the atmosphere below about 105 km. altitude.

The absorption aspect of this phenomenon has been documented by a number of workers in the northern hemisphere, and the study by Thomas (1962) includes a survey of much of available work. The absorption phenomenon has received relatively little attention in the southern hemisphere, although an early study by White and Straker (1939) contains evidence that the phenomenon did exist at 43° S. Similarly, Appleton and Piggott (1954) mention the existence of the phenomenon in the Falkland Islands at 52° S.

The related aspect of the phenomenon which appears in various forms of radio-wave scatter studies, has conversely received relatively little attention in the northern hemisphere. Workers using high power vertical incidence sounders have noted the existence of "low echoes" on certain winter days (Dieminger 1952). In their early study of the characteristics of forward scatter propagation, Bailey et al. (1955) suggested that a winter enhancement of scatter signal strength at medium to high latitudes in the northern hemisphere was related to the winter anomaly of ionospheric absorption. In the southern hemisphere a similar effect has been noted on a forward scatter path over a distance of approximately 800 km. (Gregory and Mawdsley, to be published). At 43° S some extensive studies have been made by high-sensitivity vertical incidence sounding techniques, and these are given in more detail below.

2. Mesospheric Partial Reflections

The results of a year's observations of vertical incidence soundings at a fixed frequency of 1.75 m/s. have been published (Gregory 1956, 1961). The first of these studies showed the great variability of the strength and fading rates of partial reflections as a function of altitude which could be observed in the mesosphere during the winter period. The second study shows that the heights of the reflections decrease markedly during the winter to values below 55 km. altitude. In contrast, reflections during the summer months of January and February often were absent below 65 km. It is to be noted that although these studies

refer to a period of high sunspot activity, from September 1956 to August 1957, the essential results have been duplicated throughout the solar cycle. It has not been possible to maintain an exact comparison of the scatter characteristics throughout all this time, but it is evident that the amplitude of the winter effect does respond to the variation of solar activity throughout the cycle.

Closely allied to the downward extension of the heights of scattering in winter is an increase in strength of scatter signals, again variable. This increase in strength is demonstrated in two ways, shown in Figs. 1 and 2. In Fig. 1 a series of monthly mean profiles of scatter signal strength, as recorded at hourly intervals for 3 hr. around local noon, is presented. These measurements are derived from an apparatus which used a plane-polarized array for both transmission and reception. Hence any polarization effects, and also the effects of absorption on ordinary and extraordinary components, have not been separated or allowed for in the data. It is obvious that at the lower altitudes the signals are essentially the extraordinary reflected component, while at the higher altitudes the ordinary component predominates. Examination of Fig. 1 shows that in general the scatter strength increases with altitude. A number of discontinuities can be observed, for example, around 80 km. in the summer months of January and February. Later work suggests that the location of these discontinuities may be related to the position of gradients of larger value than at other months. Discontinuities also exist at other heights in different months, e.g. May and June. The significance of these is not clear. The outstanding feature of Fig. 1 is the increase in scatter signal strength which occurs from March onwards to September, reaching a maximum in the months of June and July. In the latter month the signal strength is higher at all altitudes than at any other month. Fig. 1 also suggests that there is a second maximum of signal strength apparent at above 80 km. in the summer months. An alternative presentation is, however, desirable to show the latter point more clearly.

Fig. 2 shows a larger assemblage of data for the years 1956 to 1959 inclusive. The strength of vertically back-scattered waves at 1.75 Mc/s is shown for altitude ranges of 10 km. intervals. The data relate to noon values in most years, but for the period 1956-1957 three-hourly readings centered around noon have been included. Fig. 2 shows that the strength of the scattered waves varies throughout a period of six months from March to September-October, reaching a maximum in mid-winter at June-July. A minor maximum may be seen at the two higher altitudes between 74 and 94 km. in summer. At the two lower altitudes this minor maximum disappears and at the lowest altitude it has been necessary to accept data lying outside the noon period in order to continue the probable trend of the curve. The outstanding feature of this assemblage of data is that the seasonal variation of strength is entirely at variance with what would be expected from considerations of photoionization alone. The major winter maximum lasting half a year dominates the behavior of the scatter signal strength. As a check on the effect of solar zenith angle, a more limited selection of data throughout 1956 and 1957 has been analyzed at constant zenith angle conditions of $\cos \psi = 0.4$, and also at noon. The trends shown in Fig. 2 are confirmed and there is negligible difference between the constant zenith angle values of scatter signal strength and the noon values of scatter signal strength. It should be borne in mind that this analysis has not attempted to correct for variations of sunspot activity which could introduce fluctuations over a scale of the order of a few months. However, the assemblage of data for four years shows that sunspot activity is not a major factor in the over-all seasonal behavior of the scattered signals. Again the effect of ionospheric absorption at low altitudes, which might reduce the strength of scattered signals from higher altitudes, has not been included.

One further aspect of the back-scattering phenomenon affords some insight into the origin of the variability under discussion. Observations of back-scatter signals during hours of darkness show that at 43° S partial reflections are consistently reflected from heights in the region 80 to 85 km.; but not below this altitude. Early observations showed that reflection heights were lower than usual on nights following days of high absorption. This behavior has been investigated in more detail. In order to reduce the spread of values, monthly means of lowest heights of reflection for one year 1956-57 were compiled from 2 hr. after sunset to 2 hr. before sunrise. Data were arranged in two groups, (a) including all values in this period, and (b) omitting those values which followed days of high absorption. Since some exercise of judgment was often necessary to determine which values should be omitted, no statistical significance can be attached to this presentation of data. The two sets of monthly means are shown in Fig. 3. It will be observed that between September and March, the two sets of data differ by a negligible amount, indicating both that few periods of high absorption were involved and that night heights were little affected by daytime absorption. From March to August, the data for all values show a steady decrease to a mid-winter height, and then a recovery; while the data omitting values associated with high absorption show much less decrease in height. The portion of the year during which heights decrease coincides with the winter period of increased noon scatter strength (see Fig. 1). The association of lower than usual night heights with high absorption during day is thus seen to be a winter effect, with maximum decrease of monthly mean height in mid-winter. The period of decrease of monthly mean heights, during winter months, coincides with the winter decrease of pressure and density at 80 km., as tabulated by Kantor and Cole (1965) for 45° latitude (substituting southern for northern hemispheres). However, it is clear that the cause of the difference in monthly mean heights when high absorption conditions are omitted cannot be ascribed to a readjustment of monthly mean values of pressure or density. The effect implies an association of downward displacement of scattering heights with increased absorption, and since the latter is a fluctuating effect on a scale of days, a fluctuation of these scattering heights is also suggested.

Theories of radio wave scattering (Booker, 1959) show that the amplitude of scattered waves received at a distant location is essentially determined by the extent to which a macroscopic, or ambient, electron density is perturbed. Thus the data of Figs. 1 and 2 may involve variations in either or both of the ambient density or the perturbing mechanism. It is therefore desirable to examine ionospheric data in which one of these two factors is not involved. The only data available in sufficient quantity comprise the f-min. parameter from a local ionosonde (Godley Head). These data involve another factor, namely the possible variation of electron collision frequencies. However, f-min. values for the years 1958 to 1963 have been analyzed to determine the variation of monthly mean values. Constant zenith angle conditions of $\cos \psi = 0.4$ have been selected. Although a solar cycle variation is clearly evident throughout these six years, the basic seasonal variation remains unchanged, and is shown by the mean curve for the total period given in Fig. 4a. The seasonal variation of the f-min. parameter reveals in general the same basic feature as does the scatter data, namely, an increase to a maximum in mid-winter with minima in March and October, and a smaller maximum in summer months. The f-min. data differ from the scatter data in that the winter maximum is not symmetric and maintains higher values between July and September than does the scatter data. Since the f-min. parameter is determined by the total column concentration of electrons below the height of reflection, usually in E region, weighted by the effect of collision frequencies at each altitude, it is not possible to make an altitude comparison as was done for the scatter data.

It is possible to write down in principle the functional dependence of the scatter signal and the f-min. values on the three possible variables of perturbed electron density, ambient electron density, and collision frequency. When this is done it would appear that the only factor that is common to the two sets of data is the ambient electron density. However, this argument fails to show the variation of electron density with altitude, although the curves of Fig. 2 suggest that the increase in the latter may be largest at the higher altitudes, i.e. above 74 km. It is therefore necessary to turn to more precise measurements of electron densities.

3. The Variation of Electron Densities

In assembling the data of Figs. 1 to 3, monthly mean values have been used. While this has served to show the existence of a marked seasonal variation contrary to that expected from a supposedly solar dominated phenomenon, the period of a month is still long in comparison with other known fluctuations of mesospheric values. The "winter anomaly of ionospheric absorption" has always been associated with the occurrence of "winter days of high absorption". The duration of groups of these days of high absorption is generally short compared with a month and therefore a more detailed time scale of investigation is desirable.

It may be commented at this juncture that the existence of a close link between days of high absorption and days of enhanced back-scatter from mesospheric heights was established early in the scatter studies made at 43° S. At the working frequency of 1.75 Mc/s, a series of observations on particular winter days of high absorption would often present a remarkable aspect. The absorption would be sufficient to render signals reflected from the E region of the ionosphere undetectable, but at altitudes usually above about 67 km. and not above 85 km., the scatter signals would be enhanced by as much as 24 db, while at the same time their fading rate was greatly increased. An illustration of the connection between ionospheric absorption and the strength of scatter signals in the height range 75 to 80 km. has been published (Gregory, 1965). Viewed from the aspect of the scattering of radio waves, the winter phenomenon is one of great variability, and it appeared to be more logical to inquire as to the reason for the variability from day to day than to attempt to ascertain monthly average values, e.g. of electron densities. A study of the electron density profiles was therefore commenced, having as one of its primary objects the determination of the cause of the day-to-day variability and also the seasonal aspects which are implicit in the data of Figs. 1 to 3.

The application of differential absorption techniques to measurements of electron densities at 43° S, with particular reference to periods of high absorption in winter, has been described previously (Gregory, 1965). The essential finding in relation to one major absorption period, of nine days duration, was the change in stratospheric temperatures which accompanied the absorption change. When isopleths of electron density shifted to lower heights in the mesosphere, stratospheric temperatures increased, and when the electron density contours restored to original heights, temperatures decreased. This linkage of behavior, over an altitude distance in excess of 50 km., suggested that vertical motion was occurring simultaneously in the two regions.

A more detailed study of this effect has now been made, with attention to the circulation patterns existing in the troposphere and the stratosphere, up to the limit of meteorological balloon observations at about 30 km. or 10 mb. Calculations of vertical motion in the stratosphere have been made by New Zealand Meteorological Service. The adiabatic method of calculation was employed, and although some deficiencies of data resulted in reduced accuracy, the sign and approximate magnitude of the stratospheric vertical motion has been determined. A gap in total available data exists from 30 km., the meteorological balloon limit, to just below 60 km., where partial radio wave reflections provide usable information. At this juncture, no positive measurement of vertical motion above 30 km. is available in relation to the periods studied.

An assemblage of data for the period 21 to 29 June, 1963 is shown in Fig. 5. At A, the variation of noon electron density isopleth heights, previously given by Gregory (1965), is shown. The electron density profiles from which the curves of Fig. 5A were plotted were derived on the assumption of a collision frequency profile which did not change throughout the period. This assumption is probably invalidated by the further data of Fig. 5. A detailed investigation has been made of the possible effect of change of collision frequency on the resulting electron density profiles. In summary, this investigation shows that the errors in the profiles will be of opposite sign above and below a particular altitude, at which the normalized differential absorption maximizes. In present work, that altitude occurs for the collision frequency model adopted at 73 km. Since the trends of isopleths in Fig. 5A are similar above and below 73 km., it is unlikely that the changes evident in Fig. 5A are attributable to change of collision frequency alone.

The changes in stratospheric temperatures which accompanied the isopleth height changes of Fig. 5A have been described above. The vertical motion in the stratosphere is shown in Fig. 5B. It will be noted that downward motion in the stratosphere occurs while electron densities increase with time in the mesosphere, and upward motion occurs while densities decrease. The time of changeover from downward to upward motion agrees, within the sampling period of one day, with the change of slope of the isopleths.

Further investigation of stratospheric and tropospheric conditions shows that a well-defined pressure ridge passed over the observing site within one day of the time of change of slope of isopleths, i.e. on 27 June. Fig. 5C shows the height, in geopotential meters, of the 20 mb. surface, during the period. Fig. 5D shows the approximate position of the pressure ridge, as judged from successive daily 200 mb. charts, along the zonal direction. Fig. 6 shows the 200 mb. chart for June 25, 1963. The ridge whose position is plotted in Fig. 5D lies with its axis commencing in the Australian Bight and extending slightly east of south. It is noticeable that a large trough, extending over 40° of latitude, precedes the ridge. The sudden drop in isopleth heights, evident in Fig. 5A between 21 and 22 June, is simultaneous to within one day with a rapid increase of heights of all constant-pressure levels from 20 mb. down to below 300 mb.

This instance of the passage of a pressure ridge in the westerly winter flow, accompanied by electron density increases and presumably also collision frequency increases, has been shown through continuing studies to be typical of groups of "days of high absorption" at various periods of winter in the years 1956-64 at 43° S. At this juncture, the following interim findings may be listed:

(1) In the southern hemisphere, the increases of ionospheric absorption, which can be recognized through the characteristic increase of f-min. values between 0900 and 1700 hours local time on winter days, are the accompaniment of pressure ridges overhead to within a 24-hour period. More than 80 per cent of the groups of "winter days of high absorption" in 6 years show this association.

(2) Similarly the passage of troughs can be associated with a decrease of f-min., though, due to technical factors, notably the change of sensitivity with frequency of ionosondes, the effect is less evident. (More accurate ionospheric measurements are expected to confirm this trough decrease association.)

(3) Allowing for a probable but uncertain change in electron collision frequency, electron densities in the mesosphere at given heights are positively correlated with the pressures in the stratosphere and troposphere.

(4) The atmosphere below 30 km., often down to 3 km. (700 mb.), shows a coherent behavior during the passage of these pressure systems, i.e. the changes of pressure are closely paralleled in this range of altitudes.

(5) If the vertical displacements of isopleths of electron densities are real and not apparent, the accompanying vertical velocities in the mesosphere are in the range up to 10 cm./sec. The corresponding actual vertical velocities in the stratosphere are nearer 1 cm./sec.

(6) Simultaneous studies of mesospheric winds have shown the variation in height of transition of westerly to easterly zonal flow. This transition height rises to a maximum of about 105 km. in the winter so far studied at 43° S (G.J. Fraser, private communication). Preliminary studies indicate that there is a correlation between this transition altitude and the maximum altitude at which increases in electron densities can be detected.

4. Discussion

A sufficient number of examples of mesospheric electron density increases has now been studied in detail to confirm an essential similarity of behavior. In each instance, the increase is associated with a pressure change at lower altitudes. However, a pressure change at a lower altitude does not necessarily imply a change in the pressure profile, for example, in the mesosphere. In this respect, the existence of strong vertical motion is more acceptable. The main requirement of the process which underlies ionospheric absorption increases is the establishment of larger electron densities in a region of given pressure, i.e. of collision frequency. This requirement can be met in principle by sufficiently rapid vertical transport of minor constituents.

From a dynamical viewpoint, the observable stratospheric pressure changes are an aspect of the passage of baroclinic waves, moving at about 500 to 1000 km./day in the westerly flow of the southern hemisphere. The role which longer or slower moving waves, such as Rossby waves, may play in affecting the mesosphere has yet to be determined. However, it is evident that a number of findings by Thomas (1962) concerning the "winter anomaly" can be explained on the hypothesis of wave motion, involving vertical transport, in the mesosphere. While the actual consequences of wave penetration from the lower atmosphere into the mesosphere remain to be established, it is instructive to re-examine the ionospheric scatter and absorption evidence presented in Figs. 1 to 4.

Since the wave motion is a fluctuation, with a time scale shorter than a month, it is to be expected that mesospheric values, e.g. of absorption, should also show a fluctuation aspect. Accordingly, the coefficient of variation of f-min. values, defined as standard deviation/mean, has been computed for a number of locations and years, by month, using the 5-hourly readings centered around noon. Fig. 4b shows the mean of four years' data for Godley Head, 43° S. A minimum coefficient is reached in March, and again in November, with maximum in June. Other southern hemisphere mid-latitude stations show similar behavior, but the coefficient of variation varies from year to year for a particular winter month, and is less in summer months. Thus the fluctuations repeat the essential seasonal features of the monthly mean values.

The basic winter ionospheric behavior thus stretches from autumn equinox, where it is clearly defined, to beyond the spring equinox, where it is less well defined. At latitudes around 40° to 50° S, the winter effect is in general not less than seven months duration. This period is also that of the growth and decay of the westerly mid-latitude circulation. No detailed studies of that circulation for latitudes poleward of 40° S, and for altitudes up to 100 km., exists. The study reported by Rofe (1963), shows that a westerly regime from surface to 60 km., in latitudes greater than 40° S, is to be inferred. It remains to be determined whether this regime will support the upward penetration of baroclinic waves, and what development of the wave takes place in the vertical direction. The ionospheric evidence suggests that the upward propagation does occur in the westerly flow, and that the associated vertical motion, which may affect highest altitudes in mid-winter, has an important mixing action in redistributing minor atmospheric constituents in both upward and downward directions.

Finally, since various analyses at constant zenith angle have shown summer maxima, of less amplitude than the winter maxima, it appears possible that some wave propagation may be effective in the easterly regimes of the summer circulation.

Acknowledgments

The experimental aspects of this work were conducted while the author was a member of the Physics Department, University of Canterbury. Financial support was given by the National Science Foundation of USA., and by the Universities Research Committee, New Zealand. The assistance of the Director and staff, New Zealand Meteorological Service, is gratefully acknowledged.

REFERENCES

Appleton, E.V. and W.R. Piggott. Ionospheric absorption measurements during a sunspot cycle. J. Atmos. Terr. Phys., 5, 141-172, 1954.

Bailey, D.K., Bateman, R. and R.C. Kirby. Radio transmission at VHF by scattering and other processes in the lower ionosphere. Proc. I.R.E., 43, 1181, 1955.

Booker, H.G. Radio scattering in the lower ionosphere. J. Geophys. Res., 64, 2164-2177, 1959.

Dieminger, W. On the causes of excessive absorption in the ionosphere on winter days. J. Atmos. Terr. Phys., 2, 340-349, 1952.

Gregory, J.B. Ionospheric reflections from heights below the E region. Aust. J. Phys., 9, 324-342, 1956.

Gregory, J.B. Radio wave reflections from the mesosphere. J. Geophys. Res., 66, 429-445, 1961.

Gregory, J.B. The influence of atmospheric circulation on mesospheric electron densities in winter. J. Atmos. Sci., 22, 18-23, 1965.

Kantor, A.J. and A.E. Cole. Monthly atmospheric structure, surface to 80 km. J. Appl. Met., 4, 228-237, 1965.

Rofe, B. Australian sounding rocket experiments. Weapons Research Establishment, Australian Department of Supply, Technical Note SAD127, (unclassified), July 1963.

Thomas, L. The winter anomaly in ionospheric absorption. Radio wave absorption in the ionosphere, 301-317, 1962. New York, Pergamon.

White, F.W.G. and T. Straker. The diurnal variation of absorption of wireless waves. Proc. Phys. Soc., 51, 865-875, 1939.

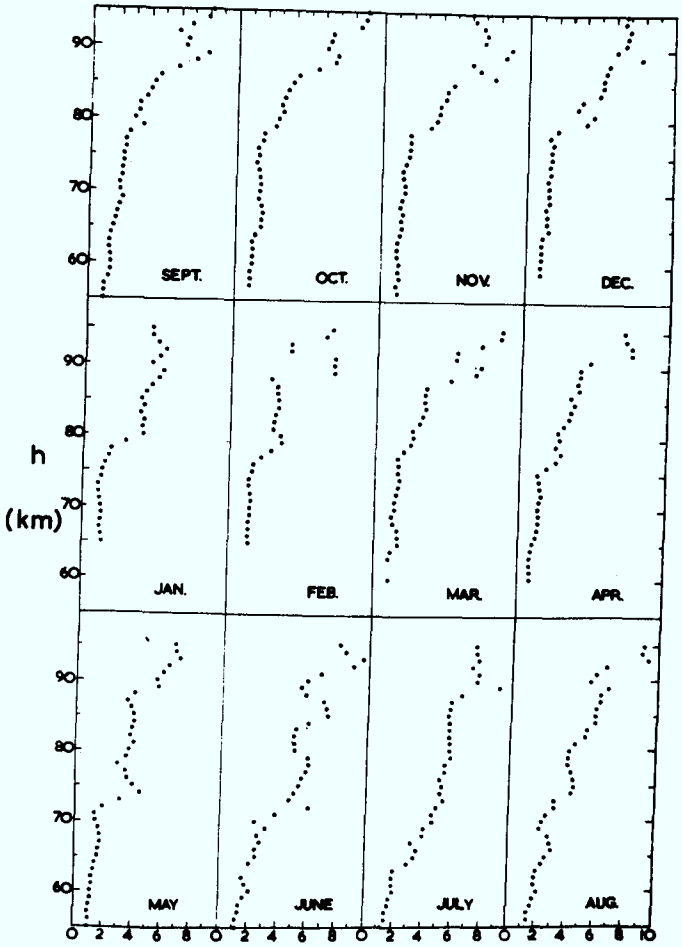

Fig. 1. Height profiles of strength of vertically back-scattered waves, 1.75 Mc/s. Points are monthly mean values of three readings at hour intervals centered on local noon, 1956–1957. Abscissae are in units of 6db.

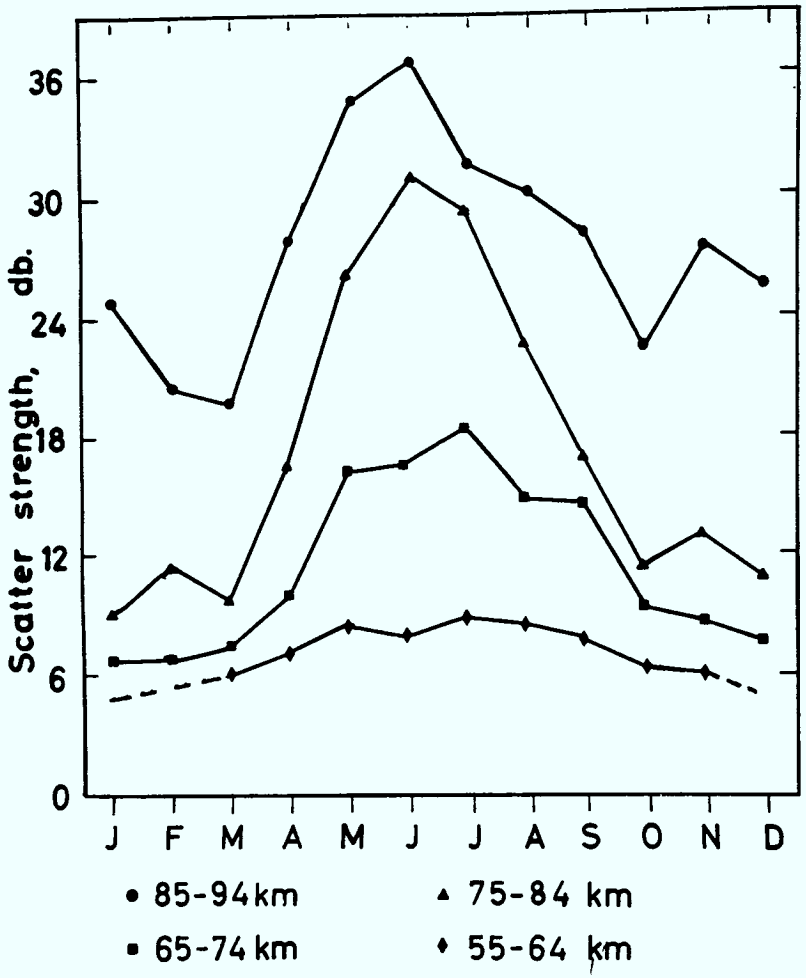

Fig. 2. Seasonal variation of strength of vertically back-scattered waves, averaged over 10 km. altitude intervals. Monthly means are of noon values from 1956–1959.

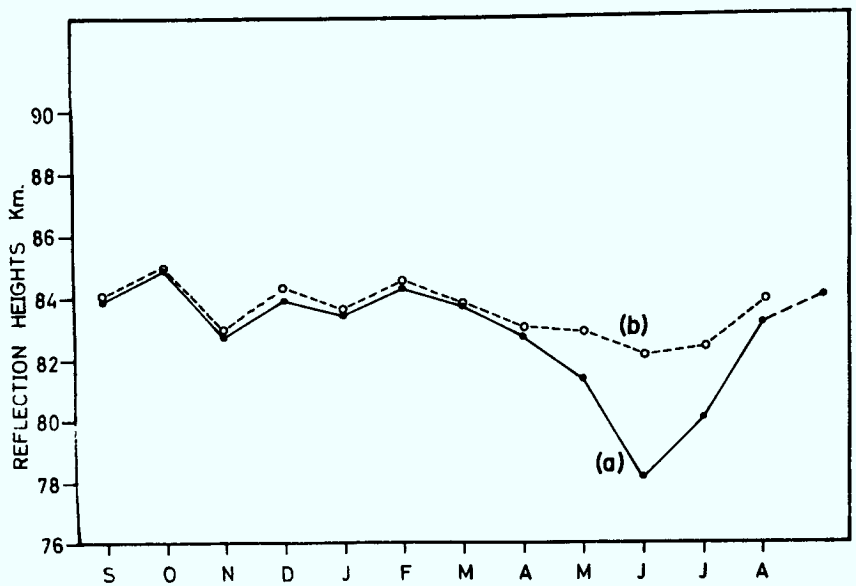

Fig. 3. Monthly mean values of lowest reflection heights at 1.75 Mc/s, night hours, (a) all values, (b) data omitted following days of high absorption, 1956–1957.

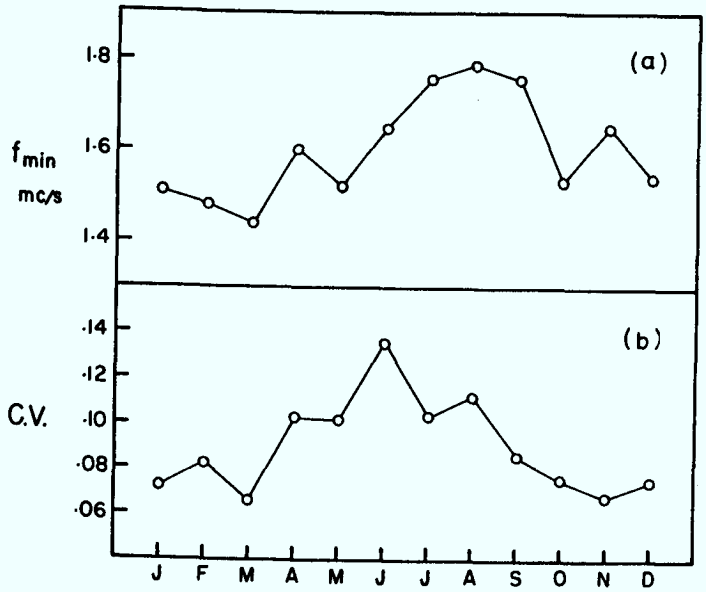

Fig. 4(a). Monthly mean values of f-min.. selected at constant zenith angle, cos x = 0.4, for the years 1958–63, at 43°S (Godley Head).

Fig. 4(b). Monthly coefficient of variation, (C V) for the data of (a).

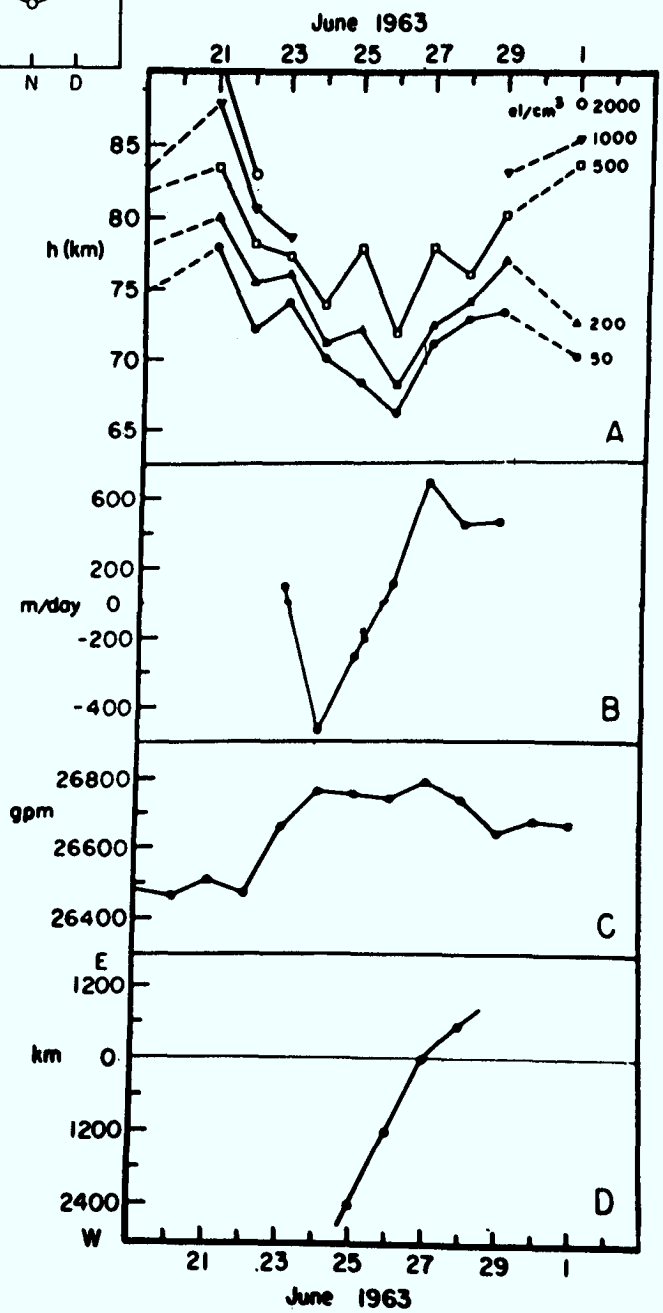

Fig. 5. Data for absorption event of 21–29 June, 1963, 43°S.
(a) Electron density isopleths.
(b) Vertical motion, meters/day, 200-150 mb. levels.
(c) Height of 20 mb. level, geopotential meters.
(d) Position of pressure ridge, with respect to Christchurch, New Zealand.

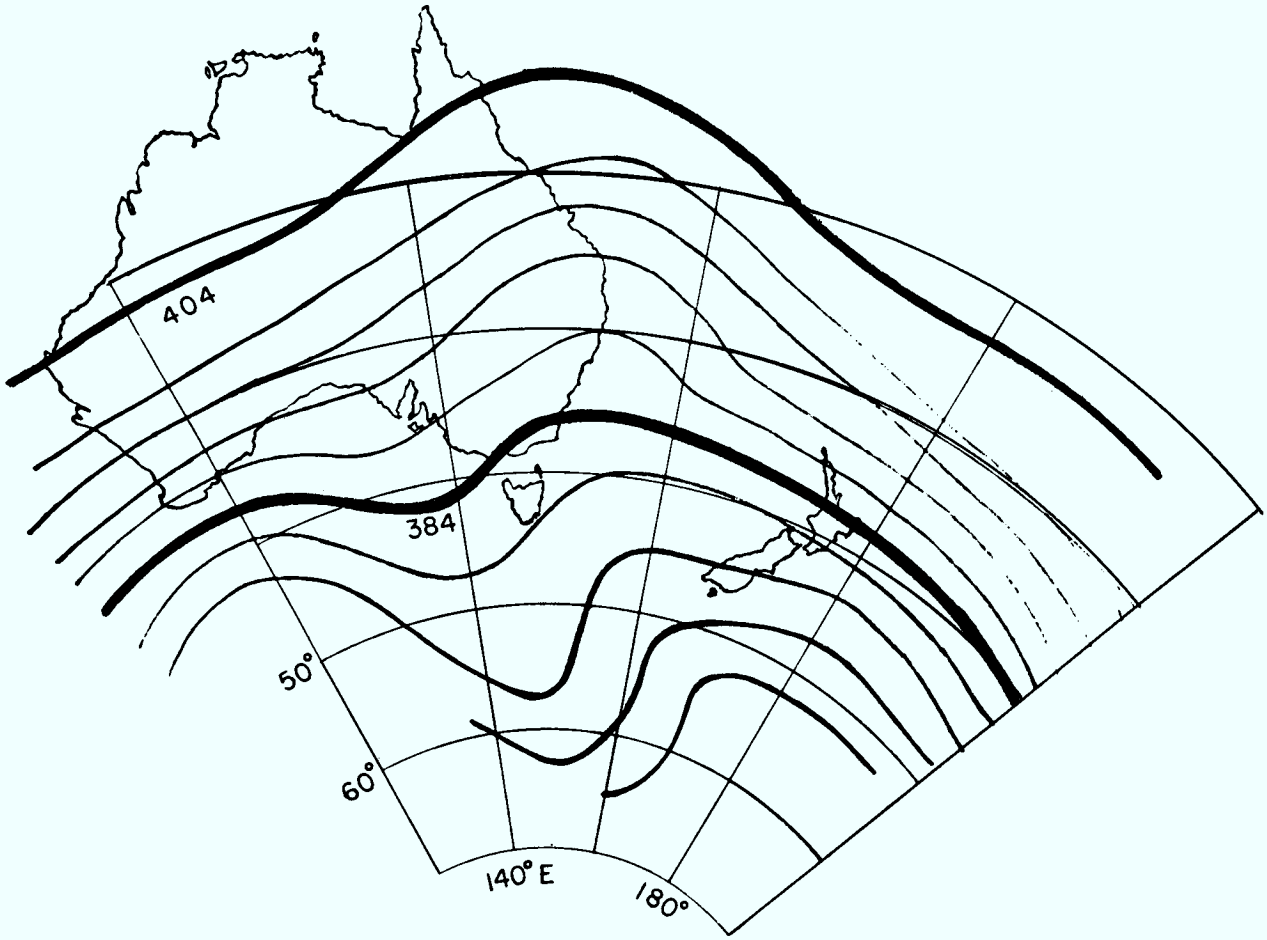

Fig. 6. 200 mb. chart for 25 June, 1963.

Discussion on Paper 2.3.5 presented by J.B. Gregory

Hewitt: Did you look at the magnetic activity at the time you saw these increased electron densities at low heights?

Gregory: Yes, we did that years ago. I think that various people at various times have adequately disposed of this question; for example, the work by Lange-Hesse in the Northern Hemisphere. Our own geomagnetic latitude is 47°, and it would be a very unusual event which would pour any sort of recognizable particle precipation into the mesosphere for six or seven days exactly in synchronism with the passage of a pressure trough. About 80 per cent of the mesospheric events are connected with the stratosphere; the fraction which connects with all K-index variations is small. I am aware that you people have seen this, but I have already pointed out that this is an effect and not a cause.

Wright: On a day of high absorption (a winter anomalous day), does the absorption increase more rapidly at sunrise?

Gregory: I couldn't say. The partial reflection experiment isn't really reliable, as Belrose has said, until a couple of hours after sunrise. I have resolutely rejected the f-min. data at sunrise and used it only between 10 o'clock and 3 o'clock, and at that time the effect is easily recognized. You can see the effects just by glancing through the f-min. sheets.

Zimmerman: You hypothesize then, that these pressure oscillations are created in the 600 mb. area?

Gregory: I didn't say that; they are a perturbation of the westerly flow, and the big question basically is what are the conditions that are necessary in the westerly flow baroclinic atmosphere for the wave to propagate upward. As I said, at the base level there are the ordinary cyclones and anticyclones. The wave motion becomes cleaner in the troposphere, and as it gets up higher into the stratosphere, it looks like a wave motion, but it looks as though it is baroclinic towards the planetary waves.

Zimmerman: The second question; from what I understand of the data, there is no phase lag?

Gregory: It is still too crude to give you an explicit answer to that. I have thought this over carefully, and we need much more data and a sophisticated technique of analysis by cross-spectral analysis to tell. I can guess at a number of things, but none of them are precise.

Whitten: Have you ever thought about what a hurricane might do?

Gregory: Yes, we had one slight advantage, we didn't have any hurricanes. Mind you, these things do enough; the big southerly fronts are associated with these things

Zimmerman: Have you analyzed the diurnal variation in your partial echo data to see if the tidal oscillations could produce a similar effect?

Gregory: I don't know what effect the tidal oscillations would have.

Zimmerman: They would all support the pressure variations, perhaps not so much in that altitude region.

Gregory: It should be remembered that these events have a time scale of days, the average scale being two, three or four days; some are as short as one day.

To make one last comment, I think that probably the southern and northern atmospheres are rather different in this respect, and that the reason that this hasn't been seen as clearly in the northern hemisphere is that the very big standing wave known to exist over the North American continent, for example, probably damps out the propagation effect, or hinders the propagation of these fast-moving baroclinic waves.

2.3.6 PARTIAL REFLECTION EXPERIMENT DURING THE 1965 ECLIPSE

by

H.A. von Biel

Cornell Aeronautical Laboratory, Buffalo

1. Introduction

As a part of the 1965 Eclipse Program, the Cornell Aeronautical Laboratory conducted a Partial Reflection Experiment on Aitutaki in the Cook Islands. This effort was sponsored by the Defense Atomic Support Agency and had the primary purpose of obtaining D region electron density profiles before, during, and after the May 30 solar eclipse, so that we can determine the variation in time of electron density associated with the eclipse.

Conceptually, the experimental technique employed by us was identical to the original experiment of this kind reported by Gardener and Pawsey. That is, the differential absorption between the characteristic modes of propagation was measured for various backscatter heights in the D region. In processing of our data, use was made of the generalized magneto ionic theory advanced by Sen and Wyller, and the tables of semi-conductor integrals published by Burke and Hara.

2. Instrumentation

Specific frequencies of operation and instrumentation details for conducting the partial reflection experiment have in the past differed substantially from experiment to experiment. In implementing the Cornell experiment, we had to work within the framework of certain fundamental constraints dictated primarily by available time.

We had exactly four months during which to design, construct and test the instrumentation, to install and make the experiment work on Aitutaki Island, and to collect the required data.

In our experiment, separate antenna arrays were used for transmission and reception. Both arrays were circularily polarized. The transmitting antenna (Fig. 1) consisted of two orthogonal six-element colinear arrays which were excited in time quadrature. The linear dimension of each six-element array, at our operating frequency of 2.4 mc, was about 1200 ft. The receiving array consisted of orthogonal halfwave dipoles also excited in time quadrature. For both arrays the polarization was changed by altering the excitation phase to one of the orthogonal legs by 180°.

The transmitter used for our experiment had a peak power capability of 200 kw. We normally operated at a power level of about 150 kw. and a pulse width of 25 μsec.

The receiver employed had a bandwidth of 40 kc. and was range-gated to display echo ranges from about 50 to 100 km. The gating circuitry was capable of a minimum range display of 45 km. and a maximum of about 300 km. Particular attention was given to the design of the receiver output stages. Two outputs were provided, the first being linear, with input, from noise level to +30 db, the second being linear from +20 db to +50 db. These outputs were displayed alternatively on a cathode ray oscilloscope. The display, in turn, was recorded on photographic film, which moved past the oscilloscope screen at a rate of 10 in. per sec.

In recording our A-scan data we alternately displayed three echo ranges from 0 to 30 db and three echo ranges from 20 db to 50 db (Fig. 2). Then we switched polarization and repeated the sequence. The time interval between successive pulses was 60 msec. corresponding to a prf of 16 2/3. Thus a complete set of O wave and X wave data required 720 msec. This rate was judged adequate in view of the echo fading rate which appeared to be of the order of several seconds.

3. Equipment Calibration and Data Collection

O-X identification was made by observing F-region splitting which occurred on several nights (Fig. 3). Antenna polarization was indicated on our film by the presence or absence of a dark line on the edge of the film. Because of the physical placement of the argon bulb which caused this line, this polarization flag starts two pulses late and ends two pulses after polarization has been switched. By this rule, and through the use of the F-region echoes, we conclude that the dark line indicates echoes of the ordinary wave. This test was repeated several times with identical results.

We also attempted to assess the amount of background noise at our frequency. Tests showed that our receiver had a threshold sensitivity of −111 dbm, and that during daylight hours the background noise and interference level was below this value. At night, however, background noise amounted to about −100 dbm to −95 dbm. No partial reflections from the D region were observable at nighttime.

4. Observational Results and Data Analysis

Partial reflection data were collected for 2 min. of every hour between sunrise and sunset on pre-eclipse and post-eclipse days. On May 30, 1965, data were collected continuously from one-half hour before totality until one-half hour after totality. For the times from T−120 min. to T+150 min. data are available in 10-min. intervals. Beyond T+150 min. the normal schedule was followed.

Data collected on pre- and post-eclipse days indicate that approximately half an hour after local sunrise, echoes are observable below 75 km; about one hour after sunrise, weak echoes are noticeable in the 50 km. range and two hours after sunrise reliable strong echoes appear at altitudes as low as 45 km. Disappearance of all echoes below 80 km. occurs within half an hour after local sunset, at which time the noise level increased very rapidly.

Statistical treatment of "non-eclipse" amplitudes at any given range and polarization has shown them to be "Rayleigh-like" distributed. Fig. 4 shows a typical example. We have encountered ranges where the amplitude distribution is definitely non-Rayleigh, but if, for example, a non-Rayleigh range exists for the O wave, the corresponding X wave range may or may not be Rayleigh-distributed. The exception to this finding occurred for all of the data collected during the eclipse which exhibit very definite "Rice-like" distributions.

In our analysis we have looked for preferred heights from which echoes originate and have not found them to exist. This conclusion is based on the technique employed to analyze our data, in which the most probable received power at any given range and polarization is computed from about 160 consecutive A-scans. The resulting curve of received power as a function of range is quite smooth and does not substantiate the "preferred height" theory. The correlation between X and O amplitudes was examined and was found to be quite low (Fig. 5). It is evident that the correlation coefficient rarely exceeds a value of 0.3. Consequently one would expect that the instantaneous ratio of the X amplitude to the O amplitude is not a meaningful quantity. For this reason, in our analysis we computed the ratio of most probable power in the X wave echo to the most probable value of power in the O wave echo at any given range.

The echo fading for data collected on non-eclipse days appears to be of the order of 2 sec. Fig. 6 shows the decorrelation times for echoes from various heights. It is interesting to note the long decorrelation time (indicative of steady echoes) at about 72 km. In general, the echoes observed below 70 km. were quite steady and showed little fading.

Our data analysis technique followed closely that reported by Belrose and Burke, with the exception that the "peak-scaling" method was not used. Fig. 7 represents a typical example of the received power ratio profile, together with a power reflection coefficient profile computed for collisional frequencies consistent with the 1959 standard ARDC atmosphere. Ideally, these two profiles should be identical up to an altitude where differential absorption becomes important. Most of our data indicate that these two profiles depart from one another at an altitude near 70 km. Below that altitude the $[Ax^2/Ao^2]$ curve exhibits a behavior which is most perplexing! Generally, in the 50- to 70-km. range, values of $[Ax^2/Ao^2]$ fluctuate considerably both plus or minus from the theoretical power reflection coefficient curve. One possible (and also highly probable) mechanism that would explain this behaviour is the reception of echoes from directions other than vertical. If one makes allowance for possible angles of arrival of 25°, the error in the observed results can be shown to be as large as plus or minus 20 percent, a magnitude which is consistent with our observations. It is for this reason that we have restricted our data analysis to altitudes in excess of 70 km.

The overall results from our experiment are shown in the following figures. Fig. 8 shows the average of 3 non-eclipse noontime profiles. The magnitudes of electron density obtained certainly appear reasonable and we conclude that the instrumentation did not have any obvious faults. Before presenting and discussing the results from data collected during the eclipse, it is of interest to examine a typical set of eclipse A-scans (Fig. 9). It is evident that there is little resemblance between normal A-scans and those observed during the eclipse. One of the more striking observations made during the eclipse was the fact that the average echo intensity was between 25 db and 30 db stronger than on normal days. This fact necessitated attenuation of both the X signal and the O signal to prevent receiver overloading. Even with 25 db of attenuation in the antenna leads, note that the 0 to 30 db range for the O wave is saturated. Also note the deep and periodic fading which is particularly noticeable in the 0 to 30 db X wave channel, but occurred just as much on the O wave channel. This observation could be explained if one assumes the existence of two, or possibly three, main scattering centers. Incidentally, the noise background during the eclipse was significantly larger than on normal days. In particular, we noticed a large amount of what appeared to be spherics activity and, for a while at least, were concerned about data contamination by this interference. Fortunately, the contaminated data are easily recognized and amount to a small percentage of the total. Fig. 10 represents a composite of electron density profiles obtained at various times during the eclipse. It is interesting to notice that the electron density in the 70- to 80-km. range was not noticeably influenced by the eclipse phenomenon. In contrast, the electron density above 80 km. appears to be substantially affected. Recovery of electron density appears to start noticeably at about 30 min. after totality. Fig. 11 shows that 80 min. after totality the altitudes above 80 km. have recovered. The eclipse noontime profile appears to be normal.

The following figures present the same data, but arranged so that the electron density history can be observed for any given altitude. Fig. 12 indicates that in the height region from 70 to 75 km. not much of anything happened. Fig. 13 shows a noticeable effect taking place at 77 km., which becomes more pronounced at 78 and 79 km. A very definite peaking in the electron density can be observed at approximately 30 min. after totality (Fig. 14). This peaking exists out to 84 km. (Fig. 15) and then appears to diminish at 86 and 87 km.

5. Concluding Remarks

The total output from the Cornell experiment amounts to about 14,000 ft. of 35-mm. film, or about 280 min. of data. On the basis of the observed echo fading rate, we consider a two-minute data sample to be adequate for reducing a D region electron density profile. On that basis, we have sufficient data for 140 electron density profiles. To date, we have transferred enough A-scan data from film onto IBM cards to compute 15 electron density profiles, and have found that, on the average, it requires one man-week to read a two-minute record. At that rate, getting all of our data in digital form will require a two and one-half man-year effort. We have been, and are continuing to investigate the use and availability of automatic film-reading equipment. So far these efforts have been discouraging. We are currently preparing for the 1966 Eclipse. The instrumentation, particularly the receiving equipment, will differ substantially from that used in 1965, and is designed to circumvent most of the data contamination problems encountered during the last experiment. We have also procured digital data recording instrumentation which will make possible the reduction and analysis of all of the data to be collected in November 1966.

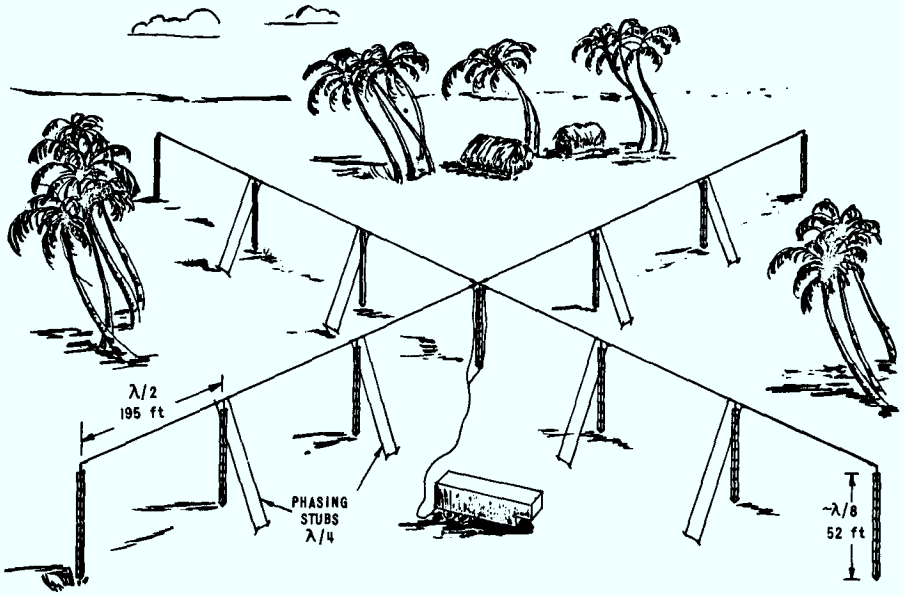

Fig. 1. Transmitting antenna array 1200 × 1200 ft.

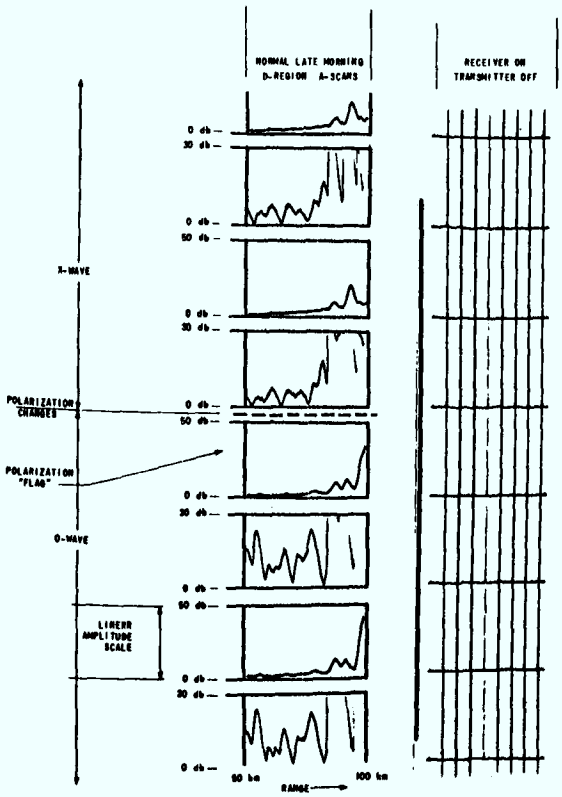

Fig. 2. Normal late morning D region A-scans.

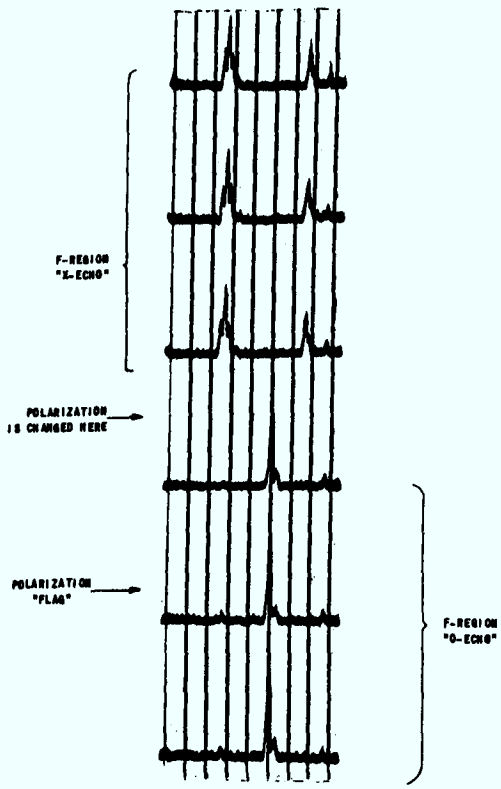

Fig. 3. O-wave and X-wave identification by F-region splitting.

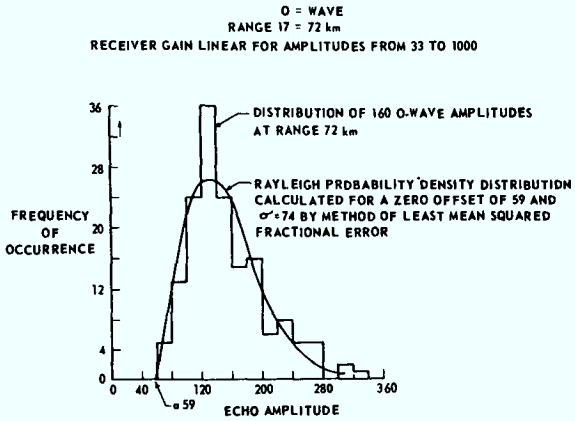

Fig. 4. Distribution of O-wave amplitudes.

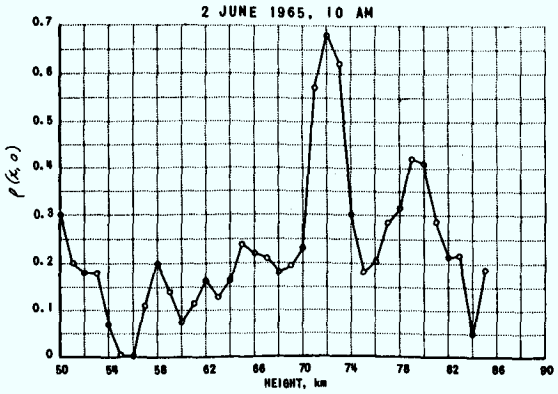

Fig. 5. Correlation coefficient ρ (x, o) for X and O amplitudes as a function of scattering height.

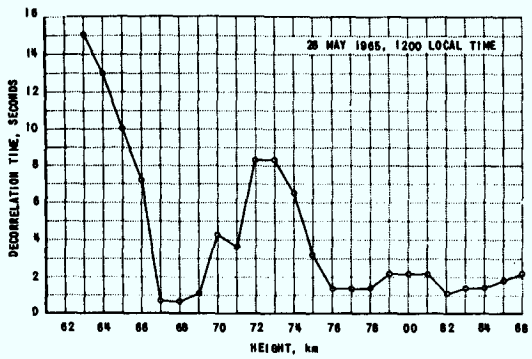

Fig. 6. Plot of O wave decorrelation time as a function of altitude.

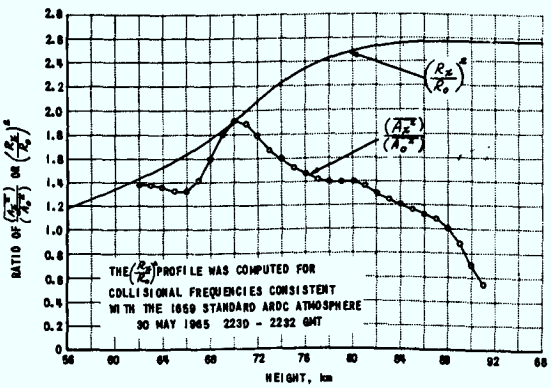

Fig. 7. Plot of the power ratio of X wave and O wave as a function of altitude (H).

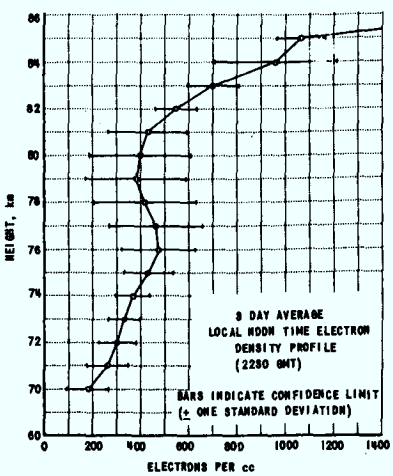

Fig. 8. Electron density profile.

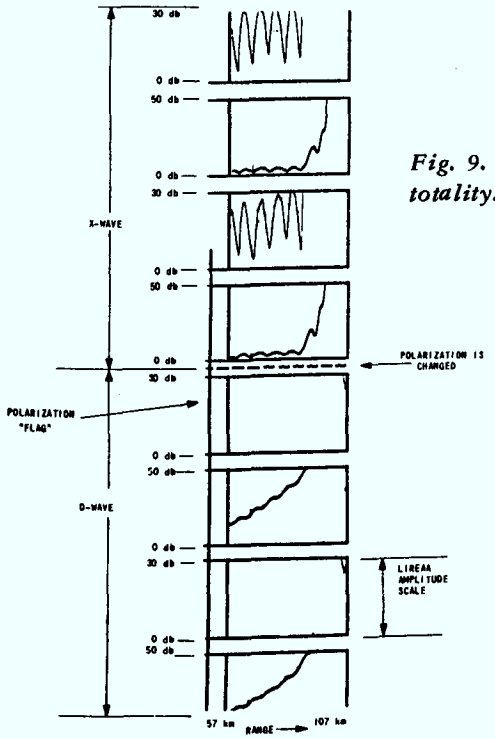

Fig. 9. D region A-scans taken at totality.

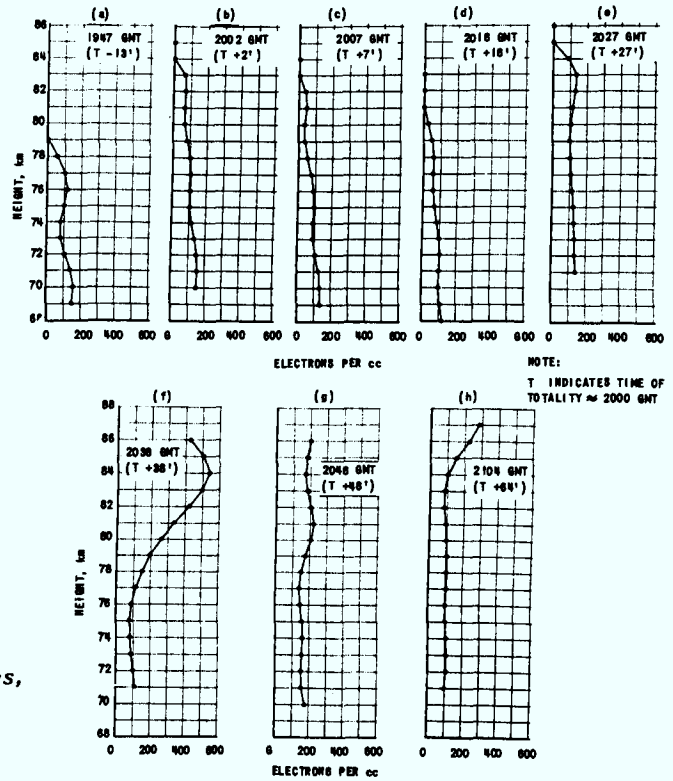

Fig. 10. Electron density profiles, 30 May, 1965.

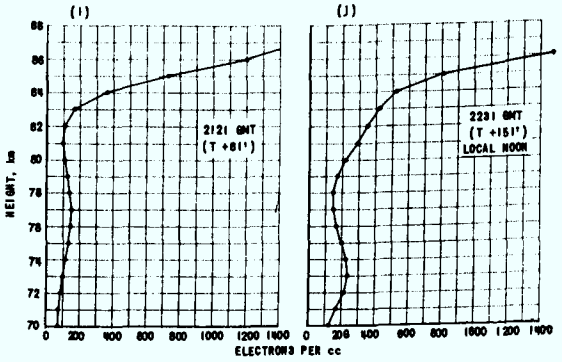

Fig. 11. Electron density profiles, 30 May, 1965.

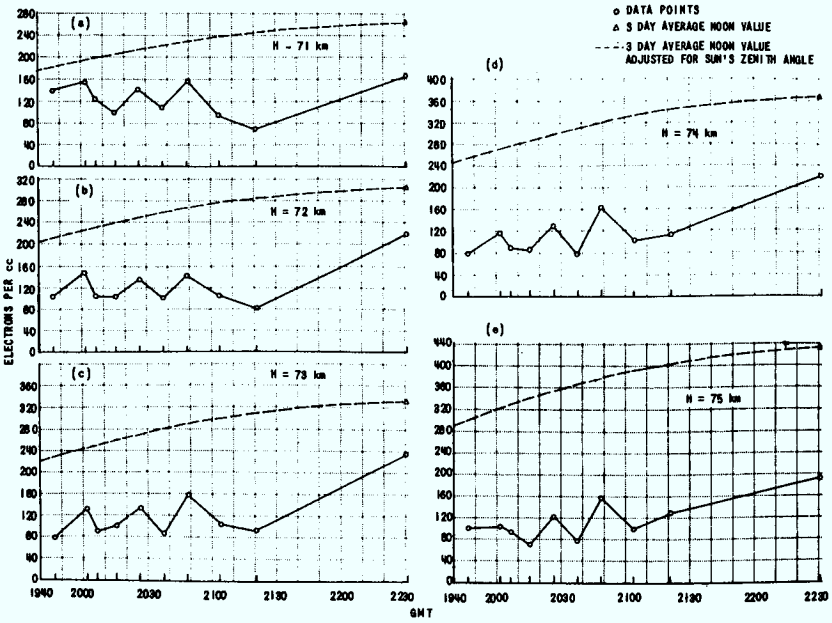

Fig. 12. Electron density time histories, 30 May, 1965.

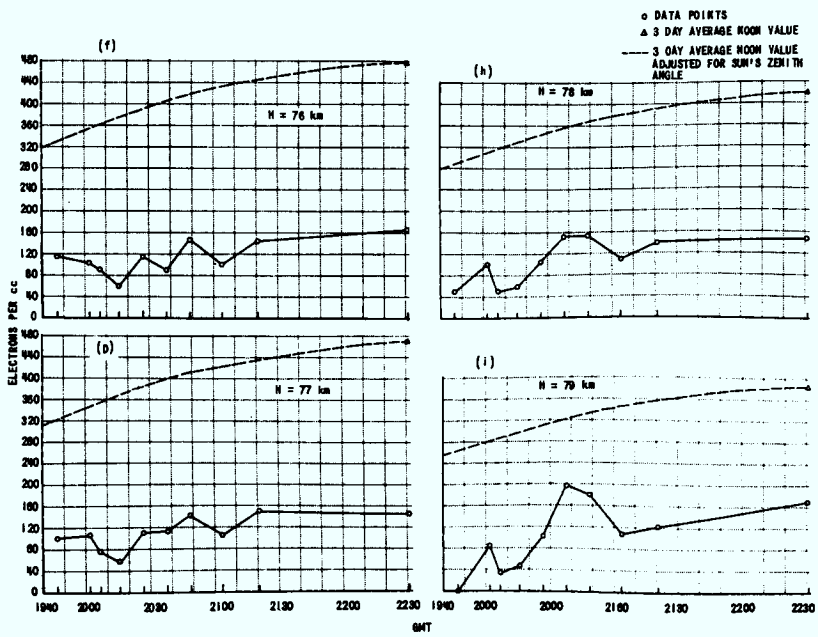

Fig. 13. Electron density time histories, 30 May, 1965.

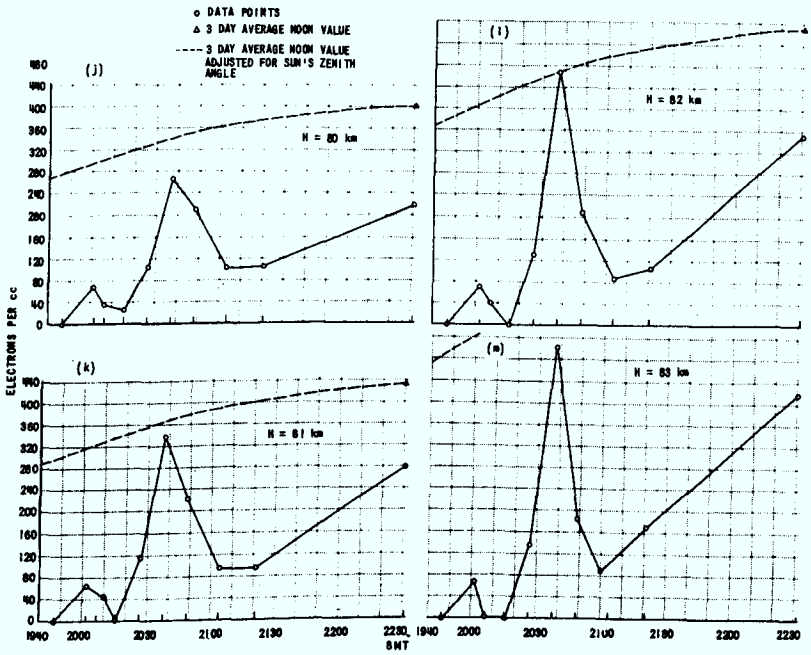

Fig. 14. Electron density time histories, 30 May, 1965.

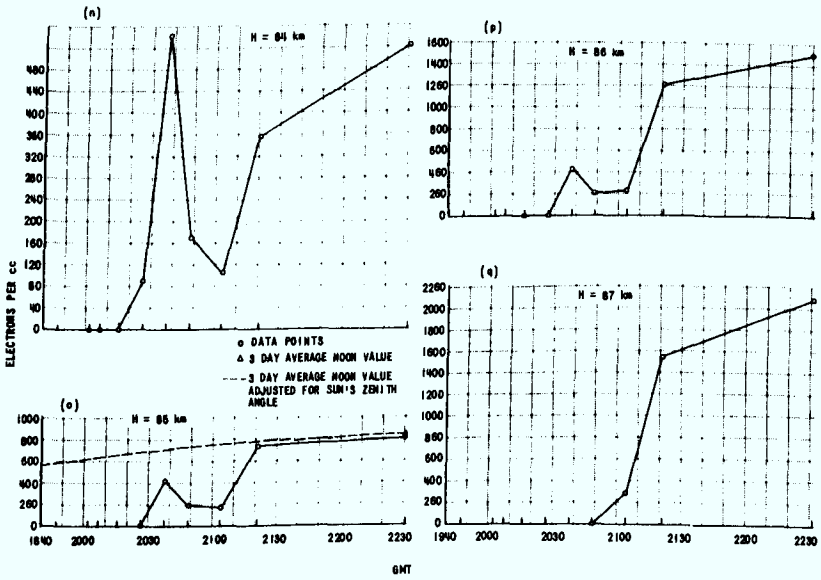

Fig. 15. Electron density time histories, 30 May, 1965.

Discussion on Paper 2.3.6 presented by H.A. von Biel

Bourne: What is the directivity of your antenna?

von Biel: We didn't measure it, but if you believe τ/d, it would be roughly 20°. We used a dipole antenna for reception.

Gregory: One of your slides seemed to show extraordinarily strong signals at lower altitudes; what was the lowest altitude, and how strong were the signals?

von Biel: The signal at 50 km. had a signal-to-noise ratio of approximately 25 d. At 80 km. we had easily 60 to 80 d signal-to-noise.

Gregory: Have you examined your data in such a way that you could throw out the possibility of sea echoes? We had similar results at a sea site and on occasion they could be completely misleading. I think your last slides, which showed the electron density at low altitudes as being negligibly altered during the eclipse, should be examined carefully since the data may be contaminated by sea echoes.

Crain: Have you made any attempt to correlate your data with theoretical estimates of the lifetime of electrons at various heights?

von Biel: We have not. These results are just off the press, and we have not tried to correlate anything.

Crain: Just looking at it, it looks scary at 85 km. with all the electrons disappearing in this time period. It is just the opposite of what I thought we saw in a northern eclipse a couple of years ago.

von Biel: We did not have any lead at all as to what to expect for the electron densities, and for this reason, I analyzed the data arbitrarily in ten-minute steps from totality to see what would happen. If something interesting should show, we would analyze more data. Eventually all these data will be analyzed.

2.4 VHF FORWARD SCATTER

by

P.A. Forsyth

University of Western Ontario

In Canada, during the last 11 years some 40 bistatic VHF scatter systems have been operated for periods ranging from 1 to 10 years. While the systems had individual differences, a typical example would consist of: (a) a transmitter radiating about 100 watts of continuous-wave power by means of a 5-element Yagi antenna located so that the principal lobe in the vertical radiation pattern illuminates the ionosphere at a height of 100 km. above the path midpoint; and (b) a receiving station (at a distance of between 700 and 2000 km.) with a similar Yagi antenna, a stable receiver with a bandwidth of 1 kc/s and a moving chart recorder which records the logarithm of the signal strength. Frequencies ranging from about 30 to 100 Mc/s have been used. From the large number of records which have been accumulated, some picture of the interaction of VHF radio waves with the disturbed and undisturbed lower ionosphere is emerging; but unfortunately an interpretation in terms of physical conditions in the ionosphere is still far from complete.

One of the earliest studies suggested that essentially four quite different kinds of scattering from ionic inhomogeneities take place in the lower ionosphere, and later studies have supported the validity of this classification. Three of these types, designated A_1, A_2, A_3, occur primarily at night, while the fourth, designated S, occurs in the daytime. It appears that A_1 events correspond to scattering from field-aligned irregularities associated with aurora (perhaps the earlier stages of the auroral process). These events are characterized by very rapid fading and are seen most often on short paths at lower latitudes. The A_2 events represent scattering from field-aligned irregularities but are less aspect-sensitive, and therefore may be seen at higher latitudes and on longer paths. Near the auroral zone A_2, events dominate the nighttime records. The A_3 and S events have much in common and, while not conclusive, the direction-finding evidence and the evidence gained from comparison of paths of different lengths seems to indicate that these events arise from scattering in the 70 to 90 km. height range from inhomogeneities that are approximately isotropic (Collins and Forsyth 1959). It is likely that these are the scatterers that were detected by D.K. Bailey and others using high power, very directive VHF radio systems. The early results suggested that the S events were enhanced by sunlight, but later results indicated that there is a systematic variation of time of peak occurrence of S events with variation in latitude, so the original observation of symmetry of occurrence about noon may have been fortuitous.

The fundamental question relating to these VHF measurements in the context of this conference is that of determining the degree of relevance of the measurements to electron density variations in the lower ionosphere. Certainly some of the observations refer only to scattering centers located at heights of about 105 km. and associated with bright auroral displays. In general these seem to be confined to the A_1 and A_2 signals which make up a small fraction of the total signals if measured with reasonable sensitivity. If looked at with low sensitivity the A_2 signals tend to predominate (Forsyth et al. 1960). Assuming that the A_3 and S events, both of which last much longer and occur more frequently than A_1 and A_2 events (at least at mod-rate latitudes), do predominate in the records, then it is

reasonable to assume that the general diurnal seasonal and solar cycle dependence of the VHF scatter events observed at mid-latitudes do refer to conditions in the lower ionosphere. Since records extending over one full solar cycle are now available for paths at approximately 45° North geographic latitude, it is worthwhile examining at least the general statistical characteristics of the recorded events. The data shown in Fig. 1 were derived from 10 years of operation of a 40 Mc/s circuit between Greenwood, Nova Scotia and Ottawa, Ontario (1955-1964 inclusive) and one year of operation of a similar circuit between Greenwood and London, Ontario (1965). The histogram shows the relative occurrence in percentage of total time of all the A and S activity by years for the 11-year period, together with a graph of the mean sunspot number for each year. There seems to be no doubt that the scatter activity (radio-aurora) is related to the sunspot activity. Fig. 2 shows the diurnal variation averaged over the 11 years. The strong noontime peak (S events) noted by Collins and Forsyth persists in this data and the post-midnight peak also persists, but (perhaps because of detection criteria which favour A_3 events over A_2) is a little later than that found previously for the Greenwood-Ottawa path. In any case the times of occurrence of these two peaks approximate very closely those required by the relation between times of maximum occurrence and geomagnetic latitude found by Forsyth et al. These results too suggest that the scattering centers are related to precipitated particles. An extension of this kind of thinking suggests that the events are, in fact, part of the auroral process and that the A_3 events, which occur later and lower than the visible aurora, are caused by a hardening of the spectrum of the precipitated particles, or even by a change in particles from, say, electrons to protons.

Whatever the cause, the nature of the ionic inhomogeneities which cause the scattering is of interest. Again, there is much evidence but little conclusive interpretation. The scattering centers seem to be fairly small (less than a few meters in diameter) and scatter nearly isotropically. That the isotropic characteristic is only approximate is indicated by the experiment of Lyon (1965). He observed simultaneously signals scattered in a generally forward direction (transmitter at Great Whale River, receiver at London) and in a nearly backward direction (transmitter at Ottawa and receiver at London) from the same body of ionization. He found great variations in the relative amplitudes of the forward and back-scattered signals and many cases in which the A_1 and A_2 signals could not be explained in terms of weak scattering. On the other hand, the A_3 signals at least admitted of interpretation in terms of weak scatterers with a scale size of say, one meter, and elongation along the magnetic field lines with an axial ratio of no greater than four, and perhaps as little as two. It has recently been indicated by Moorcroft (1966) that the interpretation of these angular results and the large number of frequency dependence results now available in terms of random assemblies of scatterers, is not satisfactory. Some further modification of the model is necessary, and the wave hypothesis advanced by Farley (1963) is attractive. Leadabrand (1965) has examined radar data, and while the presence of plasma-acoustic waves was not clearly confirmed, the possibility is not ruled out that the auroral ionization is governed by an extremely complex process to which plasma-acoustic waves contribute. More measurements of the directional characteristics would be of value in sorting out the situation. In the meantime, it seems likely that such waves do not exist below the E region and do not need to be invoked to provide a satisfactory interpretation of the A_3 and S events which are of prime importance here. While there are uncertainties, it seems adequate to consider that the inhomogeneities involved are approximately isotropic, have scale sizes of the order of meters, are located at a height of 80 to 90 km. and contain peak electron densities of the order of 10^6 electron cm^{-3}.

REFERENCES

Collins, C. and P.A. Forsyth. J. Atmos. Terres. Phys., 13, 315, 1959.

Farley, D.T. Phys. Rev. Letters, 10, 279, 1963.

Forsyth, P.A., Green, F.D. and W. Mah. Can. J. Phys., 38, 770, 1960.

Leadabrand, R.L. Radio Science 69D, 959, 1965.

Lyon, G.F. J. Atmos. Terres. Phys., 27, 1213, 1965.

Moorcroft, D.R. Planet and Space Sci. In Press. 1966.

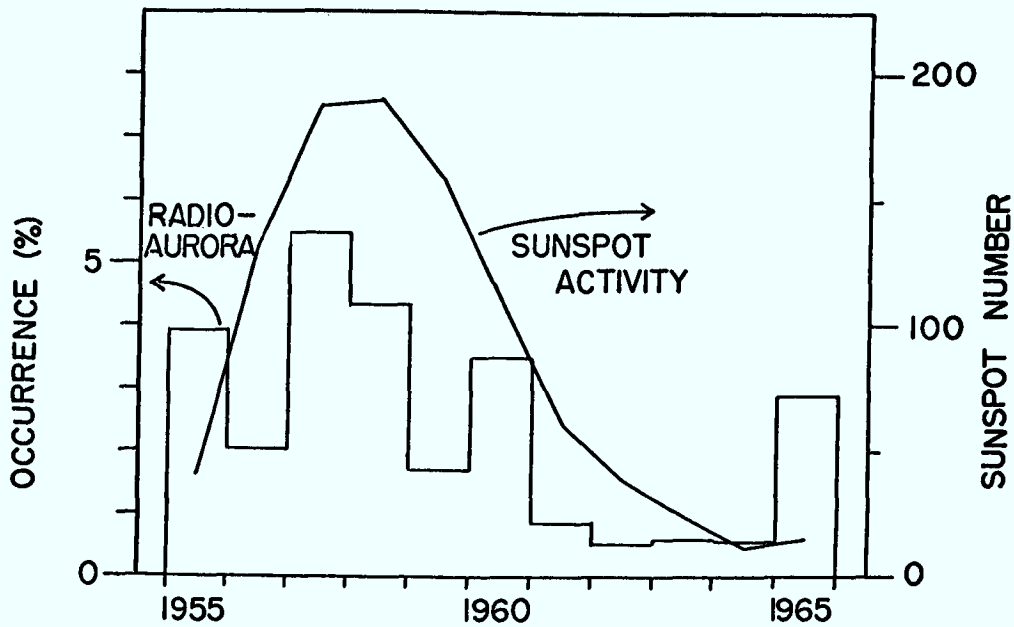

Fig. 1. Histogram showing relative occurrence of scattering events over an 11-year period compared with the sunspot activity for the same period.

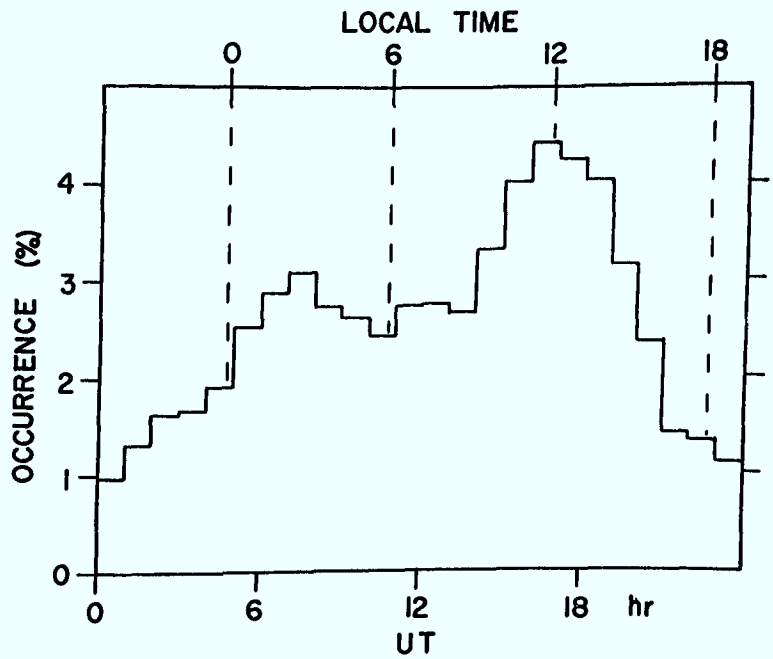

Fig. 2. Diurnal variation of scattering events.

Discussion on Paper 2.4 presented by P.A. Forsyth

Belrose: I would like to comment since I asked Dr. Forsyth to talk on this subject. Reports in the literature have indicated possible connections between the mesospheric scatter that you see at medium frequencies, and VHF scatter that we see at high latitudes in Canada. While I don't think such a connection has been positively established, some work has been initiated in New Zealand. Do you know, Dr. Gregory, whether it was carried to fruitful results?

Gregory: The medium frequency comparison made in New Zealand was for very short periods only, and wasn't in fact particularly successful due to the shortness of time. However, the basic variation of the seasonal scatter that I showed in the earlier talk was one that paralleled Bailey's very early work.

Wright: I recall that about five years ago we published a small amount of data from the southern tip of Greenland, which was not unlike similar observations made in Canada, and some of the things that have been reported in New Zealand. Our measurements were high frequency vertical incidence measurements on an ionogram which showed scatter from this same height region, 70 to 80 km., and showed maximum reflections in the 5 to 10 megacycle range – rather surprisingly high, but they were definitely scatter-type echoes, not total reflectors. At the time we thought that the returns were associated with the region responsible for some of the VHF forward scatter.

Forsyth: I might comment that an attempt has been made to associate the occurrence of scattering of this kind with the occurrence of absorption, particularly polar cap absorption, but I don't think that the connection has yet been established. Certainly in the early results there were many occasions when the two were coincident, but I am not sure a connection has been established.

2.5 LOWER IONOSPHERE ECHOES OBSERVED WITH INCOHERENT SCATTER RADARS

by

L.M. LaLonde

Cornell University, Ithaca, New York

Of the three back-scatter radars which are familiar to the author, the only successful E-region echoes, particularly nighttime echoes, have been received at Arecibo. The large back-scatter station at Jicamarca, while sufficiently sensitive and free of ground clutter, is masked by the strong coherent echoes from the electrojet over the magnetic equator. The 220-ft. dish at Millstone Hill is masked by ground clutter, and the 84-ft. dish, which can look at low elevation angles to eliminate ground clutter, is barely sensitive enough to see the daytime E region. The following remarks therefore, will be restricted to results from the Arecibo radar.

Using 40 μsec. probing pulses at peak power levels of 2 Mw., the single pulse signal-to-noise ratio from the daytime E region is greater than unity. Integration over 10,000 pulses (50 to 100 sec.) allows 1 percent statistics on the daytime E region, with time resolution of the order of 1 min. and height resolution approaching 3 km.

The nighttime E region, with an average density down two orders of magnitude or more from the daytime, presents a more difficult target, yet integrated signal-to-noise ratios are greater than unity. Horizontally stratified layers, such as Sporadic E, cause the signal-to-noise ratio at a particular range interval to increase markedly, depending of course on the layer density and thickness.

The Arecibo radar, by virtue of its large aperture and high local horizon, is free from detectable ground clutter beyond 50 km. of range. The ground return experienced is likely due to radiation from the sidelobes of the feed itself, which is only slightly above the immediately surrounding hills. Reception of echoes from a range beyond 50 km. then, is attributed to ionospheric back-scatter.

Electron density profiles are computed from these lower ionosphere echoes by solving the radar equation using an electron cross section based on incoherent scatter theory. Fig. 1 shows a typical profile near a winter noon over Arecibo. This profile is uncorrected for the electron-to-ion temperature ratio dependence of the electron cross section. On the same figure, simultaneous ionosonde critical frequency indicated densities, a theoretical profile and partial reflection experiment profile of the D and lower E region are shown (Belrose). With temperature ratios of 1.6, 1.4, 2.1, and 2.8 corresponding to heights from 107 to 215 km. where the ionosonde indicated densities are shown, E- and F-region densities are in good agreement with measurements made by other techniques.

Below 100 km., where the temperature ratio is believed to be unity throughout the day, excellent agreement is shown between the back-scatter measurement and other workers' results.

Fig. 2 is a series of sunrise profiles, averaged over 10 min. and shown approximately 20 min. apart. Again, above about 85 km. there is no basic disagreement with other workers'

The Arecibo Ionospheric Observatory is operated by Cornell University with the support of the Advanced Research Projects Agency under a contract with the Air Force Office of Scientific Research.

results. Below 85 km., in particular between 60 and 75 km., there is general disagreement, particularly in the 0650 profile which shows a thin layer at 60 km. with a density of 10^4 electrons/c.c. averaged over a 6-km. height interval.

Ionograms taken throughout this period of time show no difference in the low frequency return from the F layer. Yet the two-megacycle attenuation calculated using the COSPAR collision frequency at this altitude is 27 db for a one-way path through a large horizontal layer with the average density indicated. Therefore, if one assumes that the radar echoes are correctly interpreted as electron density, the irregularity size must be greater than 300 m., but less than a Fresnel zone at the sounder frequency, or less than 3 km.

These strong echoes have been observed to occur in the height range from 60 to 70 km. over the entire year. They occur day and night with fading rates whose periods vary from minutes to about one hour, though the faster fading echoes are most frequently observed.

The reasons for these intense echoes are not understood. One might suggest that "coherent" echoes result from the turbulence in this region and therefore electron density is over-estimated due to the increased scattering cross section over that predicted by thermal fluctuations and incoherent scatter theory. Because the echoes are not always present, and the fading rates vary widely, a model which allows a patchy ionosphere of dense clouds to drift slowly through the narrow antenna beam also fits experimental evidence. At the present time, neither of these are offered as a preferred explanation; clearly a more detailed study of the echo characteristics and simultaneous measurements by other techniques are needed.

Above 85 km., the strength of the incoherent scatter technique lies in the time and spacial resolution of electron density measurements permitted. The profiles presented in Fig. 2 represent 10-min. averages spaced over 1 hr. and 23 min. The data were taken so that one profile per minute can be generated with a signal-to-noise ratio degenerated by a factor of three from those shown here. This provides information throughout the day on the dynamics of the E region, with a height resolution of 6 km., horizontal resolution of 300 m., and time resolution of 1 min.

The results of some E-region studies of the data gathered at Arecibo have already been reported. These include:

1. The detection of the valley above the nighttime residual E peak which forms after sunset and persists until sunrise.

2. An inferred daytime electron-to-ion temperature ratio at 120 km. of about 1.5 during the quiet sun.

3. The determination of height, vertical separation, and inferred thickness of Sporadic E layers.

More recently, successful beam swinging in an attempt to resolve the horizontal distribution of Sporadic E layers has been performed. Although this scheme has not yet been attempted when heavy E_s was visible over Arecibo, the first attempt revealed interesting features of E_s.

During the afternoon of 17 February, 1966, the beam was swept from vertically overhead to 17.8° elevation angle, at an azimuth of 033°. It remained at 17.8° for 30 sec. and was returned to 17.5°. The scan rate in elevation is very nearly 1° per min. Profiles were made during the entire period with an averaging time of 30 sec., identical to those of Figs. 1 and 2, except that the receiver was "over-sampled" by sampling at a 3 μsec. rate on a 6-μsec. pulse. Simultaneous C4 ionograms were made at 10-min. intervals.

The radar profiles taken during the scan show no substantial E_s evident out to an elevation angle of 16.6° . At 16.6° the 101- and 104-km. samples rose in the fashion shown in Fig. 3. The higher density curve (top plot) is the outward motion, the dashed line remaining stationary at 17.8°, and the bottom curve represents motion toward 17.5°.

It would appear that the beam scanned over the peak of an E_s layer on the way out, and back over the peak again on the way back. The drastic drop in intensity while the beam is sitting at 17.8° implies that the layer is moving with respect to the stationary beam. The noise fluctuations, averaged over this time interval, amount to less than 10^3 electrons/c.c. The change during the time the beam was stationary therefore represents a change of 80 times the noise fluctuation.

Contours of an E_s layer drawn from this data strongly depend on the assumed motion of the layer during the measurement time. Figs. 4, 5, and 6 are examples of contours which may be drawn with different magnitudes and directions of the velocity vector of the layer.

Fig. 4 is drawn with an assumed velocity of 100 m. per. sec. with the motion perpendicular to the line of the beam scan. The figure is drawn with the northernly direction up and westerly left, but a drift velocity of 180° from that assumed would reverse the east and west directions shown here.

Fig. 5 is drawn assuming a lower velocity component perpendicular to the beam and a small component radially outward along the line of scan. This tends to narrow the layer to the order of 1 km. across on a north-south line through the layer. The lower east-west velocity also reduces the length of the layer model from that shown in Fig. 4. It should be pointed out here that the radial components of velocity assumed in Figs. 4 and 5 are small compared to the rate of motion of the beam through the ionosphere.

The points plotted on Fig. 6 point out the drastic change in north-south scale when the radial component of velocity is large compared to the rate of motion of the beam. The particular velocity assumed here is the average of the velocity vectors for moving E_s layers over Puerto Rico reported by Dueño. This assumed motion would indicate the scan across two layers in the north-south direction, with the centers being separated by about 13 km. From the profiles, there is no indication of a change in slant range to the layer, meaning that if this model is assumed, the layers are at the same height above ground.

The vertical incidence sounder located at the Observatory showed no indication of strong E_s at the time this layer was detected some 30 km. north of the radar by back-scatter. Layers which were comparable in intensity appeared on the sounder 140 min. before and 73 min. after the detection by radar. No other strong layers were observed, but low intensity E_s is evident on most soundings after the time of detection by radar of the strong layer to the north. If one were to assume that the sounder detected the same layer 73 min. after the radar, due to the southerly motion of the layer, this would require the layer to drift south at a velocity of 6.8 m. per sec. The contours of Fig. 4 would be only slightly spread in the north-south direction, due to this motion.

Even though these results are quite indefinite because of lack of knowledge of the velocity of the layer, some limits on the north-south extent of the layer may be set. The upper limit of the extent of the layer is actually set by the assumed velocity in the direction radially along the scan line. The average velocity from Dueño's work causes this limit to be approximately 10 km. A lower limit of 2 to 3 km. is implied by the measurements when low radial velocities are assumed for the irregularity.

REFERENCES

Belrose, J.S. Present knowledge of the lowest ionosphere (AGARD ograph) 74, Pergamon Press. 1963.

Dueño, B. Sporadic E as observed from Mayaguez P.R. by Back-scatter Sounders, Ionospheric Sporadic E 110-122. MacMillan 1962.

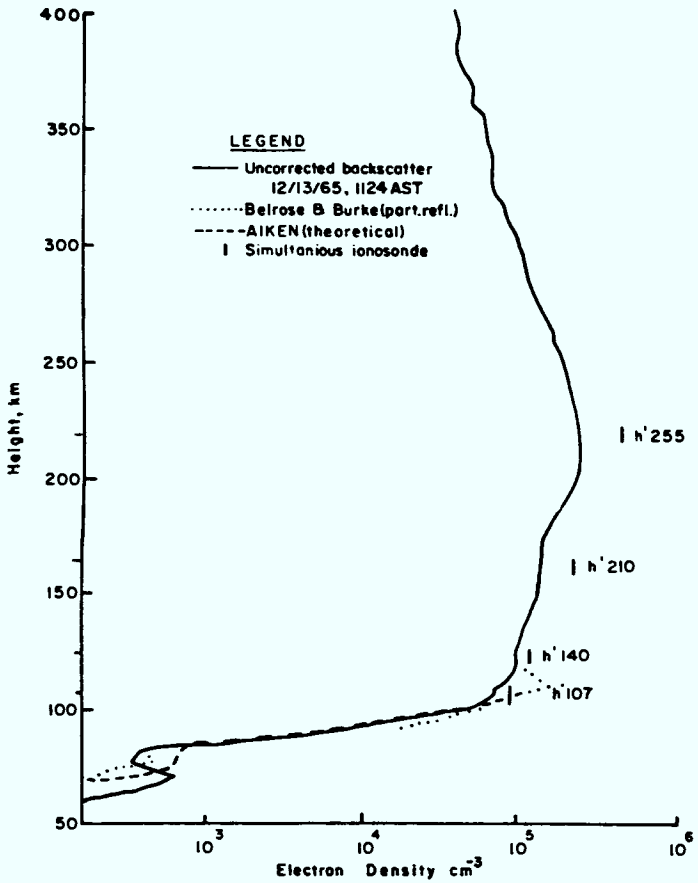
LEGEND
Uncorrected backscatter 12/13/65, 1124 AST
Belrose & Burke (part. refl.)
AIKEN (theoretical)
Simultanious ionosonde
h'255
h'210
h'140
h'107
Height, km
Electron Density cm^{-3}

Fig. 1.

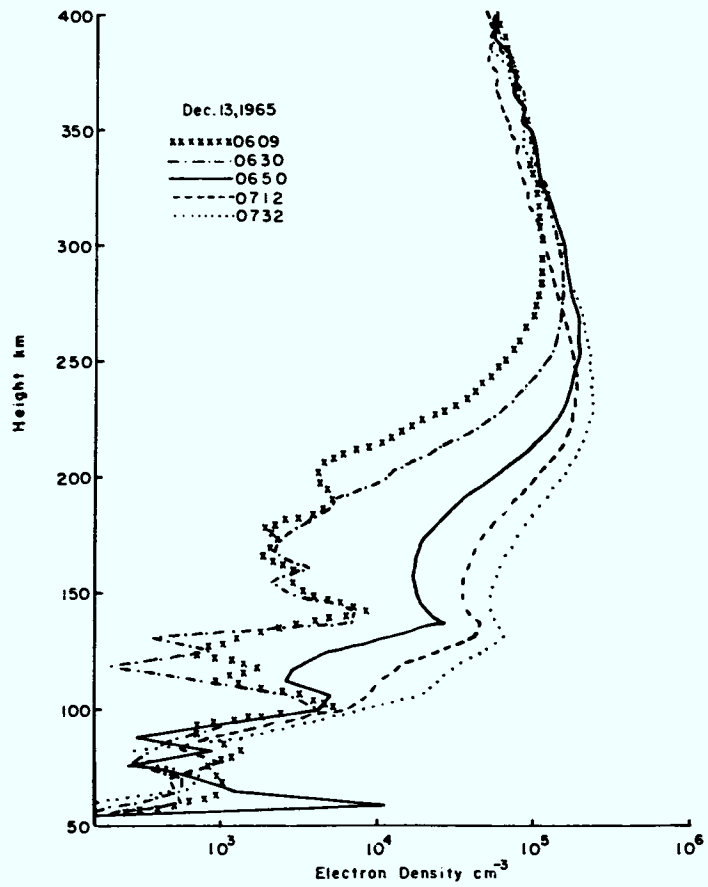
Dec. 13, 1965
0609
0630
0650
0712
0732
Height km
Electron Density cm^{-3}

Fig. 2.

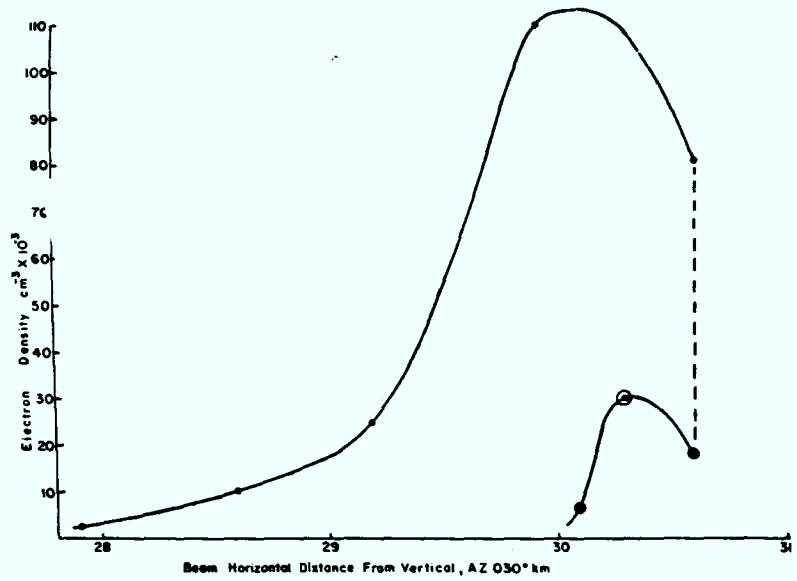

Fig. 3.

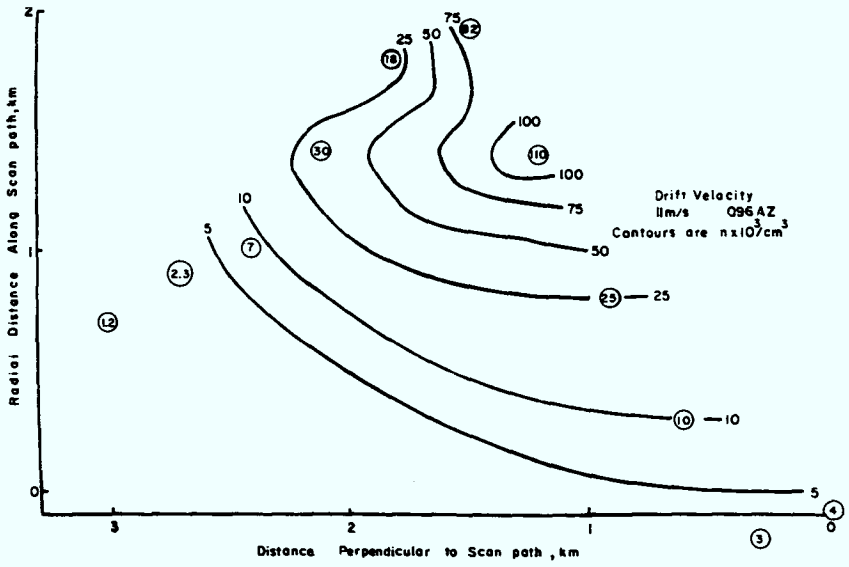

Fig. 5.

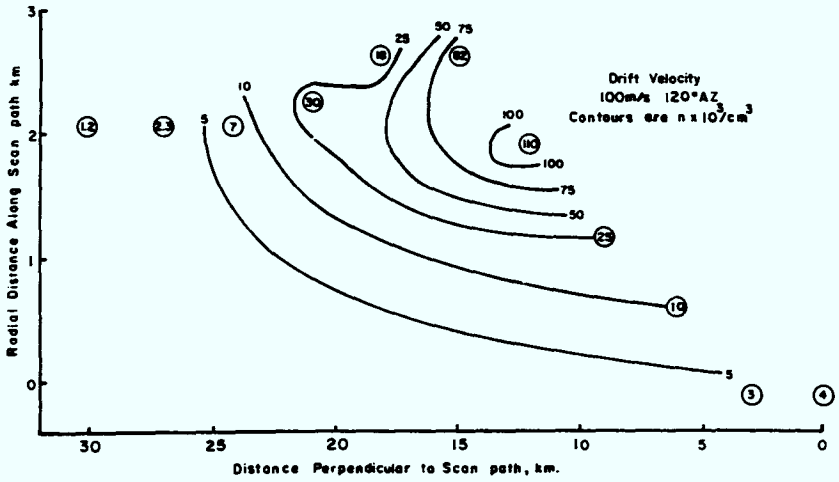

Fig.4.

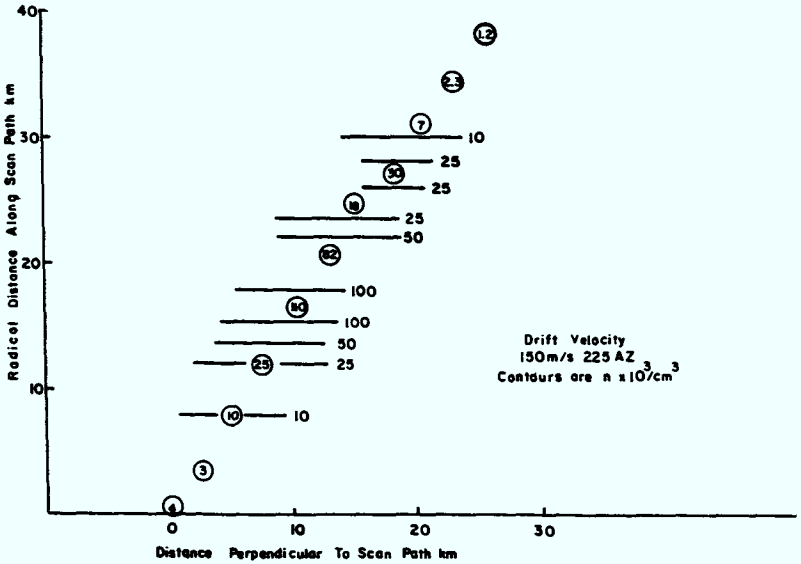

Fig. 6.

Discussion on Paper 2.5. presented by L.M. LaLonde

Wright: The height is low, but would a single, fairly strong meteor passing through the 50- to 70-km. range explain this one measurement of high electron density in the early slides?

LaLonde: I don't know. My guess is that it would, because echoes from such a trail would be very strong.

Wright: The meteor people estimate something up around 10^{10} or 10^{12} electrons c.c. on a strong trail, don't they?

LaLonde: The fading rate of these strong echoes that we observe down in the 60 to 75-km. region varies from minutes to hours. The slow variations are quite uncommon. The point is that they do vary. On one record, a layer built up over a period of something like an hour and decayed after that. The build-up and the decay were so orderly that the returns didn't fluctuate at all. These were 10-min. profiles, and if they were caused by meteors, there must be more than just an occasional meteor.

Crain: What is the antenna pattern at Arecibo in terms of side lobes? Have you ever calibrated this thing? What sort of field intensities are there on the ground?

LaLonde: No, there is really no way to calibrate it.

Crain: When in that close, I think the antenna characteristic becomes important.

LaLonde: The altitude at which the first null of the Fresnel zone lies is on the edge of the aperture, and this is where rippling should start. Rippling on the on-axis gain is in the area where we are in trouble with ground clutter, below 50 km. I think 38 km. is the right number, but I may be wrong.

Crain: If you are troubled with ground clutter, are you also bothered by aeroplanes at various ranges and altitudes?

LaLonde: If an aeroplane flies directly over the antenna certainly we are, and we do occasionally see them on the side, but it is hard to imagine an aeroplane being in the beam for an hour. We spent a considerable number of hours looking for ground clutter, and that is quite an easy thing to do because Dyce uses a technique which I think is very sensitive in this regard. You look at one line of the pulse spectrum and carefully analyze the broadening of that line. This has been done in the case of back-scatter type returns coming from vertically upwards; and you can see the narrow return, which you can attribute to ground clutter, drop right into the noise.

Crain: I was searching for other possibilities than 10^4 electrons at 65 km.

LaLonde: I don't pretend to understand it either, but it is an echo, and that was the title of my paper – "Lower Ionosphere Echoes".

Belrose: It seems peculiar that one gets echoes from say 60 km. at night. There must be a sort of half an electron there per c.c. producing scatter.

LaLonde: We have been through all of these arguments, and none of them are new. I don't pretend to know any explanation.

Shirke: I wonder what would be the absorption if such high densities do exist at these low altitudes.

LaLonde: I calculated the absorption at 2 megacycles to be 30 *db* on a one-way path through a 6-km. layer. I don't think it was this particular layer, but a little higher up. I used a collision frequency of 10^7.

SECTION 3

PULSE RADIO WAVE INTERACTION

3.1.1 SMALL PERTURBATION WAVE INTERACTION IN THE LOWER IONOSPHERE PART I

Review and Basic Theory

by

R.A. Smith

University of New England, Armidale, Australia

1. Introduction

When V.A. Bailey recognized in 1934 that electron heating by an electromagnetic wave causes the collision frequency in the ionosphere to depend on the field intensity of the wave and that this provided an explanation of an apparent wave interaction phenomenon observed in the previous year by Tellegen, he initiated a field of research, to which he made many major contributions*, and which has been actively pursued to the present day by a large number of groups and individuals.

Although electron heating is usually a negligible effect in the ionosphere, its effect on the propagation of a suitable wave can be detected without too much difficulty. The earliest method was to use a sinusoidally modulated low frequency "disturbing" wave to modulate the electron temperature, and thus the electron collision frequency, along the oblique path in the ionosphere of a continuous low frequency "wanted" wave. The low frequency for the disturbing wave enhanced its effectiveness in heating the electrons; the low frequency and long path in the ionosphere for the wanted wave made its total absorption high and thus enhanced the modulation it acquired through the periodic variations of its absorption. With the frequencies and propagation paths of the wanted and disturbing waves selected in this way, it was found using available transmitters that the depth of the modulation impressed on the wanted wave was large enough (several per cent) to be measured with simple receiving equipment. Experiments of this kind were made in England and Europe before and just after World War II and, because of the propagation conditions required, were restricted to the nighttime. This work has been reviewed by Huxley and Ratcliffe (1949) and by Huxley (1952) and was largely guided by the mathematical theory of wave interaction due to Bailey and Martyn (1934).

An important variation of the oblique incidence experiment followed a revision of the Bailey and Martyn theory by Bailey (1937a, 1938). In the revised theory Bailey correctly allowed for the influence of the earth's magnetic field and predicted that enhanced modulation would be produced by the use of a disturbing gyrowave and a suitable low frequency wanted wave. Some support for his theory of gyro-interaction was obtained by Bailey (1937b) from a series of experiments which he organized in England in 1937, but after World War II the theory became controversial through opposing observations in England (Huxley 1950, Shaw 1951) and in Italy (Cutolo et al. 1950, Cutolo 1950) and through apparent differences in theory (Shaw 1951). This controversy was resolved in favor of Bailey's theory by experiments (Bailey et al. 1952, Hibberd 1956, 1965, Smith 1957) made in Australia between 1949 and 1954 by the author in collaboration with a group from the University of Sydney headed by Bailey. The conflict in theory was resolved by a detailed theory of gyro-interaction (Smith 1957), which includes an analysis of the propagation of the oblique wanted wave. This detailed theory clarified the processes in a gyro-interaction experiment and, when used with a realistic model of the nighttime lower

* For a comprehensive list of his papers on radio wave interaction and other phenomena associated with electron heating, see Bailey (1965).

E region, gave a curve of impressed modulation as a function of disturbing frequency in good agreement with the experimental curves obtained in Australia.

The oblique incidence experiment proved an effective means of studying the phenomenon of radio wave interaction and has an assured place in its history. Nevertheless, partly because of experimental limitations and difficulties of analysis resulting from the use of an oblique wanted wave and partly because of uncertainty in the properties of near-thermal electrons in air, the experiments yielded few results on general properties of the lower ionosphere.

By pulsing both the wanted and disturbing transmitters and by using the sophisticated and sensitive detection methods summarized in Section 2, Fejer in 1955 made the first measurements of wave interaction in the daytime D region and deduced electron density and collision frequency profiles for this important region from his data. These goals are so attractive that, in spite of the marginal signal-to-noise ratio achieved by Fejer and the need for complex receiving equipment, his methods attracted immediate interest and were used again in South Africa (Fejer and Vice 1959), and have been adopted in Norway (Lied 1957, Bjelland et al. 1959, Landmark and Lied 1961, Holt et al. 1961, 1962, Barrington et al.1962, Barrington and Thrane 1962, Barrington et al. 1963), in Alaska (Rumi 1961, 1962a, b, Benson 1962, 1964a, b, Singh 1964), at Pennsylvania State University, where the Fejer technique has been extended to the measurement of very small changes in the phase of the wanted pulse, (Ferraro et al. 1963, Weisbrod 1964, Weisbrod, Lee and Ferraro 1964, Weisbrod, Ferraro and Lee 1964, Hellrich and Ferraro 1965, Day 1965, Care 1965, Bell 1966) and at the University of New England (Smith et al. 1965). Observations of wave interaction at the geomagnetic equator, using the 50 Mc/s. transmitter at the Jicamarca Observatory as the disturbing transmitter, have been reported by Klemperer (1964). Setty (1965) has described a graphical method of analysis of Type II (see Section 2) pulse wave interaction data and Georges (1965) has examined its simulation by numerical methods. Except for a few early nighttime observations in Norway and a large part of the work at the University of New England on small and large perturbation gyro-interaction, the interest in this major revival of radio wave interaction has been the D region.

The experiments referred to above have the common feature of the use of separate waves for electron heating and radio probing. The change in the properties of the medium also alters the propagation of the disturbing wave itself, as was first recognized by Bailey in 1935. "Self-interaction" or "self-distortion" are terms used to refer to this phenomenon. Self-interaction of a sinusoidally modulated wave has been discussed theoretically or by numerical methods by Vilenski (1953), Hibberd (1955, 1957), Megill (1965a) and Ginzburg and Gurevich (1960) in their extensive report on non-linear phenomena in a plasma; self-interaction of a pulsed wave has been examined by numerical methods by Smith et al. and by Georges (1965). Technically, self-interaction* is difficult to observe, but the observations of King (1959) on the self-interaction of a sinusoidally modulated wave appear definite. In a pulse wave interaction experiment, self-interaction of the disturbing pulse cannot be neglected when the perturbation of the collision frequency is large. The self-interaction can then produce indirect effects that are easily observed (Smith et al.; see also discussion of Fig. 6).

When very large radiated powers are used, the possibility of a change in electron density must be considered. Of various processes that may produce such a change, the one which would appear to require the least radiated power is the alteration of the rate of attachment of electrons to molecules of oxygen (Bailey and Goldstein 1958, Bailey 1959, Molmud et al. 1962, Molmud 1964). Rumi (1962a) has proposed that this process is effective for the pulse powers and duration normally used in a pulse wave interaction experiment, but his theoretical arguments have been shown by Benson (1964a) to be incorrect. These theories have been partially tested by Smith et al. at night using powerful (220 kw.) disturbing pulses at the gyrofrequency lasting for 30 seconds and a sensitive method for detecting the total change in the electron content of the heated region. From the negative results of their experiments it is safe to assume that in a wave interaction experiment using short pulses and normal powers the electron density remains constant. The estimated power requirements for

* Self-interaction, in the sense that we have used this term, is not to be confused with an unexplained self-demodulation phenomenon involving gyrowaves studied by Cutolo (1952, 1953a, b), Mitra (1954) and Aitchison and Goodwin (1955), which cannot be attributed to electron heating.

excitation of an airglow and to create breakdown in the ionosphere are extreme, but perhaps not impractical (Bailey 1938, 1961, Megill 1965b, Lombardini 1965).

The final papers mentioned are relevant to electron heating in the ionosphere but do not fit into the groupings above. Those on the behavior of slow electrons in air, nitrogen, and oxygen have been discussed in Paper 1.6. Farley (1963) has suggested a method for extending wave interaction observations to the F region. Non-linear phenomena in a plasma have been considered by a number of authors (see, e.g., Ginzburg and Gurevich 1960, Caldirola and Barbieri 1965, Layzer and Menzel 1965) using an approach based on the Boltzmann equation. This highly mathematical approach to wave interaction theory is necessary for the discussion of phenomena such as frequency mixing and harmonic generation, but the need for it in the interpretation of wave interaction data has as yet to be demonstrated.

The invitation to the conference asked for a review of the theory of pulse radio wave interaction and a separate review of experimental results. These requests carry the implication that the pulse methods are now the only methods that need be considered. With this implication we agree, but not because the superiority of the pulse methods has been demonstrated generally. It is an unfortunate fact that through restriction of the observations to a particular pulse sequence introduced by Fejer and failure to appreciate the experimental precision required, the experimental observations that have been reported by various workers are of very limited value. Because of this, it is felt that the objectives of this conference would best be served by taking as the central theme of this paper the problem of using pulse wave interaction methods to determine the electron density profile of the D region, since this profile has been the primary objective of much of the current research on radio wave interaction.

This paper is a melange of review, in many cases by implication, of theory, and of descriptions of experimental techniques and measurements. Section 2 on experimental techniques includes a number of photographs of wave interaction equipment at Armidale, in order that the complexity of the experimental method may be fully appreciated. It also contains a large number of figures illustrating typical records and data obtained in Australia, Norway, and at Pennsylvania State University. The figures are given to illustrate the quality of the data that have been used to deduce properties of the D region, to demonstrate that other pulse sequences beside that introduced by Fejer can be used with profit, and to show that it is possible to obtain data of high quality under small perturbation conditions.

The mathematical theory in Section 3 treats collisions by the simple, but adequate, methods of Bailey and of the Townsend school and is developed only for the case of a small perturbation. The latter restriction on the theory is deliberate, since it is believed that the considerable complexity in interpretation, which the phenomenon of self-interaction introduces, should be avoided in any experiment with synoptic applications.

The plot of the impressed modulation against the relative delays of a short disturbing pulse and the wanted echo is referred to in this paper as a Fejer curve. These curves provide information on the structure of the region in which the wave interaction occurs. Their formation is discussed in Section 4 and the problem of their practical interpretation is considered in Section 5.

Sections 3 and 4 contain a number of results for small perturbation wave interaction in thin regions, which are needed in Papers 3.2.1 and 3.2.4.

2. Pulse wave interaction techniques and measurements

The method introduced by Fejer (1955) to measure the interaction of two vertically propagated radio waves in the D region employs a train of short disturbing pulses D transmitted at half the repetition frequency f of a train of short wanted pulses W, where the time 1/f is long compared to the duration of the transient electron heating caused by a disturbing pulse. By suitably delaying one pulse train relative to the other, every second wanted pulse is made to pass through the whole or part of the D region during its transient modification. This causes these pulses to be received with an amplitude E different from the normal amplitude E_0 of each of the immediately following pulses.

The change $(E_0 - E)$ is usually only a very small fraction of E_0. To detect this change in the amplitudes of alternate pulses, Fejer selected the echo by gating the receiver

at the rate f and then applied the video pulses at a controlled level to a selective amplifier tuned to the frequency f/2. This amplifier was followed by a phase-sensitive detector to discriminate against noise, and a pen recorder. To convert the reading to a depth $(E_o - E)/E_o$ of impressed modulation, Fejer obtained a calibration reading by applying video pulses at the rate f/2, with amplitude a known fraction of E_o, to the selective amplifier. The detection method is extremely sensitive and under good observing conditions a modulation depth as small as 0.001 per cent can be detected.

The Fejer method of calibration is a convenient one and is used at the University of New England, where the unattenuated calibration pulses are obtained by gating the controlled receiver at the rate f/2. This ensures that the calibration pulses are identical in shape and magnitude with the pulses E_o of the train used in measurement. Workers in Norway and at Pennsylvania State University have obtained the calibration reading by introducing, either at the input of the receiver or within the receiver, a known change in amplitude of alternate RF pulses. Whatever method of calibration is employed during experiments, the high reading accuracy that can be achieved under good observing conditions even when the modulation depth is as small as 0.1 per cent (see, for example, Figs. 12 and 13), the "black box" nature of Fejer equipment, and the possibility of obtaining useful information about the properties of the lower ionosphere from comparisons* of modulation depths observed in different parts of the world, make it desirable for the accuracy of the method of calibration to be checked by an independent method. A network comprising resistances and a fast-acting relay, which is used at the University of New England to modulate the output of a signal generator to a number of standard depths from 0.044 per cent to 80 per cent, each accurate to about 1 per cent, is described in outline by Smith et al.

Technical details of the equipment being used at Pennsylvania State University to measure small changes in the phase of the wanted pulse are given in references cited in Section 1.

Fig. 1 shows parts of the radiofrequency circuits of the 500 kw., pulse and CW, gyrotransmitter at the University of New England. The 66 kv. sub-station for this transmitter is illustrated in Fig. 2, which also contains a view down the main trunk feeder lines towards the circularly polarized array of 40 dipoles. This unique transmitting installation (Station B) for the gyrofrequency and its associated wanted station C (Fig. 3) were constructed under Contract AF19(604)-6177 for studies of non-linear phenomena in the ionosphere at electron energies up to about 1 ev. and to test the theory of Bailey (1959) that prolonged electron heating at night will cause a significant increase in electron density near the 85-km. level by reducing the rate of attachment of electrons to molecules of oxygen. Part of the complexity of the receiving equipment evident in Fig. 3 is due to the wide variety of the pulse wave interaction experiments being performed at C and part is due to a desire to make the equipment as flexible and versatile as possible. Technical details of B and C, and of a third and earlier station A, are given by Smith et al. The experimental parameters of stations A and C are summarized in Paper 3.2.1.

In both his original experiments and his later experiments with Vice, Fejer transmitted a short (50 μsec.) disturbing pulse D at a number of delays after the wanted pulse W and before the return of the wanted echo E. This experiment has been followed in Norway, in Alaska, and at Pennsylvania State University, but is only one of a number of possible experiments. Those illustrated in Fig. 4 are classified according to the scheme used by Smith et al.

In an experiment of Type I, the pulse D precedes the pulse W and the interaction is measured at a number of delays t between the trailing edge of D and the leading edge of W. For this delay we will use the code DtW with t given in microseconds. As may be seen from the height-time diagram associated with this part of Fig. 4, the transient perturbation of the collision frequency is intercepted by the wanted pulse on both its upward and downward paths. The experiment provides no direct height information, but the decay of $\Delta\nu$ can be studied to any delay and the disturbing pulse can be of any duration.

* For these comparisons to be worthwhile, the gain of the disturbing aerial and the radiated power must also be known with high accuracy.

The Fejer experiment is classified at Type II and results in the perturbation being intercepted by the wanted pulse only on its downward path. The experiment provides direct height information but, unless the wanted pulse is reflected by the F layer, no direct information about the decay of $\Delta\nu$ is obtained. Also, since the duration T_d of the disturbing pulse can be only a fraction of the group time T_E of the wanted echo, the electron heating is small at levels where the electron relaxation time is comparable to, or longer than, T_E.

The Type III experiment combines Types I and II with superposition of the pulses D and W and thus provides direct information about height and the decay of $\Delta\nu$. The advantages of the Type III experiment for studies of the daytime D region will be demonstrated later.

The modulation depth, that would be impressed on the wanted pulse during a single transit of the disturbed region when $\Delta\nu$ is steady, is an important theoretical quantity. The depth can be deduced from experimental data of Types I to III but is best determined experimentally by using a disturbing pulse, which starts a sufficiently long time before W and ceases just before, or after, the return of the echo E. The modulation depth measured in this Type IV experiment is twice the depth for a single transit under steady conditions.

Type II and Type III experimental data should preferably be plotted against the time, in microseconds, between the leading edges of D and E. For this delay we will use the code DtE. The widespread practice of converting the delay measured in this way to a meeting height of the upgoing disturbing pulse and the downcoming wanted pulse should be discontinued. It has no merit and can give the false impression that the modulation corresponding to a given meeting height is actually impressed at that height (see also discussion of Fig. 11).

To define the problem we propose to examine in later sections of this paper and to illustrate aspects of pulse wave interaction measurement, we have shown in Figs. 5 to 17 experimental records and data of Types I to IV obtained at the University of New England by Smith et al. and typical records and data of Type II obtained in Norway and at Pennsylvania State University. Since the depth of the impressed modulation increases with the power of the disturbing pulse and it may appear from the quality of a number of the records of Smith et al. that very high disturbing powers were used, it is noted that at the frequencies of 1.78 Mc/s. and 1.515 Mc/s. (the gyrofrequency at Armidale at a height of 85 km.), the gain of the disturbing aerial at Station A is approximately equal to the gain of a pair of crossed horizontal dipoles above a perfectly reflecting ground.

The upper part of Fig. 5 shows a record of Type I obtained between 2340-2355 E.A.S.T. on 5 April, 1963 using an extraordinary wanted echo (2.12 Mc/s.) from the E layer and disturbing pulses from Station A of 5 kw. power and 820 μsec. duration radiated in the extraordinary mode at the gyrofrequency. The fraction in brackets after the delay DtW refers to the attenuator setting of the selective amplifier; the change from ½ to 1 indicates that the gain was doubled. In this experiment, the use of an extraordinary gyrowave as the disturbing wave caused the electron heating to be confined to a thin region at the base of the nighttime E layer, and the use of an extraordinary echo in place of an ordinary echo enhanced the modulation depth by a factor of about 20. The low power of 5 kw. for the disturbing pulse ensured that $\Delta\nu$ was very small throughout the disturbed region. As may be seen from the lower part of the figure, the accuracy of the value of the time constant (840 μsec.) deduced from the data is high.

The measurements we have just discussed were made during experiments to determine the value of the energy loss coefficient G at heights near 85 km. (see Paper 3.2.1). On theoretical grounds, an ordinary mode wanted echo at 2.12 Mc/s. would have served the purpose of the experiment equally well, but the modulation depth would have been too small for accurate measurement. The reduction in the modulation depth could have been off-set by the use of a much higher disturbing power, but then an effect shown in Fig. 6, in which similar data to that in the previous figure are plotted for a number of powers of the disturbing pulse, would have been produced. In Fig. 6 the order of the measurements is indicated by the number in brackets against each line and the plotted values are the derived values of the impressed decrement and not the measured values of the impressed modulation. The term "impressed decrement" is defined in Section 3, where the need for the distinction is discussed. The time constants in Fig. 6 refer to variations at small values of the impressed decrement (and thus to near-thermal relaxation) and increase from 640 μsec., when the power was 5 kw.,

to 1260 μsec., when the power was 175 kw. This change in the value of the near-thermal time constant can be attributed to the self-interaction of the disturbing pulse; the magnitude of the change corresponds to an increase of 4 km. in the mean height of the disturbed region*.

Fig. 7 shows an experimental record of Type I obtained near noon on 22 November, 1963 during experiments to determine the value of G in the lower D region (see Paper 3.2.1). The disturbing pulse (1.78 Mc/s., x-mode, 37 kw., 800 μsec.) was transmitted from Station A and the wanted echo (2.12 Mc/s., o-mode) was reflected by the E layer. Over the range − 110 μsec. to 15 μsec. for DtW, the delay was varied slowly and continuously. The time between major vertical lines on the chart was 5 min., the times printed on the chart should be ignored, and the detector integration time was about 2 sec. (These remarks apply also to the experimental records shown in Figs. 12 and 13.) For the accurate measurement of time constants as short as that deduced from the record (43 ± 2 μsec., see lower part of Fig. 7) it is necessary for the group time of the wanted echo to be constant. An output pulse from the receiver much shorter than the 50 μsec. used in this experiment is also desirable, so that the useable delay range without overlap of the disturbing pulse is increased.

Unlike other wave interaction data, it is relatively easy to compare time constants measured at different places using different experimental parameters. Since the electron relaxation time in the lower ionosphere changes by a factor of about three in 6 km. and the accuracy of measurement of a time constant is high, small changes in the mean height can be detected easily. If the time constant is found to be the same from day to day, it is a reasonable inference that both the ionization and the properties of the atmosphere are stable. These features make Type I measurements of the time constant a valuable means of studying synoptic changes in the lower ionosphere.

The experimental record of Type II shown in the upper part of Fig. 8 appears to be typical of records obtained at Kjeller and at Tromso during the period 1957 to 1960 using linearly polarized disturbing pulses. From the values of cross modulation** as a function of meeting height shown in the lower part of the figure, Landmark and Lied (1961) have deduced electron density profiles for the daytime D region and the nighttime lower E region in summer and winter and at the equinoxes. A number of other electron density profiles for the D region during quiet and disturbed conditions have also been deduced by the group in Norway from Type II data of similar quality.

In later experiments at Kjeller, the disturbing pulse (2 Mc/s., 160 kw. omni-directional power, 100 μsec.) was circularly polarized. The parts of Fig. 9 are reproduced from Barrington, Thrane, and Bjelland (1963). They give the results of experiments made throughout the day during the periods 17 March to 7 April, 16 August to 9 September, and 17 November to 16 December in 1960. The upper of the two experimental records was obtained when there was little external noise and the wanted echo was steady; the lower was obtained in the presence of appreciable external noise. Barrington et al. comment that not only the accuracy but also the sensitivity of the equipment is dependent on the noise level. The latter is not a feature of measurements at the University of New England, where the average deflection is independent, as it should be, of the external noise. The values of transferred modulation plotted against meeting height in Fig. 9 are the average values between 10 and 11 o'clock local mean time for about eight days in the equinoctial period, and each point represents the average of from 10 to 14 values. The results of Barrington, Thrane, and Bjelland from averaged data of this kind for the diurnal variation of the electron density profile have been used in other work on the D region.

---

* The absorption coefficient of an exact extraordinary gyrowave is inversely proportional to the collision frequency. Its electron heating causes the wave to be less strongly absorbed and so penetrate to a greater height, where the electron relaxation time is longer.

** In the discussion of Figs. 8, 9 and 10, the notation and terminology of the respective paper is used.

The extension of the Fejer technique to the measurement of very small changes in the phase of the wanted pulse is a major technical achievement, and it is of considerable interest that records (Fig. 10) of phase interaction T_ϕ and amplitude interaction T_A published by the group at Pennsylvania State University have similar signal-to-noise ratios. This does not always appear to be the case, however, since their quarterly reports (Lee and Ferraro 1964, etc.) list values of T_ϕ for roughly only one-third of the values of T_A. The reason for this difference is not stated and possibly this point will be clarified in the discussion. Since phase interaction is certain to play a wider role in future studies of the D region, some comment on the present experimental technique is in order. The records shown in Fig. 10 each suffer from the lack of a well-defined "zero". There is, of course, no difficulty in establishing such a zero in the case of T_A, but there may be technical problems in the case of T_ϕ. Until these are overcome, the measurement of T_ϕ will suffer by comparison with the measurement of T_A. Also, since T_A and T_ϕ are treated analytically as independent quantities, it is essential that the experimental values originate from separate "black boxes", rather than from separate ports in the same black box.

Except for Fig. 12, Figs. 11 to 17 are taken from the report of Smith et al.

The Type II measurements in Fig. 11 were made between 0245 and 0430 E.A.S.T. on 24 October 1962 using a disturbing pulse (91 kw., 130 μsec., x-mode) at the gyrofrequency from Station A and a wanted echo (2.12 Mc/s., x-mode) from the F layer. The values of the impressed decrement extend over almost three decades of magnitude and the long group time of the wanted echo permitted the exponential variation beyond the peak to be followed to long delays. The time constant deduced from this portion of the data is 640 μsec.

The experimental data in Fig. 11 have been used by Smith et al. to associate electron relaxation time with height in the lower E region. The curve drawn in the figure is a theoretical curve, calculated and located in the manner described in Paper 3.2.1, for interaction at a height of 85 km. in an infinitesimally thin region, in which the electron relaxation time is equal to 640 μsec. The curve is almost a perfect match of the experimental data and the only evidence of thickness of the disturbed region is the difference of about 10 μsec. in delay between the start of the experimental data and the start of the theoretical curve. Had the delay axis been labelled in terms of the meeting height of the disturbing and wanted pulses, the rising part of the experimental plot would have covered about 30 km. of the height scale and the maximum meeting height would have been over 300 km. Clearly, this method of labelling the delay axis would have obscured, rather than clarified, the significance of the experimental data.

The Type II record shown in Fig. 12 was obtained in the early afternoon of 15 April, 1964 during testing of a 12 μsec. output gate for the receiver and operation at the high repetition rate of 333.3 p.p.s. for the wanted pulse. The disturbing pulse (1.78 Mc/s., x-mode, 108 kw., 60 μsec.) was transmitted from Station A and the wanted echo (2.12 Mc/s., o-mode) was from the E layer. The markers on the side of the chart for the delay DtE occur at 10 μsec. intervals and the modulation depth at the peak of the record is about 0.3 per cent. The two large spikes on the rising portion of the record can be ignored, since they were caused by an intermittent contact in the aerial feeder line of the wanted transmitter. After the peak had been reached, the wanted echo changed from a relatively steady, single echo to one with rapid and deep fades. The marked change in the signal-to-noise ratio, which this caused, is obvious. A feature of this record, which we draw particular attention to, is the absence of negative modulation at the onset.

The records of Type III shown in Fig. 13 play an important role in subsequent discussion in this paper and were obtained near noon on 4 November, 1963 with continuous variation of the delay DtE. The wanted echo (2.12 Mc/s., o-mode, 50 μsec., 166.6 p.p.s.) was from the E layer and the disturbing pulse (1.78 Mc/s., 63 μsec.) was transmitted from Station A. For the upper record, the power of the disturbing pulse was 100 kw. in the extraordinary mode; for the lower record, the power was 81 kw. in the ordinary mode. In both records the modulation depth at the first peak (i.e., the peak at the smaller value of DtE) is less than the modulation depth at the second peak; the difference is small in the case of the x-mode record, but is marked in the case of the o-mode record. A second obvious difference between the two records is the much greater extent of the tail of the o-mode record.

A third difference — the earlier start, by about 20 μsec., of the x-mode record — is evident in Fig. 14, in which the plots of modulation depth against the delay DtE are scaled to a common power of 100 kw. Since the same wanted pulse was used, this difference simply reflects the fact that the modulation depth, measured using the more highly absorbed disturbing pulse, was above the threshold of detection at an earlier delay.

For comparison with the daytime Fejer curves, two nighttime curves of Type II have also been plotted in Fig. 14 with arbitrary amplitudes. The curve labelled 24.10.62 was obtained using a 130 μsec. disturbing pulse and is a smoothed plot of the experimental data in Fig. 11. The data for the curve labelled 7.9.64 were obtained between 0115 and 0150 E.A.S.T. on that date using a wanted echo (2.12 Mc/s., x-mode) from the F layer and a disturbing pulse (1.515 Mc/s., x-mode, 60 μsec.) from Station A of closely the same duration as used for the two daytime curves. The time constants deduced from the nighttime curves are nearly equal (640, 750 μsec.), indicating that the modulation was impressed on the wanted pulse at closely the same height on the two nights. Like the curve for the night of 24.10.62, the curve for the night of 7.9.64 shows minute evidence of thickness of the disturbed region. For all the curves plotted in Fig. 14, the duration of the output pulse from the receiver was the same (50 μsec.).

During the day the energy of an ordinary disturbing wave at 1.78 Mc/s. is absorbed in depth and, as we shall show in Section 5, the Type III curve in Fig. 14 for this disturbing wave provides clear evidence of this penetration. However, it is evident that if the nighttime curve for 7.9.64 were to be displaced in delay, it would be a fair match to the front part (i.e. the Type II part) of the noon o-mode curve. Since the deduction of electron density profiles for the D region from pulse wave interaction data requires the resolution of Fejer curves of the kind we have illustrated into components from different height regions, it should be evident that for this purpose Type II data have serious limitations.

In order to obtain information on the practical limits to the application of small perturbation wave interaction theory and to study electron heating under large perturbation conditions, the dependence of the modulation depth on the power of a disturbing extraordinary gyrowave has been determined at the University of New England on numerous occasions. Figs. 15 and 16 illustrate two extremes. The data plotted in the first of these figures were obtained on the night of 7 October, 1960 using 800 μsec. disturbing pulses from Station A and a wanted echo (2.12 Mc/s., x-mode) from the E layer. The disturbing pulse was located at the fixed delay D30W and the lowest power used in the measurements was 300w*. The data plotted in Fig. 16 were obtained in Type IV experiments made in January 1965 using 10 ms. disturbing pulses in the extraordinary mode from the powerful gyrotransmitter B and the wanted echoes of extraordinary (2.12 Mc/s.) and ordinary (1.78 Mc/s.) modes. When allowances are made for the different pulse durations and the different aerial gains, Fig. 15 extends the plot in Fig. 16 for the 2.12 Mc/s. wanted wave down to a power (from B) of about 10w.

Fig. 17 is the only record shown in this paper from experiments using Station B and data from the record are plotted in Fig. 16. The wanted echo at 2.12 Mc/s. from the E layer was particularly steady and, as may be seen from Fig. 17, the signal-to-noise ratio is high. Generally, however, it has been found that Station B, with its highly directive aerial, yields records of poorer quality when the echo is fading than does the disturbing Station A, with its less directive aerial. The reason for this difference cannot be established easily, but it is believed to be caused by the large cone angle of arrival of a fading echo. In experiments using highly directive disturbing aerials, the wanted aerials should ideally be more directive. The necessity to wait until the reflection of the wanted pulse is specular severely limits the use of Station B.

Huxley (1952), in discussing the proportionality between modulation depth and disturbing power observed in England in 1948 using disturbing powers up to 520 kw. at a frequency of 0.167 Mc/s., has concluded on theoretical grounds that the proportionality holds only when the perturbation of the collision frequency is small.That this conclusion is incorrect is evident from the data plotted in Figs. 6 and 15. For the maximum power plotted in the latter

* During 1962 the disturbing aerial at Station A was changed from a single horizontal dipole to the present square array of 4 dipoles. The powers plotted in Fig. 15 are the equivalent powers in the extraordinary mode for the square array.

figure, the "time constant" in Fig. 6 is significantly longer than the time constant for a near-thermal perturbation, because of the self-interaction of the disturbing pulse. A behavior for electrons in air that has been found by Smith et al. to be consistent with data such as shown in the two figures, is mentioned briefly in Section 4 of Paper 1.6.

3. Small Perturbation Wave Interaction Theory

In wave interaction theory the small changes in the mean electron collision frequency ν and the mean electron energy U occurring during a cycle of the disturbing wave are neglected and the much larger changes occurring at modulation frequencies are calculated using the energy balance equation

$$\frac{dU}{dt} + (\nu\eta) = \frac{I}{N} F^2(t) \tag{1}$$

where F(t) is the modulation function of the envelope of the disturbing wave, I is the mean power over a cycle it supplies when unmodulated (F(t) = 1) to the N electrons in unit volume, and $(\nu\eta)$, the mean rate at which an electron loses energy in collisions with the molecules of the gas, can be expressed as

$$(\nu\eta) = G'\nu(U - U_o) \tag{2}$$

where the value of the dimensionless coefficient G' is a function of U and the thermal energy U_o of the gas (see Paper 1.6).

We assume that the disturbing aerial radiates vertically a single wave mode. The power flux density Π of the disturbing wave at a height h directly above the aerial is then given by

$$\Pi = \frac{gW}{4\pi h^2} \exp\left(-2\int_o^h k_d(\nu)dh\right) \tag{3}$$

where g is the gain of the aerial referred to an isotropic radiator, W is the radiated power, $k_d(\nu)$ is the absorption coefficient of the wave mode, and Π is related to I and $k_d(\nu)$ by

$$I = 2k_d(\nu)\ \Pi \tag{4}$$

If the functions $U(\nu)$, $G(U, U_o)$ are known, then (1) can be expressed as an equation in ν which, through the term I, is coupled to the equations for lower levels in the disturbed region. This coupling is caused by the self-interaction of the disturbing wave and in general the solution $\nu(h,t)$ can be found only by numerical methods for particular models of the undisturbed ionosphere.

Let

$$\Delta\nu = \nu - \nu_o \tag{5}$$

where ν_o is the collision frequency in the undisturbed ionosphere.

When the perturbations of the electron energy and collision frequency are small throughout the disturbed region, the inequalities $U - U_o \ll U_o$, $\Delta\nu \ll \nu_o$, which then apply, allow the discussion of equations (1) to (4) to be simplified considerably. For I in (1) we can substitute I_o, its value with $\nu = \nu_o$, thus eliminating the coupling. For $G\nu$ in (2) we can substitute $G\nu_o$, where G is a function of U_o only. We can also use the approximation

$$U = U_o + \alpha \frac{U_o}{\nu_o} \Delta\nu \tag{6}$$

where

$$\alpha = \frac{\nu_o}{U_o} \left(\frac{\partial U}{\partial \nu}\right)_o \tag{7}$$

In (7) the subscript o attached to the derivative means that it is to be evaluated with $\nu = \nu_o$.

With these simplifications, equation (1) reduces to

$$\frac{d\Delta\nu}{dt} + G\nu_o \Delta\nu = \frac{\nu_o I_o}{\alpha N U_o} F^2(t) \tag{8}$$

For a rectangular disturbing pulse of duration T_d starting to act at $t = 0$ ($F(t) = 1$, $0 \leqslant t \leqslant T_d$; $F(t) = 0$, $t \geqslant T_d$) the rise of $\Delta\nu$ during the pulse is given by

$$\Delta\nu = \Delta\nu_s\left[1 - \exp(-t/\tau)\right] \tag{9}$$

and the decay following cessation of the pulse by

$$\Delta\nu = \Delta\nu_s\left[1 - \exp(-T_d/\tau)\right]\exp\left[-(t - T_d)/\tau\right] \tag{10}$$

where

$$\tau = 1/G\nu_o \tag{11}$$

and

$$\Delta\nu_s = \frac{I_o}{\alpha N G U_o} \tag{12}$$

The solutions (9) and (10) of (8) will apply for repetitive pulses if the period between pulses is long compared to the electron relaxation time τ.

In applying the preceding results to calculate the changes in the amplitude and phase of the wanted pulse, we assume that it is reflected well above the region acted on by the disturbing pulse. The modifications of the theory to allow for a change in the reflection coefficient of a partial reflection from the D region are given by Smith et al.

At the ground the field amplitude of the reflected wanted pulse is proportional to $\frac{1}{L}\exp(-\int_L k_w(\nu)dh)$, where $k_w(\nu)$ is the absorption coefficient of the wave mode and L is the total length of the up and down paths. The association of L with the integral sign means that the integral is to be evaluated over the total path with dh always considered positive. It follows that the modulation depth M_k ($= (E_o - E)/E_o$) impressed on the wanted pulse due to the change in its absorption is given by

$$M_k = 1 - \exp(-m_k) \tag{13}$$

where

$$m_k = \int_L \{k_w(\nu) - k_w(\nu_o)\}dh \tag{14}$$

The up and down paths of the wanted pulse introduce a phase lag of $\frac{\omega}{c}\int_L \mu\, dh$ radians, where ω is its angular frequency, c is the velocity of light in free space and μ is the real

refractive index. For compatibility with the definition of M_k we define the phase interaction M_ϕ to be equal to the phase of the undisturbed wanted echo minus the phase of the disturbed wanted echo. Hence,

$$M_\phi = \frac{\omega}{c}\int_L \{\mu_w(\nu) - \mu_w(\nu_o)\}dh \tag{15}$$

Formulae (13) to (15) are general and their use is not restricted to the case of a small perturbation. When $|M_k| << 1$, the approximation $M_k \doteq m_k$ can be made. When this approximation is invalid, it is preferable to consider the derived quantity m_k, which is more simply related to the wave propagation than the measured quantity M_k. No such difficulty occurs in the case of M_ϕ. The quantity m_k has been referred to by Smith et al. as the "impressed decrement", but a better name is desirable.

When $\Delta\nu << \nu_o$ we can use in place of (14) and (15) the approximate formulae

$$M_k = m_k = \int_L \left(\frac{1}{N}\frac{\partial k_w}{\partial \nu}\right)_o N\Delta\nu \, dh \tag{16}$$

and

$$M_\phi = \frac{\omega}{c}\int_L \left(\frac{1}{N}\frac{\partial \mu_w}{\partial \nu}\right)_o N\Delta\nu \, dh \tag{17}$$

where the subscript o attached to each of the partial derivatives has the significance assigned earlier, and where, for propagation under non-deviating conditions, the terms in brackets in each integral can be taken to be independent of the electron density N.

The use of the approximation (6) in a formal statement of small perturbation wave interaction theory avoids the difficulty that the relation A(c) between the collision cross-section A and the electron speed c for thermal electrons in air is unknown (see Paper 1.6) and brings out the property that except for its amplitude the transient waveform of $\Delta\nu$ (and thus of M_k and M_ϕ) is independent of this relation. The two behaviors that have been adopted in papers on wave interaction are a constant cross-section (A = const.), for which $\nu \propto U^{\frac{1}{2}}$, and $\alpha = 2$, and a cross-section proportional to electron speed ($A \propto c$), for which $\nu \propto U$ and $\alpha = 1$. The first of these behaviors was proposed by Bailey and Martyn (1934); the second was proposed by Crompton, Huxley, and Sutton (1953) and is now known to occur in nitrogen (see Paper 1.6). Since 1960, with a few exceptions, the $A \propto c$ hypothesis has been preferred.

The integrals (16) and (17) are evaluated taking into account the different times at which the disturbing pulse acts on, and the wanted pulse passes through, each section of the disturbed region. A method for doing this is described in the next section.

We now discuss the much simpler case of steady conditions in the disturbed region during the upward and downward transits by the wanted pulse. To avoid introducing a factor of 2, we consider only the upward path, which we take to extend to an infinite height.

An exact expression for the steady modulation depth M_{ks} impressed on the wanted pulse during the single transit can be obtained under the following conditions:

$$\left.\begin{array}{ll} \text{(i)} & \text{the disturbing wave incident on the ionosphere is plane.} \\ \text{(ii)} & k_w(\nu) = AN\nu, \text{ where A is a constant.} \\ \text{(iii)} & \text{the composition and temperature of the gas are uniform in the disturbed region} \\ & \text{(i.e., } \alpha, G, U_o \text{ are constants).} \end{array}\right\} \tag{18}$$

Using (12) and the conditions just given, formula (16) becomes for a single transit

$$M_{ks} = \frac{A}{\alpha G U_o} \int_o^\infty I_o \, dh$$

Since I_o is the power per unit volume at the height h absorbed from the plane disturbing wave

$$I_o = -\frac{\partial \Pi}{\partial h}$$

Hence

$$M_{ks} = \frac{A}{\alpha G U_o} \Pi_i \tag{19}$$

where Π_i is the power flux density of the disturbing wave at entry into the ionosphere. This remarkably simple formula, which shows that under the condition (18) the depth M_{ks} is independent of the electron density and collision frequency profiles and of the frequency and mode of the disturbing wave, is due to Ratcliffe* (see Shaw 1951). It seems to have been largely forgotten since the introduction of the pulse methods.

In a pulse wave interaction experiment the divergence of the spherical disturbing wave cannot be neglected and, to be able to use (19) with any accuracy, it is necessary to identify the height in free space to which Π_i refers. In making the identification we assume that the thickness of the disturbed region is small compared to its height above the ground.

Let

$$I_o = \frac{gW}{4\pi h^2} i$$

where

$$\int_o^\infty i \, dh = 1$$

The last result follows from the fact that the power gW, when radiated omnidirectionally, is totally absorbed in a sphere of infinite radius.

Consider the integral $\int_o^\infty fi \, dh$, where f is a continuous function of h. Since the i(h) function is localized to the neighborhood of its mean height $\underline{h}$, we can adopt for f an expansion of the form

$$f(h) = f(\underline{h}) \left[1 + a_1 (h - \underline{h}) + a_2 (h - \underline{h})^2 + a_3 (h - \underline{h})^3 + \ldots\right] \tag{20}$$

and obtain

$$\int_o^\infty fi \, dh = f(\underline{h}) (1 + a_2 m_2 + \ldots) \tag{21}$$

where m_2 is the second central moment of the i(h) function.

* Ratcliffe considered the situation in which the path of the wanted ray through the disturbed region is rectilinear and inclined at an angle i_w to the vertical. Then (19) is multiplied by sec i_w.

Let

$$\int_0^\infty I_o(h)dh = gW/4\pi H^2 \tag{22}$$

and $\underline{H}$ be the mean height of the I_o (h) function. By expanding h^{-2} and h^{-1} as in (20) and neglecting terms in the third and higher moments, it is easily shown that

$$H = \underline{H}\ (1 + \frac{1}{2}\ m_2/\underline{h}^2) = \underline{h}\ (1 - \frac{3}{2}\ m_2/\underline{h}^2)$$

Now, let us suppose for simplicity that the i(h) function in the lower ionosphere ($\underline{h} \geqslant 60$ km.) is rectangular. If its height extent is 5 km., then $m_2 = 2.1$ sq. km., $m_2/\underline{h}^2 \leqslant 6 \times 10^{-4}$ and the error in identifying H with $\underline{H}$ is negligible. Thus, in place of (19), we obtain

$$M_{ks} = gW/4\pi\underline{H}^2 \cdot \frac{A}{\alpha GU_o} \tag{23}$$

with an error < 0.1 per cent for the example just considered.

The condition (18) that $k_w(\nu) = AN\nu$, where A is a constant, is unduly restrictive when the disturbed region is thin. The particular case of wave interaction at night, when both wanted and disturbing waves are extraordinary gyrowaves and the term $\frac{1}{N}\frac{\partial k_w}{\partial \nu}$ for the wanted wave is a rapidly varying function of height in the disturbed region, has been discussed in the report of Smith et al. Here we give a more general discussion covering the use of wanted waves of both polarization and wave interaction in the D and lower E regions. For simplicity, we use the Appleton-Hartree magnetoionic theory.

In current wave interaction experiments the propagation of the wanted pulse in the disturbed region is quasi-longitudinal (Q.L.) and non-deviating ($\mu \doteqdot 1$). The approximations made by Booker (1935) then yield the well-known formula

$$k_{o,e} = \frac{\rho_o^{\ 2}\nu}{2c\{(\omega \pm |\Omega_L|)^2 + \nu^2\}} \tag{24}$$

where $\rho_o^{\ 2} = 3.19 \times 10^9 N$, ω is the angular wave frequency and $\Omega_L = \Omega\cos\theta$, where Ω is the angular gyrofrequency and θ is the angle between the direction of the wave propagation and the direction of the earth's magnetic field.

For the extraordinary mode, the formula in (24) fails badly near the gyrofrequency. For this mode and the propagation conditions in pulse wave interaction experiments using gyrowaves, the following formula, due to Bailey (1938), is highly accurate (see Smith et al.):

$$k_e = \frac{\rho_o^{\ 2}\nu}{4c} \cdot \frac{(1 + \cos^2\theta)}{\{(\omega - \Omega)^2 + \nu^2\}} \tag{25}$$

Formulae (24) and (25) are of the form

$$k \propto N\nu/(a^2 + \nu^2)$$

where a is independent of ν. Thus,

$$\frac{1}{N}\ \frac{\partial k}{\partial \nu} \propto (a^2 - \nu^2)/(a^2 + \nu^2)^2$$

and is zero when $\nu = a$.

In the lower ionosphere the variation of ν with height is closely exponential with a scale height of about 6 km. If h' is the height in kilometers above the level where $\nu = a$, then

$$\frac{1}{N} \cdot \frac{\partial k_w}{\partial \nu} \propto y$$

where

$$y = \frac{1 - \exp(-h'/3)}{\{1 + \exp(-h'/3)\}^2}$$

This function, whose sign is the sign of the modulation impressed at the level, is shown plotted against h' in Fig. 18 for both positive and negative values of h'.

The disturbed region starts at the base of the ionosphere, and the form and the mean height $\underline{H}$ of the $I_o(h)$ profile are determined by the frequency and mode of the disturbing pulse and the ionization present. The height of the level h' = 0 is determined by the frequency and mode of the wanted pulse, so that, in principle, it is possible to choose these parameters to locate the $I_o(h)$ profile at any part of the h'-axis. In practice, any overlap of the profile with the region h' < 0 would be avoided as far as possible and we assume that the level $\underline{H}$ is above the level h' = 0. Since the disturbed region is assumed to be localized in height, we can then use for $\frac{1}{N} \cdot \frac{\partial k_w}{\partial \nu}$ the expansion

$$\frac{1}{N} \cdot \frac{\partial k_w}{\partial \nu} = \left(\frac{1}{N} \cdot \frac{\partial k_w}{\partial \nu}\right)_{h=\underline{H}} \{1 + \alpha_1(h - \underline{H}) + \alpha_2(h - \underline{H})^2 + \ldots\}$$

where the values of the coefficients α_1, α_2 etc. are functions of h'. Plots of α_1 and α_2 against h' (h' $\geqslant$ 1 km.) are shown in Fig. 18.

Using this expansion and the property that H and $\underline{H}$ are almost identical, we obtain

$$M_{ks} = \frac{gW}{4\pi\underline{H}^2} \cdot \frac{1}{\alpha G U_o} \cdot \left(\frac{1}{N} \cdot \frac{\partial k_w}{\partial \nu}\right)_{h=\underline{H}} \{1 + O(\mu_2\alpha_2)\} \tag{26}$$

where μ_2 is the second central moment of the normalized $I_o(h)$ profile.

To illustrate the use and significance of Fig. 18, let us suppose, as before, that the i(h) profile is 5 km. thick and rectangular in form. The mean height of this profile can be taken to be the height $\underline{H}$ and for μ_2 we can use, when estimating the value of $O(\mu_2\alpha_2)$, the value 2.1 sq. km. of m_2. The plot of α_2 against h' in Fig. 18 then shows that if the height $\underline{H}$ is above the level h' = 2 km. (at this level the disturbed region extends 0.5 km. into the region where y is negative) the error from neglecting the term $O(\mu_2\alpha_2)$ does not exceed 4 per cent in magnitude and can be considerably smaller. For example, when the profile is located between h' = 0.5 km. and 5.5 km., the error is less than 0.5 per cent, in spite of the fact that the value of y (and, hence, of $\frac{1}{N} \cdot \frac{\partial k_w}{\partial \nu}$) changes in this height range by a factor of about 15.

Omitting the term $O(\mu_2\alpha_2)$ from (26) we obtain the formula

$$M_{ks} = \frac{gW}{4\pi\underline{H}^2} \cdot \frac{1}{\alpha G U_o} \cdot \left(\frac{1}{N} \cdot \frac{\partial k_w}{\partial \nu}\right)_{h=\underline{H}} \tag{27}$$

The accuracy of this simple formula for the modulation depth impressed on the wanted pulse during a single transit of a thin disturbed region under steady conditions can be high in a suitable experiment (see Paper 3.2.1).

The "thin slab" approximation to the steady phase interaction $M_{\phi s}$ is obtained by replacing the term $(\frac{1}{N} \cdot \frac{\partial k_w}{\partial \nu})_{h=\underline{H}}$ in (27) by the term $\frac{\omega}{c}(\frac{1}{N} \cdot \frac{\partial \mu_w}{\partial \nu})_{h=\underline{H}}$. The analysis for this type of wave interaction is not given here, but it is found that the accuracy of the approximation is comparable to that for M_{ks}.

The generalized magnetoionic theory of Sen and Wyller (1960) is now preferred to the theory of Appleton and Hartree in the analysis of wave propagation in the lower ionosphere. The Sen and Wyller theory is an average for a Maxwellian distribution for a collision cross-section proportional to electron speed ($\alpha = 1$), and an inconvenient numerical factor is often avoided by using a collision frequency ν_m equal to two-thirds of the mean collision frequency ν. For the same reason, it is then convenient to use an energy loss coefficient G_m such that

$$\tau = 1/G_m \nu_m = 1/G\nu \tag{28}$$

where $G_m = \frac{3}{2} G$.

To use the Sen and Wyller magnetoionic theory with any of the formulae given above, it is necessary only to put $\alpha = 1$, if the magnetoionic collision frequency is the mean value. If the magnetoionic collision frequency is taken as ν_m, then both G and ν in the formulae must be subscripted.

4. Theory of Fejer Curves

We now examine how Fejer curves of Types II and III are formed out of contributions from different levels in the disturbed region, which we consider to be divided by horizontal planes into a large number of thin, closely homogeneous sections of equal thickness Δh. The mean height of the ith section is denoted by h_i.

The time relations in a pulse wave interaction experiment are most easily visualized from a height-time diagram. In Fig. 19 time increases from left to right, W is the transmitted wanted pulse, D is the transmitted disturbing pulse, E is the wanted echo from the E or F layers and t is the time delay of the leading edge of E after the leading edge of D. With W fixed in time, the pulse D moves from right to left as the delay t is increased.

We assume that the disturbing pulse is so highly attenuated when it reaches a reflecting layer in the ionosphere that electron heating by the reflected pulse can be neglected. The perturbation $\Delta\nu_i$ at height h_i is then a single transient of the form (9) and (10) when the electron heating is small and the disturbing pulse is rectangular.

If the duration of the wanted pulse is negligible (δ-pulse), then from (16) and (17), respectively, the modulation depth and phase change impressed on it during a transit of the section at height h_i are given by

$$\left.\begin{aligned} M_{ki} &= \left(\frac{1}{N}\frac{\partial k_w}{\partial \nu}\right)_i N_i \Delta\nu_i \Delta h \\ M_{\phi i} &= \frac{\omega}{c}\left(\frac{1}{N}\frac{\partial \mu_w}{\partial \nu}\right)_i N_i \Delta\nu_i \Delta h \end{aligned}\right\} \tag{29}$$

As D moves from right to left in Fig. 19, the perturbation $\Delta\nu_i$, which moves with it, is intersected first on the downward (↓) path OE of the wanted pulse. When D overlaps, or precedes, W, the perturbation is intersected also on the upward (↑) path WO. Since from (29) the modulation depth or phase change are proportional to the value of $\Delta\nu_i$ at the time of the transit of the section by the wanted pulse, it follows that the plot of ΔM_i against the delay t consists of the parts

$$\Delta M_i(t) = \Delta M_i(t)\downarrow + \Delta M_i(t)\uparrow$$

which are identical in magnitude and have the waveform of $\Delta\nu_i$, but are displaced relative to each other as shown in the lower part of Fig. 19. If group refraction in the disturbed region is negligible, the onset of the component $\Delta M_i(t)\downarrow$ occurs at the delay $2h_i/c$ and the onset of the component $\Delta M_i(t)\uparrow$ occurs at a fixed delay T_E equal to the group time of the wanted echo. To illustrate the relative positions on the delay axis of the contributions from different sections, the two components for a height h_j, where $h_j > h_i$, have also been shown in the lower part of Fig. 19. The Fejer curve $M^\delta(t)$ from the interaction of a rectangular disturbing pulse and a δ-wanted pulse in an extended height range can thus be resolved into the sum of suitably located elementary waveforms.

Since the waveforms that produce the first peak (i.e. the Type II part) of the $M^\delta(t)$ curve are added displaced relative to each other, whereas those that produce the second peak are added without displacement, the second peak must, in general, have a greater amplitude than the first peak. The waveforms that produce the first peak will also contribute to the second peak unless their decay is complete by the delay T_E.

The calculation of the $M^\delta(t)$ curve for given experimental parameters and ionospheric conditions utilizes the following theory:

Let Π_i by the power flux density of the disturbing wave incident on the section i and δ_i be the fraction of Π_i which penetrates to the section i + 1.

Then

$$\delta_i = \exp(-2\, k_{di}\, \Delta h) \tag{30}$$

and

$$\Pi_i = \frac{gW}{4\pi h_i^2}\, \delta_1\delta_2 \cdots \delta_{i-1} \tag{31}$$

The power absorbed in a unit column of the section i is

$$P_i = (1 - \delta_i)\Pi_i \tag{32}$$

Using (9), (10), (12), and (29), the shape and magnitude of the component $M_i(t)\uparrow$ (or $M_i(t)\downarrow$) are given by

$$\left.\begin{aligned} 0 \leqslant t' \leqslant T_d; \quad & \Delta M_i(t')\uparrow = \Delta M_{si}\,\{1 - \exp(-t'/\tau_i)\} \\ t' > T_d; \quad & \Delta M_i(t')\uparrow = \Delta M_{si}\,\{1 - \exp(-T_d/\tau_i)\}\exp\{-(t' - T_d)/\tau_i\} \end{aligned}\right\} \tag{33}$$

where

$$\tau_i = 1/G_i\nu_i \tag{34}$$

and, in the case of a change in the amplitude of the wanted pulse,

$$\Delta M_{si} = \frac{1}{\alpha G_i U_{oi}} \cdot \left(\frac{1}{N}\frac{\partial k_w}{\partial \nu}\right)_i P_i \tag{35}$$

By means of (31) and (32), the last formula can be written as

$$\Delta M_{si} = Q(h_i)\ \delta_1\delta_2 \ldots \delta_{i-1}(1-\delta_i) \tag{36}$$

where

$$Q(h_i) = \frac{gW}{4\pi h_i^2}\ \frac{1}{\alpha G_i U_{oi}} \cdot \left(\frac{1}{N}\frac{\partial k_w}{\partial \nu}\right)_i \tag{37}$$

Total absorption of the power of the disturbing wave imposes the condition

$$\Sigma\{M_{si}/Q(h_i)\} = 1 \tag{38}$$

A knowledge of the experimental parameters T_d, g, and W, the time T_E and the quantity α enables the calculation of the components $\Delta M_i(t)\uparrow$ for the interaction of particular wanted and disturbing waves for given profiles N(h), $\nu(h)$, $U_o(h)$, and G(h). Summation of these components and the displaced components $\Delta M_i(t)\downarrow$ over the disturbed region yields the $M^\delta(t)$ curve. The shape of the curve is independent of the quantities α, g and W.

A number of further steps are necessary to obtain a curve that can be compared with the experimental curve.

The output pulse from the receiver has a finite duration T_w. If this pulse is rectangular and the detector responds to the average value in the pulse, then the Fejer curve is given by

$$M(t) = \frac{1}{T_w}\int_t^{t+T_w} M^\delta(t)\ dt \tag{39}$$

The onset of this averaged curve occurs at a delay earlier by T_w than the onset of the $M^\delta(t)$ curve.

In practice, the pulse from the receiver and the disturbing pulse are non-rectangular. The average (39) must then be evaluated for the shape of the pulse from the receiver and for $\Delta\nu_i$ it is necessary to use the solutions of (8) for the power envelope $F^2(t)$ of the disturbing pulse. Since non-rectangular pulses can be simulated by the sum of suitable rectangular pulses, these elaborations to obtain a Fejer curve corresponding to experimental reality require no additional theory and can easily be incorporated in a computer program. An analogue method of adding correctly shaped and averaged waveforms is described in Section 5.

The theory given above shows how a Fejer curve is formed out of contributions from different sections of the disturbed region and how the curve for a given set of ionospheric and experimental conditions may be computed. The converse problem of obtaining information on the properties of the lower ionosphere from an experimental curve is considered in the next section.

In a wave interaction experiment at night using an extraordinary gyrowave as the disturbing wave, the electron heating is confined to a region of up to about 5 km. in thickness, so that between its height extremes the electron relaxation time can vary by about a factor of three. Despite this large possible variation, experiments of Type I made at night yield a plot of modulation depth against the delay DtW, which is closely exponential. To a high accuracy a time constant τ_i can be associated with the initial decay. This has been illustrated in Fig. 6.

In Section 3 it was shown that for disturbed regions of comparable thickness the modulation depth M_{ks} under steady state conditions closely approximates the depth that would have been impressed had interaction occurred in an infinitesimally thin region located at the mean

height $\underline{H}$ of the $I_o(h)$ profile for the disturbing wave. The relation between τ_i and the electron relaxation time $\tau_{\underline{H}}$ at the height $\underline{H}$ is thus of considerable interest.

In a Type I experiment, both transits of the disturbed region by the wanted pulse occur while $\Delta\nu$ is decaying. Neglecting the duration of the wanted pulse,* it follows from (10), (11), (12), and (16) that the modulation depth $M_k(t)$ measured at the delay t (DtW) is given by

$$M_k(t) = \frac{1}{\alpha G U_o} \int_o^\infty f(h) \exp(-t/\tau) dh \tag{40}$$

where

$$f(h) = \left(\frac{1}{N} \frac{\partial k_w}{\partial \nu}\right) D(h)\ E(h)\ I_o \tag{41}$$

$$D(h) = 1 - \exp(-T_d/\tau) \tag{42}$$

$$E(h) = 1 + \exp\{-(T_E - \frac{2h}{c})/\tau\} \tag{43}$$

$$\tau = 1/G\nu \tag{44}$$

and I_o is given by (3) and (4). Here, as in Section 3, the quantities G and U_o are taken outside the integral, since the disturbed region is assumed to be confined to a narrow height range.

The time constant τ_i associated with the initial variation of $M_k(t)$ is given by

$$\left[-M_k(t) \ / \ \frac{d}{dt}\ \{M_k(t)\}\right]_{t=0}$$

and thus by

$$\tau_i = \int_o^\infty f(h)\ dh \ / \int_o^\infty \{f(h)/\tau\}\ dh \tag{45}$$

Let τ_f be the electron relaxation time at the mean height h_f of the f(h) function. Then

$$\tau = \tau_f \exp\{(h - h_f)/H_o\} \tag{46}$$

where H_o is the scale height of ν. Since the function f(h) is localized in the neighborhood of h_f it follows that, correct to the term in the second central moment μ_2' of the normalized f(h) function

$$\tau_i = \tau_f/(1 + \mu_2'/2H_o^2) \tag{47}$$

This bias of τ_i below τ_f is due to the form of (46).

The function f(h), and thus its mean height h_f, is seen in (41) to (43) to depend on the relation $k_w(\nu)$ for the wanted pulse, the echo delay T_E, the $I_o(h)$ profile, and the

* Over that part of the $M^\delta(t)$ curve which is exponential, the average (39) does not change its character.

duration T_d of the disturbing pulse. By the previous result the value of τ_i is influenced by these factors.

To examine this influence on τ_i we use the following expansions in the neighborhood of the mean height $\underline{H}$ of the $I_o(h)$ profile:

$$\left.\begin{aligned} \frac{1}{N}\frac{\partial k_w}{\partial \nu} &= \left(\frac{1}{N}\frac{\partial k_w}{\partial \nu}\right)_{h=\underline{H}} \{1 + \alpha(h - \underline{H})/H_o\} \\ D(h) &= D(\underline{H})\ \{1 + d(h - \underline{H})/H_o\} \end{aligned}\right\} \quad 48$$

$$\left.\begin{aligned} E(h) &= E(\underline{H})\ \{1 + e(h - \underline{H})/H_o\} \\ D(\underline{H}) &= 1 + \exp(-x) \\ d &= -x\ \exp(-x)/\{1 - \exp(-x)\} \end{aligned}\right\} \quad 49$$

$$\left.\begin{aligned} x &= T_d/\tau_{\underline{H}} \\ E(\underline{H}) &= 1 + \exp(-x) \\ e &= x\ \exp(-x)/\{1 + \exp(-x)\} \\ x &= (T_E - 2\underline{H}/c)/\tau_{\underline{H}} \end{aligned}\right\} \quad 50$$

In the expression for e in (50), a small term due to the transit time of the wanted pulse through the disturbed region has been neglected. From (41), (48), and the definitions of h_f and $\underline{H}$, it follows that as a first approximation

$$\underline{H} - h_f = -\mu_2\ (\alpha + d + e)/H_o \tag{51}$$

Since $|\underline{H} - h_f| << H_o$, we can make the approximation

$$\tau_f = \tau_{\underline{H}}\{1 - (\underline{H} - h_f)/H_o\}$$

Hence, using (47) and (51) we obtain, to the first power in small terms,

$$\tau_i = \tau_{\underline{H}}\ \{1 - \frac{\mu_2'}{2H_o^2} + \frac{\mu_2}{H_o^2}\ (\alpha + d + e)\} \tag{52}$$

To illustrate in Section 3 the magnitudes of terms such as those in (52), we used the value 6 km. for H_o and considered the simple example of a rectangular i(h) function extending over 5 km. and having a second central moment m_2 equal to 2.1 sq. km. This function determines the height extent of the functions f(h) and $I_o(h)$ and when estimating the magnitudes of small terms we have put $m_2 = \mu_2' = \mu_2 = 2.1$ sq. km. and $H_o = 6$ km. Then $\mu_2'/2H_o^2 = 0.03$.

The term d in (49) involves the duration T_d of the disturbing pulse and its value increases from -1 when $T_d/\tau_{\underline{H}} << 1$ to 0 when $T_d = \infty$. The corresponding range of $\mu_2 d/H_o^2$ is -0.06 to 0. When $T_d = \tau_{\underline{H}}$ the value is -0.035.

The term e in (50) involving T_E vanishes when $x = 0$ and ∞ and its value is a maximum when $x = 1.28$. Then $e = 0.28$ and $\mu_2 e/H_o^2 = +0.02$.

The coefficient α in (48) is H_o times the coefficient α_1, which was evaluated in Section 3 using the Appleton-Hartree magnetoionic theory and which is shown plotted in Fig. 18 against the height h' in kilometers above the level where $\frac{1}{N}\frac{\partial k_w}{\partial \nu} = 0$. The least height h' of practical interest in this figure is about 3 km., for which the variation of $\frac{1}{N}\frac{\partial k_w}{\partial \nu}$ with height is extremely rapid, $\alpha_1 = 0.4$ and $\mu_2\alpha/H_o^2 = +0.14$. For less extreme variations the value of the latter term decreases and is zero when the formula $k_w(\nu) = AN\nu$, where A is a constant, applies in the disturbed region.

The relaxation between τ_i and $\tau_{\underline{H}}$ in particular experiments is discussed in Paper 3.2.1.

Let $M_k(0)$ be the modulation depth measured at the delay t = 0, using a disturbing pulse of duration T_d and a wanted echo whose group time is T_E. It is then easily shown using (48) that M_{ks}, given by (27), and $M_k(0)$ are related by

$$M_{ks} = M_k\ (0)/D(\underline{H})\ E(\underline{H}) \tag{53}$$

where $D(\underline{H})$ and $E(\underline{H})$ are defined, respectively, in (49) and (50).

5. Interpretation of Fejer Curves

The theory in the preceding section shows that the shape of a Fejer curve depends on the frequency, wave mode, duration, and shape of each of the disturbing and wanted pulses, on the group time of the wanted echo (if the data are of Type III), and on the profiles N(h), $\nu(h)$, $U_o(h)$, and G(h) for the disturbed region. The absolute modulation depths are proportional to the power of the disturbing pulse and the gain of the aerial and depend, through the quantity α, on the relation between collision cross-section and electron speed. If the latter quantity and the three last profiles are known, then in principle the electron density profile N(h) can be determined.

Two methods of interpretation of Type II data were described by Fejer. One, which he did not use, referred to the simultaneous analysis of x- and o-mode curves*. By means of the other he deduced from the curve for the ordinary disturbing wave profiles of electron density and collision frequency and a value ($\sim 10^{-2}$) for G. In obtaining these results for the D region, Fejer used a value 1 for α and atmospheric data for U_{oi}.

That Fejer's methods of interpretation were invalid through a failure to allow for the durations of the wanted and disturbing pulses was recognized on theoretical grounds at the University of New England, and was confirmed in nighttime experiments in 1958 by the simple expedient of changing the duration of the disturbing pulse (e.g., see Bourne 1960). It was also recognized that information in Type II data on structure of the disturbed region is most meager and for this reason wave interaction in the D region was not studied until the completion of the wanted station C allowed the more effective Type III experiment to be employed.

The necessity of allowing for the durations of the two pulses was also recognized by the group in Norway, who have fitted their data of Type II by trial and error methods, using a computer. Early analyses were made using the Appleton-Hartree magnetoionic theory, a value of 1 for α and a value of 2×10^{-3} for G. To this value of G limits of 1×10^{-3} and 5×10^{-3}

*These refer to the wave mode of the disturbing pulse. During the day the wave mode of a medium frequency wanted echo is ordinary.

have been assigned (Landmark and Lied 1961). Later analyses have been made using the magneto-ionic theory of Sen and Wyller and the value of G_m has been taken to be twice the previous value. The collision frequency at a fixed height has been established from partial reflection data and from the transition, observed at Tromso during periods of high absorption, from negative to positive values of the impressed modulation. The latter method was suggested by Fejer, but suffers from the defect that the "meeting height" for the zero in the modulation depth bears no simple relation to the height at which $\frac{1}{N}\frac{\partial k_w}{\partial \nu}$ for the wanted wave is zero (Bourne 1964; Georges 1965; see Paper 3.2.4).

Trial and error methods, by introducing preconceived ideas into the interpretation, have obvious shortcomings when applied to the D region, whose electron density profile is largely a matter of conjecture. The desirable interpretation is by direct synthesis of the experimental data, and methods for this have been developed at the Pennsylvania State University and at the University of New England.

At Pennsylvania State University, Type II data of phase and amplitude interaction, either separately or together, are synthesized using a computer to obtain a "least squares" fit of the assigned values and to yield the electron density and collision frequency profiles and the value of G. The approach is highly mathematical (Hellrich and Ferraro 1965; Day 1965; Care 1965), but the analysis appears to have been developed only for the case of a rectangular disturbing pulse and a δ-wanted pulse.

The synthesis of data of Type II or III is effected at the University of New England by manual adjustment of the amplitudes of electronically generated waveforms of the kind discussed in the previous section. In the synthesizer proper account is taken of the shapes of the disturbing and wanted pulses and its operation is now briefly described with reference to the block diagram Fig. 20.

The double pulse generator generates two rectangular pulses, 1 and 2, each of duration T_d. Pulse 1 is fed to a tapped delay line and the delayed pulse from each tap opens a transistor gate to produce a rectangular pulse of duration T_d. Pulse 2 opens a second transistor gate (one for each tap on the delay line) to produce a pulse identical in magnitude and duration to that from the gate opened by the pulse from the tap on the delay line. The equal rectangular pulses are added before shaping to match the power envelope of the disturbing pulse and are then applied to an RC integrating circuit, which has a time constant appropriate to the height the tap on the delay line represents. The output of the desired polarity is added to the outputs of the other height channels and the sum is applied to a tapped delay line, whose total delay is equal to the duration of the output pulse of the receiver. The average (39) for the actual pulse is effected by adding the outputs of 12 taps on this line with appropriate amplitudes. The final waveform is displayed on a Dumont 766H oscilloscope and projected onto a 6 × 10 inch frosted screen. The synthesizer just described adds in height steps of 1 km. An earlier version, constructed in 1962, employed electronic tubes and added in steps of 2.25 km.

Methods of establishing the height scale of the synthesizer in terms of absolute height and of associating time constants with the height channels are described in Paper 3.2.1. Once the synthesis has been completed, the outputs of all the height channels are switched out and the gain of a calibration channel is adjusted until it gives a deflection corresponding to a known modulation depth. The amplitudes of the rectangular pulses (i.e., the pulses before the RC integration networks) of this channel and of the used height channels are then measured and the values of ΔM_{si} calculated. The derivation of the electron density profile from these values utilizes the theory given in Section 4 and requires a knowledge of the experimental parameters g and W and the properties α, $\nu(h)$, $U_o(h)$, and $G(h)$ of the disturbed region. The complicated interrelation of these many variables makes it virtually impossible to estimate the error of the derived electron density profile introduced by errors in the experimental and subsidiary data. The separate problem of the height resolution of a Fejer curve can be discussed simply, however, and this we now proceed to do.

In Figs. 13 and 14, Fejer curves of Type III obtained by Smith et al. near noon on 4 November 1963 using extraordinary and ordinary disturbing pulses at a frequency of 1.78 Mc/s.

were shown and compared. For the first of these pulses, the amplitudes of the peaks of the curve are closely equal and the time constant of the decaying tail is 42 μsec. Since from the theory in the previous section the waveforms that produce the first peak are added with time displacement, whereas those that produce the second peak are added without displacement, the close equality of the amplitudes indicates that the wave interaction was localized in height. The short time constant implies that the interaction occurred low (near 70 km.) in the D region. The disparate amplitudes of the two peaks of the o-mode curve, on the other hand, indicate that the wave interaction occurred over an extended height range, whose upper bound, implied by the value (455 μsec.) of the time constant of the slowly decaying tail, was well above a height of 80 km. These properties of the two Type III curves are consistent with the large difference between the absorption coefficients of the two wave modes.

In the discussion of Fig. 14 we have pointed out the close resemblance of the shape of the front part (i.e., the Type II part) of the noon o-mode curve for 4 November, 1963 to the shape of the corresponding part of a curve for 7 September, 1964, when the wave interaction was localized in a thin region near the base of the nighttime E region. Had a Type II experiment been made on 4 November, 1963, the o- and x-mode curves would have been limited to the parts of the first peaks with delays shorter than about 580 μsec. These parts are compared in Fig. 21, in which the amplitudes of the two peaks have been made the same and the o-mode curve has been displaced in delay so that its observed onset coincides with the observed onset of the x-mode curve. Clearly, the effect of the thickness of the disturbed region on the shape of a Type II Fejer curve is minor.

The corollary of this result is that the deduction of the structure of the disturbed region from a Type II Fejer curve requires precise experimental data. In order to illustrate the degree of precision required and the merits of the Type III experiment, we have shown in Figs. 22 and 23 by broken lines (drawn where the departure from the experimental curve can be distinguished) a number of syntheses of the o-mode curve for 4 November, 1963. The syntheses have been made using the height channels and time constants noted on the left of each figure, and the length of the horizontal line against the height channel is proportional to the value of ΔM_{si} for that channel. The top parts of Figs. 22 and 23 are the same and, except for the middle part of Fig. 23, the time constants used in the syntheses are the values deduced for the heights by the methods described in Paper 3.2.1. The time constants in the middle part of Fig. 23 have been made, arbitrarily, about twice as long.

The many implications of Figs. 22 and 23 need no stressing.

Considerable claims have been made by the group at Pennsylvania State University for the value of simultaneous Type II measurements of phase and amplitude interaction as a means of obtaining the D-region electron density profile and other basic data, which enter into the deduction of this profile. Preferably, any assessment of these claims should be made by considering the experimental data obtained by this group, but those tabulated by Lee and Ferraro (1964 etc.) are insufficiently accurate for the present purpose, and details are not given of the shapes of the disturbing and wanted pulses. Instead, we have used the propagation data for the 2.12 Mc/s. wanted wave shown in Fig. 24 and the values of the basic parameters given in Paper 3.2.1 to calculate the Fejer curves of amplitude interaction M_k and phase interaction M_ϕ for the electron density profile for noon on 4 November, 1963 given in Paper 3.2.4. This reverse process yields theoretical curves for M_k almost identical with the experimental o- and x-mode curves and it is reasonable to assume that the curves for M_ϕ are close to what would have been measured on that date. The Type III curves of M_k and M_ϕ are shown in Figs. 25 and 26 for the x- and o-mode disturbing pulses, respectively. The Type II parts of the four curves are compared in Fig. 27.

The influence of the different characteristics of $\frac{1}{N}\frac{\partial k_w}{\partial \nu_m}$ and $\frac{\omega}{cN}\frac{\partial \mu_w}{\partial \nu_m}$ is readily evident in these figures. The larger values of the latter derivative at heights below 70 km. causes the onset of the M_ϕ curve to be at a lower delay than that of the M_k curve for the same disturbing wave mode. Thus, for equivalent sensitivity, the M_ϕ curve would yield more and, since

the derivative does not have a zero or vary so rapidly with height, better information about ionization at these levels. Against this, phase interaction gives much less information at heights above about 75 km., as is evident in Fig. 26, where the time constant of the tail of the M_ϕ curve is 100 μsec. compared with 455 μsec. for the M_k curve. These different characteristics make phase and amplitude interaction valuable complements of each other.

It was shown earlier that the height resolution in a Type II Fejer curve is poor. When curves of phase and amplitude interaction are synthesized simultaneously, some improvement can be expected from the use of the additional data. However, the accuracy requirements for an effective resolution of Type II data are so high that the improvement with poor data of both kinds would be insignificant. This is illustrated in Fig. 25, where the scaled curve of phase interaction shows an effective width only 2 μsec. greater than the curve of amplitude interaction.

When Fejer curves are obtained using different disturbing or wanted waves, or when phase and amplitude interaction are measured simultaneously, information is obtained on the values of the collision frequencies, etc. Figs. 28 to 30 illustrate the use for this purpose of phase and amplitude interaction data of Type II. In each of these figures, the curve of phase interaction produced by the ordinary disturbing wave has been synthesized accurately. The values of $\Delta M_{\phi i}$ for the height channels used are represented by the length of the lines. The values of the products $(G_m \nu_m)_i'$ used in these syntheses are the correct values $(G_m \nu_m)_i$ for the height channels (Fig. 28), values 1.82 times larger (Fig. 29), and values 0.535 times smaller (Fig. 30). Let us now consider Fig. 28, for which the correct values have been used and let $\alpha = \nu_m'/\nu_m$. By multiplying the values of $\Delta M_{\phi i}$ by the ratio $\{\frac{1}{N}\frac{\partial k_w}{\partial \nu_m}/\frac{\omega}{cN}\frac{\partial \mu_w}{\partial \nu_m}\}_i$, calculated using the correct collision frequencies (i.e., with $\alpha = 1$), one obtains the components ΔM_{ki}, which should add to produce the curve of amplitude interaction. The predicted curve obtained in this way is shown as a broken line and its difference from the actual curve of amplitude interaction is very small. Except for this small relative difference the use of combined phase and amplitude interaction data has not increased the height resolution. The predicted curves for values of α equal to 0.735 and 1.34 differ significantly from the curve of amplitude interaction.

If the method is to be useful, however, it must also fix the value of $G_m \nu_m$, at some height.* In Figs. 29 and 30 no attempt has been made to obtain the value of α which yields the best agreement between the predicted and actual curves of amplitude interaction but it is evident in Fig. 29 ($(G_m \nu_m)_i'/(G_m \nu_m)_i = 1.82$) that a value for $\alpha \sim 1.25$ would give close agreement. In Fig. 30 ($(G_m \nu_m)_i'/(G_m \nu_m)_i = 0.535$) the agreement would be close for the optimum value of α, estimated to be ~ 0.8.

While the method has its limitations as a sole source of data for G_m and ν_m, it is another example of the versatility of pulse wave interaction methods.

6. Concluding Remarks

The material in this paper has been selected because of the conviction that pulse radio wave interaction has yet to play its proper important role in a global study of the lower ionosphere.

Wave interaction has a sound theoretical basis. Its correct application makes possible the effective study of a wide variety of phenomena in the lower ionosphere.

---

* The possibility of using the method to obtain individual values of $(G_m \nu_m)_i$ is considered to be beyond its capabilities.

Acknowledgments

The ideas presented in this paper crystallized during long associations with Dr. I.A. Bourne and Messrs. R.G. Loch and T.N.R. Coyne. The valuable help received from Messrs. Loch and Coyne in the preparation of this paper is gratefully acknowledged.

The experimental work at the University of New England was supported by the Air Force Cambridge Research Laboratories under Contract AF19(604)-6177, The Defense Atomic Research Agency under Subtask 0710, and the Radio Research Board of Australia.

REFERENCES

Aitchison, G.J. and G.L. Goodwin. Nuovo Cimento, 1, 722, 1955.

Bailey, V.A. World Radio, 25 January, 1935.

Bailey, V.A. Phil. Mag., 23, 929, 1937a.

Bailey, V.A. Nature, 139, 838, 1937b.

Bailey, V.A. Phil. Mag., 26, 425, 1938.

Bailey, V.A. J. Atmos. Terr. Phys., 14, 299, 1959.

Bailey, V.A. J. Res. N.B.S. 65D, (Radio Prop.), 321, 1961.

Bailey, V.A. Radio Science, 69D, 9, 1965.

Bailey, V.A. and L. Goldstein. J. Atmos. Terr. Phys., 12, 216, 1958.

Bailey, V.A. and D.F. Martyn. Phil Mag., 18, 369, 1934.

Bailey, V.A., Smith, R.A., Landecker, K., Higgs, A.J., and F.H. Hibberd. Nature, 169, 911, 1952.

Barrington, R.E., Landmark, B., and E. Thrane. "Electron Density Profiles in the Ionosphere and Exosphere"., ed. B. Maehlum, Pergamon, 1962.

Barrington, R.E. and E. Thrane. J. Atmos. Terr. Phys., 24, 31, 1962.

Barrington, R.E., Thrane, E.V. and B. Bjelland. Can. J. Phys., 41, 271, 1963.

Bell, C.D. Ionospheric Res. Sci. Rept. No. 262, Penn. State Univ., 1966.

Benson, R.F. J. Geophys. Res., 67, 2569, 1962.

Benson, R.F. Radio Science, 68D, 1109, 1964a.

Benson, R.F. Radio Science, 68D, 1123, 1964b.

Bjelland, B., Holt, O., Landmark, B., and F. Lied. Nature, 184, 973, 1959.

Bourne, I.A. M.Sc. Thesis, Univ. of New England, 1960.

Bourne, I.A. Ph.D. Thesis, Univ. of New England, 1964.

Caldirola, P. and O. De Barbieri. Radio Science, 69D, 33, 1965.

Care, K.H. Ionospheric Res. Sci. Rept. No. 248, Penn. State Univ., 1965.

Cutolo, M. Nature, 166, 98, 1950.

Cutolo, M. Nuovo Cimento, 9, 687, 1952.

Cutolo, M. Nature, 172, 774, 1953a.

Cutolo, M. Nuovo Cimento, 10, 915, 1953b.

Cutolo, M., Ferrero, R., and M. Motzo. Alta Frequenza, 19, 3, 1950.

Day, E.L. Ionospheric Res. Sci. Rept. No. 238, Penn. State Univ., 1965.

Farley, D.T. J. Geophys. Res., 68, 401, 1963.

Fejer, J.A. J. Atmos. Terr. Phys., 7, 322, 1955.

Fejer, J.A. and R.W. Vice. J. Atmos. Terr. Phys., 16, 291, 1959.

Ferraro, A.J., Lee, H.S., and S. Weisbrod. J. Geophys. Res., 68, 1169, 1963.

Georges, T.M. N.B.S. Tech. Note No. 325, 1965.

Ginzburg, V.L. and A.V. Gurevich. Soviet Physics "Uspekhi", 3, 115 and 175, 1960.

Hellrich, F.V. and A.J. Ferraro. J. Geophys. Res., 70, 1195, 1965.

Hibberd, F.H. J. Atmos. Terr. Phys., 6, 268, 1955.

Hibberd, F.H. Ph.D. Thesis, University of Sydney, 1956.

Hibberd, F.H. J. Atmos. Terr. Phys., 11, 102, 1957.

Hibberd, F.H. Radio Science, 69D, 25, 1965.

Holt, O., Landmark, B., and F. Lied. J. Atmos. Terr. Phys., 23, 318, 1961.

Holt, O., Landmark, B., and F. Lied. "Electron Density Profiles in the Ionosphere and Exosphere"., ed. B. Maehlum, Pergamon, 1962.

Huxley, L.G.H. Proc. Roy. Soc., A, 200, 486, 1950.

Huxley, L.G.H. Nuovo Cimento, 9, (Suppl.), 1, 1952.

Huxley, L.G.H. and J.A. Ratcliffe. J. Inst. Elect. Engrs., 96, III, 433, 1949.

King, J.W. J. Atmos. Terr. Phys., 14, 41, 1959.

Klemperer, W.K. N.B.S. Tech. Note No. 211, 3, 63, 1964.

Landmark, B. and F. Lied. J. Atmos. Terr. Phys., 23, 92, 1961.

Layzer, D. and D.H. Menzel. Radio Science, 69D, 59, 1965.

Lee, H.S. and A.J. Ferraro. Ionospheric Res. Sci. Rept., Nos. 207, 224, 232, 236, 239, 250. Penn. State Univ., 1964, 1965.

Lied, F. Elektroteknisk Tidsskrift, nr. 35-36, 1957.

Lombardini, P.P. Radio Science, 69D, 83, 1965.

Megill, L.R. Radio Science, 69D, 367, 1965a.

Megill, L.R. Radio Science, 69D, 77, 1965b.

Mitra, S.N. Conference on the Physics of the Ionosphere, 71, 1954.

Molmud, P. N.B.S. Tech. Note No. 211, 6, 1, 1964.

Molmud, P., Altshuler, S., and J.H. Gardner. Final Report, Contract AF19(604)-8844, 1962.

Rumi, G.C. J. Atmos. Terr. Phys., 23, 101, 1961.

Rumi, G.C. I.R.E. Transactions on Antennas and Propagation, AP-10, 594, 1962a.

Rumi, G.C. I.R.E. Transactions on Antennas and Propagation, AP-10, 601, 1962b.

Setty, C.S.G.K. J. Inst. Telecom. Engrs., 11, 127, 1965.

Shaw, I.J. Proc. Phys. Soc., B, 64, 1, 1951.

Singh, R.N. Planet. Space Sci., 12, 675, 1964.

Smith, R.A. Ph.D. Thesis, University of Sydney, 1957.

Smith, R.A., Bourne, I.A., Loch, R.G., Setty, C.S.G.K., Coyne, T.N.R., Barratt, P.H., and B.S.N. Prasad. Scientific Report No. 3 and Final Report, Contract No. AF19(604)-6177, University of New England, 1965.

Tellegen, B.D.H. Nature, 131, 840, 1933.

Vilenski, I.M. Dokl. Akad. Nauk. U.S.S.R., 92, 525, 1953.

Weisbrod, S. Ionospheric Res. Sci. Rept. No. 206, Penn. State Univ., 1964.

Weisbrod, S., Ferraro, A.J., and H.S. Lee. J. Geophys. Res., 69, 2337, 1964.

Weisbrod, S., Lee, H.S. and A.J. Ferraro. J. Geophys. Res., 69, 1448, 1964.

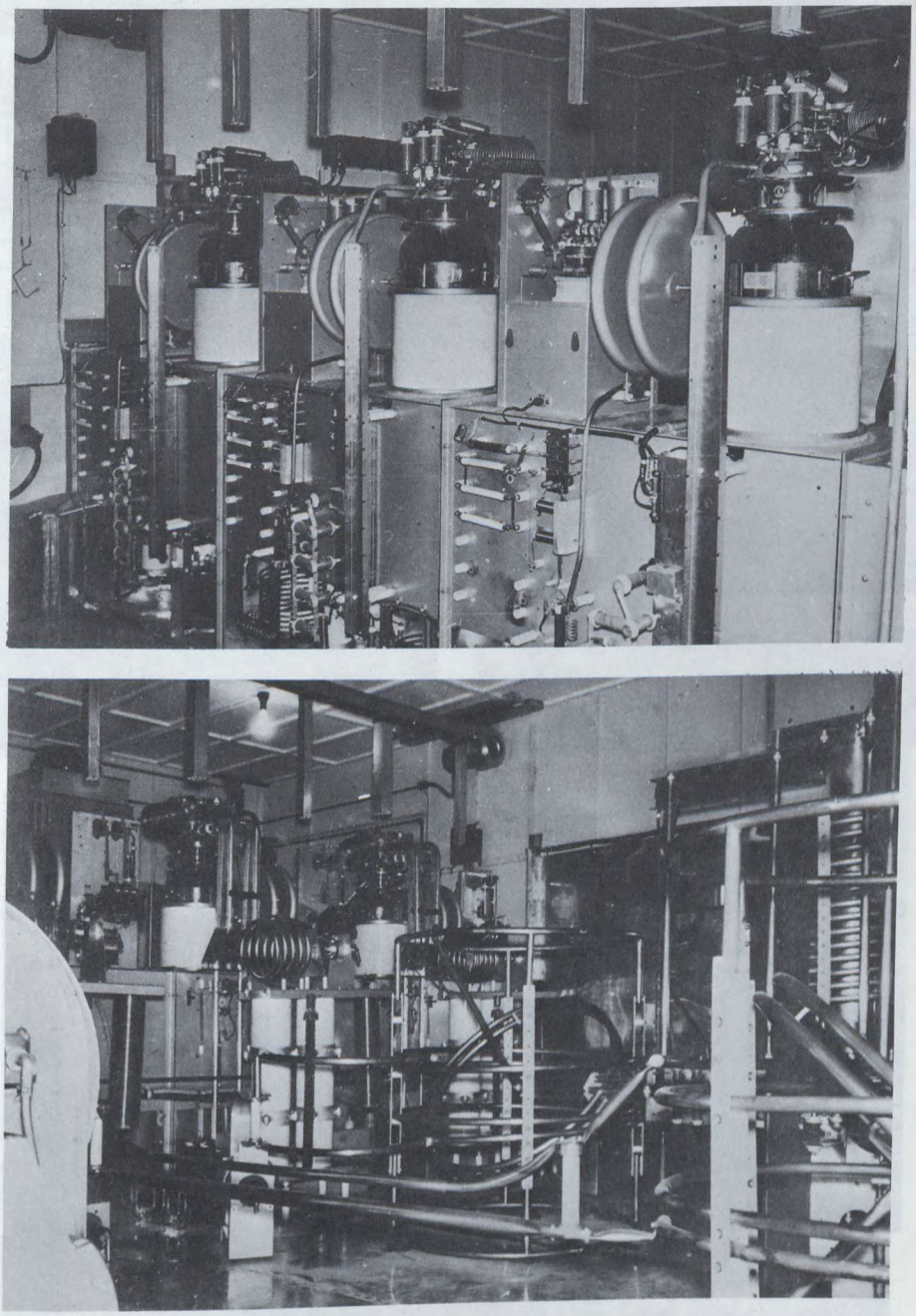

Fig. 1. 500 kw gyrotransmitter at the University of New England.

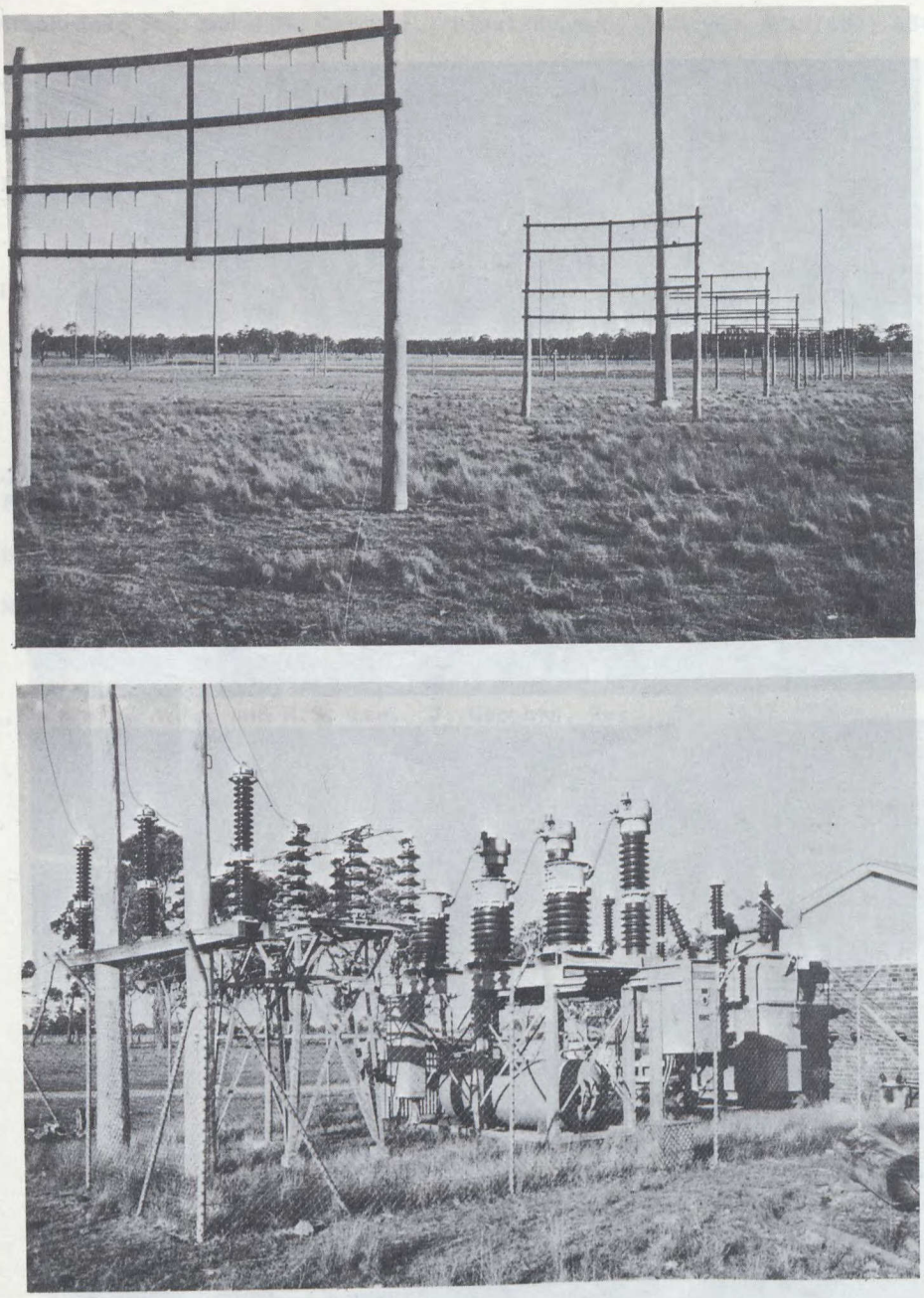

Fig. 2. Trunk feeder lines to 40-dipole array and 66 kv substation for 500 kw gyrotransmitter.

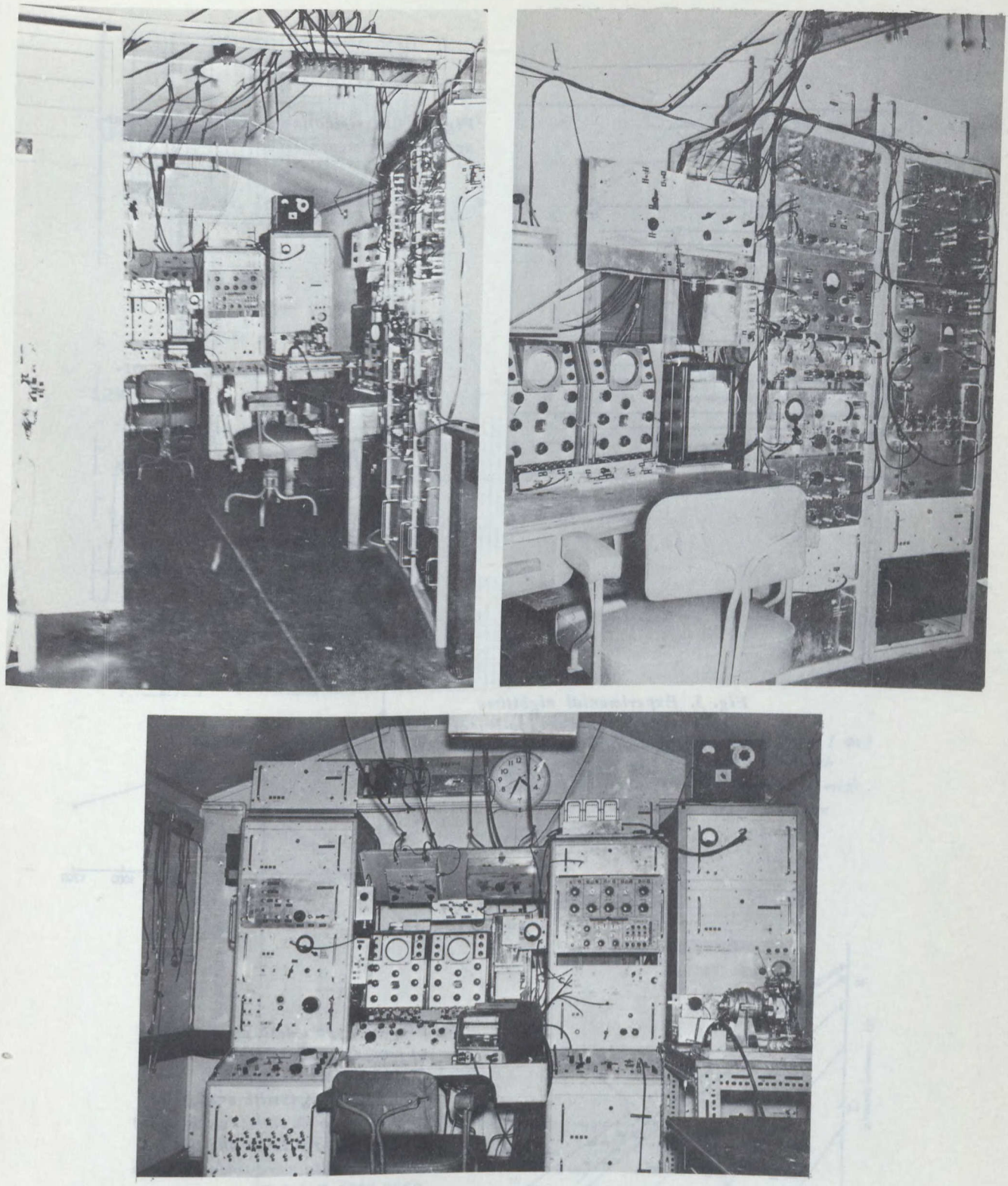

Fig. 3. Interior view of wanted station C (top left) and photographs (top right and lower) of its receiving and control equipment.

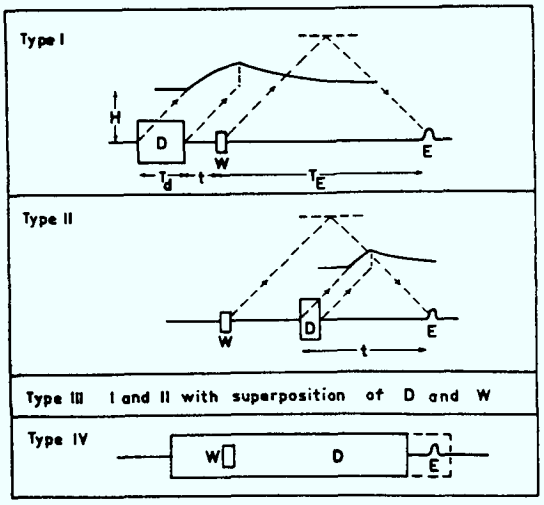

Fig. 4. Classification of pulse wave interaction experiments.

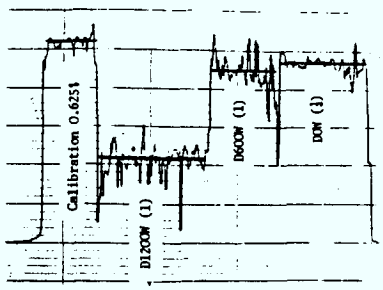

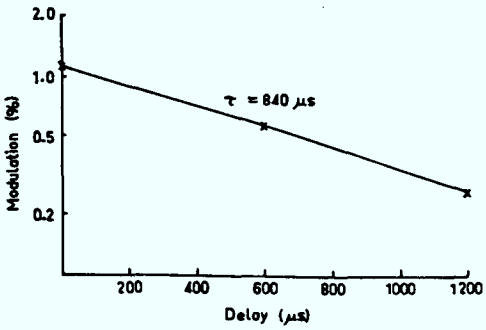

Fig. 5. Experimental nighttime record of Type I and its log-linear plot of modulation depth against the delay DtW (Smith et al.).

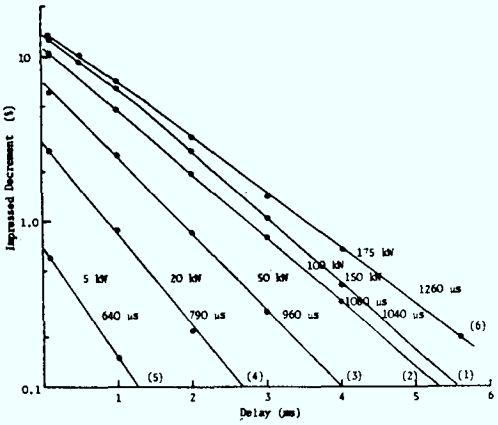

Fig. 6. Type I data for a number of powers of the disturbing pulse (1.515 Mc/s., x-mode, 800 μsec.) from Station A (Smith et al.). The wanted echo (2.12 Mc/s., x-mode) was from the F layer and the measurements were made between 0200-0350 E.A.S.T. on 7 March 1961.

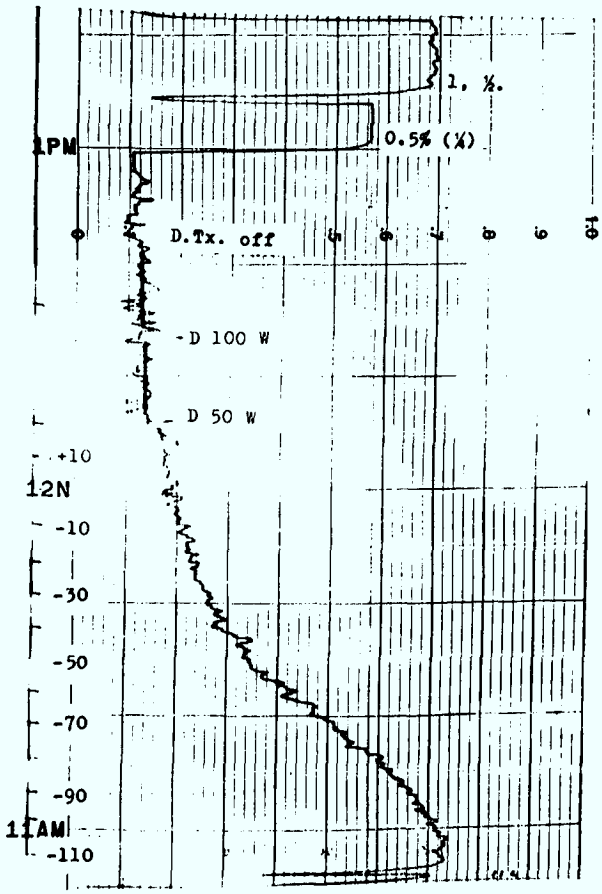

Fig. 7. Experimental record of Type I and its log-linear plot of modulation depth against the delay DtW, obtained by Smith et al. between 1140-1220 E.A.S.T. on 22 November 1963.

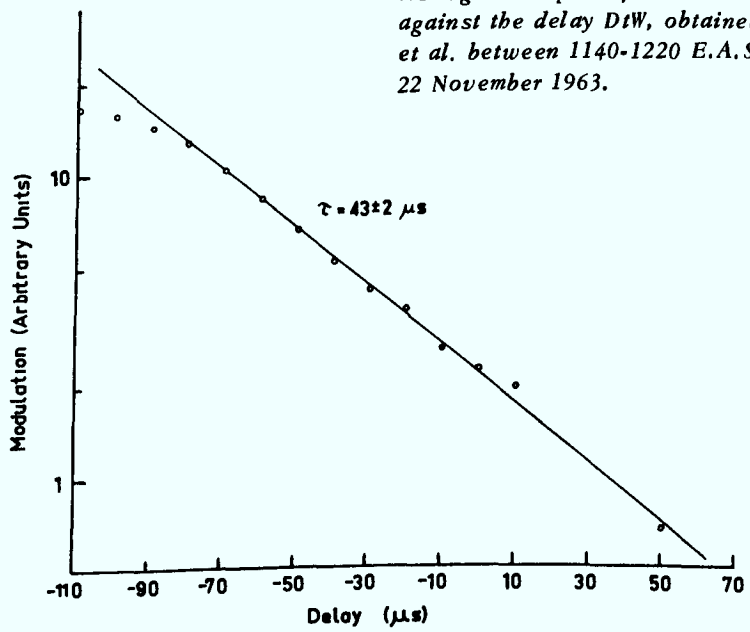

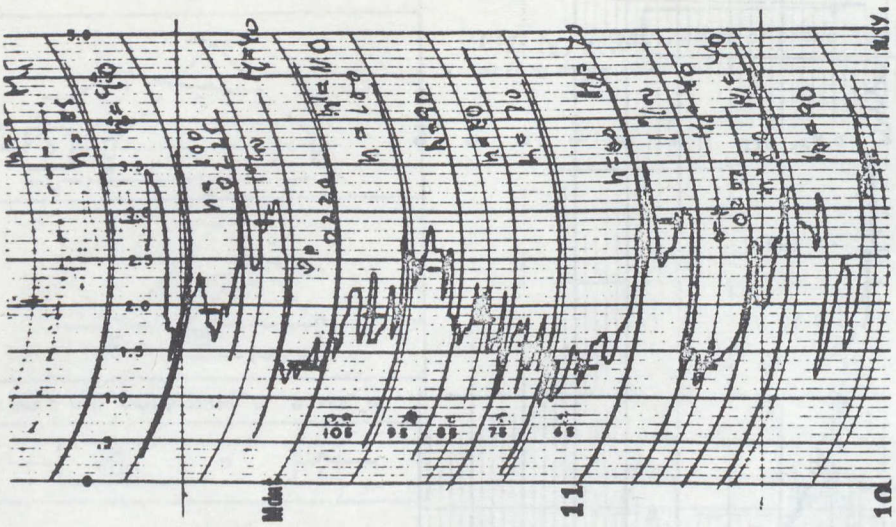

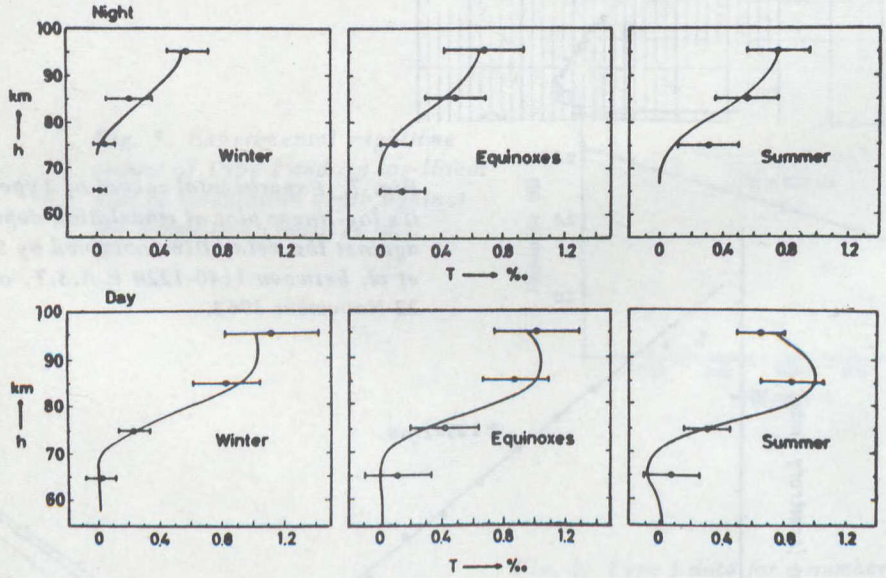

Fig. 8. Reproduction of Fig. 56 and 60 of Landmark and Lied (1961).

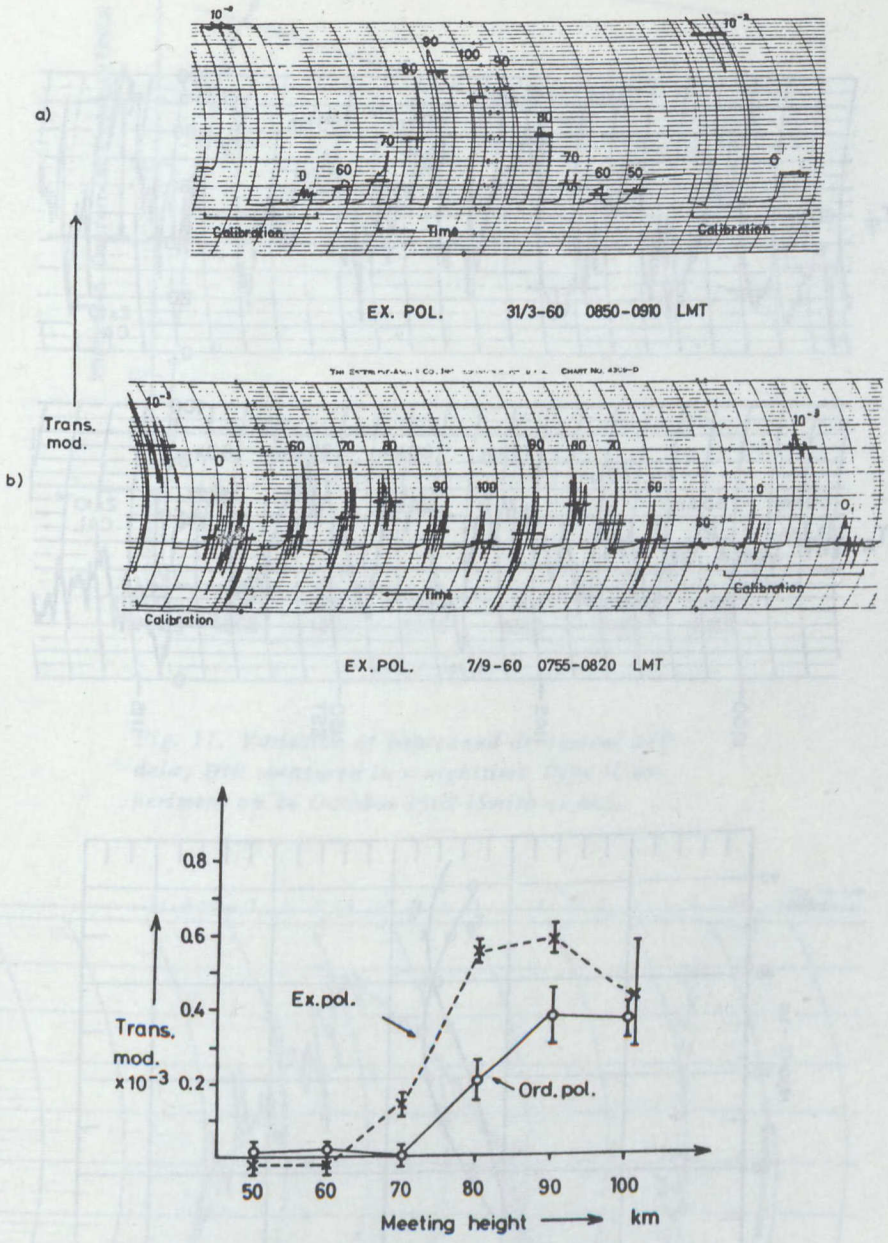

Fig. 9. Reproduction of Fig. 2 and 3 of Barrington, Thrane and Bjelland (1963).

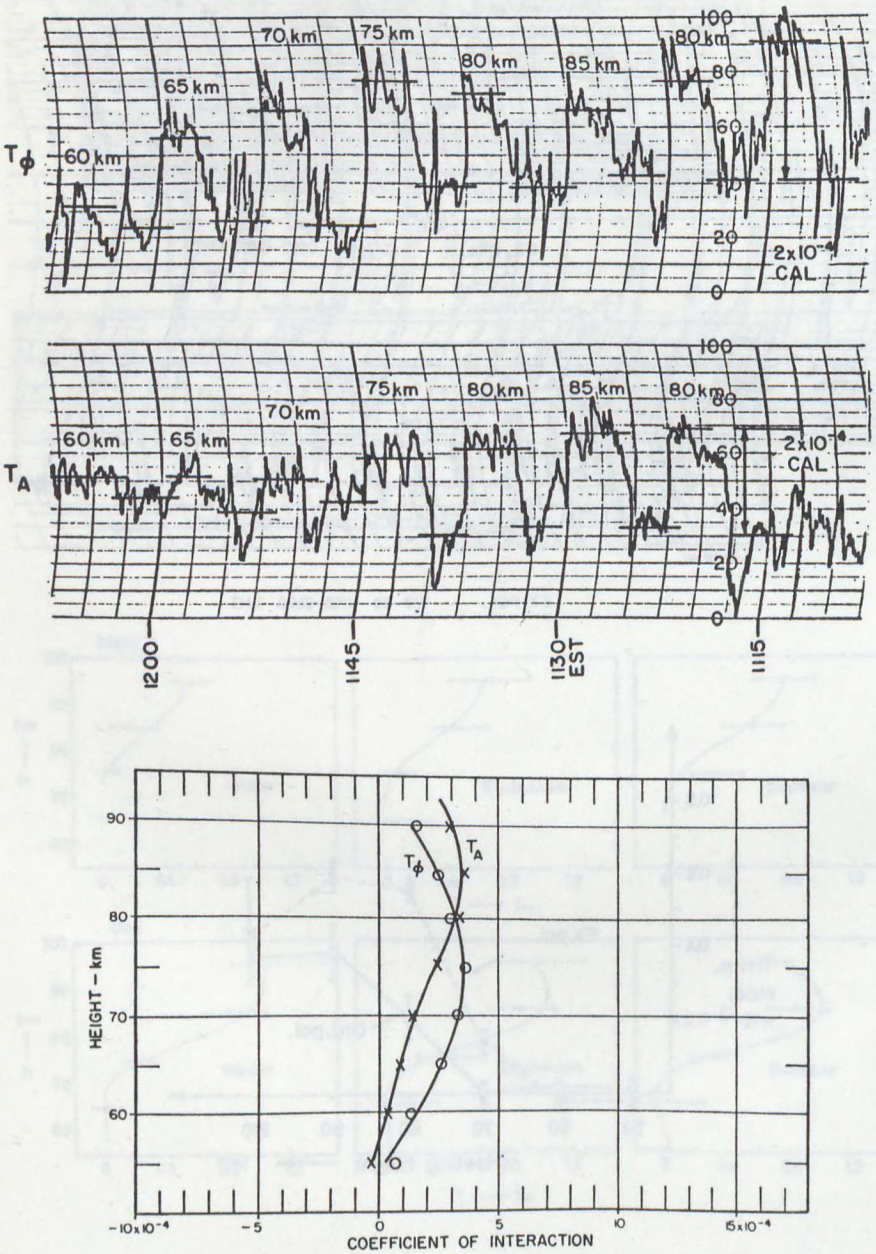

Fig. 10. Reproduction of Fig. 4 and 7 of Weisbrod, Lee and Ferraro (1964).

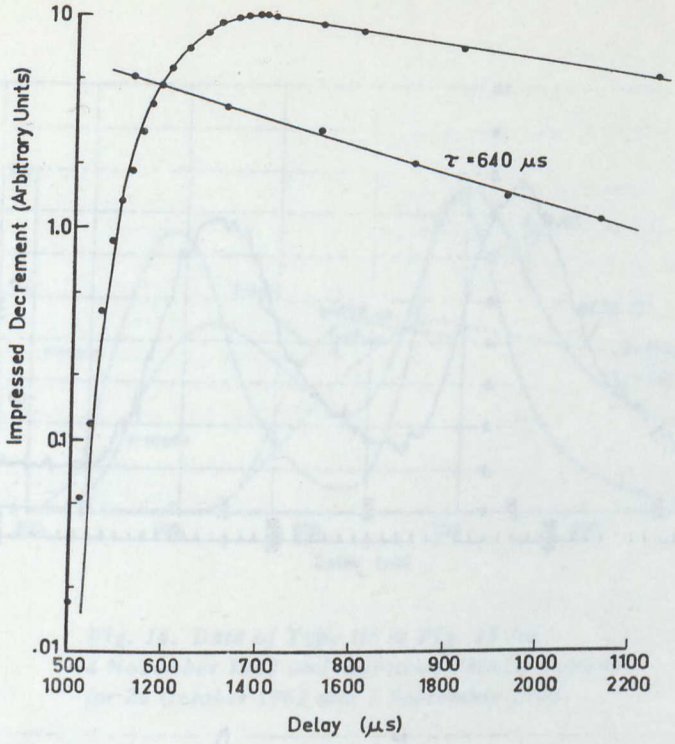

Fig. 11. Variation of impressed decrement with delay DtE measured in a nighttime Type II experiment on 24 October 1962 (Smith et al.).

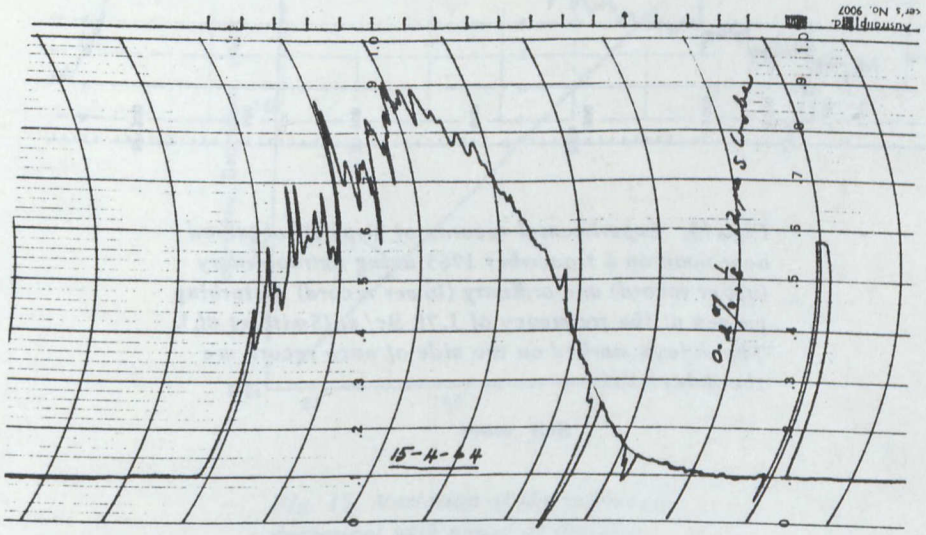

Fig. 12. Experimental record of Type II obtained at the University of New England in the early afternoon of 15 April 1964.

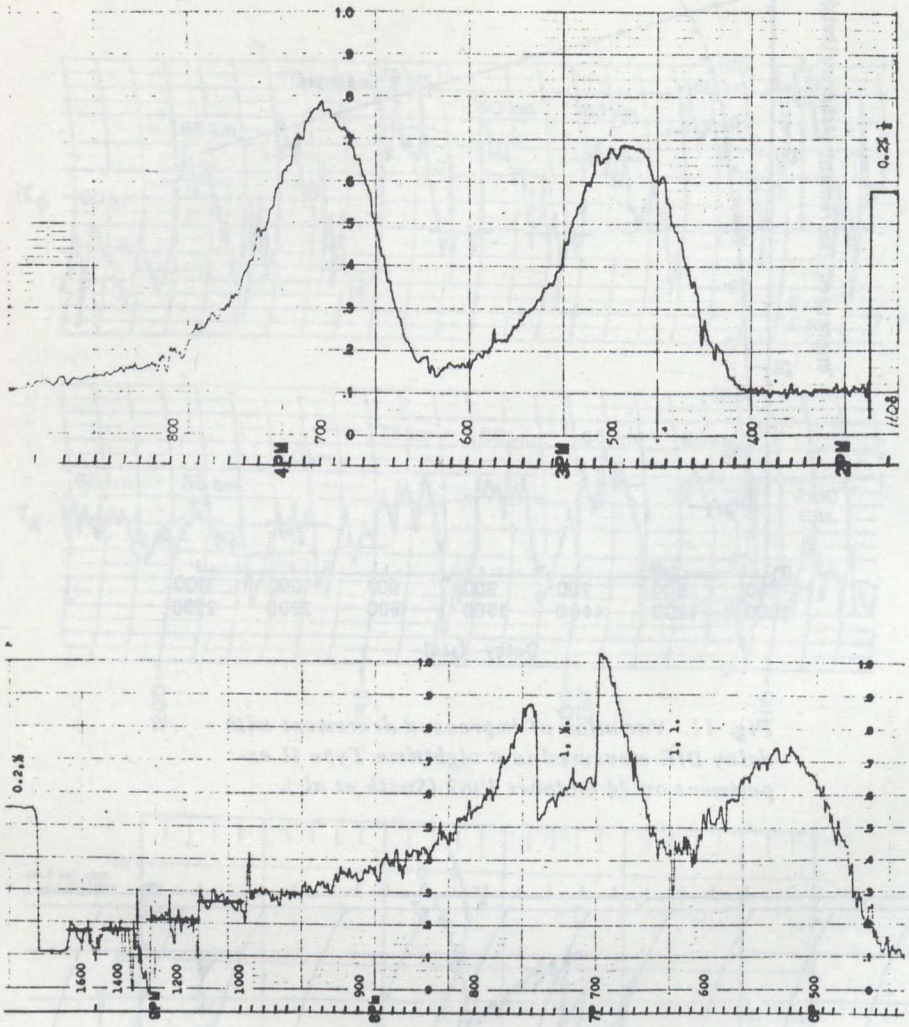

Fig. 13. Experimental records of Type III obtained near noon on 4 November 1963 using extraordinary (upper record) and ordinary (lower record) disturbing pulses at the frequency of 1.78 Mc/s. (Smith et al.). The delays marked on the side of each record are the delays DtE.

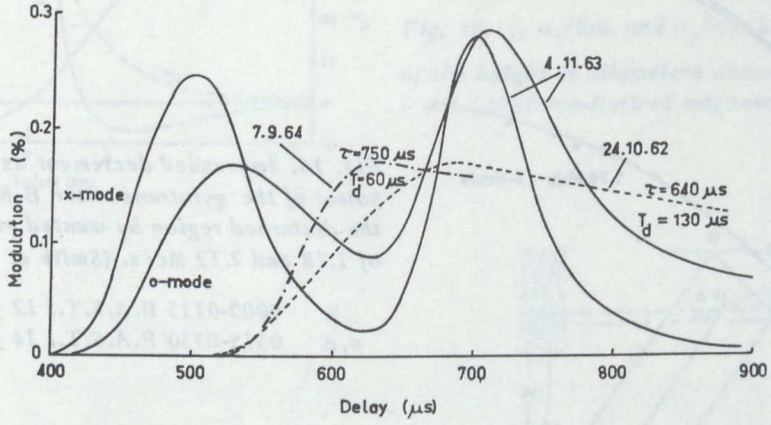

Fig. 14. Data of Type III in Fig. 13 for 4 November 1963 and nighttime data of Type II for 24 October 1962 and 7 September 1964.

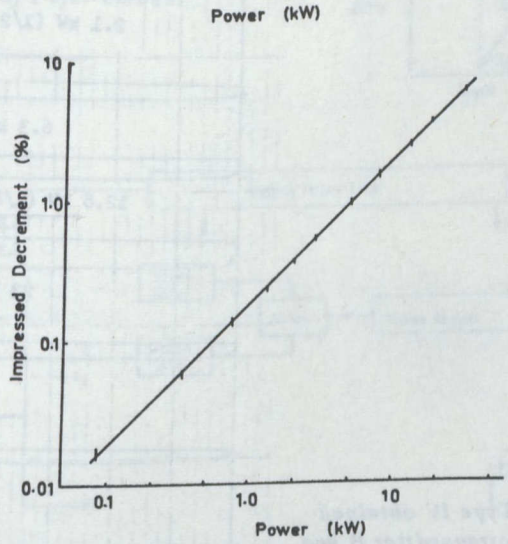

Fig. 15. Variation of the impressed decrement with power of the disturbing pulse from Station A (Smith et al.).

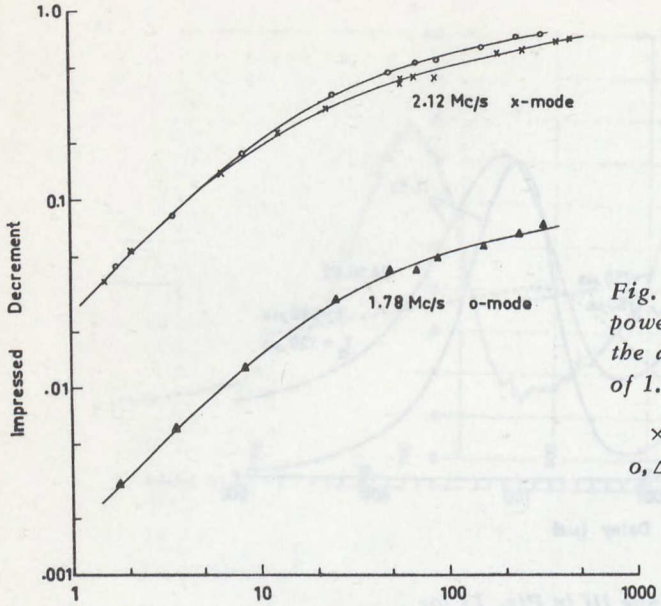

Fig. 16. Impressed decrement as a function of the power of the gyrotransmitter B for two transits of the disturbed region by wanted pulses at frequencies of 1.78 and 2.12 Mc/s. (Smith et al.)

× *0000-0115 E.A.S.T., 12 January 1965*
o, △ *0315-0350 E.A.S.T., 14 January 1965.*

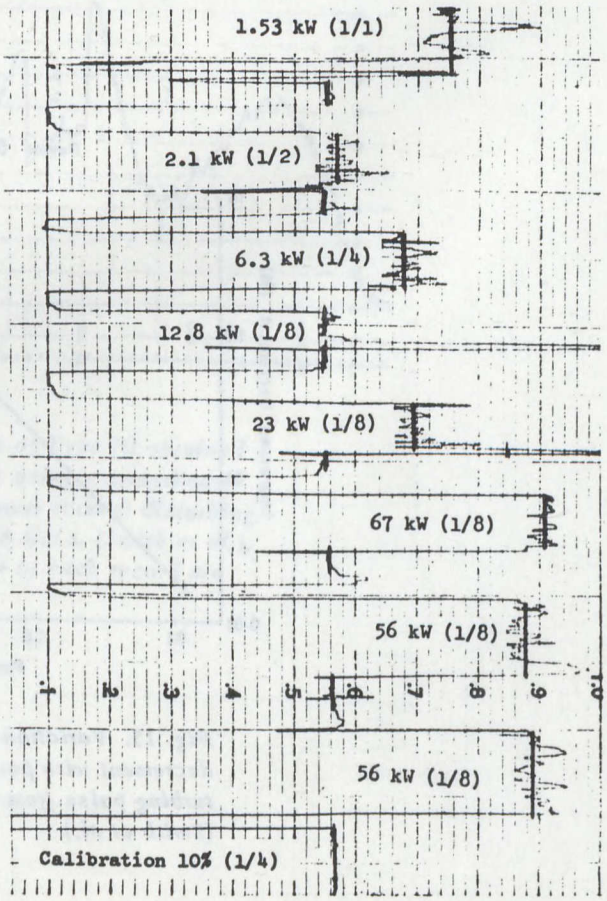

Fig. 17. Experimental record of Type IV obtained on 12 January 1965 using the gyrotransmitter B and a wanted frequency of 2.12 Mc/s. (Smith et al.). Every second deflection is a calibration record and the fractions (1/4) etc. refer to attenuator settings of the selective amplifier.

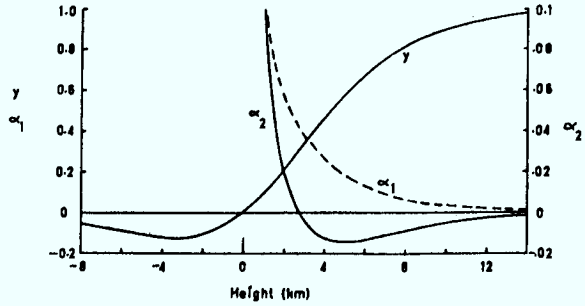

Fig. 18. y, a_1/km. and a_2/sq. km. as functions of the height in kilometers above the level where $\nu = a$ (Appleton-Hartree magnetoionic theory).

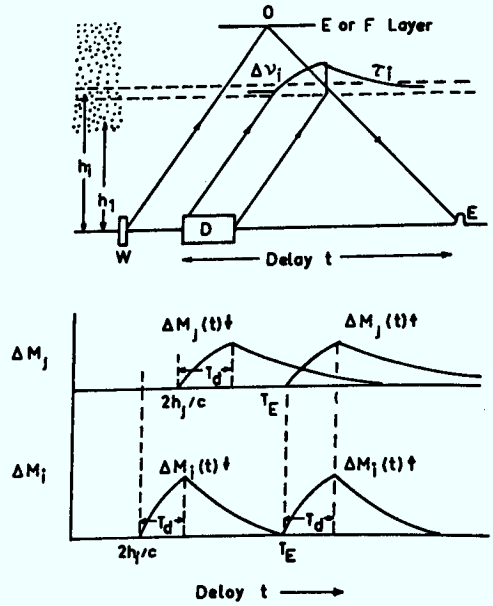

Fig. 19. Diagrams illustrating the formation of Fejer curves.

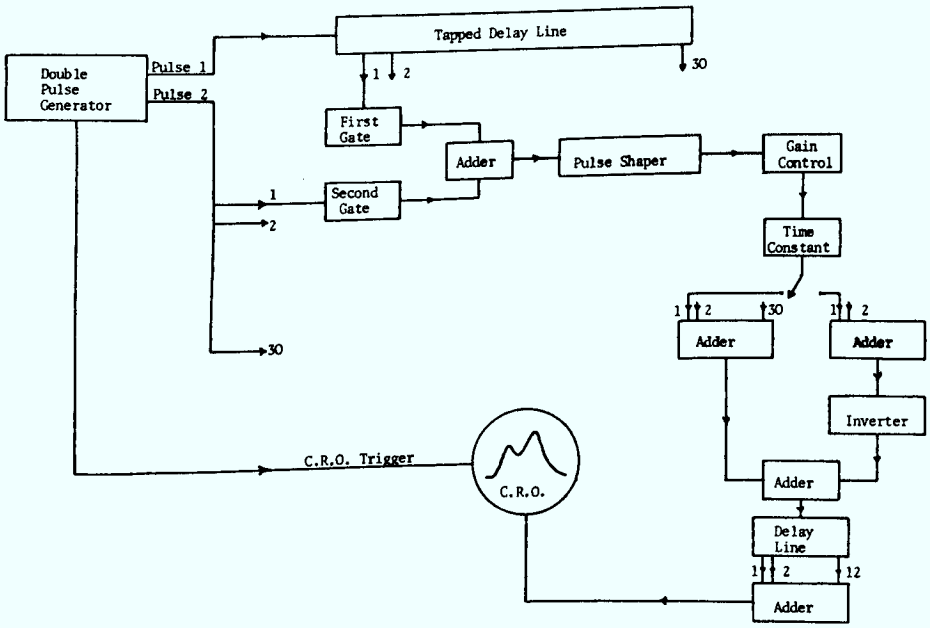

Fig. 20. Block diagram of electronic synthesizer.

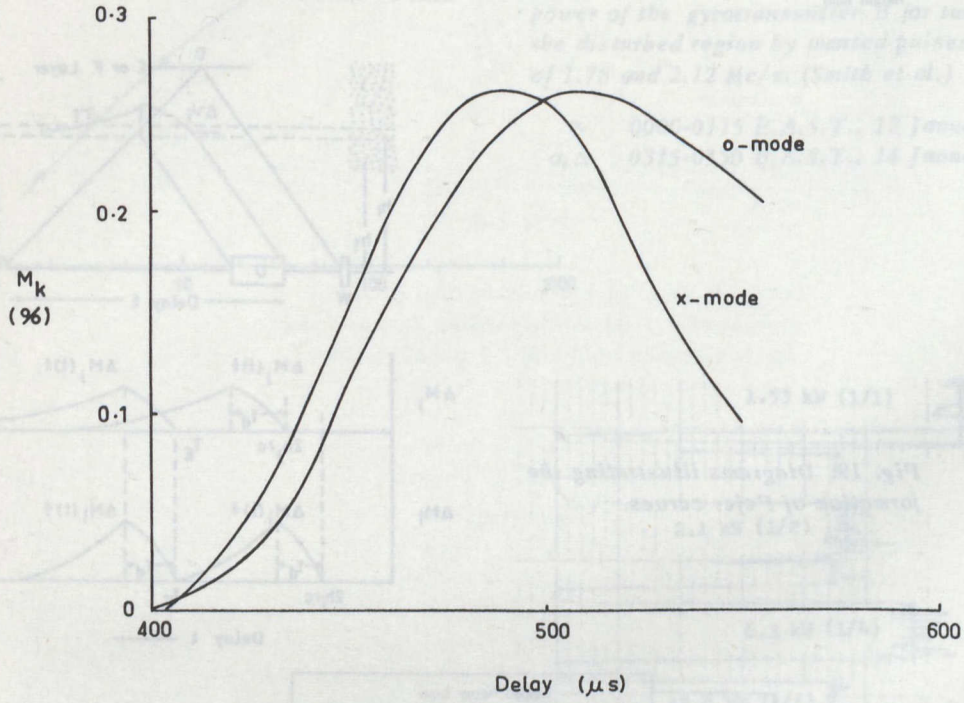

Fig. 21. Comparison of the shapes of the Type II parts of the noon x- and o-mode Fejer curves for 4 November 1963.

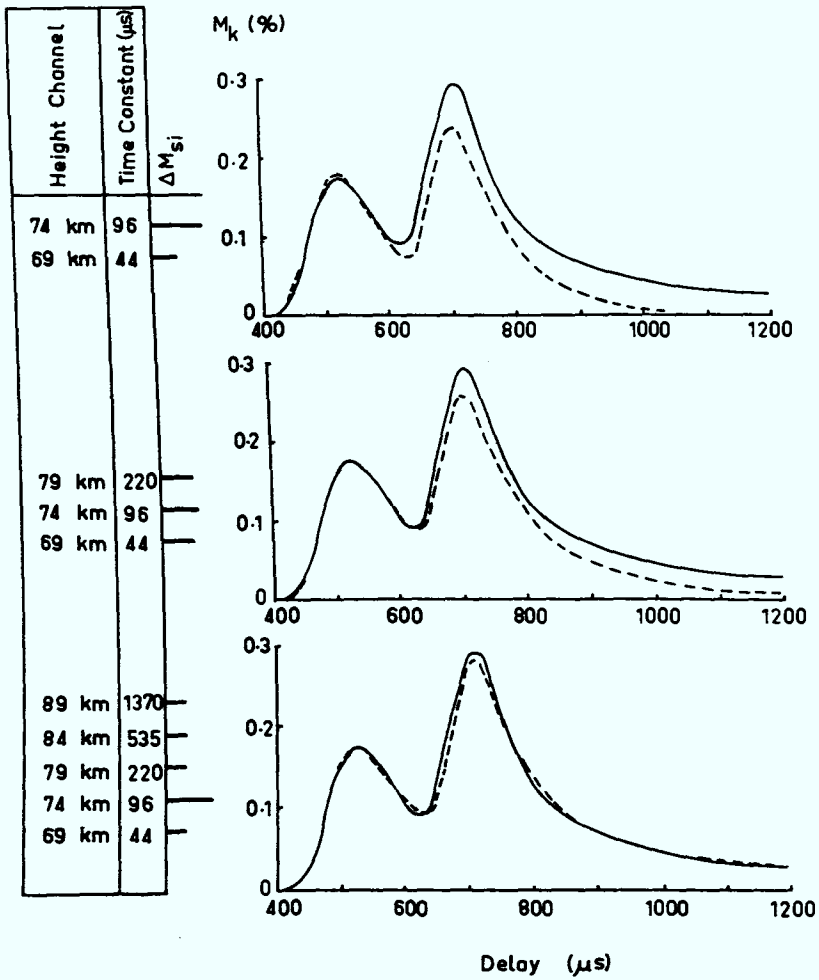

Fig. 22. Syntheses of the noon o-mode Fejer curve for 4 November 1963.

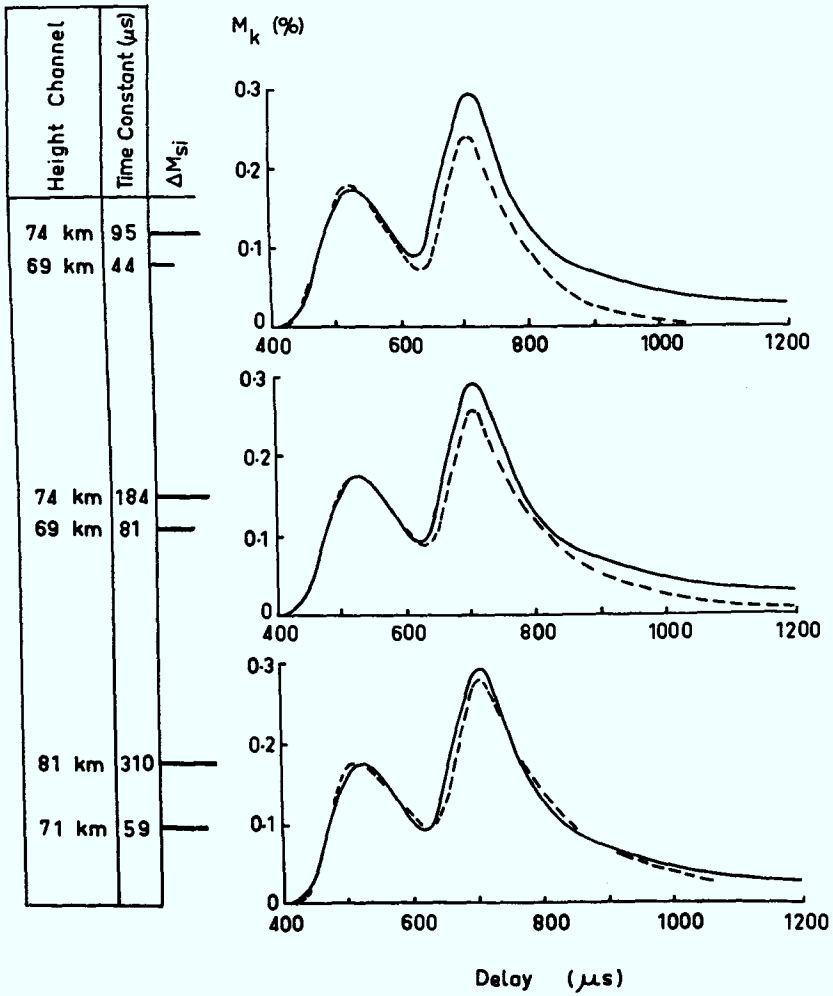

Fig. 23. Syntheses of the noon o-mode Fejer curve for 4 November 1963.

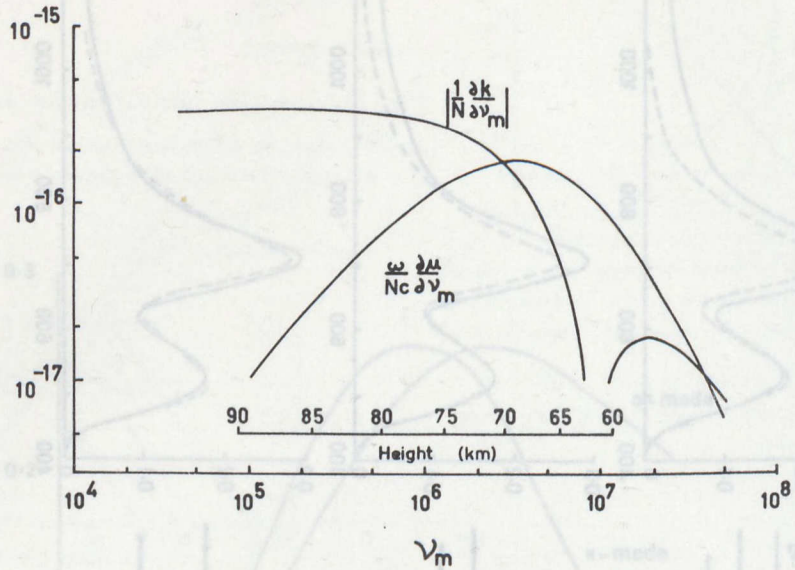

Fig. 24. Magnetoionic data for vertical propagation of the ordinary mode of the 2.12 Mc/s. wanted wave at Armidale (Sen and Wyller M.I. theory).

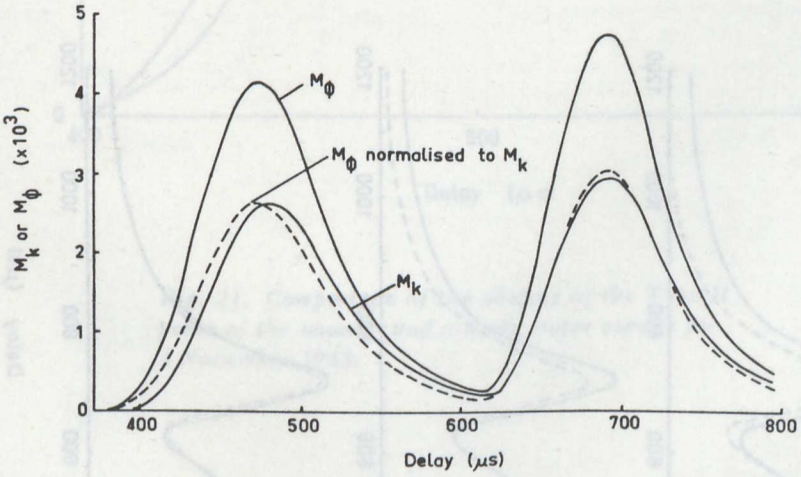

Fig. 25. x-mode Fejer curves of amplitude and phase interaction calculated for noon on 4 November 1963.

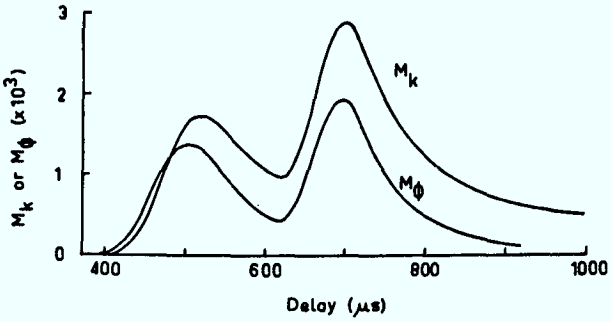

Fig. 26. o-mode Fejer curves of amplitude and phase interaction calculated for noon on 4 November 1963.

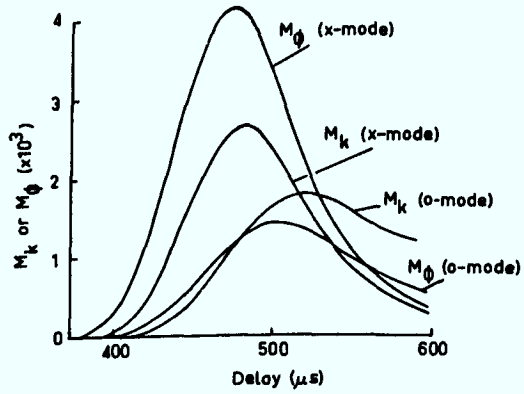

Fig. 27. Comparison of the Type II parts of the Fejer curves shown in Figs. 25 and 26.

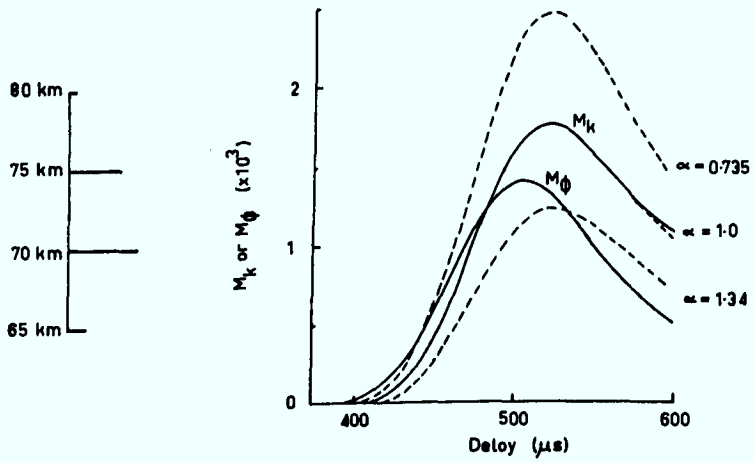

Fig. 28. Comparison of amplitude interaction curve with curves derived for several values of α from the synthesis shown of the curve of phase interaction $\left((G_m \nu_m)_i' = (G_m \nu_m)_i\right)$.

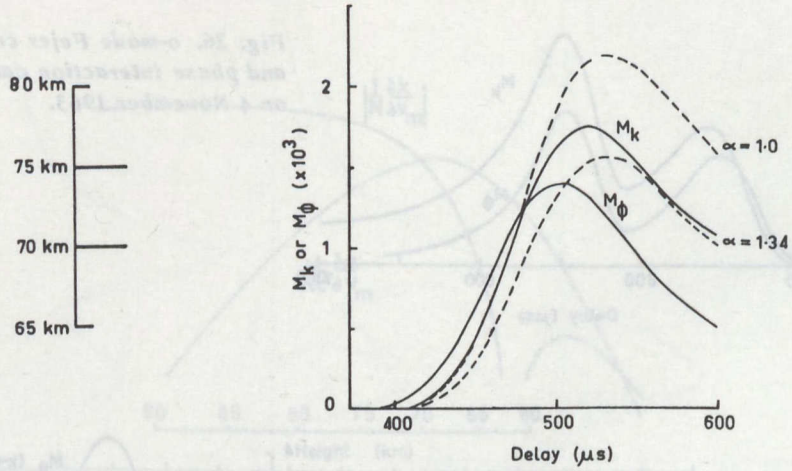

Fig. 29. Comparison of curve of amplitude interaction with curves derived for two values of a from the synthesis shown of the curve of phase interaction $\left((G_m \nu_m)_i' = 1.82(G_m \nu_m)_i\right)$.

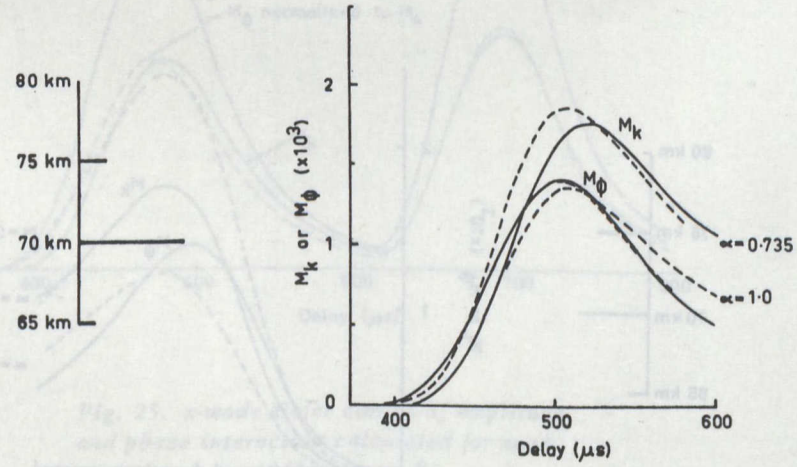

Fig. 30. Comparison of curve of amplitude interaction with curves derived for two values of a from the synthesis shown of the curve of phase interaction $\left((G_m \nu_m)_i' = 0.535(G_m \nu_m)_i\right)$.

Discussion on Paper 3.1.1 presented by R.A. Smith

Ferraro: In this technique, which is an analogue method, how do you handle underlying ionization? The interaction data are available down to some low height level, 55 km. or so, depending on the smallest interaction that you can reliably read. When you synthesize an interaction curve, do you allow for the absorption which might occur in the region for which you do not have reliable data?

Smith: In the profiles I have shown, there are a number not continued below a height of 65 km., which is the lowest height for which we are reasonably certain of the electron densities. These particular profiles are derived from data obtained using the ordinary mode of the 2.12 Mc/s. wanted wave, for which the derivative $\frac{1}{N}\frac{\partial k}{\partial v_m}$ of the absorption coefficient is zero at a height of about 61 km. Because of this zero, the power of the disturbing wave absorbed near the latter level produces no observable effect; but when records of the quality I have shown contain no evidence of negative modulation impressed at heights below 61 km., it is certain that the absorbed power is too small for neglect of it to have an appreciable effect on the magnitudes of the electron densities derived for greater heights. As I will point out tomorrow, for the height range 65 to 70 km., we have favored electron densities derived from data obtained using the extraordinary disturbing wave, since in this height range this highly absorbed wave produces much larger effects to be resolved in a synthesis than does the more weakly absorbed ordinary disturbing wave.

The "starting point" problem due to the zero in $\frac{1}{N}\frac{\partial k}{\partial v_m}$ does not occur in amplitude interaction when the zero is either well above or well below the lower bound of the disturbed region. The problem, of course, does not occur in phase interaction.

Ferraro: I don't understand your synthesis procedure, but in our digital technique it seemed important to account for the ionization below 60 or 65 km. Serious errors, at least in our technique, could be incurred if we neglected it. We have a way of accounting for it, which I will describe tomorrow. I would like to clarify a statement you made about phase interaction being measurable about one-third of the time that amplitude records were obtained. I would like to explain what would cause this. In measuring amplitude interaction, an AGC system is needed to account for the amplitude fluctuations. The AGC is entirely electronic. In making a phase measurement, some device is needed to account for phase height variations. Our present system for compensating for phase height variations is a mechanical servo device, and a situation can occur where the phase tumbling is so rapid that the mechanical goniometer cannot keep up with it, and a phase measurement cannot be made at that time. The problem is a limitation in the instrumentation.

Smith: I'm not criticizing phase interaction. I would like to have phase measurements, which would be valuable at the base of the ionosphere and complement the amplitude data, which is valuable at higher levels. The point I emphasize is that an error of 5 or 10 km. in the meeting height is unacceptable.

Ferraro: The reason for the error in meeting height is that the choice of disturbing frequency at this time is such that there is group retardation. Is this what you are referring to?

Smith: I don't know if it is caused by group retardation or by the shape of the pulse.

Ferraro: The meeting height is simply the time delay, which you measure accurately on a counter, times the speed of light.

Smith: Yes, but I think Weisbrod said in his thesis that the meeting height is not well defined, and is roughly known only up to an accuracy of approximately 5 km.

Ferraro: This is because the disturbing frequency is 300 kc/s. You have a lot of group retardation. This was our first attempt at a measurement. If we had had our choice, we would not have used 300 kc/s.

Smith: This is true.

Ferraro: In your case, the phase velocity of the wave equals the velocity of the speed of light. Consequently there is no discrepancy regardless of whether you call it time delay in seconds or Ct.

Rao: Just one question. In one of the slides I believe you showed the energy relaxation time constant as a function of the heating power, and you said that for increasing powers the time constant increased. I am not an ionospheric man, but to my knowledge the time constant τ is just $1/G\nu$. Does this mean that the collision frequency is decreasing with increasing disturbing power?

Smith: The effect is extremely complicated.

Rao: Is τ not equal to $1/G\nu$?

Smith: The properties that seem to fit our data best are; that for moderate disturbing powers $G\nu$ is independent of the mean electron energy, and that ν is proportional to the energy. When the perturbation of the collision frequency is large, there is an increase in the thickness of the disturbed region because of the self-interaction of the disturbing wave. The interpretation of the decay of the impressed modulation then becomes complicated, except at delays so long after the cessation of the disturbing pulse that the electrons have cooled to near the thermal energy. At these long delays, the decay is observed to be several times slower than that following a disturbing pulse which produces only a small perturbation.

Crain: In your critique of wave interaction results, you didn't mention Prof. Cutolo's work. I wondered if the omission meant that you approved of it.

Smith: Prof. Cutolo and his colleagues have published a large number of papers on some aspects of radio wave interaction. These papers have not been mentioned since I believe their methods and results have no bearing on the objectives of this conference.

3.1.2

RADIOWAVE PHASE INTERACTION

by

A.J. Ferraro and H.S. Lee

Ionosphere Research Laboratory
Pennsylvania State University, University Park, Pennsylvania

Presented by A.J. Ferraro

1. Introduction

This paper reviews the basic theory of radiowave phase interaction and describes a systematic procedure for the utilization of phase and amplitude interaction in the determination of the D-region electron densities, collision frequencies, and energy loss coefficient.

Radiowave phase interaction represents an extension of the amplitude interaction technique introduced by Fejer (1955). These earlier experiments have involved only the amplitude effects on the wanted echo. The basic sequence of events pertaining to a wave-interaction experiment is illustrated in Figs. 1.1 and 1.2. The local heating of the ionospheric medium by the disturbing pulses not only perturbs the imaginary part of the refractive index (χ), which accounts for the usual amplitude interaction, but also the real part of the refractive index (μ). This latter effect, which will be called phase interaction, should produce a detectable phase shift in the radio frequency carrier of the wanted wave. Measurement of both of these effects leads to a significant advantage in that the available information has been doubled and, as will be shown, one can utilize these data for determining the electron collision frequency, ν, without knowledge of the electron density, N.

Techniques for measuring this phase effect have been developed at the Ionosphere Research Laboratory (see Weisbrod et al. 1964) and have been utilized for routine measurements during the IQSY program.

2. Basic Theory

The phase and amplitude interaction effects are expressed by the complex coefficient of interaction T as

$$T = T_A + jT_\phi = \frac{(R - R')}{R} \tag{1}$$

where R' is the reflection coefficient of the disturbed sequence of wanted pulses, and R is the reflection coefficient of the undisturbed sequence of wanted pulses. Then it is clear that

$$T_A = \frac{\Delta A}{A} \text{ (amplitude interaction effect)} \tag{2}$$

$$T_\phi = \Delta\phi \text{ (phase interaction effect)} \tag{3}$$

For narrow wanted and disturbing pulses, T can be expressed as follows:

$$T(h_i) = j \int_{o}^{h_i} \Delta n(h)\, K_w\, dh \tag{4}$$

where h_i is the height at which the upgoing disturbing pulse meets the downgoing wanted pulse and K_w is the free space propagation constant for the wanted signal. In (4), $\Delta n(h)$ is the change in the refractive index due to the heating of the medium. It is assumed that the change in the index results from a change in the collision frequency, so that for small changes in $\Delta n(h)$ it can be written as

$$\Delta n(h) = \frac{\partial n}{\partial \nu} \Delta\nu \tag{5}$$

The detailed derivation of (4) for a narrow wanted pulse and a finite disturbing pulse as given by Weisbrod et al. (1964) is

$$T = \int_{o}^{h'_i} \frac{T_H(1 - e^{-G\nu\tau})}{G\nu\tau} \exp\left[\frac{-2G\nu(h'_i - h)}{c}\right] dF +$$

$$\int_{h'_i}^{h_i} \frac{T_H}{G\nu\tau}\left\{1 - \exp\left[\frac{-2G\nu(h_i - h)}{c}\right]\right\} dF \tag{6}$$

where T_H involves the longitudinal expression for $\frac{\partial n}{\partial \nu}$, G is the energy loss coefficient, τ is the disturbing pulse width, F is related to the absorption on the disturbing pulse.

3. Synthesis Techniques

Phase and amplitude interaction data can be effectively utilized for the determination of the collision frequency, ν, electron density, N, and the time constant, $G\nu$, pertaining to the D region.

A. Collision Frequency

The synthesis of ν and $G\nu$ involves a matrix technique. For the case of ν, the matrix technique is developed as follows: by approximating (6) by a summation, T_A and T_ϕ for the case of a narrow disturbing pulse are expressed by

$$T_A(h_i) = \sum_{m=1}^{n} T_{HA}(m\Delta h)\, e^{\frac{-2G\nu_m(n-m)\Delta h}{c}}\, \Delta F_m \tag{7}$$

$$T_\phi(h_i) = \sum_{m=1}^{n} T_{H\phi}(m\Delta h)\, e^{\frac{-2G\nu_m(n-m)\Delta h}{c}}\, \Delta F_m \tag{8}$$

Or, more conveniently by the matrices

$$(T_A) = (A)\ (\Delta F) \tag{9}$$

$$(T_\phi) = (\phi)\ (\Delta F) \tag{10}$$

It is easy to show that (A) and (ϕ) are triangular and contain the parameter ν and $G\nu$ while (ΔF) involves ν and N. The unknown electron density parameter can be eliminated from (9) and (10) by solving these equations simultaneously. This leads to

$$(T_A) = (A)\ (\phi)^{-1}\ .\ (T_\phi) = (M)\ .(T_\phi) \tag{11}$$

The triangular matrix (M) contains the unknowns ν and $G\nu$. If the time constant $(G\nu)^{-1}$ is assumed known, then ν can be determined either by a step-by-step method, since (M) is triangular, or by a least square error procedure for which ν is assumed exponential.

In the interpretation of wave interaction data, it is necessary to somehow account for the underlying ionization. Since data are usually available down to 60 km., it is important to include this effect. Previous workers seemed to have given no attention to this matter. If data are available down to some lower limit h_L, then the interaction expression can be written as

$$T(h_i) = \int_o^{h_i} \Lambda\Lambda\Lambda\Lambda\Lambda\Lambda\ dh = \int_o^{h_L} \Lambda\Lambda\Lambda\Lambda\Lambda\Lambda\ dh + \int_{h_L}^{h_i} \Lambda\Lambda\Lambda\ dh \tag{12}$$

The integration from zero to h_L represents the contribution of the underlying ionization to the interaction effect. If the numerical value of the integral could be evaluated and subtracted from $T(h_i)$, then the matrix approach just described could be applied to the region above h_L. The integrated effect from h_L to h_i is defined as the corrected interaction, $T_c(h_i)$. It can be shown from application of the mean value theorem that a fairly accurate expression for $T_c(h_i)$ is given by

$$T_c\ (h_i) = KT\ (h_L)\ \exp\left\{-\frac{2G\nu(h_L)}{c}\ h_i\right\} \tag{13}$$

The constant K is found from the fact that $T_c\ (h_L) = T(h_L)$, the interaction at the lowest observable height, h_L.

Fig. 2 demonstrates the importance of the correction. Interaction data was generated corresponding to the solid line collision profile. The synthesis of ν with and without corrections are given by the circles and triangles, respectively.

B The Time Constant $(G\nu)^{-1}$

For the determination of $G\nu$, a similar technique can be devised but either amplitude or phase interaction information is used, or both used if a check is desired. It can be shown for a long disturbing pulse that the relation between the interactions for a finite and narrow disturbing pulse is

$$\frac{\partial\ T^F\ (h_i)}{\partial\ h_i} = \frac{2}{c\tau}\ T^N(h_i) \tag{14}$$

where superscripts F and N refer to finite and narrow disturbing pulses, respectively. Using (14) and the summation approximation to (6), matrices for $\partial\ T^F/\partial\ h_i$ and T^N can be written as

$$(T^N) = (a)\ (\Delta F) \tag{15}$$

$$\left(\frac{\partial T^F}{\partial h_i}\right) = (b)\ (\Delta F) \tag{16}$$

or

$$(T^N) = (a)\ (b)^{-1}\ .\ \left(\frac{\partial T^F}{\partial h_i}\right) = (m)\ .\ \left(\frac{\partial T^F}{\partial h_i}\right) \tag{17}$$

The matrix (m) is triangular and contains only the unknown $G\nu$. Solutions for the height dependence of $G\nu$ are similar to those described for finding ν.

A method for finding the height dependence of $G\nu$ has not, to the authors' knowledge, been previously proposed. Other workers employing gyro-interaction have succeeded in determining this parameter at a specific height.

C. Electron Densities

The method of synthesizing electron density profiles is to assume a piecewise linear model. In this manner, it is possible to synthesize a more general electron density profile. The synthesis is performed by searching for the least squared error between the observed interaction coefficients T_A and T_ϕ and those computed from the synthesized piecewise linear electron density profile.

An alternate procedure for finding electron density profiles is based upon the matrix technique described under section (A). Using equation (10) one can solve for (ΔF), since

$$(\Delta F) = (\phi)^{-1}\ (T_\phi) \tag{18}$$

Then the quantity F, which is related to the absorption on the disturbing pulse, can be found from

$$\begin{aligned} F_1 &= F_o + \Delta F_1 \\ F_2 &= F_o + \Delta F_1 + \Delta F_2 \\ F_n &= F_o + \Delta F_1 + \ldots\ldots \Delta F_n \end{aligned} \tag{19}$$

The quantity F_o is related to the absorption occurring below the lowest observable height, h_L. If this height is low enough then $F_o \approx 1$. From F_1, F_2, ...F_n can be determined and then, in a direct manner, the electron densities, since $\Delta F_n/F_n$ is directly proportional to electron density.

This latter approach has not been used too extensively, since the piecewise linear technique with the least squared error feature provides a more satisfactory procedure to employ with noisy data. The effect of noise on the measurement of interaction is illustrated in Fig. 3. In this example, phase and amplitude data were generated corresponding to the solid line profile and then this data was modified in a random manner in an attempt to simulate the effect of noise. In this case, the signal-to-noise ratio is as low as two for the data at the lower heights. The results indicate a fairly reasonable synthesized profile of electron densities.

4. Discussion

This paper has described a systematic procedure for the measurement of D-region parameters by the wave-interaction technique. By measuring either phase or amplitude interaction for both a narrow and long disturbing pulse, a direct determination of the height profile of $G\ \nu$ is obtained. With this profile and the simultaneous measurement of pulse and amplitude interaction, the matrix technique outlined in 3A will give a collision frequency profile. Now it is possible to specify the value of G. With these values of G and ν along with a suitable temperature profile, the electron densities are computed from either the

piecewise procedure or the matrix technique. At all times it is necessary to account for the underlying ionization.

Through the use of the above described techniques, simultaneous phase and amplitude data obtained during the IQSY program are being reduced.

Acknowledgment

The research reported in this paper has been sponsored by the National Science Foundation under Grant GP-846.

REFERENCES

Fejer, J.A. The Interaction of Pulsed Radio Waves in the Ionosphere. J. Atm. Terr. Phys., 7, 322-332, 1955.

Weisbrod, S., Ferraro, A.J. and H.S. Lee. Investigation of Phase Interaction as a Means of Studying the Lower Ionosphere. J. Geophys., Res., 69, 2337-2348, 1964.

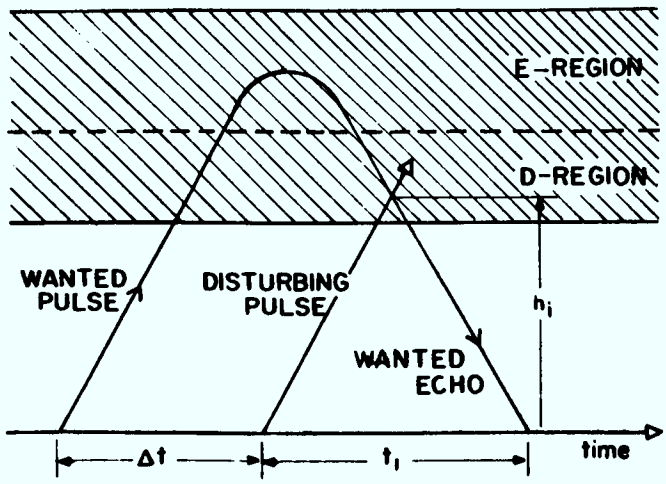

Fig. 1.1. Height of Wanted and Disturbing Pulses as a Function of Time.

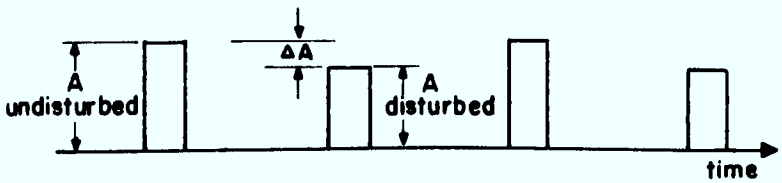

Fig. 1.2. Amplitude of Wanted Echoes as a Function of Time.

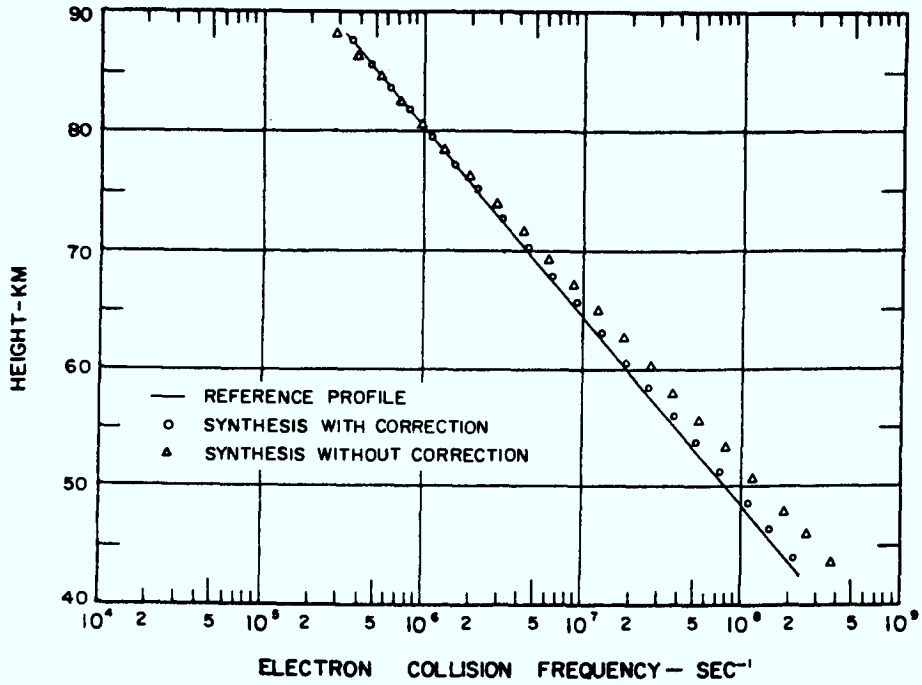

Fig. 2. Effects of Correction in Exponential Synthesis.

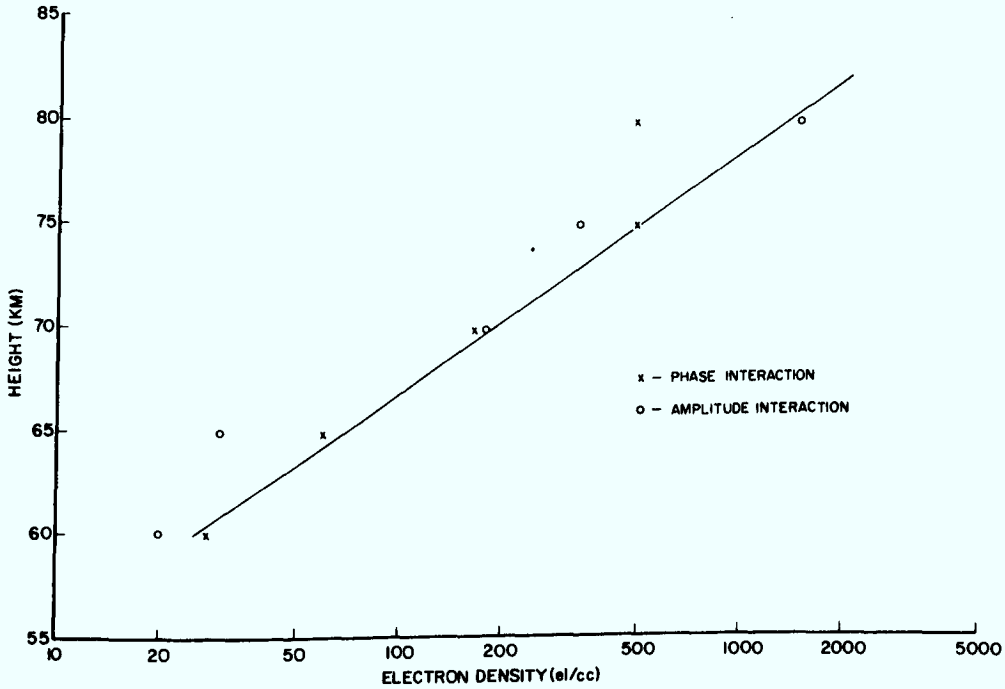

Fig. 3. Effect of Random Errors in Electron Density Synthesis.

Discussion on Paper 3.1.2 presented by A.J. Ferraro

Bourne: Could you give a brief outline on how you measure phase interaction? I have frequently noticed that many of the E-region echoes consist of two different echoes with different phase patterns, and I should think this could make the measurement rather difficult.

Ferraro: The undisturbed echoes from the E region are, of course, tumbling in phase, but because of the interaction the disturbed sequence of echoes is also tumbling in phase. What we are doing is looking at the difference in phase. Even though the phase is wild and tumbling, it does not bother us because we are looking at the difference between two things which we hope are tumbling together. This is why we can measure a small change in the phase even under conditions of rather severe phase fading. Is this what you had in mind or do you want to know about instrumentation?

Bourne: Yes and no. What happens if the echo that you are getting back from the E region actually consists of two separate echoes with different phases, which I understand is frequently the case?

Ferraro: I think the same thing happens that happens in the measurement of amplitude interactions. You don't know what you are measuring. Is that correct?

Bourne: With amplitude interaction this doesn't matter very much. You are not really worried where the signal comes from so long as it is coming from roughly the same direction and the same height.

Ferraro: This does cause some limitations because the mechanical phase-measuring device will have some difficulty in knowing what phase to correct for, and it just looks at the average phase. My answer would be that it would give an average value of the phase interaction between the two echoes.

Smith: In your analysis, do you actually allow for the shapes of your disturbing and wanted pulses?

Ferraro: At this stage, the only thing we have included is that they are rectangular. The shape has not been included. We consider a definite width of disturbing pulse but it is a rectangular pulse, not rounded. We include the fact that it is a definite width but we do not include the fact that it is probably non-rectangular.

Smith: Do you propose to extend these analyses to include the actual shape of the wanted pulse, because if you don't, I don't see what value they are?

Ferraro: At this time I don't think I know how to do it. I certainly will consider it.

Smith: This is important. You can't replace an irregularly shaped pulse by a rectangular one and hope to get the right answers.

Ferraro: Well, how do you do it, then?

Smith: We actually shape the pulse that goes into our synthesizer.

Ferraro: Well, if you can do the analog method I am sure we can do it digitally. We haven't done it, but we realize it probably should be done. It is one of the things we are considering.

3.1.3 A NUMERICAL APPROACH TO THE INTERPRETATION OF PULSE INTERACTION EXPERIMENTS*

by

T.M. Georges

ITSA/ESSA, Boulder, Colorado

Present methods of interpreting pulse interaction experiments depend on greatly simplified models of the interaction mechanism. As disturbing powers tend towards the megawatt range, the use of these models leads to errors which may no longer be negligible. Since attempts to formulate a more rigorous analytical model of the interaction process prove to be quite involved, a numerical approach would seem to be a logical one.

High-speed digital computers lend themselves well to "brute-force" methods for solving problems of this kind. Instead of solving complicated analytical interaction expressions, the computer is programmed to perform a large number of relatively simple calculations which in effect simulate the interaction process. By representing the disturbed ionosphere as a grid of a large number of "cells" in the height-time domain, probing wave interaction becomes merely the sum of interaction contributions of cells lying along appropriate height-time paths. The interaction contributions of each cell are determined by solving the electron energy balance and magnetoionic absorption equations for each cell in a height-time sequence simulating the upward passage of the disturbing pulse. Fig. 1 is a convenient way of illustrating this process.

Complete generality is retained by allowing arbitrary representations of the neutral atmosphere and ionosphere in tabular form, arbitrary energy dependences of electron collision parameters (G and ν), and the use of any version of the magnetoionic theory yielding explicit values for the complex refractive index. Other previously necessary assumptions are avoided by accounting for time-dependent coefficients of the energy balance equation (G and ν), disturbing pulse self-distortion, and disturbing pulses of arbitrary shape. Provision for time-dependent electron density is possible, although this has not yet been attempted. The simulation technique is directly applicable to vertical-incidence experiments based on the method of Fejer, including phase interaction, gyrointeraction, and cosmic noise interaction. Its flexibility allows the incorporation of future refinements in interaction theory and in laboratory measurements of collision parameters, without modification of the basic program.

The basic assumptions of the process are only that: (1) absorption in the interaction region is nondeviative, (2) an effective value of electron collision frequency can be calculated and applied to an appropriate magnetoionic theory, and (3) the medium varies so slowly in space and time that ray theory is applicable.

The central problem of the interpretation of interaction experiments is the derivation of ionosphere profiles from interaction data. Present trial-and-error methods are capable of

*Summary of a paper to appear in Radio Science, September 1966.

indicating only gross features of the D-region electron density distribution. For more accurate resolution of detailed structure, a direct synthesis process is required.

A modification of the simulation process just outlined yields a method for synthesizing D-region electron density and collision frequency profiles from interaction data. Here the data are used to reconstruct the interaction process by a bootstrap method similar to the simulation technique, where electron density and collision frequency are calculated as each height step is made. By using "data" from the simulation program, and modifying it to represent limitations in accuracy and sensitivity, checks on the accuracy of the synthesis process are possible. Fig. 2 shows errors in synthesizing an electron density profile (collision frequency assumed known), for several degrees of data quality. (L represents the smallest measurable interaction, N the number of significant digits, or accuracy, of the data.) Note that these curves apply only to the specific experimental conditions indicated. Simultaneous synthesis of electron density and collision frequency (using both phase and amplitude interaction data) significantly reduces the electron density accuracy.

A basic problem in such synthesis methods is thus the accuracy requirements imposed on the interaction data. Note that decreases in sensitivity degrade the synthesis accuracy primarily at low heights, while decreases in data accuracy affect the high end of the interaction region. Since the bottom curve of Fig. 2 represents somewhat better conditions than are at present obtainable, there is some doubt that the basic interaction experiment is capable of yielding very accurate D-region profiles. Certainly, extensive refinements in both experimental techniques and synthesis methods are necessary before it can.

The possibilities of using numerical techniques in interpreting pulse interaction experiments have been only briefly explored; however, it is believed that their development thus far indicates a profitable approach to the design, evaluation, and interpretation of these experiments.

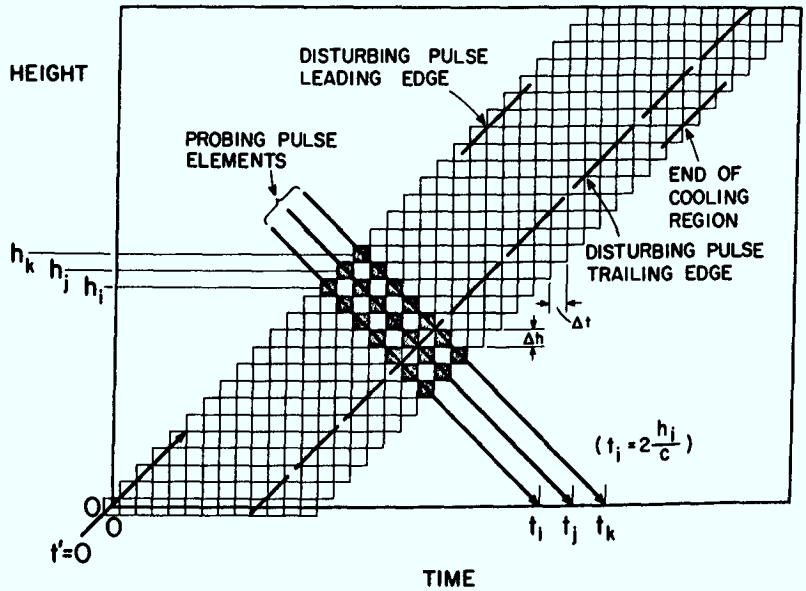

Fig. 1. A schematic representation of the method of numerical simulation by quantization of the interaction region in the height-time plane.

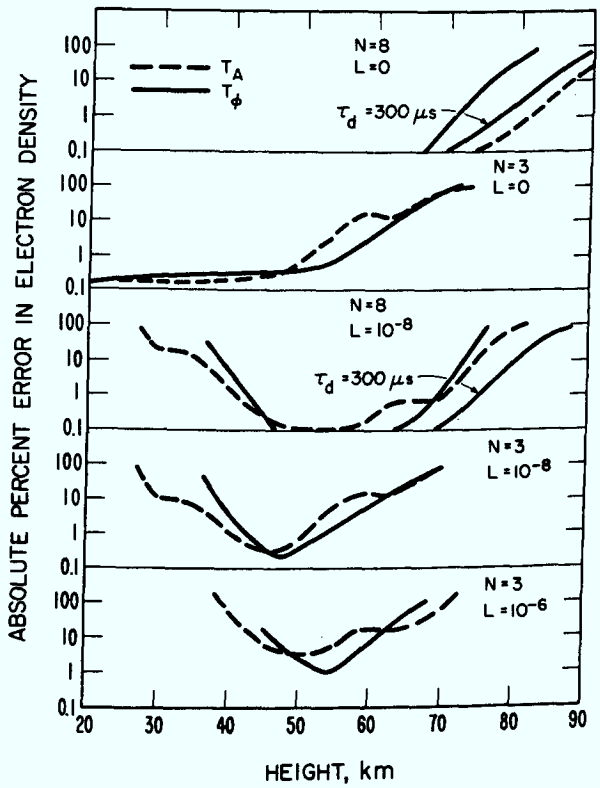

Fig. 2. Errors in synthesizing a daytime electron density profile under various simulated experimental conditions. L is an index of experimental sensitivity, and N is an accuracy parameter (see text). Collision frequency profiles are assumed given. Disturbing frequency is 10 Mc/s, power is 10 megawatts, and pulse length is 57 microseconds except as noted.

Discussion on Paper 3.1.3 presented by T.M. Georges

Ferraro: One of your slides showed a percentage error for synthesis versus altitude, and you have indicated on most of your slides that the error was very large at low heights. On a previous slide where you actually showed the computed N profile, you had good agreement below 60 km. The two curves were on top of each other, implying very small error, and yet the error bars indicated 100 per cent error?

Georges: The first slide was just limiting the sensitivity of the data and retaining all the accuracy.

Ferraro: Yes, but at your lowest heights, interactions are of the order of 10^{-8}, and sensitivity is set on 10^{-8}. (I looked at your report and saw some of your numbers, so I have some advance knowledge here.) The percentage error in the interaction records would be small at high heights but large at low heights, where you obtained a beautiful profile.

Georges: Well, I'll have to think about that; I did think about it before.

Wright: I want to observe that Dr. Bourne presented a paper on the partial reflection experiment that contained a similar assessment of the kinds of error that experiment might bring. I think it would be worthwhile to plan for Friday that you two review your conclusions and compare the two experiments for us. They contain different sources of error but for one who might wish to include such experiments in future instrumentation, it would help a great deal to see how these two experiments compare. Secondly, I would like to ask whether or not this 100 per cent error, which seemed to be about the maximum that Dr. Georges obtained, is so frightening? We have been hearing about errors by factors of ten in some of these other experiments.

Georges: Not necessarily. The computed electron densities values can be 50 per cent too low or 100 per cent too high.

Bourne: In part answer to this, I think a main aim of this conference is to assess the reliability of the various experimental methods so that installations, or combinations of installations, can be designed which will enable acceptable accuracies to be obtained in measurements of electron densities and collision frequencies. A factor of 2 is, I think, a realistic estimate of the accuracy of collision frequency and electron density measurements obtained with the partial reflection experiment. Personally, I feel it is unacceptably large from an experimental point of view; I would like to know what accuracy is required by theoreticians. We are deducing electron densities basically for their needs, and it would be very handy if we knew if accuracies of 1 per cent, 10 per cent, or 100 per cent are required so that our final objectives can be met.

Belrose: I would just like to make a comment on Dr. Georges' analysis. You said that the results in your calculations looked bad for the cross modulation experiment; well, I don't think that it does. I think that it is a very valuable piece of work that you have done. You can see how the percentage errors vary as a function of height for various conditions, and you can see that sometimes this can be very good. On the basis of the work you have done, I wonder if you would comment on the far worse situation which Dr. Smith suggested; that is if you have only the Fejer height interaction profile, you can synthesize the whole thing with only two slabs to the accuracy that he can see on his analog comparison.

Georges: I wouldn't care to explain that. The essential difference between a numerical synthesis and an analog synthesis is that in the analog method you are really synthesizing the whole profile at the same time with no knowledge of how your errors depend on the height that you are talking about.

Belrose: You suggested that you could have a very complicated profile, and if you knew the interaction curve as a function of height to sufficient accuracy you could, in fact, go back to that complicated electron density profile. Dr. Smith drew us a smooth interaction profile with a dashed line disappearing behind it,

and yet he was synthesizing the dashed curve with only two slabs! There seems to be a tremendous difference between the suggested capability of the experiment on the basis of these two methods of synthesizing electron density profiles.

Georges: Dr. Smith could probably answer that better than I could, but as I understood his remarks, he assumed the smoothest possible profile corresponding to his two knob settings.

Smith: I think the answer is very clear on that, if you have a poor curve you have to do the best you can. We can get a solution for poor interaction curves by putting bumps and hollows in the electron density profiles. You must include in the criterion that the electron density profile is smooth within the resolving power of the instrument. You must reject those wild profiles. This is a physical hypothesis that you must include.

Belrose: The uniqueness of the profile seems to be in question, according to you.

Smith: Well, I think it is the same in any method, in your method, Jack, if you have a finite resolving power then you have to reject the wildness in your curves.

Georges: It depends on the size of the cell with which you are concerned. In the numerical representation I used cell sizes about 1 km. high and 3 1/3 μs. long, and you can probably resolve the structure on the order of a kilometer in size.

Ferraro: Dr. Smith, you found several electron density profiles which gave the same interaction profile. Did you use the same $G\nu$ profiles? You indicated there were several N profiles which would give your measured interaction profile. Were they using the same $G\nu$ profiles you used or were they different $G\nu$ profiles?

Smith: The same $G\nu$.

Georges: They may look the same but I don't think they will be exactly the same.

Bourne: There is really no disagreement between Prof. Smith's analysis and Dr. Georges' computations. Dr. Georges is assuming that the wave interaction experiment is capable of detecting very small modulation depths, and is capable of measuring the interaction depth to a high degree of accuracy. The sensitivity and accuracy assumed by Prof. Smith differ by orders of magnitude from the conditions assumed by Dr. Georges. I believe Prof. Smith's work is appropriate to the best wave interaction measurements presently available. Dr. Georges' analysis is extremely valuable but, to my knowledge, the majority of the conditions that he has considered far exceed the capabilities of the present wave interaction experiments.

Smith: Under good conditions, it is realistic and practical to put the accuracy at 2 per cent. You are not going to get a better accuracy than that. We consider the experimental accuracy to be of great importance.

3.1.4 HIGH POWER INTERACTION THEORY

by

C.D. Bell and A.J. Ferraro

Ionosphere Research Laboratory, Pennsylvania State University
University Park, Pennsylvania

Presented by C.D. Bell

1. Introduction

The Ionosphere Research Laboratory in conjunction with the IQSY has been conducting a wave interaction experiment. As an extension of this experiment, in order to increase the accuracy of experimental data, the disturbing power will be increased considerably. At present the wanted wave frequency is 2.2 Mc/s., the disturbing wave frequency is 300 kc/s, and the peak radiated disturbing power is 100 kw. The new disturbing transmitter will have a frequency of 4.5 Mc/s. and a peak radiated power variable to 15 Mw. The pulse width will be variable to 1 ms.

With this increased energy, certain nonlinearities not accounted for using low power or small perturbation theory are more noticeable. In view of this, a re-evaluation of this low power approximation must be made before using high power. In order to facilitate synthesis of ionospheric parameters, suitable analytic nonlinear approximations for the interaction coefficients should be found. The details of this study have been given by Bell (1966).

2. Theoretical Studies

(a) Perturbation in the electron densities

The perturbation of the index of refraction can be expanded in a Taylor series with respect to the change in electron collision frequency and the change in electron density. In the past the perturbation due to change of electron density has been ignored. Taking the dominant temperature dependent processes in the D region to be the ion-ion recombination coefficient and the three-body attachment coefficient, a measure of the effect of the interaction due to changes in electron density can be obtained.

When interaction coefficients were obtained considering interaction due to changes in collision frequency only and changes in electron density only for characteristic D-region parameters, 2.3 Mc/s. wanted frequency, and a 100 μsec. disturbing pulse width, it was found that the ratio of interaction due to electron change to interaction due to collision frequency change was 0.12 for amplitude interaction and 0.06 for phase interaction at 40 km. At 50 km. these ratios were a hundred times smaller. In view of this it seems apparent that the expansion of the perturbation of the index of refraction due to changes of electron density can be ignored without incurring significant error.

(b) Non-linear heating

At these higher powers, a suitable expression for the energy change of the electrons due to the disturbing wave has been developed. Considering the energy balance for an electron after the passage of the disturbing pulse,

$$\frac{\partial \Delta Q}{\partial t} + G\nu\Delta Q = 0$$

where G is the energy loss coefficient and ν is the electron collision frequency, and using the energy relation derived from the curves given by Phelps (1963),

$$G(Q) = 4.7 \times 10^{-4}\, Q^{-.55}$$

and $$\nu(Q) = 9.7 \times 10^{-8}\, Q^{.978}\, n_m$$

where the energy, Q, is in electron volts and n_m is the neutral particle concentration, a nonlinear energy balance equation can be obtained,

$$\frac{\partial \Delta Q}{\partial t} + A\Delta Q + B\Delta Q^2 = 0.$$

This rectifies the error in low power theory that G and ν are independent of energy change. The solution to this equation is

$$\Delta Q(h) = \frac{\Delta Q_o\, e^{-At}}{1 + \Delta Q_o \frac{B}{A}(1-e^{-At})}$$

where ΔQ_o is the maximum energy change. By applying an energy production term, C, to the energy balance equation, a suitable expression for the energy build-up within the disturbing pulse can be obtained,

$$\Delta Q(h) = \frac{2C\,(1-e^{-\sqrt{A^2+4BC}\,t})}{A + \sqrt{A^2+4BC} - (A - \sqrt{A^2+4BC})\, e^{-\sqrt{A^2+4BC}\,t}}$$

where $$C = \frac{P}{2\pi\, h^2\, N}\left(-\frac{\partial F}{\partial h}\right)$$

P being peak radiated power and $\frac{\partial F}{\partial h}$ the differential absorption. By saying that C is a constant at any height, self-distortion is neglected since C is a function of ν.

The accuracy of these expressions was evaluated with respect to accurate numerical integration of the non-linear energy balance equation including the effect of self-distortion. Fig. 1 shows the maximum percentage energy change for representative D-region parameters using 100 μsec. pulse width and a frequency of 4 Mc/s. using the numerical solution, the non-linear approximation and low power or linearized approximation. By 30 Mw. the non-linear approximation is in error by less than 2 per cent while the linearized approximation is in error by about 22 per cent. This would indicate that the neglect of self-distortion is not sufficient to invalidate the worth of the non-linear approximation.

(c) Taylor expansion of the change of index

The inaccuracy in terminating the Taylor series expansion of $\Delta\mu$ and $\Delta\chi$ after the first term, as in low power theory, was investigated. This was done by using the time-height cell approach similar to that described by Georges (1965). Fig. 2 shows a comparison of interaction coefficients using for the exact coefficients the $\Delta\mu$'s and $\Delta\chi$'s, the first term of the Taylor series with exact heating, and the first and second terms of the Taylor series using exact heating at 15 Mw. The maximum error in the first term approximation is about 3 per cent; but the inclusion of the second term does not improve the error significantly. This would mean that many more terms would be needed to cancel all error. This would make the equation too bulky to handle. The conclusion is that the lack of accuracy is not enough to warrant the increased complexity.

Figs. 3 and 4 compare the exact interaction coefficients with those using the first term approximation and linear and non-linear heating at 15 and 30 Mw. respectively. The non-linear approximation gives much better accuracy than the linear approximation in both cases.

(d) Electron density and collision frequency synthesis

Based upon the foregoing discussion, an analytical expression for the interaction effect was developed which appears fairly accurate up to at least 30 Mw. peak power. With this expression it is possible to develop techniques for the synthesis of the electron density and collision frequency profiles. However, it is instructive to examine the accuracy of synthesis techniques based upon low-power theory when utilized with high-power data. Figs. 5 and 6 summarize these results. Assuming exponential collision frequency and electron density profiles, interaction data were generated by the linear theory (low-power theory) and by the more exact theory employing numerical integration described previously. Fig. 5 shows these results for high-power data up to 50 Mw. At 15 Mw., the error is tolerable and would be considerably smaller if phase alone were used in the synthesis rather than simultaneous use of phase and amplitude. Not shown is the synthesis using amplitude alone at 15 Mw. This resulted in an electron density so poor that it even went negative about 70 km. The derived collision frequencies based upon low-power synthesis theory are also acceptable at 15 Mw., as shown in Fig. 6.

3. Conclusions

A suitable expression for interaction for disturbing powers up to 30 Mw. was derived. Low-power synthesis theory appears reasonably adequate up to 15 Mw. if both phase and amplitude interaction are used. If more accuracy is desired, then the more exact expressions must be used to derive a new synthesis procedure.

Acknowledgments

The research reported in this paper has been sponsored by the Office of Naval Research under Grant NONR656(35), NR087-164/8-13-65 (Field Projects Branch) and in part by the National Science Foundation under Grant GP-4622.

REFERENCES

Bell, C.D. Investigation of Problems Encountered in Wave Interaction Experiments at High Power. Ionosphere Research Scientific Report No. 262, Ionosphere Research Laboratory, Pennsylvania State University, January 10, 1966.

Georges, T.M. Numerical Simulation of Ionospheric Wave Interaction Experiments. NBS Tech. Note No. 325, October 25, 1965.

Phelps, A.V. Non-linear Interaction Coefficients for Electrons in Nitrogen and Air. Presented at the Conference on Non-linear Processes in the Lower Ionosphere, December 16-19, 1963, NBS Tech. Note No. 211.

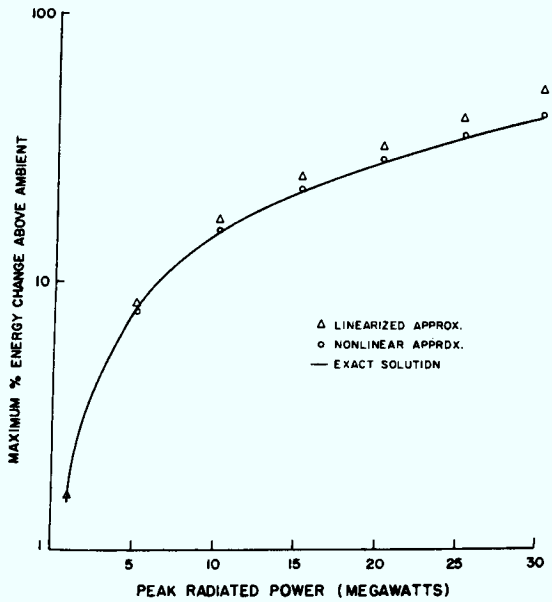

Fig. 1. Maximum energy buildup at end of 100 μsec. pulse at 67 km., the height of maximum energy change, 4 mc. extraordinary mode.

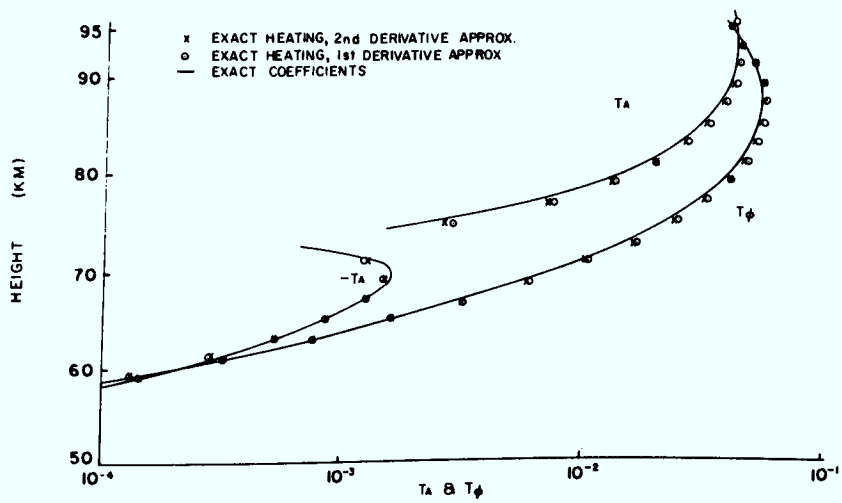

Fig. 2. Interaction coefficients using 2.3 mc. wanted, ordinary mode; 4 mc. 15 Mw. disturbing, extraordinary mode.

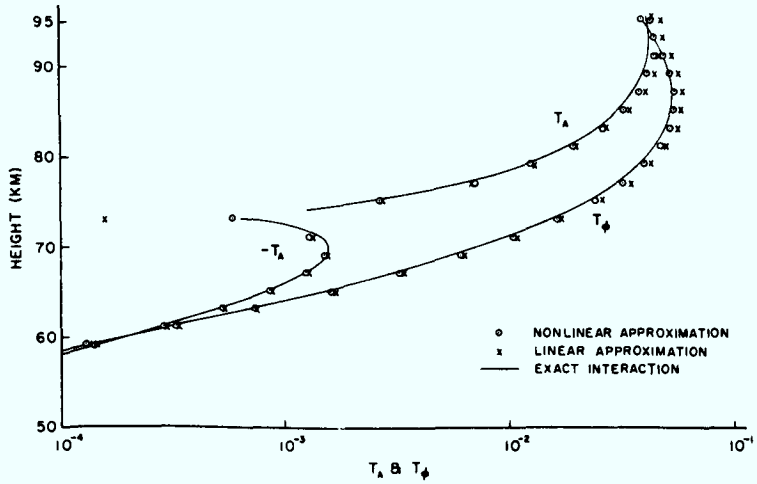

Fig. 3. Interaction coefficients using 2.3 mc.wanted, ordinary mode; 4 mc. 15 Mw. disturbing, extraordinary mode.

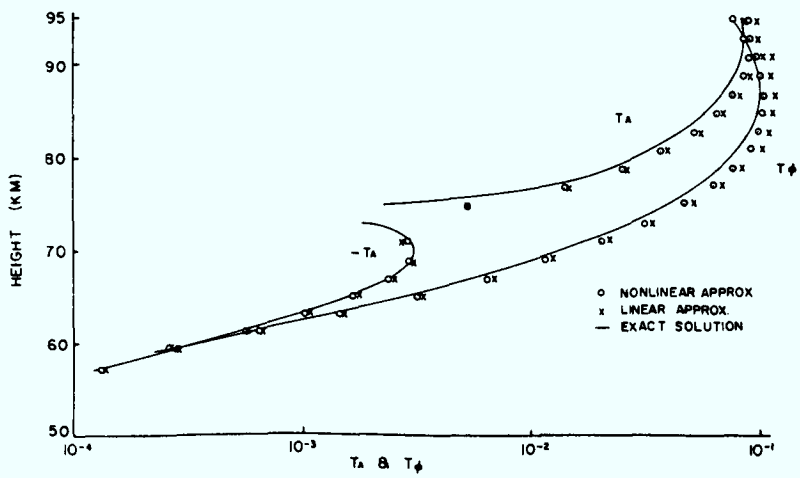

Fig. 4. Interaction coefficients using 2.3 mc.wanted, ordinary mode; 4 mc. 30 Mw. disturbing, extraordinary mode.

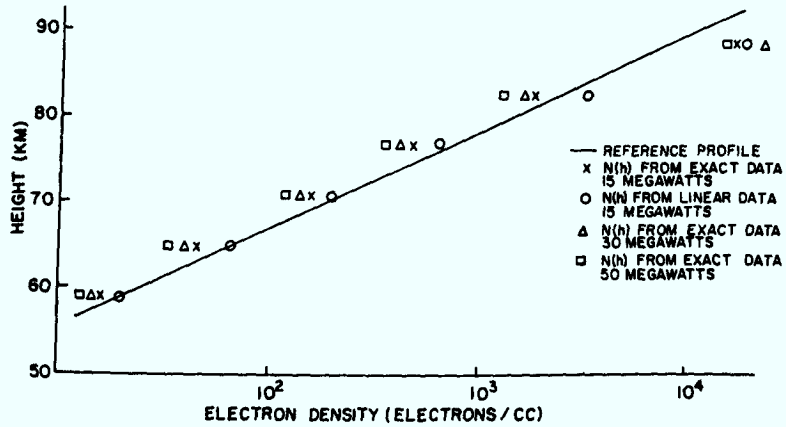

Fig. 5. Electron density synthesized from linear and exact interaction coefficients.

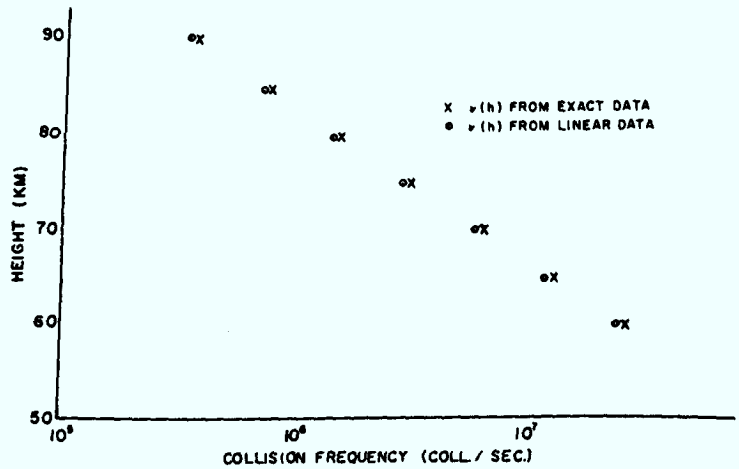

Fig. 6. Collision frequency synthesized from linear interaction coefficients and exact interaction coefficients at 15 Mw.

3.2.1 SMALL PERTURBATION WAVE INTERACTION IN THE LOWER IONOSPHERE

PART 2

MEASUREMENTS OF BASIC PARAMETERS

by

R.A. Smith, I.A. Bourne*, R.G. Loch and T.N.R. Coyne
University of New England, Armidale, Australia

* Now at DRTE, Ottawa, Canada

1. Introduction

Experiments on gyro-interaction at night have been made at the University of New England since 1949. Those to 1954 have been referred to in Paper 3.1.1 and employed an obliquely reflected continuous wanted wave at a frequency of 0.59 Mc/s. In these early experiments the need for two transmitters and a receiving station at widely spaced points prevented frequent observations, and selective fading of the wanted wave was often troublesome. Also, the experiments provided no direct height data. Since these defects from the use of an oblique wanted wave were eliminated in the pulse experiment of Fejer (1955), Smith and Bourne began using his pulse methods in 1958 to assess their value in a gyro-interaction experiment at night. It soon became evident that a small modulation depth with a marginal signal-to-noise ratio, as in the experiments of Fejer, was not a necessary defect of the pulse experiment. At night the modulation depth could be enhanced by factors of 20 or more by using as the wanted wave an extraordinary gyrowave instead of the more strongly reflected and less absorbed ordinary mode of a medium frequency wave. This allowed full advantage to be taken of the sensitivity and inherent accuracy of the detection methods and, as a consequence, of the simple and precise interpretation which is possible in a wave interaction experiment using two vertically propagated waves.

With development of transmitting facilities for the disturbing gyrowave, particularly those made under Contract AF19(604)-6177, the experiments at night have been extended progressively to higher degrees of electron heating. Studies of wave interaction in the D region were not undertaken until mid-1962 when, following completion of an isolated receiving and transmitting station for the wanted pulse, it became possible to superimpose the disturbing and wanted pulses and thus use the more effective Type III experiment described in Paper 3.1.1.

In the account of wave interaction theory given in Paper 3.1.1 the electron heating was assumed to produce only a small perturbation of the electron collision frequency. This limitation on the magnitude of the perturbation is the usual condition in a pulse wave interaction experiment and simplifies the theory by allowing the self-interaction of the disturbing pulse to be neglected and propagation data for the wanted pulse to be evaluated for ambient conditions. The use of the Bailey and Martyn formula for energy loss in collisions can be justified on general grounds, and the introduction of an explicit relation $U(\nu)$ between the electron energy U and the collision frequency ν is unnecessary. The unknowns for the behavior of near-thermal electrons in air which appeared in the theory are the energy loss coefficient G and a second dimensionless quantity α related to the gradient of the $U(\nu)$ function. Both G and α must, in general, be considered as functions of the ambient temperature.

There has been a long-standing need in wave interaction research for quantitative data for G and the $U(\nu)$ relation in air. Without such information the effectiveness of small perturbation wave interaction in studies of the general properties of the lower ionosphere is severely limited, and a start cannot be made on the quantitative interpretation of large perturbation phenomena (Smith et al. 1965). The determination of these basic data for near-thermal collisions and the testing of the limits of applicability of small perturbation wave interaction theory were the initial objectives of the experimental program started in 1958. The latter aspect of the research has been referred to briefly in Paper 3.1.1. More detailed accounts have been given by Bourne (1960, 1964) and Smith et al.

Details of experimental equipment used for the investigations in this paper and in Paper 3.2.4 are summarized in Section 2.

Section 3 outlines the principles of the methods used to determine the values of G, ν, and electron relaxation time in the nighttime lower E region. Experimental results for this region are summarized in Section 4 along with some observations on its general behavior. A feature of the methods is that the properties of the collisions can be inferred to a close approximation without taking account of the electron density profile of the region where the interaction occurs. This is most valuable, since the profile in the lower ionosphere is not easily determined by wave interaction or other methods.

Results for electron collisions in the lower D region, obtained using similar methods, are summarized in Section 5.

Evidence from the investigations on the form of the $U(\nu)$ relationship for near-thermal electrons in the lower ionosphere is discussed in Section 6.

2. Experimental Details

Between 1958 and 1962 measurements of pulse wave interaction were made at the University of New England, using disturbing and wanted transmitters and receiving equipment at a field station A within the grounds of the University. Subsequent measurements, which form the main body of this and the later paper 3.2.4 were made using the disturbing transmitter at A and transmitters and receivers for the wanted pulse at a field station C, 9 km. from A. A number of photographs of Station C and the higher power gyrotransmitter B, 1.5 km. from C, are shown in Paper 3.1.1. Technical details of the three stations are given in Smith et al.

The disturbing transmitter at A has a maximum pulse power of 200 kw. and a maximum pulse duration of 800 μsec. at this power. Both power and pulse duration are continuously adjustable. Transmissions in the frequency range 1.26 - 1.8 Mc/s. about the gyrofrequency (1.515 Mc/s.) are allowed between midnight and 0500 E.A.S.T. under a permit that has continued from the early experiments on gyro-interaction. The permitted frequency during the day is 1.78 Mc/s.

The aerial for the disturbing transmitter was changed at the end of 1961 from a single horizontal half-wave folded dipole suspended between 150 ft. towers to a square array of four similar dipoles. This array has been matched in the circularly polarized condition at the frequencies of 1.515 and 1.78 Mc/s., and stub coils are permanently mounted on the feeder lines with plug and socket connections for speed in changing between these frequencies. At each of these frequencies the power radiated in the suppressed mode is negligible.

The question of the stability of the gain of the disturbing aerial is an important consideration when wave interaction observations are compared over long periods. The aerial at station A is on a poor site and the aerial has no ground mat. Nevertheless, it would appear from the constancy of the input impedance and from general considerations of ground reflection at these frequencies that the gain of the aerial is little affected by ground conditions.

The wanted station C contains two receiving units of the Fejer type, two wanted transmitters (7 kw., 70 μsec.) and timing and control equipment for synchronous operation of the three stations. The wanted frequencies are 1.78 and 2.12 Mc/s. during the night and 2.12 Mc/s. during the day. Separate receiving and transmitting aerials are used at each of these frequencies, the aerials being square arrays of 4 dipoles at 2.12 Mc/s. and crossed dipoles at 1.78 Mc/s. The transmitting aerials are co-phased using artificial $\frac{\lambda}{4}$ - sections and the rejection ratios are about 20/1. The receiving aerials are co-phased using the circuit of Gardner and Pawsey (1953), which gives a higher rejection ratio of about 40/1. The 40-dipole array at Station B can also be fed to station C by means of an underground 4-wire feeder line, to act as a polarized receiving aerial for the wanted pulse. The use of the large array for this purpose appears to make a slight improvement to the signal-to-noise ratio of the measured modulation when the echo is fading severely.

The repetition rate (27.75, 55.5, 166.6 or 333.3 p.p.s.) of the wanted pulses is generated by division of the frequency of a 100 kc/s. crystal oscillator and the dividing chain provides time calibration pulse trains (pulses 10 or 100 μsec. apart) for each of the monitoring oscilloscopes. Of these repetition rates, the lowest is used only in some experiments with Station B and the second was used generally until late in 1963. The rate of 166 p.p.s. was then added to assess the value of a higher rate in experiments during the day. When this change was found to improve the quality of the records, the rate of 333.3 p.p.s. was added for the dawn experiments described in Paper 3.2.4.

A number of the experimental records shown in Papers 3.1.1 and 3.2.4 have been obtained with continuous variation of the relative delays of the disturbing pulse from A and the wanted pulse from C. The variable delay generator is at C and for all the records shown it has controlled the triggering of equipment at C and not the triggering of the disturbing pulse from A. This method of introducing the delay places more demands on the smoothness of the variation, but is preferred when the virtual height of the wanted echo is steady since it causes the monitored disturbing pulse from A to be at a fixed location relative to the time calibration pulses. Any small drift of the disturbing pulse over long periods can then be checked easily at C. Other methods of introducing the variable delay to cope with a wanted echo, whose virtual height is changing, are described in Smith et al.

The duration (50 μsec.) of the output pulse from the receiver is made shorter than the duration of the transmitted wanted pulse and the AGC circuit controls the area rather than the amplitude of the output pulse of the receiver. These practices give a sharp video pulse for accurate measurement of the delay and make the measurement of the modulation depth more tolerant of movement of the echo relative to the strobe pulse for the receiver. Other practices are the recording of the AGC.bias voltage and the use of a short (2 - 5 sec.) integration time for the phase-sensitive detector. The parts of the record when the echo was steady can then be identified readily and the recovery of the detector from noise bursts is rapid.

Magnetic data for Armidale (30°30'S, 151°30'E, altitude 1000 m.) supplied by the Bureau of Mineral Resources, Department of National Development, yield the following values for the gyrofrequency f_H at a height of 85 km., when calculated using the dipole model of the earth's magnetic field:

Epoch 1959.5: Smoothed (1.515 Mc/s.) Station (1.511 Mc/s.)

Epoch 1963.5: Smoothed (1.518 Mc/s.) Station (1.514 Mc/s.)

The smoothed values are derived from magnetic data read off isomagnetic maps of New South Wales; the station values are derived from measurements at Armidale. The Bureau commented that the station and surrounding districts appeared to be undisturbed magnetically.

Magnetoionic data used in this paper and Paper 3.2.4 are calculated for a gyrofrequency of 1.515 Mc/s. and a propagation angle of 29°14'. This value for the gyrofrequency agrees with the value from the wave interaction measurements described in Section 2 of Paper 3.2.4 and its difference from any of the values above is negligible when considered in terms of the "Q" of the resonance in the absorption coefficient of the extraordinary mode. The value for the propagation angle is based on the magnetic data supplied by the Bureau.

3. Some theoretical properties of gyro-interaction at night

Since the significance of experimental data on wave interaction is more readily appreciated with a previous knowledge of the properties predicted by theory, the relevant parts of small perturbation wave interaction theory in Paper 3.1.1 are summarized in this section. The formulae are expressed for use with the generalized magnetoionic theory of Sen and Wyller (1960) and the collision frequency (unperturbed) is taken as ν_m.

For vertical propagation the power $I_o(h)$ per unit volume absorbed at a height h from a disturbing wave with an absorption coefficient $k_d(\nu_m)$ is given by

$$I_o(h) = \frac{gW}{2\pi h^2} k_d(\nu_m) \exp\{-2\int_o^h k_d(\nu_m)dh\} \qquad (1)$$

where W is the radiated power and g is the gain of the polarized disturbing aerial. An exact extraordinary gyrowave is the most strongly absorbed wave of all and its use as the disturbing wave confines the electron heating to the thinnest possible region. Fig 1. shows two $I_o(h)$ profiles calculated for this wave at Armidale using the collision frequencies $\nu_m = 2.30 \times 10^5 \exp(-0.17\ h)$. Profile (i) has been calculated for the electron density

distribution derived in Paper 3.2.4 for the night of 6 September 1963, while the broader profile (ii) is that for the electron density model $N = 17 \exp(0.6h)$. In the expressions for N and ν_m, the height h is in kilometers above the 85 km. level.

When the disturbed region is localized in height the modulation depth M_{ks} for a single transit by the wanted pulse under steady state conditions is given, to a close approximation, by

$$M_{ks} = \frac{gW}{4\pi \underline{H}^2} \frac{1}{G_m U_o} (k'_w/N)_{h=\underline{H}} \tag{2}$$

where k'_w is the partial derivative of the absorption coefficient of the wanted wave with respect to ν_m, G_m is the energy loss coefficient associated with ν_m, U_o is the thermal energy of the gas, and $\underline{H}$ is the mean height of the $I_o(h)$ function.

The magnitude of the error in the approximation (2) is $O(\mu_2\alpha_2/H_o^2)$, where μ_2 is the second central moment of the normalized $I_o(h)$ function, H_o is the scale height of ν_m and α_2 is the second coefficient in the expansion

$$k'_w/N = (k'_w/N)_{h=\underline{H}} [1 + \alpha_1\{(h-\underline{H})/H_o\} + \alpha_2((h-\underline{H})/H_o\}^2 + \ldots] \tag{3}$$

When the localized electron heating is produced by a rectangular disturbing pulse of duration T_d, the modulation depth $M_k(t)$ measured using a short wanted pulse transmitted at a delay t after cessation of the disturbing pulse is given by

$$M_k(t) = M_{ks}\, D(\underline{H})\, E(\underline{H}) \exp(-t/\tau_i) \tag{4}$$

where

$$\left.\begin{aligned} D(\underline{H}) &= 1 - \exp(-T_d/\tau_{\underline{H}}) \\ E(\underline{H}) &= 1 + \exp\{-(T_E - 2\underline{H}/c)/\tau_{\underline{H}}\} \end{aligned}\right\} \tag{5}$$

$\tau_{\underline{H}}$ $(= 1/G_m\nu_{\underline{H}})$ is the electron relaxation time at the height $\underline{H}$, T_E is the group time of the wanted echo and

$$\tau_i = \tau_{\underline{H}}(1 + \gamma) \tag{6}$$

where

$$\gamma \doteqdot (\alpha_1 + d + e - 0.5)\, \mu_2/H_o^2 \tag{7}$$

$$\left.\begin{aligned} d &= -x \exp(-x)/\{1 - \exp(-x)\} \\ e &= X \exp(-X)/\{1 + \exp(-X)\} \\ x &= T_d/\tau_{\underline{H}} \\ X &= (T_E - 2\underline{H}/c)/\tau_{\underline{H}} \end{aligned}\right\} \tag{8}$$

Formula (4) applies for delays short compared to $\tau_{\underline{H}}$.

The above theory is the basis of the methods used in Sections 4 and 5. The following discussion is concerned with the experimental conditions in Section 4 and in it we use the profile (ii) of Fig. 1, which is broader than the typical nighttime $I_o(h)$ profile. Since both the error in (2) and the magnitude of γ are proportional to μ_2, and, thus, are proportional to the square of the width of the $I_o(h)$ profile, the use of the broader profile

provides a good test of the accuracy of the theory as applied to the nighttime experiments. For profile (ii), μ_2 = 2.7 sq. km., $\underline{H}$ = 84.9 km. and $\tau_{\underline{H}}$ = 635 μsec.

The wanted waves used in the experiments of Section 4 were extraordinary gyrowaves at frequencies of 1.78 and 2.12 Mc/s. Fig. 2 shows k'_w/N for each of these waves as a function of ν_m and as a function of height. Over the height range of profile (ii), the variation of k'_w/N for 1.78 Mc/s. is large, while that for 2.12 Mc/s. is small. For the 1.78 Mc/s. wave, the value of α_1/H_o at the height $\underline{H}$ is 0.157; for the 2.12 Mc/s. wave, it is 0.048*. For each of these waves the value of α_2/H_o^2 is ∿0.005, so that the term $O(\mu_2\alpha_2/H_o^2)$ introduces a correction of about one per cent to (2).

For a single (upward) transit by the wanted pulse, values of $M_k(0)$ and M_k(500 μsec.) have been calculated from the exact equations (40) to (44) of Paper 3.1.1 for the experimental conditions shown in the first two columns of Table 1. The time constants given in the third column of the table are for an assumed variation between these two delays. They show a small dependence on T_d and the propagation properties of the wanted wave. The values in the fourth column have been calculated from (7) and (8) with e = 0, $\tau_{\underline{H}}$ = 635 μsec., μ_2 = 2.7 sq. km., and are each close to 4 per cent smaller than the corresponding values in the third column. This difference arises because the variation of $M_k(t)$ with delay is not an exact exponential.

By means of the methods used in Paper 3.1.1 to relate τ_i and $\tau_{\underline{H}}$, it can be shown that at a delay t the instantaneous time constant τ_t is given by

$$\tau_t = \tau_i(1 + \beta) \tag{9}$$

where, for delays less than about $\tau_{\underline{H}}$,

$$\beta \doteqdot t\ \mu_2/H_o^2\tau_{\underline{H}} \tag{10}$$

For t = 500 μsec., β = 0.06 and, since β is small, the time constant derived from the values of $M_k(0)$ and $M_k(500)$ is equal to $\frac{1}{2}(\tau_{500} + \tau_i)$. It should thus exceed τ_i by 3 per cent. With this correction the values of the time constants in the third and fourth columns of the table agree to within one per cent.

TABLE 1. Calculated and predicted time constants for various experimental conditions.

Duration of disturbing pulse (1.515 Mc/s., x-mode)	Wanted pulse	Time constant (μsec.)	
		Calculated from $M_k(0)$ and M_k(500 μsec.)	τ_i
∞	2.12 Mc/s., o-mode	627	611
∞	2.12 Mc/s., x-mode	648	621
∞	1.78 Mc/s., x-mode	686	660
800 μsec.	2.12 Mc/s., x-mode	624	601
800 μsec.	1.78 Mc/s., x-mode	663	636

* The values in Smith et al. of 0.21 and 0.05 respectively were obtained using the Appleton-Hartree magnetoionic theory.

While a particular model of the electron density profile has been used to demonstrate the accuracy of the theory, it is stressed that the theory is developed without consideration of the profile that causes the wave interaction to be localized.

If the steady modulation depths are measured simultaneously at two wanted frequencies f_1 and f_2, it follows from (2) that

$$(M_{ks})_{f_1}/(M_{ks})_{f_2} = \{(k'_w/N)_{f_1}/(k'_w/N)_{f_2}\}_{h=\underline{H}} \tag{11}$$

The right-hand side of this equation is a function of collision frequency only and is plotted in Fig. 2 for the extraordinary 1.78 and 2.12 Mc/s. waves. Simultaneous measurements of the two steady state modulation depths then yield the value of the collision frequency at the height $\underline{H}$. Association of this collision frequency with $\tau_{\underline{H}}$ then yields the value of G_m. To a first approximation $\tau_{\underline{H}}$ can be taken equal to the time constant measured using either wanted wave. In a more accurate association the dependence of the time constant on the factors discussed above must be considered. Calculations for electron density profiles giving $I_o(h)$ curves of various thicknesses have shown that for the experimental procedures and conditions in Section 4, an association with the mean of the measured time constants for the 1.78 and 2.12 Mc/s. wanted waves recovers to within 2 per cent the value of G_m adopted initially.

A consequence of (11) is that the measured ratio of the modulation depths cannot exceed the limiting value of the right-hand side when $\nu_m \to 0$. At Armidale the limiting value is 5.2 for extraordinary 1.78 and 2.12 Mc/s. waves and 25.2 for extraordinary and ordinary 2.12 Mc/s. waves.

4. Gyro-interaction in the nighttime lower E region

Before the introduction of pulse wave interaction methods in 1955, considerable emphasis was placed on the measurement of the quantity $G\nu$. This quantity was deduced either from the variation of the depth of the impressed modulation with the modulation frequency of a sinusoidally modulated disturbing wave or, as in the experiments of Bailey et al. (1952), from the time constant of the transient decrease in the amplitude of the received continuous wanted wave caused by a pulsed disturbing gyrowave.

The modern counterpart of these early experiments with a vastly greater scope for precise experimentation and interpretation and for optimization of the experimental parameters for particular purposes is the experiment classified in Section 2 of Paper 3.1.1 as Type I. The experiment is made with the disturbing pulse D preceding the wanted pulse W and the impressed modulation $M_k(t)$ is measured as a function of the delay DtW between the trailing edge of D and the leading edge of W. Both transits of the disturbed region by the wanted pulse occur while the electrons are cooling to the ambient condition and the modulation depth 'decays' with the increase of the delay. When the distinction discussed in Paper 3.1.1 is necessary, the experimentally measured modulation depths should be converted to impressed decrement before analysis. The Type I experiment is of greatest value when the disturbed region is localized in height and the disturbing pulse is long enough to create near steady state conditions.

The transmitter at Station A was used after midnight on about 400 nights over the five years to 1963 to study gyro-interaction in the lower E region. Almost all of the experiments were of Type I but a few, to associate electron relaxation time with height, were of Type II. The investigations had as their general objective the establishment of an interpretation of small and large perturbation wave interaction phenomena compatible with the high accuracy with which the impressed modulation was measured, and fall under the following headings:

(i) Dependence of the impressed decrement on the power of the disturbing pulse (D-- 1.515 Mc/s., x-mode, 800 μsec.; W-- 2.12 Mc/s., x- and o-modes; 1.78 Mc/s., x-mode; 1.7 Mc/s., x-mode; Type I experiment with the delay DtW fixed at about 50 μsec.).

(ii) Variation of the decay of Type I data with the power of the disturbing pulse (D-- 1.515 Mc/s., x-mode, 800 μsec.; W-- 2.12 Mc/s., x- and o-modes).

(iii) Variation of the decay of the impressed modulation with the frequency of the extraordinary disturbing gyrowave (D-- 1.4-1.8 Mc/s., x-mode, 800 μsec.; W-- 2.12 Mc/s., x-mode).

(iv) Wave interaction produced by the ordinary mode of the disturbing gyrowave.

(v) Determination of the properties of electron collisions in the lower ionosphere.

Experimental data from the investigations (i) and (ii) have been shown in Paper 3.1.1. Such measurements are necessary to establish the maximum disturbing power that can be used before an interpretation based on small perturbation wave interaction theory is invalid and in this connection we wish to comment on a feature of the Type I data plotted in Fig. 6 of that paper. Except for the highest powers, the variation of the impressed decrement with the delay is exponential, which is the predicted variation for a small perturbation.* Thus, had the measurements been made for a single power, the incorrect conclusion could have been reached that the time constant of the variation referred to a near-thermal perturbation. The investigations (iii) are the basis of the method described in Paper 3.2.4 for determining the electron density profile of the nighttime lower E region and (iv) have been described by Loch (1966). Here, we summarize the results from the investigations (v).

Were gyro-interaction at night to occur in an infinitesimally thin region at a height $\underline{H}$ where the electron relaxation time is $\tau_{\underline{H}}$, then the modulation depth $M_k(t)$ measured in a small perturbation Type I experiment would be given by (4) and (5) with $\tau_i = \tau_{\underline{H}}$ and would be proportional to the value of k'_w/N at the height $\underline{H}$. Also, the decay would be exponential with a time constant $\tau_{\underline{H}}$. When the disturbed region has a finite thickness it was shown in Section 3 that as in this hypothetical case the modulation depth $M_k(0)$ at $t = 0$ is evaluated at a definite height $\underline{H}$. However, the variation with t is then not an exact exponential and its initial time constant τ_i is different from $\tau_{\underline{H}}$ and depends on factors such as the duration of the disturbing pulse and the propagation properties of the wanted pulse. These departures in the decay characteristics of $M_k(t)$ from those for interaction in an infinitesimally thin region increase in proportion to the square of the thickness of the disturbed region. For the experimental conditions shown in Table 1 and a disturbed region much thicker than the usual region in a gyro-interaction experiment at night, the values of τ_i were found to lie within 5 per cent of $\tau_{\underline{H}}$.

The determination of M_{ks} from Type I data requires the evaluation of the factors $D(\underline{H})$, $E(\underline{H})$ in (5). These factors involve the unknown relaxation time $\tau_{\underline{H}}$ and have been evaluated using the measured time constant τ_i. This practice, which leads to an error in the value for M_{ks} smaller than the error in the value used for the relaxation time, has been taken into account in the assessment given at the end of Section 3 of the accuracy of recovery of the value of G_m.

The electron relaxation time changes by about 16 per cent in a kilometer. As such a change is considerably larger than the normal error in the measurement of the time constant,

* Within the limits discussed in Section 3.

small changes in the height of the disturbed region can be detected easily. Measurements for this purpose at night have been made using the 2.12 Mc/s. extraordinary wanted wave and the 1.515 Mc/s. extraordinary disturbing wave of a low power (see Fig. 5, Paper 3.1.1). The time constants have ranged from 500 to 1200 μsec. with the great majority lying between 600 and 900 μsec. A change in the time constant of up to 100 μsec. during the night was not uncommon, but on many nights a much higher degree of stability was evident. Changes during the night appear to have no preferred sense, while those from night to night were larger in magnitude but also appear to be random.

Direct height information is obtained from Type II or Type III Fejer curves. If this information is to be associated with a simultaneous direct measurement of the time constant, it is generally necessary to use the Type III experiment. However, when the wanted echo is from the F layer, which is often the case at night, there is sufficient range of delay for this purpose in a Type II curve (see Fig. 11, Paper 3.1.1).

In Section 4 of Paper 3.1.1 the theory required to calculate Fejer curves of Type II or III for a given set of ionospheric and experimental parameters was rigorously developed. Calculation from this theory of the shape of the Type II curve for interaction in an infinitesimally thin region requires a knowledge only of the shapes of the disturbing pulse and the output pulse of the receiver and of the electron relaxation time and height of the disturbed region. The height has no effect on the shape of the curve but locates it in delay. The solid curve in Fig. 11 of Paper 3.1.1, calculated for the experimental pulses and a relaxation time of 640 μsec., has been normalized to the peak of the experimental curve. Its delay for best fit to the latter curve as a whole locates the relaxation time at a height of 85 km. above sea level. In this height determination, the error from uncertainty in the fit of the experimental curve and from errors in measurement of the receiver delay is estimated to be about ± 1 km. Since the relaxation time changes by 16 per cent in a kilometer and this change is much larger than the percentage error in the measurement of the time of 640 μsec., all error is considered to be in the height.

The electron relaxation time is inversely proportional to the product $G_m \nu_m$, where G_m may be assumed to be constant over a limited height range and ν_m is proportional to the gas density and the temperature, so that the relative variation of the relaxation time with height can be calculated using atmospheric data. The broken curve in Fig. 3 shows the variation about the value for 85 km. obtained using the data of Cole et al. (1963) for a latitude of 30°N (the latitude of Armidale is 30°30'S). Cole et al. give the winter and summer temperatures at a height of 85 km. as 191°K and 180°K respectively, and the corresponding densities as 7.81×10^{-3} and 8.33×10^{-3} gm./cu.m. These yield almost the same values for the product of density and temperature, so that at Armidale the collision frequency at 85 km. should be independent of the season. Further, as will be shown later, there is every reason to believe that the value of G_m is unaffected by the temperature change. Thus, the relaxation time at a given height near this level should remain constant throughout the year.

The relaxation time-height associations that have been made by the method above are shown in Fig. 3. Because of improved experimental technique, much greater weight is placed on those made since mid-1960, which are in good accord with the derived profile and, as expected, show no seasonal variation.

Formula (2) for the modulation depth M_{ks} impressed on the wanted pulse during a single transit of the disturbed region under steady state conditions was derived in Paper 3.1.1 without consideration of the electron density profile which caused the wave interaction to be localized. For a 2.12 Mc/s. extraordinary wanted wave the variation of k'_w/N with collision frequency and height has been shown in Fig. 1. Over the height range 85 to 90 km. the increase in k'_w/N with height is largely compensated for by the divergence term in (2), so that the value of $(k'_w/N)/\underline{H}^2$ remains constant to within 4 per cent. For temperature changes, such as have been discussed above, the product $G_m U_o$ should not vary by more than

about 5 per cent over the year. It would thus be expected that the value of M_{ks} for this wanted wave, when referred to a standard disturbing power (taken to be 100 kw.), should remain closely constant. M_{ks} values measured over the five-year period have shown no significant variation. The particular set of measurements plotted in histogram form in Fig. 4 were obtained from Type I experiments made between 15 October 1962 and 17 August 1963 using disturbing powers from Station A of 5 kw. or lower. For this group of measurements the time constants were found to lie between 570 and 1130 μsec. The corresponding range of $\underline{H}$ is 84.5 to 88 km. and the dotted lines represent the distribution of the values when standardized to a height of 85 km. This adjustment appears to have reduced the spread of the distribution slightly.

The mean experimental value for a height of 85 km. and a power of 100 kw. is (21.7 ± 0.3) per cent for E and F echoes. When considered separately, the observations for the two echoes give the same mean value.

The ratio of the steady modulation depths measured using two wanted waves has been shown in Section 3 to be a function only of the collision frequency at the mean height $\underline{H}$ of the $I_o(h)$ profile of the disturbing wave. By a suitable choice of the wanted waves the ratio can be made to be a rapidly varying function of collision frequency. Fig. 2 illustrates this variation for extraordinary wanted waves at frequencies of 1.78 and 2.12 Mc/s., and for these waves the error in the value deduced for the collision frequency at the height $\underline{H}$ is about the same as the error in the ratio of the measured modulation depths. The frequency of 1.78 Mc/s. is relatively close to the gyrofrequency and the extraordinary mode is much more highly attenuated than at the frequency of 2.12 Mc/s. At first sight this would appear to affect adversely the accuracy of measurement at 1.78 Mc/s. It has been found, however, that when the echo is single and steady the measurements are as accurate as at 2.12 Mc/s. It is noted that this does not apply at frequencies closer to the gyrofrequency (e.g. 1.7 Mc/s.) as the extraordinary echo is then much weaker and, since the ordinary mode cannot be suppressed completely, the received echo frequently contains both modes causing the observed modulation to show large fluctuations.

The accuracy of associating the collision frequency deduced from the ratio measurement with the mean of the time constants for the two wanted waves to deduce the value of G_m has been discussed in Section 3. The ratios and mean time constants given in Table 2 were obtained from Type I experiments made during October 1962 and April 1963 using an 800 μsec. extraordinary disturbing pulse at the gyrofrequency and at the powers listed. This process yields values for the collision frequency and the energy loss coefficient which depend on the magnetoionic theory used in the analysis. Table 2 shows the values deduced using the Appleton-Hartree magnetoionic theory and generalized magnetoionic theories derived for a collision cross-section A proportional to electron speed c (Sen and Wyller) and for a constant collision cross-section. For the generalized theories the relation between the mean and subscripted values are

$$A \propto c \quad : \quad G_m = \frac{3}{2} G, \quad \nu_m = \frac{2}{3} \nu$$

$$A = \text{constant}: \quad G_m = \frac{2}{\sqrt{\pi}} G, \quad \nu_m = \frac{\sqrt{\pi}}{2} \nu$$

The tabulated collision frequencies for a height of 85 km. have been calculated using the mean experimental values for the energy loss coefficient and the value of 640 μsec. for the electron relaxation time at this height.

TABLE 2. Values of G and ν at a height of 85 km. above sea level

	$\frac{(M_{ks})_{1.78^x}}{(M_{ks})_{2.12^x}}$	Mean time constant (μsec.)	G × 10^3			Power (kw.) at A
			A-H	Constant A	Sen and Wyller	
15 Oct. 1962	3.60	795	1.91	2.78	4.30	20
19 Oct. 1962	3.46	698	2.06	2.98	4.62	7.8
	3.65	680	2.27	3.34	5.17	7.8
6 Apr. 1963	4.08	1010	1.86	2.88	4.44	5.0
	4.06	955	1.94	2.93	4.57	2.5
	3.94	1005	1.76	2.66	4.15	5.0
	4.10	905	2.08	3.17	5.0	2.5
12 Apr. 1963	3.65	800	1.93	2.83	4.39	2.5
	3.65	800	1.93	2.83	4.39	2.5
17 Apr. 1963	3.96	910	1.94	2.88	4.58	2.5
25 Apr. 1963	3.31	780	1.76	2.53	3.87	2.5
	3.64	710	2.17	3.42	4.92	2.5
	3.44	800	1.79	2.58	3.98	2.5
	3.70	710	2.21	3.24	5.08	2.5
Mean values of G			2.0±0.1	2.9±0.2	4.5±0.3	
Mean values of G_m				3.3±0.2	6.8±0.3	
Collision frequency at 85 km. × 10^{-5} } ν			7.8	5.4	3.5	
Collision frequency at 85 km. × 10^{-5} } ν_m				4.7	2.30	

5. Gyro-interaction in the lower D region

During the day only the ordinary mode of the 2.12 Mc/s. wanted wave is received, but the high collision frequencies in the lower D region make k'_w/N for this mode a rapidly varying function of ν_m. The variation becomes less marked at higher wave frequencies and Fig. 5 shows as a function of ν_m the ratio of the values of k'_w/N for the ordinary modes at 2.12 and 3.85 Mc/s. This plot is similar in form to that in Fig. 2 for the extraordinary wanted waves used in the nighttime measurements of G_m and ν_m.

A Fejer curve of Type III, obtained near noon on 4 November 1963 using the 2.12 Mc/s. wanted wave and 63 μsec. disturbing 1.78 Mc/s. pulses in the extraordinary mode from Station A, was shown in Fig. 13 of Paper 3.1.1. In Section 5 of that paper, features of the curve were discussed which indicate that the wave interaction was localized in a thin region where the electron relaxation time is of the order of 40 μsec. Because of the localized interaction and the characteristics of the wanted waves discussed above, it is possible to employ the methods of the previous section to determine the values of the basic parameters in the lower D region. The short time constants impose greater technical problems for their accurate measurement, but against this a 1 ms. disturbing pulse from Station A is sufficiently long to create steady state conditions and, thus, to allow a Type IV experiment to be used for the measurement of M_{ks}.

The Fejer curves obtained in nighttime experiments using an exact extraordinary gyrowave as the disturbing wave are not significantly different from those predicted for interaction in infinitesimally thin regions, and this allowed the relaxation time-height associations of the previous section to be made in a simple manner. X-mode Fejer curves of Type III at noon, on the other hand, are sufficiently broad for the structure of the disturbed region to be resolved. Because of this a more elaborate procedure must be used to associate the time constant of the decaying tail of the curve (42 μsec. for the x-mode curve of 4 November 1963) with height. That followed involves the use of the synthesizer (Smith et al., Paper 3.1.1), which allows the Fejer curve to be simulated by the addition of electronically generated waveforms representing the components from different levels.

The only parameters* used in a synthesis are the known shapes of the disturbing and wanted pulses and the time constants of the height channels. For the latter, one datum point is the time constant of 640 μsec. at a height of 85 km. In the setting up of the synthesizer the channel for this height is located in delay so that its output matches the Fejer curve used to derive this datum point. This practice ensures that the error of ± 1 km. in the absolute value of the height determination is not reflected in the use of the synthesizer except as a constant error at all heights. A simple one slab synthesis of the curve of 4 November 1963 then shows that the time constant of 42 μsec. occurs near the 69 km. level.

As discussed in the previous section, if the assumption is made that G_m is a constant, the relative variation of the electron relaxation time with height can be calculated using atmospheric data. Using the value of 640 μsec. at 85 km., the model atmosphere of Cole et al. for mid-summer gives a value of 41 μsec. at a height of 69 km. In order to make an accurate association, the x-mode curve of 4 November 1963, and a number of other curves of similar quality, have been synthesized for best fit using time constant profiles obtained by "swinging" the profile calculated using the atmospheric data slightly about the value at 85 km. From these syntheses it has been concluded that the relaxation time at a height of 69 km. (16 km. below the 85 km. level) is 44 μsec. with a maximum error of ± 4 μsec. The close agreement between this relaxation time and that predicted using atmospheric data gives considerable confidence in the use of these data to interpolate between, and extrapolate beyond, the two measured datum points. The profile so derived is shown in Fig. 6.

The region acted on at noon by the extraordinary 1.78 Mc/s. disturbing wave has sufficient depth for its structure to be resolved. Because of this depth the accuracy of the methods of the previous section for determining the values of G_m and ν_m is less certain during the day than at night. To assess their accuracy a knowledge of the electron density profile is required and this in turn cannot be deduced without a knowledge of the values of the parameters. Thus, an iterative process must be used to obtain both the parameters and the profile accurately. Fortunately, the initial approximation of neglecting the thickness of the disturbed region leads to small errors and only a single iteration is necessary.

Experiments to determine the values of G_m and ν_m in the lower D region were made in July, August and November, 1963. The values of M_{ks} at the wanted frequencies of 2.12 and 3.85 Mc/s. were determined directly in a Type IV experiment using 1 ms. disturbing pulses of power about 35 kw. in the extraordinary mode at 1.78 Mc/s. The time constant $\tau_{2.12}$ at the wanted frequency of 2.12 Mc/s. was measured in a Type I experiment made with a continuous variation of the same disturbing pulse as used for the measurement of M_{ks} (see Fig. 7, Paper 3.1.1). Interference and rapid variations in the group height of the echo made measurement of the time constant at the frequency of 3.85 Mc/s. extremely difficult, but three fairly rough measurements suggest that the time constant was about 4 per cent lower than the value of $\tau_{2.12}$. The experiments were made near noon since the ionization is then a maximum and the disturbed region is most localized in height.

* While in theory the group time of the wanted echo is required to locate the second peak of the simulated Type III Fejer curve, this peak is so well defined that it is self-locating in a synthesis.

The values of M_{ks} (scaled to a power of 100 kw.) at the two wanted frequencies and $\tau_{2.12}$ are plotted against time of day in Fig. 7. Each set of data shows little variation for an hour or so about noon. The variation from day to day in the winter period is within the experimental error. The data for 19 and 27 November also agree within the error of measurement, while those for 22 November are slightly larger in magnitude.

The time constant data in Fig. 7 imply a high degree of stability of the noon ionization near 70 km. in the D region.* The change in the time constant from winter to summer shows the region to be under solar control. There is also more ionization present at 0830 E.A.S.T. in November than at noon in July and August. This, too, is consistent with the region being under solar control.

Through lack of one or more of the values of M_{ks} and a time constant, not all the data in Fig. 7 could be used for determining the values of G_m and ν_m. Table 3 gives the useable time constants and M_{ks} ratios, together with the energy loss coefficients deduced from them using the three magnetoionic theories. In the approximation of associating the collision frequency yielded by the ratio measurement with the value of $\tau_{2.12}$, the mean value (6.3×10^{-3}) for G_m deduced using the Sen and Wyller magnetoionic theory is lower than that at night. The mean values deduced using the other two magnetoionic theories, on the other hand, are slightly larger. Association of the above value for G_m with the relaxation time of 44 μsec. gives 3.6×10^6 as the first approximation to the value of ν_m (Sen and Wyller) at the height of 69 km.

Electron density profiles for the noon D region on 4 November 1963 and 22 June 1964 have been given by Smith et al. These profiles, for summer and winter respectively, are the first approximations in the iterative process. For the conditions in the experiments to determine the value of G_m, it has been found that for each of the profiles† the value recovered from the computed data is 10 per cent too low. Further iteration was found unnecessary and the value of G_m adopted for the lower D region is 6.9×10^{-3}. This value, in effect, is the same as that at 85 km.

The association of a relaxation time of 44 μsec. with a height of 69 km. was made by synthesizing experimental Fejer curves for best fit and is independent of the iterative process. When this relaxation time is used with the corrected value of G_m, the collision frequency ν_m at 69 km. is found to be 3.3×10^6. The collision frequency profile shown in Fig. 6 is based on this value and the value at 85 km.

The final electron density profiles and the basic data used in their deduction can be tested by comparing the computed values of M_{ks} and time constant with the experimental values for the two seasons. In the comparison below, the values in Fig. 7 for noon in the two seasons are given in brackets after the computed values. Because the experimental values for 22 November 1963 are slightly higher than the values for 19 and 27 November 1963, both sets of values are given in place of a single mean value.

---

* For the range of time constants plotted in the figure, the value of M_{ks} for the 2.12 Mc/s. wanted wave is roughly proportional to $\tau_{2.12}$. The data for M_{ks} thus supplement for this purpose the data for the time constant.

† In computations the exponential tails of both profiles were extrapolated below 65 km.

TABLE 3. Value of G at a height of 69 km. above sea level.

Date	$\frac{(M_{ks})_{2.12^0}}{(M_{ks})_{3.85^0}}$	Time constant 2.12 Mc/s. (μsec.)	$G \times 10^3$		
			A - H	Constant A	Sen and Wyller
25 Jul. 1963	1.69	54	2.22	3.12	4.43
27 Aug. 1963	1.66	55	2.11	3.00	4.21
	1.66	54	2.17	3.08	4.32
19 Nov. 1963	1.39	41	2.27	3.15	4.18
	1.36	41	2.22	3.07	4.04
22 Nov. 1963	1.41	43	2.20	3.06	4.07
	1.44	45	2.15	3.00	4.01
27 Nov. 1963	1.39	40	2.31	3.20	4.24
	1.37	39	2.34	3.23	4.27
Mean value of G			2.2±0.1	3.1±0.1	4.2±0.1
Mean value of G_m				3.5±0.1	6.3±0.1

4.11.63 2.12 Mc/s.: $M_{ks}(\%) = 0.42$ (0.44, 0.40); $\tau_{2.12}$(μsec.) = 41 (43, 40)

3.85 Mc/s.: $M_{ks}(\%) = 0.30$ (0.31, 0.29)

22.6.63 2.12 Mc/s.: $M_{ks}(\%) = 0.57$ (0.61) $\tau_{2.12}$(μsec.) = 55 (54)

3.85 Mc/s.: $M_{ks}(\%) = 0.35$ (0.36)

It was noted above that $\tau_{3.85}$ appeared to be about 4 per cent lower than $\tau_{2.12}$. The computed difference for the summer electron density profile is 5 per cent; for the winter profile, it is 6 per cent.

The correction of 10 per cent in the value of G_m arises from three main causes. The first is that the collision frequency determined by the M_{ks} ratio is not exactly that located at H, the mean height of the $I_o(h)$ profile of the disturbing wave. The second is that the increase in the value of k'_w/N with height in the disturbed region results in the value of τ_i for each of the waves being larger than the value of the electron relaxation time τ_H at the height H. The third is the result of the short time constant of the decay and the finite width of the wanted pulse. Even when the disturbing pulse has an abrupt termination, the first 50 μsec. of the decay (i.e., about one time constant) cannot be used for determining the time constant since the wanted pulse is overlapping the disturbing pulse. Since the decay in an extended region is not an exact exponential and the time constant associated with the variation increases with the delay, this results in the measured time constant being longer than τ_i.

The iteration above has been applied only to the analysis using the magnetoionic theory of Sen and Wyller. The physical basis of the correction indicates that its magnitude would be closely the same for analyses using the other magnetoionic theories.

6. Tests of the U(ν) relation for electrons in the lower ionosphere

The values of G_m and ν_m at heights of 69 and 85 km. have been deduced in the previous sections for the cases of a constant collision cross-section A and a cross-section proportional to the electron speed c. Since the values of M_{ks} are known, the energy U_o, and thus the temperature of the gas, at each of these heights may be calculated. The temperature so obtained depends on the A(c) relation used, and comparison of the temperature with that ascribed to the region by other methods provides a means of testing this relation.

For a height of 85 km. the wave interaction temperature calculated using mean values of M_{ks}, G_m and ν_m is found to be $(190 \pm 20)^{o}K$, when A is proportional to c and $(119 \pm 13)^{o}K$, when A is a constant. The uncertainty in the gain of the disturbing aerial is by far the greatest source of error in these determinations. Of the temperatures, the first is in good agreement with the mid-winter ($191^{o}K$) and mid-summer ($180^{o}K$) temperatures in the model atmosphere of Cole et al. The second is unacceptably low, even if weight is attached to the temperature of $152^{o}K$ reported by Minzner et al. (1965).

For the height of 69 km. the temperature deduced from the wave interaction data summarized in Table 3 neglecting the thickness of the disturbed region is $(233 \pm 12)^{o}K$, when A is proportional to c, and $(140 \pm 8)^{o}K$, when A is a constant. The errors quoted are those arising from the experimental scatter of the data in the table and do not include the errors, comparable to those for the temperatures at 85 km., arising from uncertainty of the disturbing aerial gain. The iteration process, applied to data analyzed using the magnetoionic theory of Sen and Wyller, requires the initial estimate of the temperature to be reduced by 10 per cent. This gives a temperature of $210^{o}K$, which compares favorably with the temperatures of 225 and $222^{o}K$ for mid-winter and mid-summer, respectively, quoted by Cole et al. for this height.

Although the temperatures derived from the wave interaction measurements have large errors, they support the use of the Sen and Wyller magnetoionic theory at both heights. Because of the uncertainty in both the wave interaction and directly measured temperatures, however, the necessity of some adjustment to the theory cannot be excluded.

For the heights of 69 and 85 km. the values deduced for ν_m using the Sen and Wyller magnetoionic theory are 3.3×10^6 and 2.3×10^5 respectively. If the collision cross-section of electrons in air is taken to be 80 per cent of that given in Paper 1.6 for nitrogen, the collision frequency at 85 km. from the data of Cole et al. is 2.5×10^5 for both summer and winter, while at 69 km. it is 4.0×10^6 at mid-summer and 3.5×10^6 at mid-winter. This method of calculating the collision frequency thus gives values that are in good agreement with those measured.

The collision frequencies obtained using the hypothesis that A is a constant are about 30 per cent larger than those using the hypothesis that A is proportional to c. When the collision frequencies are deduced from atmospheric data using the cross-sections for oxygen and nitrogen given by Phelps (1964), which were shown in Paper 1.6 to imply a constant cross-section in air, the values obtained are in just as good agreement with the corresponding measured values.

The 1 km. uncertainty in the heights (69 and 85 km.) at which the collision frequencies are measured introduces a 16 per cent uncertainty in any comparison with collision frequencies deduced by other means. When this factor is taken into consideration, the difficulty of distinguishing between the two hypotheses by comparison of collision frequencies is evident.

If the assumption is made that energy loss in near-thermal collisions in oxygen is negligible, the theories of Huxley (1959) and Dalgarno and Moffett (1962) suggest that the value of G_mT in air is 5 per cent lower at a temperature of $210^{o}K$ than at a temperature of $190^{o}K$ (see Paper 1.6). The wave interaction measurements ($A \propto c$), on the other hand, give effectively the same value of G_m at the two temperatures and hence a 10 per cent increase in the product G_mT from $190^{o}K$ to $210^{o}K$.

7. Concluding remarks

The derivation of the electron density profile for the D region from pulse wave interaction measurements requires the use of data for the electron collision frequency, relaxation time and energy loss coefficient. Values of these parameters at heights of 69 and 85 km. above sea level have been derived from wave interaction measurements. The value of the energy loss coefficient has been found to be the same at the two heights. The variation of the other two parameters with height is in close agreement with that calculated using atmospheric data, giving considerable confidence in the use of such data to interpolate between, and extrapolate beyond, the two heights. The measurements support the use of the magnetoionic theory of Sen and Wyller in the analysis of wave propagation in the lower ionosphere.

Acknowledgements

The research reported here was sponsored by the Air Force Cambridge Research Laboratories under Contract AF19(604)-6177 and supported in part by the Defense Atomic Research Agency, Washington, D.C., under Subtask 07010 and the Radio Research Board of Australia.

REFERENCES

Bailey, V.A., Smith, R.A., Landecker, K., Higgs, A.J. and F.H. Hibberd. Nature, 169, 911. 1952.

Bourne, I.A. M.Sc. Thesis, University of New England. 1960.

Bourne, I.A. Ph.D. Thesis, University of New England. 1964.

Cole, A.E., Kantor, A.J., and A. Court. Interim Notes on Atmospheric Properties - No. 32 (Rev.), Supplemental Atmospheres, AFCRL. 1963.

Dalgarno, A. and R.J. Moffett. Planet. Space Sci., 9, 439. 1962.

Fejer, J.A. J. Atmosph. Terr. Phys., 7, 322. 1955.

Gardner, F.F. and J.L. Pawsey. J. Atmosph. Terr. Phys., 3, 321. 1953.

Huxley, L.G.H. J. Atmosph. Terr. Phys., 16, 46. 1959.

Loch, R.G. M.Sc. Thesis, University of New England. 1966.

Minzner, R.A., Sauermann, G.O. and G.A. Faucher. J. Geophys. Res., 70, 739. 1965.

Phelps, A.V. NBS Techn. Note No. 211, 5, 49. 1964.

Sen, H.K. and A.A. Wyller. J. Geophys. Res., 65, 3931. 1960.

Smith, R.A., Bourne, I.A., Loch, R.G., Setty, C.S.G.K., Coyne, T.N.R., Barratt, P.H., and B.S.N. Prasad. Scientific Report No. 3 and Final Report, Contract No. AF19(604)-6177, University of New England. 1965.

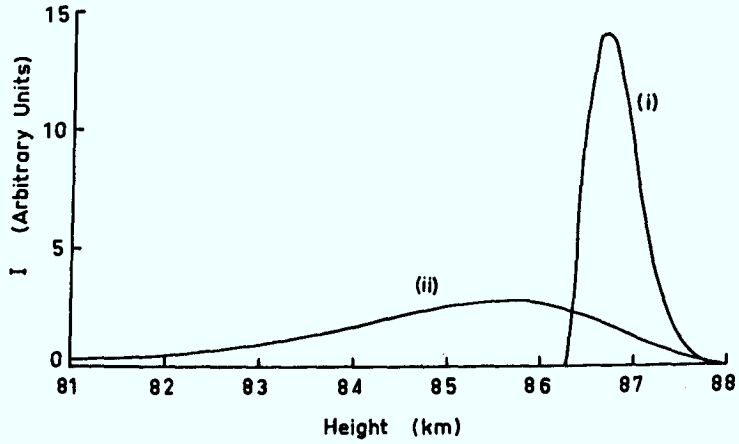

Fig. 1. $I_o(h)$ profiles at night for the exact extraordinary gyrowave. The electron densities and collision frequencies used in the calculation of the profiles are discussed in the text.

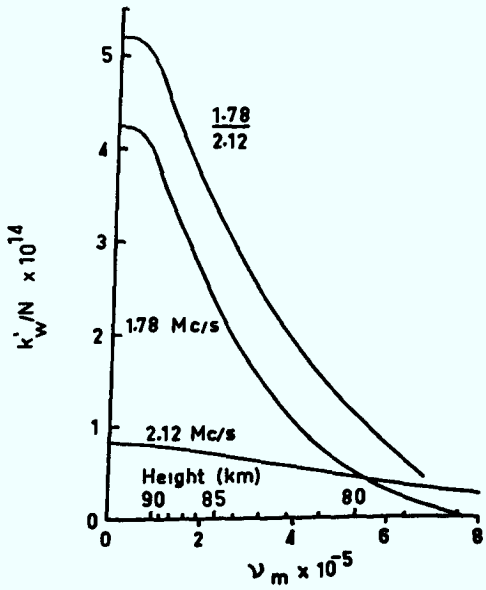

Fig. 2. The ratio and values of k'_w/N for extraordinary 1.78 and 2.12 Mc/s. waves as functions of collision frequency and height.

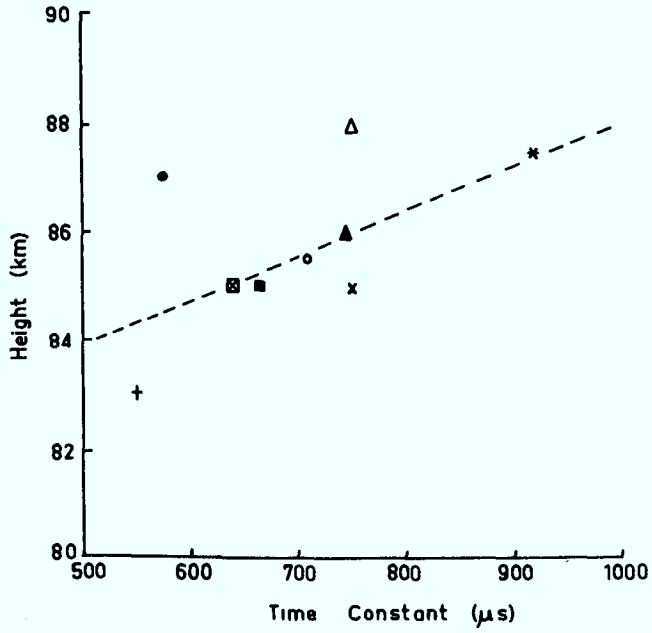

Fig. 3. Measured heights as a function of time constant:
+ 12 March, 1959; △13 March, 1959; ■ 16 March, 1959;
● 10 July, 1959; ○20 June, 1960; x 22 June, 1960;
** 19 October, 1962; ⊠ 24 October, 1962;*
▲ 7 September, 1964.

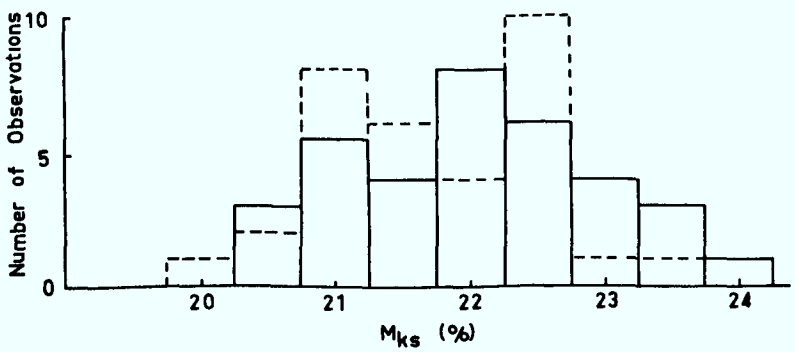

Fig. 4. M_{ks} values for the extraordinary mode of the 2.12 Mc/s. wanted wave and a disturbing power of 100 kw.; — observed, --- corrected to 85 km.

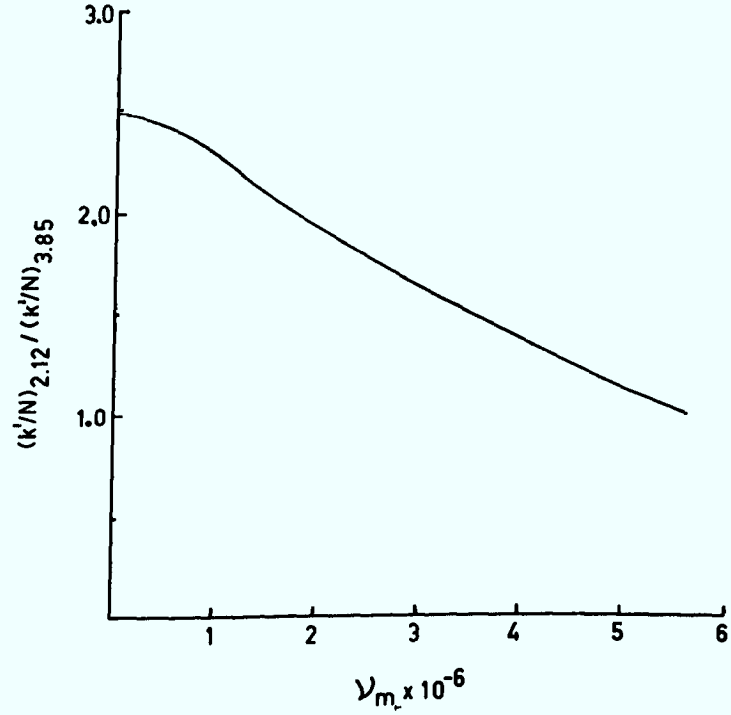

Fig. 5. Ratio of values of k'/N for ordinary 2.12 and 3.85 Mc/s. waves as a function of ν_m (Sen and Wyller M.I. theory).

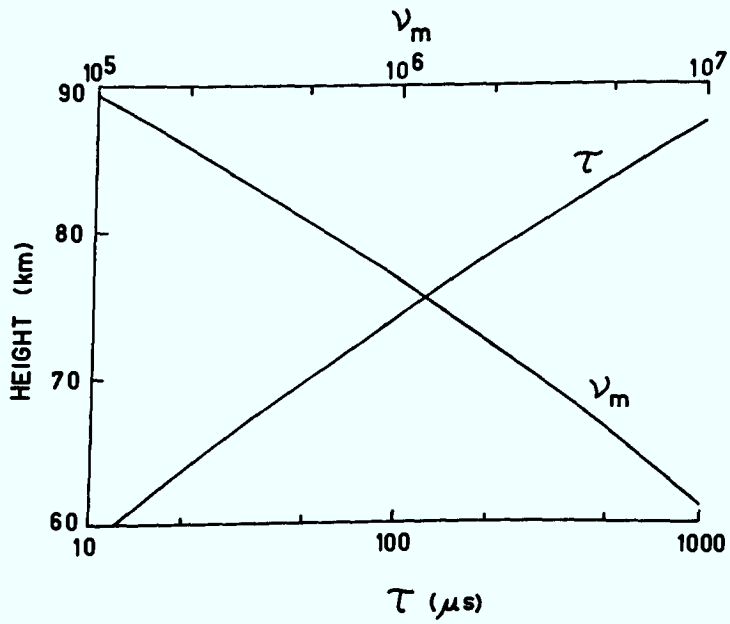

Fig. 6. Height profiles of electron collision frequency (Sen and Wyller M.I. theory) and relaxation time.

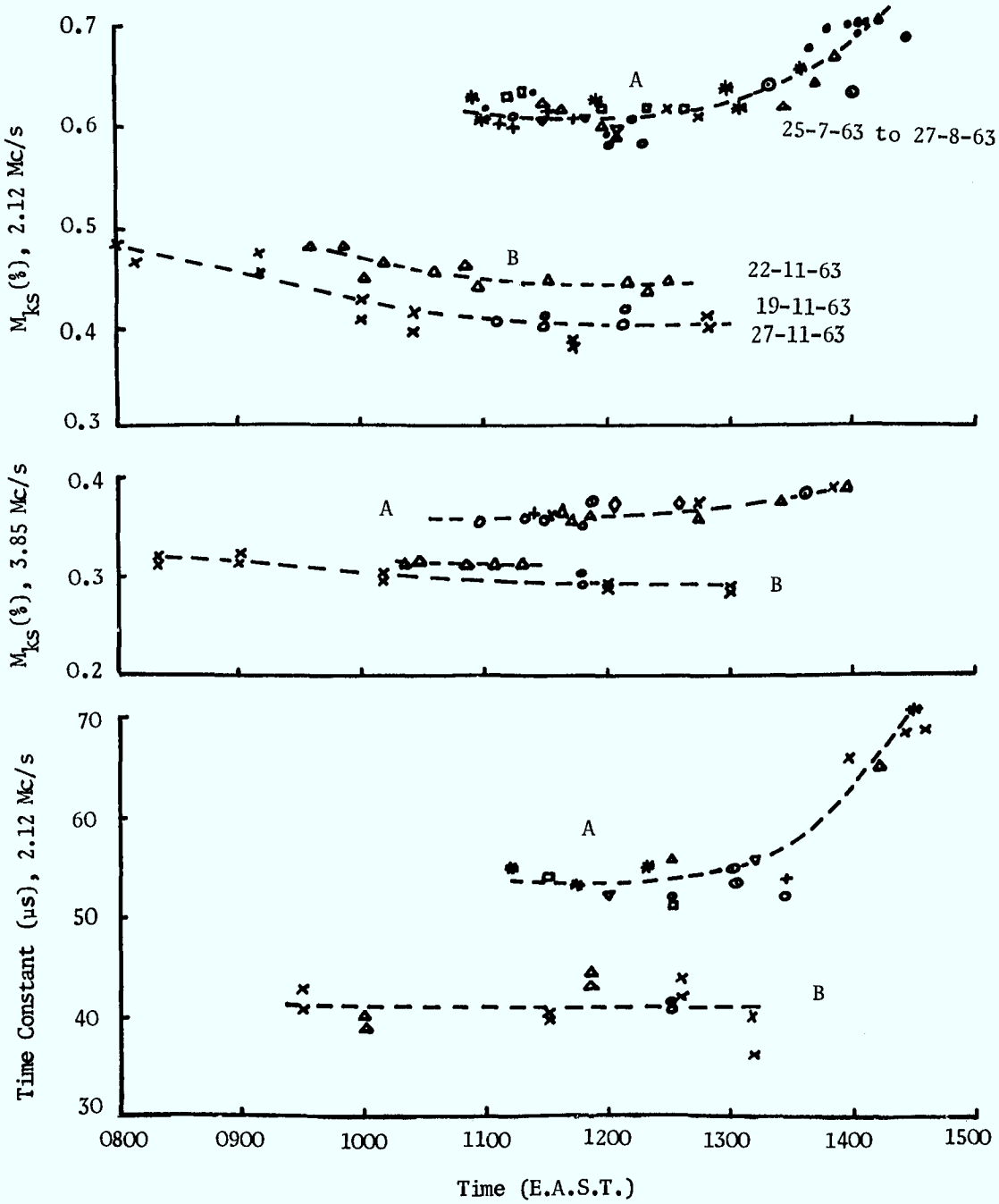

Fig. 7. M_{ks} values (100 kw.) for 2.12 and 3.85 Mc/s. ordinary wanted waves and the time constant (2.12 Mc/s.) as a function of time.

*A: x 25.7.63, + 30.7.63, o 31.7.63, ◇ 1.8.63, * 2.8.63, △ 5.8.63, □ 20.8.63, ● 21.8.63, ▽ 23.8.63, ⊙ 27.8.63,*
B: o 19.11.63, △ 22.11.63, x 27.11.63.

Discussion on Paper 3.2.1 presented by R.A. Smith

Bell: With your gyro-interaction experiment, the heating is confined to a thin slab. I can see it pins everything down well at that one height, but I think you said that to get the full profile you start to vary the disturbing frequency to get this resonant point to move. Doesn't this widen your resonant band?

Smith: I'm not quite sure which profiles you are referring to. The only time we varied the frequency was during the night to obtain the nighttime profile. We have used the 1.78 x-mode wave to obtain a thin slab as a first approximation, at low heights in the daytime. This is quite a different technique from the nighttime case because the slab near the 70 km. level is not as thin, and if you have very good data, you can determine its structure.

Bell: The band does widen, and your absorption should be an integrated effect, consequently it should not be assumed that everything happens in one very narrow band.

Smith: The beauty of this theory is that it doesn't matter within quite wide limits how thin it is. You get the same answer out, and you don't worry about how it is distributed in that region. It is independent of the N and the v profiles, provided that the slab is thin.

Bell: What is your criterion of how thin it is?

Smith: If you use the Sen and Wyller theory, and our nighttime profiles the slab is about 1 km. thick for a gyro-disturbing wave, the theory holds to within 1 per cent. In the daytime, you use the first approximation to the electron density profile to test the accuracy of the thin slab theory. We have only used thin slab theory at night to determine the parameters G and v at a particular height.

Bourne: I feel that there is some confusion here. Prof. Smith's argument is that you can determine the nighttime profile by changing the frequency of the extraordinary mode disturbing wave. The daytime profile is determined by using both the ordinary and the extraordinary mode disturbing waves. The extraordinary mode wave enables you to get a reasonably accurate electron density profile near the base of the D region (near the 70 km. level). Having obtained that part of the profile, you use the ordinary mode disturbing wave to extend the profile to greater heights.

Gregory: What is the geographic latitude of Armidale?

Smith: Approximately 30° 30'S.

Gregory: Its accurate value is important, since I would expect that the great stability which you have emphasized is a consequence of the latitude and its location relative to the edge of the westerly circulation. The second thing about this stability that you emphasized is that you really mean that every time you sampled the ionosphere, you obtained the same result; but how many times have you sampled it? You have approximately a dozen samples. That is not a big sample of a dynamical variable such as we get in meteorological conditions. I think you should be careful about saying it is stable. It is reproducible as you have seen it so far.

Smith: Yes, but what I am talking about is reproducible, not in figures that you people talk about, but it is reproducible to a few per cent.

Gregory: I think we have a different point of view here. You are sampling a medium which is inherently possibly variable. You have only made a small sample of it and therefore you shouldn't say that it is necessarily always the same; it is the same, as you have seen it. This business of a population and its sample has been mentioned in books of statistics.

Smith: I quite agree. These results are what we have seen.

Whitten: This question is really directed at all people using wave interaction. You are really interested in the inelastic collision frequency. Why do you use the quantity Gv which is some ratio times the momentum transfer collision frequency?

Smith: If you consider the energy balance equation, we can write that the power absorbed from the disturbing wave electron $= \frac{dv}{d} + R$ where v is the mean energy of the electron and R is the rate at which energy is lost by an electron to the neutral gas. In calculating the power absorbed from the disturbing

wave, we employ the momentum transfer collision frequency, and it is desirable for the sake of simplicity to use the same collision frequency in any expression for the term R. The quantity G is therefore defined to satisfy the relation $R = G\nu\,(v - v_0)$ where ν is the momentum transfer collision frequency and v_0 is the energy of the gas molecules.

Whitten: It was confusing to me when I first saw it. This is a plea to use some other notation.

Smith: Other notations have been used. Huxley tried replacing G by a term BN where B was a constant which had a lot of dimensions and N was the gas particle density. It is not convenient to use the gas particle density in radio work since it is not directly involved in the propagation parameters of the various radio waves. Of course, we know that τ the relaxation time, is equal to $\frac{1}{G\nu}$ for low power theory so that, if we wish, we can write the energy balance equation in terms of τ instead of G.

Thrane: I should like to ask you how long it takes you to get sufficient information to establish a reliable profile. The dawn profiles you have shown suggest that you need very little time to do the work.

Smith: Well, they are instantaneous profiles in the sense of one and one-half minutes.

Rao: I would like to point out that this is not a complete list for the wave interaction experiments conducted in the ionosphere. Also, when Dr. Smith commented during an earlier talk on the laboratory experiments on wave interaction (gyro-interaction in particular), I think he objected to the values of the collision frequency derived in nitrogen and oxygen. In the laboratory experiments, I think we know actually what is the neutral particle density, we know what is the region of interaction (we don't make guesses), we know exactly what are the frequencies involved, we know the plasma frequencies, we know the cyclotron frequency exactly, and we know the variation of the conductivity with collision frequency as a function of time during the disturbing pulse for every microsecond interval; I don't see that those values deduced from laboratory measurements are in any way inferior to these values obtained by gyro-interaction in the ionosphere.

Smith: I would be happy if I knew the temperature in the ionosphere. I would also like to know accurately the gain of my disturbing antenna.

Rao: I referred to your comment about the determination of the collision frequency in oxygen and nitrogen by the laboratory methods.

Smith: You haven't done it in nitrogen.

Rao: Yes, in nitrogen and in oxygen. In fact, we have done it with nitric oxide. We have the measurements of τ, equal to $1/G\nu$, in all three gases, and also as a function of gas temperature.

Smith: Has this been published?

Rao: Yes; it has been published in Phys. Rev. Letters, May 10, 1965.

Smith: Well, I apologize then. How do your values agree with Crompton?

Rao: In oxygen, the time constant is ten times faster than that in nitrogen; in nitric oxide, which has not been published as yet, the time constant is one hundred times faster than that in nitrogen. This is done in the range of gas temperatures from 300° to about 1000° Kelvin.

3.2.2 MEASUREMENTS OF IONOSPHERIC CROSS MODULATION AT A MIDDLE LATITUDE STATION

by

E.V. Thrane

Norwegian Defence Research Establishment

1. Introduction

The pulsed radio wave interaction technique for studying the lowest part of the ionosphere was first introduced by Fejer (1955) and has since been used by a number of workers — Landmark and Lied 1962; Flock and Benson 1961; Barrington and Thrane 1962; Weisbrod 1964.

The purpose of this paper is to present some results from a cross modulation experiment made during the International Quiet Sun Year at Crete, Greece (35°N, 25°E).

It proved possible to study the diurnal changes in the lower D region by means of this technique, and electron density profiles in the height range 60 to 80 km. were derived for different times of day.

In section 2 the experimental technique is briefly described, while the third section deals with the method of analysis. In the final sections the results are presented and compared with results from a partial reflection experiment made at the same station.

2. Experimental Technique

The experimental technique used in the present work is basically the same as the technique described by Barrington and Thrane (1962) and by Barrington et al. (1963). A low-noise site on the north-eastern coast of Crete was selected for the station. The geographical coordinates are 35°N, 25°E, the gyrofrequency is 1.20 MHz. and the angle of dip is 50°.

A wanted wave with frequency 2.30 MHz., pulse length 100 μsec., and pulse repetition frequency 50 Hz. was transmitted vertically. The receiving equipment was situated close to the wanted transmitter. The receiving antenna and the antenna for the wanted transmitter were single half-wave dipoles. To avoid false cross modulation the disturbing transmitter was situated about 6 km. away from the receiver. It worked on 2.00 MHz. with a PRF of 25 Hz. The peak power was about 50 kw. and the pulse width 100 μsec. A system of four horizontal half-wave dipoles forming a square permitted the transmission of circularly polarized disturbing waves of either orientation.

The equipment has been described by Bjelland (1966).

The amplitude modulation of the wanted wave was measured as a function of the meeting height of the wanted and disturbing pulses. An integration time on each meeting height of 2 to 3 min. was normally sufficient to give a reliable value. The meeting height was changed in steps of 10 km. from 60 km. to 100 km., and the polarization of the disturbing wave was changed every 20 to 25 min. The calibration was done by introducing a known degree of modulation on the wanted echo when the disturbing transmitter was turned off.

3. Method of Analysis

The method of analysis and the uncertainties involved in the experiment have been discussed in detail in the two papers referred to in the preceding section, and only a few additional remarks will be made here. Huxley (1953) gives a general expression for the fractional amplitude change T in the wanted pulse due to interaction with the disturbing pulse.

$$T(ho) = \int_{o}^{ho} \frac{\partial \kappa}{\partial T_e} \Delta T_e \, dh \tag{1}$$

The formula applies when both pulses are assumed to be of infinitesimal width. κ is the absorption index for the wanted wave, T_e is the electron temperature, and ΔT_e is the heating produced by the disturbing wave. h_o is the meeting height of the pulses. ΔT_e is a function of the absorption index of the disturbing wave and of the rate at which the electrons lose their excess energy to the neutral gas particles. Expressions for $\frac{\partial \kappa}{\partial T_e}$ and for ΔT_e have been derived using the generalized magnetoionic theory given by Sen and Wyller (1960). Since the longitudinal approximation of the formula for the complex refractive index is not accurate when applied to low and middle latitudes (Benson 1964) the complete formula has been used in this work. The finite width of the disturbing and wanted pulses has been taken into account (Landmark and Lied 1962; Bjelland and Lytomt 1961).

According to Dalgarno and Henry (1965), electron gas in the D region will cool mainly by rotational excitation of molecular nitrogen if the electron temperature T_e is less than 1300°K. For small deviations of T_e from the neutral gas temperature T_g, the cooling will be exponential with a time constant.

$$\tau = \frac{1}{G_M \, \nu_M} \tag{2}$$

G_M is the collision frequency of electrons with energy kT and $G_M = G'_M \cdot T_g^{-\frac{3}{2}}$. G'_M is a constant. In this work we have adopted the temperature variation with height given in the U.S. Standard Atmosphere (1962), and the height distribution of ν_M given by Haug and Thrane (these Proceedings). No attempts have been made to deduce the relaxation times or the collision frequency from the measurements. A value of the constant $G'_M = 14.1$ has been used. The relaxation times at 85 and 70 km. will then be $\tau_{85} = 640$ μsec., $\tau_{70} = 60$ μsec., in good agreement with the relaxation times measured at these levels by Bourne (1964). The adopted values are also in accord with results given by Dalgarno and Moffett (1962) and by Landmark and Lied (1962).

The analysis was based on a trial and error method in which a height distribution of electron density was assumed, and the cross modulation as a function of height computed and compared with the experimental data. The electron density distribution was then adjusted until satisfactory agreement between measured and computed values was obtained.

4. Experimental results

The experimental results presented here were obtained at Crete during the period 20 September to 3 October, 1964. No solar flares of importance greater than 1— were reported during the measurements. Observations of ionospheric cross modulation were made throughout the day from ground sunrise to ground sunset. Due to interference and radio noise, few reliable results were obtained at night. The measurements were averaged for every hour of the day, and Fig. 1 shows the average diurnal variation of cross modulation at each meeting

height and for both polarizations of the disturbing wave. Fig. 2 shows the measured average dependence of cross modulation on meeting height for one hour of the day. The bars indicate the quartiles. One electron density profile was derived for each set of data such as the data set shown in Fig. 2. Because of the large spread in the measurements each data set, taken separately, can be explained by a range of models. If, however, the additional assumptions are made that the electron density at each level must have a smooth diurnal variation, the range of possible models is severely restricted. Fig. 3 shows the profiles that give the best fit with the experimental data, and Fig. 4 demonstrates the agreement of the computed and observed values of cross modulation.

The measurements give no detailed information about the electron density distribution at night or below about 65 km. during the day. However, it is possible to set upper limits to the electron densities in these cases. The dashed curve in Fig. 3 give the upper limits for the electron densities below 85 km. when the solar zenith angle $\chi > 80$ km.

Below 65 km. the electron concentration at any time of the day must not exceed 50 electrons per c.c.

5. Discussion

The uniqueness of the electron density distributions presented in Fig. 3 has been tested to see whether a different set of profiles can explain the observations equally well, and to try to estimate the accuracy of the method. It was found that either of the data sets shown in Fig. 4 can be explained by simple one-layer models, but if a smooth and consistent diurnal variation of electron density is required, the two-layer structure indicated in Fig. 3 gives the best fit. The sensitivity of the experiment will vary with height and with time of day, but in general it is possible to state that the electron density at any height in the range 60 to 80 km. cannot be changed by more than 30 per cent from the models in Fig. 3 without spoiling the agreement between measured and computed values of cross modulation.

In Fig. 5 the cross modulation models are compared with the electron density distributions derived by Haug and Thrane (these Proceedings) from measurements of partial reflection.

The two sets of results agree rather well in the range 75 to 80 km., but the electron densities derived from the partial reflection experiment are smaller than those given by the cross modulation method near 70 km.

We conclude that the quiet D region at middle latitudes exhibits a fairly smooth diurnal variation.

Acknowledgments

The research described in this paper is sponsored by NATO Scientific Affairs Division under Research Grant No. 133. The measurements were made in collaboration with the Ionospheric Institute of Athens.

REFERENCES

Barrington, R.E. and E.V. Thrane. J. Atm. Terr. Phys. 24, 31, 1962.

Barrington, R.E., Thrane, E.V. and B. Bjelland. Can. J. Phys. 41, 271, 1963.

Benson, R.F. J. Res. N.B.S. 68D, 219, 1964.

Bjelland, B. In publication.

Bjelland, B. and O. Lytomt. NDRE Rep. No. 35 Parts IV-VI, Norwegian Defence Research Establishment, 1961.

Bourne, I.A. Ph.D.Thesis, Faculty of Science, Univ. New England, November 1964.

Dalgarno, A. and R.J.W. Henry. Proc. Roy. Soc. 288A, 521, 1965.

Dalgarno, A. and R.J. Moffett. Planet. Space Sci. 9, 439, 1962.

Fejer, J.A. J. Atm. Terr. Phys. 7, 322, 1955.

Flock, W.L. and R.F. Benson. Final Report Contract No. AF 19(604)-3880, Air Force Cambridge Research Laboratories, 1961.

Haug, A. and E.V. Thrane. These Proceedings.

Huxley, L.G.H. Proc. Roy. Soc. 218, 520, 1953.

Landmark, B. and F. Lied. Radio Wave Absorption in the Ionosphere. AGARDograph 53, Ed. N.C. Gerson, Pergamon Press, 1962.

Sen, H.K. and A.A. Wyller. J. Geophys. Res. 65, 3031, 1960.

Sissenwine, N., Dubin, M. and H. Wexler. US Standard Atmosphere, 1962, US Gov. Printing Office, Washington 25, DC.

Weisbrod, S. Sci. Rep. No. 206, Penn. State Univ., March 1964.

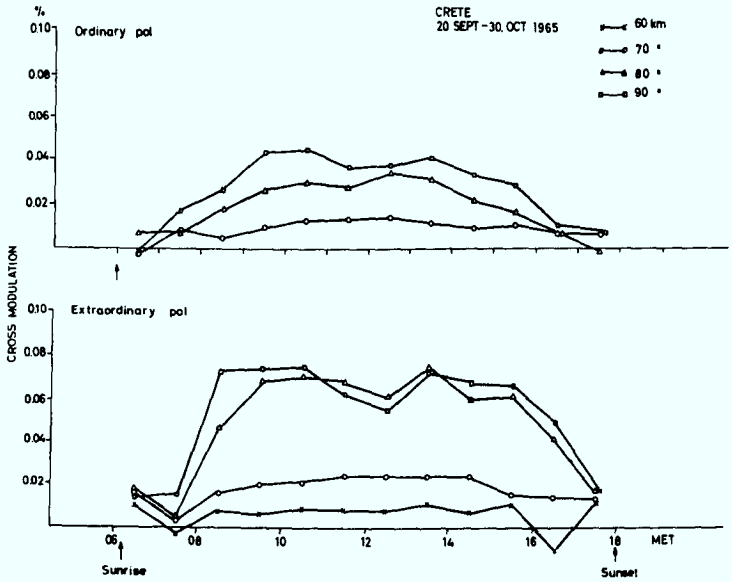

Fig. 1. Average diurnal variation of cross modulation for different meeting heights.

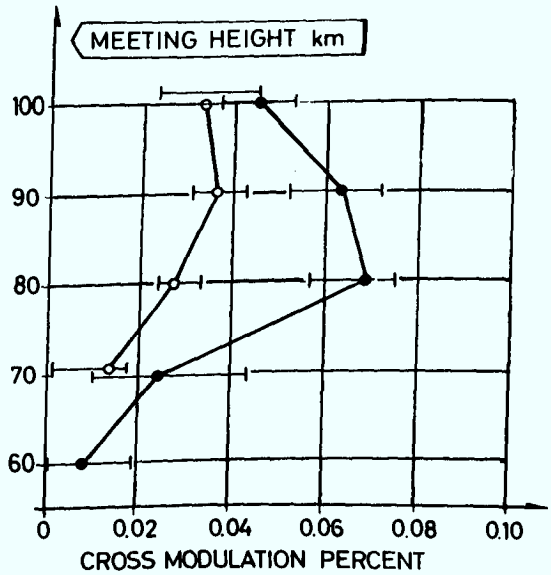

Fig. 2. Average values of cross modulation for the hour 11 – 12 LMT. The bars indicate the quartiles.
● *Extraordinary disturbing wave*
o *Ordinary disturbing wave*

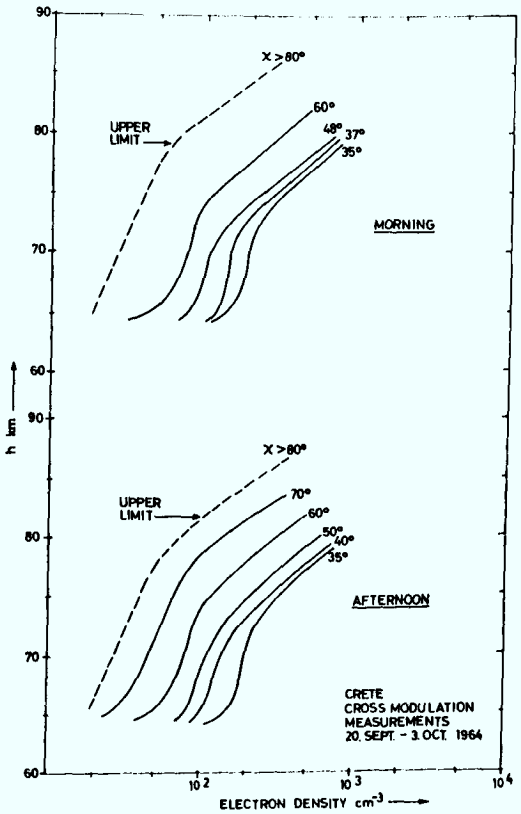

Fig. 3. Diurnal variation of electron density.

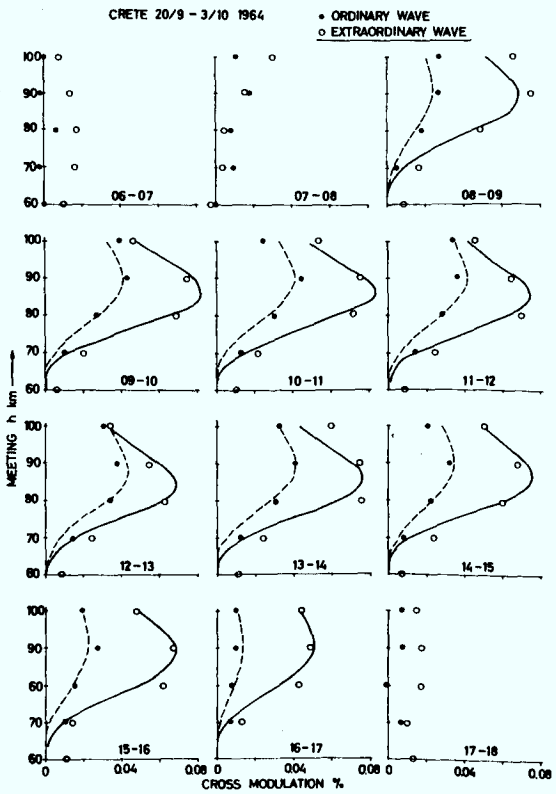

Fig. 4. Comparison between average experimental values (open and full circles) and computed values of cross modulation
------- *computed cross mod. ordinary wave*
—— *computed cross mod. extraordinary wave*

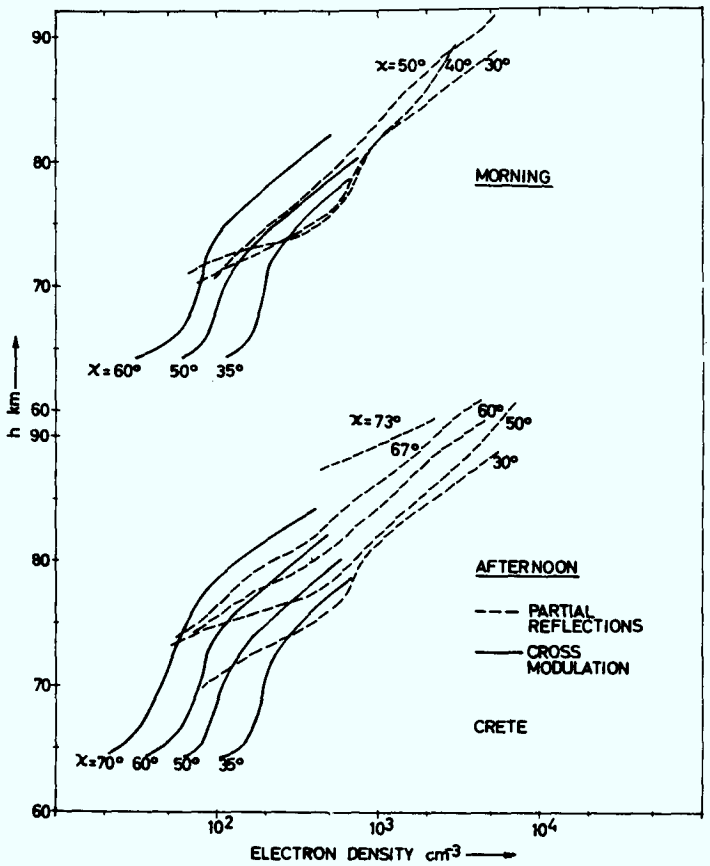

Fig. 5. Comparison between electron densities derived from measurements of cross modulation and partial reflections.

Discussion on Paper 3.2.2 presented by E.V. Thrane

Falcon: It is interesting to note that the profiles that you presented (determined by the cross modulation experiment at middle latitudes) agree with the profiles that I presented yesterday, both in approximate value and general variation. Your profiles, determined by the partial reflection experiment, showed a sharper gradient at the lower heights. Is this an inherent characteristic of some of the assumptions made in the cross modulation experiment? Your cross modulation results show a very slow variation in electron density from just below 70 km. up to around 73 or 74 km. and then a more rapid variation. This is for the same general latitudes as where we conducted our experiments, where we noted the same type of variations, during the same season, and at approximately the same solar zenith angle. Is this something which is inherent only in your assumptions, or do you feel these cross modulation figures are relatively accurate, as far as the diurnal variations are concerned?

Thrane: It is a difficult question to answer. Of course, the cross modulation profiles do depend on all the assumptions I have made, and, in particular, if the value of G was different, this might change the shape of the profiles and also the collision frequency model; but it seemed difficult to get away from that type of profile – the slow variation below 70 or below 73 km. and the change in gradient for greater heights. By pressing things I could perhaps have made it a single exponential, but this was not the model that gave the best fit.

Georges: Two speakers this morning have referred to the *definition* of amplitude interaction as

$$T_A = \int_o^{h_i} \frac{\partial a}{\partial \nu} \, \delta\nu \, dh$$

where a is the probing wave absorption coefficient. While this expression is quite accurate for all but the highest power experiments, and some gyrointeraction, it should not strictly be called a definition. Actually, the definition is

$$T_A \equiv \frac{\Delta A}{A}$$

from which

$$T_A = \frac{A}{A_o} - 1$$

$$= \exp\left[-\int_o^{h_i} \delta a \, dh \right] - 1$$

$$\approx -\int_o^{h_i} \delta a \, dh; \text{ if } T_A << 1$$

and if only perturbations in ν are considered,

$$T_A \approx -\int_o^{h_i} \frac{\partial a}{\partial \nu} \, \delta\nu \, dh.$$

Bell: I believe this should be answered. I tested this for peak radiated powers at 4 Mc. between 15 and 30 Mw., and the error was less than half a per cent.

Georges: That is probably so, but I don't think that the integral should be called the definition.

Bourne: I must agree; there are some experiments at Armidale in which you obtain a reduction of echo amplitude by 70 or 80 per cent. There are then significant differences between these two 'definitions' of modulation.

Thrane: This is so. Of course, for all small perturbations it is alright. I perhaps didn't mention that the power of the disturbing transmitter is nominally 50 kw., but because of losses it is probably much less. I can give you one approximate value; the equivalent omnidirectional flux of the disturbing pulse would be about 150 kw.

Bourne: Would you have any estimate of what the efficiency of your antenna installation would need be to explain your wave interaction observations?

Thrane: About 4 or 5 db above a single half-wave dipole; I don't know for certain because I don't really know exactly how much power went into the antennas.

Aikin: Might we have a summary of how the sunrise variations of electron density at Crete and in Australia compare, particularly around 70 km., and make a comparison with the rocket results over Wallops Island, which showed virtually no sunrise effect until after ground sunrise and 25 electrons at a zenith angle of 85°.

Kane: This figure (D1) compares the results presented yesterday by Dr. Thrane, which he obtained in Crete at a latitude of 35° in the northern hemisphere, with some of the results which we were able to obtain at 35°S latitude in New Zealand last May 30th. I plotted his data as a function of zenith angle in terms of the altitude at which the electron density has values of 100, 200, 500, and 1000, and the general meeting of our data with his is somewhat gratifying. Also plotted is the altitude at which Lyman α flux has some arbitrary constant value.

Sales: Dr. Thrane just showed that his partial reflection results near 70 km. were probably too low by a factor of five when compared with his wave interaction results. I wonder how that would affect your comparison.

Kane: I only had access to his partial reflection data.

LaLonde: Are these sunrise or sunset χ values?

Kane: Our data is at sunrise, Dr. Thrane's are taken in the afternoon.

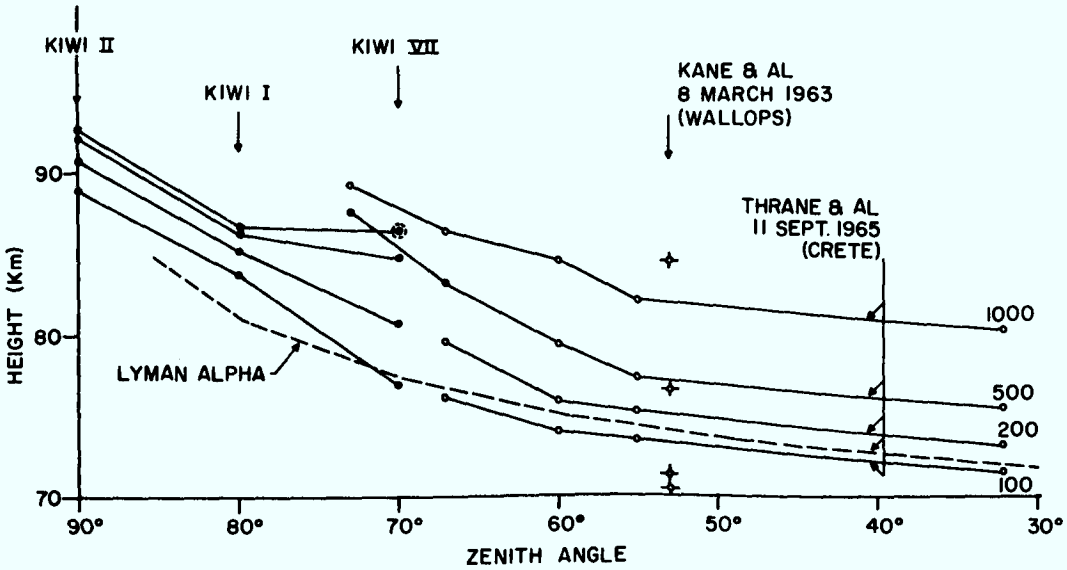

Fig. D1. Electron Density Isopleths. (Presented by Dr. J. Kane.)

3.2.3 RESULTS OF AN AMPLITUDE CROSS-MODULATION EXPERIMENT AT BIRDLINGS FLAT, 43°S

by

A.H. Manson*

Department of the Geophysical Sciences, University of Chicago, Chicago, Illinois

* Now at University of Canterbury, Christchurch, New Zealand

1. Introduction

The mesosphere has been studied by ground-based radio methods for several years, at Birdlings Flat, New Zealand. Transmitters of medium frequency (1.75, 2.40 Mc/s.) and high power have enabled partial reflections from 60 to 90 km. to be studied in detail (Gregory, 1961).

These observations have shown that the ionospheric absorption of these radio waves varies greatly throughout the winter months, and for periods of several days the lower frequency in particular may be almost totally absorbed. This so-called 'winter anomaly' has been studied in some detail by other workers (Appleton and Piggott, 1954). It was therefore decided to develop an electron density measuring facility to provide information on the mesosphere throughout the year, and particularly at these periods of high absorption. The requirements for this equipment were high resolution and accuracy, and good observational efficiency.

2. Experimental Techniques

A partial reflection experiment (Gardner and Pawsey 1953) was operational by the end of 1962, and the combination of an extremely quiet site, high transmitter power (320 kw., 2.4 Mc/s.), and good receiving equipment produced excellent results. However, this method has the basic disadvantage of providing relatively few values of electron density, N(h), at any one time, due to its dependence on natural irregularities in the mesosphere. Also, the collision frequency (ν_m) profile is required before the N(h) values can be calculated, and the method provides values of ν_m only when very low echoes near 60 km. are received. Thus, a ν_m profile has to be assumed, and since this is known to vary seasonally, certain inaccuracies will arise in the calculated N(h) profile.

It was therefore decided to develop an amplitude cross-modulation experiment, using two pulsed transmitters. This method was used initially by Fejer (1955), and promises high resolution at continuously variable heights – the use of ordinary and extraordinary components of the 'wanted transmitter' also makes possible the measurement of ν_m and N(h). The disturbing transmitter produces a 100 kw., 40 μsec. pulse, and although previous workers (Fejer and Vice, 1959; Landmark and Lied, 1961) had experienced problems in obtaining good data with similar transmitter powers, it was felt that the very quiet experimental site would enable useful observations to be made. It is frequently stated that the partial reflection experiment demands high transmitter powers and quiet sites, so that the success of this latter experiment suggested the possibility of similar success with the cross-modulation experiment.

Various instrumentations were considered, but eventually a variant of the filter detection system used by Fejer was decided upon. When completed, this was capable of measuring

amplitude modulation of one part in 10^5. Theoretical profiles of the transferred modulation, obtained from average mesospheric ν_m and N(h) values, suggested that values of the order of 1 part in 10^4 could be expected.

3. Experimental Results

The equipment was run for a period of two months — October, November 1964. Observations were made twice a week, but later only in the weekends. This restriction was imposed by strong interference recorded by local commercial radio operators who were using adjacent radio channels. Although most partial reflection experiments operate at a repetition rate of 50 p.p.s. or less, the filtering technique of the cross-modulation experiment favours a somewhat higher rate (75 p.p.s.), which is also distinct from the a.c. mains frequency. Unfortunately the receivers of the commercial operators were not filtered sufficiently at this higher repetition rate. Of those days available, however, less than 40 per cent gave usable cross-modulation profiles, and few of these provided any detailed information. During the remaining 60 per cent of the observations, a large, randomly varying signal was recorded, even when the disturbing transmitter was not operating. Apart from the radio interference already mentioned, the fading of the E-region signal during these observations was often rapid — of shorter period than the time constant of the A.G.C. in the equipment — and complete changes in the structure of the signal often occurred within the period of one observation. With the time constant used in the equipment, 20 min. was required to record the transferred modulation from 60 to 90 km.

At this stage it was not known whether the energy in the fading spectrum at the frequency of the required modulation could increase to a value above that of the transferred modulation — or if the equipment was sensitive to rapid changes in input signal, such as would occur when the structure of the E-region signal changed rapidly. Depending on the rate at which these changes occurred, this latter situation would not be as serious, since observations could be carried out between changes in echo structure. The 'noisy' portion of the record could then be identified, and not considered for purposes of analysis.

The amplitudes of series of E-region echoes were analyzed, and power spectra and autocorrelation functions were obtained on a number of representative days. Fig. 1 shows the variation in amplitude of a 1-volt signal, on days when observations were impossible, marginal and good, respectively. The noise at 37.5 c/s., on the 'quiet' day, may be calculated from Fig. 2. The peak at 25 c/s. is due to the mechanical structure of the diesel power supply. Using this peak as a reference, the noise at 37.5 c/s. can be shown to be 3.10^{-5}v. in a 1-volt signal — this value agrees with noise observed on the recording charts on the quiet days. Fig. 3 shows that there was greatly increased high frequency energy present on the day when it was impossible to make any observations of the transferred modulation. The diesel's 25 c/s. modulation cannot be seen, so that the component at 37.5 c/s. is in excess of 10^{-3}v. Although these are the extremes of observing conditions, it is apparent that a transferred modulation of 10^{-4}v.(in a 1-volt signal) is too small to enable reliable observations. Also, in addition to this relatively steady noise component, the signal-structure change undoubtedly introduces sudden increases in the 37.5 c/s. noise component, which causes severe overloading of the high-gain amplifier.

Following this analysis, the E-region echo was observed between 0930-1500 hr. on many days. One in three of the observations were in the 'quiet' category — a figure which agrees with the observational efficiency of less than 40 per cent which was mentioned above. Unfortunately, these results appear to agree with the experience of other workers in this field, who had similar problems with noise, due to insufficient 'disturbing-transmitter' power. One of the best cross-modulation profiles is shown in Fig. 4 — the N(h) profile was obtained by comparison with a theoretical cross-modulation curve derived from typical N(h), ν_m values — effectively a 'slab' analysis was used. Considering the noise on the record, and the crude analysis used, the N(h) values are in reasonable agreement with those due to the partial reflection experiment.

4. Conclusion

It appears that powers in excess of 1 Mw. would be required before reliable, accurate measurements of the transferred modulation could be made at this New Zealand site. Providing such a transmitter were available, both phase and amplitude should be measured. Ferraro and Lee (1966) and their associates have shown this to be a very powerful method, enabling ν_m, N(h), G (fractional energy loss parameter) and temperature to be obtained uniquely.* It is important that all of these be measured, not only to provide more ionospheric data, but also to verify the equation describing the energy loss mechanism that exists in the region of the interacting pulses. This process is crucial to the theory of the cross-modulation experiment, as neither the 'Bailey and Martyn' or 'Huxley' loss equations that are now used for most theoretical analyses, fully explain all cross-modulation results from 30 to 100 km.

It remains to emphasize, that with the transmitter power available, the partial reflection experiment remains a powerful method for probing the mesosphere — providing almost 100 per cent observational efficiency, and good accuracy from 60 to 80 km. The method has proved useful in studying the periods of high winter absorption during the last three years.

REFERENCES

Appleton, E. and W.R. Piggott. Ionospheric absorption measurements during a sunspot cycle. J. Atmos. Terr. Phys., 5, 141-172, 1954.

Fejer, J.A. The interaction of pulsed radio waves in the ionosphere. J. Atmos. Terr. Phys., 7, 322-332, 1955.

Fejer, J.A. and R.W. Vice. An investigation of the ionospheric D region. J. Atmos. Terr. Phys., 16, 291-306, 1959.

Ferraro, A.J. and H.S. Lee. Radio wave phase interaction. These Proceedings, 1966.

Gardner, F.F. and J.L. Pawsey. Study of the ionospheric D region using partial reflections. J. Atmos. Terr. Phys., 3, 321-344, 1953.

Gregory, J.B. Radio wave reflections from the mesosphere. J. Geophys. Res., 66, 429-455, 1961.

Landmark, B. and F. Lied. Observations of the D region from a study of ionospheric cross-modulation. J. Atmos. Terr. Phys., 23, 92-100, 1961.

Smith, R.A., Bourne, I.A., Loch, R.G., Setty, C.S.G., Coyne, T.N.R., Barratt, P.H. and B.S.N, Prasad. Radio wave interaction using gyrowaves. Scientific Report No. 3 and Final Report, AFCRL 65-460, 1965.

* Smith (1965) has also measured these parameters by using several variations of the familiar amplitude modulation technique.

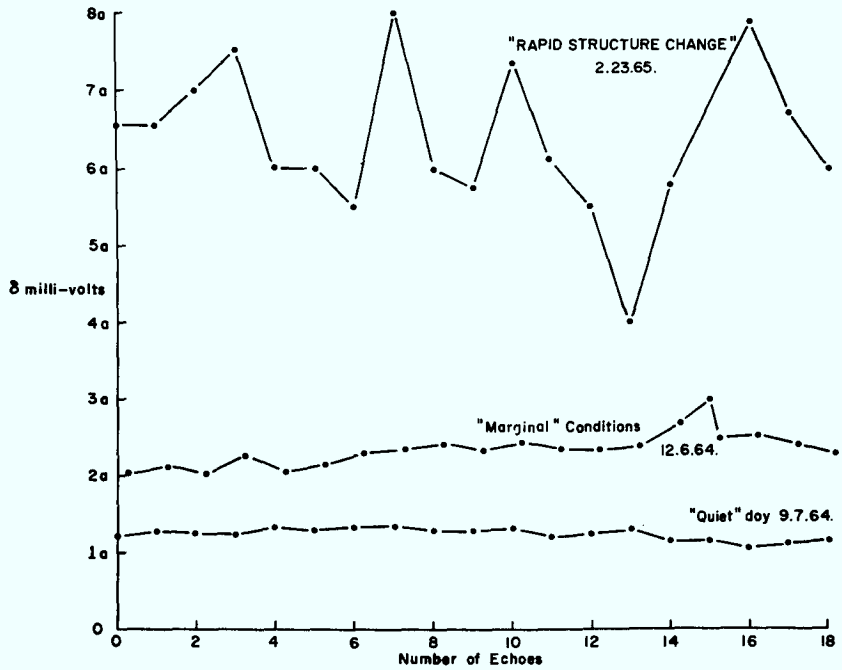

Fig. 1. E-region amplitude variations on a 1-volt signal (a = 20 mv).

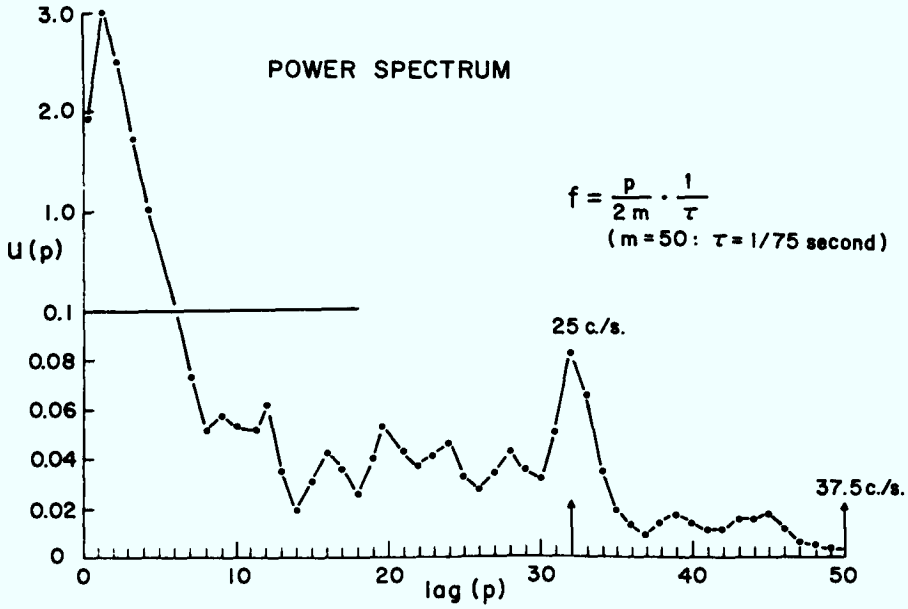

Fig. 2. "Quiet Day" analysis.

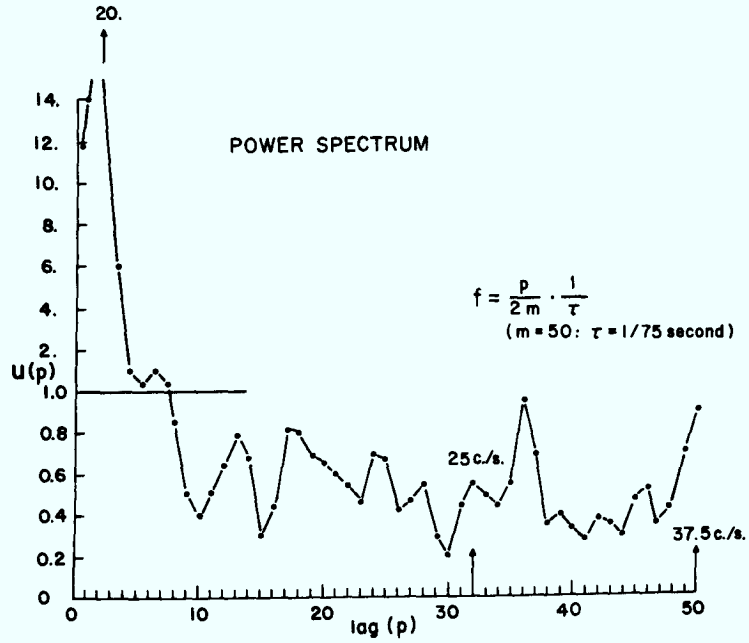

Fig. 3. "Rapid Structure Change" analysis.

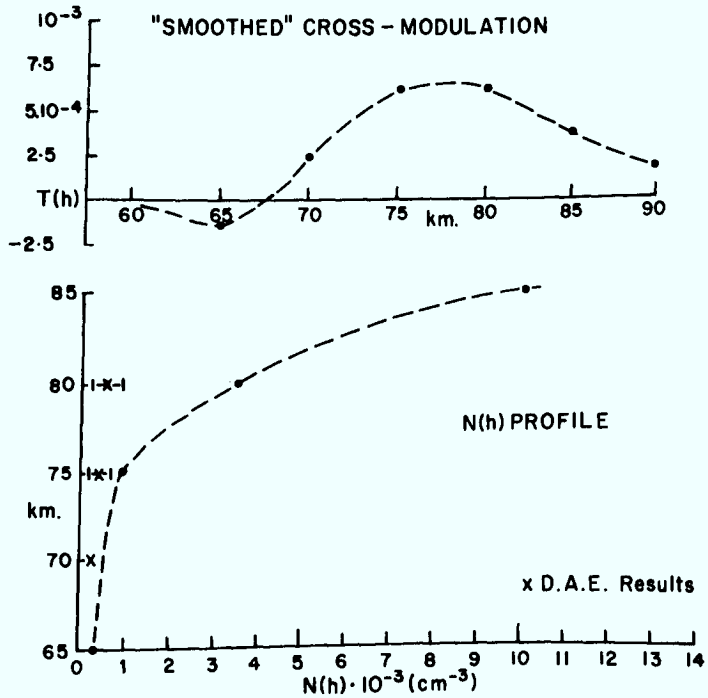

Fig. 4. Cross-modulation and electron concentration profiles.

Discussion on Paper 3.2.3 presented by A.H. Manson

Bourne: When you measured power density at various frequencies, I assume that you did not use a phase-sensitive detector. The use of these detectors should bring the effective limit of measurable transferred modulation depths down by a large factor. We noticed at Armidale that without a phase-sensitive detector there may be very large fluctuations, which were almost completely eliminated as soon as we employed the phased detector.

Manson: It will reduce it, but in our case it didn't reduce it to a point at which we could obtain reliable measurements.

Gregory: What type of aerial did you employ? Was it a square with half-wave dipoles?

Manson: Yes.

Bibl: Have you any results showing the winter anomaly?

Manson: Yesterday Dr. Gregory presented some of the partial reflection results that were obtained during periods of winter anomaly. We have no wave interaction records showing the effect.

3.2.4 SMALL PERTURBATION WAVE INTERACTION IN THE LOWER IONOSPHERE

PART 3

MEASUREMENTS OF ELECTRON DENSITIES

by

R.A. Smith, T.N.R. Coyne, R.G. Loch, and I.A. Bourne*

University of New England, Armidale, Australia

* Now at DRTE, Ottawa, Canada.

1. Introduction

Progress in the understanding of the ionosphere below 90 km. has been hampered by the difficulty of determining the diurnal change of the electron density profile. This paper is concerned with the profile for the tail of the nighttime E region (Section 2), the noon profiles for the D region in summer and winter (Section 3), the development of the sunrise D region and the further changes that occur to maximum ionization at noon (Section 4), and the residual ionization in the lower D region at night (Section 5). Section 3 also summarizes the practices which have been used in the analyses of Fejer curves, and supplements the more general discussion given in Paper 3.1.1. In technical and theoretical description the terminology and notation of that paper are used.

2. Electron density profile for the nighttime lower E region

An effective resolution of the structure of the disturbed region acted on at night by an extraordinary disturbing gyrowave cannot be made from a Fejer curve. The method described here for obtaining the electron density profile utilizes the property that the time constant of Type I data passes through a resonance minimum when the frequency of the extraordinary disturbing wave is varied about the gyrofrequency.

The experiments were made mainly during August and September 1963 using extraordinary 2.12 Mc/s. wanted pulses and extraordinary disturbing pulses of 800 μsec. duration in the frequency range 1.45 - 1.78 Mc/s. from Station A. The radiated powers were not measured but were kept to about 5 kw. to ensure the applicability of small perturbation wave interaction theory.

The minimum at the gyrofrequency (1.515 Mc/s.) in the time constant – disturbing frequency curve was generally well-defined, but often the shape of the curve varied during the night as a result of changes in the electron density profile. Because the method requires both good recording conditions for accurate measurement of the time constants and stability of the profile over the time necessary to obtain the curve and confirm its reproducibility, the amount of usable data from the experiments is limited. Fig. 1 shows observations made on the night of 9 August 1963, when the profile changed from one with a steep gradient absorbing all the disturbing frequencies in a small height range to one with a shallower gradient. Figs. 2 and 3 show observations made on 3 and 6 September 1963, respectively. On each of these nights the profile was stable and the experimental curve was reproduced closely.

The time constant of the decay of small perturbation Type I data is independent of the power of the disturbing pulse and can be evaluated for an assumed electron density profile from formula (40) in Paper 3.1.1, using data for the energy loss coefficient and the electron collision frequency given in Paper 3.2.1. Since Martyn (1935), Nertney (1953), Parkinson (1955), and Mechtly (1962) have deduced profiles for the nighttime lower E region from medium and low frequency propagation data which are closely exponential, the first profiles tested were of the form $N_o \exp(ah)$. For a given value of the gradient a, the value of N_o was adjusted during execution of the computer program to obtain agreement at the gyrofrequency between the computed and measured time constants. The time constants at frequencies of 1.53, 1.55, 1.60, 1.70 and 1.78 Mc/s. were then computed.

The time constants computed for a number of exponential models using the Appleton-Hartree magnetoionic theory are compared in Fig. 4 with the values (b in Fig. 2, c in Fig. 3) measured on the two nights. In this and the next two figures the value of N at a height of 85 km. (N_o) is given in brackets beside the value ($km.^{-1}$) of the gradient. Both experimental curves are fitted reasonably well for a gradient of 0.6, a value which is lower than that (1.0) given by Martyn, but is close to that (0.5) given by Mechtly and to the gradients of the profiles of Nertney and of Parkinson. The value of N_o for the night of 3 September 1963 is three times larger than that for 6 September 1963. Because of the limitations of this magnetoionic theory, further analysis using it was not considered worthwhile.

Similar computations have been made using the generalized magnetoionic theory for a constant collision cross-section A and the generalized theory of Sen and Wyller (1960) for a cross-section proportional to electron speed c. Using the first of these theories, the fit in each part of Fig. 5 is good for a value of the gradient of 0.85. The use of the Sen and Wyller theory, on the other hand, gives the different result that the experimental data cannot be matched using exponential profiles (Fig. 6). This difference is caused by the more pronounced resonance in the absorption coefficient of the extraordinary mode (Fig. 7) and the resonance is so sharp that, for the scale on which Fig. 6 is plotted, the shapes of the minima in the computed time constants are not evident. To offset this sharpness, a steep initial gradient of the electron density is required to limit penetration at frequencies near the gyrofrequency. The curves shown in Fig. 8 have been computed for linear models of the form $N = a(h - x)$, where h is the height in kilometers above a reference level of 80 km. For these computations, the value of x (shown in brackets in the figure beside the value of a) was adjusted to make the computed and experimental time constants agree at the gyrofrequency. It may be seen that a linear model gives a good fit to the data of 3 September 1963 and a reasonable fit to that of 6 September 1963. A non-linear profile, which gives a good fit to the latter data, is shown in Fig. 9, together with the linear profile for 3 September 1963.

3. Synthesis methods and the noon D region

The problem of deducing electron density profiles from Fejer curves has been discussed generally in Paper 3.1.1. Since the remainder of this paper is largely concerned with profiles for the D region that have been obtained by this method, relevant aspects of the previous discussion are summarized and a number of points expanded.

In general the height resolution in a Fejer curve is poor. For an effective resolution to be made, it is necessary for the accuracy of the experimental data to be high and, preferably, these data should be of Type III rather than of Type II because of the greater information content. A corollary of the accuracy requirement is that in the analysis proper account must be taken of experimental parameters, such as the shapes of the disturbing and wanted pulses, which have a marked influence on the shape of, and hence the height resolution in, a Fejer curve. It is virtually impossible to give a comprehensive estimate of the error in the derived electron density profile from errors in the measured Fejer curve and in the many subsidiary experimental and ionospheric parameters introduced in the analysis.

With regard to the problem of height resolution, our initial policy has been to deduce profiles from particular Fejer curves which are considered to be of the requisite standard, rather than to use averages of curves of poorer quality. It is stressed that the quality of the curve is determined by factors, such as the nature of the wanted echo and atmospheric noise, external to the D region, and we have no evidence to suggest that the region is abnormal at times when satisfactory records are obtained. The electronic synthesizer employed at the University of New England (Paper 3.1.1) takes proper account of the shapes of the wanted and disturbing pulses, and has a height interval of 1 km. between channels. This high density of channels is required for accurate matching of Fejer curves, such as those from interaction in restricted height ranges and those having a sharp transition from negative to positive modulation (Section 4). When synthesizing Fejer curves generally, we use all the height channels and accept the synthesis which gives maximum smoothness in the variation of the modulation depths, ΔM_{si}, with height. This ensures that structural detail beyond that permitted by the height resolution in the Fejer curve is not erroneously deduced for the electron density profile. The above method is preferred to one that makes use of channels at a height interval dictated by the limit of resolution, since the requirement of homogeneity over the basic height interval is more closely approximated.

In Paper 3.2.1, evidence in support of the use of the magnetoionic theory of Sen and Wyller in the analysis of wave propagation in the D and lower E regions was given, and accurate values of the energy loss coefficient G_m, the collision frequency ν_m, and the relaxation time τ were deduced for heights of 69 and 85 km. above sea level. It was also shown that reliance could be placed on the use of atmospheric data to extend the values of ν_m and τ over the height range in which wave interaction is observed. The profiles of ν_m and τ so obtained (Fig. 6, Paper 3.2.1) and the magnetoionic theory of Sen and Wyller have been used in the deduction of the electron density profiles shown in Fig. 9.

The values of ΔM_{si} yielded by a synthesis are related to the electron densities N_i by equations (36), (30) and (37) of Paper 3.1.1. For an analysis using the magnetoionic theory of Sen and Wyller, these equations are

$$\Delta M_{si} = Q(h_i)\ \delta_1\ \delta_2 \cdots\cdots\cdots \delta_{i-1}(1 - \delta_i) \tag{1}$$

$$Q(h_i) = \frac{gW}{4\pi h_i^2} \cdot \frac{1}{(G_m U_o)_i} \cdot (k_w'/N)_i \tag{2}$$

$$\delta_i = \exp(-2k_{di}\ \Delta h) \tag{3}$$

where

$$k_w'/N = \frac{1}{N} \cdot \frac{\partial k_w}{\partial \nu_m}$$

With a knowledge of ΔM_{si} and $Q(h_i)$, the evaluation of δ_i from (1) is straightforward. Since $(k_d/N)_i$ for the disturbing wave is known, N_i can then be found from (3).

At first sight it might appear that although the values of G_m and ν_m are known accurately, the relatively large errors quoted in Paper 3.2.1 for the gain of the disturbing aerial and the gas temperature do not allow the factors $Q(h_i)$ to be calculated accurately. This is not the case, however, as will now be shown.

It is obvious from (2) that $Q(h_i)$ is equal to the steady modulation depth that would be impressed on the wanted wave at the height h_i during a single transit of an infinitesimally thin region in which the radiated disturbing power W (taken to be 100 kw.*) is totally absorbed. It is also equal to the steady modulation depth observed when the disturbed region is localized about this height. Thus, the value of (21.7 ± 0.3)% for M_{ks} from the nighttime experiments (D--1.515 Mc/s., x-mode; W--2.12 Mc/s., x-mode) described in Section 4 of Paper 3.2.1 provides a reference value for the height of 85 km. Using this reference value, $Q(h_i)$ can be written as

$$Q(h_i) = \frac{g_D}{g_{1.515}} \cdot \frac{(84)^2}{(h_i)} \cdot \frac{(G_m U_o)_{85}}{(G_m U_o)_i} \cdot \left(\frac{M_{ks}}{k_w'/N}\right)_{85} \cdot (k_w'/N)_i \qquad (4)$$

where the height h_i above Armidale (altitude 1 km.) is expressed in kilometers, g_D is the gain of the disturbing aerial at Station A at the frequency used, $g_{1.515}$ is the gain at the frequency of 1.515 Mc/s., and the subscript 85 has an obvious meaning. Since the error in the value of $(k_w'/N)_{85}$ for the extraordinary 2.12 Mc/s. wave is also negligible, the use of the data from the nighttime experiments makes it necessary to consider, apart from the variation of k_w'/N, only the variation of $G_m U_o$ with height and the variation of the aerial gain with frequency.

In order to establish the magnitudes of the factors $Q(h_i)$ in the lower D region, two sets of experimental values of M_{ks} have been used – the summer and winter values for ordinary 2.12 and 3.85 Mc/s. wanted waves obtained using the extraordinary 1.78 Mc/s. disturbing wave (Section 5, Paper 3.2.1), and the values for an ordinary 2.12 Mc/s. wanted wave obtained near noon during November 1963 using extraordinary 1.78 and 1.515 Mc/s. disturbing waves. The latter set gives accurately the relative gain $g_{1.78}/g_{1.515}$ at the two disturbing frequencies and was taken into account in the deduction in Paper 3.2.1 by an iterative method of a value of $G_m U_o$ at 69 km. ten per cent higher than at 85 km. When evaluating the factors $Q(h_i)$ this small change in $G_m U_o$ with height has been taken to be linear. The accuracy with which the summer and winter values of M_{ks} for the 2.12 and 3.85 Mc/s. wanted waves and the time constant $\tau_{2.12}$ are predicted using the values of $Q(h_i)$ derived by the above method, and the electron density profiles given in Fig. 9 for noon on 4 November 1963 ($\chi = 15.5^o$) and 22 June 1964 ($\chi = 54^o$), respectively, have been demonstrated in Section 5 of Paper 3.2.1.

This process of normalizing the $Q(h_i)$ factors at two widely different levels to experimentally measured modulation depths makes the shape of the deduced electron density profile essentially independent of the magnetoionic theory used.

The x- and o-mode Type III Fejer curves for noon on 4 November 1963, from which the electron density profile in Fig. 9 has been derived, are reproduced in Fig. 13 of Paper 3.1.1. These curves were obtained using the ordinary 2.12 Mc/s. wanted wave, for which k_w'/N progressively decreases in magnitude below about 75 km. and passes through a zero at 61.5 km. (Fig. 10). This behavior for the wanted wave and the small electron densities does not allow an accurate deduction of the profile at heights below 65 km. For this reason the profile for 4 November 1963, and others in Fig. 9 obtained using the ordinary 2.12 Mc/s. wanted wave, have not been shown below the latter level. Since the x- and o-mode Fejer curves are essentially complementary, the combined data are of great value in the deduction of the profile. The noon profile in Fig. 9 for 22 June 1964 is also derived from combined x- and o-mode Type III data. Fig. 11 compares the o-mode Fejer curve of 4 November 1963 and its synthesis (broken line).

* For ease of comparison and analysis, experimentally measured modulation depths are scaled to a radiated power of 100 kw.

The absence of negative modulation on the experimental records in Fig. 12 and 13 of Paper 3.1.1 allows a conservative upper limit of 10 el.c.c. to be placed on the density near 58 km. This limit is consistent with extrapolations of the tails of the two noon profiles.

Measurements of wave interaction using a partial echo from the D region as a wanted echo provide a sensitive method of detecting low level ionization. The measurements of Smith et al. (1965), made during June and July 1962 using partial reflections from levels near 72 km., are consistent with the noon profile for 22 June 1964 and the extrapolation discussed above.

Each of the profiles shown in Fig. 9 has been truncated at the maximum height at which the electron density is considered to be reliable. The reason for this truncation is that, although each of the syntheses requires the use of height channels above the truncation level, the fractions of the radiated power reaching these heights are small and hence the deduced values of δ_i are unreliable.

4. The D region at sunrise

In order to facilitate discussion of the methods we have used to obtain the electron density profiles in Fig. 9 for the sunrise period, we note that the development which starts when the sun's zenith angle χ is about 98° has two aspects. One is the build-up of ionization in the tail of the nighttime E region, which continues past ground sunrise (G.S.R.). The other is the progressive formation of a distinct lower layer (C layer), which is essentially complete by G.S.R. and has an N_{max} of about 80 el.c.c. at a height of 65 km. At this stage the electron density at the ionization minimum near 80 km. is less than 10 el.c.c. Later development is shown by the other profiles in the figure.

Technically, wave interaction methods are far more difficult to apply during the twilight periods than at other times of the day because of the rapid variation and low density of the ionization and the general instability of wanted reflections from the higher regions. Fortunately, it has been possible by the use of extraordinary disturbing and wanted gyrowaves to achieve the necessary sensitivity, information rate, and echo stability during the sunrise period.

The absorption coefficients per electron of the exact extraordinary gyrowave (1.515 Mc/s.) and the extraordinary 1.78 Mc/s. wave are compared at different heights in Fig. 12. Below 65 km. the high values of the collision frequency make the absorption coefficients almost the same. Above this level the absorption coefficients progressively diverge and above 85 km. that of the exact gyrowave is larger by factors in excess of 20. These characteristics make the exact gyrowave the optimum disturbing wave in studies of the development of the C layer, but the wave has insufficient penetration to reveal much of the development of the lower E region. The use of the more penetrating 1.78 Mc/s. wave, on the other hand, shows more of the latter development, but reduces the sensitivity substantially near the top of the C layer. Broadcast restrictions confine the use of the exact gyrowave to the period from midnight to 0500 E.A.S.T., which limits the effective use of this wave in dawn studies to about three months in mid-summer.

The derivatives k_w'/N for the extraordinary and ordinary modes of the 2.12 Mc/s. wanted wave have been shown as functions of height in Fig. 10. Except in the height range 72-74 km., the magnitude of the derivative for the extraordinary mode is everywhere larger than that for the ordinary mode, by a factor of 25 at heights near 90 km. and by factors in excess of 3 in the height range 55-70 km. Since measurements must be made quickly during the sunrise period, the advantage of using the extraordinary mode for enhancement of the modulation depth is obvious. In place of the zero in k_w'/N for the ordinary mode at the height of 61.5 km., there is one at the height of 73 km. This is well above the level of maximum ionization in the C layer and the zero presents few problems.

At night the most frequently observed extraordinary 2.12 Mc/s. echo is from the F region. When χ is between 98° and 96°, the solar radiations, which have their maximum effect during the day at the peak of the E region, start producing electrons by photo-ionization in the E-F region (Setty et al. 1964). This electron production, which is simultaneous with that in the D region, first causes the group height of the F echo to increase by 50 to 100 km. in about 25 min. By this time the ionization in the E-F region has developed sufficiently for reflection and the group height falls to about 160 km. With further electron production the reflection may again change to a lower level. The initial movement of the echo does not affect the measurement of Type II Fejer curves, since the impressed modulation is a function of the delay DtE and with continuous variation of the delay of the disturbing pulse the echo may be "chased" by methods described in Smith et al. However, it can make that part of the Type III Fejer curve with the disturbing pulse preceding the wanted pulse difficult to analyze, since the time between the upward and downward transits of the disturbed region by the wanted pulse is continually changing. The echoes from the E-F region generally have a complex fluctuating structure, and satisfactory measurements using these echoes have been found to be impossible.

The extraordinary 2.12 Mc/s. echo from the sporadic E layer usually has a simple structure and a stable group height, and has been observed to persist, apart from temporary fading, in gradually diminishing strength for about an hour after G.S.R. Unfortunately, this far more satisfactory echo occurs infrequently and its duration is unpredictable, so that using it to obtain a complete set of observations covering the dawn period is a lengthy task.

The records reproduced in Fig. 13 are two of a sequence of five consecutive Type III Fejer curves obtained on 1 September 1964 using extraordinary 1.78 Mc/s. disturbing pulses of 83 kw. power and 60 μsec. duration from Station A, and an extraordinary 2.12 Mc/s. E echo. The duration of the output pulse from the receiver was 50 μsec., the integration time of the detector was about 2 sec., and the repetition rate of the wanted pulses was 333.3 p.p.s. The recording time between major vertical lines was $1\frac{1}{3}$ min. In order to reduce the time required to record a curve, the continuous drive for the delay was stopped after the first 450 μsec. of delay variation, and the decaying tail was measured at a number of fixed delays.

A feature of these records that needs some discussion is caused by the use of the high repetition rate of 333.3 p.p.s. Normally, when the time between consecutive wanted pulses is long compared to the duration of the transient heating by the disturbing pulse, zero modulation is recorded at a delay such as D350E, since the downcoming wanted pulse emerges from the D region before the upgoing disturbing pulse enters. If, because of a high pulse repetition rate, the electron cooling is incomplete by the transits of the normally undisturbed wanted pulse, then at such delays apparent negative modulation, "kickback", is recorded. In each part of Fig. 13 the instrument zero is the thickened line and the deflection for positive modulation is upwards. In the upper record the kickback is -1.5 small divisions; in the lower record it is negligible. The difference is due to the longer electron relaxation time when the upper record was taken. Effects from kickback are easily and accurately allowed for when small, as in this sequence, and are a small price to pay for the advantages in information rate from the use of the high pulse repetition rate.

The sequence of Type III Fejer curves obtained on 1 September 1964 is plotted in Fig. 14 for a disturbing power of 100 kw. Unfortunately, recording was not commenced until 0558 E.A.S.T. ($\chi = 93^{\circ}$) because of difficulties in linking the Stations A and C, but the echo persisted until 0700 E.A.S.T. allowing development to be studied to $\chi = 82^{\circ}$. Since each curve took about 11 min. to record and in this time χ changed by 2.3°, the curves cannot be regarded as "instantaneous" for deduction of electron density profiles. Such instantaneous curves, however, can be constructed from time plots of the modulation depth at fixed delays. Those shown as broken lines in the figure are derived in this way for the times at which the maxima of the negative modulation were recorded. This correction could not be made to the first curve of the sequence, since the negative part was recorded first, but could be made to the last. Corrections to the negative parts were found unnecessary,

because of the little variation between curves and the short time (∿ 2 min.) in which this part of each curve was recorded. The values of χ for the four instantaneous curves are 90.3°, 87.9°, 85.1° and 82.1°.

The Fejer curves in Fig. 14 are the sum of negative contributions with time constants shorter than 130 μsec. from the region below the level (73 km.) where k_w'/N is zero, and positive contributions with longer time constants from above this level. The positive and negative contributions overlap and their sum is zero at the delay of the "crossing point" from measured positive to negative modulation. Over the hour of measurement, the time constant of the positive decaying tail of the Fejer curve decreased from 1250 μsec., which is the value of the electron relaxation time at a height of 88.5 km., to 540 μsec., the value at 84 km. This decrease from ionization growth in the lower E region caused the sum of the positive contributions to change in shape and also, because the electron heating by the 60 μsec. disturbing pulse was more effective, to increase in magnitude. These changes, which were not accompanied after G.S.R. by any marked change in ionization below 73 km., have caused the progressive decrease by 50 μsec. in the delay of the crossing point. Syntheses have shown that the latter "eating away" of the measured negative modulation by positive modulation has not progressed to the negative peak until the last curve of the sequence ($\chi = 82.1^{\circ}$).

The insert to Fig. 15 illustrates a modified Type I experiment in which two 2.12 Mc/s. wanted pulses (labelled 2 and 3) are transmitted at fixed delays after a long (2 ms.) extraordinary disturbing pulse. This duration is sufficient to create near steady-state conditions in the lower E region and thus, to give the maximum ratio of positive to negative modulation. The first of the delays shown is long enough for the decay of negative modulation to be complete by the time that wanted pulse makes its upward transit. From the modulation depths impressed on the two wanted pulses, both the time constant and the steady value M_{ks} of the modulation impressed in the lower E region can be calculated. Electron production in this region causes the time constant to decrease but does not change the value of M_{ks}. Electrons produced below the E region absorb power from the disturbing wave and reduce the value of M_{ks}. Continuous measurements of this kind with a disturbing power of about 5 kw. were made on 23 and 30 September 1964, using the 1.78 Mc/s. disturbing wave, and on 6 January 1965 using the 1.515 Mc/s. wave. The experimental records of 6 January 1965 are reproduced in Fig. 15 and the time constants on the three mornings are plotted against χ in Fig. 16.

The fairly rough time constants measured using the more penetrating 1.78 Mc/s. disturbing wave are compatible with those given in Fig. 14, but show no clearly defined point from which the beginning of electron production in the lower E region can be inferred. Those measured using the 1.515 Mc/s. wave increase from 600 μsec. at $\chi_o = 103^{\circ}$, to 950 μsec. at 100°, and then fall, with a suggestion of a change in slope near 98°, to 500 μsec. at 92°. There is evidence, to be described elsewhere, that the initial increase in the time constant is not a peculiarity of this particular day, but is characteristic of the sunrise lower E region on many days. Some clarification of the significance of the time constant plot is provided by the records in Fig. 15 which show a well-defined onset when $\chi = 97.8^{\circ}$. Before this onset the measurements show a slow variation because of the simultaneous change in the time constant, but the calculated values of M_{ks} remain constant near the average nighttime value, indicating that the changes in the electron density profile causing the changes in the time constant were confined to the lower E region. At $\chi = 97.8^{\circ}$ the calculated value of M_{ks} starts to decrease substantially. This onset is thus due to absorption of power at levels below the E region and is presumably later than the onset of photo-detachment in the region itself.

The graphs plotted in Fig. 16 are further illustration of the variability of the ionization below 90 km. in the nighttime E region. That of 6 January 1965 shows the difficulty, because of the complex behavior of this already ionized region, of assigning a definite value to the largest zenith angle at which photo-detachment commences and, thus, of distinguishing between visible and ultraviolet solar radiation as the photo-detaching agent. (When $\chi = 98^{\circ}$, the height of closest approach to the earth of a ray reaching 85 km., assuming no refraction, is 22.3 km.; when $\chi = 99^{\circ}$, it is 6.4 km.).

On 8 and 22 June 1964, continuous measurements were made at the delay ($t_{N.P.}$) of the peak of the negative modulation at G.S.R. These, scaled to a disturbing power of 100 kw., are shown in Fig. 17 as a function of χ, together with a number of discrete values for other days in the same general period from Fejér curves obtained using the same 60 μsec. 1.78 Mc/s. disturbing pulse. The continuous measurements and some of the individual values are rather rough because of the poor quality of the wanted echoes. However, the essentially linear character of the initial increase, commencing when χ is 95.6° and complete when χ is about 91°, is definite.

When the ionization is so low that it absorbs only a small fraction of the disturbing power, the modulation depth impressed at each level is proportional to the electron density. While the C layer does not develop proportionately and simultaneously over its height range, so that an exact and simple interpretation of the plots in Fig. 17 is not possible, the change can roughly be taken as a measure of the variation of the electron density at the level (65 km.) of maximum ionization of the fully developed layer. Using the value of 80 el.c.c. for N_{max} this simple interpretation gives $\sim$ 0.06 el.c.c./sec. as the rate of increase of electron density at 65 km. The significance of the apparent small decrease in the modulation depth when $\chi < 91°$ is discussed later.

Although superior for the deduction of electron density profiles, Type III Fejer curves require a considerable recording time ($\sim$ 11 min.), which can be a handicap for studying the initial rapid development of the C layer. For this reason, a series of Type II curves was obtained on 8 January 1965 using the highly absorbed 1.515 Mc/s. disturbing wave to examine the characteristics of this development in detail rather than to be a source of electron density profiles. The power of the 60 μsec. disturbing pulse was 112 kw. and the extraordinary 2.12 Mc/s. wanted echo was from the E region. Except for the use of a wanted pulse repetition rate of 166.6 p.p.s., other experimental parameters were the same as for 1 September 1964. The measurements commenced at 0348 E.A.S.T. (χ = 104.1°) and ceased at 0521 E.A.S.T. (χ= 86.6°) when the echo disappeared. During the first 24 min. (104.1° > χ > 99.6°), the wanted echo faded periodically and four curves obtained in this time were somewhat spoilt by noise. The remainder, with superimposed dotted lines to represent the scalings, are reproduced in Fig. 18 to 22 and plotted as a sequence in Fig. 23 for a disturbing power of 100 kw. The values of χ quoted in the latter figure to identify the curves are those corresponding to the times of measurement of the start of positive modulation in the early curves and at the delay D450E in the later curves showing negative modulation (see Fig. 18-22). The absence in this sequence of records of kickback as seen in that of 1 September 1964 is due to both the lower pulse repetition rate and the shorter time constant from the use of the exact extraordinary gyrowave.

The four curves recorded when χ was between 104.1° and 99.6° show no significant variation. However, their comparison with those at 98.8° and 98.1° indicate a lower height of absorption of the disturbing wave at the latter values of χ. This is consistent with the suggestion made in the discussion of Fig. 15 and 16 that photo-detachment in the lower E region occurs before χ = 97.8°. The impressed modulation progressively moves down in delay until at χ = 95.4° the C layer has developed sufficiently below 73 km., the level of the zero in k_w'/N, for the curve at this value of χ to show negative modulation. The negative modulation continues to develop until about G.S.R.

After G.S.R. there is an apparent small decay of the C layer. The negative parts of the corresponding curves in Fig. 23 can only be synthesized with such a decay, and the same is true for the curves of 1 September 1964. It is also implied by the data plotted in Fig. 17. This decay could explain the well-known plateau observed after G.S.R. in long wave propagation data (Bracewell et al. 1951), and has considerable bearing on the rates of processes occurring in the D region. Nevertheless, it is felt that the data are as yet too scant to establish the decay unequivocally and so to justify the inclusion of electron density profiles in Fig. 9 showing this behavior.

Except for the nighttime profiles of 3 and 6 September 1963, each profile given in Fig. 9 is identified both by a date and value of χ. The four shown for 1 September 1964 have been deduced from the corresponding instantaneous Type III Fejer curves plotted in Fig. 14.

These profiles are for times later than G.S.R., and their common part below the E region tail is a mean of the profiles derived from the four Fejer curves. The use of the 1.78 Mc/s. disturbing wave and the much greater ionization at lower and higher levels have not permitted in the first three profiles an accurate deduction of the shapes of the minima near 80 km., and these minima are shown as broken lines.

The unusual and distinctive characteristics of the sunrise Fejer curves with their positive and negative modulation gives them effectively two "onsets". This greatly improves the height resolution and made possible the deduction of the profiles in Fig. 9 for 8 January 1965 from the Type II curves plotted in Fig. 23. However, the lack of complete Type III data has reduced the information available on the upper parts of the profiles and those shown above 80 km. for this day should be regarded as models of the E region development before G.S.R. which produce a match to the Fejer curves. The use of the highly absorbed 1.515 Mc/s. disturbing wave and the absence of underlying ionization have permitted the continuation of the first two of the profiles to electron densities as small as 1 el.c.c.

The profiles given in Fig. 9 for values of χ of 76.3°, 66° and 62.7° are derived from Type III Fejer curves obtained on 22 June 1964 using the extraordinary 1.78 Mc/s. disturbing pulse and an ordinary 2.12 Mc/s. wanted echo from the E region. The upper truncation of these profiles gets progressively lower in height as the penetration of the extraordinary disturbing pulse decreases.

5. Ionization in the nighttime lower D region

In Fig. 17 we showed that at the delay $t_{N.P.}$ defined in the previous section the negative modulation is above the threshold of detection for the recording sensitivities used when $\chi = 95.6^{\circ}$ and attains a maximum value of about -0.45 per cent for a disturbing power of 100 kw. just before G.S.R. Since in a simple interpretation the modulation at this delay can be taken as proportional to the electron density at the level (65 km.) of maximum ionization of the fully developed C layer, its value during the night is of considerable interest.

Since October 1962, 40 nighttime Fejer curves of Types II and III have been recorded for other purposes using extraordinary 1.515 Mc/s. disturbing pulses and extraordinary 2.12 Mc/s. wanted pulses. These curves show no evidence of negative modulation and generally allow an upper limit of about 0.01 per cent to be placed on its absolute magnitude. For a number of the curves, such as that of 24 October 1962 (Fig. 11, Paper 3.1.1), the limit can be reduced to about 0.005 per cent. For that curve the peak-to-peak noise fluctuation at the delay $t_{N.P.}$ is equivalent to a modulation depth $\sim$0.008 per cent and the mean value, to which no significance is attached, is -0.003 per cent.

The search for nighttime negative modulation, which we now describe, was made on 7 September 1964, when a strong and steady extraordinary 2.12 Mc/s. wanted echo from the E region and a low level of external noise and interference allowed the use of the maximum recording gain. The power of the 60 μsec. extraordinary 1.515 Mc/s. disturbing pulse from Station A was 127 kw., the wanted pulse repetition rate was 166.6 p.p.s., and simultaneous measurements were made using the receiving units 2 and 3 at Station C*. Duration of the output pulse from the receiver of Unit 2 was 50 μsec.; that of Unit 3 was 10 μsec. The use of the latter pulse made the records of Unit 3 slightly inferior to those of Unit 2, which are reproduced in Fig. 24. After the first two measurements shown in this figure, the integration time of the detector was increased from 5 to 20 sec.

Alternate measurements were made at the delay $t_{N.P.}$ (D476E, Unit 2; D490E, Unit 3) and at a delay (D120E, Unit 2; D134E, Unit 3) for which the true modulation depth must be zero. The measured modulation depths are given in Table 1 for a disturbing power of 100 kw.;

* Unit 1 is at Station A.

the value for the shorter delay has been caused entirely by kickback. In correcting for the kickback, we have used data from a Type III Fejer curve, which was recorded immediately before the tabulated measurements were made. This curve has a peak modulation depth of 2.96 per cent and an initial time constant of decay from this peak of 740 μsec. To illustrate how the correction has been made we show the calculations for data from Unit 2.

TABLE 1

TIME (E.A.S.T.)	Mean Modulation Depth (%)			
	UNIT 2		UNIT 3	
	D476E	D120E	D490E	D134E
0428-0432	-.0034		-.0034	
0432-0435		-.0037		-.0049
0438-0447	-.0031		-.0031	
0447-0453		-.0052		-.0055
0455-0505	-.0034		-.0043	
0505-0509		-.0032		-.0024
0509-0515	-.0032		-.0024	
0515-0517		-.0042		-.0043
MEAN	-.0033	-.0041	-.0033	-.0043
TRUE MEAN MODULATION DEPTH (%)	-.0004		-.0002	

In 6 ms., the time between consecutive wanted pulses, exponential decay with a time constant of 740 μsec. would reduce the modulation depth of 2.96 per cent to 2.96 exp(-8.1) per cent, i.e., to 0.0009 per cent. In 12 ms., the time between consecutive disturbing pulses, the modulation depth would become negligible. Thus, were the decay to be an exact exponential, the kickback at the delay D120E would be -0.0009 per cent instead of the measured value of -0.0041 per cent. The decay, however, is not an exact exponential (Paper 3.2.1), and the latter value requires an average time constant over the 6 ms. of decay of 910 μsec. The actual time constant after 6 ms. of decay will be longer than this average and has been taken to be 1100 μsec. The true mean modulation depth in per cent at the delay $t_{N.P.}$ is

$$-0.0033 + 0.0041 \exp(-356/1100)$$

where 356 is the difference in microseconds between the delays D476E and D120E and the last term is the calculated value of the kickback at the delay D476E. It is noted that the uncertainty in the value of the time constant used in the calculation of the latter term is of small consequence. Thus, had it been taken as 900 or 1300 μsec., the true mean modulation depth for Unit 2 would have been -0.0005 per cent or -0.0002 per cent, respectively, in place of the tabulated value of -0.0004 per cent.

Conservatively, we conclude that the negative modulation at the delay $t_{N.P.}$ does not exceed 0.001 per cent in absolute magnitude. Since the modulation depth of -0.45 per cent corresponds to an electron density at 65 km. of 80 el.c.c., the density near this level at night must be less than 0.2 el.c.c. If it is assumed that the electrons detected at G.S.R. have all been detached from negative ions, then the value of the nighttime negative ion to electron ratio near 65 km. is in excess of 450.

6. Concluding remarks

In this paper, electron density profiles for the lower ionosphere from night to maximum ionization at noon have been presented and an upper limit placed on the electron density at night near 65 km. The profiles show that at first light there is a growth of ionization in the lower E region and the development of a distinct layer with maximum ionization near 65 km. While the formation of the latter layer is complete by G.S.R., the lower E region continues to develop and its growth is accompanied by the formation of a ledge of ionization near 75 km., whose density is much greater than that of the original sunrise layer. While the general characteristics of the development are clear from these profiles, there are a number of aspects which require some comments, the most important of which is the question of the typicalness of the profiles.

In Paper 3.2.1, attention was drawn to the two distinct groupings of the time constants measured near noon on random days in July, August, and November 1963 using the extraordinary 1.78 Mc/s. disturbing wave. This was considered indicative of both solar control and stability of the quiet lower D region. Over the four-year period from mid-1962, more than 250 time constants, covering values of χ up to 85°, have been determined from Type I data and Type III Fejer curves using this disturbing wave. When the time constants are plotted against χ, the diurnal pattern thus established shows no statistically significant variation over this period, and a high degree of stability of the ionization in the region disturbed by this wave is evident. This simple analysis and comparison of the Fejer curves give no reason for assuming that the daytime profiles presented are not typical.

The main features of the development of the sunrise layer are without question. There are, however, insufficient data to discuss its day-to-day stability, and hence determine whether the difference between the profiles for 1 September 1964 and 8 January 1965 is a seasonal or a random fluctuation. Nor is it yet possible to establish the behavior of the layer after G.S.R.

Because of the steep gradient of the ionization, the determination of the electron density profile for the nighttime lower E region presents special problems and a resonance method has been used to derive the two profiles given in Fig. 9. Unlike those deduced from Fejer curves, the form of the profile yielded by this method is dependent on the magnetoionic theory used in the analysis. The height difference of the two profiles is typical of changes from night to night revealed by the time constant measurements discussed in Section 4 of Paper 3.2.1. Those measurements also show that changes, which have no preferred sense, occur during the night and are presumably caused by movements. Such movements make it difficult to establish the precise onset of initial dawn effects in this ionized region. As yet, the significance of an upward movement occurring on many days in the pre-dawn period cannot be assessed.

Acknowledgments

The research reported here was sponsored by the Air Force Cambridge Research Laboratories under Contract AF19(604)-6177 and supported in part by the Defense Atomic Research Agency, Washington, D.C. under Subtask 07010, by the Air Force Office of Scientific Research under Contract AF-AFOSR-952-65, and by the Radio Research Board of Australia.

REFERENCES

Bracewell, R.N., Budden, K.G., Ratcliffe, J.A., Straker, T.W. and K. Weekes. Proc. Inst. Elect. Engrs., 98, III, 221. 1951.

Martyn, D.F. Proc. Phys. Soc., 47, 334. 1935.

Mechtly, E.A. Ionospheric Res. Sci. Rept. No. 160, Penn. State University. 1962.

Nertney, R.J. J. Atmos. Terr. Phys., 3, 92. 1953.

Parkinson, R.W. J. Atmos. Terr. Phys. 7, 203. 1955.

Sen, H.K. and A.A. Wyller. J. Geophys. Res., 65, 3931. 1960.

Setty, C.S.G.K., Smith, R.A. and I.A. Bourne. Sci. Rept. No. 2., Contract No. AF19(604)-6177, University of New England. 1964.

Smith R.A., Bourne, I.A., Loch, R.G., Setty, C.S.G.K., Coyne, T.N.R., Barratt, P.H. and B.S.N. Prasad. Sci. Rept. No. 3 and Final Rept., Contract No. AF19(604)-6177, University of New England. 1965.

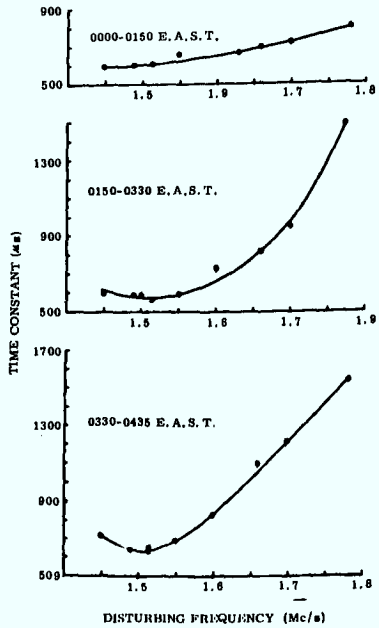

Fig. 1. Variation of the time constant of Type I data with disturbing frequency observed on 9 August 1963.

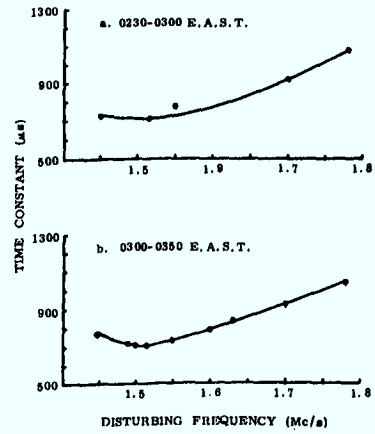

Fig. 2. Variation of the time constant of Type I data with disturbing frequency observed on 3 September 1963.

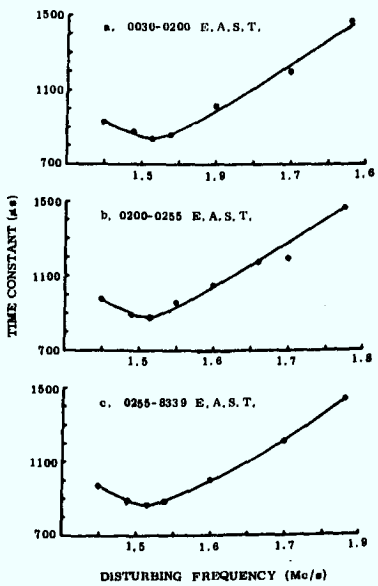

Fig. 3. Variation of the time constant of Type I data with disturbing frequency observed on 6 September 1963.

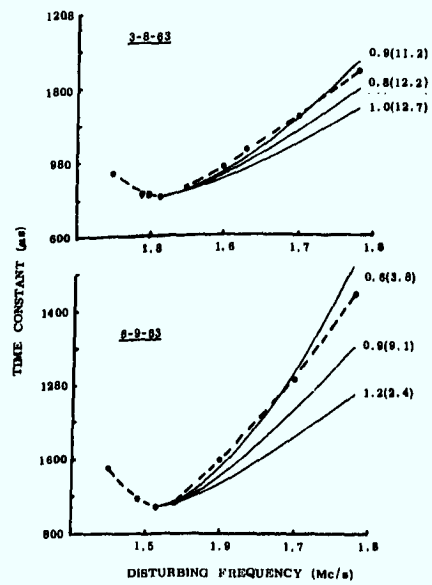

Fig. 4. Comparison of the observed dependence of time constant on disturbing frequency and that computed using exponential electron density profiles (Appleton-Hartree magnetoionic theory).

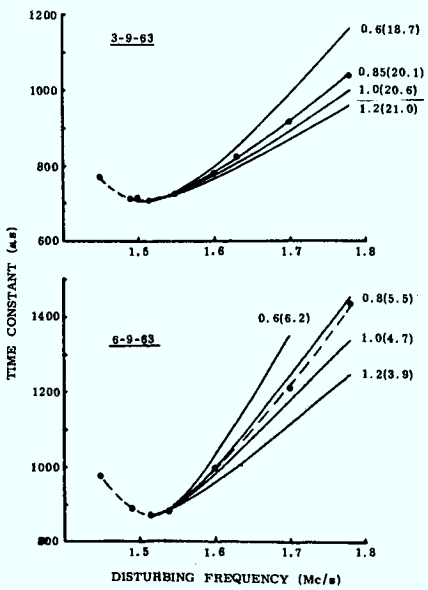

Fig. 5. Comparison of the observed dependence of time constant on disturbing frequency and that computed using exponential electron density profiles (generalized magnetoionic theory for a constant collision cross-section).

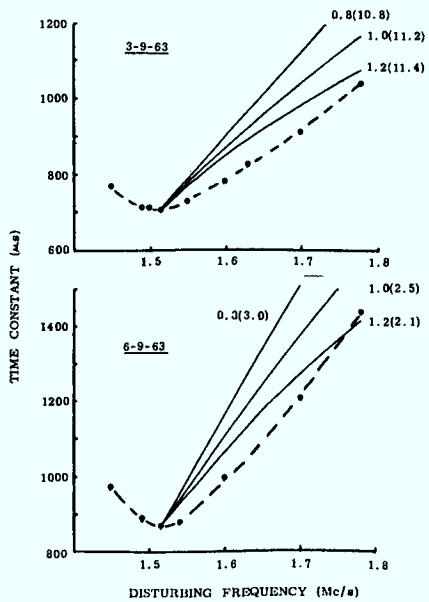

Fig. 6. Comparison of the observed dependence of time constant on disturbing frequency and that computed using exponential electron density profiles (generalized magnetoionic theory of Sen and Wyller).

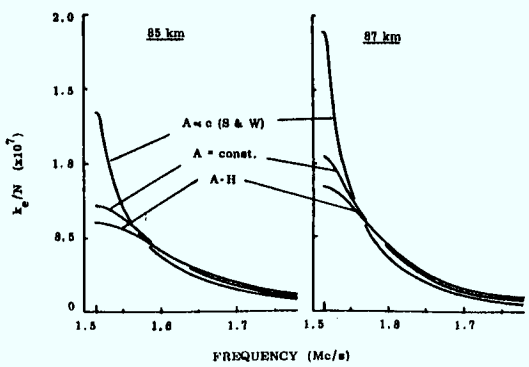

Fig. 7. k_e/N for the extraordinary mode as a function of wave frequency at heights of 85 and 87 km. for the three magnetoionic theories.

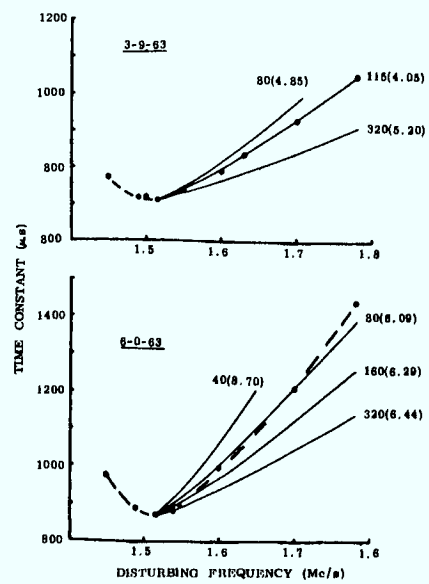

Fig. 8. Comparison of the observed dependence of time constant on disturbing frequency and that computed using linear electron density profiles (generalized magnetoionic theory of Sen and Wyller).

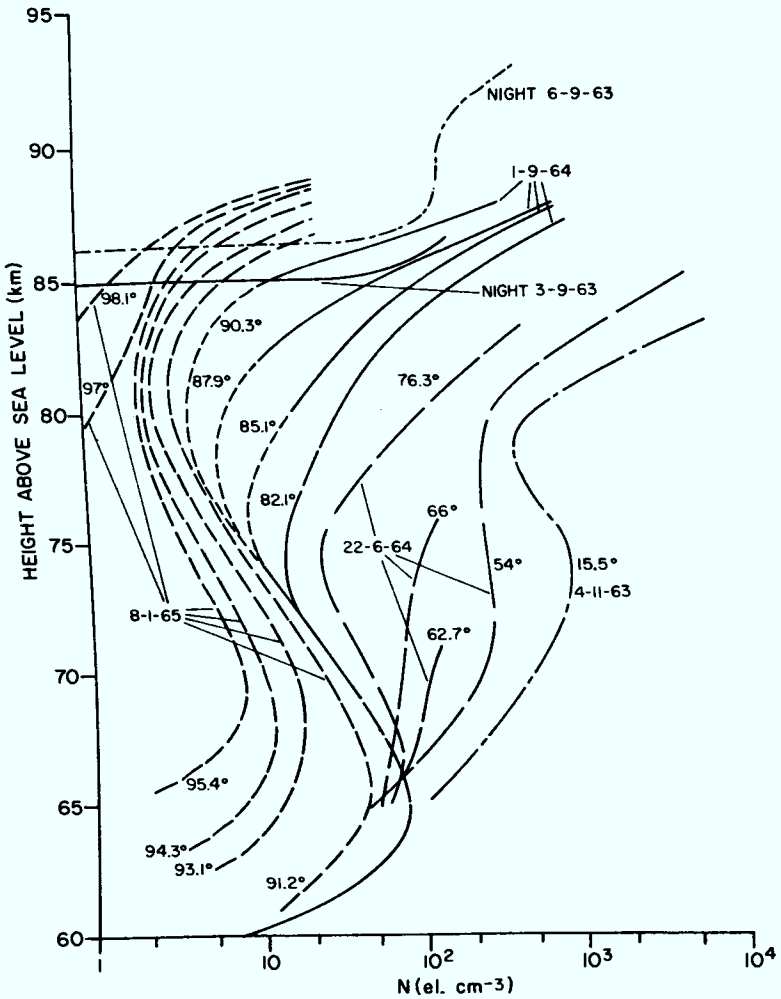

Fig. 9. Electron density profiles for night, dawn and daytime periods.

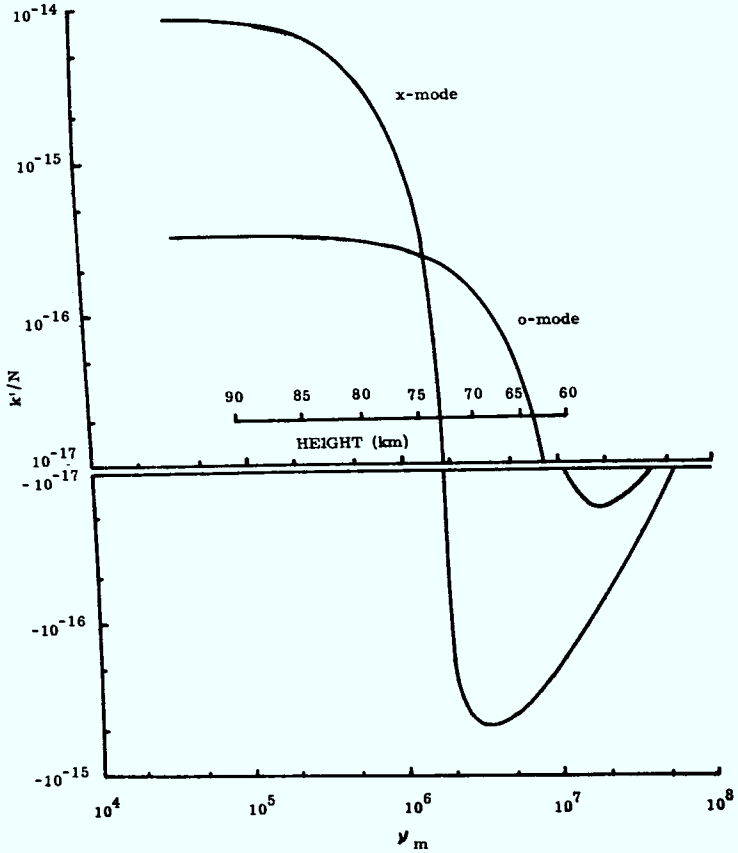

Fig. 10. Variation of k'/N for ordinary and extraordinary 2.12 Mc/s. waves with height and collision frequency (Sen and Wyller magneto-ionic theory).

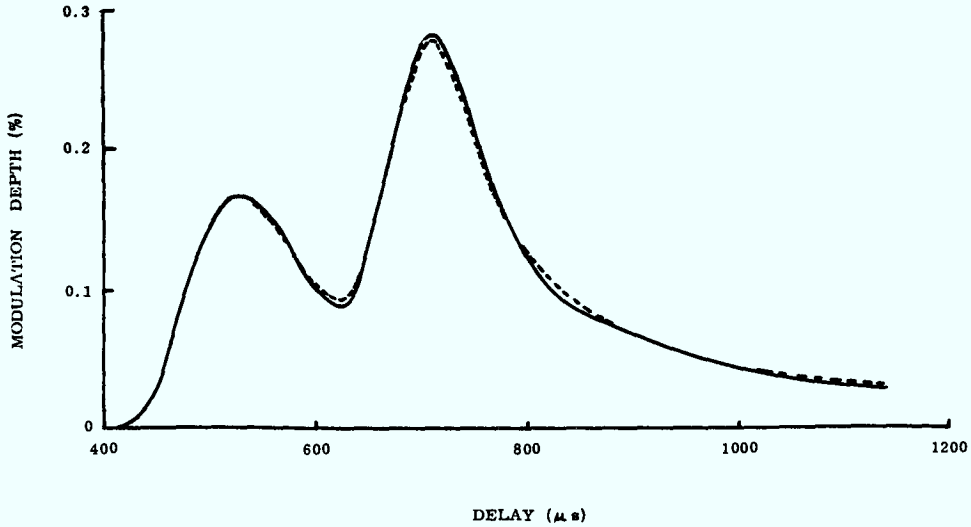

Fig. 11. Comparison of the noon o-mode Fejer curve of 4 November 1963 and its synthesis (broken line).

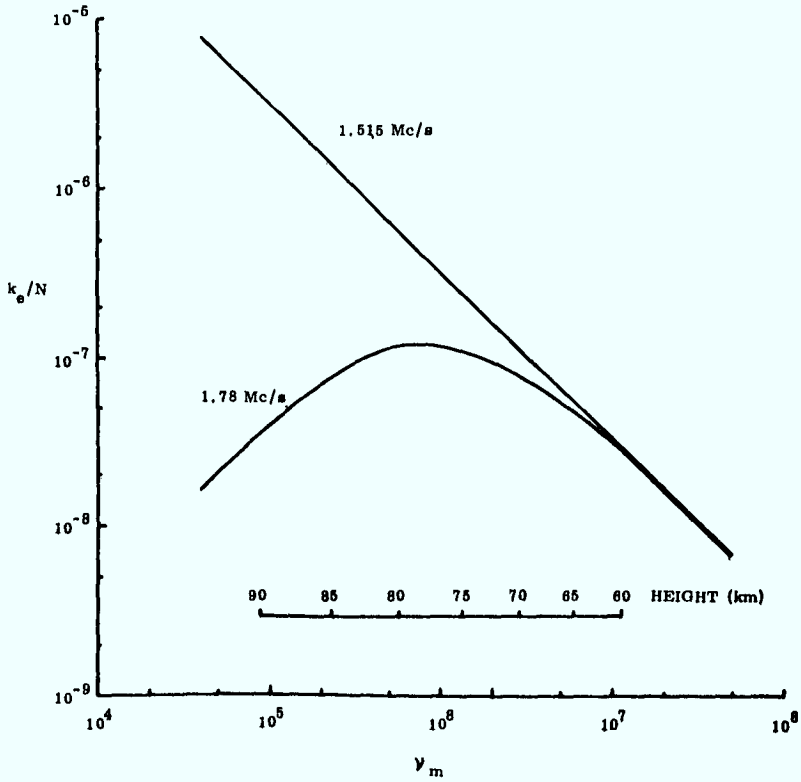

Fig. 12. Variation of k_e/N for extraordinary 1.515 and 1.78 Mc/s. waves with height and collision frequency (Sen and Wyller magnetoionic theory).

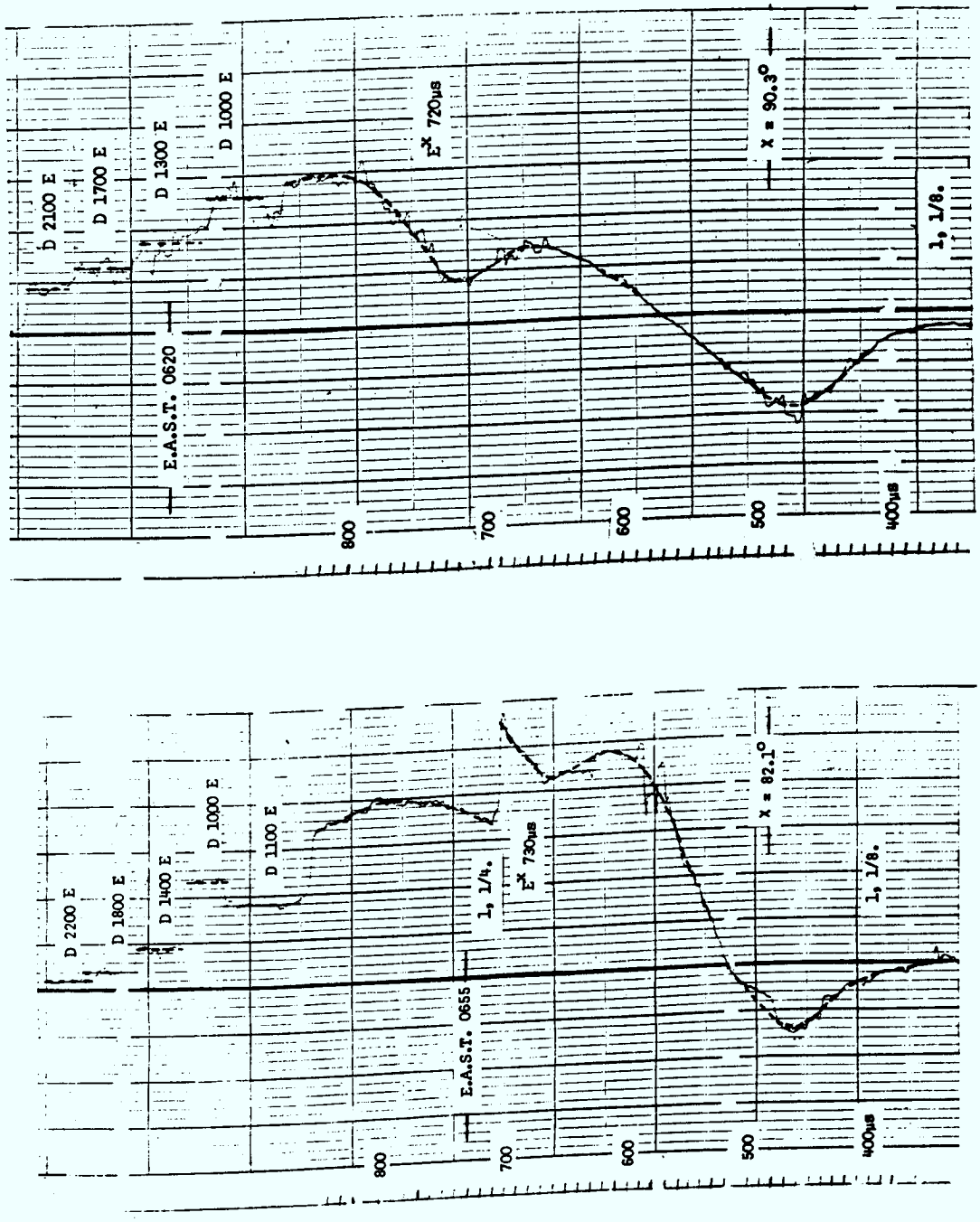

Fig 13. Two of the sequence of five Type III Fejer curves obtained near sunrise on 1 September 1964.

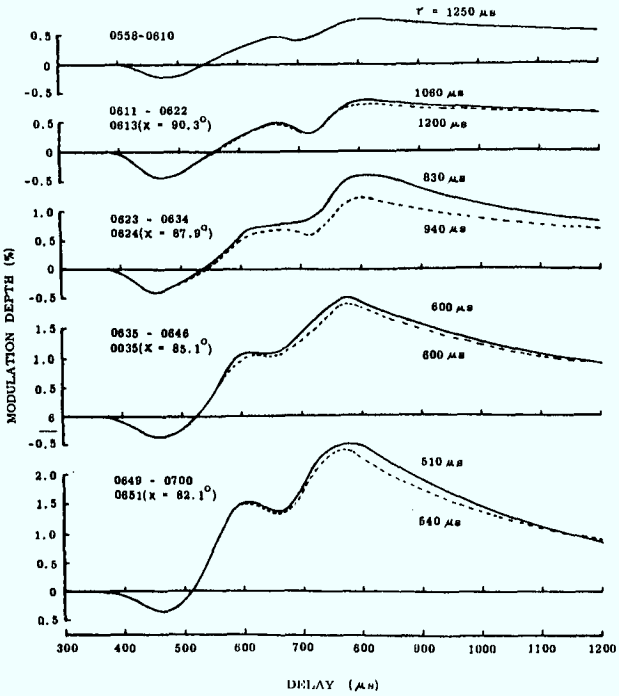

Fig. 14. Fejer curves obtained near sunrise on 1 September 1964 scaled to a power of 100 kw. The solid curves are smooth plots of the actual measurements in the time intervals shown. The broken lines show the instantaneous curves for the times at which the peaks of the negative modulation were recorded.

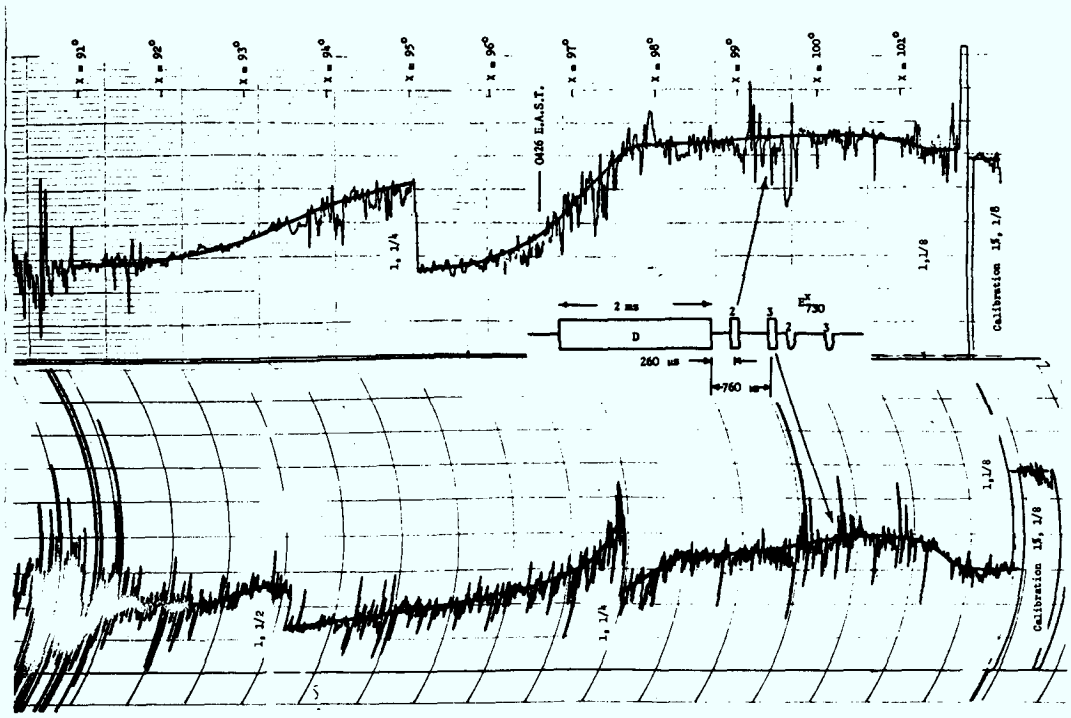

Fig. 15. Continuous Type I records obtained near sunrise on 6 January 1965.

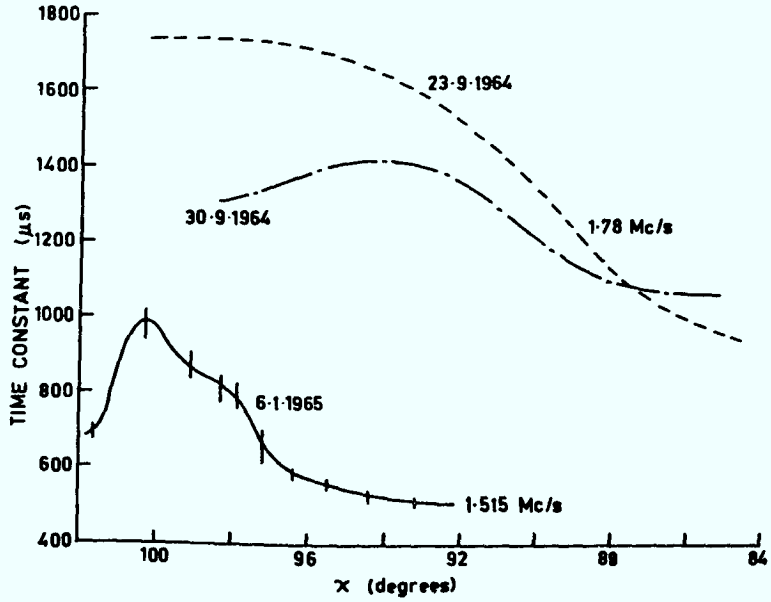

Fig. 16. Variation of time constant with χ near sunrise.

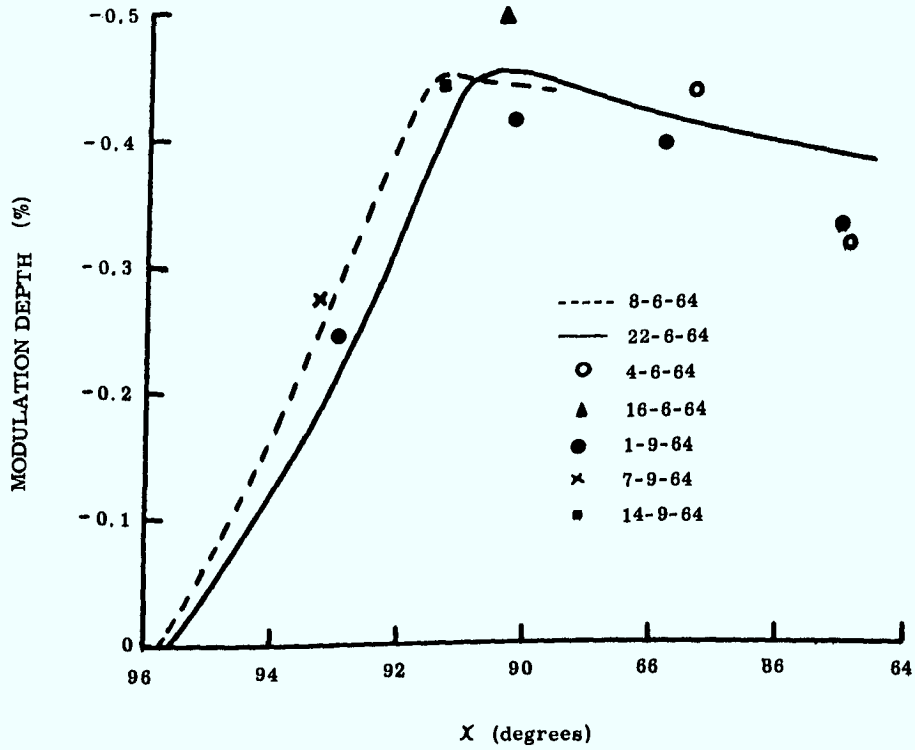

Fig. 17. Negative modulation at a fixed delay as a function of χ.

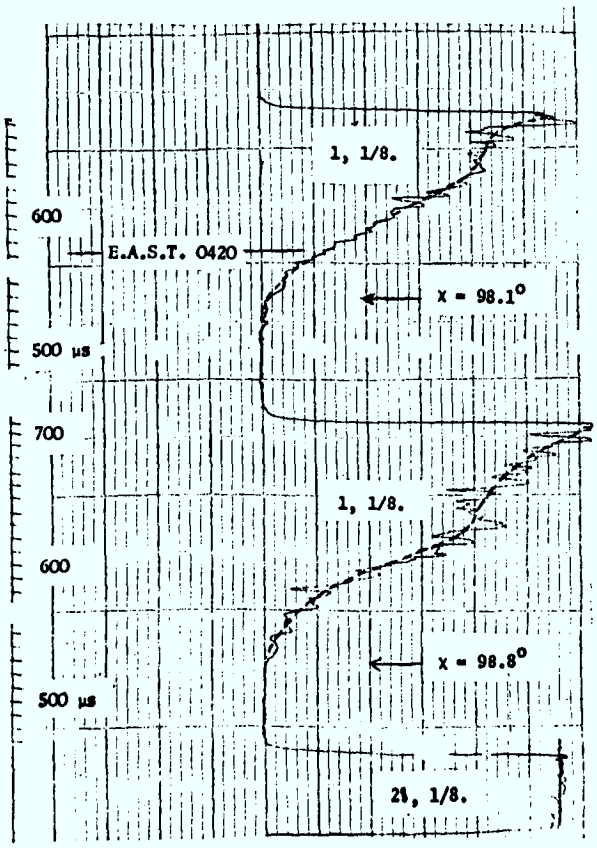

Fig. 18. Type II Fejer curves obtained near sunrise on 8 January 1965.

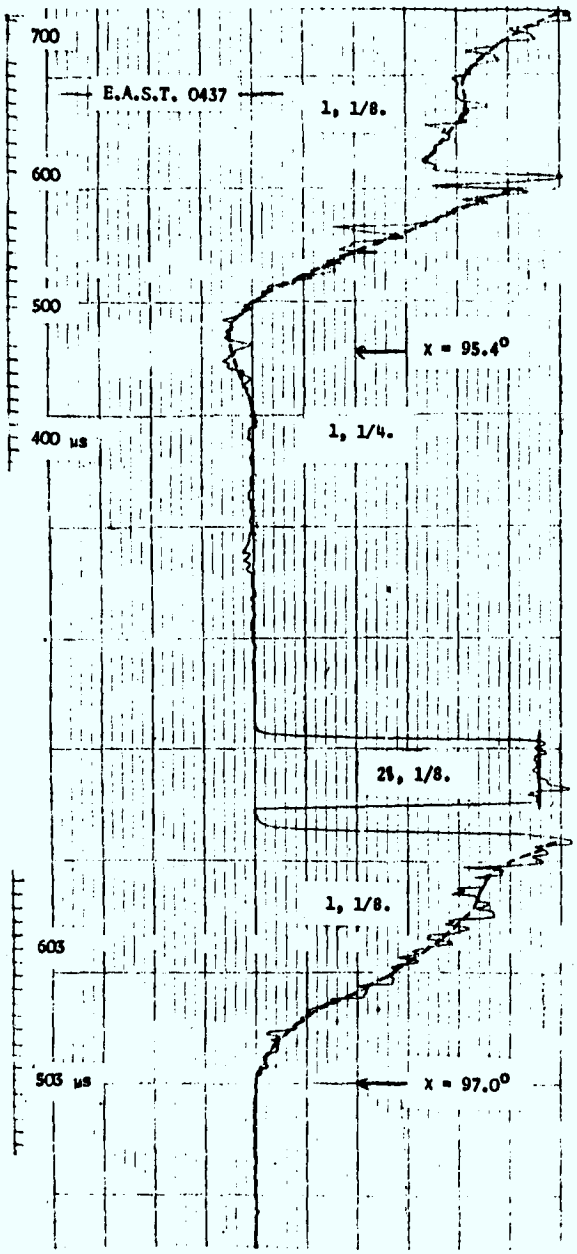

Fig. 19. Type II Fejer curves obtained near sunrise on 8 January 1965.

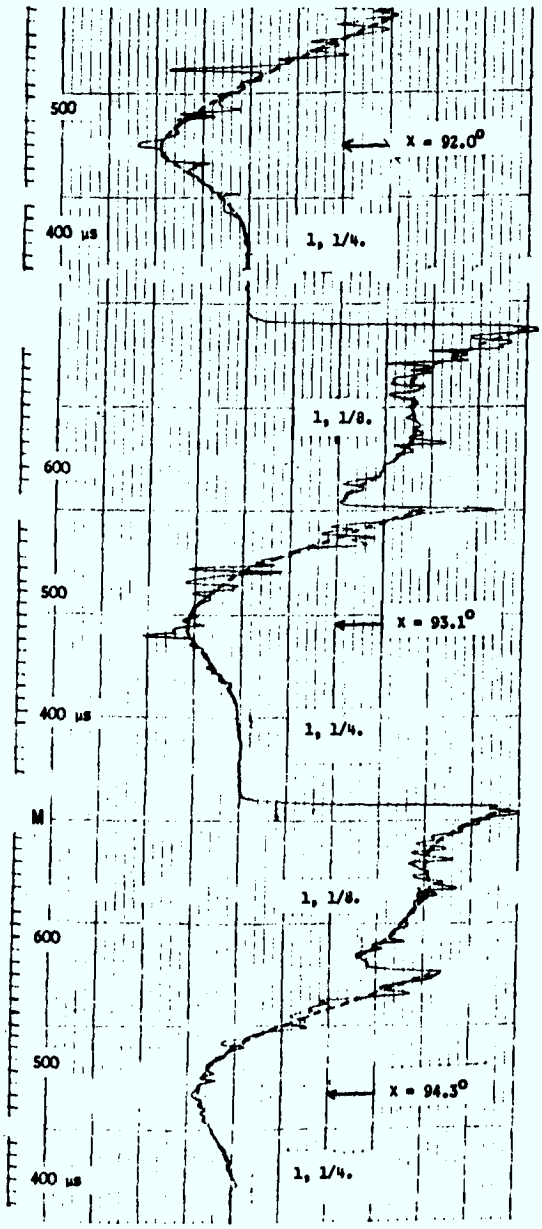

Fig. 20. Type II Fejer curves obtained near sunrise on 8 January 1965.

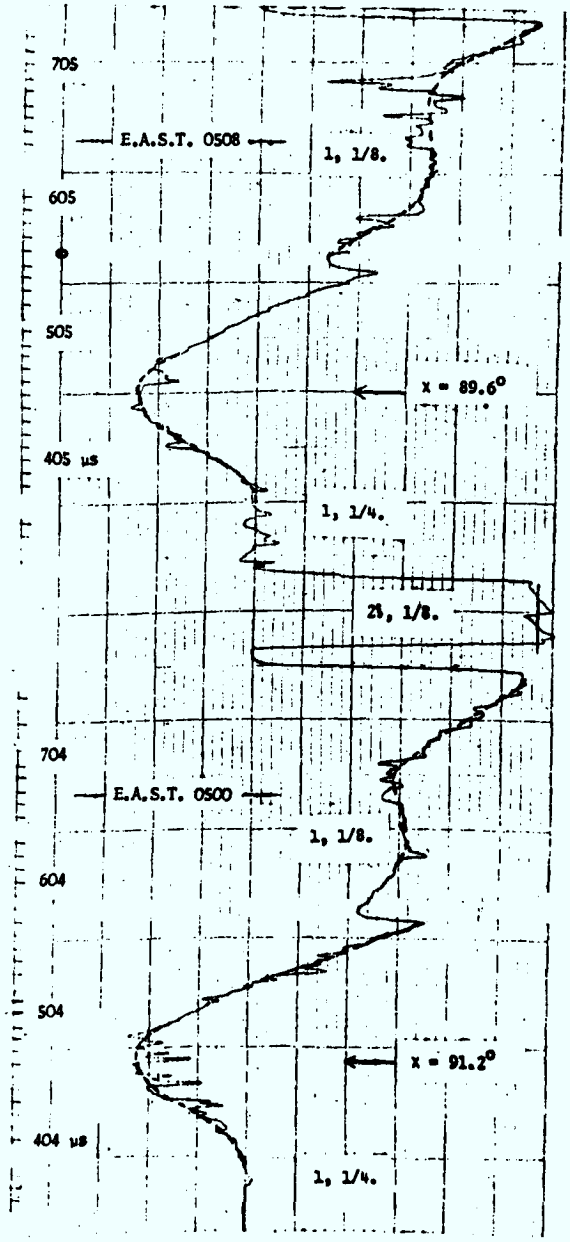

Fig. 21. Type II Fejer curves obtained near sunrise on 8 January 1965.

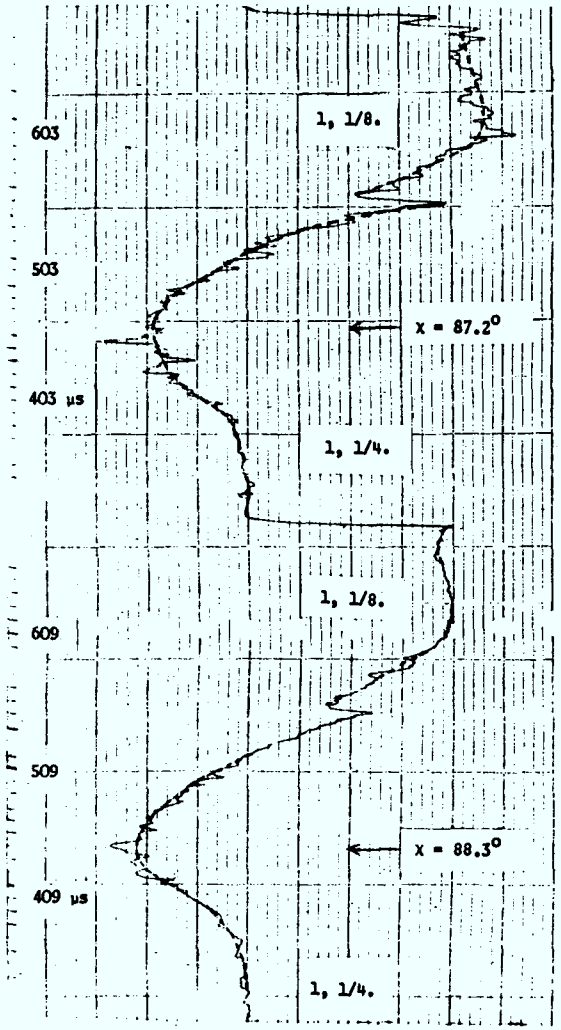

Fig. 22. Type II Fejer curves obtained near sunrise on 8 January 1965.

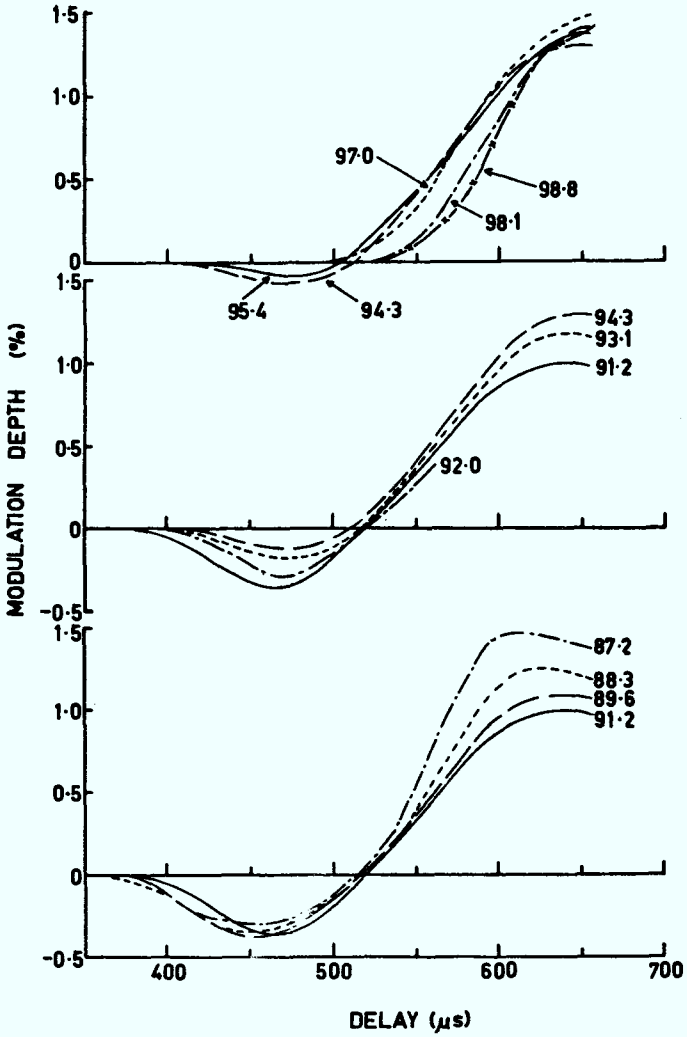

Fig. 23. Smooth plots, scaled to a disturbing power of 100 kw., of the Type II Fejer curves obtained near sunrise on 8 January 1965.

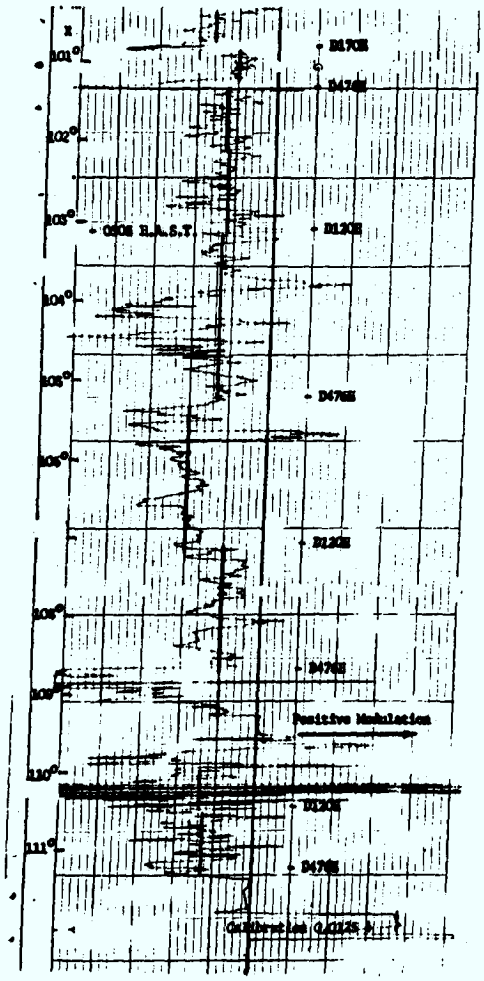

Fig. 24. Experimental record of 7 September 1964 in search for pre-dawn negative modulation.

Discussion on Paper 3.2.4 presented by R.A. Smith

Pfister: Did I understand that you first notice the sunrise effect when the visible light strikes the height level that you are studying?

Smith: The effect is seen at $\chi = 85^\circ$ when the ground glazing visible light strikes the region.

Pfister: Your data show a smooth variation. The VLF data have shown in quite a number of cases that the sunrise occurs in two steps. The implication was that we were dealing with the ultraviolet and the visible light which came at different times. If I remember correctly, Bowhill concluded from his rocket experiment that there is no effect from the visible light and that only the effect of the ultraviolet light is evident.

Smith: You cannot expect this type of work to produce lots of data unless you spend a lot of time and work hard at it. The data we have is consistent with what I have shown. If you want me to look for a discontinuity, day after day, in the downward development, then I would say I will need a dozen men to do it.

It is hard work but there is no question about the heights or about the time or about the release of 1 or 2 electrons up there. The discontinuities can be studied, but it might take a year or two to get a lot of data for just this one type of observation. The point is that it can be done.

3.3.1 HARMONIC GENERATION IN THE IONOSPHERE

by

R.E. Barrington

Radio Physics Laboratory
Defence Research Telecommunications Establishment
Ottawa, Canada

Although the propagation of radio waves within the ionosphere has, in general, been treated using a linearized theory, it is well known that the equations governing such propagation contain several non-linear terms. These non-linear terms can usually be neglected because of the rather low amplitude, within the ionosphere, of radio signals radiated from the ground. With the development of increasingly powerful transmitters, coupled to antenna systems of narrow beamwidth and the advent of rocket- and satellite-borne radio transmitters, the importance of and interest in non-linear effects within the ionosphere has steadily increased.

Certainly the ionospheric non-linearity that has received the greatest attention up to the present is that associated with the "Luxembourg effect" or cross-modulation. This is essentially a DC phenomenon in that changes that occur within a wave period are not important compared with the average change in collision frequency produced by the disturbing wave over many wave periods. Nevertheless, the very existence of this phenomenon means that the ionospheric collision frequency is sensitive to the energy of the colliding electrons and hence is a source of non-linear behavior.

In addition to the non-linearities introduced by collisional terms, there are at least three others that occur in the equations governing the ionosphere, even in a non-relativistic mean-value theory of homogeneous plane-wave propagation. In such a theory, the macroscopic electronic current must be evaluated and this is given by the product of mean particle density N, and mean particle velocity U, and since both these quantities have components varying in space and time, the electronic current has non-linear terms associated with it. The mean particle acceleration produced by an electromagnetic wave in the ionosphere is $\frac{dU}{dt} = \partial U/_{\partial t} + U.\nabla U$. The term $U.\nabla U$ is non-linear. Finally the magnetic force acting on the ionospheric electrons depends on UXH where H the macroscopic magnetic field has a varying component due to the magnetic field of the wave in addition to the steady component of the earth's magnetic field.

Since several different mechanisms may contribute to the non-linear behavior of ionospheric propagation, it is of interest to assess the relative importance of these processes. If consideration is restricted to harmonic generation or frequency mixing, the most important parameter is the ratio of the amplitudes of the harmonic or combination frequency components to the amplitudes of the exciting waves. It can be shown that this ratio may be of order $\frac{nU}{c}$ for the non-linearities of the current density, the magnetic force, and the acceleration terms. Here n is the refractive index of the wave, U is the mean electron velocity due to

the wave, and c is the velocity of light. If it is assumed that the electron collision frequency is proportional to electron energy, then the non-linearity of the collision term leads to a ratio of linear to non-linear terms of order $\frac{\nu}{\omega}\left(\frac{U}{V_{rms}}\right)^2$ where ν is collision frequency, ω is wave frequency, and V_{rms} is the root mean square velocity of the electrons. It should be emphasized at this point that these are only order of magnitude evaluations of this ratio, and refer only to the amplitude of the harmonic or combination frequency components of the electronic current at a point in the medium rather than to wave amplitude ratios.

These simple expressions lead to two important conclusions about non-linear behavior in the ionosphere. From the expression $\frac{nU}{c}$ it is seen that some non-linearities become important only when the electron velocity approaches c or, more importantly, when the refractive index becomes large, i.e. in the vicinity of a resonance of the medium. On the other hand, the collisional non-linearity becomes important when the electron velocity associated with the wave approaches the mean thermal velocity of the electrons, provided the wave frequency is of the order of the collision frequency. Both of these criteria for the collisional non-linearity to be important can be satisfied by some of the powerful HF transmitters available today, if attention is limited to the D and E regions of the ionosphere.

If harmonic generation or frequency mixing in the ionosphere is to be observed on the ground or at a site remote from the interaction region, then it is not sufficient that large amplitude currents at the harmonic or combination frequencies be established in the ionosphere by the exciting wave or waves. In addition, the phase relation between these currents at various points in the interaction region must be considered. Generally the requirement is that the phase relation of these currents must match that of a magnetoionic mode at the harmonic or combination frequency and propagating towards the receiver. It is not necessary that such a match exists over the entire interaction region, but only over a significant fraction of it. In general, this coherence condition on the generation of a harmonic or combination frequency may be of considerable value, since it means that the generation is restricted to small volumes of the medium at a particular height. Thus if such processes can be observed and interpreted, they would become powerful diagnostic tools for ionospheric study.

The possibility of detecting harmonic frequencies generated in the D region by collisional processes was studied both theoretically and experimentally at DRTE about three years ago. The component of the electronic current at the third harmonic of the frequency of a downward propagating wave was evaluated using Boltzman's equation and a perturbation technique, assuming a Maxwellian velocity distribution for the electrons. The calculation was done for the third harmonic component since the non-linearity associated with the energy dependence of the collision frequency produces only odd harmonic components. It was found that there is no harmonic generation for a circularly polarized wave, and that conditions are most favorable with linear polarization. Thus it appeared that the third harmonic would most likely be generated near the reflection height, since there the wave must be linearly polarized. This is, however, not the region where one would expect the highest values of ν or U. However, calculations of the amplitude that might be expected for the third harmonic indicated that for the parameters of the DRTE system, i.e., a one-megawatt peak, pulsed transmitter operating at a frequency of 2.66 Mc/s. and coupled to an antenna system with a gain of 10 to 12 db, this signal would have an amplitude of between 10^{-5} and 10^{-6} that of the main echo at the fundamental frequency. This was about the limit of sensitivity of the receiving equipment under the best possible conditions, and no positive evidence of a third harmonic component generated in the ionosphere was found.

The advent of topside sounder satellites, with powerful transmitters (up to 400 watts peak pulse power) has made possible the observation of non-linear behavior associated with resonances of the medium. The sounder experiments that have been orbited are not ideal from this point of view, since the receiver is invariably tuned to the transmitter frequency. In

spite of this limitation, echoes associated with a non-linear response in a region remote from the satellite have been observed. It was found that delayed signals at the transmitted frequency appeared to originate at a height where the wave frequency was twice the local gyro-frequency. While the interpretation of these observations is being developed, it provides one of the first examples of ionospheric non-linear behavior in which radio frequency signals are produced, rather than merely modified in phase or amplitude as in the Luxembourg effect. Undoubtedly with a transmitter receiver system embedded in the ionosphere, but with the receiver not always tuned to the transmitter frequency, many new forms of non-linear behavior could be explored.

Discussion on Paper 3.3.1 presented by R.E. Barrington

Reinisch: What was the ratio of energy in the third harmonic to energy in the fundamental signal that you expected?

Barrington: With the experiment that we conducted, the ratio of the expected signal strengths was of the order of 10^{-5} to 10^{-6}. Our sensitivity was of this order too, so the fact that we didn't unequivocally detect something didn't worry us too much, because we felt this was easily coped with in the theory.

Reinisch: What is the amount of third harmonic energy which is contained in the transmitted pulse?

Barrington: We were conducting a pulse experiment, where the fundamental travels to the E region and is reflected; the third harmonic component of the transmitted wave would not be reflected within the E region. It may be reflected at some greater height, but there would be a considerable delay between the reception of the third harmonic that was generated in the ionosphere and the reception, after reflection, of the component originally radiated by the transmitter. Partial reflection of the third harmonic within the E region could give you problems.

Jobler: In the higher energy terms for these non-linear processes, can we neglect gradient pressure?

Barrington: No, this could also lead to non-linear effects.

Jobler: Your equation didn't show it.

Barrington: No, this would be an additional effect. I was just pointing out some of the effects that we examined.

Jobler: In other words, this is a cold plasma type of treatment.

Barrington: Exactly.

Jobler: If we looked at this as a hot plasma I suppose we could get some non-linearities from the thermodynamic processes involving the gradient of the pressure.

Barrington: Yes. Of course when we were examining this term we actually did a Boltzmann treatment to make sure that the effects we were predicting hydrodynamically did appear when you did consider a Maxwellian distribution.

Elkins: I didn't see where polarization entered your analysis, so would you please explain why you don't expect non-linear effects through circular polarization?

Barrington: Non-linear effects certainly can exist with circular polarization. However, the non-linear effects that I have considered due to the dependence of collision frequency on energy disappear, if you consider circular polarization, but exist for the case of linear polarization or, of course, for elliptical polarization.

3.3.2 IONOSPHERIC DETECTION EFFECT

by

G. Lanza*

Northeastern University, Boston, Massachusetts

1. Introduction

Several wave interaction experiments at vertical incidence were performed in Italy by Cutolo (1) in which a VHF wave modulated at the gyrofrequency was used as disturbing wave. The same type of experiments were performed by the author in Australia during 1965. In 1963, Cutolo (2) also performed the experiment at oblique incidence, propagating the wanted wave for a distance of about 1000 miles. A considerable amount of modulation was impressed on the wanted wave during this experiment. The impressed modulation was present only when the VHF disturbing wave was modulated in the vicinity of the gyrofrequency indicating the existence of a resonance. The experiments at oblique incidence were performed at night.

The physical interpretation of these results is that through the non-linearities present in the ionospheric plasma, a field at the gyrofrequency is liberated and this interacts with the wanted wave as happens in the normal Luxembourg effect. Unlike in the normal Luxembourg effect, however, in which the gyrofrequency field is absorbed at the bottom of the ionosphere, the field liberated by the detection effect can reach any height, due to the lower absorption of the VHF wave, so that its energy can be deposited where it is most efficiently used.

The analysis in the paper shows how a field at the modulation frequency can be produced by the interaction of the fields at the carrier and sidebands frequencies. The theoretical results are in essential agreement with the experimental results at oblique incidence, and indicate also that the orientation of the electric field $\vec{E}$, the geomagnetic field $\vec{B}_o$ and the direction of propagation $\vec{a}$ of $\vec{E}$ is important.

Impressed modulation three orders of magnitude smaller than those for an oblique incidence experiment are expected for vertical incidence.

* Work performed while visiting the University of New England, Armidale, N.S.W. Australia.

2. Fundamental Equations for the Propagation of an EM Wave in an Ionized Medium.

The Maxwell equations will have to be satisfied at all times by the propagating fields. These equations are:

$$\bar{\nabla} \times \vec{H} = \vec{j} + \varepsilon_o \frac{\partial \vec{E}}{\partial t} \tag{1}$$

$$\bar{\nabla} \times \vec{E} = -\mu_o \frac{\partial \vec{H}}{\partial t} \tag{2}$$

The conduction current is

$$\vec{j} = -ne\vec{v} \tag{3}$$

where $\vec{v}$ is the ordered velocity acquired by the electrons under the action of the electric field $\vec{E}$ and n is the electron concentration.

The equation employed to obtain v is the equation of conservation of momentum, which for electrons under the influence of an electric field $\vec{E}$, immersed in a uniform magnetic field B_o, and taking into consideration collisions, becomes

$$\frac{d\vec{v}}{dt} = -\eta(\vec{E} + \vec{v} \times \vec{B}) - \vec{v}\nu \tag{4}$$

where

$$\eta = {}^{-e}/_{m} = 1.76 \times 10^{11} \text{ coul.}/_{\text{kg.}}$$

ν is the collision frequency.

$$B = B_o + B_1 \quad (B_o = \text{geomagnetic field}, \; B_1 = \text{field associated with wave})$$

The system of equations can be closed with the equation of conservation of charge

$$\frac{\partial n}{\partial t} = \text{electron generation rate - loss rate} \tag{5}$$

Maxwell's equations are linear equations unless propagation occurs in a medium. Only the conduction current $\vec{j}$ can supply the non-linearity. Examining equation (3), we see that higher harmonics of the current are obtained when both $\vec{v}$ and n oscillate at the fundamental frequency, or when either $\vec{v}$ or n have higher harmonic components.

In what follows, we wish to limit ourselves to fields low enough so there is no generation of new electrons by ionization, and further we assume n to remain constant. We can hence neglect equation (5) in the subsequent calculations.

Equation (4) will therefore have to supply the non-linear terms which are the cause of the higher harmonics in the velocity.

We see in (4) that the inertial term is

$$\frac{d\vec{v}}{dt} = \frac{\partial \vec{v}}{\partial t} + \vec{v} \cdot \bar{\nabla}\vec{v}$$

and $\vec{v} \cdot \bar{\nabla}\vec{v}$ is obviously one of the non-linear terms we wish to maintain. Observing that qualitatively at least $\vec{v} \propto \vec{E}$ through the mobility equation,

$$\vec{v} \cdot \bar{\nabla}\vec{v} \propto \vec{E} \cdot \bar{\nabla}\vec{E}$$

Hence this term has to be retained whenever the electric field changes over the mean free path of an electron. At relatively low frequencies this term can be disregarded, but not at higher frequencies.

Another non-linear term is furnished by the $\vec{v} \times \vec{B}$ term. This term is of the order v/c and therefore it is usually dropped compared to the fundamental field. However, it may not be negligible compared to the higher harmonic fields and consequently we decided to retain it.

Another non-linear term is the term $\vec{v}\nu$. This term is responsible for the Luxembourg effect and it is the most known. As can be shown (3), ν varies at the second harmonic rate and therefore, the $\vec{v}\nu$ term can only produce third harmonics and not second (4).

In what follows, we will concentrate on second harmonic generation and therefore, this latter term will be neglected.

3. Second Harmonic Generation (5)

We wish to derive specific relations for the amplitude of $\vec{P}_2$, the second harmonic in volume polarization. As we have seen before, the terms responsible for second harmonic generation by velocity modulation are derived from the terms $\vec{v}\cdot\bar{v}\vec{v}$ and $\vec{v} \times \vec{B}_1$.

Let $\vec{r}_o$ be the average position of charge, $\vec{r}$ the actual position of charge, and $\vec{R}$ the displacement of charge. Values with index o will indicate corresponding value for DC case, with index 1 will denote uniform AC variable with the applied frequency. No index will indicate a non-uniform AC quantity.

The equation of motion (4) in terms of $\vec{R}$ will become

$$\ddot{\vec{R}} + \nu\dot{\vec{R}} = -\eta(\vec{E}(r)-\vec{B} \times \dot{\vec{R}}) \tag{6}$$

As was seen before, one source of non-linearity is produced by the fact that the electric field changes over the orbit of an electron. We allow for this by expanding the field in Taylor series about $r = r_o$.

$$\vec{E}(\vec{r}) = \vec{E}_1 + (\vec{R}\cdot\bar{v})\vec{E}/_{r = r_o} \tag{7}$$

If there is a non-uniformity in $\vec{E}$, there will also be one for $\vec{B}_1$. However, we disregard this as negligible.

Inserting (7) into (6) we obtain

$$\ddot{\vec{R}} + (\nu - \vec{\omega}_c x)\dot{\vec{R}} = -\eta(\vec{E}_1 + \vec{E}_2^1) \tag{8}$$

where

$$\vec{E}_2^1 = (\vec{R}\cdot\bar{v})\vec{E}/_{r = r_o} - \vec{B}_1 \times \dot{\vec{R}} \tag{9}$$

$$\vec{\omega}_c = \eta\vec{B}_o$$

The solution of the linear part of (8) is obtained by putting $\vec{E}_2^1 = 0$ in (8) and taking an $e^{i\omega t}$ dependence for the driving term. This allows us to look for a solution with the same time dependence.

Hence, calling $\vec{R}_1$ the linear part of $\vec{R}$

$$\ddot{\vec{R}}_1 + (\nu - \vec{\omega}_c x)\dot{\vec{R}}_1 = -\eta\vec{E}_1$$

Integrating

$$i\omega\vec{R}_1 + (\nu - \vec{\omega}_c x)\vec{R}_1 = -\frac{\eta}{i\omega}\vec{E}_1$$

and solving for $\vec{R}_1$ we get

$$\vec{R}_1 = -\frac{1}{i\omega}\left[A(\omega)\vec{b} \times (\vec{E}_1 \times \vec{b}) + C(\omega)\vec{b} \times \vec{E}_1 + D(\omega)\ (\vec{E}_1 \cdot \vec{b})\vec{b}\right] \tag{10}$$

where $\vec{b}$ is a unit vector in the direction of the magnetic field $\vec{B}_o$ and

$$A(\omega) = \eta\frac{\nu + i\omega}{(\nu + i\omega)^2 + \omega_c^2} \tag{11}$$

$$C(\omega) = \eta\frac{\omega_c}{(\nu + i\omega)^2 + \omega_c^2} \tag{12}$$

$$D(\omega) = \eta\frac{1}{\nu + i\omega} \tag{13}$$

Now that we have found the linear part of $\vec{R}$, we can proceed in finding the next approximation by substituting $\vec{R}_1$ for $\vec{R}$ in (9) and solving then (8) with the new value of $\vec{E}_2^1$. We have

$$\vec{E}_2^1 = (\vec{R}_1 \cdot \bar{v})\vec{E}/_{r = r_o} - \vec{B}_1 \times \dot{\vec{R}}_1$$

Now

$$\bar{v}(\vec{R}_1 \cdot \vec{E}) = (\vec{R}_1 \cdot \bar{v})\vec{E} + (\vec{E} \cdot \bar{v})\vec{R}_1 + \vec{R}_1 \times (\bar{v} \times \vec{E}_1) + \vec{E} \times (\bar{v} \times \vec{R}_1) \tag{14}$$

The second and fourth terms will disappear because $\vec{R}_1$ is uniform, using (2), the third term becomes $-\vec{R}_1 \times \vec{B}_1$ and (14) is

$$\bar{v}(\vec{R}_1 \cdot \vec{E}) = (\vec{R}_1 \cdot \bar{v})\vec{E} - \vec{R}_1 \times \dot{\vec{B}}_1$$

or

$$(\vec{R}_1 \cdot \bar{v})\vec{E} = \bar{v}(\vec{R}_1 \cdot \vec{E}) + \vec{R}_1 \times \dot{\vec{B}}_1$$

and finally $\vec{E}_2^1$ turns out to be

$$\vec{E}_2^1 = \bar{v}(\vec{R}_1 \cdot \vec{E}) + \vec{R}_1 \times \dot{\vec{B}}_1 + \dot{\vec{R}}_1 \times \dot{\vec{B}}_1 \tag{15}$$

which also can be written as

$$\vec{E}_2^1 = \bar{v}(\vec{R}_1 \cdot \vec{E}) + \overline{\vec{R}_1 \times \vec{B}_1}^{\,\bullet} \tag{16}$$

The first term in (16) arises because $\vec{E}$ may be not uniform in the direction of electron displacement. However, if this was not true, there would still be a contribution to $\vec{E}_2^1$ from the gradient of $\vec{E}$, simply because $\vec{E}$ propagates, and this is the significance of the term $\dot{\vec{B}} \times \vec{R}_1$ in (15).

Assuming

$$\overline{v(\vec{R}_1 \cdot \vec{E})} << \overline{\dot{\vec{R}}_1 \times \vec{B}_1}$$

we can take $\vec{E}_2^1 = 2\omega \vec{R}_1 \times \vec{B}_1$

and as

$$\vec{B}_1 = \vec{a} \times \vec{E}_1 \frac{1}{v_{p2}}$$

($\vec{a}$ is the direction of propagation of $\vec{E}_1$)

we get

$$\vec{E}_2^1 = \frac{4\pi}{\lambda} \vec{R}_1 \times (\vec{a} \times \vec{E}_1) = \frac{4\pi}{\lambda} \left\{\vec{a}(\vec{R}_1 \cdot \vec{E}_1) - \vec{E}_1(\vec{R}_1 \cdot \vec{a})\right\}$$

Now that $\vec{R}_1$ and $\vec{E}_2^1$ are known, the same evaluation of $\vec{R}_1$ will give us $\vec{R}_2$, where $A(\omega) \to A(2\omega)$ etc. and $\vec{E}_1 \to \vec{E}_2^1$. Hence, the second harmonic displacement will be

$$\vec{R}_2 = -\frac{1}{2i\omega} \left\{A(2\omega)\vec{b} \times (\vec{E}_2^1 \times \vec{b}) + C(2\omega)\vec{b} \times \vec{E}_2^1 + D(2\omega)(\vec{b} \cdot \vec{E}_2^1)\vec{b}\right\} \tag{17}$$

4. Detection Effect

We see from (17) that $\vec{R}_2$, the second harmonic displacement term, is proportional to $\vec{E}_2^1$, which contains the non-linear terms. In fact, if it is assumed that the electric field gradient is zero, that is, if the field is assumed to be plane and uniform, $\vec{E}_2^1$ contains products of the type $\vec{R}_1 \cdot \vec{E}_1$.

Let us assume that $\vec{E}_1$ is an amplitude-modulated field,

$$\vec{E}_1 = \vec{E}_{10}(1 + m \cos \Omega t) \cos \omega t$$

Because of the superposition principle in $\vec{R}_1$, $\vec{R}_1$ is the solution of a linear equation and will be modulated in the same way. The factors in $\vec{E}_2^1$ containing the product of $\vec{R}_1$ and $\vec{E}_1$ will now be composed by the products of two factors, each containing a carrier and two sideband terms. Of the nine terms, four will be products of carrier with sidebands, and will have a time variation

$$\cos \omega t \cos(\omega \pm \Omega)t = \tfrac{1}{2} \cos \Omega t + \tfrac{1}{2} \cos \left[(2\omega \pm \Omega)t\right] \tag{18}$$

The first term at the left-hand side of (18) varies at the modulation frequency. Focusing our attention to these terms only, in $\vec{E}_2^1$ will appear 4 $\vec{R}_1 \cdot \vec{E}_1$, where we understand that $\vec{R}_1$ and $\vec{E}_1$ are carrier and sidebands or vice versa. As the sideband has an amplitude $\frac{m}{2}$ of that of the carrier, and taking the factor of 1/2 appearing in the time term in consideration, we conclude that $\vec{E}_2^1$ will behave like mR_1E_1 and vary like $\cos \Omega t$.

We can readily attain the displacement at modulation frequency by substituting in (17) for $\vec{E}_2^1$ the new $\vec{E}_2^1$ and $2\omega \to \Omega$. This will give us

$$\vec{R}_\Omega = -\frac{m}{i\Omega}\left\{A(\Omega)\vec{b} \times (\vec{E}_2^1 \times \vec{b}) + C(\Omega)\vec{b} \times \vec{E}_2^1 + D(\Omega)(\vec{b}\cdot\vec{E}_2^1)\vec{b}\right\} \tag{19}$$

The volume polarization at the modulation frequency is

$$\vec{P}_\Omega = ne\vec{R}_\Omega$$

We have now

$$A(\Omega) = \eta\frac{\nu + i\Omega}{(\nu + i\Omega)^2 + \omega_c^2}$$

$$C(\Omega) = \eta\frac{\omega_c}{(\nu + i\Omega)^2 + \omega_c^2}$$

$$D(\Omega) = \eta\frac{1}{\nu + i\Omega}$$

We see hence, that every time an electric field is amplitude-modulated, there is a polarization term varying at the modulation frequency. If the modulation frequency is equal to the gyrofrequency, we have a resonance.

5. Calculation of $\vec{P}_\Omega$ for some Orientations of Electric and Magnetic Fields

Inserting in $\vec{E}_2^1$ the value of $\vec{R}_1$ given by (10) and substituting in (19) would allow us to find out the $\vec{P}_\Omega$ term for any orientation of the $\vec{E}$ and $\vec{B}$ field. According to the figure, we obtain for $\vec{R}_1$, $\vec{E}_2^1$ respectively

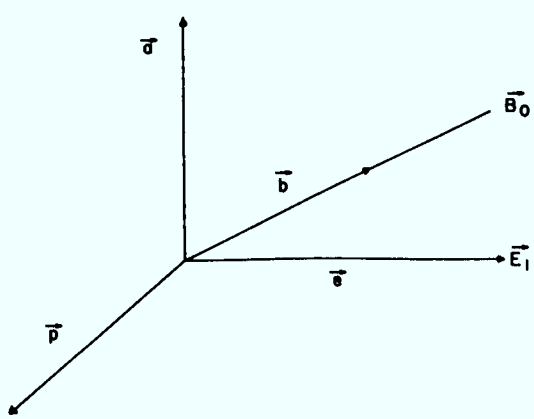

$$\vec{R}_1 = -\frac{1}{i\omega}\left\{\vec{a}\left(D(\omega)-A(\omega)\right) E_1 \cos\alpha \cos\beta + \vec{e}\left(A(\omega)E_1 + \left[D(\omega) - A(\omega)\right]E_1 \cos^2\alpha\right) - \vec{p}\left((\omega)\sin\alpha\right)\right\}$$

and

$$\vec{E}_2^1 = -\frac{4\pi}{i\lambda\omega}\left\{\left(A(\omega) - \left[D(\omega) - A(\omega)\right]\cos^2\alpha\right)E_1{}^2\vec{a} - \left(D(\omega)-A(\omega)\right) E_1{}^2 \cos\alpha \cos\beta\vec{e}\right\}$$

For $\beta = 0^o$ and $\alpha = 90^o$.

$$\vec{E}_2^1 = -\frac{4\pi}{i\lambda\omega} A(\omega)\ E_1{}^2\vec{a}$$

and substituting in (19) for $\vec{R}_\Omega$ we get

$$\vec{R}_\Omega = \frac{m4\pi}{\Omega\lambda\omega}\ |D(\Omega)A(\omega)|E_1{}^2\vec{a}$$

and finally the polarization term $\vec{P}_\Omega$

$$\vec{P}_{\Omega_1} = \frac{2mne}{c\Omega}\ |D(\Omega)A(\omega)|\ E_1{}^2\vec{a}$$

For the case of $\alpha = 0^o$ and $\beta = 90^o$ we find

$$\vec{P}_{\Omega_2} = \frac{2mne}{c\Omega}\ |C(\Omega)D(\omega)|\ E_1{}^2\ \vec{b} \times \vec{a}$$

The ratio of these two polarizations is

$$\frac{\vec{P}e_2}{\vec{P}_{\Omega_1}} = \frac{|C(\Omega)D(\omega)|}{|D(\Omega)A(\omega)|}$$

Now, at resonance, assuming $\omega >> \nu$ and $\Omega >> \nu$

$$|D(\omega)| \sim \frac{1}{\omega}$$

$$|D(\Omega)| \sim \frac{1}{\Omega}$$

$$|A(\omega)| \sim \frac{1}{\omega}$$

$$|C(\Omega)| \sim \frac{1}{2\nu}$$

$$\frac{P_{\Omega_2}}{P_{\Omega_1}} \sim \frac{\Omega}{2\nu} \sim 50$$

for $\Omega \sim 10^7$ and $\nu \sim 10^5$.

We have seen now that for the case of propagation along the magnetic field and electric vector perpendicular to it, the polarization at the gyrofrequency is given by

$$\vec{P}_{\Omega_1} = \frac{2mne}{c\Omega^2\omega}\ E_1{}^2\vec{a}$$

For the case of E parallel to magnetic field and propagation perpendicular to it

$$\vec{P}_{\Omega_2} = \frac{mne}{c\Omega\nu\omega} E_1{}^2 \cdot \vec{b} \times \vec{a}$$

and that for propagation perpendicular to magnetic field and $\vec{E}$ perpendicular to $\vec{B}_o$,

$$\vec{P}_{\Omega_3} = \frac{mne}{c\Omega\nu\omega} \left\{ \left(1 + \frac{\Omega}{\omega}\right) \cos \Omega t \vec{a} \times \vec{b} + \left(1 - \frac{\Omega}{\omega}\right) \sin \Omega t \vec{a} \right\} E_1{}^2$$

We see that $\vec{P}_{\Omega_2}$ and $\vec{P}_{\Omega_3}$ turn out to be of same order of magnitude, while the ratio of $\vec{P}_{\Omega_1}$ to either $\vec{P}_{\Omega_2}$ or $\vec{P}_{\Omega_3}$ is of the order of

$$\frac{2\nu}{\Omega}$$

that is, it is <u>at least</u> one order of magnitude smaller than the two other polarizations.

6. Comparison with Experimental Results

It has been shown how a field at the modulation frequency can be liberated in the ionosphere, essentially by the interaction of the carrier with the sidebands. Suppression of the carrier to increase modulation leads only to higher harmonics of the modulation frequency. A formula is obtained which gives the field strength produced at the modulation frequency as function of the disturbing power, for any orientation of the earth's magnetic field, direction of propagation of the disturbing wave and polarization of the electric field. If the modulation frequency is the gyrofrequency, the effect shows a resonance that greatly enhances the phenomenon.

For the situation corresponding to propagation and polarization both perpendicular to the earth's magnetic field, the electric field strength at the gyrofrequency generated by the polarization P_{Ω_2} is (6)

$$E_\Omega \simeq \frac{\omega_p{}^2}{\nu\omega} \frac{m}{c^2} \eta E_1{}^2 \Delta z \quad {}^{V}/_{m}$$

where

E_Ω is the field strength at the gyrofrequency, Ω is the gyrofrequency

ω_p is the plasma frequency

ω is the carrier frequency

m is the % modulation of disturbing wave

c is the speed of light

E_1 is the field strength of the disturbing wave at carrier frequency

Δz is the thickness of ionosphere in which the radiated fields add in phase.

Taking now

n (electron concentration) $\sim 3 \times 10^9$ electrons/c.c.

$$\omega_p{}^2 \simeq 9 \times 10^{12}$$

and using

$$E_1 \simeq \frac{10\sqrt{PG}}{d}$$

and taking

$$d = 10^5 m \qquad \omega = 3 \times 10^8 \ c/_s \qquad m = 5 \times 10^{-1}$$

$$\Delta z = 10^4 m \qquad \nu = 10^5$$

we get

$$E_\Omega \simeq 3 \times 10^{-9} \ PG$$

Knowing E_Ω allows us to calculate the power that should be radiated at the gyrofrequency to produce the same effect. In the case of Cutolo's experiment, at oblique incidence, PG ~ 1Mw, m ~ .5. The E_Ω produced is the same as if it was produced by a radiated power at the gyrofrequency of ~ 5kw. With this power at oblique incidence, a 3 per cent modulation on the wanted wave is predicted. This is in agreement with Cutolo's observation. At vertical incidence, a modulation of .003 per cent is predicted, well below the receiving capabilities of existing installation. In the calculations above, $n = 3 \times 10^9$ has been used to insure that the plasma frequency is lower than the gyrofrequency, to make sure that all the radiated fields at the gyrofrequency radiated by the various electrons are in phase for the thickness of the layer. An analysis should be made to see how an increase in plasma frequency affects Δz and the direction of propagation of the generated gyrofrequency field. The theory indicates that at a modest power level one can impress a noticeable percentage modulation on a wanted wave. Radiated disturbing powers of the order of 100 Mw are capable of producing a field at the gyrofrequency of the order of 1 V/m, depending on the value of the collision frequency and consequently on the height of interaction. These field strengths, at a pressure $p \sim 10^{-3}$ mm.of Hg, give an $\frac{E_\Omega}{p}$ ratio of the order of 10, at which breakdown of some of the constituents of air becomes possible.

The theory also predicts that, all parameters remaining unchanged in Australia, the phenomenon should be ~ 50 times less noticeable, because, due to the peculiar direction of propagation almost parallel to the magnetic field, no resonance effect is possible.

REFERENCES

1. Cutolo, M. "Propagation of radio waves at frequencies below 300 kc." W.T. Blackband editor. Pergamon Press, 1964 - AGARDograph 74.

2. Cutolo, M. - Private communication.

3. Ginzburg, V.L. and A.V. Gurevich. Soviet Physic USPEKHI, 3, 115, 1960.

4. Barrington, R.E. "Harmonic generation in the ionosphere" - this volume.

5. Verdeyen, J.T. and L. Goldstein. Scientific report No. 5, University of Illinois, AFCRL-62-488.

6. Ratcliffe, J.A. "The Magnetoionic theory and its applications to the ionosphere". Cambridge University Press, page 22, 1962.

3.3.3 AN ATTEMPT TO GENERATE COMBINATION FREQUENCIES IN THE IONOSPHERE

by

R.A. Smith, R.G. Loch, and B.S.N. Prasad

University of New England, Armidale, Australia

Presented by R.A. Smith

Since radio wave propagation in the ionosphere is non-linear, combination frequencies should be produced when two waves are superimposed. Experimental studies of this mixing, which has an extensive theoretical literature (see Ginzburg and Gurevich 1960), are limited to those of Hakefost (1936) and Green (1965). Hakefost easily detected many combination frequencies but the mixing most probably occurred in aerial structures in the neighborhood of his receiver. On several occasions during the Leonid meteor shower in 1960, Green, near Washington, D.C., observed a specular return lasting for about 20 seconds at the difference frequency (2.878 Mc/s.), but not at the sum frequency (25.026 Mc/s.), of two powerful pulsed transmissions (11.074, 13.952 Mc/s.) directed to the south. From the discussion of the experimental parameters and other information given by Green, it is difficult to attribute these returns to mixing in the vicinity of the antennas during either transmission or reception. Since the transmitted beams were not coincident and the returns at the difference frequency do not correlate with features of the returns observed at the fundamental frequencies, it is equally difficult to be certain of their origin in the ionosphere.

The three stations used at the University of New England for research on radio wave interaction are described in Paper 3.2.1, where they are referred to as A, B, and C. Of these, A and B are disturbing stations, and C, which is 9 km. from A and 1.5 km. from B, contains transmitters and receivers for the wanted wave. The disturbing transmitter at A can be pulsed at powers up to 200 kw. at frequencies within ±20 per cent of the gyrofrequency (1.515 Mc/s.). Its aerial is a circularly polarized square array of four horizontal half-wave dipoles. Less powerful circularly polarized pulse transmissions at a frequency of 2.12 Mc/s. can also be made from A. The transmitter at B is operated at the gyrofrequency and its aerial is a circularly polarized array of 40 horizontal half-wave dipoles. At the maximum power of 500 kw. into this array, it is estimated that the electron temperature near 90 km. in the nighttime lower E region produced by extraordinary mode radiation is above 5000°K. The aerials at C include circularly polarized square arrays of four dipoles for frequencies near 2.12 Mc/s., pairs of orthogonal dipoles for frequencies near 1.78 Mc/s., and delta aerials for an ionosonde. Because of its role as the wanted station, care has been taken at C to prevent non-linear effects from being produced in its aerials and receiving equipment by radiation from the two disturbing stations.

During the first week of August 1964, unsuccessful attempts were made at C using a Redifon communications receiver to detect returns from the ionosphere at combinations of the frequency f_1 (1.515 Mc/s.) of CW transmissions at a power of 220 kw. from B, and the frequency f_2 of pulsed transmissions from A. Generally, the delta aerials at C were used for reception but at frequencies for which these aerials are inefficient and at frequencies near the operating frequencies of the resonant aerials at the station, the latter were also used in both balanced and unbalanced configurations.

The exploratory searches for a combination frequency return were made at night with the transmitter at A generating pulses of 800 μsec. duration and 100 kw. power at a frequency of 1.78 Mc/s. When these searches to the 30 Mc/s. upper frequency limit of the receiver proved fruitless for each of the four combinations of the polarizations of the waves transmitted from A and B, the search was narrowed to the more

probable frequencies $|2f_1 \pm f_2|$, $|f_1 \pm 2f_2|$, $|f_1 \pm f_2|$, and the output of the diode detector of the receiver was displayed on an oscilloscope for close examination of the trace at the delays for returns from the E and F regions.

On the night of 5 August and during the day of 6 August, immediately following each search for a combination signal, the output of a pulsed signal generator was added to the aerial circuit of the receiver, and the signal level, which gave a pulse that could be clearly seen in the noise and interference picked up by the aerial, was recorded. For these two series of observations, details of the transmissions f_2 and of the combination frequencies examined are given in the table.

Detection levels in search for combination frequencies

Date	f_2	Combinations of modes	$2f_1 + f_2$ (Mc/s.)	$2f_1 - f_2$ (Mc/s.)	$\|f_1 - f_2\|$ (Mc/s.)	$f_1 + f_2$ (Mc/s.)	$f_1 + 2f_2$ (Mc/s.)	$\|f_1 - 2f_2\|$ (Mc/s.)
5 August 1964 (0000-0500 E.A.S.T.)	1.78 Mc/s. (A, 120 kw., 800 μsec., 4-dipoles)	ee, eo oe, oo	4.810 (0.7)	1.250 (75)	0.265 Heavy interference	3.295 (3)	5.075 (0.7)	2.045 (1.5)
	2.12 Mc/s. (A, 15 kw., 450 μsec., 2-dipoles)	ee, eo oe, oo	5.15 (1)	0.91 (2)	0.605 (1)	3.635 (15)	5.755 (1)	2.725 (1)
	1.848 Mc/s. (A, 80 kw., 800 μsec., 4-dipoles)	ee, eo	4.878 (5)	1.182 (not measured)	0.333 (not measured)	3.363 (15)	5.211 (2)	2.181 (3)
6 August 1964 (1200-1500 E.A.S.T.)	1.78 Mc/s. (A, 115 kw., 300 μsec., 4-dipoles)	ee, eo oe, oo	4.810 (0.5)	1.25 (5)	0.265 Long wire aerial (30)			

In this table the first letter of the notation eo, etc. gives the polarization of f_1 (o, ordinary, e, extraordinary), and the second gives the polarization of f_2. The level, in microvolts, of the signal that would have been detected is given in brackets below the combination frequency. It refers to the voltage across the 80 Ω receiver input and, with the exception noted in the table, to reception using the delta aerials. At all frequencies examined, the limit of detection was set by external noise and was thus independent of the efficiency of the delta aerials, which have an absorption cross-section of about 1500 sq. m. at frequencies above 2.5 Mc/s.

By the use of a more sophisticated detection method, by observing over long periods to find extremely quiet conditions, and by the use of a high-gain receiving aerial to discriminate against noise and interference, it might be possible to detect ionospheric returns at combination frequencies. However, when considered in relation to the powers radiated and the detection sensitivities achieved, the negative result of the present experiments indicates that the signals would need to display some feature characteristic of an origin in the ionosphere before the existence of minor effects at the ground, such as mixing of echoes from the ionosphere, could be excluded.

REFERENCES

Ginzburg, V.L. and A.V. Gurevich. Soviet Physics "Uspekhi", 3, 115 and 175, 1960.

Green, J.A. J. Geophys. Res., 70, 3244, 1965.

Hakefost, W.L. Wireless Engineer, 13, 298, 1936.

3.3.4 RADIO WAVE INTERACTION SPECTRUM ANALYSIS

by

H.S. Lee and T.D. Pinkerton

Ionosphere Research Laboratory, Pennsylvania State University

Presented by H.S. Lee

1. Introduction

Although the pulsed radio wave interaction experiment, in conjunction with the partial reflection experiment, is considered one of the two powerful ground-based techniques available to study the D region of the ionosphere, it has its shortcomings as most other techniques do. For example, in obtaining a complete interaction height profile, the delay time between the transmission of the wanted and disturbing pulses must be changed between each measurement until the whole region of interest is swept in terms of h_i. This procedure can be time-consuming, and since the state of the ionosphere can change over a period of time, the longer it takes to obtain a complete set of data the greater the error in the synthesized electron density profiles can be. Another source of error arises from the fact that the measurements can only be made down to a certain minimum height, say about 60 km., while there is interaction occurring below this height, which must somehow be taken into account.

The so-called spectrum analysis method is introduced in this paper with the belief that it could eliminate the difficulties mentioned above and bring forth some of the advantages to be discussed later. The method is different from the conventional method in that it measures the frequency spectrum of radio wave interaction. This method was developed from efforts to improve the accuracy of the interaction experiment by including the effect of finite wanted pulse width in the theory, which is discussed in Section 2 and is followed by the method of spectrum analysis in Section 3.

2. Effect of Finite Wanted Pulse Width

Most radio wave interaction theory has assumed a delta wanted pulse width and a finite disturbing pulse width. For example, the complex interaction coefficient, $T = T_A + jT_\phi$, for the amplitude and phase interaction given by Weisbrod et al. (1964)

$$T = T_A + jT_\phi = \int_0^{h_i'} \frac{T_{HA} + jT_{H\phi}}{G\nu\tau_D} (1-e^{-G\nu\tau_D}) \exp\left[\frac{-2G\nu}{c}(h_i' - h)\right](-\frac{\partial F}{\partial h})dh$$

$$+ \int_{h_i'}^{h_i} \frac{(T_H + jT_{H\phi})}{G\nu\tau_D} \left\{ 1-\exp\left[-\frac{2G\nu}{c}(h_i - h)\right] \right\} (-\frac{\partial F}{\partial h})\, dh \qquad (1)$$

where some of the symbols relevant to the subsequent discussions are:

$$h_i' = h_i - \frac{c\tau_D}{2}$$

h_i = height of interaction = height where the leading edges of the two pulses meet

τ_D = disturbing pulse width

G = energy loss coefficient

is based on such an assumption. However, the necessity of including the effect of the finite wanted pulse width in the interaction equations can be seen by referring to Fig. 1, which shows the amplitude and phase interaction coefficients for delta wanted pulse plotted against height above the ground.

The vertical dashed line in the figure represents the delta pulse concept of amplitude interaction and the solid line following the contour of the amplitude interaction curve represents true interaction. Obviously, there will be some error incurred by not accounting for the finite width of the wanted pulse, and the degree of error will depend on the manner in which the interaction coefficient is measured and will also be a function of the width of the pulse, increasing with increasing pulse width and being greatest where the slope of the interaction curve, $\frac{\partial T}{\partial h_i}$, is the greatest.

Fig. 2 shows the repetition of the interaction of the finite wanted pulse for a given value of h_i as a function of time, where T_D is the period of recurrence of the disturbing pulse. It is the mean value or the fundamental frequency component of the repetition rate of the disturbing pulse that is actually measured in practice. Thus, since the ratio of interaction of the trailing edge to the leading edge of the wanted pulse can be as great as 100 for a typical wanted pulse width, large error can be incurred if a delta pulse is assumed for the wanted pulse. As in Fig. 1, the dashed line in Fig. 2 represents the delta pulse concept, while the solid line represents true interaction.

If the finite width of the wanted pulse is accounted for in deriving the interaction equations as done by Pinkerton (1966), where both the wanted and disturbing pulses are assumed to be rectangular, the result is

$$T_{W,D}(h_i)_{ave} = \frac{p}{3\pi k} \int_0^{h_i''} \frac{k_w k_D \chi_D \nu}{\theta h^2 N} \left(\frac{\partial \chi_w}{\partial \nu} + j\frac{\partial \mu_w}{\partial \nu}\right) \cdot E_n \cdot$$

$$\exp\left(-2k_D \int_0^h \chi_D \, dh\right) dh \quad \text{for } n = 1, 2, 3, 4 \tag{2}$$

The E_n term in the above equation depends on the limits of integration, which are shown geometrically in Fig. 3 in terms of h_i introduced earlier, and on the relative widths of the wanted and disturbing pulses. In practice, the wanted pulse width is generally narrower than the disturbing pulse width, as shown in the figure, and the E_n for this case are given below.

$$E_1 = \frac{1}{(G\nu)^2 \tau_w} \left[1-\exp(-G\nu\,\tau_D)\right] \cdot \left[1-\exp(-G\nu\tau_w)\right] \cdot \exp\left[-\frac{2G\nu}{c}(h_i' - h)\right]$$

$$\text{for } 0<h<h_i'$$

$$E_2 = \frac{1}{G\nu\tau_w}\left\{\frac{2}{c}(h-h_i') + \frac{1}{G\nu}\left[1 + \left\{\exp\left[-G\nu(\tau_w+\tau_D)\right] - \exp(-G\nu\tau_w) - \exp(-G\nu\tau_D)\right\}\cdot\exp\left\{-\frac{2G\nu}{c}(h_i'-h)\right\}\right]\right\}$$

for $h_i' < h < h_{i2}$

$$E_3 = \frac{1}{G\nu\tau_w}\left\{\tau_w - \frac{1}{G\nu}\left[1-\exp(-G\nu\tau_w)\right]\cdot\exp\left[-\frac{2G\nu}{c}(h_i-h)\right]\right\}$$

for $h_{i2} < h < h_i$

$$E_4 = \frac{1}{G\nu\tau_w}\left\{\frac{2}{c}(h_i''-h) - \frac{1}{G\nu}\left[1-\exp\left\{-\frac{2G\nu}{c}(h_i''-h)\right]\right\}\right.$$

for $h_i < h < h_i''$ (3)

where τ_w = wanted pulse width.

The effect that the finite wanted pulse width has on the interaction coefficients can best be described by referring to Fig. 4, which shows the amplitude interaction height profile for several different values of the wanted pulse width, generated based on equation (2).

It is evident from this figure that large errors can be incurred if the wanted pulse width is too large for the valid usage of the delta pulse width approximation, represented by equation (1).

Fig. 5 shows an example of the error incurred in the synthesis of electron density when the delta wanted pulse width theory is used while the data is generated from the interaction equations for a finite wanted pulse width. The assumed electron density used to generate the data is given by the straight line in the figure, while the various points represent the electron density synthesized from the data generated for the height equivalent of the wanted pulse widths of 1, 5, and 10 km. This figure, as does Fig. 4, clearly shows that large error could result if the effect of the finite wanted pulse width is neglected.

The points representing the electron density synthesis of the five-kilometer wanted pulse width data and those representing the ten-kilometer wanted pulse width data are not extended above the heights of 60 and 55 km. respectively, since interaction is an integral effect, and if the first few synthesized points are not accurate, the rest of the points cannot be expected to be accurate.

3. Spectrum Analysis of Radio Wave Interaction

It has been shown that it is important to account for the finite width of the wanted pulse in radio wave interaction experiments. Unfortunately, equations 2 and 3 are complex and represent only the average value of the interaction coefficient over the width of the wanted pulse. Therefore, these equations are not only cumbersome to use but there will still be some error, since the exact form of interaction profile cannot be determined uniquely from the average values. It was because of this problem that the idea of a frequency spectrum analysis of radio wave interaction was looked into. That is, by measuring not only the amplitude and phase of the fundamental frequency component of the repetition rate of the disturbing pulses, as is done in the present experiment, but also those of some of the higher harmonics, the exact wave form of the interaction pulses shown in Fig. 2 can be found uniquely. Furthermore, if the wanted pulse width is made wide enough to cover the whole region of

interest, the exact form of interaction profile of the delta wanted pulse for that region can be found from the simultaneous measurement of the amplitude and phase of the fundamental frequency component of the repetition rate of the disturbing pulse and those of its harmonics. Such a wanted pulse width will hereafter be referred to as a wide wanted pulse width.

Fig. 6 shows the amplitude interaction profile with a very wide wanted pulse width extending from h_i to h_i'', as opposed to the narrow wanted pulse width of 5 km. shown in Fig. 1. Fig. 7 shows the repetition of the amplitude interaction of the wide wanted pulse width as a function of time, where T_D is the period of recurrence of the disturbing pulse. The radio wave interaction spectrum analysis is, in essence, the determination of Fourier coefficients, in terms of amplitude and phase, of the periodic wave form shown in Fig. 7, by applying Fourier analysis. On the other hand, if the coefficients are known, the wave form of the periodic function, which is none other than the interaction profile, can be synthesized.

Fig. 8 shows the result of a Fourier synthesis carried out by assuming that the Fourier coefficients are known up to the 600th term. The characteristics of a Fourier synthesis with a finite number of terms that are clearly visible in this figure occur at the uppermost height of the profile and at the portion below the negative peak. The deviation of the synthesized profile from the true profile at the upper end exists because a Fourier synthesis, at a point of discontinuity, results in a mid-value there. Since the point on one side of the discontinuity in Fig. 8 is zero, if the end point of the synthesis is doubled, the profile can be exactly reproduced at the upper end. The deviation of the synthesized profile from the true profile below the negative peak appears as a minute oscillation. This oscillation is actually present along the entire profile, but appears only below the negative peak because the magnitude of the profile there is comparable to that of the oscillation. This oscillation will always appear if a finite number of harmonics are used in the synthesis, but will be smaller in magnitude if a larger number of harmonics is used. It should be mentioned that although the above illustration was made with the amplitude interaction profile, the same concept can be applied equally well to the phase interaction profile.

The accuracy of synthesis exhibited in Fig. 8 is remarkable. However, in order for the frequency spectrum concept to be experimentally feasible, it is desirable to keep the number of higher harmonic components to be measured as small as possible. There are two reasons for this: firstly, it is simply not practical to measure both the amplitude and phase of 600 harmonic components simultaneously; and secondly, the harmonic components of the order of 600 are too small to measure.

The reason for requiring as many as 600 harmonics is that the convergence of the Fourier coefficients depends mainly on the factor τ_w/T_D. The smaller the factor τ_w/T_D, the larger the number of necessary harmonics becomes. Unfortunately, there is a limit as to how large this factor can be made. That is, T_D cannot be made so small that the disturbed medium does not have time to relax between disturbing pulses.

Figs. 9 and 10 show the amplitude and phase, respectively, of the first few harmonic components of the interaction profile shown in Fig. 8 plotted against the order of harmonic components. It is interesting to note in Fig. 10 that the phase points of the harmonic components fall nearly on a straight line if they are added to the proper multiple of 2π. For example, if the value of the phase of the fourth harmonic is added to 2π it falls on the dashed line as shown; if the value of phase of the ninth harmonic is added to 4π, it, too, falls on the dashed line, etc. Such linear property of phase distribution enables the determination of phase of higher harmonic components by extrapolation without actually measuring.

In regard to the amplitude distribution shown in Fig. 9, it was mentioned previously in the introduction that it is possible that the lower end of the interaction profile can be obtained from the frequency spectrum technique. Actually, amplitude of higher harmonic components of the amplitude distribution is no more measurable than the actual interaction is below about 60 kilometers. However, since the amplitude distribution is a smooth profile and becomes nearly linear at the higher harmonics, as can be seen from Fig. 9, it is

possible to obtain these unmeasurable higher harmonics components by an extrapolation from the measurable higher harmonic end of the distribution. Fig. 11 shows a Fourier synthesis of the same amplitude interaction height profile as is shown in Fig. 8, but done with only 300 harmonic components to show the increased error that occurs in the negative portion of the synthesized profile. If these first 300 terms are extrapolated to obtain the next 300 terms, the synthesized amplitude interaction height profile is much more accurate, as shown in Fig. 12. In this figure, the phase harmonic components were extrapolated linearly as described above, and the amplitude harmonic components were extrapolated exponentially from the slope of the end of the given part of the amplitude distribution. In either case, the solid line represents the synthesized profile, whereas the dashed line represents the original profile. Comparison of the two figures clearly indicates that although all 600 terms are desired in synthesizing accurate profiles, there is no need to measure all of them, in view of the possible extrapolation. Further tests indicated that even when the number of coefficients to be measured is reduced to 200, with the remainder of 400 terms extrapolated, the synthesized result is still acceptable although it is not as accurate as that shown in Fig. 12.

It should be mentioned that the distributions shown in Figs. 9 and 10 were obtained assuming that the peak power of the disturbing transmitter was 25 kw. In view of the new high power facilities to be installed at the Ionosphere Research Laboratory in the near future, the magnitude of the interaction effect will increase over 100 times, making the first 300 terms of the distributions well within the measuring capability of the equipment, thus making the application of spectrum analysis technique quite possible.

4. Conclusions

The spectrum analysis of radio wave interaction is found to be theoretically feasible, and some of its advantages over the conventional measurements made in time domain are recapitulated below. The method enables an exact interaction height profile to be obtained; it allows the data at the lower end of the profile to be reasonably extrapolated even though it is not measurable; it enables the interaction profile of the whole D region to be measured simultaneously and thus eliminates errors that could occur due to changes in the ionosphere over a long period of time; and, it allows the valid usage of the delta wanted pulse width approximations in the synthesis of both density and collision frequency.

REFERENCES

Pinkerton, T.D. "The Effect of the Finite Wanted Pulse Width on the Radio Wave Interaction Experiments". Ionosphere Research Laboratory Scientific Report No. 274, Ionosphere Research Laboratory, Pennsylvania State University. June 15, 1966.

Weisbrod, S., Ferraro, A.J. and H.S. Lee. "Investigation of Phase Interaction as a Means of Studying the Lower Ionosphere". J. Geophys. Res., 69, 2337-2348. 1964.

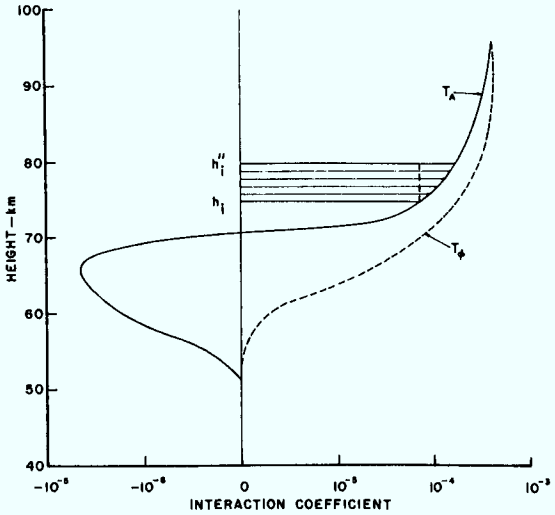

Fig. 1. Interaction coefficient vs height for finite wanted pulse width.

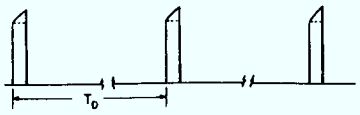

Fig. 2. Effect of interaction as a function of time.

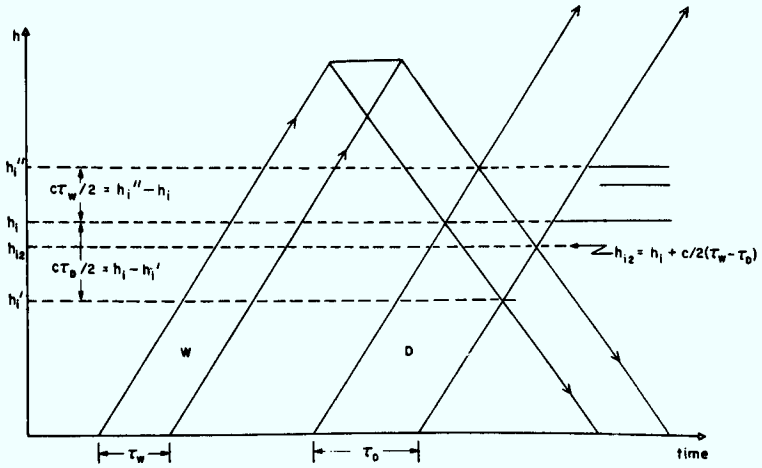

Fig. 3. Path geometry with finite wanted and finite disturbing pulse widths.

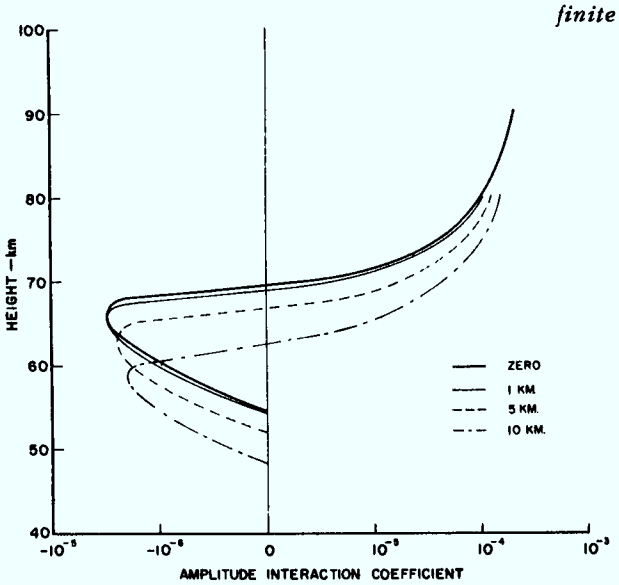

Fig. 4. Comparison between delta and finite wanted pulse width interaction coefficients.

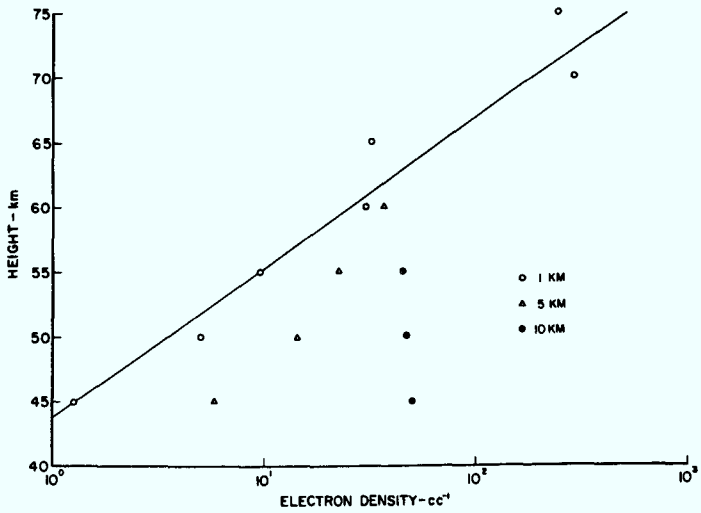

Fig. 5. Electron density synthesis assuming delta wanted pulse width.

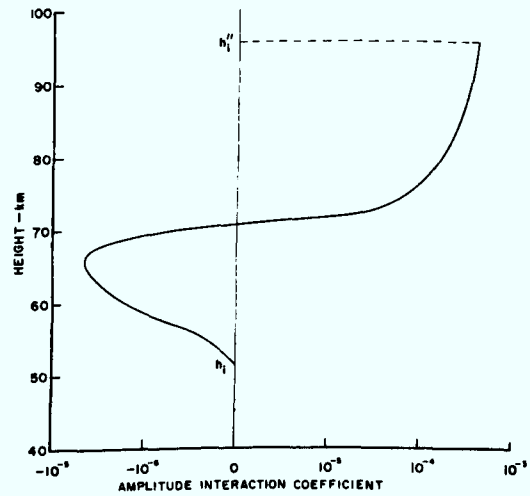

Fig. 6. Interaction coefficient vs height for a wide wanted pulse width.

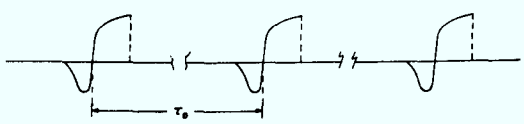

Fig. 7. Effect of interaction for a wide wanted pulse width as a function of time.

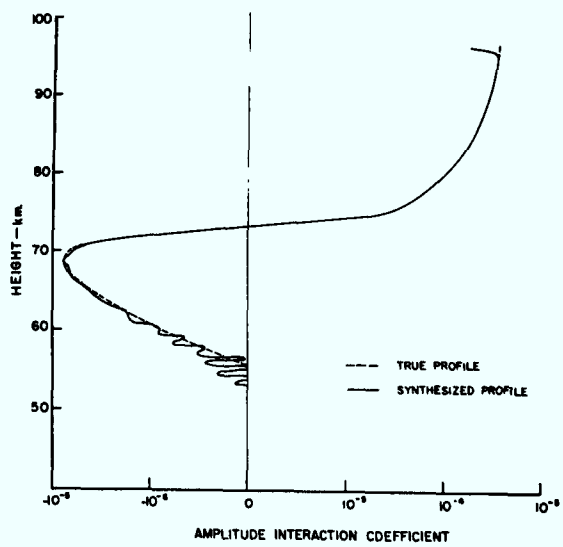

Fig. 8. Fourier synthesis of interaction profile.

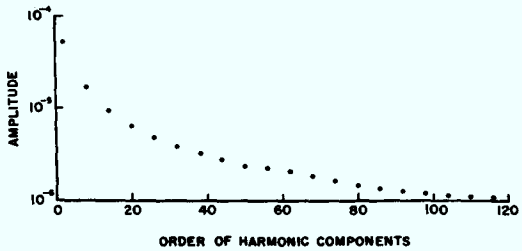

Fig. 9. Fourier amplitude distribution of interaction profile.

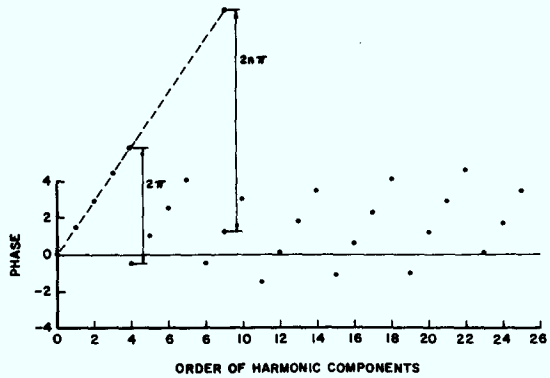

Fig. 10. Fourier phase distribution of interaction profile.

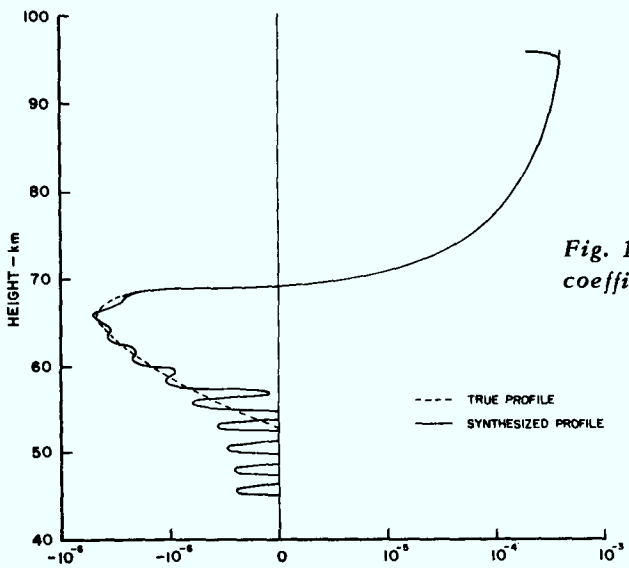

Fig. 11. Amplitude interaction coefficient.

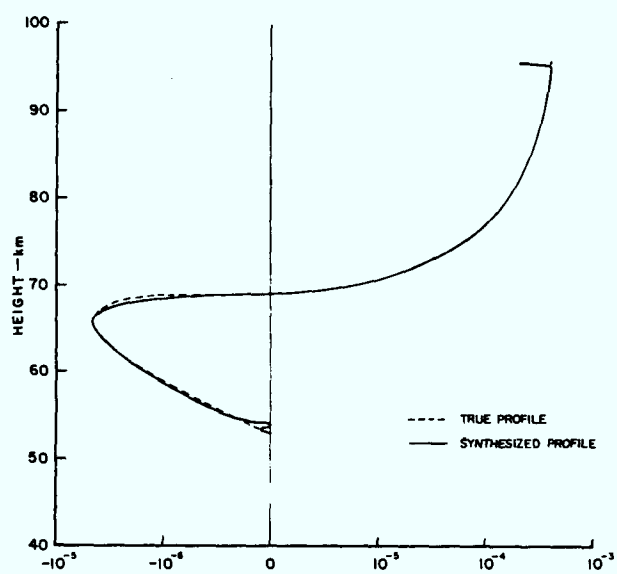

Fig. 12. Amplitude interaction coefficient.

Discussion on Paper 3.3.4 presented by H.S. Lee

Georges: Your spectrum analysis technique would appear to apply equally well to perturbations of a CW wanted wave. Would there be any advantage to using this mode of operation, assuming the interference problem could be overcome?

Lee: What we are trying to do is to determine the transferred modulation more accurately. We want to know if the measured T_A value is given by the analytical expressions we have employed.

Georges: Why do some workers refer to the amplitude interaction at low heights as being *negative,* when ΔA (the amplitude change relative to undisturbed conditions) is *positive* here?

Lee: I noticed that the signs in your profile are the opposite to ours. You have the lower modulations positive when we have them negative. I think there may be a slight difference in the definitions.

Georges: The ultimate definition comes from $\frac{\Delta A}{A}$, doesn't it?

Lee: I think so, but following that definition we did come up with the negative sign.

Elkins: On general grounds, it seems to me that if you throw away some of the components of the Fourier spectrum you are throwing away some of the resolution.

Lee: I don't think that I made it clear. I was implying that for large order harmonic components, the amplitudes and phases of the harmonic components vary almost linearly with the order of the harmonic component, so that you can interpolate or extrapolate the relation.

Elkins: Isn't the electron density profile dependent on the relation between the component amplitudes and the order of the harmonic components?

Lee: I don't want to comment on that at this time, but it is an interesting point. In the course of this study we noticed that the phase of the harmonics varied with the order of the harmonic component, and that a plot of phase of the component against the order of the harmonic components was sensitive to the chosen electron density profile. This could be due to the particular combinations of electron density and collision frequency profiles we used.

CONFERENCE ON GROUND-BASED RADIO WAVE PROPAGATION STUDIES OF THE LOWER IONOSPHERE
--Ground-based radio wave propagation studies...

DATE DUE
DATE DE RETOUR

JUN 1 - JUIN	1989		

ROGER DUHAMEL, F.R.S.C.
Queen's Printer and Controller of Stationery
Ottawa, 1968

Cat. No. DR 51-266/1